BioMed Research International

Renewable Energy and Alternative Fuel Technologies

Guest Editors: Meisam Tabatabaei, Keikhosro Karimi, Rajeev Kumar, and Ilona Sárvári Horváth

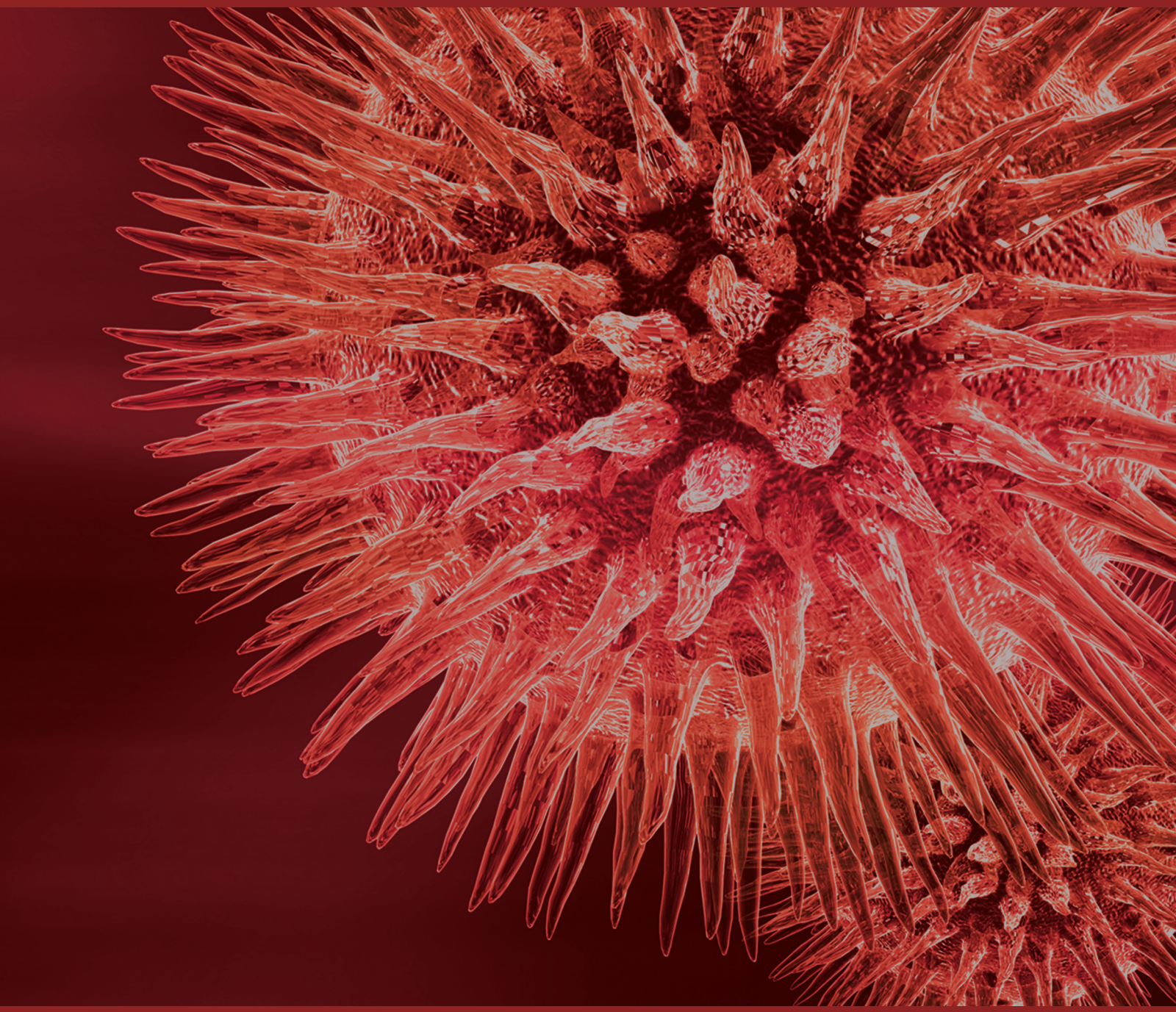

Renewable Energy and Alternative Fuel Technologies

BioMed Research International

Renewable Energy and Alternative Fuel Technologies

Guest Editors: Meisam Tabatabaei, Keikhosro Karimi, Rajeev Kumar, and Ilona Sárvári Horváth

Contents

Hindawi Publishing Corporation
BioMed Research International
Volume 2015, Article ID 245935, 2 pages
http://dx.doi.org/10.1155/2015/245935

Editorial
Renewable Energy and Alternative Fuel Technologies

Meisam Tabatabaei,[1,2] Keikhosro Karimi,[3] Rajeev Kumar,[4] and Ilona Sárvári Horváth[5]

[1]*Biofuel Research Team (BRTeam), Karaj 31438-44693, Iran*
[2]*Microbial Biotechnology and Biosafety Department, Agricultural Biotechnology Research Institute of Iran, Karaj 31359-33151, Iran*
[3]*Department of Chemical Engineering, Isfahan University of Technology, Isfahan 84156-83111, Iran*
[4]*Center for Environmental Research and Technology (CE-CERT), Bourns College of Engineering, University of California, Riverside (UCR), Riverside, CA 92507, USA*
[5]*Swedish Centre for Resource Recovery, University of Borås, 501 90 Borås, Sweden*

Correspondence should be addressed to Meisam Tabatabaei; meisam_tab@yahoo.com and Keikhosro Karimi; karimi@cc.iut.ac.ir

Received 4 December 2014; Accepted 4 December 2014

In recent years, biofuels have drawn considerable attention as clean and renewable source of energy. The most attractive types of biofuels are biogas, bioethanol, biodiesel, and biobutanol. Some of these biofuels are likely to play roles in the production of clean energy carriers as promising alternatives to fossil fuels and bring about environmental benefits globally. *Biogas* that primarily contains biomethane is produced through anaerobic digestion of organic wastes. Among the biofuels production processes, biogas process seems to be the easiest to conduct as it does not need sterilization, can be produced in simple reactors at moderate conditions using a natural consortium of microorganisms available in nature such as manure, and does not need a complicated separation and purification process. However, it is more complicated than it appears at first glance specially when high biogas yield is targeted. In fact, the microbiology and biochemistry of biogas production are the most complicated systems compared to those of the other biofuels, as four different processes, that is, hydrolysis, acidogenesis, acetogenesis, and methanogenesis are performed parallel where different types of microbes as a consortium work together. Furthermore, the substrates used for biogas production are a mixture of different components with different degradation properties. Main feedstocks are solid wastes, for example, agricultural, municipal, and food industrial wastes, and wastewater, for example, industrial and municipal wastewater. Technologies for biogas from municipal wastewater sludge are well developed; however, the recently increasing oil prices, unclear future of fossil fuels availability, and environmental impacts have led to significant interest in biogas from other resources especially from industrial and solid wastes. A number of potential substrates, for example, municipal solid waste and manure mixed with bedding materials, have a high potential; however, they contain lignocelluloses that are not easily bioconvertible. Therefore, a number of recent research activities are focused on the improvement of biogas from recalcitrant substrates, for example, lignocelluloses, and high-rate systems for biogas production.

Ethanol, the leading liquid biofuel, is widely used for transportation. Currently, sugarcane in Brazil and starchy materials, for example, corn in USA and wheat in Europe, are the main feedstocks (referred to as 1st generation), while lignocellulosic materials in the last decade (2nd generation or lignoethanol) and more recently algal biomass (3rd generation) are suggested as the raw materials. Lignoethanol seems to be the most promising type for the near future as these feedstocks are abundant and available at low prices. However, lignocelluloses are recalcitrant in nature and their processing is more complicated; the process needs a pretreatment step which is still challenging and consumption of hydrolytic enzymes should be minimized. Both of these problems are the subject of a high number of recent investigations. All in all, lignoethanol is more expensive than the 1st generation ethanol and process integration and biorefinery concepts are proposed to make the 2nd generation ethanol competitive.

Biodiesel is a promising alternative to diesel fuel, as it has a number of advantages including high cetane number, flash point, and inherent lubricity, creates less exhaust emissions, and contains no polluting chemicals like sulfur, as well as being renewable, biodegradable, and compatible to

the existing fuel distribution infrastructure. The process of biodiesel production at industrial scale is developed rather well and the most important challenging and limiting issue in biodiesel production is feedstock supply. In fact, the available feedstock is limited and accounts for over 70% of the total biodiesel production cost. "Crime against humanity" term is raised when edible sources started to be used. Therefore, the future sustainability of this industry is heavily dependent on nonedible feedstock supply and achieving more innovative, integrated, and efficient processes.

Biobutanol is considered more advanced compared to the other existing biofuels. Acetone production via acetone-butanol-ethanol (ABE) fermentation is an old process widely established during the First World War for military purposes in the Union of Soviet Socialist Republics, England, Canada, USA, Japan, China, and South Africa. Recently, ABE process attracted a high interest for the production of butanol as a renewable fuel. Main feedstocks used in the old processes were sugar-based substrates such as molasses and starchy materials such as wheat. Recently, low cost lignocellulosic wastes are suggested for ABE fermentation (lignobutanol); however, it suffers from the same problems as in lignoethanol. Furthermore, microorganisms used for biobutanol, for example, *Clostridium acetobutylicum* and *C. beijerinckii,* are more sensitive to inhibitors than the microorganisms used for biogas and ethanol production. Generally, the process of biobutanol production is more complicated than those of ethanol and biogas, as the microorganisms are strictly anaerobic; butanol-producing bacteria are severely inhibited by the process products especially butanol, and separation of products is more energy demanding and complicated. Compared to lignoethanol, lignobutanol is in its preliminary stage of research and a number of problems should be addressed in laboratory and pilot scales before the process becomes competitive to other biofuels at commercial scale.

Meisam Tabatabaei
Keikhosro Karimi
Rajeev Kumar
Ilona Sárvári Horváth

Hindawi Publishing Corporation
BioMed Research International
Volume 2015, Article ID 529808, 8 pages
http://dx.doi.org/10.1155/2015/529808

Research Article

A Comparative Study of Almond Biodiesel-Diesel Blends for Diesel Engine in Terms of Performance and Emissions

Nidal H. Abu-Hamdeh and Khaled A. Alnefaie

Mechanical Engineering Department, Faculty of Engineering, King Abdulaziz University, P.O. Box 80204, Jeddah 21589, Saudi Arabia

Correspondence should be addressed to Nidal H. Abu-Hamdeh; nabuhamdeh@kau.edu.sa

Received 6 June 2014; Revised 1 September 2014; Accepted 7 September 2014

Academic Editor: Meisam Tabatabaei

This paper investigates the opportunity of using almond oil as a renewable and alternative fuel source. Different fuel blends containing 10, 30, and 50% almond biodiesel (B10, B30, and B50) with diesel fuel (B0) were prepared and the influence of these blends on emissions and some performance parameters under various load conditions were inspected using a diesel engine. Measured engine performance parameters have generally shown a slight increase in exhaust gas temperature and in brake specific fuel consumption and a slight decrease in brake thermal efficiency. Gases investigated were carbon monoxide (CO) and oxides of nitrogen (NO_x). Furthermore, the concentration of the total particulate and the unburned fuel emissions in the exhaust gas were tested. A blend of almond biodiesel with diesel fuel gradually reduced the engine CO and total particulate emissions compared to diesel fuel alone. This reduction increased with more almond biodiesel blended into the fuel. Finally, a slight increase in engine NO_x using blends of almond biodiesel was measured.

1. Introduction

Current civilization is greatly reliant on fossil energy. Fossil fuels are the greatest energy source among all energy resources. The major part of energy requirements in the world is provided through petroleum resources such as natural gas, oil, and coal. Fossil fuel depletion is to increase with time. Since fossil resources are nonrenewable, rising demands and diminishing supplies keep fuel price rising dramatically.

The use of diesel engines resulted in numerous mechanized improvements for decreasing pollutant emissions as well as fuel usage [1]. Diesel machines are widely used in heavy-duty applications especially in the construction and farming sectors. Accordingly, the rate of reduction of diesel fuel is the greatest among gasoline fuels, which subsequently results in a greater rate of price increase of diesel fuel than other gasoline fuels. Additionally, the growing concern about environmental pollution since the 1990s has boosted the interest in alternative fuels. This has led to more financial support for research studies in energy management and conservation. Recently, the issues of steadily rising fuel prices, declining oil storage, and air contamination have resulted in the investigation of fossil fuel alternatives. These issues added to the increase in greenhouse gases such as CO_2 which is causing climate change and global warming have robustly boosted the interest in making use of biodiesel for power generation. Biodiesel is an expression usually used to refer to fatty acid methyl esters that are often created from animal fats or extracted from vegetables and have acceptable capabilities to be used in diesel engines. Because diesel fuel and vegetable oils have close cetane numbers, biodiesel made from vegetable oils might be used in current diesel engines after minor alterations [2–4].

Several studies have investigated the use of vegetable oils as alternative fuels [5–9]. Some of these research studies [10–16] reveal that there is little harm including lubricating oil thickening, injector coking, and gum formation ring sticking. The nonvolatility and excessive stickiness of pure vegetable oils were the major causes of these problems [17]. Talebi et al. [18] reported on a new software package, the BiodieselAnalyzer, for predicting the properties of a prospective biodiesel. Such software can estimate 16 different quality parameters of a biodiesel based on the fatty acid methyl ester profile of the oil feedstock used in making it.

Almonds (*Prunus dulcis*) are believed to be the most widely spread among tree nuts all over the world and are top of the list in tree nut output. They are affiliated to the Rosaceae group that also contains pears, prunes, and apples [19]. Almonds are widely produced in areas characterized by a Mediterranean climate [20], including many countries in the Mediterranean, all Middle East countries, and some countries in the Southern Hemisphere. The biggest producer of almonds in the world is the United States, specifically California; as a result, almond oil is mostly produced there [21]. Because biofuels are made from renewable sources, developing the technology to produce them must ensure the adequate supply of transporting fuel in the future as well as providing assurance against the uncertainty surrounding the petroleum resource timeline. Almond oil could be extracted from the seeds which contain a high percentage of oil [22–25]. As far as the author knows, no investigations were done on the employment of almond oil as a substitute for diesel fuel. Therefore, this study provides options for new valuable use for an existing crop.

Diesel engines are main sources of environmental pollutants such as carbon monoxide (CO), carbon dioxide (CO_2), oxides of nitrogen (NO_x), and partly burned (or burned) hydrocarbons (HC) organic compounds [26–29]. Usually, the portion of the fuel drawn in is not enough to hold great consequence on effectiveness but could be sufficient to cause severe air contamination. Such emissions have always been a critical issue in air pollution [30–32]. Engine exhaust emissions usually contain nitrogen oxides. As Lapuerta et al. [33] showed in their review paper, biodiesel exhibits an increase in NO_x concentration compared to diesel and only a few studies showed a percentage drop-off in NO_x concentration [34, 35].

This work aims to compare the various performance parameters and emissions of a single-cylinder diesel engine operating on almond biodiesel with an engine operating on pure diesel fuel through laboratory measurements in terms of exhaust gas temperature, brake specific fuel consumption, and brake thermal efficiency. Emissions investigated were carbon monoxide (CO), oxides of nitrogen (NO_x), and concentration of the total particulate and the unburned fuel emissions in the exhaust gas.

2. Materials and Methods

2.1. Extraction and Transesterification of Almond Oil. After peeling the almond seeds, they were dried at nearly 30°C and then crushed in a blender. Powdered seeds were kept at 5°C in polyethylene bags before analysis. The Bligh-Dyer method was used to extract almond oil [36]. Ground seeds were harmonized with a chloroform-methanol ($CHCl_3$/MeOH) mixture (1 : 1) and water. Two phases were obtained, aqueous layer (MeOH-water) and organic layer ($CHCl_3$). A rotary evaporator was used for evaporating off the solvent ($CHCl_3$) for the recovery of oil. A residual solvent was detached by oven drying for 1 hour at 60°C and flushing with 99.9% nitrogen. The transesterification of almond oil was performed as given by Hossain et al. [37] to guarantee fewer impurities.

2.2. Properties of Almond Biodiesel and Its Blends. The selected engine fuel was a local commercially available diesel fuel. A laboratory preparation of blends of almond biodiesel with diesel fuel was performed to operate a diesel engine and to make measurements of emissions and performance parameters. The ratios of blends selected were B0, B10, B30, and B50 on volume basis of almond biodiesel in an almond biodiesel-diesel fuel mixture. They are referred to as B0 (0% almond biodiesel-100% diesel fuel), B10 (10% almond biodiesel-90% diesel fuel), B30 (30% almond biodiesel-70% diesel fuel), and B50 (50% almond biodiesel-50% diesel fuel), respectively. These abbreviations are used throughout the current study.

Experimental measurements of the chemical and physical properties of the almond biodiesel with diesel fuel and diesel fuel alone have been performed since they directly affect emissions, fuel droplet dimension, and spray features. The analysis procedures and complete details have been followed as described in Kannan et al. [38]. The measured properties of diesel, biodiesel from almond oil, and different ratios of their blends according to ASTM standard are shown in Table 1.

2.3. Procedure and Experimental Setup. Experiments were performed to study biodiesel from almond oil as a substitute fuel to operate a diesel engine and the performance data were recorded. The exhaust gases constitution and the percentage of contaminant emissions were also measured and investigated. The experimental setup, schematically shown in Figure 1, consists of a single-cylinder, water-cooled, naturally aspirated, direct-injection (DI), and variable compression engine mounted on a standard TEQUIPMENT TD 43 test rig made in Britain. Swept volume of the engine was 583 cm^3 with a 95 mm bore and 82 mm bore by stroke. The injection system consists of an in-line fuel injection pump and throttle-type nozzle. The combustion chamber is direct injection type with a bowl-in piston design. The injection timing and injection pressure were set at 21° crank angle bTDC and 20 MPa, respectively. The cylinder pressure at each crank angle was measured and stored by a digital data acquisition system. It consisted of a Kistler water-cooled flush mounted piezoelectric pressure transducer in conjunction with Kistler charge amplifier for converting the electric charge into voltage. It could measure and store up to 200 cycles engine pressure histories. The measured data can be analyzed online or stored for postprocessing. A Chromel-Alumel (k-type) thermocouple together with a calibrated digital display was used to measure exhaust gas temperature. Load was applied through the engine's connection to an electrical generator dynamometer and could be varied by changing the control panel voltage. A rotameter was used to measure the flow rate of cooling water. The engine was similar to an engine used in a former study [39].

The differences in the measured performance and exhaust emission parameters from the "baseline" operation of the engine and all fuels tested were determined and compared. The experimental work started with a preliminary investigation of the engine running on neat diesel fuel, to determine the engine's operating characteristics and exhaust emission

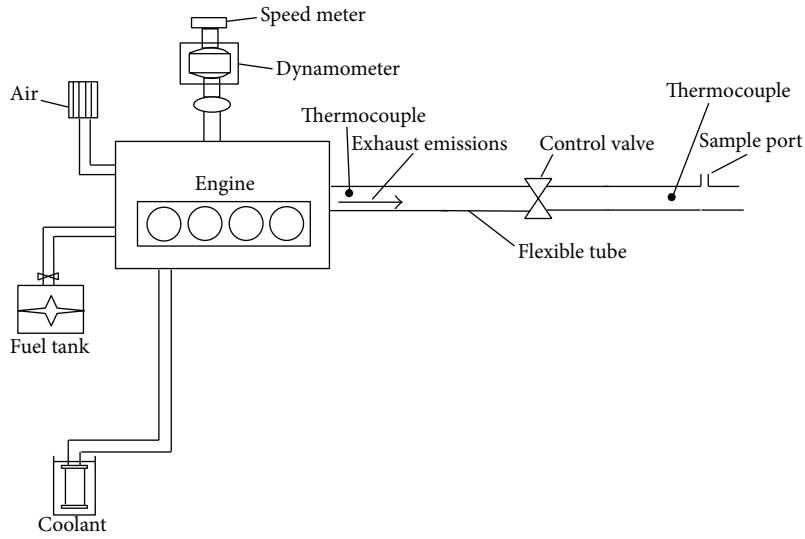

Figure 1: Schematic arrangement of the system.

Table 1: Physical and chemical specifications of fuels.

Property	Test method	100% diesel	30% almond biodiesel-70% diesel	50% almond biodiesel-50% diesel	100% almond biodiesel
Flash point (°C)	ASTM D 93	68	80	86	145
Fire point (°C)	ASTM D 93	82	97	102	154
Ash content (% by weight)	ASTM D 482	0.017	0.015	0.014	0.013
Kinematic viscosity at 40°C (cSt)	ASTM D 445	3.384	3.731	4.235	4.726
Density at 25°C (g/cm^3)	ASTM D 1298	0.848	0.856	0.870	0.911
Oxygen content (% vol.)		0	4.83	9.67	12.6
Carbon content (% by mass)	ASTM D 3176	80.6	80.8	81.0	81.1
Hydrogen content (% by mass)	ASTM D 3176	5.4	5.2	5.2	5.1
Calorific value (MJ/kg)	ASTM D 5865	48.610	44.727	43.532	41.761
Cetane number	ASTM D 613	47.48	48.31	52.54	54.32

levels constituting the "baseline." The data gathering was made at five engine torques from 4 to 20 N · m at an increment of 4 N · m each time. A control switch on the test rig was used to vary the engine torque. The time of injection was set at 21° bTDC and kept the same during all tests. In addition, the compression ratio was maintained at 18 : 1. The engine was warmed up at no load for 15 minutes to reach steady state conditions in all experiments. The speed of the engine was measured using a tachometer and it was adjusted to the rated speed of 1500 rpm by adjusting the governor connected to the fuel pump. A constant speed of 1500 rpm for the engine was used throughout this study. The same procedure was repeated for each fuel blend by repeating the same operating process for each fuel blend maintaining the same operating conditions. Before the start of the experiment with new fuel variant, the fuel used in the previous experiment was completely purged from the fuel line, filter, fuel pump, and fuel tank and the engine was left to operate for about three minutes to stabilize in its new condition. The data collected from the experimental tests included brake torque, exhaust and coolant temperatures, emissions from exhaust including carbon monoxide and nitrogen oxides, and emissions of total particulate. Engine torque, brake power, various temperatures, and air flow rate readings were taken from their meters on the test rig. Inlet and outlet cooling water temperatures were measured and recorded. Gas samples were drawn from the engine exhaust for the analysis of the contaminants.

For measuring the oxides of nitrogen (NO_x), carbon monoxide (CO), and total particulate emissions in the exhaust, a gas phase analysis scheme depicted a suggestive amount of the exhaust from the tester port. Sampling procedures and analysis performed were followed as in Abu-Hamdeh [39] in the fact that samples of the exhaust gas were

taken from the manifold of the exhaust and supplied to the analyzing instruments. NO_x measurements were obtained using Thermoelectron Model 10 AR chemiluminescent analyzer, while the samples of the exhaust were fed through a moisture trap cooled by ice and fed through a particulate filter before entering the gas analyzer. This was to ensure full drying and filtering of the gases before starting the analysis process. A gas analyzer (MSI 2000) was utilized to capture samples and evaluate the concentrations of CO in the exhaust gases. A gas extractor probe was used to remove the flue gas from the flue while measuring its temperature via a temperature sensor attached to its end. A suction pump, controlled electronically, was used to pump a constant flow rate of the gas into the evaluating compartment. After feeding throughout a constraint, same amounts of gas were pointed in the direction of electrochemical sensors via dosage compartment.

For the collection of particulate matter, unloaded clean strainers were inserted in an oven for about 24 h at 220°C. A calibrated sensitive digital balance (accuracy of ±0.02 mg) was used to weigh the strainers. The collected samples were passed out of the strainer for 3–5 min, allowing the collection of 20–90 mg of particulate matter. When the sampling process finished, the charged strainer was carefully taken off the probe. The strainer was equilibrated for a minimum of 24 hours in a controlled environment prior to being weighed for total particulate matter mass. During the equilibration period, relative humidity was maintained at a mean value of 35–40% and air temperature at a mean of 21–23°C. The particulate matter's weight was found out from the difference between the final weight of the strainer and its initial weight. The results obtained from the instruments mentioned above, accompanied by the engine torque and speed, were supplied to a data acquisition system. Each reported value for all measured parameters is the average of three replicates.

3. Results and Discussion

Density is an important property of fuel for compression ignition engines. It is worth noting that fuel density increases with the increase in the blending percentage. The 50% and 100% almond biodiesel blends have about 2.6% and 7.4% higher density, respectively, than diesel fuel. Preheating of biodiesel before injection could be done to overcome the problem of higher fuel density by taking advantage of the high temperature of the engine exhaust gas. The kinematic viscosity was measured for biodiesel from almond oil and was found to be 4.726 cSt, which is about 40% more than the kinematic viscosity of diesel (3.384 cSt). A decrease in the blending percentage of almond biodiesel decreased the kinematic viscosity of the mixture. The shape of the fuel droplets and atomization are affected by the fuel viscosity. Higher viscosity of fuel may cause problems and smoky exhaust. This requires higher spraying pressure to obtain the desired spray pattern inside the cylinder. In contrast, very low viscous fuel would prevent accurate metering of the fuel especially in older engines due to the leakage from piston walls of the injection pump [37]. Preheating of biodiesel

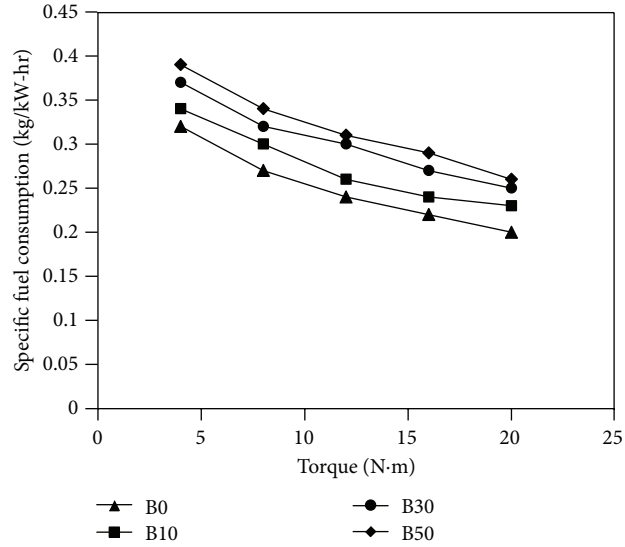

Figure 2: Variations of specific fuel consumption versus measured torque for fuels used in the study.

before injection either in the fuel tank or in the fuel lines could be done to overcome the problem of higher viscosity of biodiesel oils by taking advantage of the high temperature of the engine exhaust gas. The heating value of the almond biodiesel was measured and found to be 41.761 MJ/kg, which is 14% lower than the heating value of diesel. The flash point of almond biodiesel was 145°C while diesel has a flash point of 68°C. Transportation and safe storage are improved by higher flash point. Blending of almond biodiesel with diesel fuel reduced the value of the flash point. Still the flash point of the diesel fuel is comparatively lower than that of the different ratios of biodiesel blends. Diesel fuel and pure almond biodiesel have about equal values of carbon and hydrogen content, but in terms of ash diesel fuel contains higher percentage than almond biodiesel.

Experimental investigations of almond biodiesel on single-cylinder diesel engine were done and several parameters, such as specific fuel consumption (bsfc), brake thermal efficiency (η_b), exhaust gas temperature (T_g), carbon monoxide (CO), nitrous oxide (NO_x), particulate matter, and unburned fuel emissions, have been determined. The results obtained are shown in Figures 2 through 8.

Figure 2 shows the effect of blending ratio and measured torque on the specific fuel consumption (bsfc) at 1500 rpm. Blends of biodiesel in general have more specific fuel consumption than diesel fuel at the same torque and it increases with increasing blending ratio of biodiesel. The first reason for that is the different LHV of the biodiesel with respect to the fossil diesel. Other secondary reasons are poor atomization and the formation of mixtures with biodiesel blends because of their higher density and kinematic viscosity compared to their values with diesel fuel. That is to say, more percentages of biodiesel blends are needed to produce the same torque.

Figure 3 illustrates the change in the brake thermal efficiency (η_b) as a function of torque measured. The figure shows that for a given torque the thermal efficiency for

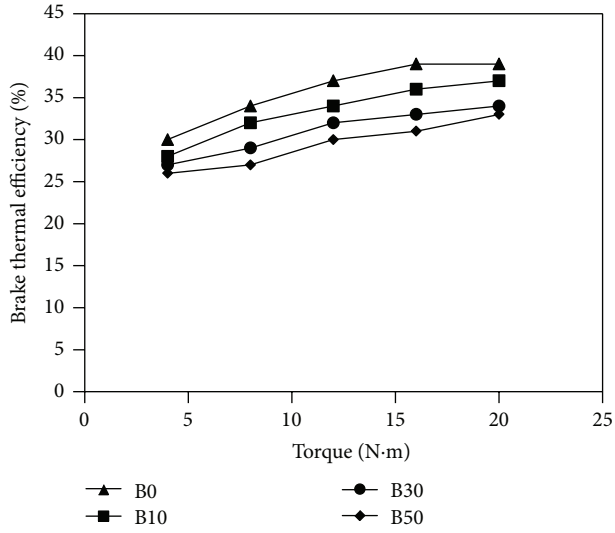

Figure 3: Variations of brake thermal efficiency versus measured torque for fuels used in the study.

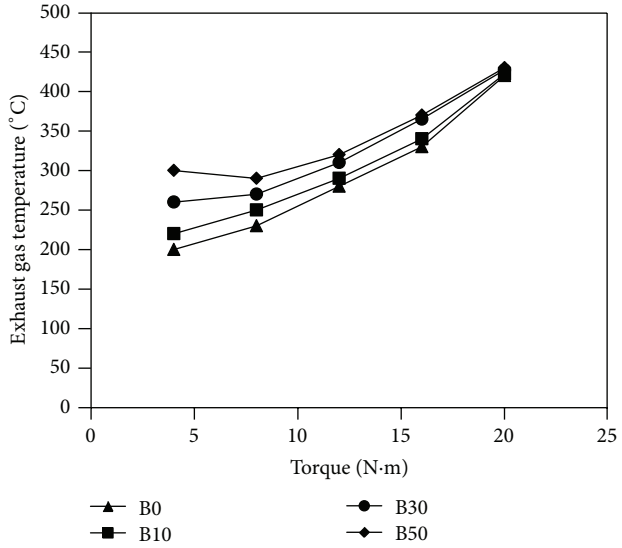

Figure 4: Variations of exhaust gas temperature versus measured torque for fuels used in the study.

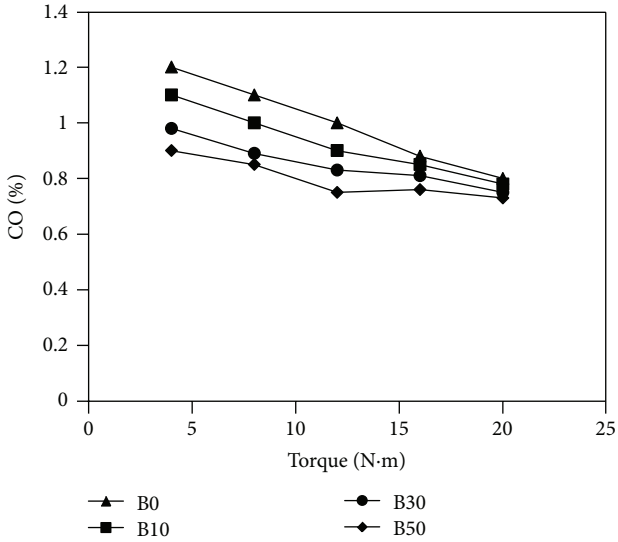

Figure 5: Variations of carbon monoxide concentration in the exhaust versus measured torque for fuels used in the study.

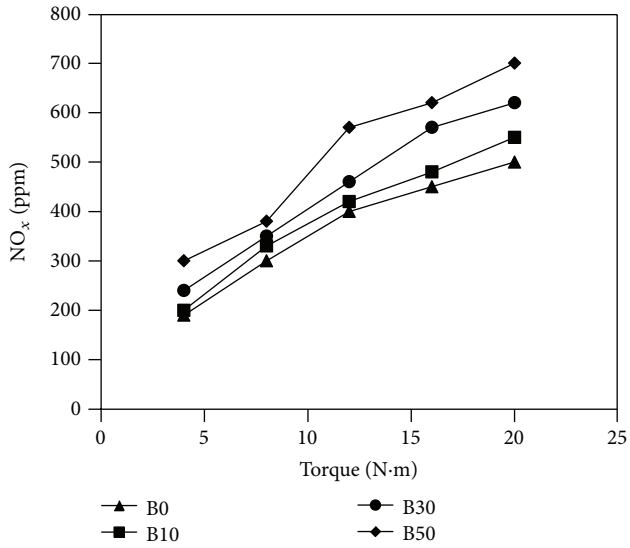

Figure 6: Variations of NO_x concentration in the exhaust versus measured torque for fuels used in the study.

biodiesel blends is less than thermal efficiency for diesel fuel. A major reason for this tendency is the higher density and viscosity of biodiesel in comparison to diesel fuel which results in poor atomization and leads to lower combustion efficiency especially at higher torques. The thermal efficiency improvement of the 10% almond biodiesel blend over the other blending ratios can be accredited to the better oxygen content which enhances combustion particularly during the stage of diffusion combustion and to the reduction of the friction loss because of higher lubricity of almond biodiesel. Further reduction in brake thermal efficiency with increasing the percentages of almond biodiesel blends can be noticed. This reduction in thermal efficiency with increasing the percentages of almond biodiesel blends can be credited to the inferior combustion characteristics of the blends due to their relatively poor volatility, high viscosity, lower calorific values, and slow burning rate and that overcomes the surplus oxygen existing in the almond biodiesel.

Figure 4 illustrates the change of exhaust gas temperature (T_g) with measured torque for the fuels used. Diesel fuel has lower exhaust gas temperature than biodiesel blends, and it increases with the blending ratio. This could mean earlier burning in case of higher blends of biodiesel due to shorter premixed combustion period. High cetane number values reduce the premixing time and move the combustion phasing earlier in the compression stroke. At higher loads, biodiesel blends and diesel fuel have comparable exhaust gas temperature.

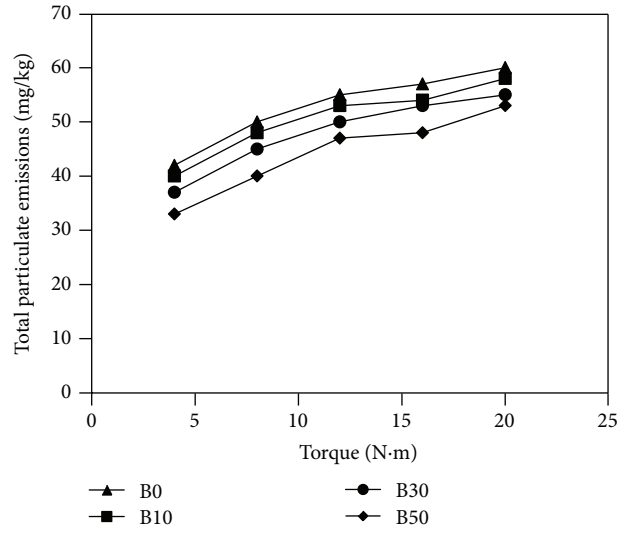

Figure 7: Total particulate emissions versus measured torque for fuels used in the study.

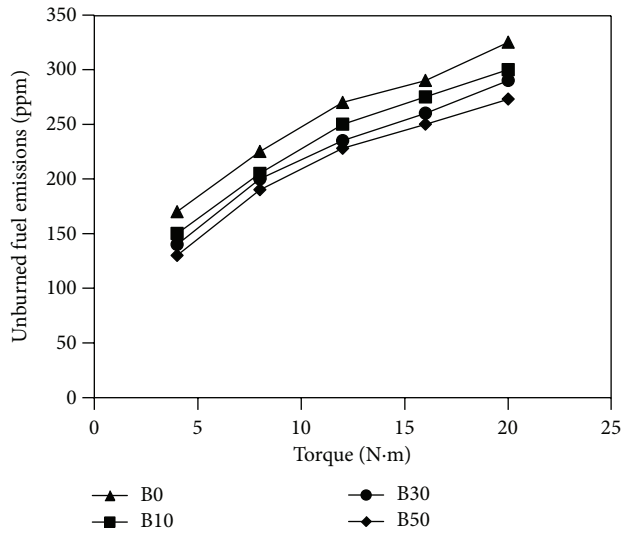

Figure 8: Unburned fuel emissions versus measured torque for fuels used in the study.

The concentration change of carbon monoxide (CO) with respect to measured torque is illustrated in Figure 5. The first observation that can be noticed in the figure is that CO emissions decrease with increasing measured torque. In all the internal combustion engines upon raising the load (and then the torque) at constant engine speed there is a significant increment of combustion temperature with remarkable conversion of CO to CO_2 and then less emission of CO at the exhaust. Furthermore, it is observed that the higher biodiesel blend value, the lower CO emissions in the exhaust gas at any measured torque. For the same load, it seems that blends of biodiesel accelerate the reaction rates and propagate the flame successfully throughout the fuel mixture resulting in improved combustion. This is a result of the existence of more oxygen content in biodiesel. This probably decreased the CO in the exhaust gas.

The variation of NO_x percentage in the exhaust gas as a function of torque measured is shown in Figure 6. NO_x concentration in all blends shows higher values compared to diesel fuel. The higher blends of biodiesel produced higher NO_x emissions. The production of NO_x is influenced by maximum temperature of the cylinder charge. Generally, the existence of oxygen in the biodiesel molecules performs as an extra factor to increase NO_x making. At higher loads, enhanced combustion and higher flame temperature increase NO_x emissions. Moreover, NO_x emissions are noticed to rise with the increase of oxygen content in the fuel. This is due to the local leaner air fuel ratio as the almond blends contain some oxygen in their molecular structure.

A glimpse at the curves in Figure 7 shows that the percentage of biodiesel blend influenced the concentration of particulate matter in the exhaust. Agglomerates of tiny carbonaceous particles are the primarily comprise of particulate emissions from diesel engines. The particulate matter character is highly vassal to the extent to which combustion progresses as preblend combustion in opposition to propagation of combustion flame [40]. Figure 7 illustrates the change in particulate emissions for different fuels used with torque measured. The particulate matter concentration was obtained as the ratio of the particulates' mass in milligrams collected by the filter from the exhaust stream to the total mass of the exhaust in kilograms passing through the filter in the same interval of time. Figure 7 points out that the increased load led to an increase in the particulate emissions. It could be read from the same figure that at any torque value there is an inverse relationship between the biodiesel blending ratio and the particulate emissions; that is, when biodiesel blending ratio increases the particulate emissions decrease. The 50% biodiesel blend produced the lowest particulate emissions compared to all fuels used in the study. Figure 8 shows the variation of unburned fuel emissions for different fuels used with torque measured. The 50% biodiesel blend produced the lowest unburned fuel emissions compared to all the test fuels. At full load conditions 50% biodiesel blend emitted 18% lower unburned fuel emissions than that of diesel fuel. At the same load, the B10 and B30 blends produced 6% and 10% lower unburned fuel emissions than diesel fuel, respectively. This shows that the particulate and unburned fuel emissions tend to reduce as the content of oxygen of the fuel increases, which leads to the particulate oxidation through the combustion interval. It is worth mentioning that the flow of the exhaust stream through oxidation catalysts reduces particulate emissions.

4. Conclusion

The emissions and performance features of a single-cylinder, naturally aspirated, diesel engine fueled with diesel-almond biodiesel blends were investigated in this study. Blends used were 10%, 30%, and 50% of almond biodiesel with diesel fuel. The blends and the diesel fuel were examined under various load conditions. In terms of engine performance, it was found

that increasing blending ratios of almond biodiesel increased the specific fuel consumption (bsfc) for biodiesel and exhaust gas temperature (T_g); on the other hand it decreased brake thermal efficiency (η_b). Blending ratio B10 has the minimum specific fuel consumption and the maximum brake thermal efficiency among other blend ratios. In terms of emissions, it was found that increasing blending ratios of almond biodiesel decreased the particulate matter, unburned fuel emissions, and CO content in the exhaust gas. However, higher blends of biodiesel produced higher NO_x emissions. In general, it is feasible to use biodiesel made from almond oil blends to run a diesel engine but more investigation is required to reach clear-cut conclusions and to give more details on the potential of this biomass as a fuel.

Conflict of Interests

The authors declare that there is no conflict of interests regarding the publication of this paper.

Acknowledgment

The project was funded by the Deanship of Scientific Research (DSR), King Abdulaziz University, Jeddah, under grant no. (162/135/1434). The authors, therefore, acknowledge with thanks DSR technical and financial support.

References

[1] R. Zhu, X. Wang, H. Miao, X. Yang, and Z. Huang, "Effect of dimethoxy-methane and exhaust gas recirculation on combustion and emission characteristics of a direct injection diesel engine," *Fuel*, vol. 90, no. 5, pp. 1731–1737, 2011.

[2] A. Srivastava and R. Prasad, "Triglycerides-based diesel fuels," *Renewable & Sustainable Energy Reviews*, vol. 4, no. 2, pp. 111–133, 2000.

[3] Y. Ali and M. A. Hanna, "Alternative diesel fuels from vegetable oils," *Bioresource Technology*, vol. 50, no. 2, pp. 153–163, 1994.

[4] R. Altin, S. Çetinkaya, and H. S. Yücesu, "Potential of using vegetable oil fuels as fuel for diesel engines," *Energy Conversion and Management*, vol. 42, no. 5, pp. 529–538, 2001.

[5] G. L. Wagner and C. L. Peterson, "Performance of winter rape (Brassica napus) based fuel mixture in diesel engines," in *Proceedings of the International Conference on Plant and Vegetable Oils as Fuels*, pp. 329–333, ASAE, St. Joseph, Mich, USA, 1982.

[6] K. S. Varde, "Some correlation of diesel engine performance with injection characteristics using vegetable oil as fuels," in *Proceedings of the International Conference on Plant and Vegetable Oils as Fuels*, pp. 303–331, Saint Joseph, Mo, USA, 1982.

[7] N. J. Schlautman, J. L. Schinstock, and M. A. Hanna, "Unrefined expelled soybean oil performance in a diesel engine," *Transactions of the American Society of Agricultural Engineers*, vol. 29, no. 1, pp. 70–80, 1986.

[8] K. Schmidt and J. H. Van Gerpen, "The effect of biodiesel fuel composition on diesel combustion and emissions," SAE Paper no. 961086, SAE, Warrendale, Pa, USA, 1996.

[9] Y. Zhang and J. H. Van Gerpen, "Combustion analysis of esters of soybean oil in a diesel engine," SAE Paper 960765, SAE, Warrendale, Pa, USA, 1996.

[10] R. A. Baranescu and J. L. Lusco, "Performance, durability and low temperature evaluation of sunflower oil as a diesel fuel," in *Proceedings of the International Conference on Plant and Vegetable Oils as Fuels*, pp. 312–332, Saint Joseph, Mo, USA, 1982.

[11] S. C. Borgelt and F. D. Harris, "Endurance tests using soybean oil–diesel fuel mixture to fuel small pre-combustion chamber engines," in *Proceedings of the International Conference on Plant and Vegetable Oils as Fuels*, pp. 364–337, ASAE, St. Joseph, Mich, USA, 1982.

[12] J. W. Goodrum, V. C. Patel, and R. W. McClendon, "Diesel injector carbonization by three alternative fuels," *Transactions of the American Society of Agricultural Engineers*, vol. 39, no. 3, pp. 817–821, 1996.

[13] C. L. Peterson, J. C. Thompson, and J. S. Taberski, "One-thousand-hour engine durability test with HySEE and using a 5X-EMA test cycle," *Transactions of the American Society of Agricultural Engineers*, vol. 42, no. 1, pp. 23–30, 1999.

[14] K. Beetul, S. B. Sadally, N. Hossenkhan, and D. Puchooa, "An investigation of biodiesel production from microalgae found in mauritian waters," *Biofuel Research Journal*, vol. 1, no. 2, pp. 58–64, 2014.

[15] H. Cao, Z. Zhang, X. Wu, and X. Miao, "Direct biodiesel production from wet microalgae biomass of *Chlorellapyrenoidosa* through *in situ* transesterification," *BioMed Research International*, vol. 2013, Article ID 930686, 6 pages, 2013.

[16] M. Shafiei, K. Karimi, H. Zilouei, and M. J. Taherzadeh, "Enhanced ethanol and biogas production from pinewood by NMMO pretreatment and detailed biomass analysis," *BioMed Research International*, vol. 2014, Article ID 469378, 10 pages, 2014.

[17] E. H. Pryde, "Vegetable oil fuel standards," in *Proceedings of the International Conference on Plant and Vegetable Oils as Fuels*, pp. 101–106, ASAE, St. Joseph, Mich, USA, 1982.

[18] A. F. Talebi, M. Tabatabaei, and Y. Chisti, "BiodieselAnalyzer: a user-friendly software for predicting the properties of prospective biodiesel," *Biofuel Research Journal*, vol. 1, no. 2, pp. 55–57, 2014.

[19] A. J. Sfahlan, A. Mahmoodzadeh, A. Hasanzadeh, R. Heidari, and R. Jamei, "Antioxidants and antiradicals in almond hull and shell (*Amygdalus communis* L.) as a function of genotype," *Food Chemistry*, vol. 115, no. 2, pp. 529–533, 2009.

[20] D. E. Kester and R. Asay, "Almonds," in *Advances in Fruit Breeding*, J. Janick and J. N. Moore, Eds., pp. 387–419, Purdue University Press, West Lafayette, Ind, USA, 1975.

[21] W. C. Evans, *Trease and Evans' Pharmacognosy*, WB Saunders, London, UK, 1996.

[22] R. Socias i Company, O. Company, J. M. Alonso, and T. M. Gradziel, "Almond quality: a breeding perspective," *Horticultural Reviews*, vol. 34, pp. 197–238, 2008.

[23] G. A. Spiller, D. J. A. Jenkins, L. N. Cragen et al., "Effect of a diet high in monounsaturated fat from almonds on plasma cholesterol and lipoproteins," *Journal of the American College of Nutrition*, vol. 11, no. 2, pp. 126–130, 1992.

[24] P. A. Davis and C. K. Iwahashi, "Whole almonds and almond fractions reduce aberrant crypt foci in a rat model of colon carcinogenesis," *Cancer Letters*, vol. 165, no. 1, pp. 27–33, 2001.

[25] F. Hotellier and P. Delaveau, "Oils of pharmaceutical dietetic and cosmetic importance," *Annales Pharmaceutiques Francaises*, vol. 30, no. 7, pp. 495–502, 1972.

[26] A. Murugesan, C. Umarani, R. Subramanian, and N. Nedunchezhian, "Bio-diesel as an alternative fuel for diesel

engines-A review," *Renewable and Sustainable Energy Reviews*, vol. 13, no. 3, pp. 653–662, 2009.

[27] Y. D. Wang, T. Al-Shemmeri, P. Eames et al., "An experimental investigation of the performance and gaseous exhaust emissions of a diesel engine using blends of a vegetable oil," *Applied Thermal Engineering*, vol. 26, no. 14-15, pp. 1684–1691, 2006.

[28] B. K. Barnwal and M. P. Sharma, "Prospects of biodiesel production from vegetable oils in India," *Renewable and Sustainable Energy Reviews*, vol. 9, no. 4, pp. 363–378, 2005.

[29] S. Sundarapandian and G. Devaradjane, "Experimental investigation of the performance on vegetable oil operated CI engine," in *Proceedings of the 19th National Conference on IC Engine and Combustion*, pp. 87–94, Annamalai University, Chidambaram, India, 2005.

[30] S. Senthil Kumar, A. Remesh, and B. Nagalingam, "Complete vegetable oil fuelled dual fuel compression ignition engine," SAE International 2001-28-0067, 2001.

[31] S. Oberweis, T. T. Al-Shemmeri, and N. Packer, "The impact of dissociation on the flame temperature in biomass combustion," in *HEATSet Conference*, Chambéry, France, 2007.

[32] A. Demirbas, *Biodiesel—A Realistic Fuel Alternative for Diesel Engines*, Springer, London, UK, 2008.

[33] M. Lapuerta, O. Armas, and J. Rodríguez-Fernández, "Effect of biodiesel fuels on diesel engine emissions," *Progress in Energy and Combustion Science*, vol. 34, no. 2, pp. 198–223, 2008.

[34] T. T. Al-Shemmeri and S. Oberweis, "Correlation of the NOx emission and exhaust gas temperature for biodiesel," *Applied Thermal Engineering*, vol. 31, no. 10, pp. 1682–1688, 2011.

[35] S. Ouenou-Gamo, M. Ouladsine, and A. Rachid, "Measurement and prediction of diesel engine exhaust emissions," *ISA Transactions*, vol. 37, no. 3, pp. 135–140, 1998.

[36] E. G. Bligh and W. J. Dyer, "A rapid method of total lipid extraction and purification," *Canadian Journal of Biochemistry and Physiology*, vol. 37, no. 8, pp. 911–917, 1959.

[37] J. Hossain, S. Biswas, and A. Islam, "Bio-diesel from mustard oil: a renewable alternative fuel for small diesel engines," *Modern Mechanical Engineering*, vol. 1, no. 2, pp. 77–83, 2011.

[38] D. Kannan, M. N. Nabi, and J. E. Hustad, "Influence of ethanol blend addition on compression ignition engine performance and emissions operated with diesel and jatropha methyl ester," SAE paper 2009-01-1808, SAE International Powertrains, Fuels and Lubricants Meeting, 2009.

[39] N. H. Abu-Hamdeh, "Effect of cooling the recirculated exhaust gases on diesel engine emissions," *Energy Conversion and Management*, vol. 44, no. 19, pp. 3113–3124, 2003.

[40] A. D. Abid, J. Camacho, D. A. Sheen, and H. Wang, "Quantitative measurement of soot particle size distribution in premixed flames—the burner-stabilized stagnation flame approach," *Combustion and Flame*, vol. 156, no. 10, pp. 1862–1870, 2009.

Hindawi Publishing Corporation
BioMed Research International
Volume 2015, Article ID 409103, 9 pages
http://dx.doi.org/10.1155/2015/409103

Research Article

Catalysis of Rice Straw Hydrolysis by the Combination of Immobilized Cellulase from *Aspergillus niger* on β-Cyclodextrin-Fe_3O_4 Nanoparticles and Ionic Liquid

Po-Jung Huang,[1] Ken-Lin Chang,[2] Jung-Feng Hsieh,[3] and Shui-Tein Chen[1,4]

[1] *Institute of Biological Chemistry, Academia Sinica, 128 Section 2, Academia Road, Nankang, Taipei 115, Taiwan*
[2] *School of Environmental Science and Engineering, Guangdong University of Technology, Guangzhou 510006, China*
[3] *Department of Food Science, Fu Jen Catholic University, Xinzhuang, Taipei 242, Taiwan*
[4] *Institute of Biochemical Sciences, College of Life Science, National Taiwan University, Taipei 115, Taiwan*

Correspondence should be addressed to Shui-Tein Chen; bcchen@gate.sinica.edu.tw

Received 5 June 2014; Revised 6 August 2014; Accepted 16 August 2014

Academic Editor: Keikhosro Karimi

Cellulase from *Aspergillus niger* was immobilized onto β-cyclodextrin-conjugated magnetic particles by silanization and reductive amidation. The immobilized cellulase gained supermagnetism due to the magnetic nanoparticles. Ninety percent of cellulase was immobilized, but the activity of immobilized cellulase decreased by 10%. In this study, ionic liquid (1-butyl-3-methylimidazolium chloride) was introduced into the hydrolytic process because the original reaction was a solid-solid reaction. The activity of immobilized cellulase was improved from 54.87 to 59.11 U g immobilized cellulase^{-1} at an ionic liquid concentration of 200 mM. Using immobilized cellulase and ionic liquid in the hydrolysis of rice straw, the initial reaction rate was increased from 1.629 to 2.739 g h^{-1} L^{-1}. One of the advantages of immobilized cellulase is high reusability—it was usable for a total of 16 times in this study. Compared with free cellulase, magnetized cellulase can be recycled by magnetic field and the activity of immobilized cellulase was shown to remain at 85% of free cellulase without denaturation under a high concentration of glucose (15 g L^{-1}). Therefore, immobilized cellulase can hydrolyze rice straw continuously compared with free cellulase. The amount of harvested glucose can be up to twentyfold higher than that from the hydrolysis by free cellulase.

1. Introduction

Recently, magnetic nanoparticles (MNPs) have been applied to enzyme immobilization because the high surface areas of such particles at the nanometer scale are beneficial to enzyme loading. In contrast, porous carrier materials would limit the rate of diffusion during enzymatic reactions [1], thus reducing the rate of reaction. The most common method for producing synthetic MNPs is the coprecipitation of ferrous and ferric ions at a molar ratio of 1 : 2 by alkali solutions. The reaction is indicated as follows:

$$Fe^{2+} + 2Fe^{3+} + 8OH^- \longrightarrow Fe_3O_{4(s)} + 4H_2O \quad (1)$$

Although this method of preparing MNPs is well known, the phase and size of MNPs are difficult to control. The properties of a nanomagnetite can be regulated by (1) temperature [2–4], (2) initial pH [2, 5], (3) stirring velocity [6], (4) different iron salt solutions with varying ratios of ferrous and ferric ions [3, 7], (5) types and concentrations of alkali [3, 8], (6) surfactants [5], and (7) ionic strength of the solution [4].

Immobilization of cellulase on MNPs allows for the recycling of the most costly ingredient of the rice straw hydrolysis process. A variety of methods [9] can be used to immobilize enzymes, including (1) physical adsorption to a solid phase [10], (2) covalent bonding to a solid phase [11], (3) covalent bonding to a soluble polymer [12, 13], (4) cross-linking with bifunctional reagents [14], (5) inclusion in a gel phase [12], and (6) encapsulation [15]. A popular technique for coupling magnetite with cellulase involves the use of silane as a linker. A functional silane compound, such as 3-aminopropyltriethoxysilane (APTES), can self-assemble onto the surface of a magnetite and form

covalent bonds [16–18]. Subsequently, the functional silane can transfer the surface of magnetite from dense hydroxyl group to amino group [19]. Therefore, modified nanomagnetite can conjugate with cellulase easily. Garcia III et al. [20] used γ-glycidoxypropyltrimethoxysilane and 3-aminopropyltriethoxysilane that were refluxed in toluene to modify the surface of magnetite. Additionally, they used PEG and PVA as ligands to improve upon the direct attachment on silanized magnetite. As a result, cellulase was immobilized onto the surface of magnetite successfully and the activity of cellulase was comparable to that of free cellulase in a phosphate buffer of pH 5.5. Furthermore, the cellulase could be immobilized onto MNPs using carbodiimide as the coupling agent [21, 22]. Their method of immobilization preserved both cellulase activity and particle size.

The purpose of this study was to immobilize cellulase from *Aspergillus niger* onto aqueous MNPs, which were modified and size-limited by β-cyclodextrin. After cellulase was bound to MNPs via 3-aminopropyltriethoxysilane (APTES) and glutaraldehyde directly, we determined the optimum operating conditions. The size and structure of MNPs were measured by Zeta-sizer and X-ray diffraction (XRD). The structure and morphology of immobilized cellulase were confirmed using X-ray photoelectron spectroscopy (XPS) and transmission electron microscopy (TEM).

2. Materials and Methods

2.1. Chemicals and Raw Materials. Ferrous chloride tetrahydrate, ferric chloride, oleic acid, kerosene, and β-cyclodextrin (all from Sigma Chemical Co., USA) and ammonium (J.T.-Baker, USA) were used to synthesize magnetic nanoparticles. Ethanol (J.T.-Baker, USA) was added to stabilize and suspend the magnetic nanoparticles during the silanization of 3-aminopropyltriethoxysilane (APTES, Sigma Chemical Co., USA). Glutaraldehyde (Sigma Chemical Co., USA) was used as the linker between cellulase and the magnetic nanoparticles. The Schiff base was reduced by sodium cyanoborohydride (Sigma Chemical Co., USA).

Acetate buffer (pH 5.5) (J.T.-Baker, USA) was prepared by dissolving acetic acid sodium acetate trihydrate in Milli-Q water. Cellulase from *Aspergillus niger* (Sigma Chemical Co., USA) was used for the hydrolysis of untreated rice straw. The enzymatic activity of cellulase was determined by the method of Ratanakhanokchai et al. [23]. The hydrolysis reaction was carried out by incubation of untreated rice straw with 150 U cellulase per gram of rice straw in 10 mL of 50 mM acetate buffer solution at pH 5.5 and 37°C. A buffer solution of 0.01% sodium azide (Sigma Chemical Co., USA) was added to prevent microorganism contamination. The hydrolytic mixture was incubated in a rotating incubator at 1.67 Hz. After incubation, samples were collected and centrifuged for sugar analysis.

Rice straws from 5-month-old plants of a japonica rice (*O. sativa* L.) variety, Tainung 67, were obtained from the experimental farm (25° 02′ 32.79″N, 121° 36′ 47.40″E with 18 m of elevation) located at the Academia Sinica campus, Taipei, Taiwan. The rice plants were transplanted to the field in the first week of March 2009 and the heading (flowering) appeared in the first week of June 2009. The straws (leaves and stems) were collected after the seeds were harvested in late July. The rice plants were approximately 100 cm tall with approximately 13~15 tillers at the time of harvest. The dried rice straws were then ground into powder and stored in sealed plastic bags at room temperature. The size distribution of the rice straws was determined by mesh sieving, and five fractions were obtained: >300 mm (3.39%); 300~150 mm (47.95%); 150~106 mm (15.52%); 106~75 mm (20.57%;) <75 mm (12.63%).

2.2. Preparation of Magnetite Nanoparticles. In this study, naked Fe_3O_4 magnetic nanoparticles were prepared by the coprecipitation method. $FeCl_3$ (2.6 g, 16 mmol) and $FeCl_2{\cdot}4H_2O$ (1.0 g, 5 mmol) were dissolved in 400 mL deionized water. The mixed solution was placed in an inert environment and purged by nitrogen for 30 minutes to prevent oxidation of the magnetite. The solution containing ferric and ferrous ions was then heated to 60°C, during which the color changed from yellow to orange. After the mixture turned orange, an ammonium solution (1.5 M, 100 mL) was added, inducing an immediate color change from orange to black and the formation of a colloid mixture. After the reduction by the alkali solution, the black colloid was heated to 80°C. Oleic acid was added to the solution, and the solution was heated for another hour until the ammonia evaporated. Subsequently, the solution was cooled to room temperature, and 100 mL kerosene was added to the coated magnetite suspension. The suspension was stirred until most of the black color had been transferred into the kerosene. The kerosene layer was collected, and the water layer was discarded. The kerosene layer was dropped onto a β-CDs solution with ratios (v/v) to black colloid of 0.02, 0.1, 0.5, and 1. The structure of the magnetic supporter Fe_3O_4-β-CDs was determined by XRD and ESCA (Electron Spectroscopy for Chemical Analysis). The particle size was measured by Zeta-sizer.

2.3. Cellulase Immobilization. A total of 150 mg Fe_3O_4-(β-CDs) magnetic nanoparticles were coated with 10% (v/v) 3-aminopropyltriethoxysilane (APTES) overnight at 40°C to form amino-functionalized magnetic nanoparticles (AFMNs). Afterwards, 10% (v/v) glutaraldehyde was added as the coupling agent to react with the AFMNs for another 12 hours. The aldehyde-functionalized magnetic nanoparticles (100 mg) were then incubated with cellulase (68 mg) from *Aspergillus niger* in a sodium cyanoborohydride (100 mg) solution to immobilize the cellulase onto the surface of magnetite. The immobilized cellulase was characterized by ESCA (Electron Spectroscopy for Chemical Analysis) and SQUID (Superconducting Quantum Interference Device). The activity of immobilized cellulase was analyzed by the FPU method.

2.4. Characterization of Nanoparticles. X-ray diffraction (XRD) patterns were recorded using a PANalytical X' Pert PRO diffractometer with the Cu Kα line (1.54 Å). Beam

divergence was restricted with a 0.15 mm silt on the source side. The X-ray diffraction studies were performed in the scan range of 2θ = 15~70° with a scan speed of 1° min^{-1} and a step size of 0.02°. Analysis of the X-ray photoelectron spectra (XPS) was performed on a thermo-ESCLAB 250 using an incident X-ray radiation (Cu Kα) as the excitation source. Particle size distribution and morphology were analyzed by a vibrating sample magnetometer at room temperature. Fourier transform infrared (FT-IR) spectra were recorded in the wave length rage of 4000~500 cm^{-1} using a Nicolet (Madison, WI) FT-IR spectrometer (model impact 410).

2.5. Sugar Determination and Cellulase Activity Measurements. The reducing sugars from hydrolyzed rice straw were measured by the dinitrosalicylic acid method (DNS) [24], and the activities of free and immobilized cellulase were determined by the FPU method. Immobilized cellulase was added to 5 mg filter paper (1 mm width × 6 mm length) overlaid with 150 μL of acetate buffer (50 mM, pH 5.5). The mixture was then incubated at 37°C. After 1 hour, 100 μL of sample was collected from the mixture and 300 μL of DNS reagent was added to this aliquot. The sample was heated at 95°C for 5 min to allow color formation. When the reaction ended, deionized water (600 μL) was added into the solution. The concentration of reducing sugar was determined at 540 nm on a HITACHI UV2010/3010.

3. Results and Discussion

3.1. Characteristics of Magnetic Nanoparticles. XRD was conducted to identify the MNPs that were prepared with ferrous and ferric salts in varying concentrations of β-cyclodextrin. Five samples were produced with the following compositions: Fe^{2+}/Fe^{3+}/CDs = 0.33/1/0, Fe^{2+}/Fe^{3+}/CDs = 0.33/1/0.02, Fe^{2+}/Fe^{3+}/CDs = 0.33/1/0.1, Fe^{2+}/Fe^{3+}/CDs = 0.33/1/0.5, and Fe^{2+}/Fe^{3+}/CDs = 0.33/1/1 (Figure 1). Other common coprecipitates, such as $Fe(OH)_3$ or Fe_2O_3, were not observed because the positions of the main peaks only matched well with those from the JCPDS card (19-0629) for Fe_3O_4. Our method of MNP preparation yielded highly pure Fe_3O_4 particles (Figure 2). Size measurement by the Zeta-sizer revealed that the average size of the Fe_3O_4 particles was 28.05 nm. The addition of oleic acid as a surfactant led to a decrease in particle size down to 10.1 nm. The subsequent addition of β-cyclodextrin to the samples with Fe^{2+}/Fe^{3+}/CDs ratios of 0.33/1/0.1 and 0.33/1/1 further reduced the average particle size down to 6.2 and 4.5 nm, respectively. Notably, as the β-cyclodextrin concentration increased, the size of the obtained Fe_3O_4 crystallite decreased. These results showed that β-cyclodextrin can be used to effectively limit the particle size of magnetite.

The Fourier transform infrared (FTIR) spectra of β-CDs, Fe_3O_4, and β-CDs-modified Fe_3O_4 revealed the following features (Figure 3). For the Fe_3O_4 magnetite, a peak at approximately 570 cm^{-1} was assigned to the stretching vibration of Fe–O (Figure 3(a)). The β-CDs spectrum showed large and abroad peaks at approximately 3344 cm^{-1} that corresponded to the O–H stretching vibration (Figure 3(c)).

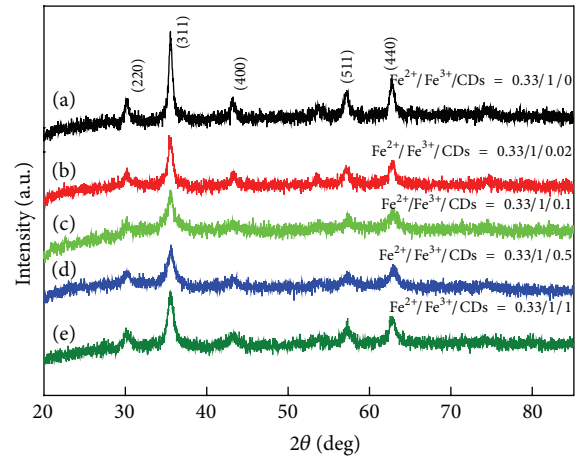

FIGURE 1: X-ray diffraction patterns of Fe_3O_4 with different ratios of ferric ion, ferrous ion, and β-CDs: (a) $Fe^{2+}/Fe^{3+}/\beta$-CDs = 0.33/1/0, (b) $Fe^{2+}/Fe^{3+}/\beta$-CDs = 0.33/1/0.02, (c) $Fe^{2+}/Fe^{3+}/\beta$-CDs = 0.33/1/0.1, (d) $Fe^{2+}/Fe^{3+}/\beta$-CDs = 0.33/1/0.5, and (e) $Fe^{2+}/Fe^{3+}/\beta$-CDs = 0.33/1/1.

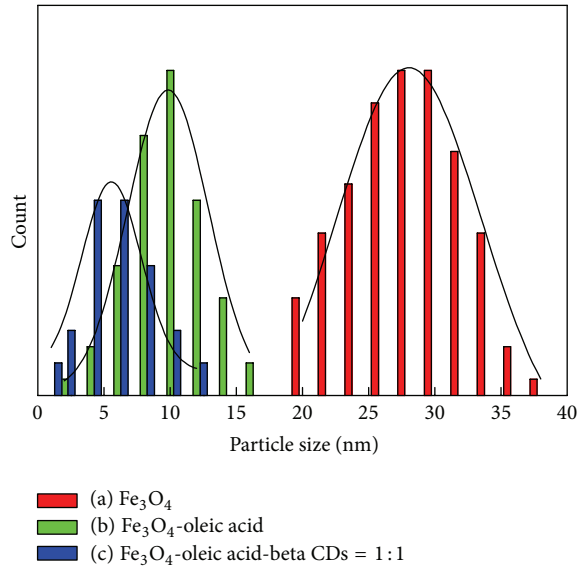

FIGURE 2: The particle size distributions of Fe_3O_4 that were synthesized under different conditions: (a) Fe_3O_4; (b) Fe_3O_4-oleic acid; (c) Fe_3O_4-oleic acid-(β-CDs): $Fe^{2+}/Fe^{3+}/\beta$-CDs = 0.33/1/1.

The peaks at approximately 2923 and 2854 cm^{-1} of the β-CD spectrum were attributed to the stretching vibration of C–H. Furthermore, the stretching vibrations of the glucose ring, such as OCH, HCH, CCH, and COH, were observed at approximately 1408, 1368, and 1332 cm^{-1}. In addition, three peaks at 1156, 1080, and 1028 cm^{-1} were indicative of the C–O–C linkage. For the Fe_3O_4-(β-CDs) conjugate, two specific peaks of oleic acid were identified with the C=O symmetric stretching vibration at 1708 cm^{-1}, the C=C stretching vibration at 1641 cm^{-1}, and the =CH bending vibration at 1004 cm^{-1} (Figure 3(b)). Moreover, the conjugation between Fe_3O_4 and β-CDs was evident from the observation that

Table 1: Saturation magnetization and coercivity values at 300 K of Fe_3O_4 nanoparticles synthesized with various iron salts.

Type of magnetic nanoparticles	Saturation magnetization (emg g^{-1})	Coercivity (Oe)
Fe_3O_4-(β-CDs)	64.7	0.288
Fe_3O_4-(β-CDs)-APTES	61.3	0.330
Fe_3O_4-(β-CDs)-AP-G	60.5	0.479
Fe_3O_4-(β-CDs)-AP-GE	50.7	3.82

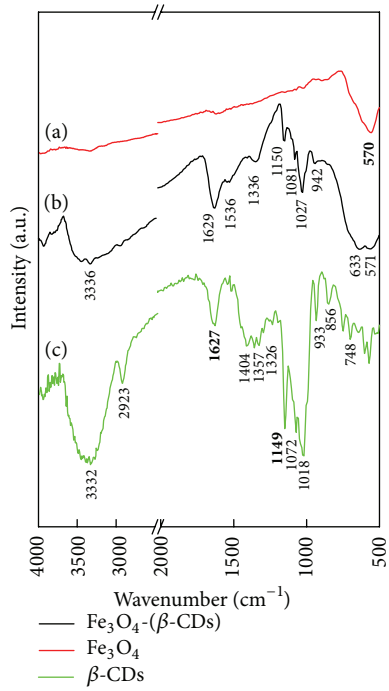

Figure 3: FTIR spectra of (a) Fe_3O_4, (b) Fe_3O_4-(β-CDs): Fe^{2+}/Fe^{3+}/β-CDs = 0.33/1/1, and (c) β-CDs.

the serial peaks of β-CDs shifted to higher wavenumbers of approximately 6–15 cm^{-1}. Therefore, the collective results of ESCA and FTIR indicated that Fe_3O_4 conjugated with β-CDs covalently.

3.2. Characteristics of Immobilized Cellulase on Magnetic Nanoparticles. The measurement of total binding energy of Fe_3O_4-(β-CDs) showed characteristic peaks of Fe at 708.2 and 722 eV, which were the binding energy of Fe 2p 3/2 and Fe 2p 1/2, respectively (Figure 4(a)). When cellulase was immobilized onto Fe_3O_4-(β-CDs) after APTES coating, the binding energy of Fe was shifted higher by 1-2 eV (Figure 4(d)). This upward shift was due to the transfer of the Fe electron density to cellulase, thus making it more difficult to emit the Fe electrons. Moreover, compared with Fe_3O_4-(β-CDs)-AP and Fe_3O_4-(β-CDs)-APGE (Figures 4(b) and 4(c)), the characteristic peak of N was clearly detected and its intensity increased after immobilization. When APTES was conjugated onto the surface of magnetite, we detected the amine functional group at approximately 400.4 eV (Figure 4(e)). After immobilization of cellulase, two peaks were shown in the spectrum of Fe_3O_4-(β-CDs)-APGE, with one at 399.8 eV, which indicated the formation of Schiff base, and the other at 401.2 eV, which corresponded to the free amine of cellulase.

The magnetic properties of the magnetite nanoparticles were measured by the Quantum Design MPMS-XL7 magnetometer with the application of field dependence of magnetization. The values of saturation magnetization and coercivity are shown in Figure 5 and tabulated in Table 1. The nanoparticles at each step were superparamagnetic in nature. However, the saturation magnetization value was gradually reduced from 64.7 to 50.7 emg g^{-1} and the coercivity value was gradually increased from 0.288 to 3.82 Oe when the nanomagnetite was modified stepwise from Fe_3O_4-(β-CDs) to Fe_3O_4-(β-CDs)-AP-GE, respectively. In other words, when cellulase was immobilized onto Fe_3O_4-(β-CDs), the barrier of magnetite was produced by each following modification. Morphological analysis of immobilized cellulase by TEM (Figure 6) and SEM (Figure 7) showed that the average particle size was approximately 30 nm.

3.3. Characteristics of Immobilized Cellulase on Magnetic Nanoparticles. Maximum and optimum amount of grafting (i.e., the production of Fe_3O_4-(β-CDs)-AP-GE) was achieved with the combination of 10% (v/v) APTES, 10% (v/v) glutaraldehyde, and 2.4% (wt) cellulase, when the dose of Fe_3O_4-(β-CDs) was 10 mg/mL. The activity of cellulase was reduced from 60.6 to 58.9 U g^{-1} enzyme after immobilization in acetate buffer (pH 5.5), which was 97% of the activity of free cellulase. The optimum operating condition was changed from acidic to weakly acidic condition. Previous studies on the immobilization of cellulase from *Trichoderma viride* onto Fe_3O_4 also showed that the optimum condition of cellulase activity shifted from acidic to weakly acidic condition [20, 21]. This change is beneficial for immobilized cellulase using magnetite as the supporter because magnetite is more prone to erosion under acidic conditions, even though an acidic condition is more suitable for free cellulase. The phase transformation was previously demonstrated [25–27], and the structure was shown to be destroyed under acidic conditions. This result was presented by SEM in Figure 7. The original immobilized cellulase had a particle size of approximately 20~30 nm and the boundary was clearly identifiable (Figure 7(d)). At pH 5.0, the surface structure of the magnetic particles was still maintained. However, at lower pH values the particle surface was eroded by the acetic acid. As the pH was lowered, we observed a surface phase transition from a smooth state to a more uneven state, and the properties of magnetization and supermagnetism were reduced or completely eliminated by acid erosion.

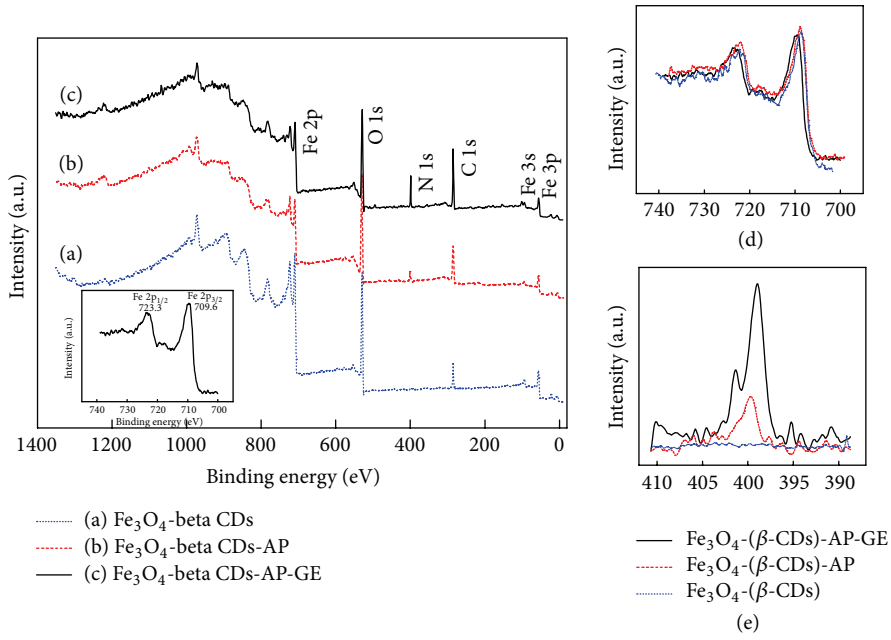

FIGURE 4: XPS spectra of total binding energies of immobilized cellulase from *Aspergillus niger* on Fe_3O_4 nanoparticles: (a) Fe_3O_4-(β-CDs); (b) Fe_3O_4-(β-CDs)-AP; (c) Fe_3O_4-(β-CDs)-AP-GE; (d) binding energy of Fe 2p; (e) binding energy of N 1s; (f) binding energy of C 1s. Dash line: Fe_3O_4-(β-CDs); dotted line: Fe_3O_4-(β-CDs)-AP; solid line: Fe_3O_4-(β-CDs)-AP-GE. The Fe_3O_4 MNPs were produced using the following ratio of ions and β-CDs: $Fe^{2+}/Fe^{3+}/\beta$-CDs = 0.33/1/1.

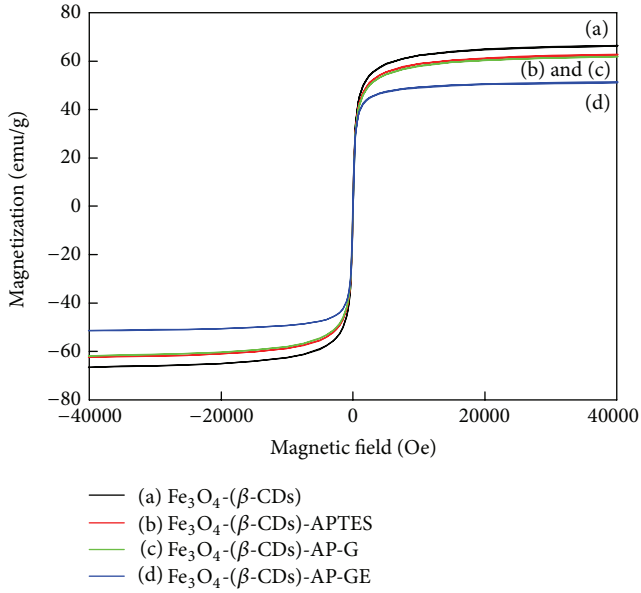

FIGURE 5: Magnetization curves and coercivity measurements at 300 K of Fe_3O_4 nanoparticles at different stages of synthesis and modification up to the immobilization of cellulase: curve (a) represents β-CD-modified Fe_3O_4; curve (b) represents APTES-modified particles; curve (c) represents glutaraldehyde-conjugated particles; curve (d) represents cellulase-bound particles.

Therefore, the weakly acidic condition is more suitable for hydrolysis catalyzed by immobilized cellulase on a magnetic supporter.

In the hydrolysis experiment, the initial rate of rice straw hydrolysis was reduced from 2.26 to 1.553 g L^{-1} hr^{-1} when cellulase was added at a concentration of 150 U g^{-1} rice straw. The ionic liquids could be used to dissolve cellulose by disrupting hydrogen bonding within cellulose [28–30]. SEM results from previous studies showed that ionic liquids not only removed the outer structural boundaries of cellulose but also improved its hydrophilicity [29, 30]. Zhao et al. [30] reported that these actions of ionic liquids could enhance cellulose hydrolysis. The hydrolysis rate would increase by fourfold compared with no ionic liquid treatment. Therefore, we tested the effects of three ionic liquids including 1-butyl-3-methylimidazolium chloride ([bmim]Cl), 1-butyl-3-methylimidazolium hydrogen sulfate ([bmim]HSO_4), and 1-ethyl-3-methylimidazolium diethyl phosphate ([emim]$PO_4(C_2H_6)_2$) on cellulose hydrolysis.

The values of the initial rate of hydrolysis and the amount of reducing sugar are shown in Figure 8 and tabulated in Table 2. All three ionic liquids increased the amount of reducing sugar (11.9–14.16 g L^{-1}) compared with the control condition with free cellulase only (5.97 g L^{-1}). Additionally, the initial rate of hydrolysis was increased from approximately 2.918 to 5.7 g L^{-1} h^{-1} after adding any of the ionic liquids. Even though immobilized cellulase was not as active as free cellulase in rice straw hydrolysis, this difference was compensated by adding ionic liquid to the reaction with the immobilized enzyme. Using immobilized cellulase, the amount of sugar produced was increased from 3.58 to 5.3 g L^{-1} h^{-1} and the initial rate of hydrolysis was increased

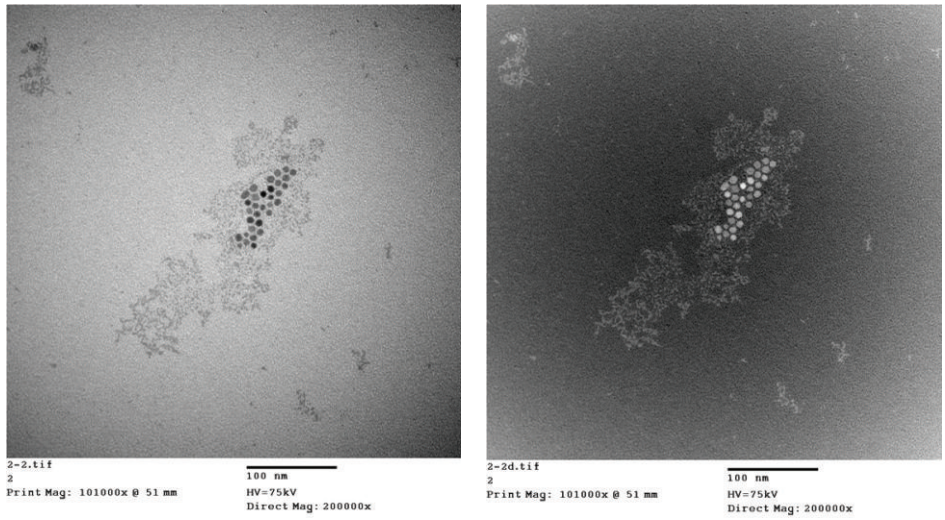

(a) (b)

Figure 6: Morphology of immobilized cellulase. (a) TEM bright field (×200 k) and (b) TEM dark field (×200 k).

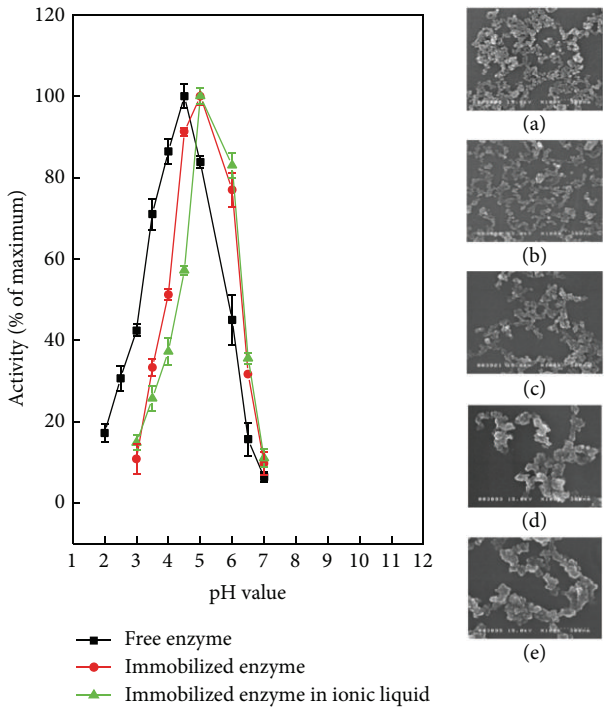

Figure 7: Effect of pH on the activity of (■) free cellulase, (●) immobilized cellulase, and (▲) immobilized cellulase + ionic liquid. Morphologies of immobilized cellulase under different pH were analyzed by SEM: (a) original immobilized cellulase; (b) pH = 5.0; (c) pH = 4.0; (d) pH = 3.0; (e) pH = 2.0.

from 1.6 g L^{-1} h^{-1} to 2.7 g L^{-1} h^{-1} on average when an ionic liquid was introduced.

Table 2: The amount of sugar produced and the initial rate of reducing sugar formation by free and immobilized cellulase with or without ionic liquid treatment.

Type of enzyme	Amount of sugar (g L^{-1}) (24 hours)	Initial rate (g L^{-1} h^{-1})
Free cellulase (FC)	5.97 ± 1.29	2.918 ± 1.89
FC + [bmim]Cl	11.91 ± 3.33	5.807 ± 3.66
FC + [bmim]HSO_4	13.56 ± 4.27	5.671 ± 1.06
FC + [emim]$PO_4(C_2H_6)_2$	14.16 ± 1.82	5.635 ± 2.57
Immobilized cellulase onto Fe_3O_4 (IC)	4.78 ± 2.44	1.629 ± 0.92
IC + [bmim]Cl	5.392 ± 2.07	2.739 ± 1.31
IC + [bmim]HSO_4	5.821 ± 1.33	2.711 ± 1.55
IC + [emim]$PO_4(C_2H_6)_2$	5.719 ± 3.49	2.595 ± 0.84

When cellulase was immobilized onto Fe_3O_4, it could be collected by magnet and reused. We found that immobilized cellulase was still active after 16 rounds of hydrolysis, with each round set for 12 hours (Figure 9). The activity of immobilized cellulase remained at 44.15% of the initial activity after 16 cycles. Furthermore, the addition of sodium cyanoborohydride during the process of immobilization could trigger reductive amidation to convert Schiff's base to a carbon-nitrogen single bond, which is more stable than Schiff's base. We assessed the activities of recycled cellulase with or without the inclusion of sodium cyanoborohydride and found that, after 16 rounds of hydrolysis, the sodium cyanohydride-containing samples retained 85% of the initial cellulase activity, while the control group without sodium cyanoborohydride only retained approximately 40% of the initial activity. Thus, the total amount of sugar from rice straw

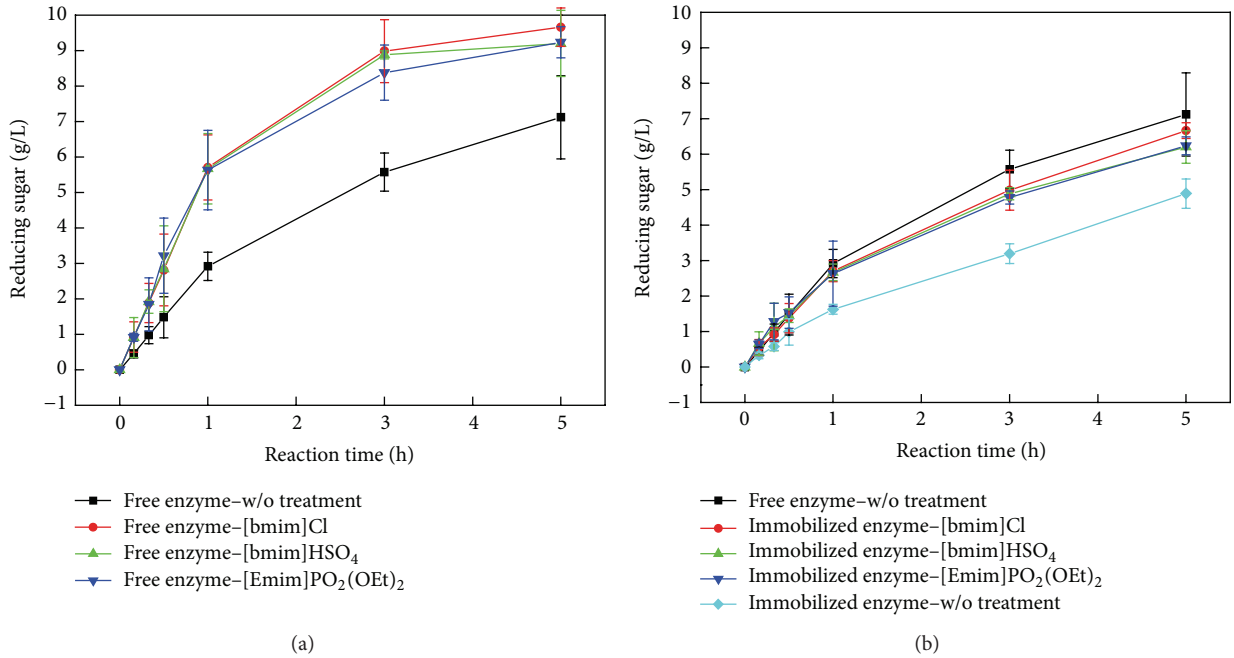

Figure 8: The concentration of reducing sugar that was produced from rice straw (150 U g^{-1}) hydrolysis in the presence of different ionic liquids at pH 5.0, 37°C, and 1.67 Hz rotation speed. (a) Free cellulase with or without ionic liquid; (b) immobilized cellulase with or without ionic liquid. ■: rice straw hydrolysis by cellulase without ionic liquid treatment; ●: rice straw hydrolysis by cellulase and 1-butyl-3-methylimidazolium chloride ([bmim]Cl); ▲: rice straw hydrolysis by cellulase and 1-butyl-3-methylimidazolium hydrogen sulfate ([bmim]HSO_4); ▼: rice straw hydrolysis by cellulase and 1-ethyl-3-methylimidazolium diethyl phosphate ([emim]$PO_4(C_2H_6)_2$); ◆: rice straw hydrolysis by immobilized cellulase without ionic liquid treatment.

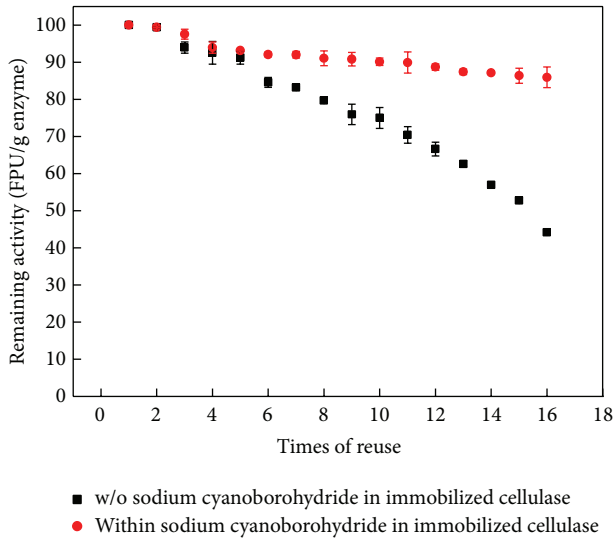

Figure 9: Activities of immobilized cellulase after repeated use.

hydrolysis was ten- to twentyfold higher when immobilized cellulase was used instead of free cellulase.

4. Conclusions

In this study, we found that β-CDs could effectively decrease the size of MNPs. The particles were reduced from 28.05 to 4.5 nm in diameter and became more uniformly distributed compared with those that were not conjugated to β-CDs. Enzymatic attachment was confirmed by XPS. After immobilization, the characteristic peak of iron was shifted to a higher binding energy by 1-2 eV. Moreover, the characteristic peak of N was detected at 399.2 eV (Schiff's base) and 401.4 eV (free amine). These data suggested that cellulase was successfully immobilized onto the surface of nanomagnetite using the silane system. The immobilized cellulase not only retained the activity of free cellulase but also gained the properties of magnetization, specifically supermagnetism. The optimum pH for the enzyme shifted from 4.0 to 5.5 after immobilization. This higher pH serves to stabilize the magnetite-associated cellulase during hydrolysis because the decrease in acidity prevents structural damage to the magnetite.

Although the activity of immobilized cellulase was reduced by 10% compared with free cellulase, the addition of an ionic liquid, such as 1-butyl-3-methylimidazolium chloride ([bmim]Cl), 1-butyl-3-methylimidazolium hydrogen sulfate ([bmim]HSO_4), and 1-ethyl-3-methylimidazolium diethyl phosphate ([emim]$PO_4(C_2H_6)_2$), could enhance rice straw hydrolysis by immobilized cellulase. The initial rate and

Table 3: The total amount of sugar from rice straw hydrolysis by free cellulase and immobilized cellulase with or without the use of $NaBH_3CN$.

Type of enzyme	Total concentration of sugar (g/L)
Free cellulase	10.5 ± 3.58
Immobilized cellulase onto Fe_3O_4 (w/o adding $NaBH_3CN$)	110.66 ± 21.11
Immobilized cellulase onto Fe_3O_4 (add $NaBH_3CN$)	208.92 ± 29.77

amount of sugar production were both increased by adding ionic liquids, and the activity of immobilized cellulase was enhanced to match that of free cellulase.

The immobilized cellulase was shown to be reusable for 16 cycles of hydrolysis while still maintaining approximately 80% residual activity. Until now, the total concentration of sugar was 208.92 g L^{-1} (Table 3), which is higher than using the free enzyme (10.5 g L^{-1}). Collectively, findings from this study suggest that immobilization of cellulase may greatly benefit the ethanol production industry.

Conflict of Interests

The authors declare that there is no conflict of interests regarding the publication of this paper.

Authors' Contribution

Ken-Lin Chang, Jung-Feng Hsieh, and Shui-Tein Chen contributed equally to this work.

Acknowledgment

The authors thank the Ministry of Science and Technology (Taiwan) for grant support (MOST 103-2313-B-030-001).

References

[1] A. K. Gupta and M. Gupta, "Synthesis and surface engineering of iron oxide nanoparticles for biomedical applications," *Biomaterials*, vol. 26, no. 18, pp. 3995–4021, 2005.

[2] G. Gnanaprakash, S. Mahadevan, T. Jayakumar, P. Kalyanasundaram, J. Philip, and B. Raj, "Effect of initial pH and temperature of iron salt solutions on formation of magnetite nanoparticles," *Materials Chemistry and Physics*, vol. 103, no. 1, pp. 168–175, 2007.

[3] K. Tao, H. Dou, and K. Sun, "Interfacial coprecipitation to prepare magnetite nanoparticles: concentration and temperature dependence," *Colloids and Surfaces A*, vol. 320, no. 1–3, pp. 115–122, 2008.

[4] L. Vayssières, C. Chanéac, E. Tronc, and J. P. Jolivet, "Size tailoring of magnetite particles formed by aqueous precipitation: an example of thermodynamic stability of nanometric oxide particles," *Journal of Colloid and Interface Science*, vol. 205, no. 2, pp. 205–212, 1998.

[5] A. P. A. Faiyas, E. M. Vinod, J. Joseph, R. Ganesan, and R. K. Pandey, "Dependence of pH and surfactant effect in the synthesis of magnetite (Fe_3O_4) nanoparticles and its properties," *Journal of Magnetism and Magnetic Materials*, vol. 322, no. 4, pp. 400–404, 2010.

[6] R. Valenzuela, M. C. Fuentes, C. Parra et al., "Influence of stirring velocity on the synthesis of magnetite nanoparticles (Fe_3O_4) by the co-precipitation method," *Journal of Alloys and Compounds*, vol. 488, no. 1, pp. 227–231, 2009.

[7] H. Iida, K. Takayanagi, T. Nakanishi, and T. Osaka, "Synthesis of Fe_3O_4 nanoparticles with various sizes and magnetic properties by controlled hydrolysis," *Journal of Colloid and Interface Science*, vol. 314, no. 1, pp. 274–280, 2007.

[8] X. Liang, X. Wang, J. Zhuang, Y. Chen, D. Wang, and Y. Li, "Synthesis of nearly monodisperse iron oxide and oxyhydroxide nanocrystals," *Advanced Functional Materials*, vol. 16, no. 14, pp. 1805–1813, 2006.

[9] M. Koneracká, P. Kopčanský, M. Timko et al., *Methods in Biotechnology: Immobilization of Enzymes and Cells*, 2nd edition, 2006.

[10] V. R. Murty, J. Bhat, and P. K. A. Muniswaran, "Hydrolysis of oils by using immobilized lipase enzyme: a review," *Biotechnology and Bioprocess Engineering*, vol. 7, no. 2, pp. 57–66, 2002.

[11] G. Baum, F. B. Ward, and H. H. Weetall, "Stability, inhibition and reactivation of acetylcholinesterase covalently coupled to glass," *Biochimica et Biophysica Acta—Enzymology*, vol. 268, no. 2, pp. 411–414, 1972.

[12] P. Chim-Anage, Y. Kashiwagi, Y. Magae, T. Ohta, and T. Sasaki, "Properties of cellulase immobilized on agarose gel with spacer," *Biotechnology and Bioengineering*, vol. 28, no. 12, pp. 1876–1878, 1986.

[13] S. Park, Y. Lee, D. N. Kim, S. Park, E. Jang, and W.-G. Koh, "Entrapment of enzyme-linked magnetic nanoparticles within poly(ethylene glycol) hydrogel microparticles prepared by photopatterning," *Reactive and Functional Polymers*, vol. 69, no. 5, pp. 293–299, 2009.

[14] A. Azem, Y. Tsfadia, O. Hajouj, I. Shaked, and E. Daniel, "Cross-linking with bifunctional reagents and its application to the study of the molecular symmetry and the arrangement of subunits in hexameric protein oligomers," *Biochimica et Biophysica Acta*, vol. 1804, no. 4, pp. 768–780, 2010.

[15] A. Takimoto, T. Shiomi, K. Ino et al., "Encapsulation of cellulase with mesoporous silica (SBA-15)," *Microporous and Mesoporous Materials*, vol. 116, no. 1–3, pp. 601–606, 2008.

[16] S. Čampelj, D. Makovec, and M. Drofenik, "Functionalization of magnetic nanoparticles with 3-aminopropyl silane," *Journal of Magnetism and Magnetic Materials*, vol. 321, no. 10, pp. 1346–1350, 2009.

[17] B. Hu, J. Pan, H.-L. Yu, J.-W. Liu, and J.-H. Xu, "Immobilization of *Serratia marcescens* lipase onto amino-functionalized magnetic nanoparticles for repeated use in enzymatic synthesis of Diltiazem intermediate," *Process Biochemistry*, vol. 44, no. 9, pp. 1019–1024, 2009.

[18] M. Yamaura, R. L. Camilo, L. C. Sampaio, M. A. Macêdo, M. Nakamura, and H. E. Toma, "Preparation and characterization of (3-aminopropyl)triethoxysilane-coated magnetite nanoparticles," *Journal of Magnetism and Magnetic Materials*, vol. 279, no. 2-3, pp. 210–217, 2004.

[19] W. D. Bascom, "Structure of silane adhesion promoter films on glass and metal surfaces," *Macromolecules*, vol. 5, no. 6, pp. 792–798, 1972.

[20] A. Garcia III, S. Oh, and C. R. Engler, "Cellulase immobilization on Fe_3O_4 and characterization," *Biotechnology and Bioengineering*, vol. 33, pp. 321–326, 1988.

[21] J. Jordan, C. S. S. R. Kumar, and C. Theegala, "Preparation and characterization of cellulase-bound magnetite nanoparticles," *Journal of Molecular Catalysis B: Enzymatic*, vol. 68, no. 2, pp. 139–146, 2011.

[22] J. Alftrén and T. J. Hobley, "Immobilization of cellulase mixtures on magnetic particles for hydrolysis of lignocellulose and ease of recycling," *Biomass and Bioenergy*, vol. 65, pp. 72–78, 2014.

[23] K. Ratanakhanokchai, K. L. Kyu, and M. Tanticharoen, "Purification and properties of a xylan-binding endoxylanase from alkaliphilic *Bacillus sp*. strain K-1," *Applied and Environmental Microbiology*, vol. 65, no. 2, pp. 694–697, 1999.

[24] G. L. Miller, "Use of dinitrosalicylic acid reagent for determination of reducing sugar," *Analytical Chemistry*, vol. 31, no. 3, pp. 426–428, 1959.

[25] J.-P. Jolivet, C. Chanéac, and E. Tronc, "Iron oxide chemistry. From molecular clusters to extended solid networks," *Chemical Communications*, vol. 10, no. 5, pp. 481–483, 2004.

[26] U. Schwertmann, J. Friedl, and H. Stanjek, "From Fe(III) ions to ferrihydrite and then to hematite," *Journal of Colloid and Interface Science*, vol. 209, no. 1, pp. 215–223, 1999.

[27] K. Przepiera and A. Przepiera, "Kinetics of thermal transformations of precipitated magnetite and goethite," *Journal of Thermal Analysis and Calorimetry*, vol. 65, no. 2, pp. 497–503, 2001.

[28] S. Datta, B. Holmes, J. I. Park et al., "Ionic liquid tolerant hyperthermophilic cellulases for biomass pretreatment and hydrolysis," *Green Chemistry*, vol. 12, no. 2, pp. 338–345, 2010.

[29] R. P. Swatloski, S. K. Spear, J. D. Holbrey, and R. D. Rogers, "Dissolution of cellose with ionic liquids," *Journal of the American Chemical Society*, vol. 124, no. 18, pp. 4974–4975, 2002.

[30] H. Zhao, C. L. Jones, G. A. Baker, S. Xia, O. Olubajo, and V. N. Person, "Regenerating cellulose from ionic liquids for an accelerated enzymatic hydrolysis," *Journal of Biotechnology*, vol. 139, no. 1, pp. 47–54, 2009.

Hindawi Publishing Corporation
BioMed Research International
Volume 2015, Article ID 824965, 10 pages
http://dx.doi.org/10.1155/2015/824965

Review Article

Current Status and Future Potential of Energy Derived from Chinese Agricultural Land: A Review

Ningning Zhai,[1,2] Chunlan Mao,[2,3] Yongzhong Feng,[1,2] Tong Zhang,[1,2] Zhenjie Xing,[2,3] Yanhong Wang,[1,2] Shuzhen Zou,[1,2] Dongxue Yin,[2,3] Xinhui Han,[1,2] Guangxin Ren,[1,2] and Gaihe Yang[1,2]

[1]*College of Agronomy, Northwest A&F University, P.O. Box 95, Yangling, Shaanxi 712100, China*
[2]*The Research Center of Recycle Agricultural Engineering and Technology of Shaanxi Province, Yangling, Shaanxi 712100, China*
[3]*College of Forestry, Northwest A&F University, Yangling, Shaanxi 712100, China*

Correspondence should be addressed to Yongzhong Feng; fengyz@nwsuaf.edu.cn and Gaihe Yang; ygh@nwsuaf.edu.cn

Received 24 February 2014; Revised 4 July 2014; Accepted 12 July 2014

Academic Editor: Keikhosro Karimi

Energy crisis is receiving attention with regard to the global economy and environmental sustainable development. Developing new energy resources to optimize the energy supply structure has become an important measure to prevent energy shortage as well as achieving energy conservation and emission reduction in China. This study proposed the concept of energy agriculture and constructed an energy agricultural technical support system based on the analysis of energy supply and demand and China's foreign dependence on energy resources, combined with the function of agriculture in the energy field. Manufacturing technology equipment and agricultural and forestry energy, including crop or forestry plants and animal feces, were used in the system. The current status and future potential of China's marginal land resources, energy crop germplasm resources, and agricultural and forestry waste energy-oriented resources were analyzed. Developing the function of traditional agriculture in food production may promote China's social, economic, and environmental sustainable development and achieve energy saving and emission reduction.

1. Introduction

With the rapid growth of the global economy, the world's energy demand will increase from approximately 12 billion tons of oil equivalents (t.o.e.) in 2009 to 17 billion or 18 billion t.o.e. by 2035. China is the second largest economy worldwide and has surpassed the US as the world's largest energy-consuming country; the energy consumption of China has reached 2.61 billion t.o.e. [1]. Consequently, the role of demand and supply of traditional fossil energy resources has become increasingly important in international relations [2, 3]. Meanwhile, carbon dioxide emissions are expected to increase from 29 Gt/yr to 36 Gt/yr or 43 Gt/yr [4], which will put great pressure on fossil energy resources and significantly affect global climate [5]. China is the largest emitter of greenhouse gases worldwide and contributed more than half of the global carbon dioxide emissions from 1990 to 2008 [6, 7]. With the establishment of the energy conservation and emission reduction target of the international community, the contradiction between economic growth and energy consumption in China has become increasingly serious [8]. Thus, energy consumption on global climate change and human survival has become increasingly critical, and energy shortage will be an important restrictive factor in economic development [9]. At present, these problems are the biggest threat to humanity.

Numerous reports on global climate change have been published [2, 10], including the Kyoto Protocol [11]. Many intergovernmental actions have already been implemented to solve these problems, such as the Intergovernmental Panel on Climate Change. These intergovernmental actions on energy sources include wind, hydro-, and biomass [12]. The Chinese government has also launched an energy project to develop renewable energy sources, such as solar, wind, hydro-, and biomass, to optimize the existing energy structure to prevent energy shortage [13].

In recent years, China has achieved considerable progress in utilizing and developing new energy resources. Based on the 12th Five-Year Plan of China, nonfossil fuel should account for 11.4% and 20% of the total primary energy consumption by 2015 and 2020, respectively. At the end of 2011, the installed generation capacity of nonfossil energy of China was 27.5%, which comprised hydropower (21.7%), nuclear power (1.19%), wind power (4.27%), and biomass power (0.41%) [14]. The development of biomass energy is relatively slow in China, but the new energy field has great potential because of its minimal negative effect on the environment, low cost of raw material, wide distribution of resources, and great energy conversion potential [14, 15]. Agricultural biomass is a preferred alternative energy source to overcome these challenges because it is environment friendly and accessible [1, 16, 17].

Agriculture is an old industry and the main provider of energy in rural areas of developing countries. In addition to providing food, clothing resources, and household energy, agriculture also provides various sources of raw materials to produce energy in the form of energy agriculture, such as oil, starch, sugar, straw, algae, trees, and livestock feces [18]. Through modern processing technologies, biomass energy production can be converted to fuel oil, gas, or electric energy, which can optimize the energy supply structure, reduce greenhouse gas emissions, and maintain urgent economic and social sustainable development. In this study, energy agriculture is an energy model to reduce CO_2 emissions and adjust the energy demand structure [11].

Energy agriculture has started earlier and developed more rapidly in other countries than in China. Since 1975, Brazil has implemented a plan that massively produces fuel alcohol using sugar cane [19, 20]. Recently, developed countries, such as the US, Japan, Canada, UK, and Germany, as well as developing countries, such as the Philippines, Indonesia, and Thailand, have formulated their own biofuel development programs [21]. From 2000 to 2005, ethanol production worldwide increased from 4.6 billion gallons to 12.2 billion gallons, a jump of 165% [22]. The biofuel production of Europe increased from 80 thousand tons in 1992 to 470 thousand tons in 1998 and that of the US rapidly increased from 30.28 million tons in 1979 to 3.63 billion tons in 1990, 4.54 billion tons in 1999, and 9.69 billion tons in 2003. The study on biodiesel of the US began in 1983, and its biodiesel production reached 450 million gallons in 2007, which increased by 80% compared with the production in 2006 [23]. The US also planned to increase the annual output to 6.1 million tons by 2015. Other countries are also actively and rapidly promoting the development of the industry, including Germany, Japan, Brazil, and India [24].

Bioenergy in China was not studied as early as the other countries. Energy agriculture had not been given close attention by law until 2006 with the establishment of the "renewable energy law" [13]. Excess rice and agricultural waste are the main raw materials of biomass energy, but the cultivation area of energy crops is continuously expanding [25]. Similarly, investigation on biodiesel produced by waste cooking oil, oil extraction residue, and forest oil fruit also started late in China [24]. Nevertheless, China has started emphasizing on energy agriculture and biomass energy industry and developed a clear program [26].

In the National Long-Term Development Plan (2005–2020), the "agricultural and forestry biomass project" is classified as a major project and an important part of the national energy strategy. The State Forestry Administration has conducted a preliminary plan for biomass energy aimed at developing 13.33 million hectares of forestland to grow biomass energy raw materials. During the 11th Five-Year (2006–2010) period, China had cultivated biomass energy plants to meet the supply requirement of 6 million tons of raw diesel and raw materials for 15 million KW installed capacity of power generation [27]. In April 2007, the Department of Science and Technology Education of the Ministry of Agriculture released an investigation and assessment letter to all provinces and cities regarding the development of suitable energy crop resources in marginal land. The investigation and assessment work started with winter fallow land that could be used for planting energy crops. The implementation of this measure will promote the planning and development of energy agriculture [28].

The development of agricultural energy in China is promising. China is currently one of the world's largest biogas production countries [29] and has set up a standard system of biomass solid fuel. About 19 agriculture industry standards presently exist in China. By the end of 2010, the number of promulgated and implemented energy standards in Chinese rural areas reached 94 [30]. At the beginning of the 21st century, China established several production enterprises and set relevant standards to develop fuel ethanol; thus, fuel ethanol has been used in cars in some provinces for several years [27]. Energy agriculture has not attracted attention in China because the policies focus on reusing excess rice and agricultural waste [31]. In the next decade, China will be focusing more attention on the energy agriculture industry, including its scientific input and policy orientation.

2. Energy Supply and Demand of the Chinese Energy Agriculture Development

2.1. Structure Characteristics of the Energy Supply and Demand. Table 1 shows the trend of the energy supply and demand of China from 1978 to 2012. According to statistics, raw coal output increased from 70.3% in 1978 to 76.5% in 2012 and showed a dominant part in China's energy supply structure despite the occurrence of certain amplitude fluctuations during this period. Meanwhile, the self-supply capacity of oil decreased from 23.7% in 1978 to 8.9% in 2012, whereas natural gas and electricity increased from 2.9% to 4.3% and 3.1% to 10.3%, respectively, in more than 30 years from 1978.

Coal consumption accounted for 76.2% of the total energy consumption in 1990, followed by a decrease of 9.6% to 66.6% in 2012. In the same period, production only was 76.5% (2012), which indicates that supply exceeded demand. The proportion of crude oil consumption decreased from 22.7% to 18.8% in 2011, which indicates a decrease of 3.9%. This result presents a great contradiction of supply and demand. The output production of natural gas increased from 1.9% in 1994 to 4.3% in 2012, and the consumption proportion

Table 1: Production and consumption of China's energy structure [45].

Year	Total energy production (10000 tons of SCE)	As percentage of total energy Production				Total energy consumption (10000 tons of SCE)	As percentage of total energy consumption			
		Coal	Crude oil	Natural Gas	Hydropower, nuclear power, wind power		Coal	Petroleum	Natural gas	Hydropower, nuclear power, wind power
1978	62770	70.3	23.7	2.9	3.1	57144	70.7	22.7	3.2	3.4
1980	63735	69.4	23.8	3	3.8	60275	72.2	20.7	3.1	4
1985	85546	72.8	20.9	2	4.3	76682	75.8	17.1	2.2	4.9
1990	103922	74.2	19	2	4.8	98703	76.2	16.6	2.1	5.1
1991	104844	74.1	19.2	2	4.7	103783	76.1	17.1	2	4.8
1992	107256	74.3	18.9	2	4.8	109170	75.7	17.5	1.9	4.9
1993	111059	74	18.7	2	5.3	115993	74.7	18.2	1.9	5.2
1994	118729	74.6	17.6	1.9	5.9	122737	75	17.4	1.9	5.7
1995	129034	75.3	16.6	1.9	6.2	131176	74.6	17.5	1.8	6.1
1996	133032	75	16.9	2	6.1	135192	73.5	18.7	1.8	6
1997	133460	74.3	17.2	2.1	6.5	135909	71.4	20.4	1.8	6.4
1998	129834	73.3	17.7	2.2	6.8	136184	70.9	20.8	1.8	6.5
1999	131935	73.9	17.3	2.5	6.3	140569	70.6	21.5	2	5.9
2000	135048	73.2	17.2	2.7	6.9	145531	69.2	22.2	2.2	6.4
2001	143875	73	16.3	2.8	7.9	150406	68.3	21.8	2.4	7.5
2002	150656	73.5	15.8	2.9	7.8	159431	68	22.3	2.4	7.3
2003	171906	76.2	14.1	2.7	7	183792	69.8	21.2	2.5	6.5
2004	196648	77.1	12.8	2.8	7.3	213456	69.5	21.3	2.5	6.7
2005	216219	77.6	12	3	7.4	235997	70.8	19.8	2.6	6.8
2006	232167	77.8	11.3	3.4	7.5	258676	71.1	19.3	2.9	6.7
2007	247279	77.7	10.8	3.7	7.8	280508	71.1	18.8	3.3	6.8
2008	260552	76.8	10.5	4.09	8.62	291448	70.3	18.3	3.7	7.7
2009	274619	77.3	9.9	4.1	8.7	306647	70.4	17.9	3.9	7.8
2010	296916	76.5	9.8	4.2	9.4	324939	68.0	19.0	4.4	8.6
2011	317987	77.8	9.1	4.3	8.8	348002	68.4	18.6	5.0	8.0
2012	331848	76.5	8.9	4.3	10.3	361732	66.6	18.8	5.2	9.4

Note: The coefficient for conversion of electric power into SCE is calculated on the basis of the data on the average coal consumption in generating electric power in the same year.

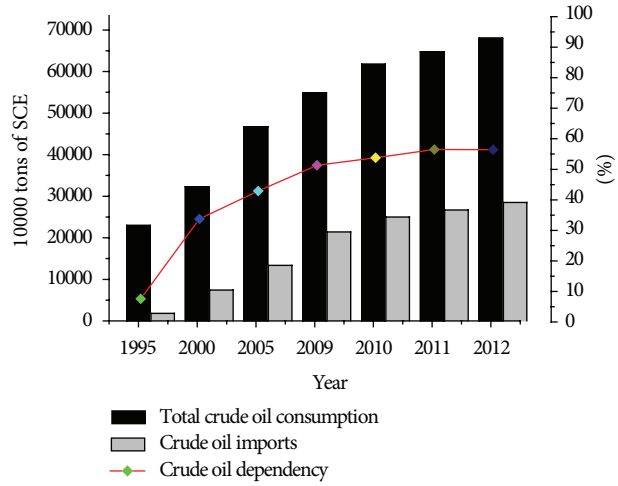

Figure 1: Consumption and imports of crude oil in China [32, 45].

increased by 1.8% in 1997 to 5.2% in 2012. The output of rapidly developing wind power, hydropower, and nuclear power increased from 3.1% in 1978 to 10.3% in 2012, which was equivalent to 3.3 times that in 1978, and consumption was equivalent to 2.8 times that in 1978, indicating an oversupply problem [31]. However, regional and seasonal power supply and demand contradiction still exists. Therefore, optimizing China's energy structure will become a priority in future development.

2.2. China's Dependence on International Energy Market. After more than half a century of exploration and development, China's energy industry has achieved significant success. However, China still shows an unbalanced relationship of energy supply and demand (Table 1) and relies on foreign imports, particularly oil. China's dependence on crude oil imports from the international crude oil market was only 7.59% in 1995, but the proportion increased continuously to 33.76% in 2000, 42.9% in 2005, and 51.3% in 2009. The foreign dependence indicated an increase at an average rate of 3% annually. In 2010, China's dependence on foreign oil remained high, but the increase was only 2.5%, which was lower than the average rate 15 years ago. The latest data shows that the crude oil dependency proportion has reached 56.5 in 2011 and 2012 (see Figure 1). The International Energy Agency forecasted that China's dependence on oil imports will reach 76.9% in 2020 [31, 32]. Based on these findings, China's energy supply will continue to rely on the international crude oil market for a long time, and the dependence rate will further increase. Therefore, changing and optimizing the energy structure at the national strategic level are significant.

3. Framework of China's Energy Agricultural Development Strategy

3.1. Basic Concept, Definition, and Characteristics of Energy Agriculture. Cultivating plant oil sources is the best explanation for energy agriculture, which is an academic concept that appeared in recent years. The first Chinese official publications on energy agriculture were "Shallow Theory of the Development of China's Energy Agriculture" by Yao [33] and "Necessity and Strategy of Development of Energy-Oriented-Agriculture" by Feng et al. [34]. Both studies discuss the concept of energy agriculture. Yao regarded energy agriculture as agricultural production and related activities for providing energy resources and transforming products. Feng et al. reported that energy agriculture aims to convert solar energy into an energy that can be used directly. The energy agriculture proposed by Lu aims to produce energy [35]. Hu and Gu [36] considered that energy agriculture includes various energy utilization patterns; the main development resource was biomass energy. According to Li [37], energy agriculture is a motivation to produce high-value crops with high biomass energy content. Biomass energy locked in biomass crops will then be translated into energy that can be directly used for economic and social development. Xu et al. and Sun et al. [21, 38] generally regarded that energy agriculture is the foundation of biomass industry and a new form of agriculture that supplies raw materials to produce biomass energy. Based on previous studies and the special role of agriculture in solving energy problem, energy agriculture can be defined as an agricultural production activity, where solar energy is fixed through photosynthesis by green energy crops and then converted into energy that can be directly used by humans (Figure 2). Energy agriculture has the following characteristics.

(1) Energy agriculture is a concept that involves interdisciplinary industry of planting, breeding, and modern energy chemical industry, as well as equipment manufacturing, electric power, and transportation. Energy agriculture also produces living resources, such as food, clothing, and housing, as well as energy. It is an integrated science based on land, crops, and artificial regulation. This concept belongs to agriculture category because the process and utilization of crops depend on land, similar to traditional planting and breeding.

(2) Energy agriculture mainly solves the contradiction between fossil energy consumption and development of the environment and economy in the human development process. The energy provided by energy agriculture is different from the traditional primary energy, such as coal, oil, and natural gas. This energy is renewable, which is fixed through photosynthesis of green plants and stored as organic energy in the body of crops.

(3) Energy agricultural production cannot be used directly and must be combined with certain processing technologies. The energy can only be used by humans after being converted under certain technical and economic conditions rather than through direct combustion of straws or firewood.

(4) Production activities of energy agriculture are very systematic. They include a series of production and research activities, such as energy crop cultivation

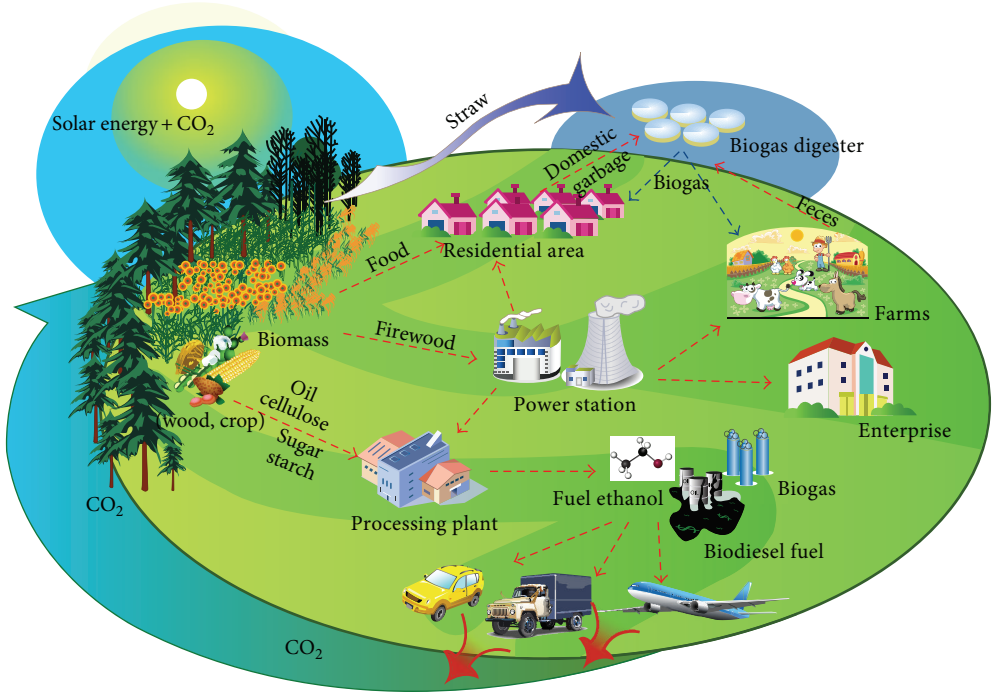

Figure 2: Diagram of energy agriculture concepts and characteristics.

and management, energy crop germplasm resource selection and breeding, processing technologies of energy agricultural production, equipment design, and development.

(5) Fixing atmospheric CO_2 is the main production process of energy agriculture. CO_2 and H_2O are released from the process of exploiting agriculture products. CO_2 emissions do not increase because of energy flow and material recycling in the ecosystem. Therefore, developing energy agriculture is suitable for controlling the concentration of greenhouse gases in the atmosphere. This process is also significant for controlling the increase of surface temperature and maintaining the ecosystem carbon balance of the earth.

(6) The prerequisite for energy agriculture development is food and energy security, which are the major challenges faced by energy agricultural development. Energy agriculture can be performed smoothly by guaranteeing food security.

3.2. Technology System for Energy Agriculture in China. According to its definition and characteristics, energy agriculture involves five sectors, namely, energy crop farming, energy forestry, energy animal husbandry, utilization of waste produced in agricultural production, and related processing industry (Figure 3) [39]. The contents of each sector are as follows.

The technology system of energy crop is nonfood crops breeding and high-yield culture technique. Nonfood crops include starchy crops, oil crops, and sugar crops. Energy forestry is cultivation and breeding technology system of germplasm resources, including firewood forest-based wood fuel, woody oil, and woody starch crops. Woody oil crops include *Jatropha*, tung tree, *Pistacia*, *Xanthoceras sorbifolia* Bunge, and oil tea camellia. Woody starch crops are mainly oak fruit (acorn).

Energy technology system in animal husbandry uses modern biobreeding techniques to directly breed existing animals with high grease conversion rate, such as pigs. This technology aims to cultivate new species of animals that can efficiently convert plant products, such as straw, wheat bran, and other nonfood products, into axunge for biodiesel processing [40]. Currently, herbivores are preferred, such as pigs and sheep.

Energy utilization technology system is a technological system for producing biogas, biodiesel, and cellulosic fuel ethanol from wastes, such as various straws, tree branches, feces, and kitchen waste, produced by farming, animal husbandry, or humans.

The manufacturing technology system of energy agricultural equipment involves designing special equipment and exploring intelligent processing technologies. Equipment and technology are mainly used to utilize energy agriculture, forestry, animal husbandry wastes, and so on. The equipment and products of producing biodiesel oil, and fuel ethanol are all included in the system (Figure 3).

3.3. Development Potential of Chinese Energy Agriculture. According to the policy and tendency of China's energy development, the priorities of energy development in China are the utilization of marginal land resources, selection and

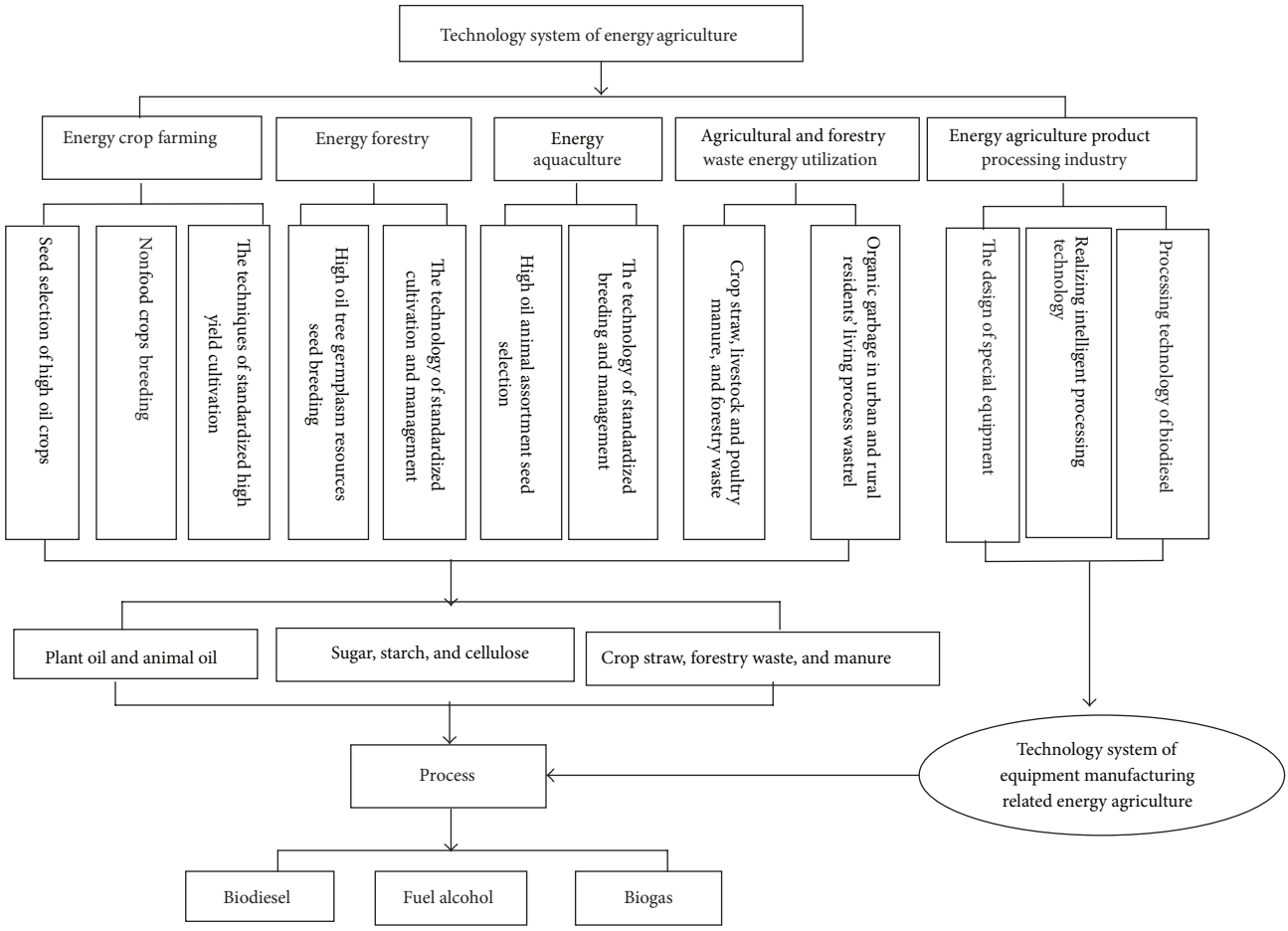

Figure 3: Technology system of energy-oriented agriculture.

cultivation of energy biomass germplasm resources, and efficient utilization of waste energy in the production process.

3.3.1. Potential of Marginal Land Resources. China has a vast territory. In addition to the 121 million hm^2 of cultivated land used to ensure the nation's grain production, China's available nonarable land area is large. According to the survey, China has 108 million hm^2 of uncultivated land, and 35.35 million hm^2 is suitable for agriculture, accounting for 32.7% of the total wasteland area. The total wasteland area may be equivalent to 36.9% of the existing arable land area. Forestry land covers 267.43 million hm^2, but only 76.62 million hm^2 of waste mountains and land is suitable for tree planting, accounting for 28.6% of the woodland area. The woodland area is equivalent to 6.2% of the existing forest area [28].

According to the information from the Science and Research Department of the Ministry of Agriculture (Science and Education Division of the Ministry of Agriculture) in April 2007, 34.2 million hm^2 of noncultivated land suitable for cultivation of energy crops is distributed in 1845 counties (cities and regions) of China. Approximately 26.8 million hm^2 of wasteland is available for farming. First-, second-, and third-class wastelands cover 4.33 million hm^2 (16.2%), 8.73 million hm^2 (32.6%), and 13.73 million hm^2 (51.2%), respectively [41]. The amount of winter-free farmland is approximately 7.4 million hm^2.

Considering crop ecological adaptability, the suitable wasteland areas for planting sweet sorghum, cassava and sugar cane are approximately 13, 5, and 15 million hm^2, respectively. If 20% to 30% of wastelands are cultivated with energy crops, the biomass energy production can be converted to 50 million tons of alcohol based on the existing technologies in China [41].

3.3.2. Potential of Germplasm Resources. According to the notice of "strengthening biological fuel ethanol project construction and management" jointly enacted by the National Development and Reform Commission and Ministry of Finance in 2006, as well as "the guidance of promotion of the healthy development of deep processing of corn" and "development planning of agricultural biomass energy (from 2007 to 2015)" promulgated by the Ministry of Finance China and the Department of Agriculture in 2007, the development of energy crops in China must adhere to the precondition of "do not compete for food with people, do not compete for land with food" [42] Therefore, the energy agricultural germplasm resources of China aim to develop nonfood energy crops. Approximately 40 kinds plants can be used

Table 2: Biological characteristics of mainly woody fuel.

Tree name	Harvest organ	Yield kg/hm^2	Oil content	C16-C18 FA	Distribution area
Jatropha curcas L	Seed	9750	More than 39.8% (kernel 64.5%)	100.00%	Guangdong, Guangxi, Yunnan, Guizhou, and Sichuan provinces etc.
Xanthoceras sorbifolia Bunge	Seed	9000	More than 35.5% (kernel 66.4%)	88.97%	North China, East China, and Northwest China
Pistacia chinensis Bunge	Seed	12000	35.1% (kernel 56.5%)	100.00%	North to Yellow River basin, south to Guangdong, Guangxi
Cyperus esculentus L	Tuber	6000	25.30%	100.00%	North to inner Mongolia, south to Jiangsu and Zhejiang provinces
Euphorbia lathyris L	seed	1650	More than 43.5% (kernel 69.2%)	99.70%	North to Jilin, south to Jiangsu and Zhejiang provinces
Swida wilsoniana	seed	12000	33%~36% (nutlet 55%–59%)	77.68%	Yellow River basin regions to their south, Hunan, Jiangxi, and Hubei provinces are the main areas

as energy crops, including short rotation trees, herbaceous crops, sugar crops, vegetable oil crops, and plants used for extracting hydrocarbons, such as sugar beets, sugar cane, sweet sorghum, *Miscanthus* crop, sweet corn, beans, peanuts, cotton, sunflower, rapeseed, palm, and castor. Studies show that the highest per unit yield is achieved by sugar cane and sweet sorghum. The biomass per unit area produced by sugar cane and sweet sorghum is 12 times as much as maize and 2.5 times as much as sweet potato and cassava. Maize is the most suitable crop for fuel ethanol production because 2.82 tons of maize can produce 1 ton of fuel ethanol. However, the fuel ethanol production per unit of land of maize is the lowest, whereas sugarcane is the highest, followed by sweet sorghum, cassava, and sweet potato. Maize is suitable for planting in almost all parts of China, cassava and sugarcane are mostly planted in southern China, and sweet potato and sweet sorghum are suitable in southwestern and northern China [43].

According to the results of the sixth forest resource inventory published in 2005, the national forest area is 175 million hm^2, with total standing volume of 13.62 billion m^3 and total woody biomass resources of more than 18 billion tons. Energy forestry mainly contains woody biomass fuel resources, woody oil plant resources, woody starch, and fiber plant resources.

China's existing firewood forest area is approximately 3.03 million hm^2, which can provide 21.24 million tons of firewood that can replace 12.11 million tons of coal equivalents. Preliminary estimates showed that approximately 60 million hm^2 of shrubs can be planted in western China. If 60% of these areas are used as energy forest, approximately 144 million tons of biomass can be obtained (if 4-ton biomass is produced per hectare annually), which can replace 93.6 million tons of coal equivalents.

Approximately 3.43 million hm^2 of woody oil crop area has been planted in China. A total of 151 energy oil plants (seed plant), 697 genera, and 1554 species exist, which account for 5% of the total seed plants in China. About 154 species of woody plants have seed oil content of more than 40%, and up to 10 species are suitable for building raw material bases and scale supply bases for improved variety using barren hills and sand. Table 2 shows the main woody oil crops.

Some inedible woody fruit trees are rich in starch; for example, the acorn of oak comprises 50% starch. The existing area of oaks is up to 18 million hm^2 in China, and more than 6.7 million hm^2 of oak area exists in Inner Mongolia, Jilin, and Heilongjiang provinces. More than 10 million tons of fruits can be harvested from these oaks annually, which contain more than 5 million tons of starch. If these fruits are fully utilized, 2.26 million tons of biological fuel alcohol can be produced. Hemp and other lignocellulose materials are widely distributed in China. The suitable planting areas are north to Heilongjiang, south to Hainan, west to Xinjiang, and east to coastal areas, which cover up to 1.06 million hm^2. The dry matter is up to 23 tons per hectare annually, and the lignocellulose content is as high as 68% to 75%. If each ton of lignocellulose can produce 0.35 tons of industrial alcohol, hemp (dry matter basis) per hectare can produce 5.75 tons of industrial alcohol average annually.

3.3.3. Potential of Agricultural Waste Resource. According to the information provided by the China Statistical Yearbook in 2012, the estimated amount of crop straw in China was 972.26 million tons in 2011. Food crop straw, oil crop straw, and other crop straws were 765.32, 60.15, and 146.79 million tons, respectively. The dung discharge was about 39.87 billion tons, in which about 54.5% was pig manure (21.7 billion tons) and 38.69% was cow dung (15.4 billion tons). Human feces emission in 2011 was about 25.73 million tons [44].

Among all the provinces and cities in China, Guangxi, Heilongjiang, and Henan were the top producers of crop straw. Xizang, followed by Shanghai and Qinghai, produced the lowest quantity of crop straw. Sichuan ranked first in terms of livestock manure emission, followed by Henan and Hunan. Shanghai, behind Beijing and Tianjin, was the lowest in the rank. Given these data, Sichuan ranked first in agricultural waste potential, and its total quantity of agricultural waste was 437.88 million tons, accounting for 8.8% of the whole country, followed by Henan and Shandong,

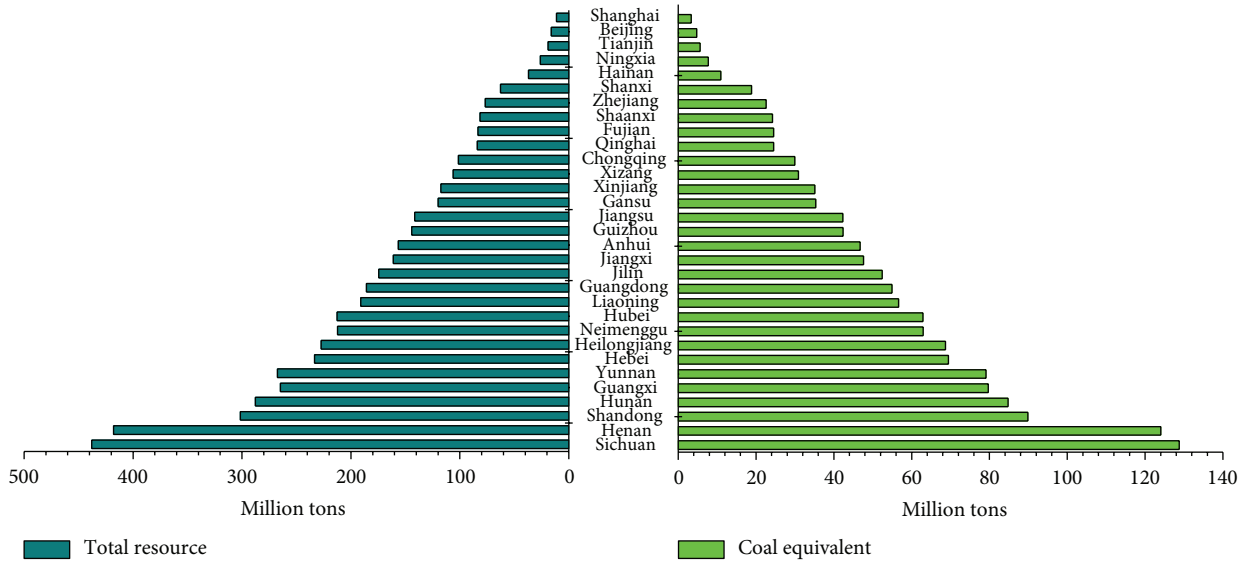

Note: Data of Taiwan area is lack

Figure 4: Resource and potential of agricultural waste of province's level in mainland China [20, 31].

accounting for 8.4% and 6.1%, respectively. Shanghai ranked last in resource potential because its quantity of agricultural waste was 11.26 million tons, accounting for 0.23%, followed by Beijing and Tianjin with 0.32% and 0.38%, respectively (Figure 4) [31, 44].

When these straws and dung were used for digestion at 35°C, the biogas yield potential of crop straws in 2011 was estimated to be 311.97 billion m^3, which is equivalent to 220 million tons of standard coal. The potential of livestock manure was 288.93 billion m^3, which is equivalent to 205 million tons of SCE (standard coal equivalent). The biogas potential of human feces was 12.5 billion m^3, which is equivalent to 8.8 million tons of SCE. The total biogas production potential of agricultural waste in 2011 was 613.43 billion m^3 or 436 million tons of SCE, accounting for 17.6% of the coal produced in the same period.

The above analysis showed that China has considerable reserves of energy agriculture resource that can potentially produce large amounts of energy when used well.

4. Conclusions

(1) China's energy agricultural development and energy supply and demand structure from 1978 to 2012 showed an increasing demand for renewable energy and decreasing demand for raw coal and oil. The supply-demand contradiction of raw coal and oil still continued, and an oversupply of the overall performance of gas and electricity existed.

(2) China's dependence on foreign oil continued to increase for a long time. Thus, strategies on optimizing and changing the energy structure must be planned at the national level.

(3) Energy agriculture is a special agricultural production activity, where solar energy is fixed through photosynthesis by energy crops and then converted into energy that can be directly used. An energy agriculture technology system was also established based on energy crop, energy forestry, energy animal husbandry, energy utilization of agricultural waste, and equipment manufacturing.

(4) China has an immense energy potential for marginal land resources, germplasm resources, and agricultural and forestry wastes. Developing energy agriculture has no limits if resources are fully utilized. Meanwhile, the ecological construction of China will improve with combined energy agriculture.

Conflict of Interests

The authors declare that there is no conflict of interests regarding the publication of this paper.

Acknowledgment

Financial support was received from the China's Technology Support Project for the 12th Five-Year Plan: High-yielded Biogas Technology Integrated Demonstration on Mixing Materials (Grant no. 2011BAD15B03).

References

[1] J. Tollefson and R. Monastersky, "The global energy challenge: Awash with carbon," *Nature*, vol. 491, no. 7426, pp. 654–655, 2012.

[2] G. A. de Leo, L. Rizzi, A. Caizzi, and M. Gatto, "Carbon emissions: the economic benefits of the Kyoto protocol," *Nature*, vol. 413, no. 6855, pp. 478–479, 2001.

[3] J.-A. M. Atkinson, D. J. Gray, A. C. A. Clements, T. S. Barnes, D. P. Mcmanus, and Y. R. Yang, "Environmental changes impacting Echinococcus transmission: research to support predictive surveillance and control," *Global Change Biology*, vol. 19, no. 3, pp. 677–688, 2013.

[4] S. Chu and A. Majumdar, "Opportunities and challenges for a sustainable energy future," *Nature*, vol. 488, no. 7411, pp. 294–303, 2012.

[5] R. Walker, "The impact of Brazilian biofuel production on Amazônia," *Annals of the Association of American Geographers*, vol. 101, no. 4, pp. 929–938, 2011.

[6] X. Guo, D. Marinova, and J. Hong, "China's shifting policies towards sustainability: a low-carbon economy and environmental protection," *Journal of Contemporary China*, vol. 22, no. 81, pp. 428–445, 2013.

[7] B. Xue and W. Ren, "China's uncertain CO_2 emissions," *Nature Climate Change*, vol. 2, no. 11, article 762, 2012.

[8] S. Wang, J. Dai, and M. Su, "Material flow analysis of fossil fuels in China during 2000–2010," *The Scientific World Journal*, vol. 2012, Article ID 625828, 8 pages, 2012.

[9] L. Chester, "Dissecting the conjunction of capitalism's environmental, energy, and economic crises: the example of one liberal, market-based economy," *Journal of Economic Issues*, vol. 47, no. 2, pp. 485–494, 2013.

[10] J. Sheffield, E. F. Wood, and M. L. Roderick, "Little change in global drought over the past 60 years," *Nature*, vol. 491, no. 7424, pp. 435–438, 2012.

[11] Q. Schiermeier, "The long road from Kyoto," *Nature*, vol. 426, no. 6968, p. 756, 2003.

[12] C. Pirlogea and C. Cicea, "Econometric perspective of the energy consumption and economic growth relation in European Union," *Renewable and Sustainable Energy Reviews*, vol. 16, no. 8, pp. 5718–5726, 2012.

[13] C. Y. Yu, "International comparison and inspiration of energy agriculture development strategy," *Chinese Rural Economy*, vol. 7, pp. 76–80, 2007 (Chinese).

[14] M. Zeng, C. Li, and L. Zhou, "Progress and prospective on the police system of renewable energy in China," *Renewable and Sustainable Energy Reviews*, vol. 20, pp. 36–44, 2013.

[15] F. H. Abanda, "Renewable energy sources in Cameroon: Potentials, benefits and enabling environment," *Renewable and Sustainable Energy Reviews*, vol. 16, no. 7, pp. 4557–4562, 2012.

[16] Z. Ming, X. Song, M. Mingjuan, and Z. Xiaoli, "New energy bases and sustainable development in China: a review," *Renewable and Sustainable Energy Reviews*, vol. 20, pp. 169–185, 2013.

[17] Y. P. Zhang, K. Q. Sun, and Y. H. Zuo, "Quantitive appraisal of potential environmental benefits from the development of energy agriculture and its geographical distribution in China," *Journal of Agro-Environment Science*, vol. 29, no. 5, pp. 826–832, 2010 (Chinese).

[18] A. H. Demirbas and I. Demirbas, "Importance of rural bioenergy for developing countries," *Energy Conversion and Management*, vol. 48, no. 8, pp. 2386–2398, 2007.

[19] E. de Paula, "Ethanol from sugar cane: a successful alternative energy strategy for Brazil," in *Proceedings of the Portland International Center for Management of Engineering and Technology, Technology Management for a Sustainable Economy (PICMET '08)*, pp. 108–118, New York, NY, USA, July 2008.

[20] M. Balat and H. Balat, "Recent trends in global production and utilization of bio-ethanol fuel," *Applied Energy*, vol. 86, no. 11, pp. 2273–2282, 2009.

[21] M. Xu, Z. Zhang, and Y. H. Zuo, "Prospect of energy agriculture in China," *Environmental Protection*, vol. 288, no. 2, pp. 55–57, 2008 (Chinese).

[22] U. E. Simonis, "Lester R. Brown, Plan B—rescuing a planet under stress and a civilization in trouble," *The Environmentalist*, vol. 28, no. 3, pp. 337–338, 2008.

[23] M. Balat, "Global bio-fuel processing and production trends," *Energy Exploration and Exploitation*, vol. 25, no. 3, pp. 195–218, 2007.

[24] L. H. Zhang, "Analysis on energy agriculture development in China," *Gansu Science and Technology*, vol. 26, no. 20, pp. 179–180, 2010 (Chinese).

[25] C. Z. Wu, Z. Q. Zhou, X. L. Yin, and W. M. Yi, "Current status of biomass energy development in China," *Transactions of the Chinese Society of Agricultural Machinery*, vol. 40, no. 1, pp. 91–99, 2009.

[26] Z. J. Sun, "Biomass industry and its developmental trends in China," *Transactions of the Chinese Society of Agricultural Engineering*, vol. 20, no. 5, pp. 1–5, 2004.

[27] Z. Y. Lei, B. Q. Li, and T. T. Zhou, "Study on development of energy agriculture and modern agriculture," *Journal of Anhui Agricultural Sciences*, vol. 39, no. 3, pp. 1662–1664, 2011 (Chinese).

[28] Department of Scientific and Education of Ministry of Agriculture of the People's Republic of China, Law on investigation and evaluation of the marginal land resources suitable for cultivation energy plants in China, no. 10, 2007. [Chinese].

[29] Y. Chen, G. Yang, S. Sweeney, and Y. Feng, "Household biogas use in rural China: a study of opportunities and constraints," *Renewable and Sustainable Energy Reviews*, vol. 14, no. 1, pp. 545–549, 2010.

[30] G. Liu, "An enacted group of rural energy agriculture in aspects of biomass energy industry standards," *Sino-Global Energy*, vol. 15, no. 10, p. 50, 2010 (Chinese).

[31] Y. P. Zhang, K. Q. Sun, and Y. H. Zuo, "A benefit evaluation and regional analysis of energy agriculture development in China," *Resources Science*, vol. 31, no. 12, pp. 2080–2085, 2009 (Chinese).

[32] British Petroleum, *BP Statistical Review of World Energy June 2012*, British Petroleum, London, UK, 2012.

[33] X. J. Yao, "Development of energy-oriented agriculture in China," *Transactions of the CSAE*, vol. 19, no. 7, pp. 6–9, 2003 (Chinese).

[34] Y. Z. Feng, G. H. Yang, G. X. Ren, and R. X. Ding, "Necessity and strategy of development of energy-oriented-agriculture in China," *Chinese Agricultural Science Bulletin*, vol. 21, no. 4, pp. 344–347, 2005 (Chinese).

[35] M. Lu, "Exploiting biomass energy, developing energy agriculture," *Qiushi*, no. 5, 2005 (Chinese).

[36] R. H. Hu and M. D. Gu, "Energy agriculture development analysis of the significance and prospects," *Journal of Anhui Agricultural Sciences*, vol. 33, no. 10, pp. 1998–2000, 2005 (Chinese).

[37] L. Li, "Development of energy agriculture is a major measure to speed up the construction of modern agriculture," *Chinese Countryside Well-off Technology*, vol. 234, no. 6, pp. 17–19, 2007 (Chinese).

[38] Y. M. Sun, Z. H. Yuan, and Z. J. Sun, "The status and future of bioenergy and biomass utilization in China," *Renewable Energy*, no. 2, pp. 78–82, 2006 (Chinese).

[39] Y. Z. Feng, G. H. Yang, Y. R. Mao, and G. X. Ren, "Constructing technology system of energy-oriented agriculture," *Journal of*

Northwest A & F University (Natural Science Edition), vol. 34, no. 1, pp. 30–34, 2006.

[40] G. H. Xie, "Progress and direction of non-food biomass feedstock supply research and development in China," *Journal of China Agricultural University*, vol. 17, no. 6, pp. 1–19, 2012 (Chinese).

[41] J. P. Kou, Y. Y. Bi, L. X. Zhao et al., "Investigation and evaluation on wasteland for energy crops in china," *Renewable Energy Research*, vol. 26, no. 6, pp. 3–9, 2008 (Chinese).

[42] Y. J. Wang, Y. Y. Bi, and H. J. Tang, "The status of producing liquid bio-fuels from energy crops and its development trend in China," *Renewable Energy Research*, vol. 27, no. 2, pp. 100–105, 2009 (Chinese).

[43] L. Zeng and G. H. Wang, "Current status, benefit analysis and developmental strategy of energy-oriented agriculture & forestry," *Trans CSAE*, vol. 1, pp. 20–24, 2006 (Chinese).

[44] China Animal Agriculture Yearbook Editor Committee, *China Animal Industry Yearbook*, China Agriculture Press, 2003, (Chinese).

[45] National Bureau of Statistics of China, *China Statistical Yearbook*, China Statistics Press, Beijing, China, 2000, (Chinese).

Hindawi Publishing Corporation
BioMed Research International
Volume 2015, Article ID 519513, 13 pages
http://dx.doi.org/10.1155/2015/519513

Review Article

Microalgae as Sustainable Renewable Energy Feedstock for Biofuel Production

Srikanth Reddy Medipally,[1] Fatimah Md. Yusoff,[1,2] Sanjoy Banerjee,[1] and M. Shariff[1,3]

[1] *Laboratory of Marine Biotechnology, Institute of Bioscience, Universiti Putra Malaysia (UPM), 43400 Serdang, Selangor, Malaysia*
[2] *Department of Aquaculture, Faculty of Agriculture, Universiti Putra Malaysia (UPM), 43400 Serdang, Selangor, Malaysia*
[3] *Department of Veterinary Clinical Studies, Faculty of Veterinary Medicine, Universiti Putra Malaysia (UPM), 43400 Serdang, Selangor, Malaysia*

Correspondence should be addressed to Fatimah Md. Yusoff; fatimahyus@gmail.com

Received 5 June 2014; Revised 13 August 2014; Accepted 16 August 2014

Academic Editor: Keikhosro Karimi

The world energy crisis and increased greenhouse gas emissions have driven the search for alternative and environmentally friendly renewable energy sources. According to life cycle analysis, microalgae biofuel is identified as one of the major renewable energy sources for sustainable development, with potential to replace the fossil-based fuels. Microalgae biofuel was devoid of the major drawbacks associated with oil crops and lignocelluloses-based biofuels. Algae-based biofuels are technically and economically viable and cost competitive, require no additional lands, require minimal water use, and mitigate atmospheric CO_2. However, commercial production of microalgae biodiesel is still not feasible due to the low biomass concentration and costly downstream processes. The viability of microalgae biodiesel production can be achieved by designing advanced photobioreactors, developing low cost technologies for biomass harvesting, drying, and oil extraction. Commercial production can also be accomplished by improving the genetic engineering strategies to control environmental stress conditions and by engineering metabolic pathways for high lipid production. In addition, new emerging technologies such as algal-bacterial interactions for enhancement of microalgae growth and lipid production are also explored. This review focuses mainly on the problems encountered in the commercial production of microalgae biofuels and the possible techniques to overcome these difficulties.

1. Introduction

World energy crisis and global warming are the two major problems human kind faces today, which are mainly due to the more population growth, fast industrialization, and increased use of fossil fuels [1]. Hence, the importance for identification of potential renewable source for sustainable energy production has gained momentum recently [2]. Currently many countries are using biomass, waste, solar, wind, hydro and geothermal energy sources as alternative to fossil based fuels [3]. International Energy Agency (IEA) recently declared that the energy from wastes and combustible sources has higher potential as alternative fuel as compared to other renewable sources [4].

Biofuel (biodiesel, bioethanol, and biogas) from combustible sources is presently being recognised as an alternate and green renewable fuel for sustainable energy production in the near future [5]. Microalgae are the photosynthetic microorganisms, which are attracting huge interest from researchers, government, and local and international entrepreneurs. Recently, the usage of liquid biofuels such as biodiesel, bioethanol, and jet fuel has increased immensely especially in the transport industry [6]. Compared to fossil diesel, biodiesel has many advantages such as it is biodegradable and nontoxic and it has lower emissions of greenhouse gases (GHG) [7].

Microalgae biofuels belong to the third generation type of biofuels, which are considered as an alternative energy source

Table 1: Comparison of oil content, oil yield, and biodiesel productivity of microalgae with the first and the second generation biodiesel feedstock source [17, 18, 21, 22].

Feedstock source	Oil content (% oil by wt. in biomass)	Oil yield (oil in litres/ha/year)	Biodiesel productivity (kg biodiesel/ha/year)
Oil palm	36	5366	4747
Maize	44	172	152
Physic nut	41–59	741	656
Caster	48	1307	1156
Microalgae with low oil content	30	58,700	51,927
Microalgae with medium oil content	50	97,800	86,515
Microalgae with high oil content	70	136,900	121,104

for fossil fuels without the disadvantages associated with the first and the second generation biofuels [8]. Generally the first generation biofuels are derived from crop plants, such as soybean, corn, maize, sugar beet, and sugar cane; palm oil; rapeseed oil; vegetable oils; and animal fats [8]. These types of biofuels have created a lot of disputes due to their negative impacts on food security, global food markets, water scarcity, and deforestation [9, 10]. In addition, the second generation biofuels derived from nonedible oils (*Jatropha curcas*, *Pongamia pinnata, Simarouba glauca,* etc.), lignocellulose biomass, and forest residues require huge areas of land otherwise that could be used for food production. Currently, the second generation biofuel production also lacks efficient technologies for commercial exploitation of wastes as source for biofuel generation [6]. Based on the above-mentioned drawbacks associated with the first and second generation biofuels, microalgae biofuel seems to be a viable alternative source of energy to replace or supplement the fossil fuels.

Several species of microalgae, such as *Botryococcus braunii*, *Nannochloropsis* sp., *Dunaliella primolecta*, *Chlorella* sp., and *Crypthecodinium cohnii,* produce large quantities of hydrocarbons and lipids. *Botryococcus braunii,* the colonial green microalgae, has the capability to produce a large number of hydrocarbons as compared to its biomass, and it also synthesizes other commercially important compounds such as carotenoids and polysaccharides [11–16]. The production level of oil content in microalgae species reaches up to 80% and the levels from 20 to 50% are quite common [16–18]. The microalga *Chlorella* has up to 50% lipids and *B. braunii* produces the highest oil content of approximately 80% [17]. In Table 1, a comparison was given between the oil yield, production, and biodiesel productivity of microalgae with some other biofuel feedstock. Other than biofuel, microalgae also synthesize different bioactive compounds and have varied applications in nutraceuticals, pharmaceuticals, and chemical and food industries [19, 20].

Microalgae biofuel production is commercially viable because it is cost competitive with fossil based fuels, does not require extra lands, improves the air quality by absorbing atmospheric CO_2, and utilizes minimal water [23]. However, microalgae biofuels have some disadvantages such as low biomass production, low lipid content in the cells, and small size of the cells that makes harvesting process very costly. These limitations can be overcome by improving the technologies for harvesting and drying and genetic engineering of metabolic pathways for high growth rate and increased lipid content. Initial evaluation of microalgae as the potential source for biofuel production began in 1970, but it was temporarily shelved due to technical and economic problems [24]. Later, subsequent studies from 1980 onwards showed high potential in microalgae biofuel production [25].

2. World Market for Biofuel Production

Large scale commercial production of microalgae began in Japan in the early 1960s by culturing *Chlorella* as food additive. Later, in the 1970s and 1980s it expanded to reach other countries such as USA, Australia, India, and Israel. By the year 2004, the microalgae industry had grown to produce 7000 tonnes of dry matter per annum [26–28].

Biofuel production in the world has increased recently, mainly in the production of bioethanol from sugar crops (e.g., sugar cane, sugar beet, and sweet sorghum) and cereals (wheat and maize). World bioethanol production in 2009 was 73.9 billion liters which showed 400% increase as compared to that in 2000, which was only 17 billion liters [29]. Based on this progress, the global bioethanol production in 2017 will be double that of 2007 [30]. United States and Brazil remained the top most bioethanol producers in the world. In Brazil, with the exception of bioethanol from sugar cane, other biofuels are economically not competitive with fossil based biofuels without subsidies [10].

The world biodiesel production in the year 2003 was around 1.8 billion litres [31]. Countries like United States, Brazil, Canada, China, India, and Japan and Europe are motivated to develop internal biofuel markets and the plans were established to use these biofuels. During the past several years, an increase in biodiesel production was observed because of the increased demand for fuels, to produce "cleaner" energy globally, to fulfil the Bali Action Plan and Kyoto Protocol requirements and establishment of alternative sources for agricultural producers [32]. Currently, the biodiesel production rates in Southeast Asian countries such as in Malaysia, Thailand, and Indonesia range between 70 and 250% [33].

Europe is also an important biofuel producer in the global market. Currently, the European Union countries have

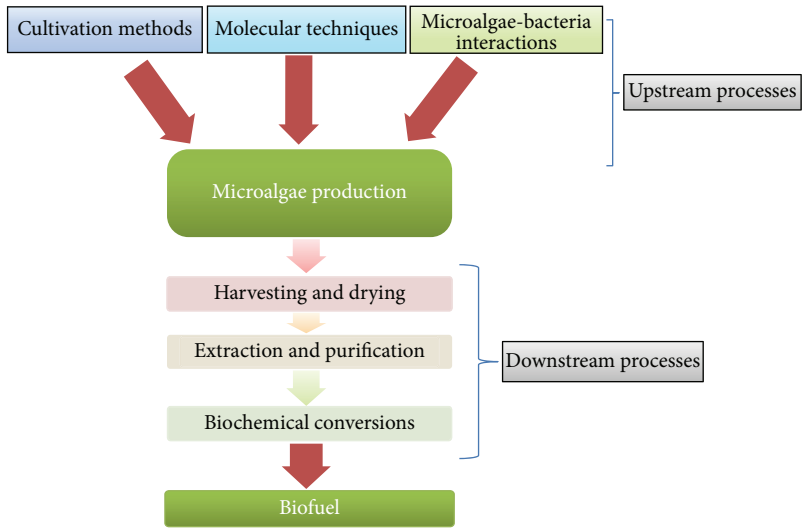

Figure 1: Different strategies involved in microalgae biomass and biofuel production.

a small share (6%) in global biofuel production. The European production levels in global market have increased 40 times from 80 tons in 1993 to 780 tons in 2001 and 3.184.000 tons in 2005 [34]. Germany is the top most biofuel producing country in Europe followed by France, Italy, and Czech Republic [35]. In Europe, biodiesel production occupies the top position (79.5%) among liquid biofuels in the year 2004 [34]. In European countries, biodiesel is generally used by applying various blends with diesel. However in some countries like Germany, Sweden, and Austria, pure biodiesel is used in adapted captive fleet vehicles. Presently in Europe about 1.4 million hectares of arable land is dedicated for biodiesel production. At the moment there are about 40 plants in the EU producing up to 3,184.00 tonnes of biodiesel yearly; and these plants are located mainly in Italy, Germany, Austria, Sweden, and France.

3. Production of Microalgae Biomass and Biofuel

Microalgae biomass and biofuel production can be developed at two major phases that involve upstream and downstream processes (Figure 1). The upstream phase involves different cultivation technologies to maximize biomass quality and quantity, whereas the downstream stage puts emphasis on harvesting technologies and sustainable production of biofuel.

3.1. Upstream Processes

3.1.1. Microalgae Cultivation Technologies. Production of microalgae biomass can be carried out by three different types of culture systems such as batch, semi-batch, and continuous systems. The growth rate and maximum biomass production of microalgae strains in these culture systems are affected by abiotic (light, temperature, pH, salinity, O_2, CO_2, nutrient stress, and toxic chemicals), biotic (pathogens and competition by other algae), and operational (shear produced by mixing, dilution rate, depth, harvest frequency, and addition of bicarbonate) factors. A number of studies have been conducted to develop different cultivation technologies for bulk production of microalgae biomass [28, 36]. Usually, microalgae can be cultivated using four types of cultivation methods such as phototrophic, heterotrophic, mixotrophic, and photoheterotrophic [37] cultivation methods (Table 2). Among these, only phototrophic cultivation is commercially feasible for large scale microalgae biomass production [26]. In addition to this, phototrophic microalgae can also capture atmospheric carbon dioxide and act as a potential carbon sink.

(1) Phototrophic Cultivation. Microalgae have high photosynthetic efficiency and growth rates when compared to higher plants [16]. In phototrophic method, microalgae can generally be cultivated in open ponds and enclosed photobioreactors.

(a) Open Pond Production. These are the oldest and simplest systems commonly used for large scale microalgae production. These microalgae cultivating methods have been practiced since the 1950s [26]. Presently, about 98% of commercial algae are produced in these systems [41]. There are various types of open pond systems which are mainly differentiated based on their size, shape, and material used for construction, type of agitation, and inclination [42]. Some common ones include raceways stirred by a paddle wheel, extensive shallow unmixed ponds, circular ponds mixed with a rotating arm, and sloping thin-layer cascade systems. Among the above-mentioned systems, raceways are the most commonly used artificial system [43]. Open pond system is the cheapest method for large scale cultivation of microalgae compared to close PBRs. Open pond systems do not compete with agricultural crops for land, since they can be established in minimal crop production areas [44]. The construction, regular maintenance, and cleaning of these systems are easy

Table 2: Biomass and lipid productivities of some microalgae under phototrophic, heterotrophic, and mixotrophic conditions.

Cultivation method	Microalgae	Biomass productivity ($g\,L^{-1}\,d^{-1}$)	Lipid content (% dry weight biomass)	Lipid productivity ($mg\,L^{-1}\,d^{-1}$)	Reference
Phototrophic method	*Chlorella vulgaris*	0.02–0.20	50–58	11.2–40	[18]
	Chlorella protothecoides	2.00–7.70	14.6–57.8	1214	
	Chlorella sorokiniana	0.23–1.47	19.0–22.0	44.7	
Heterotrophic method	*Chlorella vulgaris*	0.15	23	35	[38]
	Chlorella protothecoides	3.1–3.9	—	2400	[39]
	Chlorella sorokiniana	1.48	23.3	—	[40]
Mixotrophic method	*Chlorella vulgaris*	0.25–0.26	20.0–22.0	52.0–56.0	[37]
	Chlorella protothecoides	23.9	58.4	11,800	
	Chlorella sorokiniana	0.58	—	29.0–56.0	

and they also consume relatively low energy [45]. Open pond systems are less technical in design and are more scalable; however, they are limited by abiotic growth factors like temperature, pH, light intensity, and dissolved oxygen concentration and are easily subjected to contamination [46]. Contamination from the air and ground is often a serious limiting factor for cultivation of algae in open pond systems and therefore most of the species cultured in that systems are grown under selective environments such as high alkalinity and high salinity [47–50].

(b) Enclosed Photobioreactors (PBR). These systems are generally available in the form of tubes, bags, or plates, which are made up of glass, plastic, or other transparent materials. Algae are cultivated in these systems with adequate supply of light, nutrients, and carbon dioxide [51, 52]. Although many PBR designs are available, only a few are practically used for bulk production of algae [53]. Some common PBR designs include annular, tubular, and flat-panel reactors, with large surface areas [52, 54].

Annular Photobioreactors. These photobioreactors are more frequently used as bubble columns or airlift reactors [55]. But occasionally they are used as stirred tank reactors [56]. Generally in column photobioreactors the columns are arranged vertically, and aeration is provided from below, and light illumination is supplied through transparent walls. Column photobioreactors have the advantages of best controlled growth conditions, efficient mixing, and highest volumetric gas transfer rates [57].

Tubular Photobioreactors. In these reactor systems the algal cultures are pumped through long and transparent tubes. The mechanical pumps or airlifts create the pumping force, and the airlift also allows the exchange of CO_2 and O_2 between the liquid medium and the aeration gas [58–61].

Flat-Panel Photobioreactor. Flat-panel photobioreactors support higher growth densities and promote higher photosynthetic efficiency [45, 62]. In flat-panel system, a thin layer of more dense culture is mixed or sailed across a flat clear panel; and the incoming light is absorbed within the first few millimetres at the top of the culture [63–65].

As compared to open pond systems, photobioreactors have many advantages such as controllable growth, system efficiency, and algal purity. However, there are some disadvantages such as high costs of construction, operation, and maintenance (Table 3). Though these drawbacks can be partially compensated by higher productivities, they still limit the cost-effective production of microalgae biomass on required scale for biodiesel production.

(c) Hybrid Production Systems. In these hybrid systems both open ponds and close photobioreactors are used together in combination to get better results. In these systems, the required amount of contamination free inocula obtained from photobioreactors is transferred to open ponds or raceways to get maximum biomass yield [72, 73]. Olaizola [74] and Huntley and Redalje [75] used these hybrid systems for the production of astaxanthin from *Haematococcus pluvialis*. However this is not suitable for biofuel production because this system is more expensive and it is also a batch culture system rather than a continuous culture system.

(2) Heterotrophic Cultivation. In heterotrophic cultivation, instead of photosynthetic process, microalgae utilize organic carbon for their growth and development. As photosynthetic organisms, microalgae are usually light-limited at high cell densities during large scale cultivation [76] or they experience photoinhibition if the light is too intense, both of which lead to slow growth and production [77]. Based on these drawbacks associated with phototrophic cultivation, heterotrophic cultivation of microalgae can be considered favourably [78]. The major advantages associated with heterotrophic cultivation over phototrophic cultivation are the good control on cultivation procedure, elimination of light necessity, and low cost of biomass harvesting [79]. However, heterotrophic cultivation also has some limitations. (1) Limited number of heterotrophic capable species is a limitation. Until now only four types of heterotrophically grown microalgae such as *C. protothecoides* [80–82], *C. vulgaris* [38], *Crypthecodinium cohnii* [83], and *Schizochytrium limacinum* [84] have been identified with high lipid production. (2) Contamination from other organisms is another problem due to the presence of organic substrate [78]. (3) Glucose is the preferred organic substrate for heterotrophic growth of microalgae. However

Table 3: Comparison between open ponds and photobioreactors [51, 52, 58, 66–71].

Factor	Open ponds	Photobioreactors
Area-to-volume ratio	Large	Small
Algal species	Restricted	Flexible
Species selection	Growth competition	Shear resistance
Sterility	Low	High
Cultivation period	Limited	Extended
Water loss through evaporation	Possible	Prevented
Controlling of growth conditions	Very difficult	Easy
Light utilization efficiency	Poor/fair	Fair/excellent
Gas transfer	Poor	Low-high
Temperature	Highly variable	Required cooling
Temperature control	None	Excellent
Automatic cooling system	None	Built in
Automatic heating system	None	Built in
Cleaning	Not required	Required due to wall growth and dirt
Weather dependence	High	Medium
Process control and reproducibility	Limited	Possible within certain tolerance
Microbiology safety	None	UV
Harvesting efficiency	Low	High
Population density	Low	High
Biomass productivity	Low	High
Biomass quality	Variable	Reproducible
Air pump	Built in	Built-in
Hydrodynamic stress on algae	Difficult	Easy
Shear	Low	High
CO_2 transfer rate	Poor	Excellent
Mixing efficiency	Poor	Excellent
Volumetric productivity	High	Low
Water loss	Very high	Low
O_2 concentration	Low due to continuous spontaneous out gassing	Exchange device
CO_2 loss	High	Low
Land required	High	Low
Capital investment	Small	High
Periodical maintenance	Less	More
Operating cost	Lower	Higher
Harvesting cost	High	Lower
Most costly parameters	Mixing	O_2, temperature control
Scale-up technology for commercial level	Easy to scale up	Difficult in most PBR models

the utilization of plant-based glucose leads to food versus fuel feud because this is also used for human consumption [85]. Therefore, there is a necessity to develop an alternative technology to use lignocellulose and glycerol derived glucose. (4) Generally microalgae release the CO_2 through respiration but in heterotrophic cultivation it cannot sequester the CO_2 from atmosphere [86]. Therefore, more comprehensive LCA studies and proactive research for heterotrophic cultivation of microalgae are highly required.

(3) Mixotrophic Cultivation. Most of the microalgae utilize both the autotrophic and heterotrophic pathways for their growth and development, indicating that they are able to photosynthesize and utilize organic material [87, 88]. In mixotrophic growth system microalgae cannot depend entirely on photosynthesis because light is not a complete limiting factor, as either light or organic substrate can be utilized for growth [78, 89]. Microalgae which exhibit mixotrophic metabolism are *Spirulina platensis* (cyanobacteria) and *Chlamydomonas reinhardtii* (green algae) [78]. In these organisms, photosynthesis takes place by utilizing light, whereas aerobic respiration uses an organic carbon source for growth [87]. Here the growth of the organism is influenced by the media supplemented with glucose during the light and dark phases; hence, biomass loss during the dark phase is less [89]. A subtype of mixotrophy is called amphitrophy.

This type of organisms can survive either autotrophically or heterotrophically, depending on the availability of organic carbon source and light intensity [90].

Chojnacka and Noworyta [91] compared the growth of *Spirulina* sp. in photoautotrophic, heterotrophic, and mixotrophic cultures. Their observation indicated that cultures grown in mixotrophic conditions showed reduced photoinhibition and enhanced growth rates as compared to autotrophic and heterotrophic culture conditions. Therefore, fruitful mixotrophic production of microalgae permits the incorporation of photosynthetic and heterotrophic compounds during diurnal cycle. Mixotrophic cultivation reduces the impact of biomass loss during dark respiration and decreases the utilization of a number of organic matters during growth. Based on these features, mixotrophic cultivation plays a significant role in microalgae biofuel production.

Photoheterotrophy is also known as photometabolism or photoorganotrophy or photoassimilation. In this cultivation system, organic substrate is utilized as carbon source in the presence of light. There is no clear differentiation between photoheterotrophic and mixotrophic metabolisms, but they can specifically be defined according to the requirement of energy source for growth and particular metabolite production [90].

3.1.2. Molecular Strategies to Improve Microalgae Biomass and Biofuel Production. Manipulation of metabolic pathways by using genetic engineering in microalgae is relatively easy due to its unicellular formation. The main objective of applying genetic engineering to microalgae is to improve the biomass and biodiesel production. The progress in genetic engineering of microalgae was extremely slow until recently. Availability of the microalgae genome sequences greatly facilitates the genetic engineering technology. To date genome sequencing projects were completed for several microalgae species [92] and the sequencing projects for some other microalgae species such as *Fragilariopsis cylindrus*, *Pseudonitzschia*, *Thalassiosira rotula*, *Botryococcus braunii*, *Chlorella vulgaris*, *Dunaliella salina*, *Galdieria sulphuraria* and *Porphyra purpurea* are under progress [93, 94]. In addition to this, several sequencing projects for different species of microalgae plastids and mitochondria were completed and some projects are continuing [92, 95–97]. The development of methodologies for microalgae genetic transformation has progressed considerably in the last 15 years. Advanced methodologies were developed for green, red, and brown algae, diatoms, euglenoids, and dinoflagellates, and until now 30 microalgae strains have been successfully transformed [92]. Most of the transformation experiments were made on a model green alga *Chlamydomonas reinhardtii* at both nuclear and chloroplast levels [98, 99].

(1) Genetic Engineering for Enhanced Biomass Production. Microalgae growth is generally influenced by various environmental stress conditions such as temperature, light, salt concentration, and pH. These conditions can be controlled by engineering and manipulations of growth characteristics, but these manipulations increase the total growing costs of microalgae. Thus, it will be beneficial if the genetic engineering strategies can be developed to control these environmental stress conditions. The average light intensity which provides the maximum photosynthesis in most microalgae species is around 200–400 μM photons $m^{-2}s^{-1}$. The light intensity above this level reduces the microalgae growth. During midday, the maximum light intensity reaches up to 2,000 μM photons $m^{-2}s^{-1}$ [100]. Because of this, microalgae growth efficiency during day time is less. Therefore, several studies were carried out to improve the microalgae photosynthetic efficiency and also to reduce the effect of photoinhibition. Most of these studies were carried out by reducing the number of light-harvesting complexes (LHC) or lowering the chlorophyll antenna size to decrease light absorbing capacity of individual chloroplasts [101]. In an experiment, LHC expression in transgenic *C. reinhardtii* was downregulated to increase the resistance to photooxidative damage and to enhance the efficiency of photosynthesis by 50% [101, 102]. This alteration allowed *C. reinhardtii* to tolerate photoinhibition. In another study conducted by Huesemann et al. [103], no growth improvement was observed in algal antenna mutants cultured in outdoor ponds and also in laboratory conditions. Genes that are able to withstand other stress conditions such as temperature, pH, salt concentration, and other stimuli have also been identified.

(2) Genetic Engineering for Enhanced Biofuel Production. Genetic engineering application in the improvement of microalgae biofuel production is still in the initial stage. Some important advances have been made in the past few years such as development of genetic transformation strategies; sequencing of nuclear, mitochondrial, and chloroplast genomes; and establishment of expressed sequence tag (EST) databases [92]. The current molecular strategies required to improve microalgae biodiesel production include blocking energy rich compounds (e.g., starch) producing metabolic pathways, to decline lipid catabolism, that is, elimination of fatty acid β-oxidation that consumes TAGs; modification of lipid characteristics; direct biological synthesis of fatty acids; and secretion of TAGs, free fatty acids, alkane, and wax esters directly into the medium [92].

3.1.3. Interactions with Bacterial Biofilms to Improve Biomass and Biofuel Production. Microalgae and bacteria perform symbiotic relationship by establishing "phycosphere" [104, 105] as plants and bacteria do in the "rhizosphere" [106]. Microalgae produce extracellular products for the development of matrix like substance on their surfaces, which encourages and provides the environment for the formation of bacterial biofilms [107, 108]. Teplitski et al. [109] reported the existence of microalgae-bacteria interactions in the unicellular microalgae *Chlamydomonas reinhardtii*. To date, only limited studies have been carried out about the existence of interactions between bacterial biofilms and microalgae [110–112]. These studies suggest that the bacteria encourage the growth of microalgae by producing the vitamins and other growth factors, and the organic matters produced by the microalgae simultaneously encourage bacterial growth.

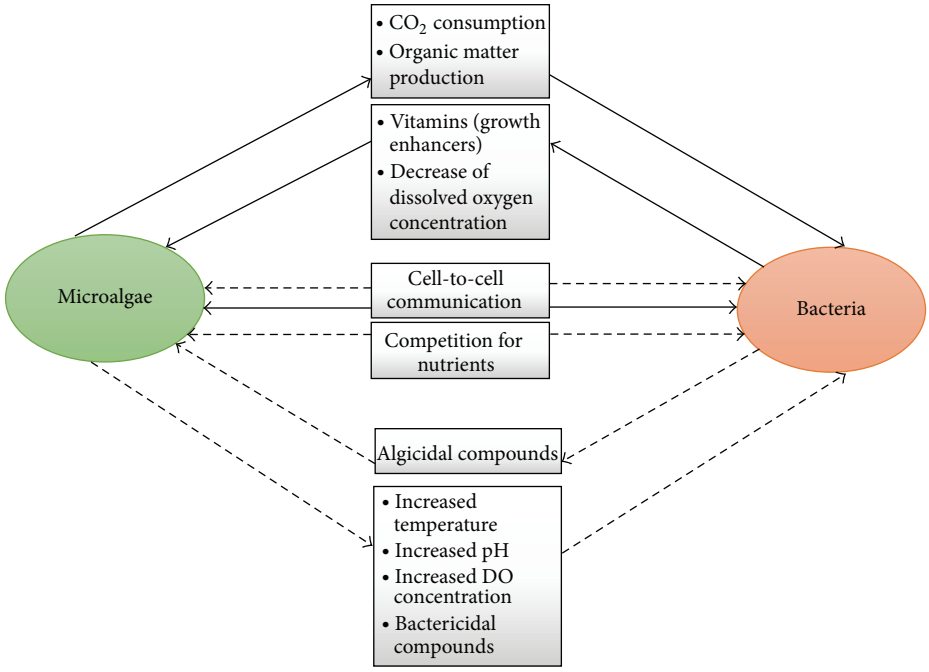

Figure 2: Possible interactions between microalgae and bacteria: solid arrows indicate the positive interactions and dashed arrows indicate the negative interactions [118, 119].

They also have negative interactions between each other; microalgae inhibit the bacterial growth by increasing the temperature, pH, and dissolved oxygen concentration (DOC) or by producing inhibitory metabolites [113, 114], and in the same manner bacteria also can inhibit the microalgae growth by secreting algicidal compounds [115] (Figure 2). Recent reports suggested that the presence of these positive interactions between microalgae and bacteria enhances the microalgae biomass and biodiesel production [116, 117].

3.2. Downstream Processes

3.2.1. Harvesting and Drying of Microalgae Biomass. After attaining sufficient biomass, the microalgae cells are separated from water and prepared for downstream processing. Generally one or more solid-liquid separation steps are required for microalgae biomass separation [23, 120, 121]. According to life cycle analysis, this separation process accounts for 20–30% of the total biofuel production costs [122]. Biomass harvesting and drying processes may constitute major energy consumption in microalgae biofuel production [123]. Therefore, there is a need to reduce energy consumption in microalgae biomass harvesting and drying processes; otherwise, it may cause major cost increase in the overall processes of microalgae biofuel production [124, 125].

3.2.2. Extraction and Purification of Lipids from Microalgae Biomass. Several methods such as presses, supercritical carbon dioxide extraction, ultrasonic-assisted extraction, osmotic shock, solvent extraction, and enzymatic extraction are available for oil extraction from microalgae biomass. The first three methods are used only at laboratory scale. The most important aspects to be considered for selection of appropriate oil extraction process are the cost, efficiency, toxicity, and ease of handling. Supercritical carbon dioxide and osmotic shock are not commercially viable methods due to high operation costs [126]. Enzymatic extraction method is commercially possible, but some efforts are needed to reduce the costs [127, 128]. However, some commercially viable methods are needed to minimize the cost, maximize the extraction of desirable lipid fractions, and reduce the coextraction contaminants.

3.2.3. Microalgae Biomass Conversion Technologies. Microalgae biomass conversion technologies are classified into different types such as biochemical conversion, thermochemical conversion, chemical reaction, and direct combustion [129] (Figure 3). Biochemical conversion can be applied to produce methanol (anaerobic digestion) and ethanol (fermentation) from microalgae biomass [28]. Thermochemical conversion processes can be categorised into pyrolysis (bio-oil, charcoal), gasification (fuel gas), and liquefaction (bio-oil) [130–132]. The energy stored in microalgae cells can be converted into electricity by using direct combustion process. In chemical conversion technologies transesterification process can be employed for the conversion of extracted lipids into biodiesel [16]. Transesterification process is quite a sensitive process as it depends on different parameters such as free fatty acids (FFAs), water content, molar ratio of alcohol to oil, catalyst, reaction temperature, and stirring [133]. Catalytic processes are more appropriate in converting biomass to biodiesel, especially nanocatalysts which have the good capacity in improving product quality and attaining best operating conditions [134].

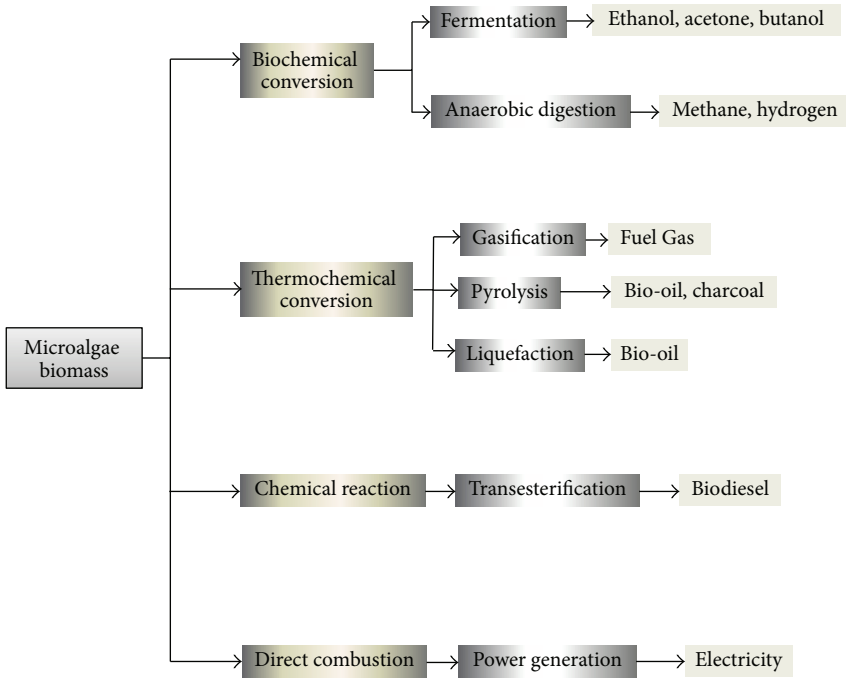

Figure 3: Microalgae biomass conversion processes [23, 135].

4. Limitations of Biofuel Production from Microalgae

In addition to many advantages, microalgae biofuels also have some disadvantages. The main limitations involved in microalgae biofuel production are the low concentration of biomass in the culture and low oil content. In addition, small size of microalgae cells makes the harvesting process quite costly. Harvesting and drying of microalgae biomass from high volume of water are an energy consuming process. Compared to the conventional agriculture practice, microalgae farming is more costly and complicated. These difficulties can be minimized or overcome by the improvement of the harvesting technology. Some of the cost effective technological strategies suggested to develop microalgae biofuel production are (1) development of biorefinery or coproduct strategy, (2) designing high photosynthesis efficiency photobioreactors, (3) development of cost-effective technologies for biomass harvesting and drying, (4) development of genetic engineering technology to modify metabolic pathways for microalgae biomass and lipid production, and (5) understanding of symbiotic interactions between microalgae and bacteria that also affects the biomass and lipid production in microalgae.

5. Economic Analysis of Microalgae Biofuel Production

Economy plays an important role in the commercial feasibility of microalgae biofuel production [136]. Microalgae oil production cost depends on various factors, such as biomass yield, oil content, scale of production systems, and cost of recovering oil from microalgae biomass. It also depends on the petroleum oil price. According to Gallagher [137], the economic feasibility of microalgae biofuel production seems to be fair and dependent on government subsidies and the future prices of oil. In addition to optimized biomass yields, the requirement of carbon neutral renewable alternatives makes microalgae one of the best future sources of biofuels [16]. Norsker et al. [138] calculated biomass production costs for three different commercial production systems such as open ponds, horizontal tubular photobioreactors, and flat-panel photobioreactors. The resulting biomass production costs for these three systems including dewatering were 4.95, 4.15, and 5.96 € per kg, respectively. The factors which influence production costs are irradiation, mixing, photosynthetic efficiency, culture medium, and CO_2. If we optimize these factors, the production cost reduces to € 0.68 per kg and at this cost microalgae become promising feedstock for biodiesel production and for other applications. Generally the following formula can be used to estimate the cost of algal oil where it can be a competitive substitute for petroleum diesel [16]:

$$C_{\text{algal oil}} = 25.9 \times 10^{-3} C_{\text{petroleum}}, \quad (1)$$

where $C_{\text{algal oil}}$ is the microalgae oil price in dollars per gallon and $C_{\text{petroleum}}$ is the crude oil price in dollars per barrel.

According to the above-mentioned formula, the algal oil roughly contains 80% of the caloric energy value of crude petroleum. For example, in order to maintain competitiveness with petroleum diesel microalgae oil should not be priced more than $ 0.70/L, if petroleum price is $ 0.62/L.

The biodiesel competitiveness depends mainly on the microalgae biomass production costs. Competitiveness can be calculated by estimating the maximum price that could

be paid for microalgae biomass with a given content of oil, if crude petroleum can be purchased at a given price as a source of energy. This estimated price can then be compared with the current cost of producing the algal biomass. According to Chisti [44] the quantity of algal biomass (M, tons), which is the energy equivalent to a barrel of crude petroleum, can be estimated as follows:

$$M = \frac{E_{\text{petroleum}}}{q\,(1-W)\,E_{\text{biogas}}} + YWE_{\text{biodiesel}}, \quad (2)$$

where $E_{\text{petroleum}}$ (~6100 MJ) is the energy contained in a barrel of crude petroleum, q ($\text{m}^3\text{ton}^{-1}$) is biogas volume produced by anaerobic digestion of residual algal biomass, W is the oil content of the biogas, Y is the yield of biodiesel from algal oil, and $E_{\text{biodiesel}}$ is the average energy content of biodiesel.

Typically, Y in (2) is 80% by weight and $E_{\text{biodiesel}}$ is ~37,800 MJ per ton. Keeping with average values for organic wastes, E_{biogas} and q are expressed to be around 23.4 MJm^{-3} and 400 $\text{m}^3\text{ton}^{-1}$, respectively. Using these values in (2), M can be calculated for any selected value of W.

Assuming that converting a barrel of crude oil to various useable transport energy products costs roughly the same as converting M tons of biomass to bioenergy, the maximum acceptable price that could be paid for the biomass would be the same as the price of a barrel of crude petroleum; thus,

$$\begin{aligned}&\text{Acceptable price of biomass } (\$.\text{ton})\\ &\quad = \text{Price of a barrel of petroleum}\frac{(\$)}{M}.\end{aligned} \quad (3)$$

By using these equations the prices of microalgae biomass can be estimated for biomass with different levels of oil content (15%–55% by weight). The feasibility of microalgae biofuel can be enhanced by designing advanced photobioreactors, developing cost-effective technologies for biomass harvesting and drying, improving molecular strategies for more biomass and lipid production, and understanding of biotic and abiotic interactions with algae.

6. Conclusions

Microalgae have the potential to be important and sustainable renewable energy feedstock that could meet the global demand. In spite of the many advantages, microalgae biofuels also have some disadvantages such as low biomass production and small cell size that makes the harvesting process costly. These limitations could be overcome by designing advanced photobioreactors and developing low cost technologies for biomass harvesting, drying and oil extraction. In addition, application of genetic engineering technology in the manipulation of microalgae metabolic pathways is also an efficient strategy to improve biomass and biofuel production. Genetic engineering technology also plays an important role in the production of valuable products with minimal costs. Biotic interaction with bacterial biofilms is also an important aspect in microalgae biomass and biofuel production. However, these technologies are still in the early stages and most have not been applied on a commercial scale. Therefore, further research in the development of novel upstream and downstream technologies will benefit the commercial production of biofuels from microalgae.

Conflict of Interests

The authors declare that there is no conflict of interests regarding the publication of this paper.

References

[1] J. Rupprecht, "From systems biology to fuel—*Chlamydomonas reinhardtii* as a model for a systems biology approach to improve biohydrogen production," *Journal of Biotechnology*, vol. 142, no. 1, pp. 10–20, 2009.

[2] K. K. Lum, J. Kim, and X. G. Lei, "Dual potential of microalgae as a sustainable biofuel feedstock and animal feed," *Journal of Animal Science and Biotechnology*, vol. 4, no. 1, article 53, 2013.

[3] M. K. Lam and K. T. Lee, "Microalgae biofuels: a critical review of issues, problems and the way forward," *Biotechnology Advances*, vol. 30, no. 3, pp. 673–690, 2012.

[4] International Energy Agency, *Key World Energy Statistics*, International Energy Agency, Paris, France, 2010.

[5] J. K. Pittman, A. P. Dean, and O. Osundeko, "The potential of sustainable algal biofuel production using wastewater resources," *Bioresource Technology*, vol. 102, no. 1, pp. 17–25, 2011.

[6] M. Tabatabaei, M. Tohidfar, G. S. Jouzani, M. Safarnejad, and M. Pazouki, "Biodiesel production from genetically engineered microalgae: future of bioenergy in Iran," *Renewable and Sustainable Energy Reviews*, vol. 15, no. 4, pp. 1918–1927, 2011.

[7] A. Demirbaş, "Production of biodiesel from algae oils," *Energy Sources Part A*, vol. 31, no. 2, pp. 163–168, 2009.

[8] L. Brennan and P. Owende, "Biofuels from microalgae—a review of technologies for production, processing, and extractions of biofuels and co-products," *Renewable and Sustainable Energy Reviews*, vol. 14, no. 2, pp. 557–577, 2010.

[9] FAO, *Sustainable Bioenergy: A Framework for Decision Makers*, United Nations Energy, 2007.

[10] FAO, *The State of Food and Agriculture*, Food and Agriculture Organization, New York, NY, USA, 2008.

[11] Z. Cohen, *Chemicals from Microalgae*, Edited by: Z. Cohen, Ben-Gurion University of the Negev, Beersheba, Israel, 1st edition, 1999.

[12] Y. Li and J. G. Qin, "Comparison of growth and lipid content in three *Botryococcus braunii* strains," *Journal of Applied Phycology*, vol. 17, no. 6, pp. 551–556, 2005.

[13] J. Qin, *Bio-Hydrocarbons from Algae: Impacts of Temperature, Light and Salinity on Algae Growth*, Rural Industries Research and Development Corporation, Australian Government, 2005.

[14] A. R. Rao, R. Sarada, V. Baskaran, and G. A. Ravishankar, "Antioxidant activity of *Botryococcus braunii* extract elucidated *in vitro* models," *Journal of Agricultural and Food Chemistry*, vol. 54, no. 13, pp. 4593–4599, 2006.

[15] J. G. Qin and Y. Li, "Optimization of the growth environment of *Botryococcus braunii* Strain CHN 357," *Journal of Freshwater Ecology*, vol. 21, no. 1, pp. 169–176, 2006.

[16] Y. Chisti, "Biodiesel from microalgae," *Biotechnology Advances*, vol. 25, no. 3, pp. 294–306, 2007.

[17] E. E. Powell and G. A. Hill, "Economic assessment of an integrated bioethanol-biodiesel-microbial fuel cell facility utilizing yeast and photosynthetic algae," *Chemical Engineering Research and Design*, vol. 87, no. 9, pp. 1340–1348, 2009.

[18] T. M. Mata, A. A. Martins, and N. S. Caetano, "Microalgae for biodiesel production and other applications: a review," *Renewable and Sustainable Energy Reviews*, vol. 14, no. 1, pp. 217–232, 2010.

[19] F. M. Yusoff, M. A. B. Habib, and S. M. Phang, "Growth and biochemical composition of tropical marine microalgae," *Journal of Aquaculture in the Tropics*, vol. 19, pp. 165–177, 2004.

[20] V. Pasquet, J.-R. Chérouvrier, F. Farhat et al., "Study on the microalgal pigments extraction process: performance of microwave assisted extraction," *Process Biochemistry*, vol. 46, no. 1, pp. 59–67, 2011.

[21] T. Leela, B. Naresh, M. Srikanth Reddy, N. C. H. Madhusudhan, and P. D. Cherku, "Morphological, physico-chemical and micropropagation studies in *Jatropha curcas* L. and RAPD analysis of the regenerants," *Applied Energy*, vol. 88, no. 6, pp. 2071–2079, 2011.

[22] B. Naresh, M. S. Reddy, P. Vijayalakshmi, V. Reddy, and P. Devi, "Physico-chemical screening of accessions of *Jatropha curcas* for biodiesel production," *Biomass and Bioenergy*, vol. 40, pp. 155–161, 2012.

[23] B. Wang, Y. Li, N. Wu, and C. Q. Lan, "CO_2 bio-mitigation using microalgae," *Applied Microbiology and Biotechnology*, vol. 79, no. 5, pp. 707–718, 2008.

[24] W. C. W. Barkley, R. A. Lewin, and L. Cheng, *Development of Microalgal Systems for the Production of Liquid Fuels*, Edited by T. Sadler, Elsevier Applied Science, Villeneuve d'Ascq, France, 1987.

[25] Y. Li, M. Horsman, N. Wu, C. Q. Lan, and N. Dubois-Calero, "Biofuels from microalgae," *Biotechnology Progress*, vol. 24, no. 4, pp. 815–820, 2008.

[26] M. A. Borowitzka, "Commercial production of microalgae: ponds, tanks, tubes and fermenters," *Journal of Biotechnology*, vol. 70, no. 1–3, pp. 313–321, 1999.

[27] O. Pulz and K. Scheinbenbogen, "Photobioreactors: design and performance with respect to light energy input," in *Bioprocess and Algae Reactor Technology, Apoptosis*, vol. 59 of *Advances in Biochemical Engineering Biotechnology*, pp. 123–52, Springer, Berlin, Germany, 1998.

[28] P. Spolaore, C. Joannis-Cassan, E. Duran, and A. Isambert, "Commercial applications of microalgae," *Journal of Bioscience and Bioengineering*, vol. 101, no. 2, pp. 87–96, 2006.

[29] Renewable Fuels Association (RFA), *Ethanol Industry Outlook: Climate of Opportunity*, 2010, http://ethanolrfa.org/page/-/objects/pdf/outlook/RFAoutlook2010_fin.pdf?nocdn=1.

[30] OECD-FAO, *OECD-FAO Agricultural Outlook 2008–2017*, OECD-FAO, Paris, France, 2008.

[31] L. Fulton, "International Energy Agency (IEA) biofuels study–interim report: result and key messages so far," in *Biomass and Agriculture Sustainability, Markets and Policies*, pp. 105–112, Organisation for Economic Co-operation and Development, 2004.

[32] S. I. Mussatto, G. Dragone, P. M. R. Guimarães et al., "Technological trends, global market, and challenges of bio-ethanol production," *Biotechnology Advances*, vol. 28, no. 6, pp. 817–830, 2010.

[33] USDA, *US Department of Agriculture*, 2007, http://www.usda.gov.

[34] Commission of the European Communities (CEC), "An EU strategy for biofuel, Communication from the commission, COM (2006) 34 final, SEC (2006) 142," Brussels, Belgium, http://ec.europa.eu/energy/res/biomass_action_plan/doc/2006_02_08_comm_eu_strategy_en.pdf.

[35] T. Kurevija and N. Kukulji, "Algae biofuels as a possible alternative to environmentally doudtful conventional methods of biodiesel production," in *Survival and Sustainability, Environmental Earth Sciences*, H. Gokcekus, Ed., pp. 499–510, Springer, Berlin, Germany, 2011.

[36] M. H. Huesemann and J. R. Benemann, "Biofuels from Microalgae: review of products, processes and potential, with special focus on *Dunaliella* sp," in *The Alga Dunaliella: Biodiversity, Physiology, Genomics, and Biotechnology, Enfield*, A. Ben-Amotz, J. E. W. Polle, and D. V. Subba Rao, Eds., Science Publishers, 2009.

[37] J. Wang, H. Yang, and F. Wang, "Mixotrophic cultivation of microalgae for biodiesel production: status and prospects," *Applied Biochemistry and Biotechnology*, vol. 172, no. 7, pp. 3307–3329, 2014.

[38] Y. Liang, N. Sarkany, and Y. Cui, "Biomass and lipid productivities of *Chlorella vulgaris* under autotrophic, heterotrophic and mixotrophic growth conditions," *Biotechnology Letters*, vol. 31, no. 7, pp. 1043–1049, 2009.

[39] Y.-H. Chen and T. H. Walker, "Biomass and lipid production of heterotrophic microalgae *Chlorella protothecoides* by using biodiesel-derived crude glycerol," *Biotechnology Letters*, vol. 33, no. 10, pp. 1973–1983, 2011.

[40] Y. Zheng, *Two-stage heterotrophic and phototrophic culture technology for microbial biofuel production [Ph.D. thesis]*, Department of Biological Systems Engineering, Washington State University, 2013.

[41] J. Sheehan, V. Camobreco, J. Duffield, M. Graboski, and H. Shapouri, "An overview of biodiesel and petroleum diesel life cycles," US Department of Agriculture and Energy Report, 1998.

[42] M. A. Borowitzka, "Culturing microalgae in outdoor ponds in," in *Algal Culturing Techniques*, R. A. Anderson, Ed., pp. 205–18, Elsevier, London, UK, 2005.

[43] C. Jiménez, B. R. Cossío, D. Labella, and F. X. Niell, "The feasibility of industrial production of *Spirulina* (Arthrospira) in Southern Spain," *Aquaculture*, vol. 217, no. 1–4, pp. 179–190, 2003.

[44] Y. Chisti, "Biodiesel from microalgae beats bioethanol," *Trends in Biotechnology*, vol. 26, no. 3, pp. 126–131, 2008.

[45] L. Rodolfi, G. C. Zittelli, N. Bassi et al., "Microalgae for oil: strain selection, induction of lipid synthesis and outdoor mass cultivation in a low-cost photobioreactor," *Biotechnology and Bioengineering*, vol. 102, no. 1, pp. 100–112, 2009.

[46] R. Harun, M. Singh, G. M. Forde, and M. K. Danquah, "Bioprocess engineering of microalgae to produce a variety of consumer products," *Renewable and Sustainable Energy Reviews*, vol. 14, no. 3, pp. 1037–1047, 2010.

[47] A. Belay, "Mass culture of *Spirulina* outdoors—the Earthrise Farms experience," in Spirulina platensis *(Arthrospira): Physiology, Cell-Biology and Biochemistry*, A. Vonshak, Ed., pp. 131–158, Taylor & Francis, London, UK, 1997.

[48] G. R. Cysewski and R. T. Lorenz, "Industrial production of microalgal cell-mass and secondary products-species of high potential: *Haematococcus*," in *Microalgal Culture: Biotechnology and Applied Phycology*, A. Richmond, Ed., pp. 281–288, Blackwell Science, Oxford, UK, 2004.

[49] N. R. Moheimani and M. A. Borowitzka, "The long-term culture of the coccolithophore *Pleurochrysis carterae* (Haptophyta) in outdoor raceway ponds," *Journal of Applied Phycology*, vol. 18, no. 6, pp. 703–712, 2006.

[50] M. A. Borowitzka, "Carotenoid production using microalgae," in *Single Cell Oils: Microbial and Algal Oils*, Z. Cohen and C. Ratledge, Eds., pp. 225–240, American Oil Chemists' Society, Urbana, Ill, USA, 2010.

[51] O. Pulz, "Photobioreactors: production systems for phototrophic microorganisms," *Applied Microbiology and Biotechnology*, vol. 57, no. 3, pp. 287–293, 2001.

[52] A. P. Carvalho, L. A. Meireles, and F. X. Malcata, "Microalgal reactors: a review of enclosed system designs and performances," *Biotechnology Progress*, vol. 22, no. 6, pp. 1490–1506, 2006.

[53] C. U. Ugwu and H. Aoyagi, "Microalgal culture systems: an insight into their designs, operation and applications," *Biotechnology*, vol. 11, no. 3, pp. 127–132, 2012.

[54] Y. Chisti, "Microalgae as sustainable cell factories," *Environmental Engineering and Management Journal*, vol. 5, no. 3, pp. 261–274, 2006.

[55] H.-S. Lee, M.-W. Seo, Z.-H. Kim, and C.-G. Lee, "Determining the best specific light uptake rates for the lumostatic cultures in bubble column photobioreactors," *Enzyme and Microbial Technology*, vol. 39, no. 3, pp. 447–452, 2006.

[56] T. M. Sobczuk, F. G. Camacho, E. M. Grima, and Y. Chisti, "Effects of agitation on the microalgae *Phaeodactylum tricornutum* and *Porphyridium cruentum*," *Bioprocess and Biosystems Engineering*, vol. 28, no. 4, pp. 243–250, 2006.

[57] N. T. Eriksen, F. K. Riisgård, W. S. Gunther, and J. J. Lønsmann Iversen, "On-line estimation of O_2 production, CO_2 uptake, and growth kinetics of microalgal cultures in a gas-tight photobioreactor," *Journal of Applied Phycology*, vol. 19, no. 2, pp. 161–174, 2007.

[58] L. Travieso, D. O. Hall, K. K. Rao, F. Benítez, E. Sánchez, and R. Borja, "A helical tubular photobioreactor producing *Spirulina* in a semicontinuous mode," *International Biodeterioration and Biodegradation*, vol. 47, no. 3, pp. 151–155, 2001.

[59] E. Molina, J. Fernández, F. G. Acién, and Y. Chisti, "Tubular photobioreactor design for algal cultures," *Journal of Biotechnology*, vol. 92, no. 2, pp. 113–131, 2001.

[60] D. O. Hall, F. G. Acién Fernández, E. C. Guerrero, K. K. Rao, and E. M. Grima, "Outdoor helical tubular photobioreactors for microalgal production: modeling of fluid-dynamics and mass transfer and assessment of biomass productivity," *Biotechnology and Bioengineering*, vol. 82, no. 1, pp. 62–73, 2003.

[61] A. Converti, A. Lodi, A. Del Borghi, and C. Solisio, "Cultivation of *Spirulina platensis* in a combined airlift-tubular reactor system," *Biochemical Engineering Journal*, vol. 32, no. 1, pp. 13–18, 2006.

[62] N. T. Eriksen, "The technology of microalgal culturing," *Biotechnology Letters*, vol. 30, no. 9, pp. 1525–1536, 2008.

[63] Q. Hu, N. Kurano, M. Kawachi, I. Iwasaki, and S. Miyachi, "Ultrahigh-cell-density culture of a marine green alga *Chlorococcum littorale* in a flat-plate photobioreactor," *Applied Microbiology and Biotechnology*, vol. 49, no. 6, pp. 655–662, 1998.

[64] J. Degen, A. Uebele, A. Retze, U. Schmid-Staiger, and W. Trösch, "A novel airlift photobioreactor with baffles for improved light utilization through the flashing light effect," *Journal of Biotechnology*, vol. 92, no. 2, pp. 89–94, 2001.

[65] A. Richmond, Z. Cheng-Wu, and Y. Zarmi, "Efficient use of strong light for high photosynthetic productivity: interrelationships between the optical path, the optimal population density and cell-growth inhibition," *Biomolecular Engineering*, vol. 20, no. 4–6, pp. 229–236, 2003.

[66] A. Vonshak and A. Richmond, "Mass production of the blue-green alga *Spirulina*: an overview," *Biomass*, vol. 15, no. 4, pp. 233–247, 1988.

[67] R. Rosello Sastre, Z. Csögör, I. Perner-Nochta, P. Fleck-Schneider, and C. Posten, "Scale-down of microalgae cultivations in tubular photo-bioreactors—a conceptual approach," *Journal of Biotechnology*, vol. 132, no. 2, pp. 127–133, 2007.

[68] P. M. Schenk, R. Skye, T. Hall et al., "Second generation biofuels: high-efficiency microalgae for biodiesel production," *Bioenergy Resources*, vol. 1, pp. 20–43, 2008.

[69] FAO, "Algae based biofuel: a review of challenges and opportunities for developing countries," FAO, Rome, Italy, 2009, http://www.fao.org/bioenergy/aquaticbiofuels/en/.

[70] S. Amin, "Review on biofuel oil and gas production processes from microalgae," *Energy Conversion and Management*, vol. 50, no. 7, pp. 1834–1840, 2009.

[71] R. Harun and M. K. Danquah, "Influence of acid pre-treatment on microalgal biomass for bioethanol production," *Process Biochemistry*, vol. 46, no. 1, pp. 304–309, 2011.

[72] J. U. Grobbelaar, "Physiological and technological considerations for optimising mass algal cultures," *Journal of Applied Phycology*, vol. 12, no. 3-5, pp. 201–206, 2000.

[73] H. C. Greenwell, L. M. L. Laurens, R. J. Shields, R. W. Lovitt, and K. J. Flynn, "Placing microalgae on the biofuels priority list: a review of the technological challenges," *Journal of the Royal Society Interface*, vol. 7, no. 46, pp. 703–726, 2010.

[74] M. Olaizola, "Commercial production of astaxanthin from *Haematococcus pluvialis* using 25,000-liter outdoor photobioreactors," *Journal of Applied Phycology*, vol. 12, no. 3–5, pp. 499–506, 2000.

[75] M. E. Huntley and D. G. Redalje, "CO2 mitigation and renewable oil from photosynthetic microbes: a new appraisal," *Mitigation and Adaptation Strategies for Global Change*, vol. 12, no. 4, pp. 573–608, 2007.

[76] Z.-Y. Wen and F. Chen, "Heterotrophic production of eicosapentaenoic acid by microalgae," *Biotechnology Advances*, vol. 21, no. 4, pp. 273–294, 2003.

[77] J. Myers and G. O. Burr, "Studies on photosynthesis: some effects of light of high intensity on *Chlorella*," *Journal of General Physiology*, vol. 24, no. 1, pp. 45–67, 1940.

[78] F. Chen, "High cell density culture of microalgae in heterotrophic growth," *Trends in Biotechnology*, vol. 14, no. 11, pp. 421–426, 1996.

[79] F. Chen and M. R. Johns, "Effect of C/N ratio and aeration on the fatty acid composition of heterotrophic *Chlorella sorokiniana*," *Journal of Applied Phycology*, vol. 3, no. 3, pp. 203–209, 1991.

[80] H. Xu, X. Miao, and Q. Wu, "High quality biodiesel production from a microalga *Chlorella protothecoides* by heterotrophic growth in fermenters," *Journal of Biotechnology*, vol. 126, no. 4, pp. 499–507, 2006.

[81] W. Xiong, X. Li, J. Xiang, and Q. Wu, "High-density fermentation of microalga *Chlorella protothecoides* in bioreactor for microbio-diesel production," *Applied Microbiology and Biotechnology*, vol. 78, no. 1, pp. 29–36, 2008.

[82] Y. Cheng, W. Zhou, C. Gao, K. Lan, Y. Gao, and Q. Wu, "Biodiesel production from Jerusalem artichoke (*Helianthus*

tuberosus L.) tuber by heterotrophic microalgae *Chlorella protothecoides*," *Journal of Chemical Technology and Biotechnology*, vol. 84, no. 5, pp. 777–781, 2009.

[83] R. M. Couto, P. C. Simões, A. Reis, T. L. Da Silva, V. H. Martins, and Y. Sánchez-Vicente, "Supercritical fluid extraction of lipids from the heterotrophic microalga *Crypthecodinium cohnii*," *Engineering in Life Sciences*, vol. 10, no. 2, pp. 158–164, 2010.

[84] M. B. Johnson and Z. Wen, "Production of biodiesel fuel from the microalga *Schizochytrium limacinum* by direct transesterification of algal biomass," *Energy and Fuels*, vol. 23, no. 10, pp. 5179–5183, 2009.

[85] O. Perez-Garcia, F. M. E. Escalante, L. E. de-Bashan, and Y. Bashan, "Heterotrophic cultures of microalgae: metabolism and potential products," *Water Research*, vol. 45, no. 1, pp. 11–36, 2011.

[86] Y. Li, M. Horsman, B. Wang, N. Wu, and C. Q. Lan, "Effects of nitrogen sources on cell growth and lipid accumulation of green alga *Neochloris oleoabundans*," *Applied Microbiology and Biotechnology*, vol. 81, no. 4, pp. 629–636, 2008.

[87] X.-W. Zhang, Y.-M. Zhang, and F. Chen, "Application of mathematical models to the determination optimal glucose concentration and light intensity for mixotrophic culture of *Spirulina platensis*," *Process Biochemistry*, vol. 34, no. 5, pp. 477–481, 1999.

[88] L. E. Graham, J. M. Graham, and L. W. Wilcox, *Algae*, Pearson Education, San Francisco, Calif, USA, 2nd edition, 2009.

[89] M. R. Andrade and J. A. V. Costa, "Mixotrophic cultivation of microalga *Spirulina platensis* using molasses as organic substrate," *Aquaculture*, vol. 264, no. 1–4, pp. 130–134, 2007.

[90] K. Chojnacka and F. J. Marquez-Rocha, "Kinetic, Stoichiometric relationships of the energy and carbon metabolism in the culture of microalgae," *Biotechnology*, vol. 3, no. 1, pp. 21–34, 2004.

[91] K. Chojnacka and A. Noworyta, "Evaluation of *Spirulina sp.* growth in photoautotrophic, heterotrophic and mixotrophic cultures," *Enzyme and Microbial Technology*, vol. 34, no. 5, pp. 461–465, 2004.

[92] R. Radakovits, R. E. Jinkerson, A. Darzins, and M. C. Posewitz, "Genetic engineering of algae for enhanced biofuel production," *Eukaryotic Cell*, vol. 9, no. 4, pp. 486–501, 2010.

[93] K. Liolios, K. Mavromatis, N. Tavernarakis, and N. C. Kyrpides, "The Genomes On Line Database (GOLD) in 2007: status of genomic and metagenomic projects and their associated metadata," *Nucleic Acids Research*, vol. 36, no. 1, pp. D475–D479, 2008.

[94] S. Sasso, G. Pohnert, M. Lohr, M. Mittag, and C. Hertweck, "Microalgae in the postgenomic era: a blooming reservoir for new natural products," *FEMS Microbiology Reviews*, vol. 36, no. 4, pp. 761–785, 2012.

[95] J. M. Archibald, M. B. Rogers, M. Toop, K.-I. Ishida, and P. J. Keeling, "Lateral gene transfer and the evolution of plastid-targeted proteins in the secondary plastid-containing alga Bigelowiella natans," *Proceedings of the National Academy of Sciences of the United States of America*, vol. 100, no. 13, pp. 7678–7683, 2003.

[96] T. R. Bachvaroff, G. T. Concepcion, C. R. Rogers, E. M. Herman, and C. F. Delwiche, "Dinoflagellate expressed sequence tag data indicate massive transfer of chloroplast genes to the nuclear genome," *Protist*, vol. 155, no. 1, pp. 65–78, 2004.

[97] E. A. O'Brien, L. B. Koski, Y. Zhang et al., "TBestDB: a taxonomically broad database of expressed sequence tags (ESTs)," *Nucleic Acids Research*, vol. 35, no. 1, pp. D445–D451, 2007.

[98] V. Lumbreras, D. R. Stevens, and S. Purton, "Efficient foreign gene expression in *Chlamydomonas reinhardtii* mediated by an endogenous intron," *Plant Journal*, vol. 14, no. 4, pp. 441–447, 1998.

[99] M. Fuhrmann, A. Hausherr, L. Ferbitz, T. Schödl, M. Heitzer, and P. Hegemann, "Monitoring dynamic expression of nuclear genes in *Chlamydomonas reinhardtii* by using a synthetic luciferase reporter gene," *Plant Molecular Biology*, vol. 55, no. 6, pp. 869–881, 2005.

[100] A. Melis, "Solar energy conversion efficiencies in photosynthesis: minimizing the chlorophyll antennae to maximize efficiency," *Plant Science*, vol. 177, no. 4, pp. 272–280, 2009.

[101] J. H. Mussgnug, S. Thomas-Hall, J. Rupprecht et al., "Engineering photosynthetic light capture: impacts on improved solar energy to biomass conversion," *Plant Biotechnology Journal*, vol. 5, no. 6, pp. 802–814, 2007.

[102] J. Beckmann, F. Lehr, G. Finazzi et al., "Improvement of light to biomass conversion by de-regulation of light-harvesting protein translation in *Chlamydomonas reinhardtii*," *Journal of Biotechnology*, vol. 142, no. 1, pp. 70–77, 2009.

[103] M. H. Huesemann, T. S. Hausmann, R. Bartha, M. Aksoy, J. C. Weissman, and J. R. Benemann, "Biomass productivities in wild type and pigment mutant of *Cyclotella* sp. (Diatom)," *Applied Biochemistry and Biotechnology*, vol. 157, no. 3, pp. 507–526, 2009.

[104] J. J. Cole, "Interactions between bacteria and algae in aquatic ecosystems," *Annual Review of Ecology Systems*, vol. 13, no. 1, pp. 291–314, 1982.

[105] M. Sapp, A. S. Schwaderer, K. H. Wiltshire, H.-G. Hoppe, G. Gerdts, and A. Wichels, "Species-specific bacterial communities in the phycosphere of microalgae?" *Microbial Ecology*, vol. 53, no. 4, pp. 683–699, 2007.

[106] T. Danhorn and C. Fuqua, "Biofilm formation by plant-associated bacteria," *Annual Review of Microbiology*, vol. 61, pp. 401–422, 2007.

[107] C. E. Riquelme and Y. Ishida, "Chemotaxis of bacteria to extracellular products of marine bloom algae," *The Journal of General and Applied Microbiology*, vol. 34, pp. 417–23, 1988.

[108] H. W. Paerl and J. L. Pinckney, "A mini-review of microbial consortia: their roles in aquatic production and biogeochemical cycling," *Microbial Ecology*, vol. 31, no. 3, pp. 225–247, 1996.

[109] M. Teplitski, H. Chen, S. Rajamani et al., "*Chlamydomonas reinhardtii* secretes compounds that mimic bacterial signals and interfere with quorum sensing regulation in bacteria," *Plant Physiology*, vol. 134, no. 1, pp. 137–146, 2004.

[110] K. Kogure, U. Simidu, and N. Taga, "Effect of *Skeletonema costatum* (Grev.) Cleve on the growth of marine bacteria," *Journal of Experimental Marine Biology and Ecology*, vol. 36, no. 3, pp. 201–215, 1979.

[111] L. Verschuere, G. Rombaut, P. Sorgeloos, and W. Verstraete, "Probiotic bacteria as biological control agents in aquaculture," *Microbiology and Molecular Biology Reviews*, vol. 64, no. 4, pp. 655–671, 2000.

[112] C. E. Riquelme and R. E. Avendaño-Herrera, "Microalgae and bacteria interaction in the aquatic environment and their potential use in aquaculture," *Revista Chilena de Historia Natural*, vol. 76, no. 4, pp. 725–736, 2003.

[113] W. J. Oswald, "My sixty years in applied algology," *Journal of Applied Phycology*, vol. 15, pp. 99–106, 2003.

[114] G. Schumacher, T. Blume, and I. Sekoulov, "Bacteria reduction and nutrient removal in small wastewater treatment plants by an algal biofilm," *Water Science and Technology*, vol. 47, no. 11, pp. 195–202, 2003.

[115] K. Fukami, T. Nishijima, and Y. Ishida, "Stimulative and inhibitory effects of bacteria on the growth of microalgae," *Hydrobiologia*, vol. 358, pp. 185–191, 1997.

[116] M. O. Rivas, P. Vargas, and C. E. Riquelme, "Interactions of *Botryococcus braunii* cultures with bacterial biofilms," *Microbial Ecology*, vol. 60, no. 3, pp. 628–635, 2010.

[117] Y. Tanabe, S. Kato, H. Matsuura, and M. M. Watanabe, "A *Botryococcus* strain with bacterial ectosymbionts grows fast and produces high amount of hydrocarbons," *Procedia Environmental Science*, vol. 15, pp. 22–26, 2012.

[118] R. Muñoz and B. Guieysse, "Algal-bacterial processes for the treatment of hazardous contaminants: a review," *Water Research*, vol. 40, no. 15, pp. 2799–2815, 2006.

[119] F. M. I. Natrah, P. Bossier, P. Sorgeloos, F. M. Yusoff, and T. Defoirdt, "Significance of microalgal-bacterial interactions for aquaculture," *Reviews in Aquaculture*, vol. 6, no. 1, pp. 48–61, 2014.

[120] Z. T. Harith, F. M. Yusoff, M. S. Mohamed, M. S. Mohamed Din, and A. B. Ariff, "Effect of different flocculants on the flocculation performance of microalgae, *Chaetoceros calcitrans*, cells," *African Journal of Biotechnology*, vol. 8, no. 21, pp. 5971–5978, 2009.

[121] Z. T. Harith, F. M. Yusoff, M. Shariff, and A. B. Ariff, "Effect of different separation techniques and storage temperatures on the viability of marine microalgae, *Chaetoceros calcitrans*, during storage," *Biotechnology*, vol. 9, no. 3, pp. 387–391, 2010.

[122] C. Gudin and C. Therpenier, "Bioconversion of solar energy into organic chemicals by microalgae," *Advance Biotechnology Processes*, vol. 6, pp. 73–110, 1986.

[123] K. Sander and G. S. Murthy, "Life cycle analysis of algae biodiesel," *International Journal of Life Cycle Assessment*, vol. 15, no. 7, pp. 704–714, 2010.

[124] N. Munir, N. Sharif, N. Shagufta, F. Saleem, and F. Manzoor, "Harvesting and processing of microalgae biomass fractions for biodiesel production (a review)," *Science Technology and Development*, vol. 32, pp. 235–243, 2013.

[125] X. Zeng, C. X. Quek, M. K. Danquah, M. W. Woo, Y. Lu, and X. D. Chen, "Falling film evaporation characteristics of microalgae suspension for biofuel production," *Applied Thermal Engineering*, vol. 62, no. 2, pp. 341–350, 2014.

[126] M. Awasthia and R. K. Singh, "Development of algae for the production of bioethanol, biomethane, biohydrogen and biodiesel," *International Journal of Current Science*, vol. 1, pp. 14–23, 2011.

[127] P. Mercer and R. E. Armenta, "Developments in oil extraction from microalgae," *European Journal of Lipid Science and Technology*, vol. 113, no. 5, pp. 539–547, 2011.

[128] R. Halim, M. K. Danquah, and P. A. Webley, "Extraction of oil from microalgae for biodiesel production: a review," *Biotechnology Advances*, vol. 30, no. 3, pp. 709–732, 2012.

[129] N. Pena, *Biofuels for Transportation: A Climate Perspective*, Pew Centre on Global Climate Change, 2008.

[130] A. Hirano, K. Hon-Nami, S. Kunito, M. Hada, and Y. Ogushi, "Temperature effect on continuous gasification of microalgal biomass: theoretical yield of methanol production and its energy balance," *Catalysis Today*, vol. 45, no. 1–4, pp. 399–404, 1998.

[131] T. Minowa and S. Sawayama, "Novel microalgal system for energy production with nitrogen cycling," *Fuel*, vol. 78, no. 10, pp. 1213–1215, 1999.

[132] D. Chiaramonti, A. Oasmaa, and Y. Solantausta, "Power generation using fast pyrolysis liquids from biomass," *Renewable and Sustainable Energy Reviews*, vol. 11, no. 6, pp. 1056–1086, 2007.

[133] V. K. Sohpal and A. Singh, "Optimization of alkali catalyst for transesterification of jatropha curcus using adaptive neuro-fuzzy modeling," *Biofuel Research Journal*, vol. 2, pp. 70–76, 2014.

[134] M. Akia, F. Yazdani, E. Motaee, D. Han, and H. Arandiyan, "A review on conversion of biomass to biofuel by nanocatalysts," *Biofuel Research Journal*, vol. 1, pp. 16–25, 2014.

[135] K. Tsukahara and S. Sawayama, "Liquid fuel production using microalgae," *Journal of the Japan Petroleum Institute*, vol. 48, no. 5, pp. 251–259, 2005.

[136] A. Sun, R. Davis, M. Starbuck, A. Ben-Amotz, R. Pate, and P. T. Pienkos, "Comparative cost analysis of algal oil production for biofuels," *Energy*, vol. 36, no. 8, pp. 5169–5179, 2011.

[137] B. J. Gallagher, "The economics of producing biodiesel from algae," *Renewable Energy*, vol. 36, no. 1, pp. 158–162, 2011.

[138] N.-H. Norsker, M. J. Barbosa, M. H. Vermuë, and R. H. Wijffels, "Microalgal production—a close look at the economics," *Biotechnology Advances*, vol. 29, no. 1, pp. 24–27, 2011.

Hindawi Publishing Corporation
BioMed Research International
Volume 2015, Article ID 281934, 6 pages
http://dx.doi.org/10.1155/2015/281934

Research Article

Production and Characterization of Biodiesel Using Nonedible Castor Oil by Immobilized Lipase from *Bacillus aerius*

Sunil Kumar Narwal,[1] Nitin Kumar Saun,[1] Priyanka Dogra,[2] Ghanshyam Chauhan,[2] and Reena Gupta[1]

[1]*Department of Biotechnology, Himachal Pradesh University, Summer Hill, Shimla 171005, India*
[2]*Department of Chemistry, Himachal Pradesh University, Summer Hill, Shimla 171005, India*

Correspondence should be addressed to Reena Gupta; reenagupta_2001@yahoo.com

Received 3 June 2014; Revised 8 September 2014; Accepted 9 September 2014

Academic Editor: Meisam Tabatabaei

A novel thermotolerant lipase from *Bacillus aerius* was immobilized on inexpensive silica gel matrix. The immobilized lipase was used for the synthesis of biodiesel using castor oil as a substrate in a solvent free system at 55°C under shaking in a chemical reactor. Several crucial parameters affecting biodiesel yield such as incubation time, temperature, substrate molar ratio, and amount of lipase were optimized. Under the optimized conditions, the highest biodiesel yield was up to 78.13%. The characterization of synthesized biodiesel was done through FTIR spectroscopy, ^{1}H NMR spectra, and gas chromatography.

1. Introduction

Sustainability is a key principle in natural resource management and it has become increasingly obvious that continued dependence on fossil fuel energy resources is unsustainable in the long run because of depleting resources and the contribution of these fuels to environmental and health problems [1]. Thus transesterification of vegetable oils can be used for the synthesis of fatty acid methyl esters with properties similar to petroleum-based diesel fuel which is renewable source of energy and this process is increasingly researched as a means of producing an environmentally acceptable alternative fuel [2]. The use of lipases as biocatalysts in the transesterification of triacylglycerides allows mild reaction conditions and easy recovery of glycerol, without need for further purification or chemical waste production [3]. Enzymatic production of biodiesel by methanolysis of triglycerides using lipase as the catalyst offers several advantages compared to chemical processes. The cost of lipase production is one of the main obstacles for industrial application of lipases. Immobilization of lipases decreases cost of production by their reusability, which is necessary to make them more attractive and potent for industrial applications such as thermostability, activity in nonaqueous media, to improve handling, recovery, and recycling of biocatalyst [4]. Different vegetable oils are used for the biodiesel production, including sunflower oil [2, 5], waste cooking oil [6], soybean oil, [7], pomace oil [8], and palm oil [9]. Competition between food and biofuel leads to the search for fat sources which are not used as food, such as nonedible oils and restaurant waste lipids [10]. The production of biodiesel on a large scale using edible and nonedible oils promotes plantation of crops resulting in recycling of CO_2 and minimizing its impact on the greenhouse effect [1].

In the present work, microbial lipase from *Bacillus aerius* was immobilized by adsorption onto silica matrix. Immobilized enzyme was used for biodiesel production by transesterification of castor oil with methanol. The effects of enzyme concentration, incubation time, relative molar concentration of reactants, and reaction temperature on the rate of synthesis of biodiesel were separately evaluated. Synthesized biodiesel from the methanolysis of castor oil was characterized by FTIR and NMR spectroscopy to get the evidence for the formation of products. No such research has been found in the literature using this organism which consequently leads to its novelty.

2. Materials and Methods

2.1. Chemicals and Enzyme. Silica gel matrix 60–150, glutaraldehyde, *p*-nitrophenyl acetate (*p*-NPA), *p*-nitrophenyl benzoate (*p*-NPB), *p*-nitrophenyl formate (*p*-NPF), and *p*-nitrophenyl palmitate (*p*-NPP) were purchased from Lancaster Synthesis, England; Tris buffer and castor oil were purchased from HIMEDIA Laboratory Ltd., Mumbai, India; and methanol was from MERCK, Mumbai, India. All chemicals were of analytical grade and were used as received. The lipase producing bacteria were isolated from the water sample of a hot spring named Tattapani, Kullu, Himachal Pradesh. The thermophilic *Bacillus aerius* (identified at IMTECH, Chandigarh) was grown in the medium of the following composition: yeast extract (2 g/L), peptone (5.0 g/L), sodium chloride (5.0 g/L), beef extract (1.5 g/L), ammonium chloride (1.0 g/L), and cottonseed oil (10 mL/L) (emulsified with 0.5% Gum Acacia) at pH 8.5. The seed culture (7.5% inoculum) was transferred to 50 mL production medium (250 mL Erlenmeyer flask) for 48 h under shaking conditions at 110 rpm at 55°C. The culture broth was centrifuged at 10,000 rpm for 10 min at 4°C. The lipase activity was assayed both in the supernatant as well as in pellet for determining extracellular and intracellular enzyme activity, respectively. The enzyme produced by thermophilic *Bacillus aerius* was purified to 9-fold with 7.2% recovery by ammonium sulfate precipitation and DEAE-cellulose column chromatography. The enzyme was found to be a monomeric protein having a molecular weight of 33 kDa on SDS-PAGE.

2.2. Determination of Lipase Activity. The activity of free and silica-bound lipase was measured by a colorimetric method [11]. The reaction mixture contained 60 μL of *p*-nitrophenol palmitate (*p*-NPP) stock solution (20 mM *p*-NPP prepared in isopropyl alcohol) and 40 μL lipase and Tris buffer (0.1 M, pH 9.5) to make final volume of 3 mL. The reaction mixture was incubated at 55°C for 10 min in a water bath. Keeping the reaction mixture at −20°C for 10 min stopped the reaction. The absorbance of *p*-nitrophenol released was measured at A_{410}. The enzyme activity was defined as the micromoles of *p*-nitrophenol released per minute by the hydrolysis of *p*-NPP by 1 mL of soluble enzyme or 1 mg of silica-bound enzyme (weight of matrix included) under standard assay conditions. The protein was assayed by a standard method [12].

2.3. Immobilization of Lipase onto Silica. The silica gel matrix (60–150 mesh) was washed with 0.1 M Tris buffer (pH 7.0) and then centrifuged at 10,000 rpm at 4°C for 10 min. The supernatant was discarded and pellet was washed 4-5 times with Tris buffer. The matrix was then kept at 4°C overnight in Tris buffer. Then 1–5% glutaraldehyde (cross linking agent) solution was added to the 4 g matrix and kept at 35°C under shaking conditions for different time periods. The matrix was washed 3-4 times with Tris buffer (pH 7.0) to remove unbound glutaraldehyde. 8 mL (1.91 U/mL) of purified lipase from *Bacillus aerius* was then incubated with the matrix for 1 h under shaking condition. The supernatant was discarded.

2.4. Methanolysis of Castor Oil and Analysis of Biodiesel. Methanol (1 M) and nonedible castor oil (1 M) were taken in a screw-capped glass vial. To this mixture, enzyme (*Bacillus aerius* lipase ~1.44 U/mg) as a catalyst was added and incubated with constant shaking at 250 rpm. The effects of reaction time (24–120 h), temperature (40 and 60°C), oil to methanol molar ratio (1 : 1 to 1 : 6), and immobilized lipase amount (1–7% of oil weight) on biodiesel production were investigated in the reaction system. The reaction mixture was washed with distilled water to remove the glycerol and excess methanol. The quantification of ester was done by FTIR spectroscopy on Nicollet 5700 in KBr pallets, ^{1}H NMR was done (Advance Buker II-400 MHz) in deuterated chloroform ($CDCl_3$) solution with internal standard TMS (0 ppm), and chemical shifts were recorded in parts per million (δ/ppm) and GLC equipped with a flame ionization detector and a column (10% SE-30 Chrom WHP, 2-meter length, mesh size 80–100, internal diameter 1/8 inches, and maximum temperature limit 300°C; Netel Chromatograph, Thane, India). Nitrogen was used as a carrier gas (30 cm^3/min). The injector was warmed to 250°C, and the detector was set at 280°C. The quantification was accomplished by intern standardization. Methyl ricinoleate was the internal standard used. The methyl ester yield was determined using GLC and % yield method as follows:

$$\%\ \text{yield} = \frac{\text{weight of biodiesel formed (g)}}{\text{Total weight of reaction mixture (g)}} \times 100. \quad (1)$$

3. Results and Discussion

In the present study lipase activity from *Bacillus aerius* was found to be 1.44 U/mg and this activity is comparable with that reported in the previous study [4].

3.1. Effect of Reaction Time on Transesterification. The effect of reaction time on the transesterification was investigated by varying the reaction time from 24 to 120 h. The yield of biodiesel increased on increasing incubation time from 24 to 96 h (Figure 1). At 96 h, approximately 54.08% of biodiesel was produced. Thus in the subsequent transesterification reactions, a reaction time of 96 h at 55°C for immobilized-lipase was considered optimum for the synthesis of biodiesel. Longer reaction time led to the reduction of biodiesel formation, because the transesterification reaction reverses and thus results in loss of methyl esters as well as soap formation [13, 14]. Li et al. observed the incubation time of 72 h to be optimal for the synthesis of biodiesel [15]. Since the activity of different lipases is different so Li et al. found 72 h as optimum incubation time as compared to 96 h.

3.2. Effect of Reaction Temperature. Changes in the reaction temperature can affect the activity and stability of the enzyme and thus the rate of reaction. The effect of temperature on the lipase activity was examined using a temperature range of 40°C to 60°C as shown in Figure 2 with castor oil (1 M) and methanol (1 M) in a solvent free system for 96 h. The maximum biodiesel synthesis (54.08%) was observed at 55°C (Figure 2) under the above reaction conditions. Previously

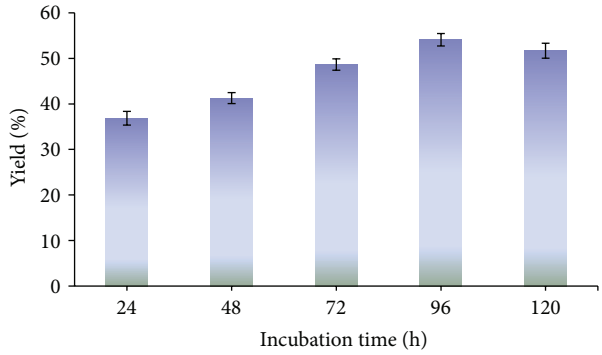

Figure 1: Time course of biodiesel synthesis tested at 55°C. Reaction conditions: methanol/oil 1 : 1 (mol/mol); 2% lipase by oil weight.

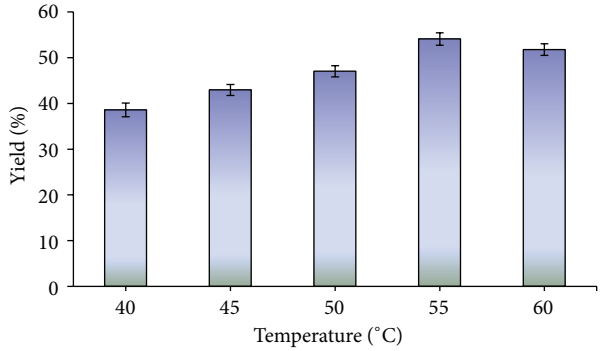

Figure 2: Effect of temperature on the synthesis of biodiesel. Reaction conditions: reaction time 96 h, methanol/oil 1 : 1 (mol/mol) and 2% lipase by oil weight.

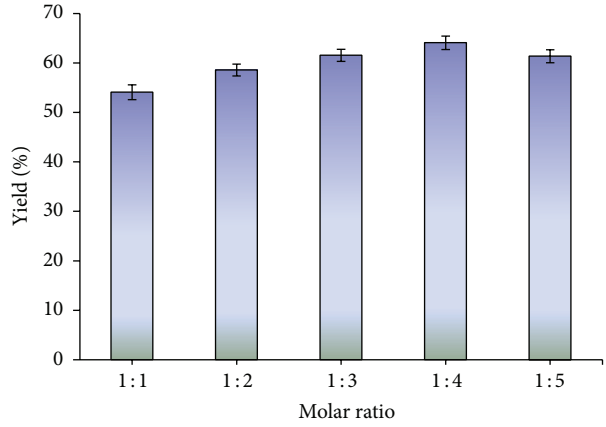

Figure 3: The effect of methanol/oil molar ratio on the methanolysis of castor oil. Reaction conditions: reaction temperature 55°C, 2% lipase by oil weight, and reaction time 96 h.

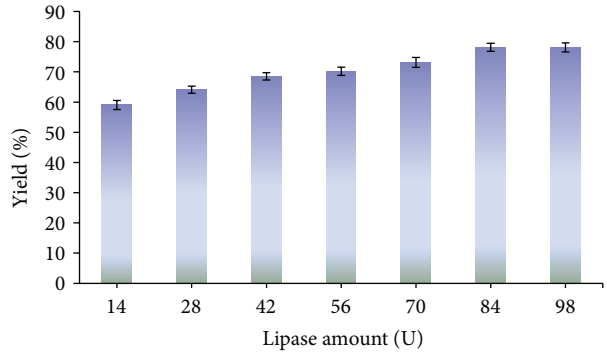

Figure 4: Effect of concentration of lipase on the synthesis of biodiesel. Reaction conditions: reaction time 96 h, reaction temperature 55°C, and methanol/oil 1 : 4 (mol/mol).

the optimum reaction temperature of 60°C was observed for the synthesis of biodiesel [16]. In a recent study, the optimum temperature of 37°C was observed for the synthesis of biodiesel [17], so this shows mesophilic nature of enzyme but the lipase from *Bacillus aerius* was thermotolerant; therefore maximum biodiesel production was observed at 55°C.

3.3. Effect of Methanol/Castor Oil Molar Ratio. One of the most important variables affecting the yield of ester is the molar ratio of methanol to oil. A set of experiments was performed in which the oil/methanol molar ratio was varied in the range 1 : 1–1 : 5 (mol/mol). The results obtained (Figure 3) showed that the methyl ester yield (64.08%) was highest at 1 : 4 oil/methanol molar ratio. However further increase in molar ratio beyond the optimal level led to decrease in biodiesel yield. This might be due to the deactivation of the lipase by exposure to methanol. In a recent study, the 1 : 4 substrate molar ratio was found to be the best for the maximum yield of biodiesel [17]. Previously 6 : 20 (oil : methanol) molar ratio was found to be optimum for the synthesis of biodiesel [18].

3.4. Effect of Amount of Lipase. The influence of enzyme quantity on the methanolysis of castor oil has been shown in Figure 4. The maximum yield of biodiesel (78.13%) was obtained with 84 U of immobilized lipase. It was observed that, with an increase of enzyme concentration, initial rate of esterification was increased from 14 to 84 U and remained almost constant with increase in lipase amount beyond 84 U. The castor oil contains 85–90% of ricinoleic acid; thus methyl ricinoleate was used as internal standard.

3.5. Characterization of Ester by Analytical Methods. The Characterization of ester was also done by various analytical/spectroscopic methods which are FTIR, ^{1}H NMR spectroscopy (Table 1) and gas chromatography. The FTIR spectrum of methyl ricinoleate shows the peak at 1743.39 cm^{-1} which is due to (–C=O stretching of ester), at 1648 cm^{-1} due to the (–C=C– stretching) but it has high intensity as the presence of ester group resulted in electronegativity of the neighboring groups and a peak at value 2942 cm^{-1} (–C–H– stretching) clearly confirms the formation of biodiesel (Figure 5). But when the above spectra were compared with their precursors in literature it was clearly found that the peak at value 1680 cm^{-1} is absent in Figure 5 which was due to –COOH group clearly confirming that esterification took

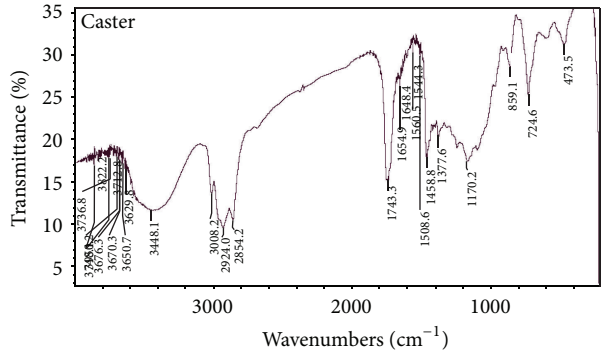

Figure 5: FTIR spectrum of transesterified castor oil.

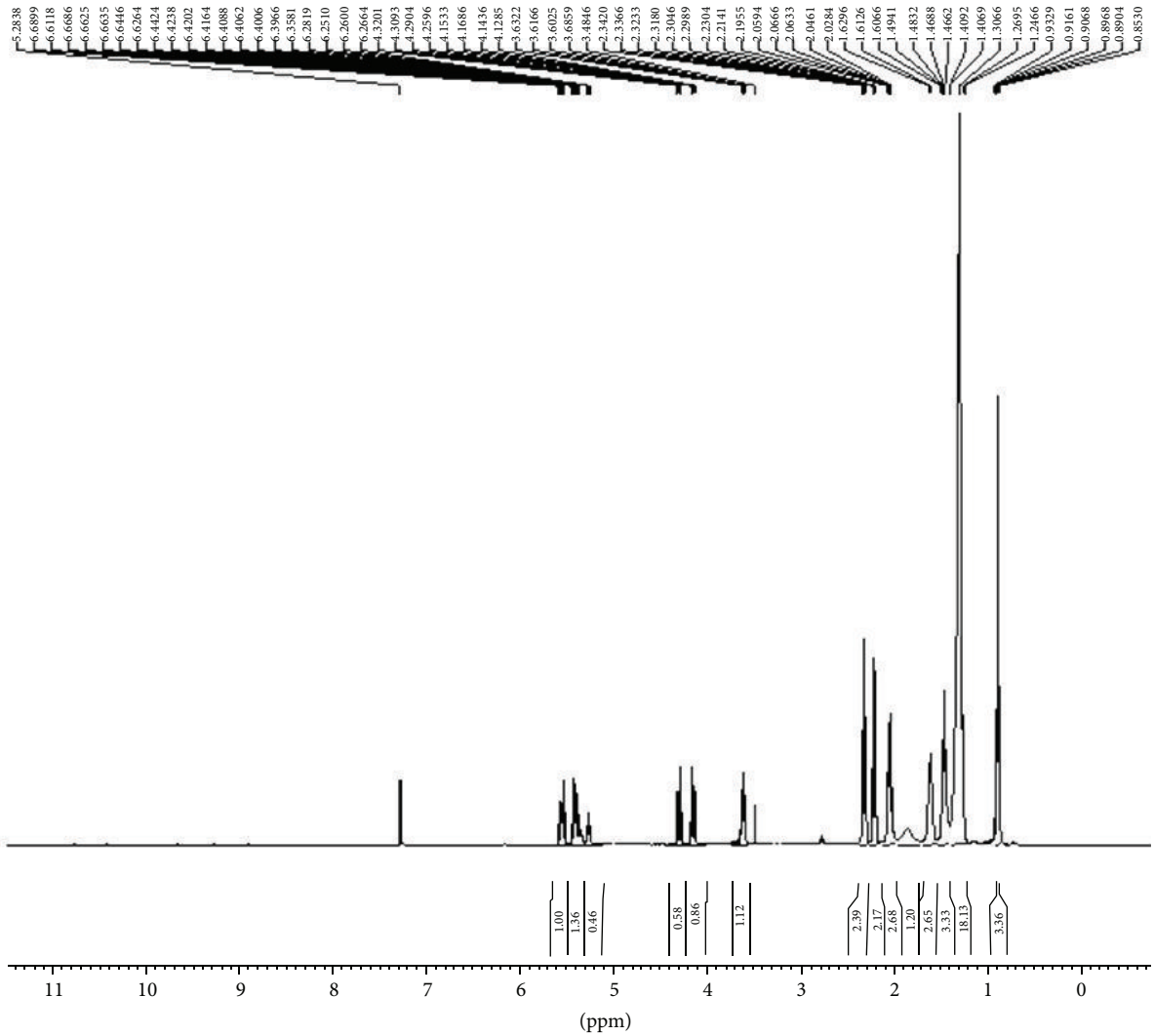

Figure 6: NMR spectrum of transesterified castor oil.

place at this position and all other peaks remained; only the intensity of the peaks changed because of some new functional groups added in it. The ^{1}H NMR spectra of methyl ester are shown in Figure 6. Signals at values 2.32 ppm and 4.21 ppm were due to presence of –CH_2–O–C–O and –C=O functional groups of ester bond which were absent in the spectrum of their precursor. Also in the precursor molecule a signal at value 12.05 ppm is due to –OH group but in its ester form this signal is absent clearly confirming that the reaction took place at this position. All other peaks remained the same.

Table 1: Characteristic peaks of methyl ricinoleate taken as a standard.

S. number	Compound	FTIR peaks		NMR peaks	
		Functional groups	Values in cm^{-1}	Functional groups	Values in ppm
1	Methyl ricinoleate	–C=O, OH	1743.39, 3481	$–CH_2–O–C–O$, –C=O	2.32, 4.21
		–C=C–	1648	–C=C–	5.32
		–CH– stretching	2942	$–CH_2$, –CH–	2.82, 1.29
2	Ricinoleic acid	–C=O, OH	1680, 3481	–C=O, OH	6.00, 12.05
		–C=C–	1616	–C=C–	5.42
		–CH–	2942	$–CH_2$, –CH	2.52, 1.29

The spectra of the products formed at various steps were matched with the ChemDraw Ultra 10 which unambiguously confirms the formation of biodiesel and also compared with its precursor molecules. From the % yield method and GLC analysis, it was observed that the yield of biodiesel produced was approximately the same.

4. Conclusion

Methanolysis of nonedible castor oil with lipase immobilized on silica to yield biodiesel through transesterification has been investigated. Biodiesel was successfully synthesized by silica-bound lipase in 96 h under shaking at 55°C using 1 : 4 oil/methanol molar ratio. Effect of the interaction among the different parameters for transesterification and enzyme kinetics was needed to be known to catalyze a reaction. *Bacillus aerius* lipase showed promising results and immobilizing the enzyme on inexpensive silica matrix could reduce cost as well as improve yield of ester.

Conflict of Interests

The authors declare that they have no conflict of interests with themselves and with the parent institution.

Acknowledgment

The financial support from Department of Biotechnology, Ministry of Science and Technology, Government of India, to Department of Biotechnology, Himachal Pradesh University, Shimla (India), is thankfully acknowledged.

References

[1] S. K. Narwal and R. Gupta, "Biodiesel production by transesterification using immobilized lipase," *Biotechnology Letters*, vol. 35, no. 4, pp. 479–490, 2013.

[2] M. Mittelbach, "Lipase catalyzed alcoholysis of sunflower oil," *Journal of the American Oil Chemists' Society*, vol. 67, no. 3, pp. 168–170, 1990.

[3] J. Yan, X. Zheng, L. Du, and S. Li, "Integrated lipase production and in situ biodiesel synthesis in a recombinant Pichia pastoris yeast: An efficient dual biocatalytic system composed of cell free enzymes and whole cell catalysts," *Biotechnology for Biofuels*, vol. 7, no. 1, article 55, 2014.

[4] S. K. Narwal, N. K. Saun, and R. Gupta, "Characterization and catalytic properties of free and silica-bound lipase: a comparative study," *Journal of Oleo Science*, vol. 63, no. 6, pp. 599–605, 2014.

[5] B. Selmi and D. Thomas, "Immobilized lipase-catalyzed ethanolysis of sunflower oil in a solvent-free medium," *Journal of the American Oil Chemists' Society*, vol. 75, no. 6, pp. 691–695, 1998.

[6] S. Hama, S. Tamalampudi, T. Fukumizu et al., "Lipase localization in *Rhizopus oryzae* cells immobilized within biomass support particles for use as whole-cell biocatalysts in biodiesel-fuel production," *Journal of Bioscience and Bioengineering*, vol. 101, no. 4, pp. 328–333, 2006.

[7] Y. Liu and X. Hua, "Production of biodiesel using a nanoscaled immobilized lipase as the catalyst," *Catalysis Letters*, vol. 144, no. 2, pp. 248–251, 2014.

[8] Y. Yucel, "Biodiesel production from pomace oil by using lipase immobilized onto olive pomace," *Bioresource Technology*, vol. 102, no. 4, pp. 3977–3980, 2011.

[9] P. Winayanuwattikun, C. Kaewpiboon, K. Piriyakananon, W. Chulalaksananukul, T. Yongvanich, and J. Svasti, "Immobilized lipase from potential lipolytic microbes for catalyzing biodiesel production using palm oil as feedstock," *African Journal of Biotechnology*, vol. 10, no. 9, pp. 1666–1673, 2011.

[10] K. Stein, "Food vs biofuel," *Journal of the American Dietetic Association*, vol. 107, no. 11, pp. 1872–1878, 2007.

[11] U. K. Winkler and M. Stuckmann, "Glycogen, hyaluronate, and some other polysaccharides greatly enhance the formation of exolipase by *Serratia marcescens*," *Journal of Bacteriology*, vol. 138, no. 3, pp. 663–670, 1979.

[12] O. H. Lowry, N. J. Rosebrough, A. L. Farr, and R. J. Randall, "Protein measurement with the Folin phenol reagent," *The Journal of Biological Chemistry*, vol. 193, no. 1, pp. 265–275, 1951.

[13] F. Ma, L. D. Clements, and M. A. Hanna, "The effects of catalyst, free fatty acids, and water on transesterification of beef tallow," *Transactions of the American Society of Agricultural Engineers*, vol. 41, no. 5, pp. 1261–1264, 1998.

[14] T. Eevera, K. Rajendran, and S. Saradha, "Biodiesel production process optimization and characterization to assess the suitability of the product for varied environmental conditions," *Renewable Energy*, vol. 34, no. 3, pp. 762–765, 2009.

[15] L. Li, W. Du, D. Liu, L. Wang, and Z. Li, "Lipase-catalyzed transesterification of rapeseed oils for biodiesel production with a novel organic solvent as the reaction medium," *Journal of Molecular Catalysis B: Enzymatic*, vol. 43, no. 1–4, pp. 58–62, 2006.

[16] L. Batistella, L. A. Lerin, P. Brugnerotto et al., "Ultrasound-assisted lipase-catalyzed transesterification of soybean oil in organic solvent system," *Ultrasonics Sonochemistry*, vol. 19, no. 3, pp. 452–458, 2012.

[17] A. Arumugam and V. Ponnusami, "Biodiesel production from *Calophyllum inophyllum* oil using lipase producing *Rhizopus oryzae* cells immobilized within reticulated foams," *Renewable Energy*, vol. 64, pp. 276–282, 2014.

[18] F. L. P. Pessoa, S. P. Magalhes, and P. W. De Carvalho Falcao, "Production of biodiesel via enzymatic ethanolysis of the sunflower and soybean oils: modeling," *Applied Biochemistry and Biotechnology*, vol. 161, pp. 238–244, 2010.

Hindawi Publishing Corporation
BioMed Research International
Volume 2015, Article ID 494182, 6 pages
http://dx.doi.org/10.1155/2015/494182

Research Article

Improvement of Biogas Production from Orange Peel Waste by Leaching of Limonene

Rachma Wikandari,[1] Huong Nguyen,[2] Ria Millati,[3] Claes Niklasson,[2] and Mohammad J. Taherzadeh[1]

[1]*Swedish Centre for Resource Recovery, University of Borås, Allégatan 1, 50190 Borås, Sweden*
[2]*Department Chemical and Biological Engineering, Chalmers University of Technology, 41296 Gothenburg, Sweden*
[3]*Department of Food and Agricultural Product Technology, Faculty of Agricultural Technology, Universitas Gadjah Mada, Bulaksumur, Yogyakarta 55281, Indonesia*

Correspondence should be addressed to Rachma Wikandari; rachma.wikandari@hb.se

Received 6 June 2014; Revised 16 August 2014; Accepted 23 August 2014

Academic Editor: Ilona Sárvári Horváth

Limonene is present in orange peel wastes and is known as an antimicrobial agent, which impedes biogas production when digesting the peels. In this work, pretreatment of the peels to remove limonene under mild condition was proposed by leaching of limonene using hexane as solvent. The pretreatments were carried out with homogenized or chopped orange peel at 20–40°C with orange peel waste and hexane ratio (w/v) ranging from 1 : 2 to 1 : 12 for 10 to 300 min. The pretreated peels were then digested in batch reactors for 33 days. The highest biogas production was achieved by treating chopped orange peel waste and hexane ratio of 12 : 1 at 20°C for 10 min corresponding to more than threefold increase of biogas production from 0.061 to 0.217 m^3 methane/kg VS. The solvent recovery was 90% using vacuum filtration and needs further separation using evaporation. The hexane residue in the peel had a negative impact on biogas production as shown by 28.6% reduction of methane and lower methane production of pretreated orange peel waste in semicontinuous digestion system compared to that of untreated peel.

1. Introduction

Orange as the main citrus fruit is one of top-five fruit commodities that dominate the global fruit market. According to Food and Agriculture Organization, global orange production reached 68 million tons representing 8.5% of the total fruit production [1]. The largest orange producers are Brazil, United States of America, China, India, and Mexico in 2012 [1]. Approximately, 40–60% of oranges are processed for juice production, of which 50–60% ends up as waste including seed, peel, and segment membrane [2, 3]. The generation of these solid wastes is estimated to be in the range of 15 to 25 million tons per year [3]. Among these wastes, citrus peel is the major constituent accounting for approximately 44% of the weight fruit mass [4].

Citrus waste for different applications such as production of pectin, flavonoid, fiber, and animal feed production has been proposed by several researchers [5–8]. However, a large amount of this waste is still dumped every year [9], which causes both economic and environmental problems such as high transportation cost, lack of dumping site, and accumulation of high organic content material [10]. Therefore, more effective and sustainable alternatives for using orange peel wastes such as biogas are highly desirable.

Biogas is gaseous material produced during anaerobic digestion of organic compound. Biogas holds wide applications such as fuel for electricity, car, cooking, lightening, and heating. Among these applications, conversion of orange peels wastes into fuel is attractive, since it gives benefits in terms of both energy recovery and environmental aspects. Orange peel waste contains both soluble and insoluble carbohydrates that can be digested to biogas [11]. However, the main challenge to produce biogas from orange peel is the presence of an antimicrobial compound "D-limonene." This

chemical constitutes 90% of oranges essential oil as 2-3% of dry matter of the orange [11]. Limonene has been reported to be highly toxic to anaerobic digestion [11–13]. It causes ultimate failure of the process at concentration of 400 μL/L on mesophilic digestion [11] and in the range of 450 to 900 μL/L on thermophilic digestion [14].

A number of investigations have been carried out to tackle the inhibition challenges by limonene [14, 15]. These methods can be classified into three categories of limonene removal, limonene recovery, and conversion of limonene into less toxic compound. Among these methods, limonene recovery seems to be the best alternative since this chemical is a valuable compound used in several industries such as perfumery, chemicals, cosmetics, medical, and food flavor [16, 17]. There are several methods that have been reported for limonene recovery including steam explosion [14], steam distillation [13], and acid hydrolysis [12]. However, these methods are performed under harsh conditions, which require high energy consumption. In addition, using acid for the pretreatment, a further neutralization is essential and expensive equipment should be applied to handle the corrosive behavior of the material. Furthermore, the acids used have a negative impact on the subsequent digestion process. On the other hand, since the goal of the pretreatment is to improve the biogas as a source of energy, the consumption of energy during the production process should be minimized. Hence, pretreatment of the orange wastes under ambient temperature is favorable.

Leaching or solid-liquid extraction is an alternative pretreatment performed in room temperature. In this technique, the limonene in the orange peel waste is leached into a solvent that has contact with the peel [18]. This technique is widely used to extract organic compounds from natural materials, where these compounds are present at low concentration. To the best of our knowledge, this technique has not been employed for pretreatment of orange peel wastes. Therefore, the objective of this work was to examine leaching technique for orange peel waste pretreatment with focus on biogas production.

2. Material and Methods

2.1. Material. Orange peel wastes were collected from Brämhults Juice AB (Borås, Sweden). The wastes were from orange juice process and contained 21.3% total solid (TS). It was then chopped or homogenized prior to pretreatment process. Inoculum was collected from a thermophilic biogas plant (Borås Energy and Environment AB, Borås, Sweden). The inoculum was kept at 55°C for 3 days before the digestion process. Chemicals including hexane, diethyl ether, and sodium sulfate were purchased from Sigma-Aldrich.

2.2. Methods. Pretreatment of the wastes by leaching was conducted in Erlenmeyer flasks. Four different solvents including hexane, diethyl ether, dichloromethane, and ethyl acetate were used. These chemicals are toxic and/or inflammable and should be treated properly. In the experiment to select the solvent, each solvent was added to the orange peel with orange peel waste and hexane ratio of 1 : 4. The mixture of solvent and orange peel was shaken vigorously for 10 minutes followed by incubation for 20 minute at room temperature. In the optimization of pretreatment study, hexane was used as a solvent. Two levels of four parameters including temperature (20°C and 40°C), time (10 min and 300 min), orange peel wastes and hexane ratio (1 : 2 and 1 : 12), and the wastes size (homogenized or chopped) were selected. Forty grams of the wastes was dissolved with a certain amount of hexane in the flasks, followed by shaking vigorously for a determined period of time. After the settlement, the extracts were removed from residuals by vacuum filtration. The residual, pretreated orange waste was then washed three times with water in order to remove remaining hexane. Finally, the pretreated waste was digested to produce biogas.

Digestion processes were performed in batch and semicontinuous reactors. The determination of biogas potential of the orange peels in batch digestion was carried out according to a previous study [19]. In the experiment to select the solvent, the digestion was conducted with different concentration of volatile solids (VS) ranging from 0.5 to 2%. In the optimization study, two percent of VS of the untreated and pretreated peels were placed in 120 mL glass bottle. The total volume of the mixture was 30 mL including 20 mL of inoculum and the rest was orange peel and water. The reactors were then flushed with a mixed gas containing 80% of N_2 and 20% of CO_2 for 2 min. The reactors were incubated at 55°C for 33 days. Reactors containing only water and inoculum were used as a blank. The experiments were performed in triplicate. At the end of the digestions, the pH of the digestates was measured. For semicontinuous digestions, the pretreated wastes were chosen based on the results obtained from the batch digestion. The semicontinuous digestions were performed in 2 L reactors (Automatic Methane Potential Test System I, Bioprocess Control, Sweden) with a liquid volume of 1.8 L. The reactors were placed in a water bath at 55°C. The organic loading rates (OLR) for both untreated and treated orange peels were set at 1 g VS/L/day during the starting up period and gradually increased to 3 g VS/L/day. The hydraulic retention time was set at 30 days. Gas production, pH, volatile fatty acids, and buffer capacity ratio were monitored during the digestion process.

Total solid and volatile solid of the untreated and pretreated wastes were determined using a gravimetric method. The gas production was measured using a gas chromatograph (Varian 450 GC, USA) equipped with a packed column (J&W Scientific GS-Gas Pro, 30 m × 0.320 mm) and a thermal conductivity detector (TCD). Gas samples of 100 μL were withdrawn using a 250 μL pressure tight syringe (VICI, Precision Sampling Inc., USA). The carrier gas was nitrogen with the flow rate of 2 mL/min. The temperature for injection, oven, and detector was 75, 100, and 120°C, respectively.

Hexane content of the orange wastes was analyzed by dissolving the wastes into 10 mL methanol. The methanol extract was then injected to gas chromatography-flame ionized detector (Clarus 400, Perkin Elmer) equipped with ZB-WAX-Plus, 30 m × 0.25 mm × 0.25 μm.

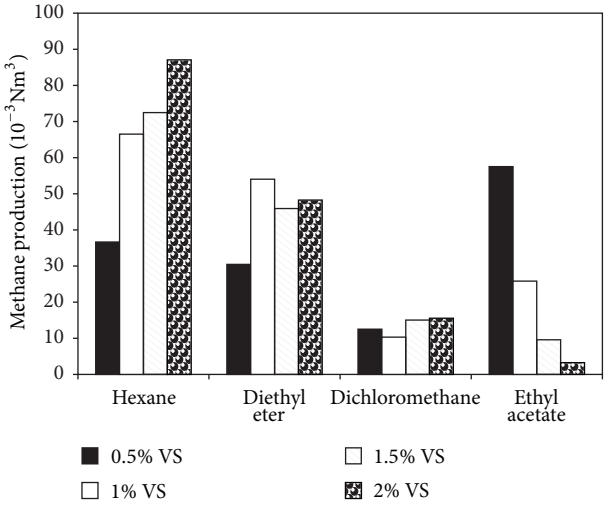

Figure 1: Methane production of pretreated orange peel waste by different solvents and digestion at different concentration of volatile solids.

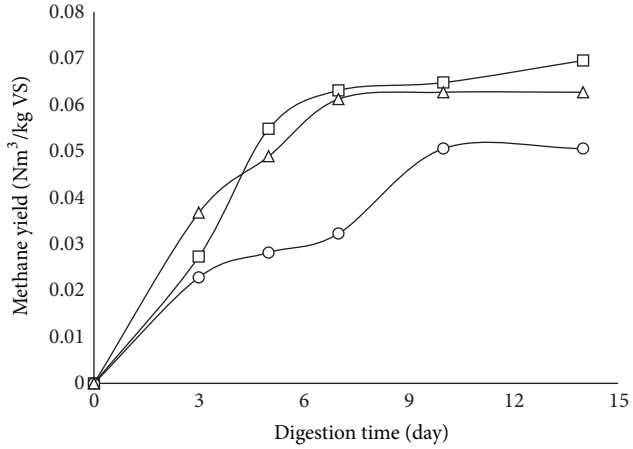

Figure 2: Effect of hexane (○) and limonene (Δ) on biogas production compared to control (□).

For statistical analysis, normal probability method and analysis of variance (ANOVA) were performed using Design-Expert 8 package.

3. Results and Discussion

Orange waste is a potential feedstock for biogas production. Orange waste contains ca 74.5% carbohydrate, 7.7% protein, and 10.6% fat [20]. Even though the theoretical methane yield is 0.45 Nm^3/kg VS, the methane yields of 0.061 and 0.131 Nm^3/kg VS were obtained in this experiment from chopped and homogenized peel, respectively. This indicated the strong inhibition by the limonene. Therefore, this compound should be separated from the orange peel before the digestion process. In the current study, the limonene was recovered from the orange peel by solid-liquid pretreatment using solvent to extract the limonene.

3.1. Leaching of Orange Wastes and Subsequent Digestion. In order to select a proper solvent for limonene recovery, four solvents including hexane, diethyl ether, dichloromethane, and ethyl acetate were used to extract the limonene followed by digestion of the pretreated orange peel waste for confirmation. The pretreated orange peel waste was digested at different concentration of volatile solids ranging from 0.5 to 2%. The results show that, for all VS concentration added, the orange peel pretreated with hexane gave the highest methane yield (Figure 1). Hence, the pretreatment using hexane was further investigated in order to obtain the best pretreatment method.

In the optimization study for pretreatment using hexane, four factors of leaching with two levels including temperature (20 and 40°C), time (10 and 300 min), orange peel waste and hexane ratio (1 : 2 and 1 : 12), and the citrus waste size (homogenized and chopped) were investigated. The pretreated orange waste was then digested to select the best condition of pretreatment. The results are summarized in Table 1. According to the statistical analysis, waste size was the only factor that was significant for the methane yield.

Table 1 showed that, for chopped peel, the pretreated wastes had higher methane production than the untreated ones. The pretreatment of the wastes increased methane production to the value of 0.076–0.217 m^3/kg VS corresponding to 25–350% of improvement. The best pretreatment condition based on the methane yield obtained was for chopped peel treated at 20°C for 10 min with orange peel waste and hexane ratio of 1 : 12. This pretreatment increased the methane yield by more than three times. On the other hand, in the case of homogenized peel, the pretreatment resulted in lower methane production.

3.2. Hexane Inhibition in Digestion. The toxic effect of hexane on anaerobic digesting microorganism might be responsible for the low yield obtained from the pretreated wastes. In order to confirm this hypothesis, batch digestion with addition of hexane to the digesting system was conducted. For comparison, the toxicity of limonene was also examined using the same method. The result showed that, at the same concentration, hexane was more toxic than limonene to anaerobic digesting system. Addition of hexane at concentration of 13 g/L resulted in 28.6% reduction of methane production compared with the control experiment (Figure 2).

The toxicity of hexane might explain the lower methane yield of the orange peel pretreated with homogenization. The smaller size of homogenized peels enabled greater contact surface between hexane and the peel resulting in higher hexane residue left in the peel. In addition, proportions of methane in biogas from pretreated homogenized orange wastes (45% to 68.5%) were lower than that of the pretreated chopped wastes (62.3% to 78.4%) (data not shown).

In order to further examine the accumulation effect of hexane in the system, semicontinuous digestion was conducted. The pretreated orange peel was compared with the untreated orange peel at organic loading rate of 3 g VS/L/day. Biogas production of the untreated and pretreated orange

Table 1: Methane yield of pretreated orange peel waste at different temperature, time, and peel/solvent ratio.

Temperature (°C)	Time (min)	Peel/solvent ratio	Citrus waste size	Methane yield (Nm^3/kg VS)
	Untreated		Homogenized	0.131 ± 0.008
20	10	1 : 2	Homogenized	0.101 ± 0.011
40	10	1 : 2	Homogenized	0.097 ± 0.009
20	300	1 : 2	Homogenized	0.040 ± 0.004
40	300	1 : 2	Homogenized	0.051 ± 0.010
20	10	1 : 12	Homogenized	0.071 ± 0.006
40	10	1 : 12	Homogenized	0.074 ± 0.006
20	300	1 : 12	Homogenized	0.094 ± 0.016
40	300	1 : 12	Homogenized	0.060 ± 0.014
	Untreated		Chopped	0.061 ± 0.004
20	10	1 : 2	Chopped	0.177 ± 0.011
40	10	1 : 2	Chopped	0.162 ± 0.015
20	300	1 : 2	Chopped	0.134 ± 0.016
40	300	1 : 2	Chopped	0.102 ± 0.017
20	10	1 : 12	Chopped	0.217 ± 0.009
40	10	1 : 12	Chopped	0.076 ± 0.011
20	300	1 : 12	Chopped	0.120 ± 0.005
40	300	1 : 12	Chopped	0.121 ± 0.016

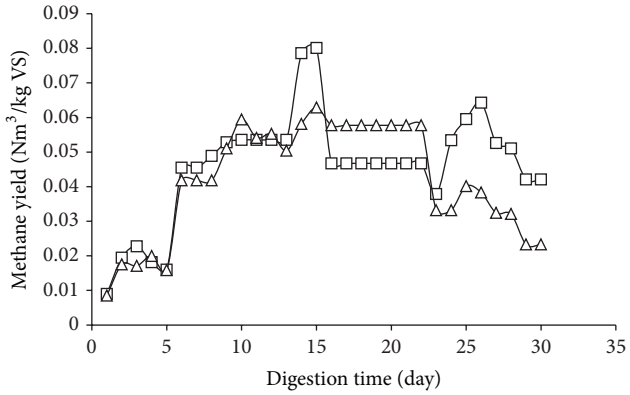

Figure 3: Methane production of untreated (□) and pretreated (Δ) orange peel wastes in semicontinuous digestion at organic loading rate of 3 g VS/L/day.

wastes is presented in Figure 3. The results show that the biogas production of the pretreated peel was lower than that of the untreated peel which might be due to the accumulation of hexane in the system.

3.3. Hexane Removal from Pretreated Orange Wastes. It was shown that hexane has inhibitory effect on anaerobic digesting system (Figure 2), and thus hexane residue in the peel must be removed prior to the digestion. Vacuum filtration was able to separate 90% of hexane and caused the hexane content of the pretreated orange wastes to be 0.2 mL/g of orange peel waste, which corresponds to concentration of 26 g/L hexane in the digesting system. This hexane residue was two times higher than the hexane concentration used in toxicity test (13 g/L). Hence, the hexane residue in the peel should be minimized or eliminated prior to the digestion process for both economic and technical reasons. Since hexane is a highly volatile hydrocarbon, removal of hexane can be performed by normal or vacuum evaporation process. In order to find the best condition, the evaporation was conducted at different temperatures and time. The range of temperature was between 30 and 70°C. Evaporation at temperature beyond 70°C made the orange peel very dried. In addition, boiling point of hexane is 68°C which is already below the maximum evaporation temperature. The low range of temperature gave advantages in which destruction of nutrients can be minimized and the energy consumption can be kept low. Hexane residue in the peel after evaporation was then analyzed. The result shows that 66% of hexane can be removed by evaporation at 50°C for 10 min corresponding to 9 g/L of hexane in the peel (Table 2).

3.4. The Overall Process of Methane Production and Limonene Extraction. One benefit of leaching pretreatment method is to recover the limonene that is a flavor compound in orange belonging to terpenoid group. As flavor compound, limonene holds widespread application in food, feed, cosmetic, chemical, and pharmaceutical industry. In the market of flavor, food and beverages is the largest which contributes to 47% of total demand in 2003 [21].

In this process (Figure 4), orange peel is fed to grinding unit using a conveyer for size reduction. The chopped peel is mixed with hexane for 10 min at 20°C with peel and solvent ratio of 1 : 2, where limonene is extracted from the peels and dissolved in the organic phase of hexane. The peel is then separated from the hexane by vacuum filtration which separates ca 90% of the hexane. Since the remaining hexane in the peel inhibits the digestion, it should be separated and

Table 2: Hexane residue in pretreated orange peel waste after evaporation in different conditions.

Pretreated peel waste	Evaporation temp. (°C)	Evaporation Time (min)	Hexane concentration (ml/g orange peel waste)	% hexane removal
Unevaporated (control)	—	—	0.12 ± 0.00	—
Evaporated	30	10	0.12 ± 0.01	0
Evaporated	30	30	0.06 ± 0.03	54
Evaporated	50	10	0.04 ± 0.00	66
Evaporated	50	30	0.07 ± 0.00	45
Evaporated	70	10	0.08 ± 0.02	31
Evaporated	70	30	0.09 ± 0.01	28

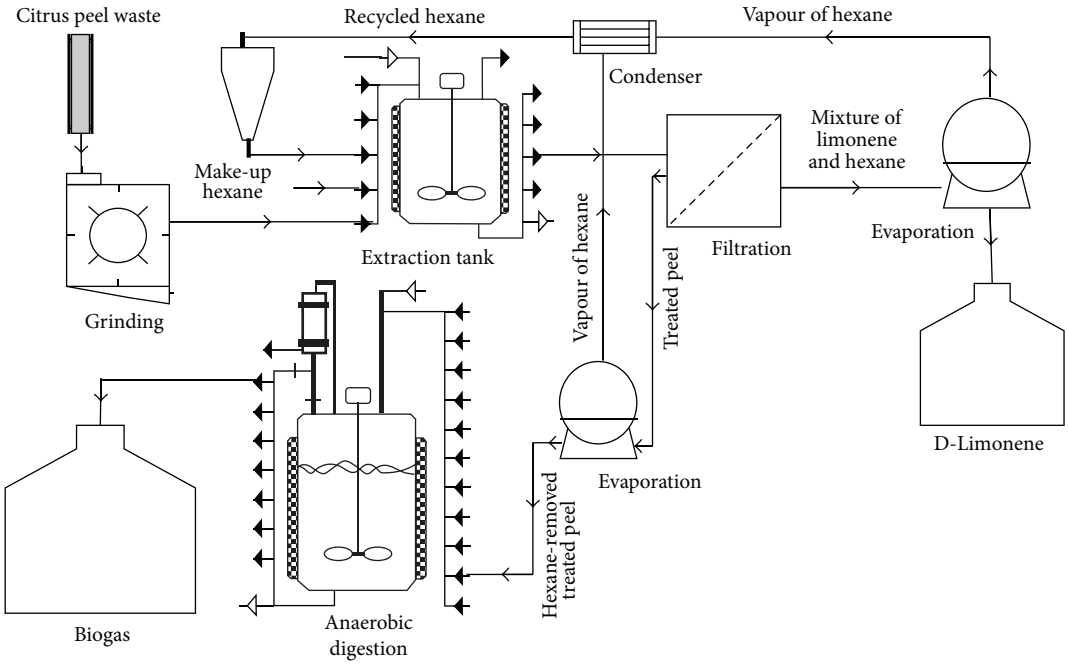

Figure 4: Block flow diagram of biogas production from treated orange peel waste by leaching pretreatment and limonene extraction.

recycled using normal or vacuum evaporation. The treated peel is fed into anaerobic digester to produce methane. The mixture of hexane and limonene out from filtration which has about 0.55 L limonene per m^3 of hexane is fed into rotary vacuum evaporator operated at 70°C in order to evaporate the volatile hexane and separate it from the limonene. The vapor of hexane is condensed and recycled back to the pretreatment vessel for extraction of more limonene from fresh peels.

The VS content of the treated orange peel is 11% and the methane yield was 0.177 Nm^3/kg VS. Thus, every ton of orange wastes produced 19.47 Nm^3 of biogas and 1.4 L of limonene as by-product. The best pretreatment condition obtained in this work increased the methane yield by 350% compared to the untreated peel. This improvement is lower than that obtained from steam-explosion pretreatment which could increase the methane yield by 426% [14]. However, in this current work the pretreatment was conducted at room temperature for 10 minutes, whereas the steam explosion pretreatment was carried out at 150°C for 20 minutes [14]. Thus, this pretreatment can be considered as low energy demanding. However, selection of the solvent is a critical point to avoid inhibition problem from the solvent on anaerobic digesting system.

4. Conclusion

Leaching of limonene from orange wastes can be a low energy demanding method for removing the inhibition effects of the wastes in the digestion process. The highest methane yield was obtained by pretreatment of the substrate at 20°C for 10 min with orange peel waste and hexane ratio of 1 : 12 which results in three times higher methane yield compared to the untreated wastes.

Conflict of Interests

The authors declare that there is no conflict of interests regarding the publication of this paper.

Acknowledgment

The authors express their gratitude to Swedish International Development Agency (SIDA) for the financial support of this work.

References

[1] FAO, Food and Agriculture Organization, 2014, http://www.faostat.org/.

[2] K. Grohmann and E. A. Baldwin, "Hydrolysis of orange peel with pectinase and cellulase enzymes," *Biotechnology Letters*, vol. 14, no. 12, pp. 1169–1174, 1992.

[3] F. R. Marín, C. Soler-Rivas, O. Benavente-García, J. Castillo, and J. A. Pérez-Alvarez, "By-products from different citrus processes as a source of customized functional fibres," *Food Chemistry*, vol. 100, no. 2, pp. 736–741, 2007.

[4] W. Widmer, W. Zhou, and K. Grohmann, "Pretreatment effects on orange processing waste for making ethanol by simultaneous saccharification and fermentation," *Bioresource Technology*, vol. 101, no. 14, pp. 5242–5249, 2010.

[5] T. Inoue, S. Tsubaki, K. Ogawa, K. Onishi, and J.-I. Azuma, "Isolation of hesperidin from peels of thinned *Citrus unshiu* fruits by microwave-assisted extraction," *Food Chemistry*, vol. 123, no. 2, pp. 542–547, 2010.

[6] Y. Jiang, Y. Du, X. Zhu, H. Xiong, M. W. Woo, and J. Hu, "Physicochemical and comparative properties of pectins extracted from Akebia trifoliata var. Australis peel," *Carbohydrate Polymers*, vol. 87, no. 2, pp. 1663–1669, 2012.

[7] W. C. Kim, D. Y. Lee, C. H. Lee, and C. W. Kim, "Optimization of narirutin extraction during washing step of the pectin production from citrus peels," *Journal of Food Engineering*, vol. 63, no. 2, pp. 191–197, 2004.

[8] D. Mamma, E. Kourtoglou, and P. Christakopoulos, "Fungal multienzyme production on industrial by-products of the citrus-processing industry," *Bioresource Technology*, vol. 99, no. 7, pp. 2373–2383, 2008.

[9] M. Pourbafrani, G. Forgács, I. S. Horváth, C. Niklasson, and M. J. Taherzadeh, "Production of biofuels, limonene and pectin from citrus wastes," *Bioresource Technology*, vol. 101, no. 11, pp. 4246–4250, 2010.

[10] M. M. Tripodo, F. Lanuzza, G. Micali, R. Coppolino, and F. Nucita, "Citrus waste recovery: a new environmentally friendly procedure to obtain animal feed," *Bioresource Technology*, vol. 91, no. 2, pp. 111–115, 2004.

[11] E. Mizuki, T. Akao, and T. Saruwatari, "Inhibitory effect of Citrus unshu peel on anaerobic digestion," *Biological Wastes*, vol. 33, no. 3, pp. 161–168, 1990.

[12] M. Lohrasbi, M. Pourbafrani, C. Niklasson, and M. J. Taherzadeh, "Process design and economic analysis of a citrus waste biorefinery with biofuels and limonene as products," *Bioresource Technology*, vol. 101, no. 19, pp. 7382–7388, 2010.

[13] M. A. Martín, J. A. Siles, A. F. Chica, and A. Martín, "Biomethanization of orange peel waste," *Bioresource Technology*, vol. 101, no. 23, pp. 8993–8999, 2010.

[14] G. Forgács, M. Pourbafrani, C. Niklasson, M. J. Taherzadeh, and I. S. Hováth, "Methane production from citrus wastes: process development and cost estimation," *Journal of Chemical Technology and Biotechnology*, vol. 87, no. 2, pp. 250–255, 2012.

[15] E. Mizuki, T. Akao, and T. Saruwatari, "Inhibitory effect of *Citrus unshu* peel on anaerobic digestion," *Biological Wastes*, vol. 33, no. 3, pp. 161–168, 1990.

[16] S. Raeissi, S. Diaz, S. Espinosa, C. J. Peters, and E. A. Brignole, "Ethane as an alternative solvent for supercritical extraction of orange peel oils," *The Journal of Supercritical Fluids*, vol. 45, no. 3, pp. 306–313, 2008.

[17] G. Forgács, *Biogas Production from Citrus Wastes and Chicken Feather: Pretreatment and Co-Digestion*, Chalmers University of Technology, Göteborg, Sweden, 2012.

[18] J. D. Seader and E. J. Henley, *Separation Process Principles*, John Wiley & Sons, New York, NY, USA, 2nd edition, 2006.

[19] T. L. Hansen, J. E. Schmidt, I. Angelidaki et al., "Method for determination of methane potentials of solid organic waste," *Waste Management*, vol. 24, no. 4, pp. 393–400, 2004.

[20] N. Oktavia, "Karakterisasi Sampah Buah Pasar Buah Gamping sebagai Bahan Baku Alternatif Produksi Biogas," in *Teknologi Pengolahan Hasil Pertanian*, Universitas Gajdah Mada, Yogyakarta, Indonesia, 2009.

[21] A. B. P. Medeiros, S. C. Rossi, and C. R. SoccoL, "Cell culture for flavor production," in *Handbook of Fruit and Vegetable Flavors*, Y. H. Hui, Ed., John Wiley & Sons, Hoboken, NJ, USA, 2010.

Hindawi Publishing Corporation
BioMed Research International
Volume 2015, Article ID 325905, 10 pages
http://dx.doi.org/10.1155/2015/325905

Research Article

Effects of Extrusion Pretreatment Parameters on Sweet Sorghum Bagasse Enzymatic Hydrolysis and Its Subsequent Conversion into Bioethanol

Erick Heredia-Olea, Esther Pérez-Carrillo, Manuel Montoya-Chiw, and Sergio O. Serna-Saldívar

Centro de Biotecnología FEMSA, Escuela de Ingeniería y Ciencias, Tecnológico de Monterrey, Avenida Eugenio Garza Sada 2501 Sur, 64849 Monterrey, NL, Mexico

Correspondence should be addressed to Sergio O. Serna-Saldívar; sserna@itesm.mx

Received 4 June 2014; Revised 28 August 2014; Accepted 28 August 2014

Academic Editor: Rajeev Kumar

Second-generation bioethanol production from sweet sorghum bagasse first extruded at different conditions and then treated with cell wall degrading enzymes and fermented with *I. orientalis* was determined. The twin extruder parameters tested were barrel temperature, screws speed, and feedstock moisture content using surface response methodology. The best extrusion conditions were 100°C, 200 rpm, and 30% conditioning moisture content. This nonchemical and continuous pretreatment did not generate inhibitory compounds. The extruded feedstocks were saccharified varying the biocatalysis time and solids loading. The best conditions were 20% solids loading and 72 h of enzymatic treatment. These particular conditions converted 70% of the total fibrous carbohydrates into total fermentable C5 and C6 sugars. The extruded enzymatically hydrolyzed sweet sorghum bagasse was fermented with the strain *I. orientalis* at 12% solids obtaining a yield of 198.1 mL of ethanol per kilogram of bagasse (dw).

1. Introduction

There are many pretreatments that can be used to prepare or obtain the fermentable sugars from lignocellulosic raw materials. The most popular pretreatments include acid hydrolysis, steam explosion, ammonia fiber expansion, alkaline wet oxidation, and hot water pretreatment [1, 2]. However, all the mentioned treatments work at high temperatures and pressures generating hazardous compounds derived from sugar degradation [3]. For this reason the search of novel pretreatments able to disrupt cell walls which render more available cellulose and hemicellulose without inhibitors for the subsequent enzymatic hydrolysis is relevant [4]. Thermoplastic extrusion is a promising technique for the biomass processing to bioethanol production [1, 5]. Extrusion provides a continuous reaction system in which the feedstock is effectively mixed, compressed, melted, and plasticized at the barrel end changing the raw material's physical-chemical properties. This high productivity process employs short residence time and is easily adaptable and scalable [4]. In addition, extrusion does not generate solids losses nor hazardous byproducts and effluents and has an efficient water use [6]. The twin-screw extruders have shown superiority over single screw counterparts [7] because of their versatility due to the easy build-up of different elements along the screw shaft providing different functionalities [8]. The extrusion parameters like barrel temperature, screws speed, and moisture have remarkable effects in the processing of the raw materials like increasing in the surface area and porosity [3]. The use of enzymatic hydrolysis provides a specific sugar production treatment with mild process conditions and ample sugar yields [2]. The combination of the extrusion and enzymatic treatments provides a process free of unwanted wastes.

The sweet sorghum is an excellent crop for bioethanol production due to its dual capacity of providing a sugar juice (rich in glucose, fructose, and sucrose) and spent lignocellulosic biomass (rich in C5 and C6 sugars) that are

efficiently converted into first and second-generation ethanol [9]. The integral use of these feedstocks enables the possibility of a reduction of the ethanol production cost [10]. The objective of this research was to determine optimum extrusion parameters (last zone of the barrel temperature, screws speed, and feedstock moisture content) of sweet sorghum bagasse for its subsequent sugar enzymatic hydrolysis and fermentation with the strain *Issatchenkia orientalis* 20381 into bioethanol.

2. Materials and Methods

2.1. Materials. Sweet sorghum (*Sorghum bicolor* (L.) Moench) bagasse was procured from the research plots of the Instituto Nacional de Investigaciones Forestales, Agrícolas y Pecuarias (INIFAP) C.E., located in Celaya, Guanajuato, at 1760 m above sea level (coordinates $20^{\circ}34'47''$N, $100^{\circ}49'13''$W). After mechanical juice extraction, the bagasse was transported to the Tecnológico de Monterrey, Monterrey Campus, and dried at 50–60°C for 24 h. The dry bagasse was ground in a knife mill (Wiley Mill, Swedesboro, NJ) equipped with a 1 mm sieve.

2.2. Chemical Characterization. Moisture was determined using the AACC standard assay 44–15. For the structural carbohydrates assay the sweet sorghum bagasse (SSB) was washed of any soluble component in water or ethanol according to the methods recommended by the National Renewable Energy Laboratory (NREL) [11]. Then, the insoluble fiber was hydrolyzed and filtered for HPLC analysis as recommended by Sluiter et al. [12].

2.3. Extrusion Pretreatment. A twin-screw corotating extruder (BTSM-30, Bühler AG, Uzwil, Switzerland) with a barrel composed of 5 zones and two independent feeders for the solid raw material and water was used. The temperature of the fifth zone of the barrel was controlled by a heat exchanger device (Tool Temp, Bühler AG, Uzwil, Switzerland). The total length and outer diameter of the screws were of 800 mm and 30 mm, respectively, and the L/D ratio was 20. A die with a single 4 mm hole was used. The screws configuration was composed of three different sections: inlet/conveying elements section (for the introduction and transport of the dry feedstock and water), mixing elements section, and the final work elements section composed for kneading and reverse elements.

2.3.1. Experimental Design and Extrusion Conditions. A central composite design was used. Three different factors were evaluated: conditioning moisture content, screws speed, and temperature applied in the last section of the extruder barrel. Each independent variable had two levels: 30 or 50% moisture, 100 or 200 rpm, and 50 or 100°C, respectively. A center point with the conditions 40% moisture, 150 rpm, and 75°C was employed. Four center points were performed and three replicates were used for each design point. The solid feed rate was set constant at 5.7 $kg{\cdot}h^{-1}$ for all conditions.

2.4. Enzymatic Saccharification. The biocatalysis assays were made with a total volume of 100 mL in 500 mL flasks using 10% solid bagasse fraction for the central composite design and 10, 12, 14, 16, 18, 20, 22, 24, 26, or 28% solids for the loading assays. Citrate (50 mM) buffer adjusted to pH 5 with 10 mM of sodium azide was used for all hydrolyses. Biocatalyses were carried out in an orbital shaking incubator (VWR Model 1575) set at 50°C and 150 rpm for 24, 48, 72, or 96 h of reaction time. For all other assays, 72 h reaction time was employed. Novozymes enzymes NS22086, NS22083, NS22118, NS22119, NS22002, and NS22035 and dosages of 5, 0.25, 0.6, 0.4, 2, and 0.06% with respect to the solids loading were used, respectively. These enzymes consist in a fibrolytic cocktail of β-glucosidase, β-glucanase, arabinase, hemicellulase, pectinase, xylanase, and glucoamylase. The declared activity for each enzyme was 1,000 endoglucanase units (EGU)/g, 250 cellobiase units (CBU)/g, 100 fungal β-glucanase units (FBG)/g (13,700 polygalacturonase units (PGU)/g), 2,500 fungal xylanase units (FXU-S)/g, 45 FBG/g, and 750 PGU. The dosages used were 5.00, 0.60, 0.40, 0.25, 2.00, and 0.06% w/w total solids, respectively.

2.5. Fermentation Process. The fermentation was performed with the strain *Issatchenkia orientalis* ATCC 20381 in 500 mL Erlenmeyer flasks with 200 mL of the hydrolysates by triplicate. Beforehand, the strain was incubated in Difco YM broth (Becton, Dickinson and Company, USA) in an orbital shaking incubator (VWR Model 1575) set at 28°C and 100 rpm. The hydrolysates were adjusted to 12% solids with citrate buffer pH 5. A concentration of 1×10^6 $cells{\cdot}mL^{-1}{\cdot}°Brix^{-1}$ was inoculated into each prepared reaction flask. Aliquots of the fermentation broth were taken at 0, 12, 24, 48, and 72 h of fermentation. The aliquots were centrifuged at 4500 rpm and filtered through a 0.22 μm filter. The total sugars, inhibitors, and ethanol of the filtered samples were analyzed by HPLC while the free amino nitrogen (FAN) was determined after reaction with ninhydrin. The amount of FAN was determined in a spectrophotometer set at 420 nm. The calibration curve was constructed using glycine as standard [13].

The fermentation was performed without any nutrient supplementation at 28°C in an incubator (VWR Model 1575) under anaerobic conditions.

2.6. HPLC Quantification of Sugars and Inhibitors. The enzymatic saccharified samples were treated as described in previous research [14]. Analytes were separated by a Shodex SH1011 column (300 × 7.8 mm) with a flow rate of 0.6 mL per minute of HPLC-grade water containing 5 mM H_2SO_4 for the quantification of inhibitors and ethanol. The sugar quantification was performed with a Shodex SP0810 column and a cation/anion deasher (Biorad). The column temperature was set at 60 and 85°C for inhibitors and sugars, respectively. Also, the detector was at 50°C and the autosampler (refractive index detector Waters 2414) was at 4°C. Standards of ethanol, cellobiose, D-glucose, D-xylose, L-arabinose, D-mannose, D-galactose, acetic acid, 5-hydroxymethylfurfural, and furfural (Sigma Chemical Co., St. Louis, MO) were used. The run

times for sugars and inhibitors quantifications were 20 and 45 min, respectively.

2.7. Calculations. The sugar yields were expressed per gram of hydrolyzed sweet sorghum bagasse. The calculations for total and individual sugar yields and recoveries were the following:

$$Y_i = \frac{S_i \times V_T}{X_T},$$

$$Y_T = \sum Y_i,$$

$$R_i = \frac{Y_i}{B_i} \times 100,$$

$$B_i = \text{Glucans, mannans, or galactans} \times 1.11, \quad \text{and arabinans or xylans} \times 1.14, \tag{1}$$

$$R_T = \frac{Y_T}{B_T} \times 100,$$

$$E_Y = \frac{E \times V_T}{X_T},$$

$$R_E = \frac{E_Y}{Y_T} \times 100,$$

$$E_V = \frac{E_Y}{\rho_E},$$

where Y_i = individual sugar yield [mg·g^{-1}], S_i = individual sugar detected with HPLC [mg·mL^{-1}], V_T = total volume recovered [mL], X_T = total hydrolyzed solids [g], Y_T = total sugars [mg·g^{-1}], R_i = individual sugar yield recovered [%], B_i = individual structural sugar per gram of sweet sorghum bagasse [mg·g^{-1}], R_T = total sugars yield recovered [%], B_T = total structural sugars per gram of sweet sorghum bagasse [mg·g^{-1}], E_Y = ethanol yield [mg·g^{-1}] per gram of bagasse, E_V = ethanol volume [mL·g^{-1}], ρ_E = ethanol density [0.789 g·mL^{-1}], E = ethanol detected with HPLC [mg·mL^{-1}], and R_E = ethanol yield [%].

2.8. Statistical Analysis. The analysis of data generated by the central composite design and ANOVA were performed with software Minitab 14 with a statistical significance (α) of 0.05 to determine significant differences between treatments and the correlations coefficients (R^2). For the enzymatic and fermentation data a t-test were used and means were compared using the Fisher's exact tests. The response surfaces were plotted with the Statgraphics Centurion XVI software.

3. Results and Discussion

3.1. Chemical Characterization. The sweet sorghum bagasse chemical composition was the following: 31.48% of glucans, 9.33% of xylans, 0.94% of mannans, 2.94% of arabinans, 3.37% of galactans, 25.42% of water extractives, 7.79% of ethanol extractives, 0.07% of acetyl groups, 4.90% of acid ashes, and 13.03% of total lignin. This meant that the SSB contained about 50% fiber components (537.4 mg of total sugars per gram of dry bagasse). The high lignin content is a strong barrier for the cellulose and hemicellulose accessibility [2]. Shen et al. [10] reported SSB with 10% more sugars, but 5% more lignin than the counterpart tested herein. Cao et al. [15] reported SSB with 49.78% cellulose and 27.72% hemicellulose. This feedstock also contained higher amounts compared with that SSB used in this research. However, although our SSB had low glucose concentration, its low lignin content could be advantageous for the extrusion pretreatment because it has been shown that lignin decreases the pretreatment efficiency and acts as a physical barrier against chemicals and enzymes [16, 17]. These differences were probably due to variety differences, agronomical conditions, and crop maturation.

3.2. Extrusion Effect

3.2.1. Release of Total Sugars. A high linear correlation coefficient of 93.1 was obtained for the total sugars with respect to temperature, screws speed, and moisture (Figures 1(a1), 1(a2), and 1(a3)). The moisture content and the interaction between temperature and moisture were the most significant extrusion parameters with a P value = 0.000 followed by the screws speed with a P value = 0.013. As expected, the amounts of total free sugars as well as the C5 and C6 sugars concentrations were strongly affected by the extrusion parameters. Higher sugar yields were obtained at low tempering moisture, high screws speeds, and high temperature (Figure 1(a1)). The crystalline cellulose structure represents a strong barrier for the active sites of enzymes [5]. In this nonchemical pretreatment, the extruder shear stress was the mean way of action to enhance the decrystallization of cellulose and its porosity and susceptibility to fibrous degrading enzymes. The tempering moisture of the feedstock was the main factor affecting disruption of fiber components because it directly affected the shear stress rate [3]. When the tempering moisture was increased, the SSB ran more easily through the extruder. Thus, with higher moistures the shear stress was reduced decreasing the susceptibility of the extruded feedstock for the subsequent enzymatic hydrolysis step. The extruder temperature and the screws speeds also affected the yield of individual sugars specially those belonging to the C5 group (Sections 3.2.2 and 3.2.3). It was observed that at high extruder temperatures a lower feedstock viscosity inside the barrel was obtained [3], and this effect improved when the speed of the screws was increased. Karunanithy et al. [18] extruded different varieties of switchgrass, big bluestem, and prairie corn finding a better glucose recovery after enzyme treatment when extruding the feedstocks at 200 rpm in a single screw extruder. In this research, the optimum extruding conditions were 30°C, 200 rpm screws speed, and 30% feedstock moisture content. With these conditions it was possible to release the maximum amounts of sugar after the subsequent enzyme treatment. Approximately 70.4% of the sugars were released from the fiber matrix. Thus, the extruded feedstock processed under the conditions mentioned above was further converted into fermentable sugars and ethanol. The utilization of higher

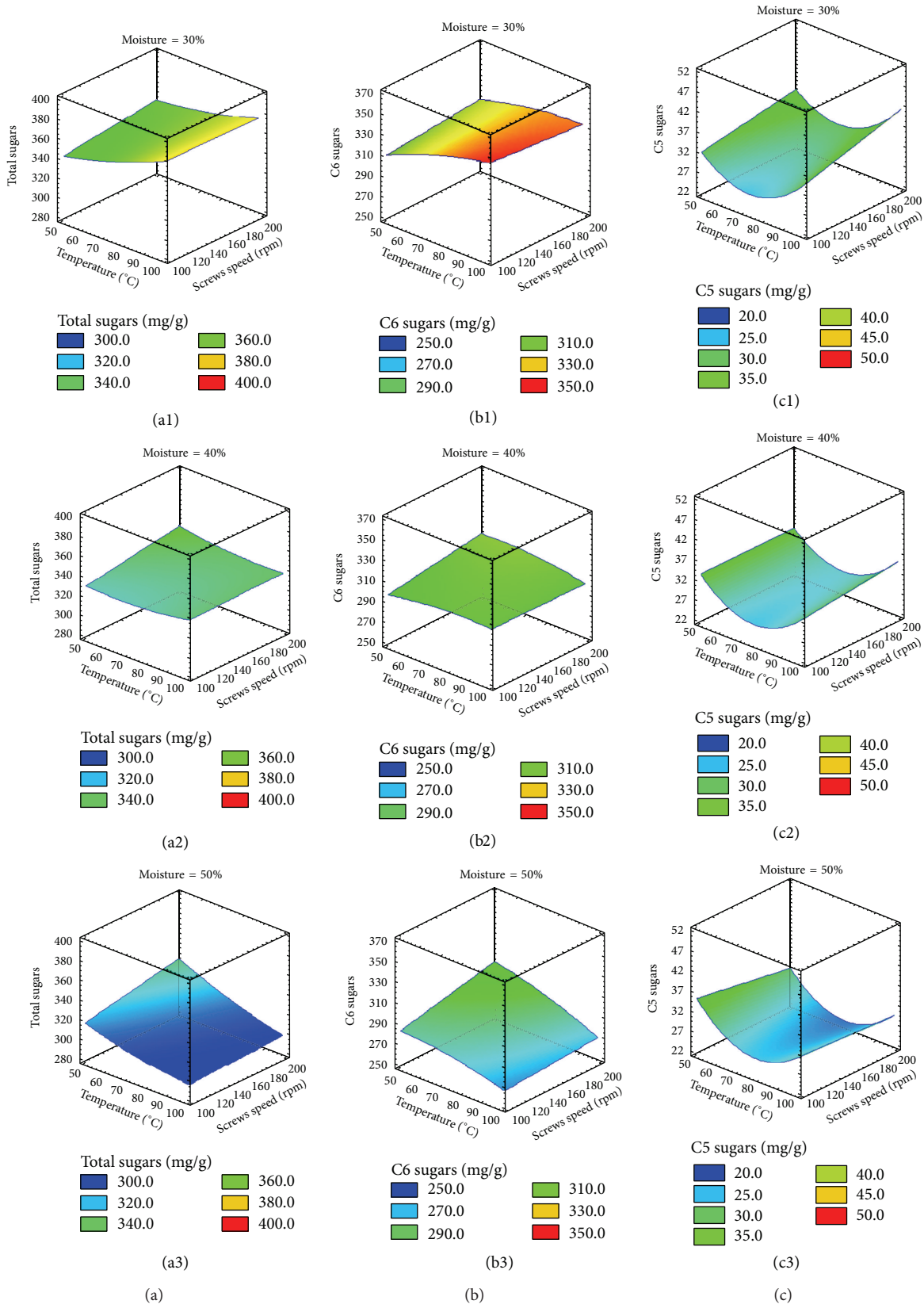

Figure 1: Response surfaces for total sugars ((a1), (a2), and (a3)), C6 ((b1), (b2), and (b3)), and C5 ((c1), (c2), and (c3)) generated from sweet sorghum bagasse extruded at different temperatures (50, 75, or 100°C), screws speeds (100, 150, or 200 rpm), and moistures inside the barrel (30, 40, or 50%) hydrolyzed with fiber degrading enzymes expressed in sugars milligrams per gram of bagasse (dw).

screws speeds (400 or 500 rpm) decreased sugar recovery to only 52.2 and 58.6%, respectively. According to Karunanithy and Muthukumarappan [6], the heat produced from the higher screws speeds affected negatively the viscosity of the feedstock inside the barrel and in some instances caused the blocking of the extruder. The same author [3] obtained an overall yield of 44.5% sugars associated to cell walls of switchgrass without the generation of inhibitory compounds when operating a single screw extruder at 50 rpm, 150°C, and 15% moisture content. Karunanithy et al. [18] employed 4 heaters to maintain the barrel temperature and increase the efficiency of transformation of lignocellulose materials. In this investigation, only one heat exchanger was used to maintain the barrel at high temperature. Only the last section of the extruder was heated because the screw configuration was designed to cause friction and intrinsic heat to properly treat the SSB. Regarding the extruder specific mechanical energy (SME) Lamsal et al. [5] obtained good sugar recoveries in a range of 222 up to 639 $Wh{\cdot}kg^{-1}$. The SME at 100, 150, and 200 rpm were 266.8, 276.0, and 314.8 $Wh{\cdot}kg^{-1}$ when extruding 30% tempered SSB, respectively. The results indicated that the thermoplastic extrusion was an adequate continuous pretreatment for second-generation bioethanol production without the generation of hazardous compounds that decrease the efficiency of fermentation of hydrolyzed lignocellulosic feedstocks.

3.2.2. Release of C6 Sugars. After the enzymatic hydrolysis, it was possible to release significant amounts of cellobiose, glucose, galactose, and mannose from the extruded SSB. The mathematical models for C6 sugars were linear with correlation coefficients greater than 85% (Figures 1(b1), 1(b2), and 1(b3)). Almost all the factors and their interactions had significant effects over the efficiency of the subsequent step of enzymatic hydrolysis. For cellulose hydrolysis, all the independent factors, double and triple interactions, had significant effects (P value ≤ 0.009). The same effects were observed with galactose with the exception that the feedstock moisture content did not have a significant effect. On the other hand, for glucose and mannose all the effects and interactions were statistically significantly different except for temperature (P value ≤ 0.010). Karunanithy and Muthukumarappan [3] used a single screw extruder to pretreat switchgrass and found that at 150 rpm there was a better sugar release. Also, these researchers found that at 100°C and low tempering moisture contents the glucose recovery was higher. Although not all the extrusion parameters were significant for every sugar released, all these variables needed to be optimized in order to have an efficient pretreatment. The interaction between extrusion parameters allowed the efficient C6 sugars release from SSB.

3.2.3. Release of C5 Sugars. A linear correlation was obtained for the enzymatic release of arabinose with R^2 = 72.63%. The main effects were the moisture content and the interactions temperature-screw speed and screws speed-feedstock moisture content (P values ≤ 0.002). On the other hand, the enzymatic release of xylose fitted as a quadratic correlation (P value = 0.000) with R^2 = 74.27%. The main extrusion effects for xylose hydrolysis were the square temperature and the interactions temperature-moisture, screws speed-moisture, and temperature-screws speed-moisture content. The square temperature and the screws speed-moisture interactions had a P value = 0.037, which meant less significance than the other values that had a P value = 0.000. The modeling of both C5 sugars fitted as a quadratic correlation temperature dependent (R^2 = 51.72, P value = 0.010). The arabinose linear modeling was overshadowed by the quadratic effect of the xylose modeling mainly for the higher amount of this sugar compared to arabinose. Karunanithy et al. [18] found that the temperature had a positive effect on the xylose release from diverse lignocellulosic raw materials. Similar to the C6 sugars, it was found that the feedstock moisture and the extrusion parameters interactions had a positive effect over the SSB enzymatic hydrolysis. Furthermore, the feedstock moisture had a direct effect over the temperature due to the shear stress effect. The heat is a very important condition for hemicellulose conversion to sugars [2]. The use of higher feedstock moisture contents reduced the heat exchange and therefore sugars yields [3].

Even if the arabinose had a correlation coefficient similar to that of xylose, the global behavior of C5 enzymatic release had a quadratic correlation (Figures 1(c1), 1(c2), and 1(c3), resp.). As discussed independently for xylose and arabinose, the feedstock moisture content was the main factor affecting the C5 sugar release. A low feedstock moisture yielded more sugars. On the other hand, at higher moistures (40 and 50%) the sugars concentrations were reduced significantly, especially when the extruder was operated at screws speeds higher than 100 rpm. Also, the interaction of temperature with other effects was important specifically for the susceptibility of hemicellulose to enzymatic hydrolysis. The quadratic effects had a strong influence in the center conditions when the C5 sugars concentrations drop to lower concentrations. The effect of the significant interactions was positive for sugars recovery, especially at 30% moisture content, 100°C, and 200 rpm. The opposite effect was obtained at 50% feedstock moisture content, where the sugar concentrations with 100°C and 200 rpm were significantly less compared to 50°C and 100 rpm (Figure 1(c1)). Despite this specific effect, the C5 sugar concentrations remained higher using a feedstock moisture content of 30%.

3.2.4. Inhibitors Compounds. As expected, any enzymatic hydrolysate did not contain significant amounts of acetic acid, furfural, or HMF. These inhibitors are produced in large quantities in fiber feedstocks pretreated with acid or alkaline chemicals. Karunanithy et al. [18] and Karunanithy and Muthukumarappan [3] reported slight amounts of acetic acid in some of their enzymatically saccharified lignocellulosic extruded materials. The acetic acid is generated from the disruption of the hemicellulose [1, 19]. The hydrolysates obtained in this research did not contain acetic acid, indicating that the heat applied during extrusion was not enough to release the acetic groups from lignocellulose. Furfural and HMF are produced from the C5 and C6 sugars dehydration [20] after

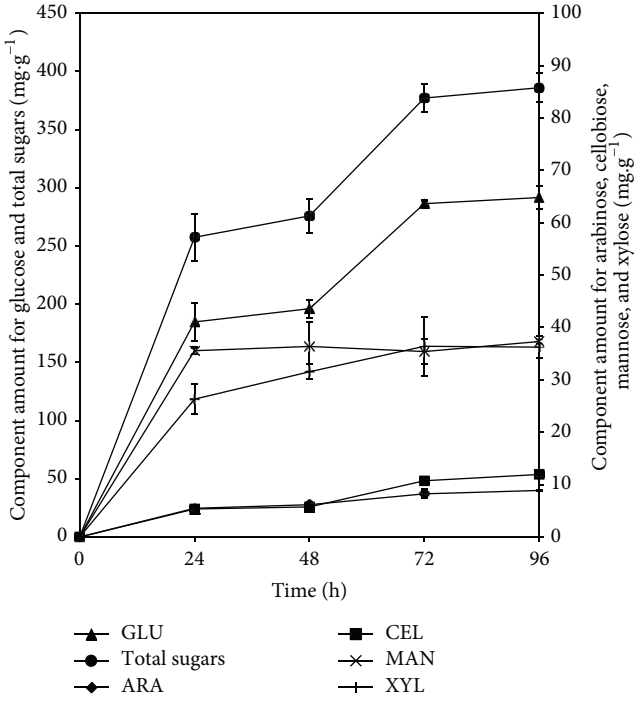

Figure 2: Sugars generated from sweet sorghum bagasse extruded at 30% moisture, 200 rpm, and 100°C at 10% solids loading after 24, 48, 72, and 96 h treatment with fiber degrading enzymes.

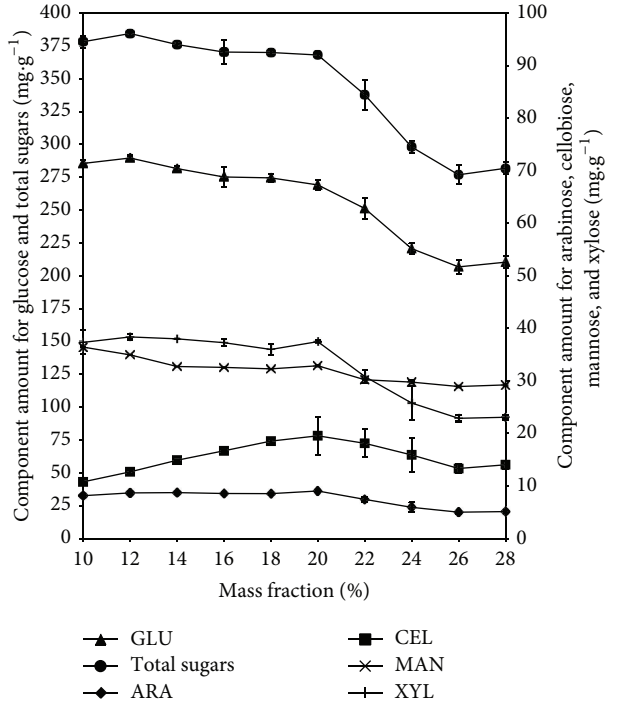

Figure 3: Sugars generated per g bagasse (dmb) at 10, 12, 14, 16, 18, 20, 22, 24, 26, or 28% loading of sweet sorghum bagasse extruded at 30% moisture, 200 rpm, and 100°C and subsequently treated with fiber degrading enzymes for 72 h.

chemical pretreatments. The residence time of the feedstock and the temperatures inside the extruder were not enough to degrade sugars into these types of inhibitors [7].

3.3. Enzymatic Studies

3.3.1. Enzymatic Saccharification Time Effect. The major glucose and total fermentable sugar release occurred after 24 h hydrolysis. At this point in time 52.8% of the glucose and 47.9% of the total sugars were released from the extruded SSB (Figure 2). There were no significant differences between the total amounts of sugars at 24 and 48 h of enzymatic saccharification. In the case of the xylose concentration, there were no significant differences after 48 h of hydrolysis. The mannose reached its maximum concentration after 24 h hydrolysis with no significant differences throughout the proposed biocatalysis step. The amounts of sugars were not significantly different when hydrolysates produced after 72 and 96 h of saccharification were compared. Regarding glucose, the maximum concentration was reached at 72 h where 82% of the total available glucose was produced. Arabinose was the only sugar which reached the maximum concentration after 96 h of hydrolysis. Even if the major amount of sugars was released during the first 24 h, hydrolyses times between 48 and 72 h were necessary to release the remaining 22% of the total sugars. During the saccharification, the hydrolyzed sugars block the active site of the enzymes [21]. For this reason, the SSB hydrolysis had an apparent time of slow enzymatic activity between the 24 and 48 h reactions. According to Pandey [1] cellulases are inhibited approximately 75% when the glucose concentration reached 3 g·L^{-1}. After 24 h of enzymatic hydrolysis the hydrolysates contained 18.47 g·L^{-1} of glucose, enough amount to produce cellulase inhibition. There were no significant differences in total sugars concentrations when hydrolysates generated after 72 and 96 h were compared. Thus, 72 h of biocatalysis was selected as the best hydrolysis time. At this time 73% of the total sugars were released.

Shen et al. [10] reported maximum sugars concentrations after 96 h enzymatic hydrolysis using SSB that was previously steam-pretreated. These particular conditions only achieved 68% of glucose hydrolysis. A previous research that tested the use of thermoplastic extrusion of SSB tempered to 30% moisture [22] obtained 67.5% of total sugars recovery. The feedstock was extruded at 150°C and 100 rpm and then saccharified using 5% bagasse loading. With the new extrusion conditions it was possible to hydrolyze 70% sugars using the double amount of SSB.

3.3.2. Solids Loading Assay. The effects of different mass loading fractions in the enzymatic hydrolysis performance of the extruded sweet sorghum bagasse are depicted in Figure 3. Xylose and arabinose were detected in significant amounts whereas galactose was not generated during the biocatalysis step. There were no statistical differences between total sugars concentrations when the 10 and 20% mass fractions were compared. It was possible to hydrolyze around 70% of the

total sugars at the loading of these solids. Xylose and arabinose were generated similarly during the proposed enzyme hydrolysis. The maximum concentrations were observed in the 10% mass hydrolysates and remained with no significant change when compared with hydrolysates elaborated with 12, 14, 16, 18, or 20% mass fractions. At 22% or higher solids, the C5 sugars concentration decreased although the detrimental effect was not observed in the 26 and 28% bagasse fractions. Mannose reached its higher concentration in hydrolysates containing 10 to 20% mass loading. After these solid loadings there were no significant differences when 14, 16, 18, or 20% mass loadings were compared. The mannose in hydrolysates produced with 22% solids maintained the same average concentration compared to the rest of the higher solid mass fractions tested. Regarding cellobiose, it increased constantly in hydrolysates produced with 10 to 20% mass loadings. The maximum concentrations (18 $mg \cdot g^{-1}$ bagasse) were achieved in hydrolysates containing 18 to 24% bagasse loadings. At higher solid concentrations cellobiose decreased to values under 15 $mg \cdot g^{-1}$ bagasse. The increase in cellobiose concentration was related to the reduction in glucose concentrations. The accumulation of cellobiose likely occurred due to its product inhibitory effect on endoglucanases, exoglucanases, and β-glucosidases [18, 23]. When more solids were used, higher amounts of cellobiose were released and enzymes inhibited yielding lower amounts of sugars especially in hydrolysates containing 22% solids. The maximum glucose concentration was achieved at 10% SSB loading. After this concentration there were no significant differences between the group of hydrolysates containing 12, 14, 16, or 18% solids and the other group containing 16, 18, or 20% SSB solids. The glucose concentrations in hydrolysates containing 22, 24, or 26–28% were significantly different. The hydrolysate containing 20% extruded bagasse loading was not significantly different compared to the counterpart containing 10% solids. The proposed thermoplastic extrusion pretreatment favored cellulose decrystallization and increased the surface area and porosity of the feedstock increasing the amount of soluble fiber [6, 8]. Due to these effects it was possible to increase the bagasse loading during the fiber degrading enzymatic step. The hydrolysate containing 10% SSB solids contained 37.8 $g \cdot L^{-1}$ of total sugars whereas its counterpart at 20% solids achieved 73.6 $g \cdot L^{-1}$. Therefore, the hydrolysate with 20% solids contained almost twice the sugar amount compared to the 10% solid counterpart. It was possible to employ high solid concentrations with extruded SSB without seriously affecting enzymes performance. However, the use of higher mass fractions did not further improve sugar generation. Although the extrusion pretreatment improved the subsequent enzymatic hydrolysis, the water to solid ratio became a limiting factor in hydrolysates containing more than 20% solids. The role of free water is relevant because it acts as solvent enhancing the contact between substrate and enzymes. Also the water has a direct effect over the viscosity and the enzyme mass transfer in the hydrolysates [21]. The use of higher than 20% extruded SSB loadings decreased free water necessary to enhance enzyme performance and sugars yields. In addition, the cellobiose amounts increased indicating the likely enzymatic inhibition by products. These results indicated that the 20% mass fraction achieved high sugars yield using relatively lower amounts of water. This particular hydrolysate contained 7.3% total sugars suited for the following fermentation step. Despite the chemical composition, the enzymatically saccharified extruded SSB using a 20% mass loading contained 10% more total sugars compared to counterparts produced by Shen et al. [10].

3.4. Extruded Sweet Sorghum Bagasse Fermentation. There were no significant differences between the sugar consumption and ethanol generation in hydrolysates with and without insoluble solids (Table 1). Although all the soluble sugars were metabolized by the yeast, the main carbohydrate source was glucose. After the first 12 h fermentation, 23.6 and 32.2% of the total sugars were consumed in hydrolysates free of insoluble solids and counterparts containing insoluble solids. After 24 h fermentation, 99.4 and 96.5% of the glucose were consumed in hydrolysates with and without insoluble solids, respectively (Table 1). During the first 12 h fermentation, only 23.6% of the total sugars in hydrolysates containing insoluble solids content were consumed. This particular system generated 21.78 mg ethanol$\cdot g^{-1}$ extruded bagasse. For the fermentation of the counterpart free of insoluble solids, 32.2% of the total sugars were consumed at the first 12 h. The arabinose was not detected after 12 h in both fermenting broths, which indicated the effective consumption of this sugar by the *I. orientalis* strain. On the other hand, 25% of the available xylose was consumed after 12 h fermentation in hydrolysates containing insoluble solids and this sugar was not further fermented during the posterior 60 h fermentation. Similarly, the fermentation of hydrolysates without insoluble solids consumed 25.6% of the total xylose present in the broth. The low and high xylose and glucose consumptions were previously documented [22]. Galactose was metabolized slowly along the fermentation of hydrolysate with insoluble solids. On the other hand, the fermented counterpart without solids consumed all the galactose after 48 h biocatalysis. After two days of fermentation, the sugars consumed were transformed into 200 Ml ethanol$\cdot g^{-1}$ SSB in hydrolysates with and without insoluble solids, respectively. These ethanol conversions efficiencies were 40.9 and 41.4%, respectively. There were no significant differences in ethanol concentrations when 24 and 48 h fermentation times were compared. After 48 h fermentation, the yeast only used the remaining sugar to survive and did not generate significant amounts of ethanol. In both cases, the mannose was not used and therefore it increased its concentration in both fermented broths. Interestingly, in both types of fermentation, the cellobiose decreased with the reaction time, but the fermentation in presence of insoluble solids decreased significantly after 24 h. Probably the *I. orientalis* had a cellulosic enzymatic activity with solids presence. Regarding the alpha amino nitrogen consumption, it followed a similar trend compared to sugars consumption. During the first 12 h fermentation, only 5.6 and 4.1% of FAN were consumed in hydrolysates with and without insoluble solids. However, FAN consumption increased to 50% after 24 h fermentation. This behavior

Table 1: Different sugars and ethanol concentrations from extruded sweet sorghum bagasse at 100°C, 200 rpm, and 30% moisture, fermented with *Issatchenkia orientalis* 20381 at 12% solids fraction after 72 h enzymatic saccharification[1,2].

Compound [mg·g^{-1}]	*Issatchenkia orientalis* ATCC 20381 at 12% solids loading ferementation					*Issatchenkia orientalis* ATCC 20381 without solids				
	0 h	12 h	24 h	48 h	72 h	0 h	12 h	24 h	48 h	72 h
Arabinose	4.20 ± 0.08	ND	ND	ND	ND	4.26 ± 0.07	ND	ND	ND	ND
Cellobiose	3.94 ± 0.27	12.29 ± 2.32	12.07 ± 0.06	6.30 ± 0.25	2.75 ± 0.05	3.31 ± 0.15	12.84 ± 0.36	12.92 ± 0.36	10.41 ± 0.13	9.88 ± 0.77
Galactose	3.71 ± 0.28	2.90 ± 0.12	1.51 ± 0.15	0.47 ± 0.01	0.16 ± 0.01	3.69 ± 0.06	0.27 ± 0.04	ND	ND	ND
Glucose	337.01 ± 1.10	250.78 ± 13.76	2.00 ± 0.35	1.48 ± 0.44	ND	326.92 ± 4.25	213.83 ± 5.26	11.45 ± 3.96	ND	ND
Mannose	ND	1.22 ± 0.08	2.30 ± 0.19	2.70 ± 0.03	3.09 ± 0.05	2.07 ± 0.03	1.46 ± 0.08	1.63 ± 0.17	2.01 ± 0.01	2.03 ± 0.19
Xylose	36.80 ± 0.29	27.60 ± 0.53	28.30 ± 0.53	26.61 ± 0.22	23.39 ± 2.12	32.51 ± 0.18	24.16 ± 1.03	28.45 ± 1.82	26.96 ± 1.70	22.23 ± 0.91
Total sugars	385.66 ± 6.79	294.79 ± 11.71	45.90 ± 0.48	37.56 ± 0.01	29.39 ± 2.05	372.76 ± 4.74	252.60 ± 6.77	54.44 ± 1.12	39.37 ± 1.56	31.14 ± 1.87
Ethanol	ND	21.78 ± 1.10	160.06 ± 3.10	157.89 ± 3.03	147.63 ± 1.81	ND	16.94 ± 0.49	154.34 ± 3.24	156.36 ± 1.15	127.63 ± 5.66
Free amino nitrogen[3]	98.65 ± 0.95	93.13 ± 4.00	49.46 ± 4.76	47.57 ± 3.24	47.30 ± 0.95	144.88 ± 0.38	138.81 ± 3.43	75.74 ± 1.52	75.45 ± 1.72	50.94 ± 3.81

[1]The compounds are in milligrams of sugar per gram of sweet sorghum bagasse dry basis.
[2]The compounds not detected by the HPLC were reported with the acronym ND.
[3]The free amino nitrogen is in milligrams per liter.

together with the glucose consumption marked the final stage of the fermentation. Only hydrolysates without insoluble solids kept producing significant amounts of ethanol and consumed FAN during the last stage of the programed fermentation. This indicates that the *I. orientalis* metabolized these components for survival in the absence of glucose.

Fermentation of enzymatically saccharified extruded SSB adjusted to 12% solids generated 19.20 and 18.53 g of ethanol·L^{-1} in hydrolysates prepared with and without insoluble solids, respectively. Shen et al. [10] obtained similar yields of 19.8 g etnaol·L^{-1} after fermenting enzymatically saccharified steam pretreated SSB with different strains of *S. cerevisiae*. Choi et al. [4] performed simultaneous saccharification and fermentation of rapeseed straw pretreated with H_2SO_4 in a twin-screw extruder obtaining 16.01 g of ethanol per L. The combination of diluted acid pretreatment and extrusion achieved a good ethanol yield, but the process recommended the washing of the chemically and mechanically treated feedstock to remove inhibitors.

The efficacy of the physical pretreatment proposed herein without the use of chemicals is ideally suited to the subsequent saccharification step and yields hydrolysates with high amounts of potentially fermentable C5 and C6 sugars without inhibitors that are effectively fermented into bioethanol by yeast strains such as *I. orientalis*. In this research, hydrolysates were diluted due to the utilization of a regular fermentation strain. The utilization of an osmotolerant yeast will likely make it possible to ferment without diluting. Assuming that the sweet sorghum cultivar yields around 85 ton per hectare [9] with 50% of sweet juice it is possible to convert the spent lignocellulose biomass into 4309 L·Ha^{-1} of ethanol. Thus, the integral use of sweet sorghum to generate first-generation ethanol from the sweet juice and second-generation ethanol from bagasse processed by the technology proposed herein can yield more than 7369 L bioethanol·Ha^{-1}.

4. Conclusions

Extrusion was a viable pretreatment for second-generation bioethanol using SSB because it did not generate inhibitors and enhanced the subsequent enzymatic conversion into fermentable sugars. The SSB extruded at 100°C and 200 rpm and with 30% moisture generated up to 70% of the total sugars after treatment with fiber degrading enzymes. After 72 h enzyme hydrolysis and using 20% mass fraction 73.6 g·L^{-1} total sugars were obtained. Fermentation of these hydrolysates yielded about 200 mL ethanol·kg^{-1} of extruded SSB. Interestingly, it was not necessary to remove the insoluble solids of the enzymatically treated SSB hydrolysate for a successful fermentation.

Conflict of Interests

The authors declare that there is no conflict of interests regarding the publication of this paper.

Acknowledgments

The authors would like to thank the Consejo Nacional de Ciencia y Tecnología and Escuela de Ingeniería y Ciencias for the support provided. They gratefully recognize the help of Novozymes for providing the enzymes used in this work.

References

[1] A. Pandey, *Biofuels: Alternative Feedstocks and Conversion Processes*, Academic Press, Oxford, UK, 1st edition, 2011.

[2] E. C. Bensah and M. Mensah, "Chemical pretreatment methods for the production of cellulosic ethanol: technologies and innovations," *International Journal of Chemical Engineering*, vol. 2013, Article ID 719607, 21 pages, 2013.

[3] C. Karunanithy and K. Muthukumarappan, "Effect of extruder parameters and moisture content of switchgrass, prairie cord grass on sugar recovery from enzymatic hydrolysis," *Applied Biochemistry and Biotechnology*, vol. 162, no. 6, pp. 1785–1803, 2010.

[4] C. H. Choi, J. S. Kim, and K. K. Oh, "Evaluation the efficacy of extrusion pretreatment via enzymatic digestibility and simultaneous saccharification & fermentation with rapeseed straw," *Biomass and Bioenergy*, vol. 54, pp. 211–218, 2013.

[5] B. Lamsal, J. Yoo, K. Brijwani, and S. Alavi, "Extrusion as a thermo-mechanical pre-treatment for lignocellulosic ethanol," *Biomass and Bioenergy*, vol. 34, no. 12, pp. 1703–1710, 2010.

[6] C. Karunanithy and K. Muthukumarappan, "Influence of extruder and feedstock variables on torque requirement during pretreatment of different types of biomass—a response surface analysis," *Biosystems Engineering*, vol. 109, no. 1, pp. 37–51, 2011.

[7] Z. Lin, L. Liu, R. Li, and J. Shi, "Screw extrusión pretreatments to enhance the hydrolysis of lignocellulosic biomass," *Journal of Microbial & Biochemical Technology*, vol. 12, p. 5, 2012.

[8] L. Moscicki, *Extrusion-Cooking Techniques: Applications, Theory and Sustainability*, Wiley-VCH, Weinheim, Germany, 1st edition, 2011.

[9] S. O. Serna-Saldivar, C. Chuck-Hernandez, E. Pérez-Cariillo, and E. Heredia-Olea, "Chapter 3: sorghum as a multifunctional crop for the production of fuel ethanol: current status and future trends," in *Bioethanol*, M. A. Pinheiro Lima and A. P. Policastro Natalense, Eds., pp. 51–74, InTech, Rijeta, Croatia, 2012.

[10] F. Shen, J. Hu, Y. Zhong, M. L. Y. Liu, J. N. Saddler, and R. Liu, "Ethanol production from steam-pretreated sweet sorghum bagasse with high substrate consistency enzymatic hydrolysis," *Biomass & Bioenergy*, vol. 41, pp. 157–164, 2012.

[11] A. Sluiter, R. Ruiz, C. Scarlata, J. Sluiter, and D. Templeton, *Determination of Extractives in Biomass: Laboratory Analytical Procedure (LAP)*, National Renewable Energy Laboratory, Golden, Colorado, 2008.

[12] A. Sluiter, B. Hames, R. Ruiz et al., *Determination of Structural Carbohydrates and Lignin in Biomass. Laboratory Analytical Procedure (LAP)*, National Renewable Energy Laboratory, Golden, Colo, USA, 2008.

[13] D. W. Wright, "The determination of free amino nitrogen in proteins," *The Journal of Biological Chemistry*, vol. 56, pp. 191–201, 1923.

[14] E. Heredia-Olea, E. Pérez-Carrillo, and S. O. Serna-Saldívar, "Effects of different acid hydrolyses on the conversion of sweet sorghum bagasse into C5 and C6 sugars and yeast inhibitors using response surface methodology," *Bioresource Technology*, vol. 119, pp. 216–223, 2012.

[15] W. Cao, C. Sun, R. Liu, R. Yin, and X. Wu, "Comparison of the effects of five pretreatment methods on enhancing the enzymatic digestibility and ethanol production from sweet sorghum bagasse," *Bioresource Technology*, vol. 111, pp. 215–221, 2012.

[16] T. Scheper and L. Olsson, *Advances in Biochemical Engineering/Biotechnology*, vol. 108, Springer, Berlin, Germany, 2007.

[17] Y. Sun and J. Cheng, "Hydrolysis of lignocellulosic materials for ethanol production: a review," *Bioresource Technology*, vol. 83, no. 1, pp. 1–11, 2002.

[18] C. Karunanithy, K. Muthukumarappan, and W. R. Gibbons, "Effects of extrudr screw speed, temperature, and enzyme levels on sugar recovery from different biomasses," *ISRN Biotechnology*, vol. 2013, Article ID 942810, 13 pages, 2013.

[19] A. Rodríguez-Chong, J. A. Ramírez, G. Garrote, and M. Vázquez, "Hydrolysis of sugar cane bagasse using nitric acid: a kinetic assessment," *Journal of Food Engineering*, vol. 61, no. 2, pp. 143–152, 2004.

[20] S. Gámez, J. J. González-Cabriales, J. A. Ramírez, G. Garrote, and M. Vázquez, "Study of the hydrolysis of sugar cane bagasse using phosphoric acid," *Journal of Food Engineering*, vol. 74, no. 1, pp. 78–88, 2006.

[21] J. B. Kristensen, C. Felby, and H. Jørgensen, "Yield-determining factors in high-solids enzymatic hydrolysis of lignocellulose," *Biotechnology for Biofuels*, vol. 2, article 11, 2009.

[22] E. Heredia-Olea, E. Pérez-Carrillo, and S. O. Serna-Saldívar, "Production of ethanol from sweet sorghum bagasse pretreated with different chemical and physical processes and saccharified with fiber degrading enzymes," *Bioresource Technology*, vol. 134, pp. 386–390, 2013.

[23] F. C. Corazza, L. P. V. Calsavara, F. F. Moraes, G. M. Zanin, and I. Neitzel, "Determination of inhibition in the enzymatic hydrolysis of cellobiose using hybrid neural modeling," *Brazilian Journal of Chemical Engineering*, vol. 22, no. 1, pp. 19–29, 2005.

Hindawi Publishing Corporation
BioMed Research International
Volume 2014, Article ID 649453, 12 pages
http://dx.doi.org/10.1155/2014/649453

Review Article

Computational Approaches for Microalgal Biofuel Optimization: A Review

Joseph Koussa, Amphun Chaiboonchoe, and Kourosh Salehi-Ashtiani

Division of Science and Math and Center for Genomics and Systems Biology (CGSB), New York University Abu Dhabi, P.O. Box 129188, Abu Dhabi, UAE

Correspondence should be addressed to Kourosh Salehi-Ashtiani; ksa3@nyu.edu

Received 6 June 2014; Revised 28 August 2014; Accepted 1 September 2014; Published 21 September 2014

Academic Editor: Meisam Tabatabaei

The increased demand and consumption of fossil fuels have raised interest in finding renewable energy sources throughout the globe. Much focus has been placed on optimizing microorganisms and primarily microalgae, to efficiently produce compounds that can substitute for fossil fuels. However, the path to achieving economic feasibility is likely to require strain optimization through using available tools and technologies in the fields of systems and synthetic biology. Such approaches invoke a deep understanding of the metabolic networks of the organisms and their genomic and proteomic profiles. The advent of next generation sequencing and other high throughput methods has led to a major increase in availability of biological data. Integration of such disparate data can help define the emergent metabolic system properties, which is of crucial importance in addressing biofuel production optimization. Herein, we review major computational tools and approaches developed and used in order to potentially identify target genes, pathways, and reactions of particular interest to biofuel production in algae. As the use of these tools and approaches has not been fully implemented in algal biofuel research, the aim of this review is to highlight the potential utility of these resources toward their future implementation in algal research.

1. Introduction

Biofuel production from microalgae has been receiving attention as an alternative energy source due to its high biomass productivity and minimal land resource requirement. However, there is still a need to improve algal productivity in order to make algal-based bioproducts economically viable. Metabolic network reconstructions of algae can offer insight into genetic modification strategies that can be used to improve microalgal strains. A large number of computational tools have been developed, allowing a range of analyses and predictions, based on genetic and thermodynamic constraints embedded in in the network, to identify bioengineering strategies that can result in enhanced biofuel production of the engineered algal strain. Although a fair number of algal genomes have been fully sequenced, only a few metabolic network models have been reconstructed for these species, hampering algal bioengineering progress [1].

The utilities of metabolic network models span over several types of applications. On one hand, these models help contextualizing high throughput experimental data, for example, integrating gene expression data with metabolic pathways under different growth conditions [2]. Metabolic models can also unveil targets for metabolic engineering approaches, which can lead to increased production of target metabolites [3] or preferentially increase respiration rates [4]. On the other hand, with the availability of large and diverse biological data sets, metabolic network models can provide a framework to integrate such omics data and allow the formulation and testing of downstream hypotheses. Last, cross-species metabolic comparison represents one more utility of such reconstructions through which identification of differentially activated metabolic pathways can be achieved among other comparative analyses [5]. Herein we review the reconstruction of metabolic network models and major computational tools and pipelines that hold the potential to contribute to the optimization of algal strains for biofuel production. We describe a number of tools that remain mostly unused by the algal research community. This is reflected from the observation that only 7 algal-based PGDBs

Table 1: Databases and tools for metabolic network reconstruction.

Database	Link
Algal Functional Annotation Tool	http://pathways.mcdb.ucla.edu/algal/index.html
BiGG	http://bigg.ucsd.edu/
BioCyc	http://biocyc.org/
Biomart	http://www.biomart.org/index.html
BRENDA	http://www.brenda-enzymes.info/
COBRA	http://opencobra.sourceforge.net/openCOBRA/
ExPASy	http://www.expasy.org/
KBASE	http://kbase.us
KEGG	http://www.genome.jp/kegg/
Model SEED	http://www.theseed.org/wiki/Main_Page
MetaCyc	http://metacyc.org/
Pathway Tools	http://pathwaytools.org/
Reactome	http://www.reactome.org/PathwayBrowser/
UniProt	http://www.uniprot.org

(Pathway/Genome Database) are available in Pathway Tools [6], while approximately 3,500 PGDBs are available for non-algal species (please see below for more information). The use of some of the herein discussed tools, already applied to the multitude nonalgal organisms, ranging from human to *E. coli*, provides strategies for algal biofuels optimization with major enhancement potential.

2. Metabolic Network Model Reconstruction

Metabolic network reconstruction from genomic and large-scale experimental data can help understand and predict metabolic processes and pathways. A number of tools and databases have been developed specifically to facilitate metabolic network reconstruction. In addition, new analysis tools and approaches are being developed along with the expansion of relevant databases and resources. Table 1 presents some of the existing databases and tools for metabolic network reconstruction.

Metabolic network reconstruction requires information on gene-protein-reaction associations to reconstruct evidence-based, species-specific networks. Protein database resources and tools help to link information between enzymes, EC numbers, genes, proteins, pathways, and substrates. These include BRENDA [7], ExPASy [8], and UniProt (Universal Protein Resource) [9]. BRENDA (BRaunschweig ENzyme DAtabase) enzyme portal is the enzyme information system, which integrates information from seven databases to provide functional biochemical and molecular data. To explore and visualize metabolic networks as maps of metabolic pathways, a number of freely available pathway databases exist. For example, BioCyc, MetaCyc [10], KEGG (Kyoto Encyclopedia of Genes and Genomes) [11], Reactome [12], and BiGG [13] can be named. In turn, common metabolic reconstruction tools include COBRA (more specifically its rBioNet component) [14–16], Model SEED [17], and Pathway Tools [6].

Pathway Tools [6, 18] is an integrated software tool that can create in a semiautomated manner organism-specific network and pathways databases (called Pathway/Genome Database, or PGDB). The PGDBs are essentially knowledge bases that users can query and visualize. For instance, dead-end metabolite analysis and visualization of predicted reaction fluxes can be done easily under "cellular overview" option of the software (Figure 1(a)). A collection of approximately 3,530 PGDBs can be found in BioCyc, which users can visualize, manage, and analyze. Out of these 3,530 PGDBs, only 7 relate to algae (both prokaryotic and eukaryotic), namely, *Thalassiosira pseudonana*, *Nannochloropsis gaditana*, *Acaryochloris marina*, *Anabaena cylindrica*, *Anabaena variabilis*, *Synechococcus elongatus,* and *Chlamydomonas reinhardtii*. None of the aforementioned algal PGDBs are well-curated with most of them having had slight validation. One of the intensively curated PGDBs is MetaCyc [19–21], which serves as a generic knowledge base that organism-specific networks can be reconstructed from. *Homo sapiens* (HumanCyc), *E. coli* (EcoCyc), and *Arabidopsis* (AraCyc) are some examples of curated, species-specific knowledge bases that can be found in BioCyc (http://biocyc.org/). Kbase (http://kbase.us/) and Biomart [22] are other examples of knowledge bases and knowledge-management platforms that are freely available and allow integration and reconciliation of a variety of data sources.

Genome-scale metabolic reconstructions have continued to expand along with the increased availability of sequenced, annotated genomes. Recent reviews describe the timeline of the appearance of publicly available metabolic models since 1999 for eukaryotes, prokaryotes and archea, and the algorithms that were used [23, 24]. The processes require inputs from different databases and experimental validations. A standard procedure for the reconstruction of genome-scale metabolic networks has been described in detail by Thiele and Palsson [25].

The process of network reconstruction, starting from genome sequences to the finished reconstructed network, is generally time-consuming and labor-intensive. Therefore, automation of the process has been of interest. A limited number of software tools for automated reconstruction are

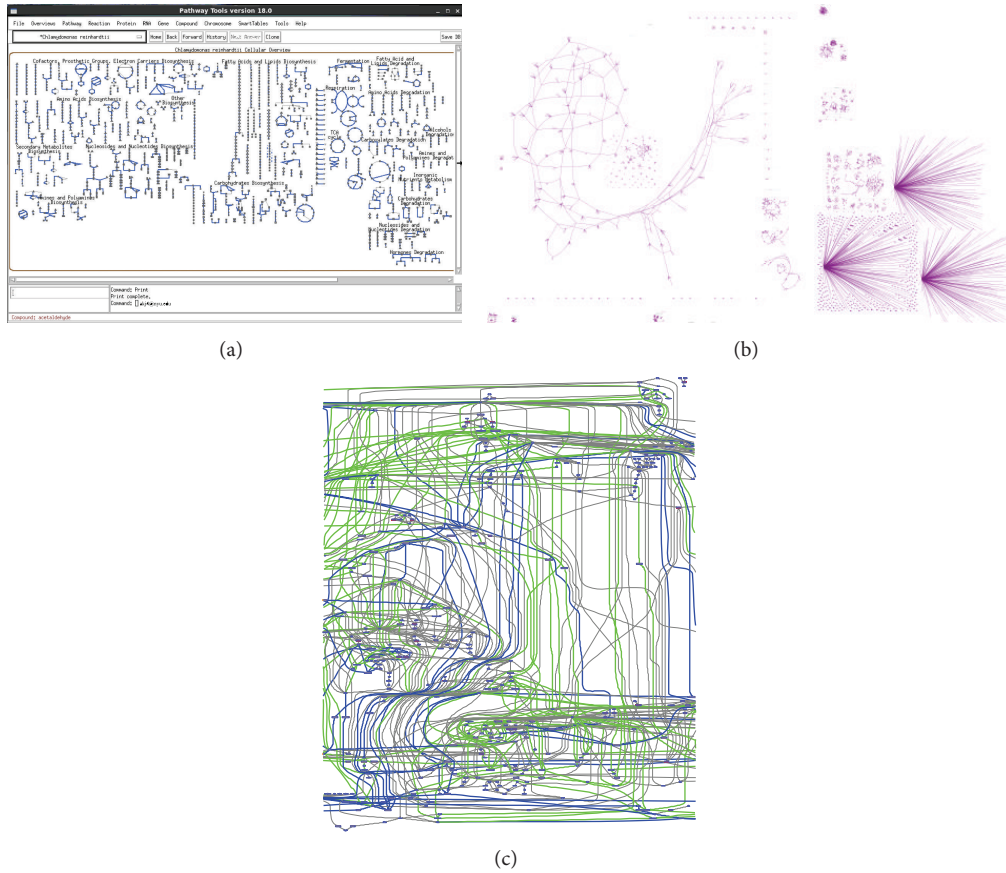

(a) (b)

(c)

Figure 1: A screen shot of (a) Pathway Tools based on *C. Reinhardtii* (unpublished data) (b) Metdraw (based on the *C. reinhardtii* iRC1080 metabolic model [82]) (c) Paint4net visualization of *C. reinhardtii* central metabolism (based on iAM303 model [84]) flux distribution is shown with forward and reverse fluxes (green and blue, respectively).

Table 2: Selected software for genome-scale metabolic reconstruction (adapted from Liao et al., 2012 [27]; Agren et al., 2013 [33]; and Hamilton and Reed, 2014 [34]).

	RAVEN	Model SEED	SuBliMinal	GEMSiRV	Pathway Tools	COBRA toolbox
Input	Annotated genome sequence	Genome annotated in RAST	Species name	Model in sbml format	Annotated genome sequence	Model in sbml format
Reference databases	KEGG	SEED	KEGG, MetaCyc	KEGG	MetaCyc	N/A
Interface	MatLab	Web	Command line	Software	Web, software	MatLab
License	Free (requires a MatLab license)	Free	Free	Free	Free for academic and government use	Free (requires a MatLab license)
Simulation	Yes	Yes	No	Yes	Yes	Yes
Visualization	Yes	Yes (with Cytoscape plug-in)	No	Yes	Yes	Yes (with plug-in)

currently available (some examples are given in Table 2); for instance, AUTOGRAPH [26], GEMSiRV [27], MicrobesFlux [28], MetRxn [29], Model SEED [17, 30], SuBliMinaL Toolbox [31], FAME [32], and RAVEN Toolbox [33] can be named. A systematic comparison between some of these platforms can be found in [34]. While draft metabolic models can be generated through such software tools, intensive manual curation is still needed to resolve errors; wrong assignments, fill gaps and reconcile inconsistencies in the generated network.

3. Pathway Visualization

Visualization is a powerful approach to leverage understanding of pathways and reconstructed metabolic networks. In

metabolic networks, nodes represent metabolites and edges denote reactions. There are a number of web-based tools to visualize biochemical and metabolic pathways; for example, Biocarta (http://www.biocarta.com/), ExPaSy (Expert Protein Analysis System, http://www.expasy.org/), and KEGG (Kyoto Encyclopedia of Genes and Genomes) can be named; however, most are static pages with only a few resources allowing authorized users to edit the pathways. The advantages that BioCyc/MetaCyc offer compared to KEGG include the ability to carry out pathway analysis, operon prediction, or comparative pathway analysis (for more details see [35]) and visualize the results.

Cytoscape [36, 37] is a biological network visualization and data integration tool that can be used to visualize the results from FBA studies (please see Constraint Based Analysis section for information on FBA). CytoSEED [38] is a Cytoscape plug-in to visualize results from the Model SEED. Fluxviz [39] is another Cytoscape plug-in to visualize flux distribution in the molecular interaction network. VANTED [40, 41] is another data visualization and data integration tool which can be utilized as a stand-alone tool. FluxMap [42] and FBA-SimVis [43] are VANTED plug-in for visualization of metabolic flux after FBA analysis. In addition, Paint4net [44] is a tool to automatically generate maps of reaction fluxes in conjunction with COBRA toolbox (Figure 1(c)).

Most recently, MetDraw [45], a new tool for visualization of genome-scale metabolic networks, has been developed (Figure 1(b)). This tool is compatible with systems biology markup language (SBML) file inputs and allows export of the map image as SVG files. It also allows visualization of metabolomics and reaction fluxes added to gene-protein expression data and overlays all of them on the reconstructed network map. The range of file formats available for data export render the postmodification of the maps, with commonly used image editing software, a simple task.

4. Model Refinement and Gap Filling

Although the generation of metabolic network models has been gaining momentum, these models may not provide a complete or accurate representation of metabolism. Particularly, automated modeling has allowed the faster generation of network models, yet reconciliation between the model itself and the biochemical and genomic data is invariably needed. Such model refinements lead to a more accurate reconstruction, allowing more accurate downstream analyses. A common step in such reconstruction refinements is filling reaction gaps to decrease the numbers of dead-end metabolites and enhance the network connectivity. Several tools and algorithms have been set in place to address gap finding and gap filling in metabolic network reconstructions. Some of these tools include, but are not limited to, Gapfill, MEP, GrowMatch, BNICE, and the hole filler in Pathway tools.

4.1. Gapfind and Gapfill. These tools have been developed using two distinct algorithms that initially identify (Gapfind) what the authors have called a "no production" or "no consumption" metabolites [46] through analyzing the production or consumption fluxes in the metabolic model. Subsequently, the identified no production/consumption metabolites are considered as "gaps" and the Gapfill algorithm will attempt to fill them through four major ways. Initially, the algorithm will consider all of the available reactions in the model and reverse them; it will then attempt to import reactions that involve the metabolites from well-curated databases such as MetaCyc [10]. Lastly, it will attempt to fill these gaps by adding transport reactions either internal transport ones, as in from one cellular compartment to the other, or external transport reactions that can either take from or excrete to the extracellular medium.

4.2. MEP and Pathway Tools Hole Filler. On the other hand MEP and Pathway Tools hole filler represent an alternative approach that tackles the gap filling issue identifying missing genes rather than missing reactions, and these tools achieve this goal using expression data and species homology, respectively. As such, this will eventually lead to the expansion of the reconstructed model to include more genes and enzymes and possibly rewire the connectivity of the network [47, 48].

4.3. GrowMatch. This tool has been developed as a model refinement tool rather than a gap filler tool where the aim of such an application would be to reconcile inconsistencies between metabolic model predictions *in silico* and growth data *in vivo*. This computational tool can suggest suppression of specific genes to resolve what is referred to as Growth No Growth (GNG) inconsistencies and alternatively adds functionalities to genes to resolve No Growth/Growth (NGG) inconsistencies [49].

4.4. BNICE. It is a framework that considers specific pathways rather than the full-scale model and allows for the optimization of the pathways. It identifies all possible chemical compounds that can be produced by the reactions and enzymes of the pathway [50]. Although this tool is not a model refinement tool *per se*, the outcome of the pathway optimization can ultimately lead to provisional addition of compounds to the metabolic model and subsequent searches (independently from the tool) for the corresponding genes to provide genomic evidence for the pathway. This approach is similar in outcome to the Gapfind/Gapfill approach.

All of the above and many more tools are of critical importance in the manual curation of metabolic network models. Although the above-mentioned tools ultimately lead to a similar outcome, each may present unique advantages and has specific requirements (Table 3). The choice and use of such tools would thus lead to a higher quality reconstruction and most importantly a higher predictive power.

5. Constraint-Based Modeling, FBA, and Integration of Expression Data

Subsequent to generation of well-curated metabolic network models of organisms, several downstream applications can be used to explore the emergent system's properties. Having

Table 3: A comparative table contrasting some of the major model refinement tools.

	Gapfind and Gapfill	GrowMatch	BNICE	MEP	Pathway Tools hole filler
Require a reconstructed metabolic model	Yes	Yes	No	Yes	Yes
Additional requirements	External databases, e.g., MetaCyc	Requires *in vivo* data collection	Requires the translation of reactions and substrates into mathematical matrices	Requires expression data analysis	Requires species homology analysis
Refinement strategy	Identifies missing reactions or reverses available reactions	Suppresses genes or adds functionalities associated with genes in the initial model to reconcile the model with *in vivo* data	Optimizes pathways in a way that can provide feedback into the model adding compounds and substrates	Identifies missing genes in the model	Identifies missing genes in the model

a network set in place, the fluxes of each of the component reactions can be evaluated and moreover modified in an attempt to increase or decrease the production or consumption of key metabolites. In the case of algal biofuel optimization, it is of high interest to achieve directional overproduction of lipids that constitute the basis for algal biofuels. Making use of the known metabolic networks and via a constraint based modeling approach, the identification of genes, pathways, and knockout strategies, that interfere or alter, the expression profiles relevant to production of enzymes related to lipid synthesis and metabolites involved in lipid synthesis pathways is readily achievable. This can be done through a number of computational tools with the outcomes evaluated *in silico* using flux balance analysis (FBA) [51] and further validated by *in vivo* experiments.

FBA constrains the metabolite fluxes and their biochemical reactions by four main parameters: mass conservation, thermodynamics (reaction reversibility), steady state assumption for internal metabolite concentrations, and nutrient availability. Based on these constraints, reaction boundaries are set, and a system of linear differential equations is solved with a biologically relevant objective function optimized. The solution space for an FBA can be reduced in size by more constraints and boundaries imposed on reactions and fluxes where the optimal flux distribution achieving the optimized function is a feasible solution for the problem.

Some of the available tools and algorithms that are able to perform such tasks include (but are not restricted to) Optknock, Optstrain, Optflux, MTA, iMAT, BioMet toolbox, PROM, GIMME, E-Flux, MADE, SIMUP, and TIGER, with some allowing the integration of expression data to the metabolic model. These tools are described below.

5.1. GIMME, iMAT, and MADE. Gene inactivity moderated by metabolism and expression (GIMME) [52] is a tool that allows for the integration of expression data to metabolic networks yet optimizing the functionality of the model towards a set objective function by minimizing the use of reaction categorized as inactive. GIMME reduces the sets of reactions to a binary on/off mode whereas each reaction flux is compared to a set threshold and deemed "off" if the flux does not reach that value [53, 54]. Similarly, integrative metabolic analysis tool (iMAT) [55] performs the same task as GIMME in such a way that transcript levels of genes are compared and the corresponding reactions are then assigned value of −1, 0, and 1 to refer to low, moderate, or high levels of expression. Further ahead, the algorithm will then optimize the model to make use of as many reactions having "1" coefficient and decreases the reactions with "−1" coefficient in order to achieve a set objective function. Here too, a threshold needs to be set for expression data comparison to be done. As both iMAT and GIMME require a manually set threshold, this gives rise to biases. In an attempt to evade such a complication, MADE [56], or metabolic adjustment by differential expression, has been developed to carry out similar tasks as the previous two tools yet without the need of manual assignment of a threshold. It will rather require as input expression data originating from more than one condition and will then comparatively, based on the differential expression of each of the genes under each of the conditions, set a threshold based on which the reactions will then be reduced to binary on/off code [53, 54].

5.2. E-Flux. While the above-mentioned tools allow the incorporation of expression data to metabolic model reconstructions and subsequently allow optimization of these models towards a set objective function by suppressing reactions categorized as inactive or of low activity, E-flux allows for this optimization through constraining the upper bounds of the metabolite fluxes based on the expression data by imposing tight constraints on metabolites and reactions where the fluxes will not reach a set value and vice versa [57].

Table 4: A comparative table contrasting major constraint based modeling tools (adapted from Blazier and Papin 2012 [53]).

	GIMME	iMAT	MADE	E-Flux	SIMUP	MTA
Description	Determines sets of active versus inactive reactions comparing expression levels to a set threshold optimizing the model towards a set objective function	Categorizes reactions into high, moderate, and low expression and solves mathematical equation to optimize for an objective function	Establishes a differential expression profile using several datasets originating from different growth conditions	Sets upper bounds for lowly expressed reactions using an externally set threshold to evaluate expression data sets	Identifies bioengineering strategies that force the cell to coutilize substrates achieving a state of "synthetic survival"	Predicts gene knockout strategies that would alter the metabolic fluxes in a cell in order to achieve the objective function assumed
Advantages	Requires one set of expression data	Requires no knowledge of metabolic functions	Requires no externally set threshold for expression levels	Requires no reduction of expression data to an on/off categorization	Achieves the coutilization of two sugars	Categorizes cell metabolism as "source" or "target" with no necessary *a priori* knowledge of functionalities
Disadvantages	Requires an externally set threshold for mRNA transcript values	Categorizes genes into high, moderate, and low expression	Requires more than one dataset of expression data to establish differential expression profiles	Sets an upper bound on fluxes using a specific function converting expression data	So far only applicable to sugars	Requires gene expression profiles in order to identify knockout strategies

5.3. Optknock, Optstrain, and Optflux. These tools have been used to identify gene knockout strategies (Optknock) [58] that lead to the overproduction of a target metabolite or overexpression strategies (Optstrain) [59] that result into an optimized strain with respect to a set objective function. Optflux on the other hand uses evolutionary algorithms and the previously mentioned Optknock algorithm to identify metabolic engineering targets as well as a range of other applications from phenotype simulations to metabolic flux analysis and calculation of elementary flux mode [60].

5.4. BioMet Toolbox. It is a web-based resource that can be used to perform stoichiometric analyses and integration of transcriptome and interactome data to a metabolic network. It also allows performing linear programming simulations, optimizing for an increased or decreased growth rate, as well as substrate consumption and production. Single or double knockout simulations can also be achieved as well as the detection of key metabolites around which high transcriptional activity is noted [61].

5.5. MTA. Metabolic transformation algorithm [62] is an alternative approach that leads to the prediction of gene knockout strategies able to shift the metabolism of a cell and alter its state from a "source" state to a "target" state. Gene expression profiles are used in order to predict knockouts that modify the flux distribution of the source state in a way to match the desired target state.

5.6. TIGER. It is a toolbox that can be used to integrate expression, metabolic and regulatory information into a genome scale model. It also accounts for gene-protein-reaction associations and couples it with its regulatory profile. One of its added values is its ability to identify model inconsistencies and thus it allows for a modification of the reconstructed network above and beyond being an integration tool [63].

5.7. SIMUP. Most recently, this algorithm was reported offering one unique feature with respect to all of the above introduced tools. The algorithm aids in identifying metabolic engineering strategies that can force the cell to coutilize two different sugar substrates thus, in effect, placing the cell in a "synthetic survival" state in a way that the cell is now forced to metabolize two different sugars simultaneously instead of preferentially consuming one. The net effect can be to simplify the fermentation cycle [64, 65].

In the context of biofuels, all of the above algorithms and tools present huge potential for achieving higher production of the desired bioproducts in microorganisms. The preferential use of one tool over the other may depend on the nature of data available rather than the ultimate goal (Table 4). The identification of knockout strategies that could alter the lipid metabolism by overproducing it, or the detection of highly regulated key metabolites in the lipid pathway, or even achieving a strain able to coutilize two separate sources of energy for its survival, all represent promising outcomes of such applications and several attempts have been already made making use of such algorithms (the results could be found in more detail in the published articles [66, 67]).

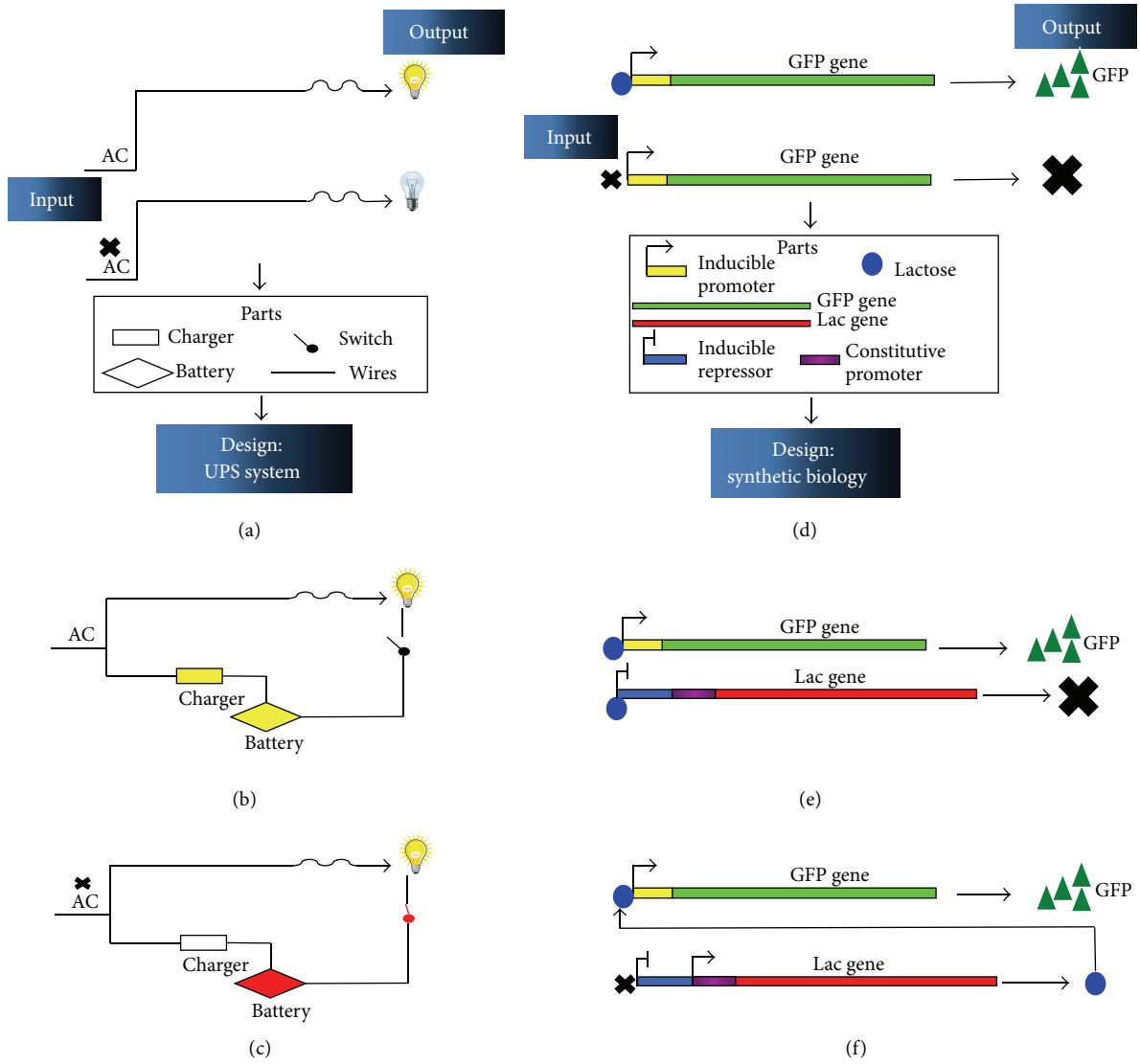

FIGURE 2: A schematic representation of a comparative design of electrical and analogous biological circuit. (a) and (d) represent the initial states of the circuits in presence and absence of the input. (b), (c), (e), and (f) represent the designed circuit, addressing the issue raised by the "wild type" design of (a) and (d) when the input signal is interrupted or is not present.

6. Omics Data Integration Tools

Beyond the integration of expression data to network models, a deeper understanding of the functional model requires further integration of proteomics, metabolomics, fluxomics, and phenotypic data with transcriptomics data. Computational tools and algorithms have been recently set forth to achieve the aforementioned integrations. IOMA, MASS, and MBA are examples of such endeavors.

6.1. IOMA. Integrative omics-metabolic analysis is an algorithm that allows the integration of metabolomics and proteomic data to the metabolic network model and also evaluates the kinetics of the reactions included [68].

6.2. MASS. Mass action stoichiometric simulation [69] achieves integration of fluxomic data on top of the metabolomics and proteomics data sets which leads to the dynamic reconstruction of the model in place.

6.3. MBA. Model-building algorithm [70] has been recently reported with an added feature allowing it to also integrate phenotypic data on top of all the above-mentioned omics data sets, thus potentially leading to tissue-specific model reconstruction.

With respect to phenotypic data, one interesting tool that may generate such type of data and can be used in conjunction with MBA, for example, is the Biolog phenotype microarray technology [71, 72]. The Biolog is a powerful technology providing high-throughput quantitation of phenotypic data, useful in identifying additional biochemical assays and improving a metabolic model reconstruction.

The phenotype microarray (PM) technology developed by Biolog (Hayward, CA, USA) can be used for the

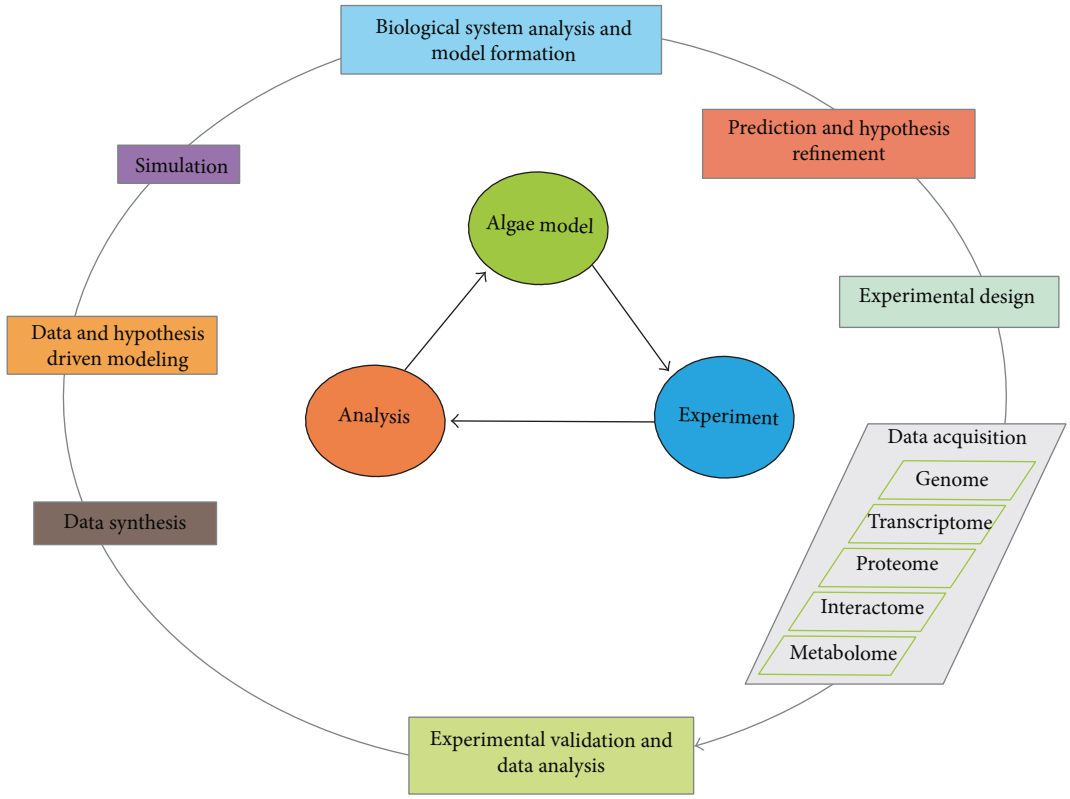

FIGURE 3: A conceptual representation of algal model reconstruction and refinement, integrating various sets of omics data and experimental validation of predictions (based on Manichaikul et al., 2009 [84]).

phenotypic analysis. Biolog is an *in vitro* assay that measures the respiration of cells as a function of time in hundreds of microwells simultaneously. Each PM plate contains 96 wells seeded with different metabolite and monitored automatically over time via the OmniLog machine. Metabolite utilization within the cell is determined by the amount of color development produced by a tetrazolium-based redox dye. Various 96-well metabolite plates (or PMs) can be used to measures carbon source, nitrogen, sulfur, and phosphorus utilization phenotypes. Some plates were used to test for osmotic/ion and pH effects. Data analysis is performed using the opm software package [73]. The Biolog technology has also been successfully used to fill gaps in metabolic networks to enhance models [74].

7. Bioengineering, Parts and Circuits

With all of the above tools readily available to use and many others currently in use but not described in this review, the identification of new pathways and reactions has been made easier than ever before. In the context of bioengineering, the significance of these computational tools is in guiding wet-bench experimental design as opposed to providing solely theoretical insight into the system as a whole. More specifically, with regard to biofuel production, the identification of knockout strategies or differential expression of genes or enzymes that might lead to overproduction of biofuels would be only of theoretical value if not coupled with more applicable approaches to achieve the targets *in vivo*. This is where the contributions of synthetic biology approaches are of crucial importance and significance. Once the target pathways have been identified, the parts forming those pathways, in engineering terms, are to be made available in order to mimic the cell metabolic circuitry and alter it. Parts are defined as genes and ribosomal binding sites, promoters, terminators, and polymerases [75]. Most recently, Talebi et al. have successfully achieved a 12% increase in the total lipid content of the microalgae *Dunaliella salina*, transforming it witha bioengineered plasmid comprising specific parts, genes, and inducible promoters, driving the cellular carbon flux into the fatty acids biosynthesis pathway [76].

Biological circuits are furthermore defined as a designed device made out of a set of parts and engineered in a way to confer an added functionality to a system. Figure 2 illustrates, in a comparative approach to electrical circuits, what a newly designed biological circuit can achieve. A number of biological circuits have been previously realized [77–79] and genetic parts are now made available through a number of databases such as the MIT Registry of Standard Biological Parts' (http://partsregistry.org/). A more in-depth review on the tools and applications that lead to the design of circuits was published by Marchicio et al. and can be referred to for more details [80].

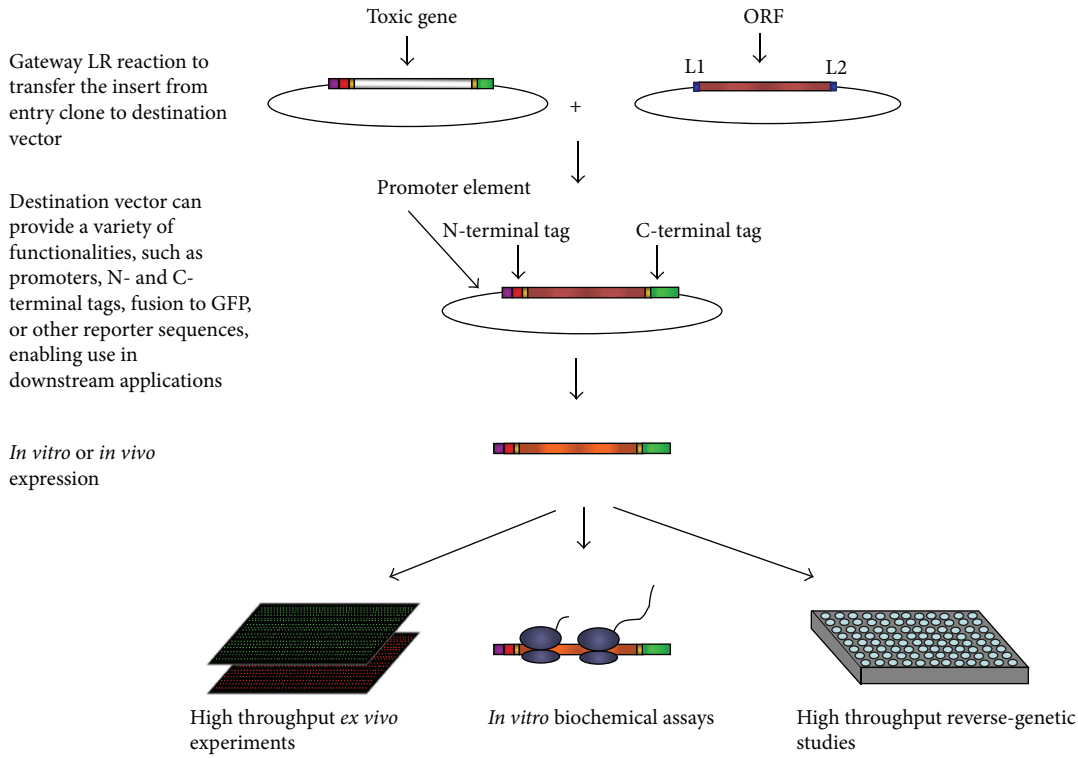

Figure 4: A summary figure representing recombinational transferring of an ORF from a gateway vector in which the initial cloning was done into destination vectors for downstream applications, including high throughput experiments and biochemical assays. Once an ORF is cloned into an "entry vector," the ORF can easily be transferred into many "destination vectors" with desired expression capabilities and tags [87].

8. Emerging Algal-Specific Computational and Experimental Resources

Optimizing algae for biofuel production requires a deep understanding of algal metabolic networks with genomic, fluxomics, proteomics, and metabolomics data integration. Figure 3 conceptualizes an integrative approach to build, refine, and validate an algae based metabolic model with predictive power to guide potential bioengineering targets aimed at optimizing algae for biofuel production.

Furthermore, a better understanding of the biological system through functional modeling using data generated from the sequencing technologies is still one of the research challenges. Functional modeling requires gene ontology (GO) annotation for enrichment analysis. GO enrichment analysis tools identify GO terms with statistical significance in the reference set. Algal Functional Annotation Tool is the algae-specific genome annotation tool that uses gene lists from AUGUSTUS, JGI, or phytozome gene models for *Chlamydomonas reinhardtii* and *Chlorella* NC64A [81] to perform functional term enrichment. This functional annotation tool provides analytical power for interpretation of obtained large-scale experimental data.

Interestingly, a new approach in bioengineering, transcription factor engineering approach (TFE) [67], is regarded as a highly promising approach and considers transcription factors as parts able to modify biological circuits. An ongoing work (in the authors' laboratory) is now attempting to systematically clone transcription and chromatin factors (TF and CF) of *C. reinhardtii* thus making available to the scientific community a full library of TF and CF parts that can easily be introduced as part of a new design. Figure 4 represents one step further downstream the initial cloning and describes the transfer of cloned ORFs from the entry vector to the destination vector of choice. These ORFs can be considered as potential parts to be used in bioengineering endeavors when model-based predictions call for their use. Furthermore, the metabolic ORFeome of *C. reinhardtii* has been previously generated and the reconstruction of its central metabolic network has been done [82–84]. Following that, genome-scale reconstructed networks of *C. reinhardtii* were released accounting for around 2000 reactions and their associated genes and metabolites [82, 85]. Added to these models, a PGDB for *C. reinhardtii* has been made available as ChlamyCyc [86] making use of Pathway Tools platform and thus making the investigations of the metabolic and regulatory networks of such algae far more at hand. Prior and in parallel to these advances a species specific resource, Chlamydomonas Resource Center (http://chlamycollection.org/), has served the algal community offering a library of Chlamydomonas strains amongst other parts and tools, which provide needed resources for experimental protocols targeting various aspects of algal biology, including the metabolism of lipids and biofuels in this organism.

9. Conclusion

The above reviewed computational tools and approaches in conjunction with the high interests of the scientific community in synthetic biology offer a new perspective in accelerating biofuel production and microalgal optimization research. The pressing economical and environmental challenges of the use of fossil fuels will furthermore lead to a positive selective pressure towards the use of these strategies aiming at the optimization of biofuel producing strains. A large set of biofuel types can serve as alternative energy sources which currently include ethanol, n-butanol, iso-butanol, short chain alcohols, short chain alkanes, biodiesel (FAMEs), and fatty alcohols. These tools and applications are promising yet much more optimizations need to be achieved in order for biofuel production to compete with available fossil fuels. With the "green revolution" and the more environmentally conscious population, we expect this field to expand significantly in the coming years, building on the available resources for systems and synthetic biology and achieving the generation of strains optimized for biofuel production.

Conflict of Interests

The authors declare that there is no conflict of interests.

Acknowledgments

Major support for this work was provided by New York University Abu Dhabi Institute grant G1205 and NYU Abu Dhabi Faculty Research Funds AD060. The authors thank Basel Khraiwesh and Ashish Jaiswal for designing some of the figures and Bushra Saeed Dohai for discussions.

References

[1] J. E. Koskimaki, A. S. Blazier, A. F. Clarens, and J. A. Papin, "Computational models of algae metabolism for industrial applications," *Industrial Biotechnology*, vol. 9, no. 4, pp. 185–195, 2013.

[2] R. Usaite, K. R. Patil, T. Grotkjær, J. Nielsen, and B. Regenberg, "Global transcriptional and physiological responses of Saccharomyces cerevisiae to ammonium, L-alanine, or L-glutamine limitation," *Applied and Environmental Microbiology*, vol. 72, no. 9, pp. 6194–6203, 2006.

[3] R. M. Zelle, E. de Hulster, W. A. van Winden et al., "Malic acid production by Saccharomyces cerevisiae: engineering of pyruvate carboxylation, oxaloacetate reduction, and malate export," *Applied and Environmental Microbiology*, vol. 74, no. 9, pp. 2766–2777, 2008.

[4] M. Izallalen, R. Mahadevan, A. Burgard et al., "Geobacter sulfurreducens strain engineered for increased rates of respiration," *Metabolic Engineering*, vol. 10, no. 5, pp. 267–275, 2008.

[5] M. A. Oberhardt, B. Ø. Palsson, and J. A. Papin, "Applications of genome-scale metabolic reconstructions," *Molecular Systems Biology*, vol. 5, no. 1, article 320, 2009.

[6] P. D. Karp, S. M. Paley, M. Krummenacker et al., "Pathway Tools version 13.0: integrated software for pathway/genome informatics and systems biology," *Briefings in Bioinformatics*, vol. 11, no. 1, Article ID bbp043, pp. 40–79, 2009.

[7] I. Schomburg, A. Chang, S. Placzek et al., "BRENDA in 2013: integrated reactions, kinetic data, enzyme function data, improved disease classification: new options and contents in BRENDA," *Nucleic Acids Research*, vol. 41, no. 1, pp. D764–D772, 2013.

[8] P. Artimo, M. Jonnalagedda, K. Arnold et al., "ExPASy: SIB bioinformatics resource portal," *Nucleic Acids Research*, vol. 40, no. 1, pp. W597–W603, 2012.

[9] T. U. Consortium, "Ongoing and future developments at the Universal Protein Resource," *Nucleic Acids Research*, vol. 39, supplement 1, pp. D214–D219, 2011.

[10] R. Caspi, T. Altman, R. Billington et al., "The MetaCyc database of metabolic pathways and enzymes and the BioCyc collection of Pathway/Genome databases," *Nucleic Acids Research*, vol. 42, no. 1, pp. D459–D471, 2014.

[11] M. Kanehisa, S. Goto, Y. Sato, M. Furumichi, and M. Tanabe, "KEGG for integration and interpretation of large-scale molecular data sets," *Nucleic Acids Research*, vol. 40, no. 1, pp. D109–D114, 2012.

[12] D. Croft, G. O'Kelly, G. Wu et al., "Reactome: a database of reactions, pathways and biological processes," *Nucleic Acids Research*, vol. 39, supplement 1, pp. D691–D697, 2011.

[13] J. Schellenberger, J. O. Park, T. M. Conrad, and B. T. Palsson, "BiGG: a Biochemical Genetic and Genomic knowledgebase of large scale metabolic reconstructions," *BMC Bioinformatics*, vol. 11, article 213, 2010.

[14] S. A. Becker, A. M. Feist, M. L. Mo, G. Hannum, B. Ø. Palsson, and M. J. Herrgard, "Quantitative prediction of cellular metabolism with constraint-based models: the COBRA Toolbox," *Nature Protocols*, vol. 2, no. 3, pp. 727–738, 2007.

[15] J. Schellenberger, R. Que, R. M. T. Fleming et al., "Quantitative prediction of cellular metabolism with constraint-based models: the COBRA Toolbox v2.0," *Nature Protocols*, vol. 6, no. 9, pp. 1290–1307, 2011.

[16] S. G. Thorleifsson and I. Thiele, "rBioNet: a COBRA toolbox extension for reconstructing high-quality biochemical networks," *Bioinformatics*, vol. 27, no. 14, Article ID btr308, pp. 2009–2010, 2011.

[17] S. Devoid, R. Overbeek, M. DeJongh et al., "Automated genome annotation and metabolic model reconstruction in the SEED and model SEED," in *Systems Metabolic Engineering*, pp. 17–45, 2013.

[18] P. D. Karp, S. Paley, and P. Romero, "The pathway tools software," *Bioinformatics*, vol. 18, supplement 1, pp. S225–S232, 2002.

[19] R. Caspi, T. Altman, J. M. Dale et al., "The MetaCyc database of metabolic pathways and enzymes and the BioCyc collection of pathway/genome databases," *Nucleic Acids Research*, vol. 38, supplement 1, Article ID gkp875, pp. D473–D479, 2009.

[20] R. Caspi, T. Altman, K. Dreher et al., "The MetaCyc database of metabolic pathways and enzymes and the BioCyc collection of pathway/genome databases," *Nucleic Acids Research*, vol. 40, no. 1, pp. D742–D753, 2012.

[21] R. Caspi, H. Foerster, C. A. Fulcher et al., "The MetaCyc database of metabolic pathways and enzymes and the BioCyc collection of Pathway/Genome databases," *Nucleic Acids Research*, vol. 36, supplement 1, pp. D623–D631, 2008.

[22] A. Kasprzyk, "BioMart: driving a paradigm change in biological data management," *Database*, vol. 2011, Article ID bar049, 2011.

[23] T. Y. Kim, S. B. Sohn, Y. B. Kim, W. J. Kim, and S. Y. Lee, "Recent advances in reconstruction and applications of genome-scale

metabolic models," *Current Opinion in Biotechnology*, vol. 23, no. 4, pp. 617–623, 2012.

[24] M. A. Oberhardt, J. Puchałka, V. A. P. M. dos Santos, and J. A. Papin, "Reconciliation of genome-scale metabolic reconstructions for comparative systems analysis," *PLoS Computational Biology*, vol. 7, no. 3, Article ID e1001116, 2011.

[25] I. Thiele and B. Ø. Palsson, "A protocol for generating a high-quality genome-scale metabolic reconstruction," *Nature Protocols*, vol. 5, no. 1, pp. 93–121, 2010.

[26] R. A. Notebaart, F. H. J. van Enckevort, C. Francke, R. J. Siezen, and B. Teusink, "Accelerating the reconstruction of genome-scale metabolic networks," *BMC Bioinformatics*, vol. 7, article 296, 2006.

[27] Y.-C. Liao, M.-H. Tsai, F.-C. Chen, and C. A. Hsiung, "GEM-SiRV: a software platform for GEnome-scale metabolic model simulation, reconstruction and visualization," *Bioinformatics*, vol. 28, no. 13, Article ID bts267, pp. 1752–1758, 2012.

[28] X. Feng, Y. Xu, Y. Chen, and Y. J. Tang, "MicrobesFlux: a web platform for drafting metabolic models from the KEGG database," *BMC Systems Biology*, vol. 6, article 94, 2012.

[29] A. Kumar, P. F. Suthers, and C. D. Maranas, "MetRxn: A knowledgebase of metabolites and reactions spanning metabolic models and databases," *BMC Bioinformatics*, vol. 13, no. 1, article 6, 2012.

[30] C. S. Henry, M. Dejongh, A. A. Best, P. M. Frybarger, B. Linsay, and R. L. Stevens, "High-throughput generation, optimization and analysis of genome-scale metabolic models," *Nature Biotechnology*, vol. 28, no. 9, pp. 977–982, 2010.

[31] N. Swainston, K. Smallbone, P. Mendes, D. Kell, and N. Paton, "The SuBliMinaL Toolbox: automating steps in the reconstruction of metabolic networks," *Journal of Integrative Bioinformatics*, vol. 8, article 186, no. 2, 2011.

[32] J. Boele, B. G. Olivier, and B. Teusink, "FAME, the flux analysis and modeling environment," *BMC Systems Biology*, vol. 6, no. 1, p. 8, 2012.

[33] R. Agren, L. Liu, S. Shoaie, W. Vongsangnak, I. Nookaew, and J. Nielsen, "The RAVEN toolbox and its use for generating a genome-scale metabolic model for penicillium chrysogenum," *PLoS Computational Biology*, vol. 9, no. 3, Article ID e1002980, 2013.

[34] J. J. Hamilton and J. L. Reed, "Software platforms to facilitate reconstructing genome-scale metabolic networks," *Environmental Microbiology*, vol. 16, no. 1, pp. 49–59, 2014.

[35] T. Altman, M. Travers, A. Kothari, R. Caspi, and P. D. Karp, "A systematic comparison of the MetaCyc and KEGG pathway databases," *BMC Bioinformatics*, vol. 14, article 112, 2013.

[36] M. E. Smoot, K. Ono, J. Ruscheinski, P.-L. Wang, and T. Ideker, "Cytoscape 2.8: new features for data integration and network visualization," *Bioinformatics*, vol. 27, no. 3, pp. 431–432, 2011.

[37] R. Saito, M. E. Smoot, K. Ono et al., "A travel guide to Cytoscape plugins," *Nature Methods*, vol. 9, no. 11, pp. 1069–1076, 2012.

[38] M. DeJongh, B. Bockstege, P. Frybarger, N. Hazekamp, J. Kammeraad, and T. McGeehan, "CytoSEED: a Cytoscape plugin for viewing, manipulating and analyzing metabolic models created by the model SEED," *Bioinformatics*, vol. 28, no. 6, pp. 891–892, 2012.

[39] M. König and H. Holzhütter, "Fluxviz-cytoscape plug-in for visualization of flux distributions in networks," in *Proceedings of the International Conference on Genome Informatics*, 2010.

[40] H. Rohn, A. Junker, A. Hartmann et al., "VANTED v2: a framework for systems biology applications," *BMC Systems Biology*, vol. 6, article 139, 2012.

[41] B. H. Junker, C. Klukas, and F. Schreiber, "Vanted: a system for advanced data analysis and visualization in the context of biological networks," *BMC Bioinformatics*, vol. 7, article 109, 13 pages, 2006.

[42] H. Rohn, A. Hartmann, A. Junker, B. H. Junker, and F. Schreiber, "FluxMap: A VANTED add-on for the visual exploration of flux distributions in biological networks," *BMC Systems Biology*, vol. 6, article 33, 2012.

[43] E. Grafahrend-Belau, C. Klukas, B. H. Junker, and F. Schreiber, "FBA-SimVis: interactive visualization of constraint-based metabolic models," *Bioinformatics*, vol. 25, no. 20, pp. 2755–2757, 2009.

[44] A. Kostromins and E. Stalidzans, "Paint4Net: COBRA Toolbox extension for visualization of stoichiometric models of metabolism," *BioSystems*, vol. 109, no. 2, pp. 233–239, 2012.

[45] P. A. Jenseny and J. A. Papin, "MetDraw: automated visualization of genome-scale metabolic network reconstructions and high-throughput data," *Bioinformatics*, vol. 30, no. 9, pp. 1327–1328, 2014.

[46] V. Satish Kumar, M. S. Dasika, and C. D. Maranas, "Optimization based automated curation of metabolic reconstructions," *BMC Bioinformatics*, vol. 8, article 212, 2007.

[47] P. Kharchenko, D. Vitkup, and G. M. Church, "Filling gaps in a metabolic network using expression information," *Bioinformatics*, vol. 20, supplement 1, pp. i178–i185, 2004.

[48] M. L. Green and P. D. Karp, "A Bayesian method for identifying missing enzymes in predicted metabolic pathway databases," *BMC Bioinformatics*, vol. 5, article 76, 2004.

[49] V. S. Kumar and C. D. Maranas, "GrowMatch: an automated method for reconciling *In Silico*/*In Vivo* growth predictions," *PLoS Computational Biology*, vol. 5, no. 3, 2009.

[50] V. Hatzimanikatis, C. Li, J. A. Ionita, C. S. Henry, M. D. Jankowski, and L. J. Broadbelt, "Exploring the diversity of complex metabolic networks," *Bioinformatics*, vol. 21, no. 8, pp. 1603–1609, 2005.

[51] M. Lakshmanan, G. Koh, B. K. S. Chung, and D.-Y. Lee, "Software applications for flux balance analysis," *Briefings in Bioinformatics*, vol. 15, no. 1, pp. 108–122, 2014.

[52] S. A. Becker and B. O. Palsson, "Context-specific metabolic networks are consistent with experiments," *PLoS Computational Biology*, vol. 4, no. 5, Article ID e1000082, 2008.

[53] A. S. Blazier and J. A. Papin, "Integration of expression data in genome-scale metabolic network reconstructions," *Frontiers in Physiology*, vol. 3, article 299, 2012.

[54] D. Machado and M. Herrgård, "Systematic evaluation of methods for integration of transcriptomic data into constraint-based models of metabolism," *PLoS Computational Biology*, vol. 10, no. 4, Article ID e1003580, 2014.

[55] H. Zur, E. Ruppin, and T. Shlomi, "iMAT: an integrative metabolic analysis tool," *Bioinformatics*, vol. 26, no. 24, pp. 3140–3142, 2010.

[56] P. A. Jensen and J. A. Papin, "Functional integration of a metabolic network model and expression data without arbitrary thresholding," *Bioinformatics*, vol. 27, no. 4, pp. 541–547, 2011.

[57] C. Colijn, A. Brandes, J. Zucker et al., "Interpreting expression data with metabolic flux models: predicting Mycobacterium tuberculosis mycolic acid production," *PLoS Computational Biology*, vol. 5, no. 8, Article ID e1000489, 2009.

[58] A. P. Burgard, P. Pharkya, and C. D. Maranas, "Optknock: a bilevel programming framework for identifying gene knockout strategies for microbial strain optimization," *Biotechnology and Bioengineering*, vol. 84, no. 6, pp. 647–657, 2003.

[59] P. Pharkya, A. P. Burgard, and C. D. Maranas, "OptStrain: a computational framework for redesign of microbial production systems," *Genome Research*, vol. 14, no. 11, pp. 2367–2376, 2004.

[60] I. Rocha, P. Maia, P. Evangelista et al., "OptFlux: an open-source software platform for in silico metabolic engineering," *BMC Systems Biology*, vol. 4, no. 1, article 45, 2010.

[61] M. Cvijovic, R. Olivares-Hernandez, R. Agren et al., "BioMet Toolbox: genome-wide analysis of metabolism," *Nucleic Acids Research*, vol. 38, supplement 2, Article ID gkq404, pp. W144–W149, 2010.

[62] K. Yizhak, O. Gabay, H. Cohen, and E. Ruppin, "Model-based identification of drug targets that revert disrupted metabolism and its application to ageing," *Nature Communications*, vol. 4, 2013.

[63] P. A. Jensen, K. A. Lutz, and J. A. Papin, "TIGER: toolbox for integrating genome-scale metabolic models, expression data, and transcriptional regulatory networks," *BMC Systems Biology*, vol. 5, no. 1, article 147, 2011.

[64] P. Gawand, P. Hyland, A. Ekins, V. J. J. Martin, and R. Mahadevan, "Novel approach to engineer strains for simultaneous sugar utilization," *Metabolic Engineering*, vol. 20, pp. 63–72, 2013.

[65] J.-H. Kim, D. E. Block, and D. A. Mills, "Simultaneous consumption of pentose and hexose sugars: an optimal microbial phenotype for efficient fermentation of lignocellulosic biomass," *Applied Microbiology and Biotechnology*, vol. 88, no. 5, pp. 1077–1085, 2010.

[66] S. K. Lee, H. Chou, T. S. Ham, T. S. Lee, and J. D. Keasling, "Metabolic engineering of microorganisms for biofuels production: from bugs to synthetic biology to fuels," *Current Opinion in Biotechnology*, vol. 19, no. 6, pp. 556–563, 2008.

[67] N. M. D. Courchesne, A. Parisien, B. Wang, and C. Q. Lan, "Enhancement of lipid production using biochemical, genetic and transcription factor engineering approaches," *Journal of Biotechnology*, vol. 141, no. 1-2, pp. 31–41, 2009.

[68] K. Yizhak, T. Benyamini, W. Liebermeister, E. Ruppin, and T. Shlomi, "Integrating quantitative proteomics and metabolomics with a genome-scale metabolic network model," *Bioinformatics*, vol. 26, no. 12, Article ID btq183, pp. i255–i260, 2010.

[69] N. Jamshidi and B. Ø. Palsson, "Mass action stoichiometric simulation models: incorporating kinetics and regulation into stoichiometric models," *Biophysical Journal*, vol. 98, no. 2, pp. 175–185, 2010.

[70] L. Jerby, T. Shlomi, and E. Ruppin, "Computational reconstruction of tissue-specific metabolic models: application to human liver metabolism," *Molecular Systems Biology*, vol. 6, article 401, 2010.

[71] B. R. Bochner, "Global phenotypic characterization of bacteria," *FEMS Microbiology Reviews*, vol. 33, no. 1, pp. 191–205, 2009.

[72] B. R. Bochner, "New technologies to assess genotype-phenotype relationships," *Nature Reviews Genetics*, vol. 4, no. 4, pp. 309–314, 2003.

[73] L. A. I. Vaas, J. Sikorski, V. Michael, M. Göker, and H.-P. Klenk, "Visualization and curve-parameter estimation strategies for efficient exploration of phenotype microarray kinetics," *PLoS ONE*, vol. 7, no. 4, Article ID e34846, 2012.

[74] J. L. Reed, T. R. Patel, K. H. Chen et al., "Systems approach to refining genome annotation," *Proceedings of the National Academy of Sciences of the United States of America*, vol. 103, no. 46, pp. 17480–17484, 2006.

[75] M. H. Medema, R. van Raaphorst, E. Takano, and R. Breitling, "Computational tools for the synthetic design of biochemical pathways," *Nature Reviews Microbiology*, vol. 10, no. 3, pp. 191–202, 2012.

[76] A. F. Talebi, M. Tohidfar, A. Bagheri et al., "Manipulation of carbon flux into fatty acid biosynthesis pathway in Dunaliella salina using AccD and ME genes to enhance lipid content and to improve produced biodiesel quality," *Biofuel Research Journal*, vol. 1, no. 3, pp. 91–97, 2014.

[77] E. Andrianantoandro, S. Basu, D. K. Karig, and R. Weiss, "Synthetic biology: new engineering rules for an emerging discipline," *Molecular Systems Biology*, vol. 2, no. 1, Article ID msb4100073, 2006.

[78] S. A. Benner and A. M. Sismour, "Synthetic biology," *Nature Reviews Genetics*, vol. 6, no. 7, pp. 533–543, 2005.

[79] D. A. Drubin, J. C. Way, and P. A. Silver, "Designing biological systems," *Genes and Development*, vol. 21, no. 3, pp. 242–254, 2007.

[80] M. A. Marchisio and J. Stelling, "Computational design of synthetic gene circuits with composable parts," *Bioinformatics*, vol. 24, no. 17, pp. 1903–1910, 2008.

[81] D. Lopez, D. Casero, S. J. Cokus, S. S. Merchant, and M. Pellegrini, "Algal functional annotation tool: a web-based analysis suite to functionally interpret large gene lists using integrated annotation and expression data," *BMC Bioinformatics*, vol. 12, no. 1, article 282, 2011.

[82] R. L. Chang, L. Ghamsari, A. Manichaikul et al., "Metabolic network reconstruction of Chlamydomonas offers insight into light-driven algal metabolism," *Molecular Systems Biology*, vol. 7, article 518, 2011.

[83] N. R. Boyle and J. A. Morgan, "Flux balance analysis of primary metabolism in Chlamydomonas reinhardtii," *BMC Systems Biology*, vol. 3, article 4, 2009.

[84] A. Manichaikul, L. Ghamsari, E. F. Y. Hom et al., "Metabolic network analysis integrated with transcript verification for sequenced genomes," *Nature Methods*, vol. 6, no. 8, pp. 589–592, 2009.

[85] C. G. de Oliveira Dal'Molin, L.-E. Quek, R. W. Palfreyman, and L. K. Nielsen, "AlgaGEM—a genome-scale metabolic reconstruction of algae based on the *Chlamydomonas reinhardtii* genome," *BMC Genomics*, vol. 12, no. 4, article S5, 2011.

[86] P. May, J. O. Christian, S. Kempa, and D. Walther, "ChlamyCyc: an integrative systems biology database and web-portal for Chlamydomonas reinhardtii," *BMC Genomics*, vol. 10, article 209, 2009.

[87] A. J. M. Walhout, G. F. Temple, M. A. Brasch et al., "GATEWAY recombinational cloning: application to the cloning of large numbers of open reading frames or ORFeomes," *Methods in Enzymology*, vol. 328, pp. 575–592, 2000.

Hindawi Publishing Corporation
BioMed Research International
Volume 2014, Article ID 921291, 10 pages
http://dx.doi.org/10.1155/2014/921291

Research Article

Simultaneous Coproduction of Hydrogen and Ethanol in Anaerobic Packed-Bed Reactors

Cristiane Marques dos Reis and Edson Luiz Silva

Department of Chemical Engineering, Federal University of São Carlos, Washington Luis Road, km 235, 13565-905 São Carlos, SP, Brazil

Correspondence should be addressed to Edson Luiz Silva; edsilva@ufscar.br

Received 6 June 2014; Revised 11 August 2014; Accepted 23 August 2014; Published 11 September 2014

Academic Editor: Ilona Sárvári Horváth

This study evaluated the use of an anaerobic packed-bed reactor for hydrogen production at different hydraulic retention times (HRT) (1–8 h). Two reactors filled with expanded clay and fed with glucose (3136–3875 mg L^{-1}) were operated at different total upflow velocities: 0.30 cm s^{-1} (R030) and 0.60 cm s^{-1} (R060). The effluent pH of the reactors was maintained between 4 and 5 by adding $NaHCO_3$ and HCl solutions. It was observed a maximum hydrogen production rate of 0.92 L H_2 h^{-1} L^{-1} in R030 at HRT of 1 h. Furthermore, the highest hydrogen yield of 2.39 mol H_2 mol^{-1} glucose was obtained in R060. No clear trend was observed by doubling the upflow velocities at this experiment. High ethanol production was also observed, indicating that the ethanol-pathway prevailed throughout the experiment.

1. Introduction

Hydrogen produced during acidogenesis stage of the anaerobic digestion is of significant interest, commercially and environmentally. It is also considered a clean fuel and, thus, it does not release greenhouse gases during combustion. However, to produce hydrogen from organic waste anaerobically, it is important to eliminate the methanogenic stage of the process by inactivating microorganisms responsible for methane conversion. It is necessary to adopt different operating strategies because the reactional environment should adapt in response to the condition applied. Some methods of inhibiting methanogenesis include pretreating the inocula to inactivate the methanogens and maintaining the pH of the system at specific values.

Furthermore, the choice of the reactor to produce hydrogen anaerobically is an important factor in optimizing hydrogen production. Good mixing conditions and high microbial biomass retention are desirable, and thus the right reactor configuration is essential. Attached growth reactors such as anaerobic packed-bed reactors (APBRs) appear to provide the best conditions. These reactors have a larger surface area available for microorganism deposition, and as a result, they are often used in research on hydrogen production [1–9].

Regarding APBR, various aspects have already been investigated. Some of these aspects include substrate, pH, temperature, inoculum, and support material for biomass adhesion. Several studies have investigated APBR with various sources of carbon, including sucrose [1, 2, 8], glucose [3, 5, 6, 9–11], domestic or industrial wastewater [12, 13], synthetic industrial paper effluent [14], palm extraction oil [15], and mixed fruit peel [16].

Studies in batch reactors [17, 18] have shown that pH is crucial for hydrogen production and metabolite formation. However, there is no consensus on the ideal pH for hydrogen production. In APBR, some researchers have opted to work in the 6-7 pH range [2, 4, 9] whereas others have preferred not to change the feed solution leading to a pH between 5 and 6 [1, 3, 5, 8]. Another important aspect in studies on APBR is related to the selection of the support material for biomass adhesion. Activated carbon [1, 2], packing rings [8], polyurethane foam [9], expanded clay [1, 5] are some of the materials that have been employed in recent studies.

Because of the diversity of parameters adopted by researchers, it appears to have no agreement about the best operation ranges to produce hydrogen. Even in studies that employ the same carbon source (glucose) and support

material (expanded clay) as we did, the reported results have differed [1, 5].

Studies in attached-growth reactors, specially in fluidized-bed reactors [19–21], suggested that hydrodynamic factors may have significant results in hydrogen production since good mixing conditions can favor mass transfer among phases in anaerobic digestion. Parameters such as upflow velocity, effluent recycle rate, and porosity are among the factors that could be studied in order to reach higher hydrogen production rates. However, there is still a lack about the impact of hydrodynamics impacts in packed-bed reactors.

As a category of attached-growth reactors, APBR shows as primary feature a good biomass retention. The use of immobilized inoculum helps to create a stable environment for hydrogen production. Enhancing the mass transfer between biofilm and bulk, for instance, appears to have an important role in anaerobic digestion. The adjustment of the hydrodynamic parameters turns in a key point in hydrogen production in attached-growth reactors. Therefore, to contribute to a better operational understanding of anaerobic packed-bed reactors in hydrogen production, a study was conducted to investigate the influence of HRT and upflow velocity on hydrogen production in two reactors filled with expanded clay and fed with synthetic wastewater containing glucose as carbon source (approximately 3500 mg L^{-1}).

2. Materials and Methods

2.1. Anaerobic Packed-Bed Reactors. The study employed two APBRs constructed from acrylic (5.3-cm diameter and 190-cm height, each) and filled with expanded clay (diameter = 2.8–3.3 mm and density = 1.5 g cm^{-3}). Figure 1 shows a basic outline of the process employed.

The inoculum was adapted to the reactors under batch mode for 48 hours, and following the 48-hour period, the reactors operated under continuous mode. The reactors began operation at HRT of 8 h, which was subsequently reduced to 1 h. The HRT was reduced when hydrogen production and glucose conversion stabilized. The choice of upflow velocities (V_{up}) was selected based on the minimum fluidization velocity (V_{mf}, for expanded clay: V_{mf} = 1.24 cm s^{-1}). The reactors were named based on the velocity at which they were operated. R030 is the reactor with V_{up} of 0.30 cm s^{-1} (24% of V_{mf}), and R060 is the reactor with V_{up} of 0.60 cm s^{-1} (48% of V_{mf}). R030 and R60 operated continuously for 217 days.

2.2. Synthetic Wastewater and Inoculum. The APBRs were fed with synthetic wastewater that contained glucose at a concentration of 3500 mg L^{-1}. The nutrient concentrations were as follows (in mg L^{-1}): $CO(NH_2)_2$ (125); $NiSO_4 \cdot 6\,H_2O$ (1); $FeSO_4 \cdot 7\,H_2O$ (5); $FeCl_3 \cdot 6H_2O$ (0.5); $CaCl_2 \cdot 6H_2O$ (47.0); $CoCl_2 \cdot 2H_2O$ (0.08); SeO (0.07); KH_2PO_4 (85.0); K_2HPO_4 (21.7); and $Na_2HPO_4 \cdot 2H_2O$ (33.4) [22]. Hydrochloric acid (30%) and sodium bicarbonate (0.84 g L^{-1}) were also added as buffer solutions to maintain the pH in the reactors at 4-5. Reactors inoculation was performed only once during the first 48 h with sludge from a treatment plant for swine waste.

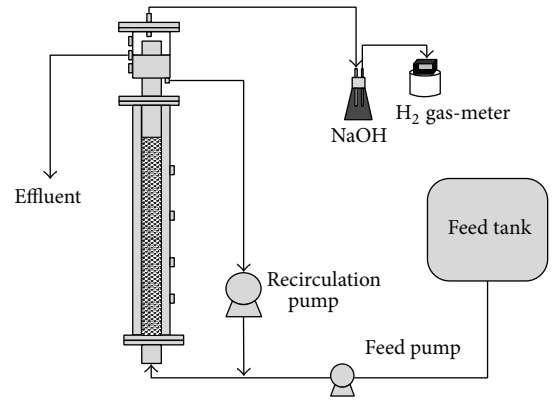

Figure 1: Schematic description of anaerobic packed-bed reactor (APBR).

The H_2 productivity of the sludge was enhanced by heat treatment [23]. The reactors were inoculated at a rate of 3.5% of sludge feed volume.

2.3. Chemical Analyses. The chemical oxygen demand (COD), pH, and solids (total solids, TS; volatile suspended solids, VSS; and total volatile solids, TVS) were measured in accordance with standard methods [24]. The glucose concentration was measured with an enzymatic GOD-PAP method [25].

The biogas hydrogen content was determined by gas chromatography (GC-2010, Shimadzu, Japan) using a thermal conductivity detector (TCD) with argon as the carrier gas, and the column was packed with Supelco Carboxen 1010 Plot (30 m × 0.53 mm i.d.) [26]. A gas meter (Type TG1; Ritter Inc., Germany) was used to measure the amount of hydrogen generated.

The concentrations of volatile fatty acids (VFA) and alcohols were also measured using a gas chromatography system (GC-2010, Shimadzu, Japan) that was equipped with FID and COMBI-PAL headspace injection (AOC 5000 model) and a HP-INNOWAX column (30 m × 0.25 mm i.d. × 0.25 μm film thickness) [26].

3. Results and Discussion

3.1. Effect of HRT and Upflow Velocity on H_2 Production. Figure 2 shows glucose conversion as a function of the HRT variation in the reactors. Glucose conversion was calculated as [influent glucose concentration, effluent glucose concentration] per influent glucose concentration. Each reactor operated at a different upflow rate to facilitate the analysis of the operating behavior at different HRTs.

As shown in Figure 2, throughout operation, R030, which was under an upflow velocity of 0.30 cm s^{-1}, presented similar conversion rates compared to R060, which operated at 0.60 cm s^{-1}, when taking in account the deviations. HRT of 2 h was an exception; at this HRT, R030 was slightly more efficient than R060. The maximum conversion rates were achieved in both reactors at HRT 8 h, and the conversion rates dropped when the HRT decreased. Conversion rates ranged

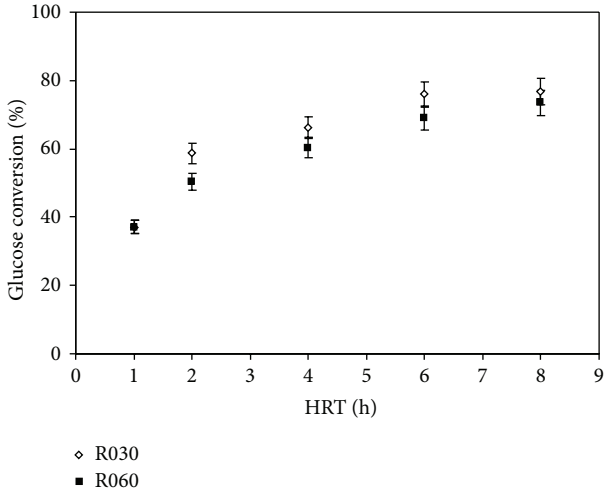

Figure 2: Effect of HRT on glucose conversion in R030 and R060.

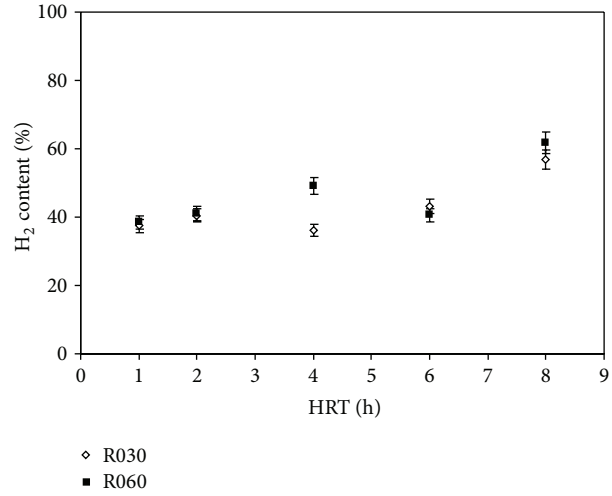

Figure 3: Effect of HRT on H_2 content in R030 and R060.

from 30.4% to 80.0% in R030 and from 33.1% to 77.9% in R060. The conversion rate decreased greatly at HRT 1 h. It is possible that the substrate residence time in the reactor was shorter than that required for organic matter degradation, leading to a reduction in glucose conversion in expanded bed reactors at HRT 1 h just like it was observed by De Amorim et al. [27] in fluidized-bed reactor when glucose concentration was elevated. The results obtained in our study are in agreement with literature data for other studies in APBR regarding HRT 1 h.

Figure 3 shows H_2 content in R030 and R060. Biogas was composed of H_2 and CO_2. Methane was not detected. For all HRT applied, with the exception of HRT 6 h, R060 showed slightly higher H_2 concentrations in the biogas than R030. The H_2 concentration was maximal at HRT of 8 h for both R030 (56.8%) and R060 (61.8%). When HRT was 8 h or higher, the H_2 concentration was reduced, appearing to stabilize at subsequent HRT. The minimum values achieved were 37.4% and 38.5% for R030 and R060, respectively.

The H_2 and CO_2 produced are released from the water medium into the gas phase. At first, the beneficial effect of the upflow velocity on mass transfer parameters is not conclusive. The presence of H_2 in biogas generated in our work agrees with studies available in the literature on APBR. Chang et al. [1] obtained H_2 content in biogas ranging from 9.5% to 45.8%. Lee et al. [2] showed that this content varied between 30% and 40%, while Li et al. [8] reported the H_2 content in biogas to be between 28.5% and 40.8%. Other studies have achieved higher concentrations. Zhang et al. [3] obtained 74% H_2 content, and Leite et al. [5] reported values ranging from 75% to 90%.

Figure 4 shows the hydrogen production rate (HPR) as a function of HRT in R030 and R060. HPR was calculated as liters of hydrogen produced per hour per reactional volume of the reactor.

As shown in Figure 4, both reactors show an increase in HPR due to a decrease in HRT from 8 h to 1 h. HPR remained stable with only a slight variation between HRT 8 h and 4 h.

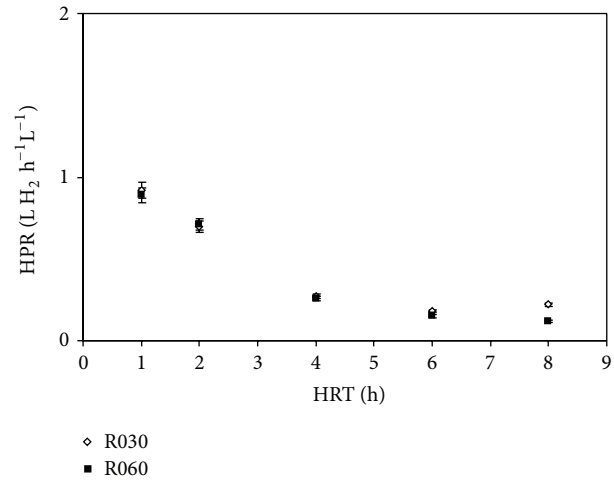

Figure 4: Effect of HRT on hydrogen production rate in R030 and R060.

However, from HRT of 4 h to 1 h, HPR increased in both reactors.

According to Chang et al. [1] and Lee et al. [2], the presence of suspended cells between bed particles (voids) favors hydrogen production because it allows for microbial growth. However, the nature of the particle bed allows for good retention of biomass in the form of biomass or as extracellular polymeric substances. Still, empty space in the reactor may be increased by increasing the upflow rate applied to the particle bed [1, 2]. Furthermore, Kumar and Das [28] investigated a pure culture of IIT-BT 08 *Enterobacter cloacae* for hydrogen production by varying the recycling rate and observed that an increase in the recycle rate led to an increase in hydrogen production due to the reduction of the resistance to mass transfer. Also studying the recycle rate on hydrogen production, Ngoma et al. [19] verified in fluidized-bed reactors with an external gas-disengager that an increase in the recycle rate (1.3 to 3.5 L min^{-1}) leads to

an increase in the H_2 productivity (2.1 to 8.7 L H_2 h^{-1} L^{-1}) under 45°C. Same effect was obtained under 70°C (2.8 to 14.9 L H_2 h^{-1} L^{-1}). According to the authors, vigorous mixing process within the gas-disengager due to high rates of effluent recycling permits an efficient removal of undissolved or nonsolibilized H_2 that may be present in the effluent. This gas removal associated with the enhanced mass transfer induces the hydrogen production. Also in fluidized-bed reactors, Dos Reis and Silva [20] verified that it should have an optimum upflow velocity range that could maximize the hydrogen production. According to them, due to the good mixing conditions inside the reactors resulted from a high velocity (1.24 cm s^{-1}) they obtained a hydrogen production rate of 2.21 L H_2 h^{-1} L^{-1}. In another research, Obazu et al. [21], when testing the relation between the reactor volume and the recycle rate in fluidized-bed reactors, also verified that the high degree of fluid turbulence is good for hydrogen release, enhancing hydrogen production.

These findings should be considered when employing different upflow velocities in face of the increase of the turbulent conditions. Thus, because R060 was operated at a rate twice as high as that of R030, it was capable of presenting better hydrogen production results. However, quantitative results show that the HPR ranged from 0.22 to 0.92 L H_2 h^{-1} L^{-1} in R030 but only from 0.12 to 0.89 L H_2 h^{-1} L^{-1} in R060.

The divergence between the expected results and our results indicates that the upflow rate range employed in our study had no effect on hydrogen production. Maybe a higher upflow velocity till the limit of the minimum fluidization velocity would be more suitable for analyzing this parameter. R030 and R060 presented lower HPR than those reported by Chang et al. [1] (1.32 L H_2 h^{-1} L^{-1} at HRT 2 h), Lee et al. [2] (7.4 L H_2 h^{-1} L^{-1}), and Jo et al. [9] (0.3 L H_2 h^{-1} L^{-1}) but higher than those reported by Li et al. [8] (0.26 L H_2 h^{-1} L^{-1} at HRT 2 h). The literature indicates that a small applied HRT results in a high HPR.

Figure 5 shows the hydrogen yield (HY) as a function of HRT in R030 and R060. HY was calculated as moles of hydrogen produced per mole of glucose converted.

Figure 5 shows that hydrogen yield values and the behavior of HPR for the two reactors were similar. The yield values for the reactors were similar when HRT decreased. This result indicates that the rates adopted for the APBR in question did not enable us to clearly identify a positive influence of increasing upflow velocities on hydrogen production. In general, HY increased when HRT decreased, with the highest yield occurring at HRT 1 h for both reactors.

When examining the combined results of HPR and HY, it appears that at HRT 1 h, R060 performed best with regard to H_2 production. When comparing our results to other studies, the HY values obtained in our work with R030 (1.23 mol H_2 mol^{-1} glucose to 2.16 mol H_2 mol^{-1} glucose) and R060 (1.16 mol H_2 mol^{-1} glucose to 2.39 mol H_2 mol^{-1} glucose) are in agreement with HY values obtained in APBR. Chang et al. [1] obtained yield values ranging from 0.08 mol H_2 mol^{-1} sucrose to 1.14 mol H_2 mol^{-1} sucrose; the peak was observed at HRT 2 h. However, Lee et al. [2] reported HY values between 2.9 mol H_2 mol^{-1} sucrose and 3.9 mol H_2 mol^{-1} sucrose when HRT varied from 0.5 h to 4 h. Li et al. [8] obtained HY values from 0.78 mol H_2 mol^{-1} glucose to 1.22 mol H_2 mol^{-1} glucose with maximum and minimum HY at HRT of 14 h and 2 h, respectively.

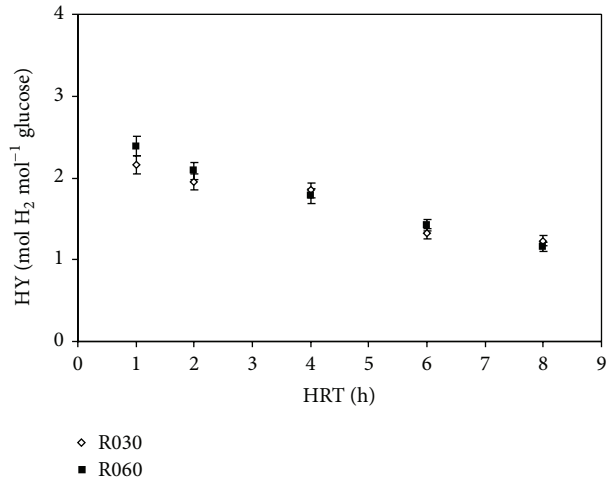

Figure 5: Effect of HRT on hydrogen yield in R030 and R060.

The hydrogen production results vary greatly due to different experimental conditions such as microorganism cultures, substrates, and pH values. Table 1 summarizes the results from several studies on APBR to show this diversity.

The acetic pathway illustrated by the following indicates that four moles of hydrogen are produced for each mol of glucose degraded:

$$C_6H_{12}O_6 + 2H_2O \longrightarrow 2CH_3COOH + 2CO_2 + 4H_2 \quad (1)$$

The acetic pathway is deemed the most effective pathway for hydrogen production. If this pathway is used as a reference, the highest HY value obtained so far was reported by Lee et al. [2] at HRT of 0.5 h. They reported 49% of the highest theoretical HY for sucrose (8 mol H_2 mol^{-1} sucrose). However, this yield is lower than what was obtained by Leite et al. [5] who reported 62% (2.39 mol H_2 mol^{-1} glucose) of the maximum theoretical value for glucose (4 mol H_2 mol^{-1} glucose).

Table 1 also provides the range of upflow velocities employed by the studies. The best yield was presented by Lee et al. [2] when the upflow rates adopted ranged between 0.001 cm s^{-1} and 0.01 cm s^{-1}, with the best results at 0.01 cm s^{-1}. However, Li et al. [8] who also worked with sucrose and a mixed culture at upflow velocities between 0.03 cm s^{-1} and 0.39 cm s^{-1} showed a lower yield than that obtained by Lee et al. [2].

However, our study with glucose as the substrate and employing higher upflow rates than Lee et al. [2] obtained higher H_2 yields. Leite et al. [5], who also employed glucose as the substrate and used expanded clay as the support material for biomass adhesion, showed H_2 yields similar to ours, even though we adopted a higher range of upflow rates.

The effect of upflow velocity applied to reactors for APBR is not relevant when it comes to increasing or decreasing

Table 1: Comparison of studies in packed-bed reactors for hydrogen production.

Reference	Substrate/ concentration ($g\,L^{-1}$)/ ORL ($kgDQO{\cdot}m^{-3}{\cdot}d^{-1}$)	Inoculum/ pretreatment method	Support material	V_{up} ($cm\,s^{-1}$)	Temperature (°C)	pH	HRT (h)	HY ($mol\,H_2{\cdot}mol^{-1}$ substrate)	HPR ($L\,L^{-1}\,h^{-1}$)
Chang et al. [1]	Sucrose 17.8/85–854	Municipal sewage sludge Acid	Expanded clay	—	35.0	6.7	0.5–5.0	0.1–1.3*	0.2–0.4
Chang et al. [1]	Sucrose 17.8/213–854	Municipal sewage sludge Acid	Activated carbon	—	35.0	6.7	0.5–2.0	0.5–1.4*	0.6–1.3
Lee et al. [2]	Sucrose 17.8/106–854	Municipal sewage sludge Acid	Activated carbon	—	35.0	6.7	0.5–4.0	2.9–4.0*	1.2–7.4
Zhang et al. [3][a]	Glucose 10.5/194	*Clostridium acetobutylicum*	Glass beads	0.005*	30.0	4.9	1.3**	0.9	0.2
Wu et al. [4]	Sucrose 17.8/107	Municipal sewage sludge Acid	Polyethylene-octane elastomer (POE)	—	35.0	6.0	4.0	0.4	0.3*
Wu et al. [4]	Glucose 18.9/113	Municipal sewage sludge Acid	Polyethylene-octane elastomer (POE)	—	35.0	6.0	4.0	0.7	0.4*
Wu et al. [4]	Fructose 18.9/113	Municipal sewage sludge Acid	Polyethylene-octane elastomer (POE)	—	35.0	6.0	4.0	0.6	0.2*
Leite et al. [5]	Glucose 2/96	Mixed culture Natural fermentation	Expanded clay	0.024	30.0	3.9–7.3	0.5	1.8–2.5	—
This study	Glucose 3.5/10–84	Swine slaughterhouse sludge Heat-shock	Expanded clay	0.3	25.0	4-5	1.0–8.0	1.2–2.2	0.2–0.9
This study	Glucose 3.5/10–84	Swine slaughterhouse sludge Heat-shock	Expanded clay	0.6	25.0	4-5	1.0–8.0	1.2–2.4	0.1–0.9

*Based on article data, [a]unsaturated flow reactor, and **HRT = reactor volume/influent flow rate.

H_2 production. Other aspects, such as adopted substrate and support material and/or chosen type of inoculum pretreatment, appear to have a higher influence on H_2 production. Furthermore, based on the literature reported in Table 1, the highest hydrogen production values are achieved at the shortest HRT. However, yield values do not show this trend [8], although H_2 yield increased as applied HRT decreased in our study.

3.2. Influence of HRT and Upflow Velocity on Production of VFA and Alcohols. Table 2 shows the distribution of soluble metabolite products (SMP) generated in R030 and R060 in relation to the HRT. The main SMPs were ethanol (EtOH) and acetic acid (HAc). Butyric acid (HBu), propionic acid (HPr), and methanol (MetOH) were also generated.

The production of metabolites did not vary significantly with regards to the upflow velocity range used, resulting in similar concentrations for R030 and R060. Thus, the use of different upflow velocities does not necessarily lead to different configurations in SMP distribution. Our results indicated that EtOH production was favored over HBu production, which is commonly associated with hydrogen production. HAc production was also relevant throughout our study.

The HAc/HBu ratio is commonly used as an indicator of bioprocess efficiency in hydrogen production. Although this parameter increased as HRT was decreased in both R030 and R060, it should not be used as the only parameter to indicate H_2 production effectiveness. HAc production prevailed over HBu production, which decreased when HRT changed. The low presence of HBu compared to EtOH and HAc which indicates the presence of a metabolic pathway to produce hydrogen differs from that of HAc and HBu because there was no H_2 production decrease when HBu production declined. HAc production remained constant when the HRT was changed. However, EtOH production increased drastically from 31% to 57% in R030 and from 29% to 50% in R060 when the HRT was decreased from 6 h to 4 h.

This change in metabolites occurred when there was a decrease in HBu production in the reactors, indicating that the HBu pathway was favored over the EtOH pathway. Because HAc production varied only slightly, it is suggested that H_2 production occurred simultaneously with HAc production. Ren et al. [29] presented a way of producing H_2 in which one mol of HAc, two moles of H_2, and one mol of EtOH were generated for each mol of glucose degraded, as shown in the following:

$$C_6H_{12}O_6 + H_2O \longrightarrow C_2H_5OH + CH_3COOH + 2H_2 + 2CO_2 \quad (2)$$

Based on the traditional pathway of EtOH production from glucose, H_2 production was expected to decrease due to increased production of solvents [29]. However, in both reactors in our study, the H_2 production increased up to HRT 1 h. It is unclear what may have caused this change in metabolic pathway. Zhu et al. [30] worked with a batch reactor and glucose to study the metabolic pathways as a function of pH. They found that the presence of different metabolic pathways depended on the pH range adopted and that the production of organic acids increased at pH values between 5.5 and 6.0.

However, EtOH production did not depend on the pH range adopted. The production of metabolites was limited at pH values lower than 4.5. Furthermore, Zhu et al. [30] found EtOH and H_2 production at pH 5.5. At this pH, the main metabolic pathways present in their study were mainly conducive to HAc, EtOH, and H_2 production. As in our study with APBR, there was simultaneous production of Hac, EtOH, and H_2. These results confirm that EtOH production without decreasing H_2 production is possible as shown in (2) proposed by Ren et al. [29].

Our results also indicate that the HAc/EtOH ratio shows the variation in the metabolic pathway for the main products obtained. Furthermore, these data also point to the production of HAc and especially EtOH, which always prevailed over the HAc production (HAc/EtOH < 1). The ethanolic pathway predominated at HRTs ranging from 6 h to 4 h. When the HRT was reduced to 2 h, the HAc production became dominant again in both R030 and R060. The highest production of HAc and H_2 occurred at HRT 1 h. Furthermore, this phase was also the only one in which HAc production prevailed over EtOH production.

Table 3 shows the data for production of hydrogen, organic acids, and alcohols in several studies with APBR. These data refer to metabolites produced at maximum H_2 production. EtOH production did not prevail in any of these studies, with the exception of Wu et al. [4], who obtained 60% EtOH along with other SMPs.

The predominant metabolites generated were HAc and HBu. Chang et al. [1] obtained low HBu production when H_2 production peaked, and EtOH appeared to be one of the major SMPs generated. This result, combined with the results obtained for R030 and R060, shows that butyric and ethanolic pathways compete with each other, while HAc production and EtOH production occur simultaneously or use the same metabolic pathway.

Table 3 shows the distribution of generated metabolites in diverse studies in packed-bed reactors compared to the present study.

The results of Chang et al. [1] indicate that an increase in upflow rate leads to a decrease in ethanol production. However, Lee et al. [2] suggest that an increase in upflow rate has no significant impact on the distribution of metabolites, which also appears to be true in the present study. Lee et al. [2] reported the highest production of volatile acids. However, at the HRT where production of volatile acids was the highest, the ethanol production was the lowest. Furthermore, the butyric pathway was favored when metabolite production was relevant.

4. Conclusions

The adoption of two different upflow rates 0.30 cm s^{-1} and 0.60 cm s^{-1} in APBR (R030 and R060, respectively) at varying HRTs was observed to have a nonsignificant influence on hydrogen production. Our results verified that a long HRT increased the volumetric hydrogen production obtained, with a maximum value of 0.92 L H_2 h^{-1} L^{-1} obtained in R030.

Table 2: Distribution of generated metabolites as a function of HRT for R030 and R060.

APBR	HRT (h)	EtOH/SMP (%)	HAc/SMP (%)	HPr/SMP (%)	HBu/SMP (%)	MetOH/SMP (%)	TVFA (mmol L^{-1})	SMP (mmol L^{-1})	HAc/HBu*	HAc/EtOH*
R030	8	32.7	31.8	0.3	28.8	6.5	18.8	30.9	1.1	0.9
	6	31.7	29.1	15.0	15.6	8.6	19.3	32.3	1.9	0.9
	4	57.5	21.1	9.7	4.6	7.1	17.3	48.7	4.7	0.4
	2	59.7	18.5	9.7	3.0	9.1	14.6	46.9	6.2	0.3
	1	39.2	36.5	11.5	3.9	8.8	19.8	38.1	9.3	0.9
R060	8	33.0	29.6	2.9	27.5	6.9	14.9	24.9	1.2	0.9
	6	29.1	25.2	23.5	14.3	7.9	18.9	29.9	1.8	0.9
	4	50.5	25.8	12.3	5.2	6.3	20.4	47.1	4.9	0.5
	2	40.1	27.0	21.7	5.0	6.2	11.0	20.5	5.4	0.7
	1	36.5	39.4	13.1	5.2	5.9	20.2	35.1	7.6	1.2

TVFA: total volatile fatty acids, TVFA = HAc + HBu + HPr, and SMP = TVFA + EtOH.
*Molar ratio.

Table 3: SMP distribution in studies using APBRs for hydrogen production.

Reference	Substrate (support material)	HRT (h)	EtOH/SMP (%)	HAc/SMP (%)	HPr/SMP (%)	HBu/SMP (%)	MetOH/SMP (%)	HVl/SMP (%)	HCpr/SMP (%)	TVFA ($mmol\,L^{-1}$)	SMP ($mmol\,L^{-1}$)	HAc/HBu*	HAc/EtOH*
Chang et al. [1]**	Sucrose (expanded clay)	5	46.3	27.2	17.4	9.1	—	—	—	29.9	55.8	2.9	0.6
		2	42.7	24.9	24.6	7.8	—	—	—	44.5	77.7	3.2	0.6
		1	25.3	31.1	33.9	9.7	—	—	—	50.7	67.9	3.2	1.2
		0.5	19.5	29.4	39.3	11.7	—	—	—	64.2	79.9	2.5	1.5
Lee et al. [2]**	Sucrose (activated carbon)	4	1.6	31.3	36.8	29.7	—	0.6	—	94.9	96.5	1.1	19.3
		2	21.0	20.8	16.6	37.8	—	3.9	—	89.2	112.8	0.6	1.0
		1	9.6	19.2	23.4	41.8	—	6.0	—	147.4	163.0	0.5	2.0
		0.5	10.3	20.6	24.7	41.2	—	3.2	—	136.2	151.8	0.5	2.0
Zhang et al. [3]	Glucose (glass beads)	1.3***	—	70.6	—	29.4	—	—	—	1.7	1.7	2.4	—
Wu et al. [4]	Fructose (POE)	4	52.8	25.1	10.1	12.1	—	—	—	355.7	616.3	2.1	0.5
Wu et al. [4]	Sucrose (POE)	4	62.0	29.9	1.9	6.2	—	—	—	605.7	1302.2	4.8	0.5
Wu et al. [4]	Glucose (POE)	4	69.2	22.3	1.3	7.1	—	—	—	418.5	1064.4	3.1	0.3
Leite et al. [5]	Glucose (expanded clay)	0.5	—	57.9	3.0	34.0	—	—	5.1	12.9	12.9	1.7	—

HVl: valeric acid. HCpr: caproic acid.
*Molar ratio, **based on article data, and ***HRT = reactor volume/influent flow rate.

Hydrogen yield was highest in R060, reaching 2.39 mol H_2 mol^{-1} glucose at HRT 1 h. The main metabolites generated were ethanol and acetic acid, indicating that the ethanol-type pathway prevailed throughout the experiment.

Conflict of Interests

The authors declare that there is no conflict of interests regarding the publication of this paper.

Acknowledgments

The authors gratefully acknowledge the financial support of CNPq, FAPESP, and CAPES.

References

[1] J.-S. Chang, K.-S. Lee, and P.-J. Lin, "Biohydrogen production with fixed-bed bioreactors," *International Journal of Hydrogen Energy*, vol. 27, no. 11-12, pp. 1167–1174, 2002.

[2] K.-S. Lee, Y.-S. Lo, Y.-C. Lo, P.-J. Lin, and J.-S. Chang, "H_2 production with anaerobic sludge using activated-carbon supported packed-bed bioreactors," *Biotechnology Letters*, vol. 25, no. 2, pp. 133–138, 2003.

[3] H. Zhang, M. A. Bruns, and B. E. Logan, "Biological hydrogen production by *Clostridium acetobutylicum* in an unsaturated flow reactor," *Water Research*, vol. 40, no. 4, pp. 728–734, 2006.

[4] K.-J. Wu, C.-F. Chang, and J.-S. Chang, "Simultaneous production of biohydrogen and bioethanol with fluidized-bed and packed-bed bioreactors containing immobilized anaerobic sludge," *Process Biochemistry*, vol. 42, no. 7, pp. 1165–1171, 2007.

[5] J. A. C. Leite, B. S. Fernandes, E. Pozzi, M. Barboza, and M. Zaiat, "Application of an anaerobic packed-bed bioreactor for the production of hydrogen and organic acids," *International Journal of Hydrogen Energy*, vol. 33, no. 2, pp. 579–586, 2008.

[6] M. A. Rachman, Y. Nakashimada, T. Kakizono, and N. Nishio, "Hydrogen production with high yield and high evolution rate by self-flocculated cells of *Enterobacter aerogenes* in a packed-bed reactor," *Applied Microbiology and Biotechnology*, vol. 49, no. 4, pp. 450–454, 1998.

[7] S.-Y. Wu, C.-N. Lin, and J.-S. Chang, "Hydrogen production with immobilized sewage sludge in three-phase fluidized-bed bioreactors," *Biotechnology Progress*, vol. 19, no. 3, pp. 828–832, 2003.

[8] C. Li, T. Zhang, and H. H. P. Fang, "Fermentative hydrogen production in packed-bed and packing-free upflow reactors," *Water Science and Technology*, vol. 54, pp. 95–103, 2006.

[9] J. H. Jo, D. S. Lee, D. Park, and J. M. Park, "Biological hydrogen production by immobilized cells of *Clostridium tyrobutyricum* JM1 isolated from a food waste treatment process," *Bioresource Technology*, vol. 99, no. 14, pp. 6666–6672, 2008.

[10] E. Palazzi, B. Fabiano, and P. Perego, "Process development of continuous hydrogen production by *Enterobacter aerogenes* in a packed column reactor," *Bioprocess Engineering*, vol. 22, no. 3, pp. 205–213, 2000.

[11] G. Chittibabu, K. Nath, and D. Das, "Feasibility studies on the fermentative hydrogen production by recombinant *Escherichia coli* BL-21," *Process Biochemistry*, vol. 41, no. 3, pp. 682–688, 2006.

[12] M. F. Colmenarejo, E. Sánchez, A. Bustos, G. García, and R. Borja, "A pilot-scale study of total volatile fatty acids production by anaerobic fermentation of sewage in fixed-bed and suspended biomass reactors," *Process Biochemistry*, vol. 39, no. 10, pp. 1257–1267, 2004.

[13] L. M. Alzate-Gaviria, P. J. Sebastian, A. Pérez-Hernández, and D. Eapen, "Comparison of two anaerobic systems for hydrogen production from the organic fraction of municipal solid waste and synthetic wastewater," *International Journal of Hydrogen Energy*, vol. 32, no. 15, pp. 3141–3146, 2007.

[14] Y. Ueno, M. Tatara, H. Fukui, T. Makiuchi, M. Goto, and K. Sode, "Production of hydrogen and methane from organic solid wastes by phase-separation of anaerobic process," *Bioresource Technology*, vol. 98, no. 9, pp. 1861–1865, 2007.

[15] K. Vijayaraghavan and D. Ahmad, "Biohydrogen generation from palm oil mill effluent using anaerobic contact filter," *International Journal of Hydrogen Energy*, vol. 31, no. 10, pp. 1284–1291, 2006.

[16] K. Vijayaraghavan, D. Ahmad, and C. Soning, "Bio-hydrogen generation from mixed fruit peel waste using anaerobic contact filter," *International Journal of Hydrogen Energy*, vol. 32, no. 18, pp. 4754–4760, 2007.

[17] S. van Ginkel, S. Sung, and J.-J. Lay, "Biohydrogen production as a function of pH and substrate concentration," *Environmental Science & Technology*, vol. 35, no. 24, pp. 4726–4730, 2001.

[18] S. K. Khanal, W.-H. Chen, L. Li, and S. Sung, "Biological hydrogen production: effects of pH and intermediate products," *International Journal of Hydrogen Energy*, vol. 29, no. 11, pp. 1123–1131, 2004.

[19] L. Ngoma, P. Masilela, F. Obazu, and V. M. Gray, "The effect of temperature and effluent recycle rate on hydrogen production by undefined bacterial granules," *Bioresource Technology*, vol. 102, no. 19, pp. 8986–8991, 2011.

[20] C. M. Dos Reis and E. L. Silva, "Effect of upflow velocity and hydraulic retention time in anaerobic fluidized-bed reactors used for hydrogen production," *Chemical Engineering Journal*, vol. 172, no. 1, pp. 28–36, 2011.

[21] F. O. Obazu, L. Ngoma, and V. M. Gray, "Interrelationships between bioreactor volume, effluent recycle rate, temperature, pH, $\%H_2$, hydrogen productivity and hydrogen yield with undefined bacterial cultures," *International Journal of Hydrogen Energy*, vol. 37, no. 7, pp. 5579–5590, 2012.

[22] A. R. Barros, E. L. C. de Amorim, C. M. Reis, G. M. Shida, and E. L. Silva, "Biohydrogen production in anaerobic fluidized bed reactors: effect of support material and hydraulic retention time," *International Journal of Hydrogen Energy*, vol. 35, no. 8, pp. 3379–3388, 2010.

[23] S.-H. Kim, S.-K. Han, and H.-S. Shin, "Effect of substrate concentration on hydrogen production and 16S rDNA-based analysis of the microbial community in a continuous fermenter," *Process Biochemistry*, vol. 41, no. 1, pp. 199–207, 2006.

[24] APHA, *Standard Methods for the Examination for Water and Wastewater*, American Public Health Association/American Water Works Association/Water Environmental Federation, Washington, DC, USA, 20th edition, 1998.

[25] G. M. Shida, A. R. Barros, C. M. D. Reis, E. L. C. D. Amorim, M. H. Rissato Zamariolli Damianovic, and E. L. Silva, "Long-term stability of hydrogen and organic acids production in an anaerobic fluidized-bed reactor using heat treated anaerobic sludge inoculum," *International Journal of Hydrogen Energy*, vol. 34, no. 9, pp. 3679–3688, 2009.

[26] S. I. Maintinguer, B. S. Fernandes, I. C. S. Duarte, N. K. Saavedra, M. A. T. Adorno, and M. B. Varesche, "Fermentative hydrogen production by microbial consortium," *International Journal of Hydrogen Energy*, vol. 33, no. 16, pp. 4309–4317, 2008.

[27] E. L. C. de Amorim, L. T. Sader, and E. L. Silva, "Effect of substrate concentration on dark fermentation hydrogen production using an anaerobic fluidized bed reactor," *Applied Biochemistry and Biotechnology*, vol. 166, no. 5, pp. 1248–1263, 2012.

[28] N. Kumar and D. Das, "Continuous hydrogen production by immobilized Enterobacter cloacae IIT-BT 08 using lignocellulosic materials as solid matrices," *Enzyme and Microbial Technology*, vol. 29, no. 4-5, pp. 280–287, 2001.

[29] N. Ren, B. Wang, and J. C. Huang, "Ethanol-type fermentation from carbohydrate in high rate acidogenic reactor," *Biotechnology and Bioengineering*, vol. 54, pp. 428–433, 1997.

[30] H. Zhu, W. Parker, R. Basnar et al., "Buffer requirements for enhanced hydrogen production in acidogenic digestion of food wastes," *Bioresource Technology*, vol. 100, no. 21, pp. 5097–5102, 2009.

Hindawi Publishing Corporation
BioMed Research International
Volume 2014, Article ID 320254, 13 pages
http://dx.doi.org/10.1155/2014/320254

Research Article

Economic Impact of NMMO Pretreatment on Ethanol and Biogas Production from Pinewood

Marzieh Shafiei,[1] Keikhosro Karimi,[1,2] Hamid Zilouei,[1] and Mohammad J. Taherzadeh[3]

[1] *Department of Chemical Engineering, Isfahan University of Technology, Isfahan 84156-83111, Iran*
[2] *Industrial Biotechnology Group, Institute of Biotechnology and Bioengineering, Isfahan University of Technology, Isfahan 84156-83111, Iran*
[3] *Swedish Centre for Resource Recovery, University of Borås, 501 90 Borås, Sweden*

Correspondence should be addressed to Marzieh Shafiei; m.shafiei@ce.iut.ac.ir

Received 3 June 2014; Accepted 15 July 2014; Published 7 September 2014

Academic Editor: Meisam Tabatabaei

Processes for ethanol and biogas (scenario 1) and biomethane (scenario 2) production from pinewood improved by N-methylmorpholine-N-oxide (NMMO) pretreatment were developed and simulated by Aspen plus. These processes were compared with two processes using steam explosion instead of NMMO pretreatment ethanol (scenario 3) and biomethane (scenario 4) production, and the economies of all processes were evaluated by Aspen Process Economic Analyzer. Gasoline equivalent prices of the products including 25% value added tax (VAT) and selling and distribution expenses for scenarios 1 to 4 were, respectively, 1.40, 1.20, 1.24, and 1.04 €/l, which are lower than gasoline price. The profitability indexes for scenarios 1 to 4 were 1.14, 0.93, 1.16, and 0.96, respectively. Despite the lower manufacturing costs of biomethane, the profitability indexes of these processes were lower than those of the bioethanol processes, because of higher capital requirements. The results showed that taxing rule is an effective parameter on the economy of the biofuels. The gasoline equivalent prices of the biofuels were 15–37% lower than gasoline; however, 37% of the gasoline price contributes to energy and carbon dioxide tax which are not included in the prices of biofuels based on the Swedish taxation rules.

1. Introduction

Ethanol and biomethane are two common biofuels which are already available in the market in some countries. Ethanol is mainly produced from sugar and starch based raw materials. However, wide investigations are performed for replacement of these food based raw materials with cheaper and more abundant lignocellulosic materials [1]. Biogas is currently produced in wastewater treatment plants or from various organic wastes such as municipal solid waste, manure, and industrial and agricultural wastes [2]. Biogas from wastes is mainly used in the power plants, and the compressed biomethane is commercially available beside the compressed natural gas (CNG) as a vehicle fuel. Considering the predicted expansion of methane usage in Sweden, there would be an increasing market for biomethane to be used as a vehicle fuel. Moreover, further developments in natural gas grid support more injection of biomethane in the grid [3].

A pretreatment step prior to biofuel production from lignocellulosic materials is essential for improvement of the low yields [1, 5–9]. Pretreatment with N-methyl morpholine-N-oxide (NMMO) is among the novel and efficient methods [5–7]. NMMO is a nontoxic cellulose solvent, does not produce toxic wastes, and can be recycled over 98% [6]. NMMO pretreatment modifies the structure of lignocellulosic materials to obtain higher yields of enzymatic hydrolysis and anaerobic digestion. During pretreatment, NMMO dissolves cellulose which is inside of the cell wall of wood. Afterwards, addition of water regenerates cellulose, and less crystalline and amorphous cellulose precipitates on the biomass surfaces. The hydrolysis of regenerated cellulose is much more convenient than the intact cellulose inside the cell wall. Furthermore, the pretreatment process increases the biomass porosity and consequently accessibility of degrading enzymes or bacteria to the inside of the biomass. Better accessibility to the inside of biomass results in enhanced

yields of enzymatic hydrolysis and anaerobic digestion [5]. One of the important features of NMMO pretreatment is that physical removal of lignin and hemicellulose is not necessary to obtain a high cellulose hydrolysis yield. The modifications made by NMMO pretreatment are so efficient that the subsequent enzymatic hydrolysis yield is significantly higher than the yield after most of the other pretreatments, for example, steam explosion.

Another promising pretreatment process is steam explosion. Although it has a lower efficiency compared with NMMO pretreatment, it is a simple method that is well investigated in laboratory and pilot scales and is suggested for industrial scale applications [1].

Biofuel production from lignocellulosic materials is a developing technology and still challenging with technical and economical bottlenecks. Technoeconomic analysis helps to overcome these problems using process simulation tools together with economic analysis [10]. Several technoeconomic analyses were performed for bioethanol production from lignocelluloses [10–12]. The economics of biogas production from lignocellulosic materials were also studied [2, 3, 13]. However, no reference was detected for technoeconomic comparison of NMMO and steam explosion pretreatment for both bioethanol and biogas production from lignocellulosic materials.

Significant improvements in the ethanol and biogas yields from NMMO treated pinewood were observed [5]. In the current study, based on the experimental results, the economics of the processes for bioethanol and biogas productions with NMMO pretreatment were compared with two processes using continuous steam explosion pretreatment for similar products. The processes were simulated and optimized using Aspen plus, and the economics were evaluated with Aspen Process Economic Analyzer (PEA). A sensitivity analysis was also performed to determine the effective parameters.

2. Methods

Four scenarios for production of bioethanol and biogas using steam explosion or NMMO pretreatment were developed. The process for each scenario was simulated by Aspen plus, and then the economy was studied by Aspen PEA. The selected raw material was pinewood because of availability of the experimental results [5]; however, other lignocellulosic feedstocks can be used with some minor modifications.

2.1. Process Development. This study includes four main scenarios. In the first two scenarios, NMMO pretreatment is used for improvement of ethanol and biogas production (scenario 1) and for only biogas production (scenario 2). The other two scenarios are for the production of the similar products but steam explosion pretreatment is used instead of NMMO pretreatment (scenarios 3 and 4).

2.1.1. Scenario 1: NMMO Pretreatment for Improvement of Ethanol and Biogas Production. The raw materials are unloaded from trucks to storage area and conveyed for size reduction. All of the scenarios include similar units for the feedstock handling area. In scenario 1 (Figure 1), raw materials are reduced in size and then pretreated with NMMO for 3 hours at 120°C (Figure 2). Then, the materials are regenerated by addition of hot water, washed with water to remove NMMO, and then sent to the biofuel production process. An optimized evaporation unit is used for the recovery and concentration of NMMO (Table 1) [12].

In scenario 1, the wood is washed with water after the pretreatment and the water containing 70% NMMO is sent to evaporation. The evaporation concentrates NMMO to 85%, and it is reused in the pretreatment. A makeup stream for NMMO is considered in the process to supply the amount of NMMO which is not recovered during the washing of the treated wood. Based on the calculations, the NMMO recovery of 99.5% is required to have an economically feasible process. Efficient multistage countercurrent equipment for solid washing is considered to provide this recovery. During the pretreatment, addition of antioxidant agents prevented the oxidation and degradation of NMMO.

Ethanol production includes hydrolysis, nonisothermal simultaneous saccharification and fermentation (NSSF), distillation, and dehydration. After pretreatment, the raw materials are hydrolyzed with Cellic CTec3 enzyme (Novozymes) for 24 hours. It is claimed that this newly developed enzyme has a higher efficiency compared with the previous types of the Cellic enzymes [12, 14]. Because of improvements in the enzyme efficiency, the enzyme is loaded at the rate of 1.8% w/w of cellulose [12]. The hydrolysis temperature is set to 45°C for better stability. Afterwards, the hydrolysate is cooled down to 37°C for SSF fermentation for 24 hours [12]. Four main fermenters and four hydrolysis reactors are designed with volumes of 800 m^3. For each of the hydrolysis and fermentation reactors, seed fermenters with relative volume ratio of 1 : 10 until volume of 80 l are used for inoculum preparation. All fermenters and auxiliary equipment are made up of stainless steel 304.

The distillation, dehydration, and wastewater treatment (WWT) units are similar to the systems presented by Shafiei et al. [12] with modifications for the new raw material and lower capacity. The distillation unit system (Figure 3 and Table 2) purifies ethanol to 95.5%. For further purification to 99.9%, a molecular sieve unit is used. The ethanol recovery was assumed to be 96% in the distillation unit. Afterwards, the wastewater from the striper column is filtered for solid removal and then sent to an anaerobic digester of UASB type for biogas production. This system removes 90% of the COD, and the effluent is further purified using aerobic digestion [12]. The biogas produced in this process is not sufficient to have an economically feasible upgrading; therefore, it is sold to a nearby combined heat and power (CHP) plant. An amount of 6% biogas loss was assumed during the storage [15].

2.1.2. Scenario 2: NMMO Pretreatment for Improvement of Biogas Production. The block flow diagram (BFD) for scenario 2 is presented in Figure 4. Similar to scenario 1, units for feed handling and NMMO pretreatment were assumed for this scenario. The treated materials are then conveyed to the

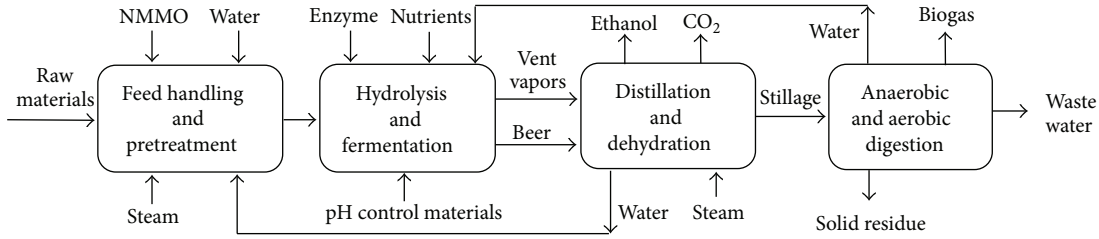

Figure 1: Block flow diagram (BFD) of scenario 1: NMMO pretreatment for production of ethanol and biogas.

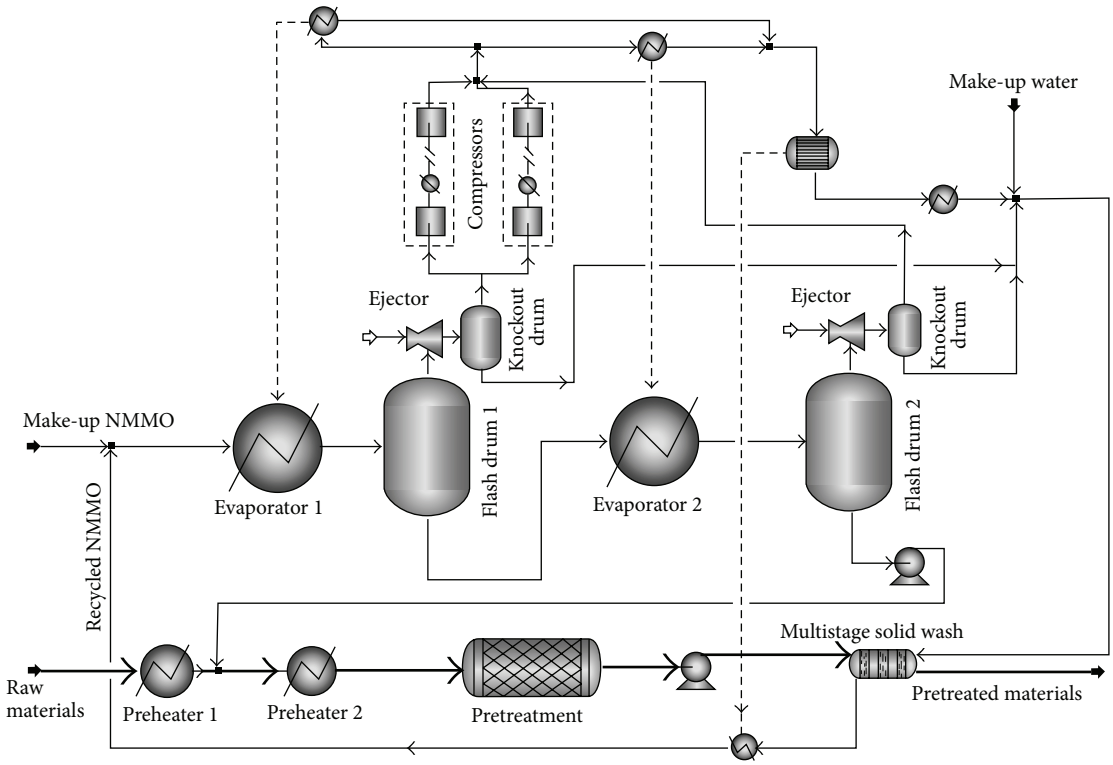

Figure 2: PFD of NMMO pretreatment unit. The optimized mechanical vapor recompression (MVR) system was used for the evaporators (scenarios 1 and 2).

solid-state biogas production unit presented by DRANCO (Germany) [16] (Figure 5). Seven digesters with volume of 3200 m^3 made of acid resistant coated carbon steel are used in the process. The digesters are vertical cone bottom vessels and are fed using screw pumps. A portion of the outflow is mixed with the pretreated wood and nutrients are sent back to the top of digesters so the overall retention time of materials is 20 days [13, 16]. The digested materials are dewatered to 30% solid content and sold as a byproduct for combustion. Macrofilters and reverse osmosis system are used for water purification, while 80% of the water is recycled to the process [17]. The effluent water is treated using aerobic digestion [12]. The produced biogas is upgraded to 97% with water scrubbing technology with regeneration and then pressurized for further application as fuel. Methane losses are estimated to be 1.5% in the upgrading process and 6% during the storage [15].

2.1.3. Scenario 3: Steam Explosion Pretreatment for Improvement of Ethanol and Biogas Production. The BFD for scenario 3 is presented in Figure 6. The feedstock is handled in an area similar to the previous scenarios. Afterwards, the feedstock is conveyed to the pretreatment area where it is subjected to continuous steam explosion pretreatment (Figure 7). The process design was similar to the process presented by Shafiei et al. [13] with some modifications for the new raw material and lower capacity. Briefly, the system consists of three parallel pretreatment units, each of them has screw conveyors, presteamer, flash vessel, pretreatment reactor, and expansion tank. The treated materials are used for bioethanol production in a process similar to scenario 1. Moreover, the dehydration and wastewater treatment units are similar to scenario 1 [12]. The raw biogas is sold as a byproduct for heat and power generation.

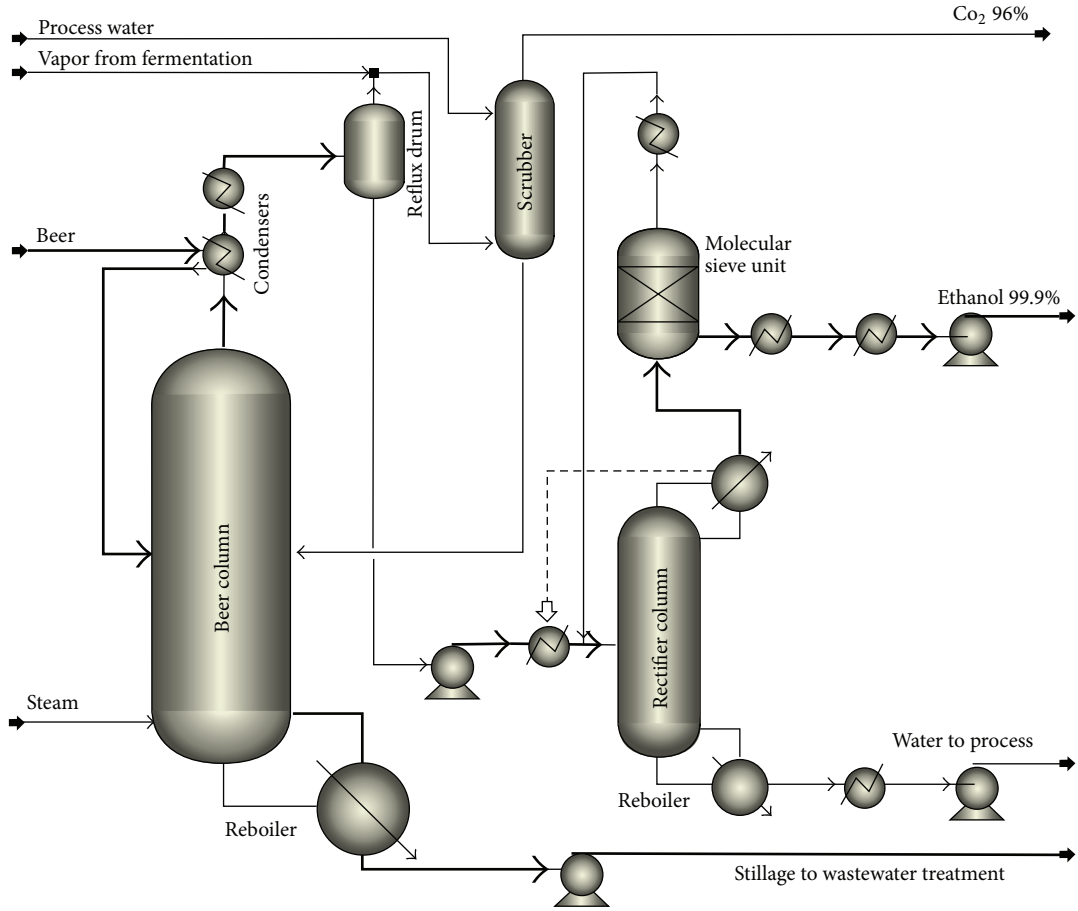

Figure 3: PFD of distillation unit. Beer is processed by a beer column, a rectifier column, and a molecular sieve unit and the product is fuel ethanol (scenarios 1 and 3).

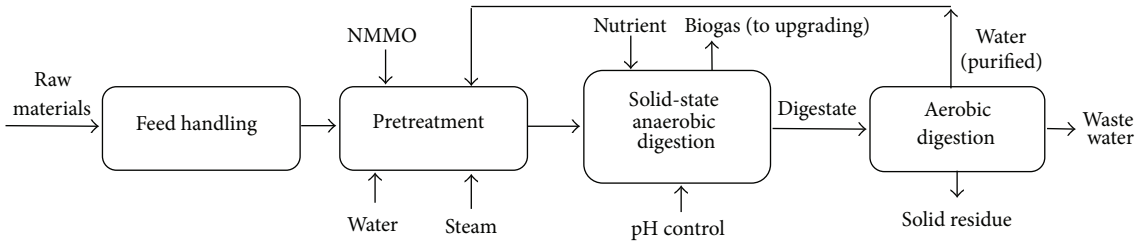

Figure 4: BFD of scenario 2: NMMO pretreatment for production of biomethane.

Table 1: The process conditions for the equipment of NMMO pretreatment in Figure 2.

Equipment/ conditions	Preheater 1	Preheater 2	Pretreatment	Multistage solid wash	Evaporator 1	Flash drum 1	Evaporator 2	Flash drum 2	Compressor
Input T (°C)	20	90	120	120[a], 45[b]	87.3	79.8	79.8	90	100
Output T (°C)	90	120	120	45[a], 62[b]	79.8	79.8	90	90	170
Input P (barg)	0	0	0.5	3	0	−0.78	−0.78	−0.97	0
Output P (barg)	0	0.5	0.5	3	−0.78	−0.78	−0.97	−0.97	0.64

[a]The temperature of main streams.
[b]Temperature of washing water.

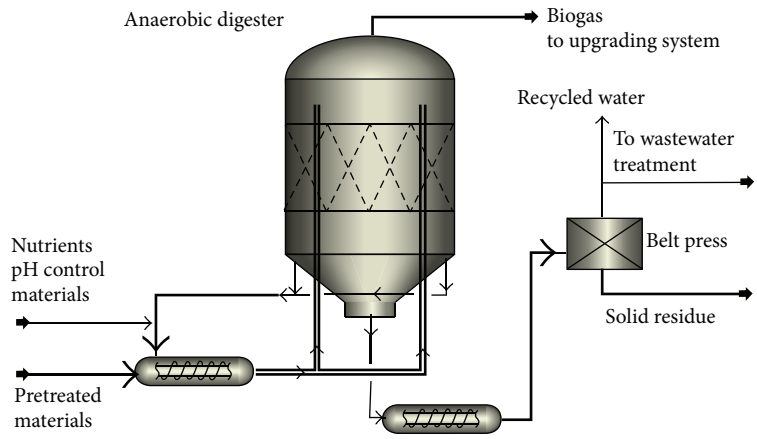

Figure 5: PFD of solid-state biogas production unit (scenarios 2 and 4).

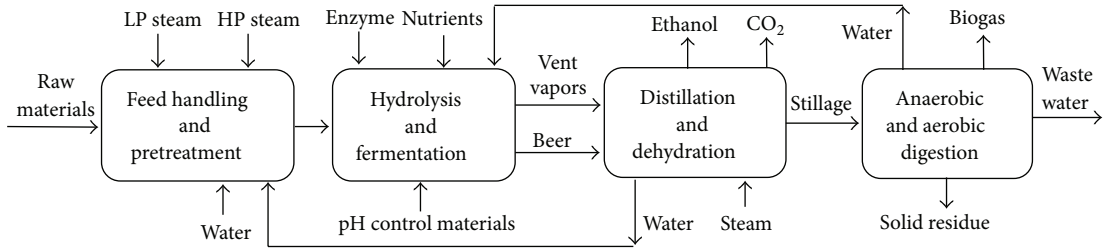

Figure 6: BFD of scenario 3: steam explosion pretreatment for production of ethanol and biogas.

2.1.4. Scenario 4: Steam Explosion Pretreatment for Improvement of Biogas Production. In scenario 4 (Figure 8), the feedstock handling and pretreatment area are similar to scenario 3. However, the materials are sent for solid-state biogas production in a process similar to scenario 2. The water from the process is purified using macrofilters and reverse osmosis system and partially recycled to the process. Complete recycling is not possible due to accumulation of some ions and chemicals in the process. The biogas is upgraded and pressurized in a process similar to scenario 2 [17, 18].

2.2. Plant Location and Capacity. Sweden was selected for the plant location because of its large biofuel vehicle fleet in Europe [19]. In order to support the economy of the biofuel production plant, it is necessary to locate it nearby a CHP plant. In such a way, a part of capital costs for steam and electricity production is reduced. Several CHP plants are already built in Sweden for production of energy from wood, municipal waste, and forest biomass. Most of the CHP plants in the main cities of Sweden are large enough to support the electricity and steam requirement of the biofuel plant. For instance, each of the CHP plants in Stockholm area produces 800–1700 GW heat and 200–750 GW electricity [20]. Finally, the availability of raw material and transportation costs would affect the final decision for exact selection of the plant location.

Wood is already used in Sweden for energy production. For example, in Brista plant in Stockholm, 350,000 ton per year of wood chips is used [20]. In this study, the plants were designed for utilization of 100,000 ton/year pinewood which have a half of the capacity of previous studies [12]. The wooden raw material required for this plant is around 1% of the total amount of 16 million m^3 of sawn wood (spruce and pine) produced in Sweden [21].

Biogas, the byproduct of scenarios 1 and 3, can be sold to the CHP plant for combustion. Solid residue, another byproduct of the processes, contains about 30% dry material. Over 70% of the dry material of solid residue is lignin, and other main materials are cellulose, hemicellulose, and biomass. Solid residue may be further used in gasification, pyrolysis, or combustion processes. However, presence of water in the solid residue is one of the major challenges for gasification and pyrolysis [22]. Thus, solid residue is sold to the CHP plant for burning.

2.3. Process Simulation and Economic Evaluation. The main equipment of the four processes was simulated by Aspen

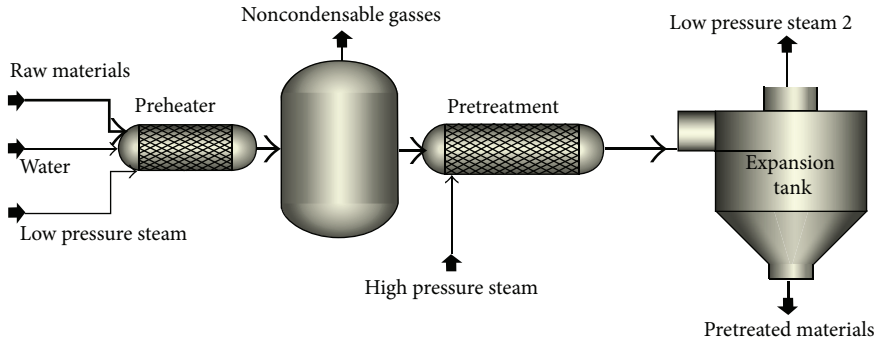

Figure 7: PFD of steam explosion pretreatment unit (scenarios 3 and 4).

Table 2: The process conditions for equipment of ethanol distillation in Figure 3.

Equipment/conditions	Beer column	Scrubber column	Rectifier column	Molecular sieve unit
Top input T (°C)	50[a], 40[b]	25	—	—
Bottom input T (°C)	110	39	90	106
Top output T (°C)	60	39	106	103
Bottom output T (°C)	67.6	40	132	103
Top input P (barg)	0.5[a], 0.5[b]	1	—	—
Bottom input P (barg)	0.43	0	3	1.9
Top output P (barg)	−0.81	−0.1	1.9	0.8
Bottom output P (barg)	−0.61	0	2.2	0.8
Number of trays	30	10	35	Packed

[a]The temperature of feed stream.
[b]The temperature of stream from scrubber.

plus simulation software. Unique features of this software are handling of materials in solid state and broad property data bank, which are beneficial for the best design, simulation, and optimization of the processes [23]. The software does the rigorous calculations for the equipment using a detailed model and determines the mass and energy in all streams of the process. For the physical and thermodynamic properties of the wood, a data bank prepared by NREL (National Renewable Energy Laboratory, USA) [24] was introduced to the software.

Based on the results from simulation, equipment sizing and optimization were performed using Aspen plus and Aspen PEA. Afterwards, the costs were estimated for all major equipment with Aspen PEA. The cost for some units was estimated based on the literature: ethanol dehydration unit [25], steam explosion equipment [25], and biogas upgrading and pressurizing [26]. Basic assumptions for economic evaluation are similar to the previous studies [13] with the following modifications.

(i) The capacity is reduced to 100,000 ton of dry materials per year.

(ii) Chemical engineering cost index of 2014 was used for the cost estimations.

(iii) The construction periods for scenarios 1 to 4 are 20, 36, 21, and 30 weeks per Aspen PEA suggestion.

The manufacturing costs of ethanol and biomethane were calculated according to the method presented by Peters and Timmerhaus [27]; however, the credit of the byproducts was subtracted from the manufacturing cost.

2.4. Sensitivity Analysis. A sensitivity analysis was performed to determine the most effective parameters (among the raw materials and byproducts) in the economy of the process. For the better comparison of four scenarios, the gasoline equivalent prices of the products were calculated using the lower heating values of the fuels which are 36.1 MJ/Nm^3 for biomethane, 21.2 MJ/l for bioethanol, and 32.0 MJ/l for gasoline.

3. Results and Discussion

Based on the experimental results [5], two scenarios for production of bioethanol and biogas using NMMO pretreatment were developed. The economy of these two scenarios was compared with the economy of two similar scenarios with steam explosion pretreatment.

3.1. Mass and Energy Balances. Four scenarios for the production of bioethanol and biogas were simulated by Aspen plus (Figures 2, 3, 5, and 7). Based on the simulation results, the required raw materials and utilities as well as product specifications are shown in Table 3. Because of the better

Table 3: The amount of raw materials/products and utilities used/produced in each scenario.

	Scenario 1	Scenario 2	Scenario 3	Scenario 4	Price (€/kg)
Raw materials (tpy)[1]					
Pinewood (wet)	105,263	105,263	105,263	105,263	0.06
Nutrients	1100	200	1100	200	0.6
pH control	200	1220	200	1220	0.24/0.15[2]
Enzymes	1,512		1,512		1.226
NMMO	1,536	1,536			4
Products (tpy)[3]					
Methane (m^3/y)		21,387,468		16,538,970	1.15[4]
Biogas (m^3/y)	5,952,956		5,217,778		0.75[5]
Solid residue (lignin)	51,317	51,248	56,884	59,112	0.04
LP steam 2[6]			61,912	61,920	0.003
Ethanol (m^3/y)	30,015		22,132		0.85[7]
CO_2	21,921		18,480		0.05
Sludge from WWT	250	3,879	232	3,612	0.04
Utilities (tpy)[3]					
Process water	166,324	123,815	121,424	62,264	0.0001
LP steam[6]			30,500	30,500	0.004
HP steam[8]	32,324	3,154	89,171	60,000	0.008
Electricity (Mwh)	17,964	18,076	14,086	14,379	30

[1]tpy: ton per year
[2]The main material for controlling pH in fermentation is NaOH solution (0.24 €/kg). In anaerobic digestion sodium carbonate (0.15 €/kg) is mainly added for maintaining the buffering capacity.
[3]tpy: ton per year, unless stated.
[4]The biomethane is sold at price of 1.15 €/m^3, which excludes VAT and selling and distribution costs.
[5]The biogas is sold at price of 0.75 €/m^3, which excludes VAT and selling and distribution costs.
[6]LP steam: low pressure steam.
[7]The price unit is 0.85 €/lit of bioethanol (99.9%). The price excludes VAT and selling and distribution costs.
[8]HP steam: high pressure steam.

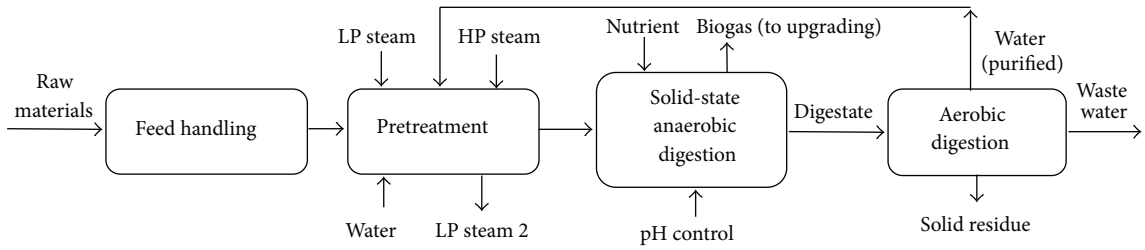

Figure 8: BFD of scenario 4: steam explosion pretreatment for production of biomethane.

efficiency of the NMMO pretreatment, the amount of ethanol and biogas in scenarios 1 and 2 was higher compared to scenarios 3 and 4. Therefore, better hydrolysis and digestion in scenarios 1 and 2 lead to production of less solid residues. After steam explosion, the exhaust steam from the expansion tanks can be returned to the CHP plant to be reused in the process. This steam contains 0.15% volatile furans which must be removed before being reused. Carbon dioxide is produced in all of the processes. The purity of carbon dioxide from bioethanol process is over 99%, and it can be sold as a byproduct; however, in the biomethane scenarios, it contributes to about 50% of the raw biogas and cannot be sold.

3.2. Total Project Investment. Total project investments calculated by Aspen PEA for scenarios 1 to 4 were 44.0, 69.7, 40.5, and 65.1 million €, respectively. The required capital for NMMO pretreatment was significantly higher than that for the steam explosion pretreatment (Table 4). Although ethanol production required more operating units, that is, hydrolysis, distillation, and dehydration, the facilities for biogas production were more expensive than the equipment required for ethanol production. The digesters were more expensive since the anaerobic digestion requires longer retention time of the materials (20 days) compared with 48 hours for the hydrolysis and fermentation in the ethanol production (Table 4). Additionally, the capital for the biogas upgrading

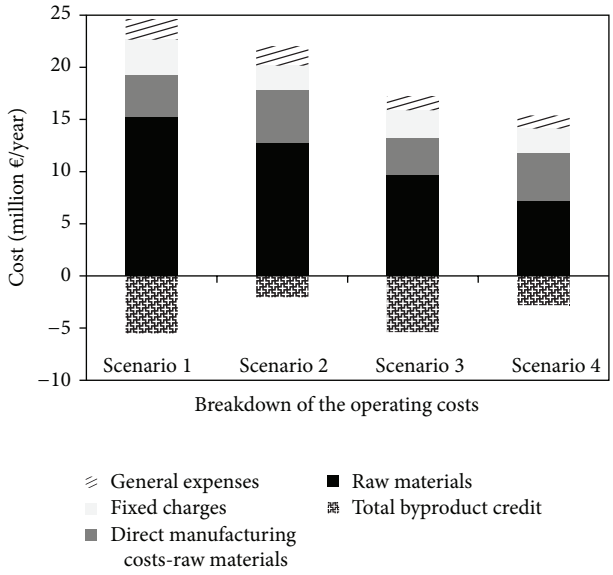

Figure 9: Breakdown of the operating costs for different scenarios.

and pressurizing was more expensive compared with the equipment for distillation and dehydration of ethanol.

3.3. Cost Distributions. The breakdown of the operating costs is depicted in Figure 9. The direct manufacturing costs include the costs for raw materials; operating labor and direct supervisory; utilities, maintenance, and repairs; and operating charges. The fixed charges include 30% taxation on the plant income as well as the plant overhead. General expenses include the costs for research and development and financing (10% return rate) and administrative costs. NMMO, lignocellulosic feedstock, and the enzymes are the most costly raw materials. The byproducts of bioethanol plants are biogas, solid residue, and carbon dioxide, while solid residue is the only byproduct of the biogas plants.

3.4. Manufacturing Costs and Gasoline Equivalent Prices. In Sweden, taxes are applied on the plant income as well as 25% value added tax on the final price of the products. Additionally, two other taxes are applied on the fossil fuels, but not on the biofuels, which are taxes for energy and carbon dioxide. The amounts of these taxes for gasoline were correspondingly 2.97 and 2.38 SEK/l in 2013. Therefore, tax contributes to 58% of gasoline price [4]. The portion of each of the taxes on the final prices of the biofuels is presented in Table 5. The average price of E85 (fuel ethanol) [28] was 1.14 €/l (9.85 SEK/l converted based on the average Euro price in 2013 [29]). The manufacturing costs were calculated with considering all the parameters presented in Figure 9, including 30% tax on the plant income. The manufacturing costs of ethanol for scenarios 1 and 3, excluding VAT and selling and distribution costs, were calculated to be 0.64 or 0.54 €/l, respectively. The final price for bioethanol including the costs for selling and distribution and the taxes for scenarios 1 and 3 would be 0.93 €/l and 0.83 €/l, respectively. These prices are still lower than the fuel ethanol as well as gasoline (Table 5). The manufacturing costs of the biomethane (97%, pressurized, including plant income tax, VAT, and selling and distribution costs) for scenarios 2 and 4 were calculated to be 1.35 and 1.17 €/Nm^3 methane, respectively.

The gasoline equivalent prices of the final products, ready for selling at station, are presented in Table 5. The gasoline equivalent prices of all scenarios are lower than the average of gasoline price; however, the safe margin for scenario 1 is lower than other processes. Scenario 4 presents the best product price while scenario 1 shows the highest product price. Despite the better efficiency of the NMMO pretreatment, higher capital and higher raw material expenses of this process have led to higher manufacturing costs for ethanol (scenario 1 compared with scenario 3) and biogas (scenario 2 compared with scenario 4). Another point is that the processes for production of biogas were not as profitable as the ethanol processes, since investment costs for biomethane production are significantly higher than those of the bioethanol process.

The gasoline equivalent expenses of E85 and biomethane 100 are 4% and 16% lower than gasoline, and the prices for the four scenarios are 15–37% less than the fossil fuel. However, only addition of energy and carbon dioxide taxes to the fossil fuels helped the competition of biofuels in the fuel market. Furthermore, there are other bonuses for biofuel vehicles, such as discount on car insurance, free parking spaces, lower annual registration taxes, and exemption from Stockholm congestion tax. Note that the manufacturing cost must be lower than the selling price to earn enough profit.

3.5. Sensitivity Analysis. The effects of price of the most important raw materials on the production cost of ethanol and methane are presented in Figure 10. While other raw materials, for example, nutrients and utilities, did not significantly affect the operating expenses (data not shown), the results of sensitivity analysis indicate that NMMO price had the most significant effect on the manufacturing cost of the products (Figures 10(b), 10(e), and 10(g)) (scenarios 1 and 2). For example, 50% increase in the price of NMMO results in 11% increase in the gasoline equivalent prices. The next two effective parameters are the price of the lignocellulosic feedstock (Figures 10(a), 10(d), and 10(f)) and the enzyme price (Figures 10(c) and 10(h)). Increasing 50% in the wood price has led to 8%, 8%, 13%, and 12% of the gasoline equivalent prices of scenarios 1 to 4, respectively. About 50% increase in the enzyme price for scenarios 1 and 3 has led to 3% and 4% increase in the gasoline equivalent prices, correspondingly. The processes for production of bioethanol had the least safe margin if they are compared with the average petrol price (1.65 €/l) in Sweden market (Figure 10).

The effects of byproduct prices on the manufacturing cost of the main products are presented in Figure 11. The data present the comparison of earning no profit from the byproduct or 50% increase in the byproduct price with the base cases. For scenarios 1 and 3, the credit from biogas and solid residue significantly affected the manufacturing costs (Figures 11(a) and 11(c)). For both scenarios 1 and 3, CO_2

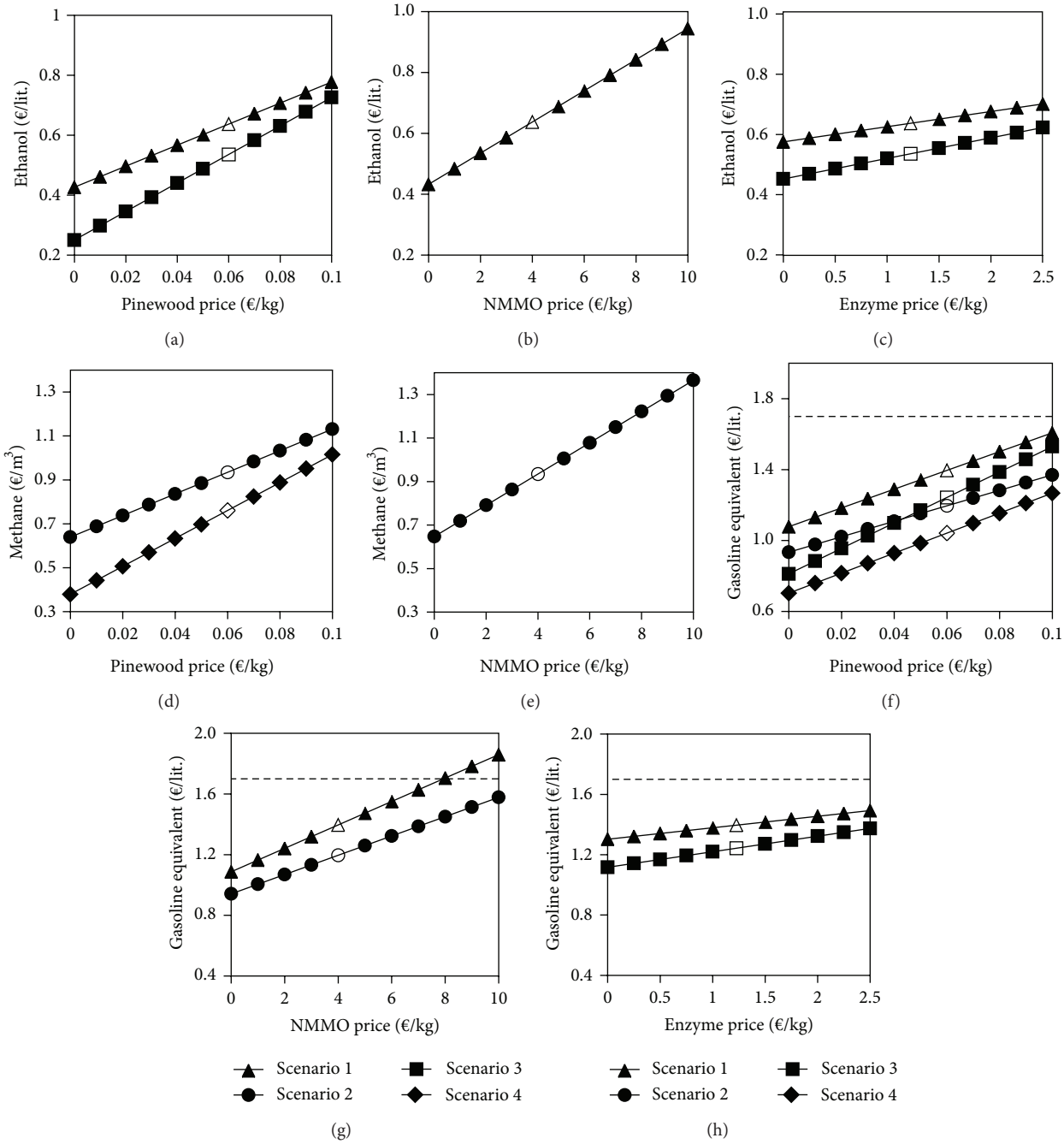

Figure 10: Effects of the price of wood, NMMO, and enzymes on the manufacturing cost of ethanol ((a), (b), and (c)), methane ((d), (e)), and the gasoline equivalent prices ((f), (g), and (h)) for scenarios 1 (▲), 2 (●), 3 (■), and 4 (◆). The dashed line corresponds to average gasoline price in the market. The empty shapes represent the base case values of manufacturing costs. The plant income tax is included in the calculation of the values, but VAT and selling and distribution costs were not added. The gasoline equivalent prices are the prices of ready products and include all expenses (c.f. Table 5).

had the least influence on the ethanol price. The price of solid residue was more effective in the manufacturing cost of methane in scenario 4 compared with scenario 2 (Figures 11(b) and 11(d)). The reason was lower efficiency of steam explosion pretreatment compared to NMMO pretreatment which results in lower digestion yield (scenario 4) and production of more solid residues (Table 3).

3.6. Profitability of the Processes. Discounted cash flow analysis for each scenario was performed using total capital investment and the annual operating costs. The costs include interests and time value of money. The payback period (payout period) for each scenario was calculated (Table 6) as the minimum length of time to recover the original capital investment. The payback period of the biogas plants was more than that

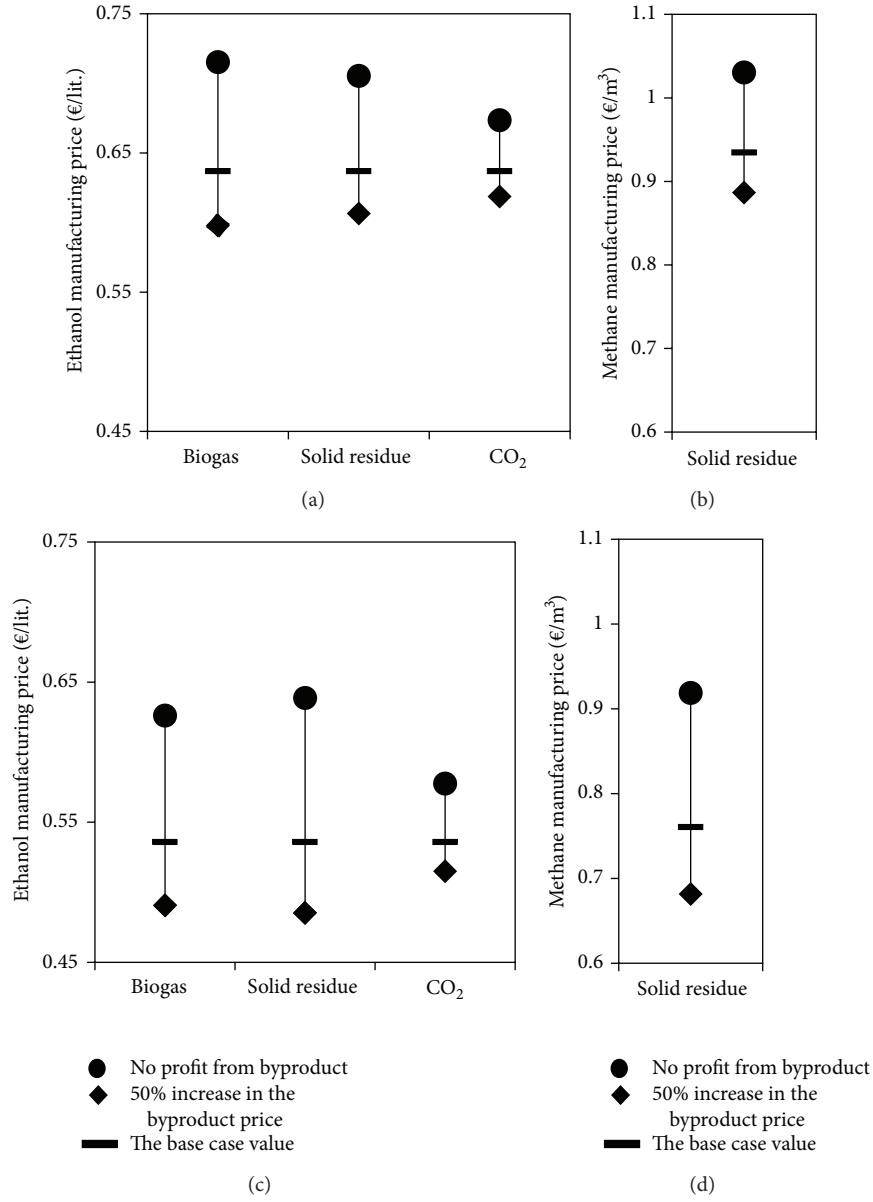

Figure 11: Effect of byproduct price on the manufacturing cost of ethanol and methane for scenarios 1 (a), 2 (b), 3 (c), and 4 (d). The values are prices before addition of VAT and selling and distribution costs.

of the bioethanol plant because of the higher capitals requirements. Net rate of return (NRR) shows the profitability of the processes and was calculated by dividing the net present value (NPV) by the present value (PV) of cumulative outflows. The NRR for ethanol production processes was positive while processes for biomethane production had negative NRR (Table 6).

The relative profitability of the processes is presented by profitability index (PI) (Table 6). PI shows the present value of benefits relative to the present value of costs; thus, the PI of a profitable project must be greater than one. The processes for ethanol production (scenarios 1 and 3) were profitable (PI > 1) and the processes for production of biomethane were not profitable (PI < 1).

4. Conclusions

Both NMMO and steam explosion led to economically feasible processes for ethanol production (PI > 1); however, none of the biomethane production processes were profitable (PI < 1). Therefore, production of biomethane as the only product from wood may not be economically profitable. However, biogas production from the waste streams of ethanol process considerably helps the economy of the process and reduces the negative environmental impacts. The processes using steam explosion pretreatment were more economically profitable compared to the processes with NMMO pretreatment. Although the pretreatment type significantly affects the yield of final product and consequently the economy of the

Table 4: Total project investment and its breakdown for the scenarios.

Scenario	1	2	3	4
Pretreatment	NMMO	NMMO	Steam explosion	Steam explosion
Product	Ethanol/biogas	Biomethane	Ethanol/biogas	Biomethane
Investment cost (million €)				
Feed handling	5.6	5.0	5.6	5.0
Pretreatment	10.2	10.0	6.4	6.4
Hydrolysis and fermentation	9.0	—	10.1	—
Distillation and dehydration	7.8	—	7.7	—
Biogas production	—	21.9	—	21.7
Biogas upgrading/compression	—	21.8	—	21.5
Water treatment	2.3	1.3	2.3	1.3
Utility	4.5	2.6	4.4	2.5
Storage	1.5	3.6	1.3	3.4
Working capital	3.1	3.5	2.7	3.3
Total project investment	44.0	69.7	40.5	65.1

Table 5: The manufacturing cost of biofuels and the tax portion of the final prices.

Cost (€/L) or (€/m^3)	Product cost	30% tax on plant income	Energy tax	Carbon dioxide tax	25% VAT[1]	Final Price	Final price (gasoline equivalent)
Gasoline[2]	0.70	—	0.34	0.28	0.33	1.65	1.65
E85[3]	0.82	—	0.05	0.04	0.23	1.14	1.59
Biomethane 100[4]	1.26	—	—	—	0.31	1.57	1.39
Manufacturing cost[5]							
Bioethanol[6] (scenario 1)	0.63	0.07	—	—	0.23[7]	0.93	1.40
Biomethane[8] (scenario 2)	0.97	0.07	—	—	0.31[9]	1.35	1.20
Bioethanol[6] (scenario 3)	0.50	0.10	—	—	0.23[7]	0.83	1.24
Biomethane[8] (scenario 4)	0.77	0.09	—	—	0.31[9]	1.17	1.04

[1]VAT is calculated as 25% of the product prices of biomethane which were 10.9 SEK/m^3 (1.26 €/Nm^3) and ethanol which were 7.9 SEK/L (0.82 + 0.05 + 0.04 = 0.91 €/L). Therefore, VAT for biomethane = 1.26 ∗ 0.25 = 0.31 €/Nm^3 and VAT for E85 = 0.91 ∗ 0.25 = 0.23 €/L.
[2]Average of gasoline (95% octane) in 2013 [4]. The gasoline includes 5% bioethanol.
[3]E85 is a blend of bioethanol and 15% gasoline. During winter time, the portion for gasoline increases to 25%. The portion of fossil fuel in E85 includes energy and CO_2 tax.
[4]Biomethane 100 contains 100% methane from biological sources and is sold in Sweden along with CNG.
[5]Manufacturing cost includes selling and distribution expenses which were 0.06 €/L for ethanol and 0.1 €/Nm^3 for biomethane.
[6]The plant product is 99.9% bioethanol.
[7]It is assumed that the product will be sold to the market in the same price of E85. Thus, VAT was assumed to be similar to VAT for E85.
[8]The plant product is 97% biomethane.
[9]It is assumed that the product will be sold to the market in the same price of biomethane 100. Thus, VAT was assumed to be similar to VAT for biomethane 100.

Table 6: The profitability parameters of the processes.

Scenario	1	2	3	4
Pretreatment	NMMO	NMMO	Steam explosion	Steam explosion
Product	Ethanol/biogas	Biomethane	Ethanol/biogas	Biomethane
Payback period (year)	6.3	8.3	6.2	7.6
Net return rate (NRR) (%)	14.6	−6.3	16.7	−3.0
Profitability index (PI)	1.14	0.93	1.16	0.96

NMMO process, higher capital as well as more expensive raw materials reduced the overall profitability of the processes with NMMO pretreatment. The technoeconomic study for production of biomethane or ethanol shows that the average gasoline equivalent price of biomethane was 16% lower than that of ethanol and both were 18–39% lower than the taxed gasoline. The energy and carbon dioxide taxes on the gasoline significantly help this competition in favor of the biofuels. Application of cheaper cellulose solvents improves the economy of the process while maintaining high yields of biofuels.

Conflict of Interests

The authors declare that there is no conflict of interests regarding the publication of this paper.

Authors' Contribution

All experiments and paper preparation were done by Marzieh Shafiei, and the rest of the authors supervised the experiments and revised the paper.

Acknowledgments

The authors are grateful for the financial support from the Swedish Energy Agency and Institute of Biotechnology and Bioengineering, Isfahan University of Technology.

References

[1] M. J. Taherzadeh and K. Karimi, "Pretreatment of lignocellulosic wastes to improve ethanol and biogas production: a review," *International Journal of Molecular Sciences*, vol. 9, no. 9, pp. 1621–1651, 2008.

[2] J. Yliopisto, "Evaluation of potential technologies and operational scales reflecting market needs for low-cost gas upgrading systems," Seventh framework programme theme energy, Biowaste as feedstock for 2nd generation, 2009, http://www.valorgas.soton.ac.uk/deliverables.htm.

[3] M. Linné and O. Jönsson, *Summary and Analysis of the Potential for Production of Renewable Methane (Biogas and SNG) in Sweden*, 2004, http://www.biogasmax.co.uk/media/summary_and_analysis_april2005__022436100_1644_26042007.pdf.

[4] "Så här byggs bensinpriset upp," http://www.preem.se/templates/page____791.aspx.

[5] M. Shafiei, K. Karimi, H. Zilouei, and M. J. Taherzadeh, "Enhanced ethanol and biogas production from pinewood by NMMO pretreatment and detailed biomass analysis," *BioMed Research International*, vol. 2014, Article ID 469378, 10 pages, 2014.

[6] M. Shafiei, K. Karimi, and M. J. Taherzadeh, "Pretreatment of spruce and oak by N-methylmorpholine-N-oxide (NMMO) for efficient conversion of their cellulose to ethanol," *Bioresource Technology*, vol. 101, no. 13, pp. 4914–4918, 2010.

[7] N. Poornejad, K. Karimi, and T. Behzad, "Improvement of saccharification and ethanol production from rice straw by NMMO and [BMIM][OAc] pretreatments," *Industrial Crops and Products*, vol. 41, no. 1, pp. 408–413, 2013.

[8] A. Goshadrou, K. Karimi, and M. Lefsrud, "Characterization of ionic liquid pretreated aspen wood using semi-quantitative methods for ethanol production," *Carbohydrate Polymers*, vol. 96, no. 2, pp. 440–449, 2013.

[9] N. Poornejad, K. Karimi, and T. Behzad, "Ionic liquid pretreatment of rice straw to enhance saccharification and bioethanol production," *Journal of Biomass to Biofuel*, vol. 1, pp. 8–15, 2014.

[10] A. Aden and T. Foust, "Technoeconomic analysis of the dilute sulfuric acid and enzymatic hydrolysis process for the conversion of corn stover to ethanol," *Cellulose*, vol. 16, no. 4, pp. 535–545, 2009.

[11] A. Ekman, O. Wallberg, E. Joelsson, and P. Börjesson, "Possibilities for sustainable biorefineries based on agricultural residues—a case study of potential straw-based ethanol production in Sweden," *Applied Energy*, vol. 102, pp. 299–308, 2013.

[12] M. Shafiei, K. Karimi, and M. J. Taherzadeh, "Techno-economical study of ethanol and biogas from spruce wood by NMMO-pretreatment and rapid fermentation and digestion," *Bioresource Technology*, vol. 102, no. 17, pp. 7879–7886, 2011.

[13] M. Shafiei, M. M. Kabir, H. Zilouei et al., "Techno-economical study of biogas production improved by steam explosion pretreatment," *Bioresource Technology C*, vol. 148, pp. 53–60, 2013.

[14] "Product benefits of Cellic CTec3," http://bioenergy.novozymes.com/en/cellulosic-ethanol/CellicCTec3/product-description/Pages/default.aspx.
CellicCTec3/product-description/Pages/default.aspx.

[15] J. D. Murphy and N. Power, "Technical and economic analysis of biogas production in Ireland utilising three different crop rotations," *Applied Energy*, vol. 86, no. 1, pp. 25–36, 2009.

[16] L. D. Baere, *The Dranco Technology: A Unique Digestion Technology for Solid Organic Waste*, 2010, http://www.ows.be/wp-content/uploads/2013/02/The-DRANCO-technology-2012.pdf.

[17] M. Abdal, *Private Communications*, Sepahan Biological Products Company, Isfahan, Iran, 2014.

[18] M. Sadeghi, *Private Communications*, Parsian Pooya Polymer Company, Isfahan, Iran, 2014.

[19] A. Sanches-Pereira and M. F. Gómez, "Towards a cleaner vehicle fleet: the dynamics of the Swedish biofuel system," in *International Workshop Advances in Cleaner Production*, UNIP, Sao Paulo, Brazil, 2013.

[20] "Combined heat and power production in Sweden," http://www.fortum.com/en/energy-production/combined-heat-and-power/sweden/pages/default.aspx.

[21] L. Borden and M. S. Arwidson, "Products from the forest—a natural choice," The Swedish Forest Industry's Sustainability, 2008.

[22] S. Kumar, "Hydrothermal processing of biomass for biofuels," *Biofuel Research Journal*, vol. 1, no. 2, pp. 34–43, 2014.

[23] "Optimize design and operations with Aspen ONE Engineering," http://www.aspentech.com/products/aspenone-engineering/.

[24] R. J. Wooley and V. Putsche, "Development of an Aspen Plus physical property database for biofuels components," Tech. Rep. NREL/MP-425-20685, National Renewable Energy Laboratory, US Department of Energy Laboratory, 1996.

[25] A. Aden, M. I. Ruth, K. Ibsen et al., "Lignocellulosic biomass to ethanol process design and economics utilizing co-current dilute acid prehydrolysis and enzymatic hydrolysis for corn stover," NREL/TP 510-32438, National Renewable Energy Laboratory, US Department of Energy Laboratory, 2002.

[26] M. Persson, "Evaluation of upgrading techniques for biogas," 2003, http://cdm.unfccc.int/filestorage/E/6/T/E6TUR2NNQW9O83ET10CX8HTE4WXR2O/Evaluation%20of%20Upgrading%20Techniques%20for%20Biogas.pdf?t=WGd8bXpud2dpfDApZg3J-NNGYnJKCGkI9FnI.

[27] M. S. Peters and K. D. Timmerhaus, *Plant Design and Economics for Chemical Engineers*, McGraw Hill, New York, NY, USA, 1991.

[28] Price history, 2014, http://www.jet.se/sv_SE/pg1334073843105/private/Priser/Prishistorik.html.

[29] Convert Euros to Swedish Krona, 2014, http://www.currency.me.uk/convert/eur/sek.

Hindawi Publishing Corporation
BioMed Research International
Volume 2014, Article ID 691537, 6 pages
http://dx.doi.org/10.1155/2014/691537

Research Article

Fast Synthesis of Multilayer Carbon Nanotubes from Camphor Oil as an Energy Storage Material

Amin TermehYousefi,[1] Samira Bagheri,[2] Kawasaki Shinji,[3] Jalal Rouhi,[4] Mohamad Rusop Mahmood,[4] and Shoichiro Ikeda[1]

[1] *ChECA IKohza, Department of Environmental & Green Technology (EGT), Malaysia Japan International Institute of Technology (MJIIT), University Technology Malaysia (UTM), Kuala Lumpur, Malaysia*
[2] *Nanotechnology & Catalysis Research Centre (NANOCAT), IPS Building, University of Malaya, 50603 Kuala Lumpur, Malaysia*
[3] *Nagoya Institute of Technology, Gokiso-Cho, Showa-Ku, Nagoya 466-8555, Japan*
[4] *NANO-SciTech Centre, Institute of Science, Universiti Teknologi MARA (UiTM), Shah Alam, Selangor, Malaysia*

Correspondence should be addressed to Samira Bagheri; samira_bagheri@um.edu.my

Received 18 June 2014; Revised 29 July 2014; Accepted 31 July 2014; Published 2 September 2014

Academic Editor: Meisam Tabatabaei

Among the wide range of renewable energy sources, the ever-increasing demand for electricity storage represents an emerging challenge. Utilizing carbon nanotubes (CNTs) for energy storage is closely being scrutinized due to the promising performance on top of their extraordinary features. In this work, well-aligned multilayer carbon nanotubes were successfully synthesized on a porous silicon (PSi) substrate in a fast process using renewable natural essential oil via chemical vapor deposition (CVD). Considering the influx of vaporized multilayer vertical carbon nanotubes (MVCNTs) to the PSi, the diameter distribution increased as the flow rate decreased in the reactor. Raman spectroscopy results indicated that the crystalline quality of the carbon nanotubes structure exhibits no major variation despite changes in the flow rate. Fourier transform infrared (FT-IR) spectra confirmed the hexagonal structure of the carbon nanotubes because of the presence of a peak corresponding to the carbon double bond. Field emission scanning electron microscopy (FESEM) images showed multilayer nanotubes, each with different diameters with long and straight multiwall tubes. Moreover, the temperature programmed desorption (TPD) method has been used to analyze the hydrogen storage properties of MVCNTs, which indicates that hydrogen adsorption sites exist on the synthesized multilayer CNTs.

1. Introduction

Research and development of energy in the 21st century focused on a wide range of renewable energy sources, due to concerns over fossil fuel and its ever-aggravating impact on global warming, environments, and the crisis of natural resource depletion [1, 2]. Carbon nanotubes have gained significant research interest for their potential applications, such as generating electricity [3] and electricity storage [4], that is, the administrable ability to capture, store, and deliver generated power. The properties of CNTs depend on the arrangement of their graphitic rings and the diameter of their helical structure [5].

CVD is a common CNTs synthesis method based on thermal decomposition of hydrocarbon vapors [6]. The properties of CNTs depend not only on the deposition condition but the starting precursor as well [7]. For various kinds of the deposition process, graphite target is commonly used for the preparation of carbon-based materials [8]. Natural essential oils, a major source of renewable energy, are regarded as promising to the world's thirst for energy [9, 10]. Camphor oil is found in wood of the camphor laurel (*Cinnamomum camphora*), which is a large evergreen tree found in Asia, Dryobalanops aromatica, a giant of the Bornean forests, and some other related trees in the laurel family, notably Ocotea usambarensis. Camphor readily ignites and burns without producing any residue. However, camphor ($C_{10}H_{16}O$), which consists of both sp^2 and sp^3 carbons, is an attractive new material for carbon-based preparation, since graphite has only sp^2 carbon [11].

The petroleum-based precursors for synthesis of CNTs have been investigated in detail, and the easy availability of high-grade precursors has resulted in the production and process optimization of different types, structure, dimension, and orientations of CNTs. However, the naturally occurring hydrocarbon precursors have generated some interest because of the possibility of production of CNTs from the bank of hydrocarbons that are being renewably produced by nature in a carbon-neutral manner [12]. So, it becomes important to search for new natural renewable precursors that are easily available and are low in cost, such as essential oils. Of course, it calls for studies that are related to yield and quality of the CNTs being produced and the applications of the resultant CNTs.

Grown MVCNTs arrays with different diameter distribution feeding gas velocity (sccm) have significant effects on CNTs, especially on their diameter distribution [13]. To date, the cause of diameter alterations in single CNTs structures has yet to be clearly understood [14]. Heterostructured multilayer CNTs are fabricated via conventional methods separated by continuous steps, which may be repeated to provide three or more layers of CNTs [15]. Various catalyst formulations and reaction conditions have also been developed to enable the formation of multiple layers of CNTs through the use of appropriate catalysts for different layers [16]. Obtaining a comprehensive understanding of the CNTs growth mechanism is necessary to achieve better control of CNTs growth and design possible nanostructures [17].

Several researchers have reported different types of CNTs based on variations in the parameters in multiple processes [18]; however, to the best of our knowledge, the single step developed in this study is a new method that allows for the control of the diameter of CNTs on PSi. In the present study, MVCNTs were successfully synthesized on a PSi substrate in a one-step process using renewable natural camphor oil via CVD. Moreover, the diameter of CNTs produced through the optimized growth condition is limited by controlling the diffusion of feedstock and also hydrogen storage characteristic of the synthesized multilayer CNTs being analyzed.

2. Experimental Procedure

The experimental setup is based on horizontal electronic furnaces used to cover the quartz tube during CNTs fabrication. A mass flow controller was used to adjust the velocity of the carrier gas by means of syringe pump into Psi, which was fabricated via selective doping [19].

Camphor oil as a precursor was mixed with ferrocene and then introduced to the inlet of the quartz tube fitted by the first furnace to release the vaporized CNTs. The reaction temperature was increased to 180°C and maintained for 30 min to ensure that the precursor and catalysts were completely pyrolyzed. Ferrocene decomposes to form the iron catalyst necessary for the experiment, while camphor acts as a carbon source (feedstock) of the substrate in the second furnace. The CVD experiments commenced when the deposition temperature of the second furnace reached the optimal temperature (between 750 and 850°C). The exhaust argon gas in the quartz tube induced movement of the amorphous vaporized carbon into the second furnace by means of a mass flow controller, thereby allowing CNTs growth on the surface of the proposed substrate [20]. To identify the relation between the flow rate and CNTs diameter on the substrate, three flow rates were employed at 1 bar. Argon gas was injected into the inlet of the quartz tube at a maximum velocity of 600 sccm. After 10 min, the velocity was gradually decreased to 400 sccm as its median range of the flow rate. Then, after 20 min, the flow rate was decreased to 200 sccm until complete consumption of the carbon source. After 1 h of reaction time, the reactor was cooled down slowly to room temperature in Ar ambient space after the synthesis.

The CNTs were characterized by FESEM (ZEISS Supra 40VP) operated at 5 kV to evaluate the structure and diameter of the samples. Raman spectra were obtained using micro-Raman spectroscopy (Horiba Jobin Yvon-DU420A-OE-325), with Ar^+ ions at 514.5 nm to determine the adsorption, desorption, and surface area of the samples. The surface structure of the CNTs was confirmed by a VECTOR33 FT-IR instrument. The chemisorption analyses of the synthesized CNTs were done by TPDRO 1100.

During the TPD analysis, the sample, adequately pretreated, is submitted at an increasing temperature at a constant rate and is swept by an inert gas such as helium. The sample surface desorbs the gas that has been previously chemisorbed, and a suitable detector monitors the process. In the TPD studies, the solid system is previously equilibrated until saturation, with a probe gas in isothermal conditions at a given partial pressure [21].

3. Results and Discussion

As shown in Figure 1, vertically-aligned CNTs with high uniformity and nearly identical diameters were fabricated. FESEM images confirm that well-aligned CNTs with three different diameters were synthesized. As the flow rate decreases, the CNTs gradually thicken [22]. The duration of carrier gas feeding and its flow rate into the reaction zone are key parameters controlling the CNTs diameter [18]. The growth rates of the active ends of the CNTs vary proportionally to the flow rate of argon gas until complete consumption of the carbon source [23]. Alteration of the flow velocity during deposition and limited gas-flow rate control the growth conditions of the CNTs [24].

Considering the influx of vaporized CNTs to the PSi, the diameter distribution increases as the flow rate decreased in the reactor. The quantity of carbons covalently attached to the active end of the tube increased with decreasing flow rates [25]. Various diameters of CNTs are evident during structural transition of the feedstock around the substrate. During the first stage of the experiment, the average diameter of the tubes is approximately 30 nm, and high uniformity is observed. Reducing the flow rate during deposition process changes the diameters of the tubes and produces a central layer with uniformity that is identical to that in the first layer, with an average diameter of 75 nm. The minimum flow rate generates the last layer of multilayer CNTs with the different geometry

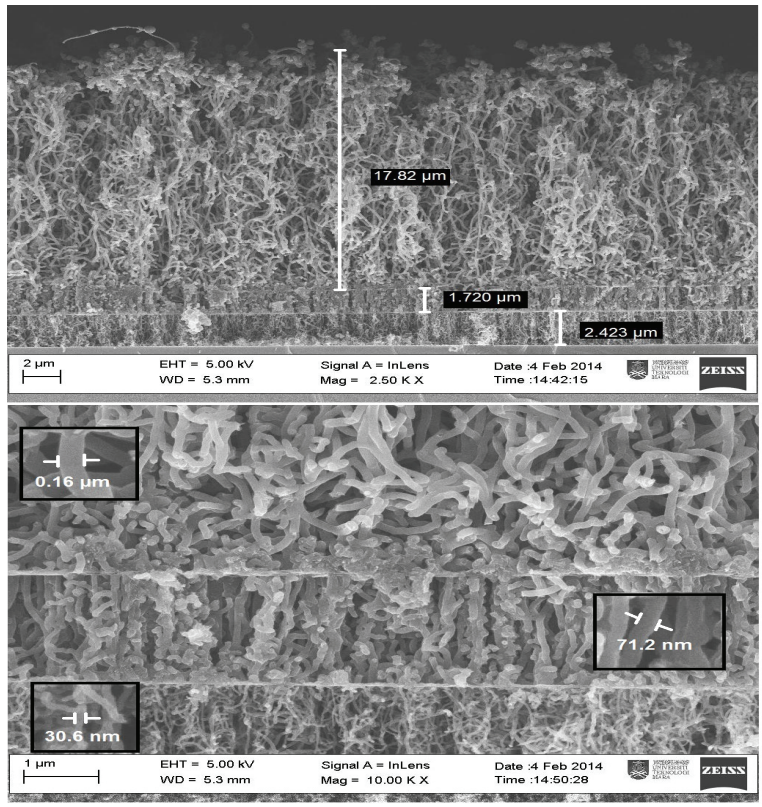

Figure 1: FESEM images of the heterostructured fast synthesized multilayer carbon nanotubes.

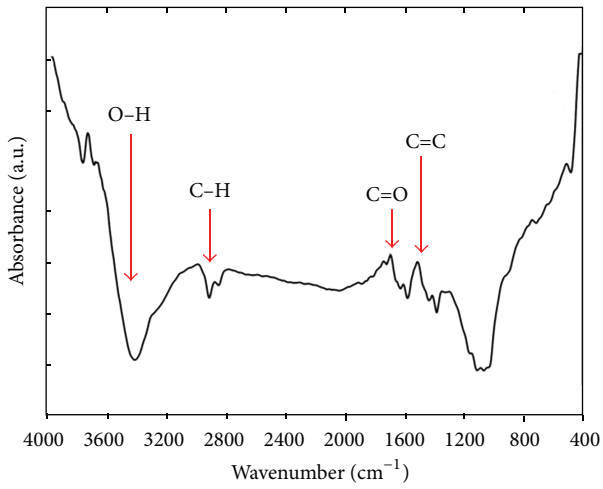

Figure 2: FT-IR spectrum of the fast synthesized multilayer carbon nanotubes.

as the previous layers and average diameter to up to 1 μm; this final layer is obtained by terminating the carbon source.

FESEM images show that variations in flow rate could systematically change the diameter distribution of the CNTs. We propose that at any given flow rate an optimal diameter exists for the CNTs. Varying the carrier gas flow rate during the growth process can be employed to control the growth of CNTs [13].

Table 1: FT-IR spectroscopy absorption bands of multilayer carbon nanotubes.

Frequency (cm^{-1})	Possible assignment
3424	H-bonded OH groups
2928	C–H bending, stretching
1699	C=O stretching
1540	C=C stretching

Given that other parameters, such as carbon feeding rate, temperature, and type of carrier gas, can be altered during CNTs synthesis, our hypothesis also can be developed due to alteration of the other parameters involved with growth process such as multilayer growth of CNTs dependence on temperature [26]. At low temperatures, only small nanoparticles are activated; altering the temperature parallel to the flow rate can change the growth efficiency and aspect ratio of the CNTs [25].

The FT-IR spectrum (400 cm^{-1} to 4000 cm^{-1}) of the fabricated CNTs is shown in Figure 2, and the related peaks are summarized in Table 1. The spectra were recorded using pressed disks of the pure solid powders combined with KBr. Only a small C–C stretch and a peak at 1532 cm^{-1} to 1560 cm^{-1} were observed, which indicates the presence of a carbon double bond (C=C); this finding confirms the hexagonal structure of the CNTs [27]. Figure 3 shows the Raman spectra of the CNTs.

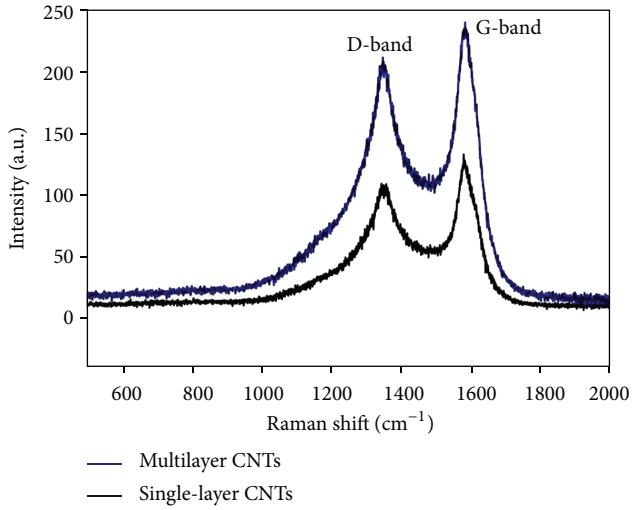

Figure 3: Raman spectra of the fast synthesized multilayer carbon nanotubes.

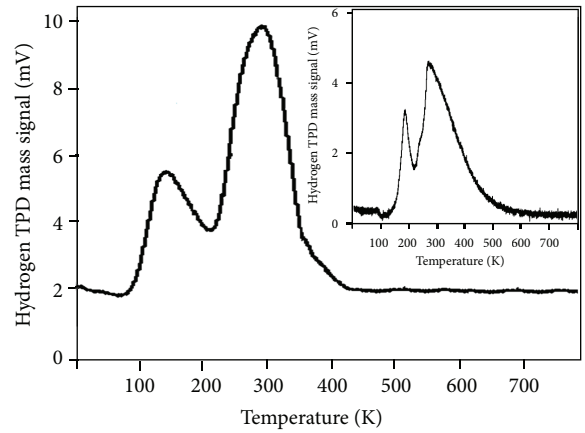

Figure 4: Hydrogen TPD spectra of the fast synthesized multilayer carbon nanotubes. Inset figure represents hydrogen TPD spectra of single layer carbon nanotubes.

The Raman results have been compared with the growth CNTs in a unique flow rate to ensure the effect of the transitive gas flow on the growth process. Accordingly, two main peaks are found at 1348 cm^{-1} and 1577 cm^{-1}; these peaks correspond to the D and G bands, respectively [28]. The I_D/I_G ratio suggests that the crystallinity of the synthesized CNTs under varying flow rates is identical to those grown under a fixed flow rate [29]. The I_D/I_G ratio for both types of CNTs is approximately 1.12. As such, the crystalline quality of the CNTs shows no major variation despite changes in flow rate [30].

The growth carbon nanotubes might be a suitable nanostructure for hydrogen storage devices, since for multiwall carbon nanotubes the hydrogen storage capacity is independent of tube's diameter [31]. Furthermore, there are also repulsive forces present between the H and C atoms. This energy tends to become larger as the diameter of tube increases. The potential of nanostructured materials is not only limited to energy storage and conversion devices but also to nanotransistors [32], actuators [33], electron field emission [34], and biological sensing devices [35].

The hydrogen adsorption properties of the fast synthesized multilayer CNTs were explored in Figure 4. Accordingly, the sample was degassed to 100°C and exposed to hydrogen at 760 Torr to obtain a TPD spectrum. For comparison, a TDP spectrum of a single layer CNTs also was degassed in the same condition, which was shown in the inset in Figure 4. In both cases, the sample was cooled to ~190 K, while the H_2 gas was evacuated [36]. These results indicate that unique hydrogen adsorption sites exist on the fast synthesized multilayer CNTs and display a hydrogen adsorption capacity at near ambient conditions that is ~2x greater than that of single layer CNTs. Therefore, conclusively, it can be concluded that multilayer CNTs may also be promising candidates for vehicular hydrogen storage applications [37].

4. Conclusion

Well-aligned CNTs with three different diameters have been synthesized by employing different flow rates. FESEM images show that varying the flow rate could systematically change the diameter distribution of the CNTs. Reducing the flow rate during deposition process changes the diameter of the tubes, thereby producing a central layer of CNTs with the same uniformity as that in the first layer. The minimum flow rate generates the last layer of the CNTs structure with the same geometry as the previous layers and high average diameter. FT-IR spectrum indicates the presence of carbon double bonds (C=C), which confirms the integrity of the hexagonal structure of the CNTs. The obtained Raman spectra indicate that the crystallinity of the CNTs structure exhibits no major variation despite changes in flow rate. According to the TPD method for the hydrogen storage properties of MVCNTs, the fast synthesized multilayer CNTs for the hydrogen adsorption capacity at near ambient conditions are ~2x greater than the single-layer CNTs. These results demonstrate a new geometric combination of CNTs based on heterostructured multilayer nanotubes, which can be used in energy storage devices because of their nanosize distribution of carbon nanotubes, accessible surface area, and high stability.

Conflict of Interests

The authors declare that they have no conflict of interests.

Acknowledgments

This work was supported by the University Malaya Research Grant (BK018-2014) and High Impact Research Grant UM.C/HIR/MOHE/ENG/44 from the Ministry of Higher Education (MOHE), Malaysia.

References

[1] Z. Cao and B. B. Wei, "A perspective: carbon nanotube macro-films for energy storage," *Energy Environmental Science*, vol. 6, no. 11, pp. 3183–3201, 2013.

[2] J. Sundaramurthy, N. Li, P. S. Kumar, and S. Ramakrishna, "Perspective of electrospun nanofibers in energy and environment," *Biofuel Research Journal*, vol. 1, no. 2, pp. 44–54, 2014.

[3] B. J. LeRoy, S. G. Lemay, J. Kong, and C. Dekker, "Electrical generation and absorption of phonons in carbon nanotubes," *Nature*, vol. 432, no. 7015, pp. 371–374, 2004.

[4] A. S. Aricò, P. Bruce, B. Scrosati, J.-M. Tarascon, and W. Van Schalkwijk, "Nanostructured materials for advanced energy conversion and storage devices," *Nature Materials*, vol. 4, no. 5, pp. 366–377, 2005.

[5] M. Liu and J. M. Cowley, "Structures of the helical carbon nanotubes," *Carbon*, vol. 32, no. 3, pp. 393–403, 1994.

[6] C. J. Lee, D. W. Kim, T. J. Lee et al., "Synthesis of aligned carbon nanotubes using thermal chemical vapor deposition," *Chemical Physics Letters*, vol. 312, no. 5-6, pp. 461–468, 1999.

[7] Y. Chen, C. Gan, T. Zhang, G. Yu, P. Bai, and A. Kaplan, "Laser-surface-alloyed carbon nanotubes reinforced hydroxyapatite composite coatings," *Applied Physics Letters*, vol. 86, no. 25, Article ID 251905, pp. 1–3, 2005.

[8] K. Koziol, B. O. Boskovic, and N. Yahya, "Synthesis of carbon nanostructures by CVD method," *Advanced Structured Materials*, vol. 5, pp. 23–49, 2011.

[9] S. R. Bull, "Renewable energy today and tomorrow," *Proceedings of the IEEE*, vol. 89, no. 8, pp. 1216–1226, 2001.

[10] M. Akia, F. Yazdani, E. Motaee et al., "A review on conversion of biomass to biofuel by nanocatalysts," *Biofuel Research Journal*, vol. 1, no. 1, pp. 16–25, 2014.

[11] G. Kasiraman, B. Nagalingam, and M. Balakrishnan, "Performance, emission and combustion improvements in a direct injection diesel engine using cashew nut shell oil as fuel with camphor oil blending," *Energy*, vol. 47, no. 1, pp. 116–124, 2012.

[12] Z. Sadeghian, "Large-scale production of multi-walled carbon nanotubes by low-cost spray pyrolysis of hexane," *New Carbon Materials*, vol. 24, no. 1, pp. 33–38, 2009.

[13] C.-S. Kuo, A. Bai, C.-M. Huang, Y.-Y. Li, C.-C. Hu, and C.-C. Chen, "Diameter control of multiwalled carbon nanotubes using experimental strategies," *Carbon*, vol. 43, no. 13, pp. 2760–2768, 2005.

[14] A. T. Yousefi, S. Ikeda, M. R. Mahmood et al., "Simulation of nano sensor based on carbon nanostructures in order to form multifunctional delivery platforms," *Advanced Materials Research*, vol. 832, pp. 778–782, 2014.

[15] L. Dai and S. Huang, "Multilayer carbon nanotube films and method of making the same," Google Patents, 2004 .

[16] A. M. Cassell, M. Meyyappan, and J. Han, "Multilayer film assembly of carbon nanotubes," *Journal of Nanoparticle Research*, vol. 2, no. 4, pp. 387–389, 2000.

[17] Q. Zhang, J. Q. Huang, M. Q. Zhao, W. Z. Qian, Y. Wang, and F. Wei, "Radial growth of vertically aligned carbon nanotube arrays from ethylene on ceramic spheres," *Carbon*, vol. 46, no. 8, pp. 1152–1158, 2008.

[18] C. Singh, M. S. P. Shaffer, and A. H. Windle, "Production of controlled architectures of aligned carbon nanotubes by an injection chemical vapour deposition method," *Carbon*, vol. 41, no. 2, pp. 359–368, 2003.

[19] T. E. Bell, P. T. J. Gennissen, D. Demunter, and M. Kuhl, "Porous silicon as a sacrificial material," *Journal of Micromechanics and Microengineering*, vol. 6, no. 4, pp. 361–369, 1996.

[20] Y. Hao, Z. Qunfeng, W. Fei, Q. Weizhong, and L. Guohua, "Agglomerated CNTs synthesized in a fluidized bed reactor: agglomerate structure and formation mechanism," *Carbon*, vol. 41, no. 14, pp. 2855–2863, 2003.

[21] M. Fadoni and L. Lucarelli, "Temperature programmed desorption, reduction, oxidation and flow chemisorption for the characterisation of heterogeneous catalysts. Theoretical aspects, instrumentation and applications," in *Studies in Surface Science and Catalysis*, A. Dąbrowski, Ed., pp. 177–225, Elsevier, 1999.

[22] A. G. Kurenya, D. V. Gorodetskiy, V. E. Arkhipov, and A. V. Okotrub, "Evaluation of the optimal carrier gas flow rate for the carbon nanotubes growth," *Technical Physics Letters*, vol. 39, no. 3, pp. 258–261, 2013.

[23] M. Kumar and Y. Ando, "Chemical vapor deposition of carbon nanotubes: a review on growth mechanism and mass production," *Journal of Nanoscience and Nanotechnology*, vol. 10, no. 6, pp. 3739–3758, 2010.

[24] C. Lu and J. Liu, "Controlling the diameter of carbon nanotubes in chemical vapor deposition method by carbon feeding," *Journal of Physical Chemistry B*, vol. 110, no. 41, pp. 20254–20257, 2006.

[25] C. J. Lee, S. C. Lyu, Y. R. Cho, J. H. Lee, and K. I. Cho, "Diameter-controlled growth of carbon nanotubes using thermal chemical vapor deposition," *Chemical Physics Letters*, vol. 341, no. 3-4, pp. 245–249, 2001.

[26] C. J. Lee, J. Park, Y. Huh, and J. Yong Lee, "Temperature effect on the growth of carbon nanotubes using thermal chemical vapor deposition," *Chemical Physics Letters*, vol. 343, no. 1-2, pp. 33–38, 2001.

[27] R. Yudianti, H. Onggo, Y. Saito, T. Iwata, and J.-I. Azuma, "Analysis of functional group sited on multi-wall carbon Nanotube surface," *Open Materials Science Journal*, vol. 5, pp. 242–247, 2011.

[28] Y. Yadav, V. Kunduru, and S. Prasad, "Carbon nanotubes: synthesis and characterization," in *Nanopackaging*, pp. 325–344, Springer, 2008.

[29] R. A. DiLeo, B. J. Landi, and R. P. Raffaelle, "Purity assessment of multiwalled carbon nanotubes by Raman spectroscopy," *Journal of Applied Physics*, vol. 101, no. 6, Article ID 064307, 2007.

[30] C. Vallés, M. Pérez-Mendoza, W. K. Maser et al., "Effects of partial and total methane flows on the yield and structural characteristics of MWCNTs produced by CVD," *Carbon*, vol. 47, no. 4, pp. 998–1004, 2009.

[31] S. M. Lee and Y. H. Lee, "Hydrogen storage in single-walled carbon nanotubes," *Applied Physics Letters*, vol. 76, no. 20, pp. 2877–2879, 2000.

[32] W. B. Choi, J. U. Chu, K. S. Jeong et al., "Ultrahigh-density nanotransistors by using selectively grown vertical carbon nanotubes," *Applied Physics Letters*, vol. 79, no. 22, pp. 3696–3698, 2001.

[33] I. Chen, Z. Liang, B. Wang, and C. Zhang, "Charge-induced asymmetrical displacement of an aligned carbon nanotube buckypaper actuator," *Carbon*, vol. 48, no. 4, pp. 1064–1069, 2010.

[34] W. A. de Heer, A. Châtelain, and D. Ugarte, "A carbon nanotube field-emission electron source," *Science*, vol. 270, no. 5239, pp. 1179–1180, 1995.

[35] F. Chekin, S. Bagheri, and S. A. Hamid, "Electrochemistry and electrocatalysis of cobalt(II) immobilized onto gel-assisted synthesized zinc oxide nanoparticle-multi wall carbon nanotube-polycaprolactone composite film: application to determination of glucose," *Analytical Methods*, vol. 4, no. 8, pp. 2423–2428, 2012.

[36] A. C. Dillon, K. E. H. Gilbert, P.A. Parilla et al., "Hydrogen storage in carbon single-wall nanotubes," in *Proceedings of the US DOE Hydrogen Program Review*, 2002.

[37] A. Züttel, P. Sudan, P. Mauron, T. Kiyobayashi, C. Emmenegger, and L. Schlapbach, "Hydrogen storage in carbon nanostructures," *International Journal of Hydrogen Energy*, vol. 27, no. 2, pp. 203–212, 2002.

Hindawi Publishing Corporation
BioMed Research International
Volume 2014, Article ID 731731, 7 pages
http://dx.doi.org/10.1155/2014/731731

Research Article

Evaluation of Dried Sweet Sorghum Stalks as Raw Material for Methane Production

Leonidas Matsakas, Ulrika Rova, and Paul Christakopoulos

Biochemical Process Engineering, Division of Chemical Engineering, Department of Civil, Environmental and Natural Resources Engineering, Luleå University of Technology, 971-87 Luleå, Sweden

Correspondence should be addressed to Paul Christakopoulos; paul.christakopoulos@ltu.se

Received 14 June 2014; Revised 17 July 2014; Accepted 23 July 2014; Published 19 August 2014

Academic Editor: Ilona Sárvári Horváth

The potential of utilizing dried sweet sorghum stalks as raw material for anaerobic digestion has been evaluated. Two different treatments were tested, a mild thermal and an enzymatic, alone or in combination. Thermal pretreatment was found to decrease the methane yields, whereas one-step enzymatic treatment resulted in a significant increase of 15.1% comparing to the untreated sweet sorghum. Subsequently, in order to increase the total methane production, the combined effect of enzyme load and I/S on methane yields from sweet sorghum was evaluated by employing response surface methodology. The obtained model showed that the maximum methane yield that could be achieved is 296 mL CH_4/g VS at I/S ratio of 0.35 with the addition of 11.12 FPU/g sweet sorghum.

1. Introduction

Replacement of fossil fuels with renewable energy carriers is now more urgent than ever in order to minimize the negative impacts of human activities on the environment. Biogas provides a renewable alternative to the traditional fossil fuels and is produced from anaerobic digestion of organic materials [1, 2]. Anaerobic digestion is a complex biochemical process which takes place in the absence of oxygen and involves several steps (hydrolysis, acidogenesis, acetogenesis, and methanogenesis) where each of them is catalyzed by different category of microorganisms and all together form a unique system where the products of one step are the raw materials of the next [3–5]. Taking into account the resource efficiency, biogas production is considered to have a better ratio of output to input energy comparing to ethanol production [6]. Special care should be taken in order not to inhibit the methanogenesis process, as it is more sensitive compared to the other steps [4].

The main components of the biogas are methane (CH_4) and carbon dioxide (CO_2) and the ratio between them affects the total energy of biogas which is estimated to vary between 18,630 and 26,081 kJ/m^3 [7]. Biogas has different applications, as it can be used for electricity and heat production or as vehicle fuel [6]. Another important benefit of biogas production is that the resulted digestate can be utilized as biofertilizer as it presents increased nutrient availability and favorite elemental composition [1, 4, 5].

Different kinds of organic materials have been utilized as raw material for anaerobic digestion, such as sewage, different animal manures, various food residues [8–10]. There is a great interest of exploiting solid biomass for biogas production and more specifically lignocellulosic biomass which is a highly abundant resource and available at low cost [11]. One important and crucial step during anaerobic digestion of lignocellulosic material is the efficient hydrolysis of the complex carbohydrates cellulose and hemicellulose [5, 7]. Improving the efficiency of this step is of great importance in order to achieve high biogas production yields.

Biomass could be derived, for example, from agricultural, such as different straws, or forest residues. An alternative source of biomass could be energy crops like sweet sorghum.

Cultivation of sweet sorghum presents several benefits as it requires fewer inputs (like fertilizers) and due to the high photosynthetic activity that presents high amounts of soluble and insoluble carbohydrates are produced in a short period [12–14]. Moreover it is tolerant to harsher climate conditions (like drought and high soil salinity) and can exploit lands that are not suitable for the cultivation of other crops [13, 15]. On the other hand, presence of soluble sugars in stalks results in low storage stability of sweet sorghum, which in turn makes storage of stalks a challenge and all-around year availability of them difficult. This problem can be solved by drying of stalks, as has previously been demonstrated [16, 17].

The aim of this work was to evaluate the potential use of dried sweet sorghum stalks as raw material for the production of biogas using a thermophilic sludge. Utilization of thermophilic conditions rather than mesophilic presents some benefits such as more thermodynamically favorable conditions, leading to higher methanogenic activity and in turn faster digestion, and less contamination problems from other microorganisms [11, 18]. Different treatments of sweet sorghum stalks were also evaluated concerning the improvement of methane production yields.

2. Materials and Methods

2.1. Feedstock and Inoculum. During this work the Keller variety of sweet sorghum was utilized, which was cultivated in Voiotia region of central Greece. Preparation of dried sweet sorghum stalks was done as previously described [16]. The particle size after drying and milling was 0.75 mm. Volatile solids (VS) concentration of sweet sorghum stalks was 93.44% w/w, whereas total solids (TS) content was 95.69% w/w. The composition of sweet sorghum stalks per dry weight is as follows (% w/w): sucrose, 34.4; glucose, 8.2; fructose, 8.1; cellulose, 19.6; hemicellulose, 15.2; acid insoluble lignin, 3.2 [16].

Anaerobic sludge which was used as inoculum was collected from the biogas plant in Boden, Sweden, where biogas is produced by thermophilic codigestion of sewage sludge and food wastes at 55°C. The VS and TS content of the inoculum were 1.17% w/w and 2.04% w/w, respectively.

2.2. Thermal and Enzymatic Treatment. During this work two different treatments were applied to improve methane yields, one thermal and one enzymatic, alone or in combination. Thermal treatment was performed using an autoclave apparatus at 105°C for 1 hour with sweet sorghum's concentration of 20% w/w.

During enzymatic treatment, a mixture of the commercial enzyme solutions Celluclast 1.5 L and Novozym 188 (Novozymes A/S, Denmark) at 5 : 1 v/v ratio was used at the same enzyme loading that was previously found optimal for sweet sorghum saccharification during ethanol production [16]. Two different process configurations were evaluated during the enzymatic treatment, namely, one-step and two-step processes. In one-step process, the enzymes were directly added in the sludge, whereas in the two-step process sweet sorghum was enzymatically presaccharified prior to the addition to sludge. During the two-step process the saccharification was performed at 50°C for 8.6 hours at 20% w/w DM content. In order to avoid the hydrolysis of sucrose by Novozym 188 endogenous invertase activity and subsequent inhibition of cellulases, the enzymatic solution was added in the startup of anaerobic digestion stage.

2.3. Analytical Methods. TS content was measured as weight difference before and after drying the samples at 105°C for 24 hours. The VS content was measured after drying the sample at 550°C for 2 hours and abstracted this weight difference from the TS content.

Enzyme activity of the commercial enzyme solutions was measured according to the method developed by Ghose [19] and found to be 83 FPU/mL for the mixture.

2.4. Biochemical Methane Potential (BMP). BMP assays were performed at the Automatic Methane Potential Test System (AMPTS II) of Bioprocess Control AB (Lund, Sweden). Incubation took place in 500 mL glass bottles containing 400 g of total sample (inoculum and substrate). Slow mixing of the sludge was conducted by motors on the top of each flask at intervals of 10 min mixing and 1 min resting. Every bottle was connected with a CO_2-fixing unit, which consists of 100 mL glass flasks containing approximately 80 mL of 3 M NaOH and thymolphthalein as pH indicator. Finally, the volume of the methane was measured at the gas flow meter unit.

In every batch of experiments two different controls were also included. One with only the inoculum in order to calculate the methane production from the organic load already present in the sludge and one with the inoculum and the enzymes in order to calculate methane production from the digestion of the enzymes. Finally, a positive control experiment was also included to evaluate the quality of the sludge, containing avicel cellulose. During the first batch of experiments the inoculum to substrate ratio (I/S ratio) in terms of VS was equal to 2, whereas in the second batch it varied as described in Section 2.5. Each flask was supplemented with salt and trace element solution as described by Antonopoulou and Lyberatos [12]. Prior to startup of the digestion each flask was sparged with nitrogen for 90 sec. Incubation of the flasks took place in a water bath at 55°C until no significant amounts of methane were produced. All the experiments lasted a maximum of 21 days.

2.5. Experimental Design. An experimental design (response surface methodology (RSM)) was employed during this work in order to evaluate the combined effect of enzyme loading and I/S ratio on the methane yield. RSM allows the estimation of the interactions of the chosen factors and their effect in one or more responses and can result in improvement of the process factors. According to the specific experimental design employed, different combinations of the chosen factors, which vary at certain levels, are generated. The responses of these combinations can be graphically represented and a quadratic or cubic model can describe the behavior of the responses. During this work a Box-Wilson circumscribed

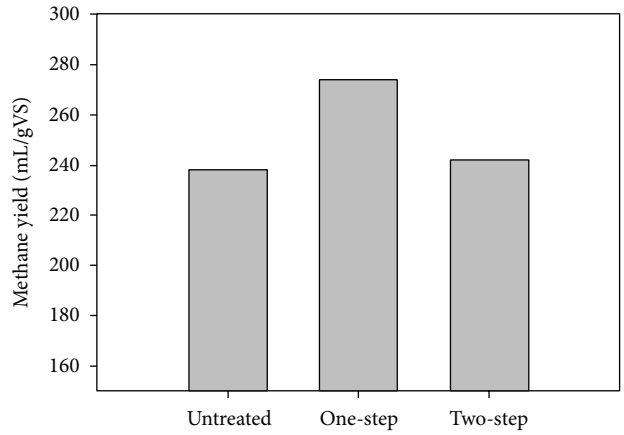

Figure 1: Effect of enzymatic treatment on methane yields. Enzymatic treatment was performed either in one step or in two steps. The values presented are the average of duplicate experiments.

central composite (CCC) design was employed generating 11 experimental combinations (3 replicates of the central points) which were done in duplicates (Table 1). The quadratic model applied was the following:

$$\text{Met} = \beta_0 + \beta_1 \cdot X_1 + \beta_2 \cdot X_2 - \beta_3 \cdot X_1^2 - \beta_4 \cdot X_2^2 - \beta_5 \cdot X_1 \cdot X_2, \quad (1)$$

where met represents the methane yield per gram of VS (mL CH_4/g VS), X_1 the enzyme loading (FPU/g sweet sorghum), and X_2 the I/S ratio and with β_i the different coefficients. Fitting of the model according to multiple linear regression (MLR) and statistical analysis of the obtained model was done using the software MODDE v.10 of Umetrics.

3. Results and Discussion

3.1. Evaluation of Different Treatments on Methane Potentials. Sweet sorghum stalks contain both soluble (glucose, fructose, and sucrose) and insoluble carbohydrates (cellulose and hemicellulose) which could be utilized for methane production. Despite the fact that the methane producing consortia can hydrolyze insoluble carbohydrates, the methane yields could be lower when the lignocellulosic materials are utilized without any kind of treatment [6, 20, 21]. One way to increase digestibility of insoluble carbohydrates is the application of a physicochemical pretreatment process, such as hydrothermal, dilute acid, and steam explosion. On the other hand pretreatment of sugar crops like sweet sorghum, which contain high amounts of soluble sugars, can result in formation of inhibitors (such as furfural and HMF) leading to a significant decrease of the available sugars. For this reason the application of a physicochemical pretreatment at harsh conditions (e.g., high temperature or treatment duration) is not feasible. On the other hand, addition of hydrolytic enzymes could facilitate the hydrolysis of both cellulose and hemicellulose and in turn increase the methane yield.

During this work an enzymatic treatment was evaluated by employing a mixture of Celluclast 1.5 L and Novozyme 188 at a ratio of 5 : 1 volumes, at a concentration equivalent to 8.32 FPU/g sweet sorghum (as previously found optimal for sweet sorghum saccharification by Matsakas and Christakopoulos [16]). In order to evaluate the effect of enzymatic treatment, two different process configurations were evaluated, namely, a one-step and two-step process which resemble the SSF (simultaneous saccharification and fermentation) and SHF (separate saccharification and fermentation) processes during bioethanol production from lignocelluloses.

When no treatment was applied to sweet sorghum stalks methane yield reached 238 mL/g VS. In contrast, addition of enzymes improved the overall methane production yields (Figure 1). It is worth noticing that when a two-step process configuration was applied the increase of methane yield was only 1.7%, whereas during the one-step process the increase was 15.1% reaching a methane production of 274 mL/g VS with the most probable reason being the presence of higher initial sugar concentration in the startup of anaerobic digestion stage during the two-step process, which could result in production of higher amounts of volatile fatty acids (VFAs), which in combination with lowering the pH below optimal could have a negative impact on methane production [22, 23].

Subsequently the effect of a mild thermal pretreatment (105°C for 1 h) on sweet sorghum digestibility was evaluated without the addition of any acid or basic catalyst which could result in severe degradation of soluble sugars. It was previously reported that a thermal pretreatment under mild conditions could enhance methane production from sweet sorghum stalks [12]. Despite the fact that Antonopoulou and Lyberatos [12] found a positive effect of thermal pretreatment on sorghum digestibility, during this work the methane production of pretreated sweet sorghum was 5.46% less compared to the untreated one, resulting in a methane production of 225 mL/gVS. This could be attributed to the minor degradation of soluble sugars and formation of inhibitors. Addition of enzymes to the thermally pretreated sweet sorghum increased the methane production but the overall yield was less compared to the yield obtained by the untreated sweet sorghum (Figure 2). The same negative effect of the two-step process was also observed during utilization of thermally pretreated sweet sorghum stalks.

3.2. Evaluation of the Combined Effect of Enzyme Loading and I/S Ratio on Methane Production. From the previous experiments it was concluded that a one-step enzymatic treatment step increases the methane yields from sweet sorghum. During anaerobic digestion the I/S ratio is considered to play a very important role on the methane yields [2, 24]. If this ratio is low, there is high possibility of inhibition of methane production due to the accumulation of VFAs [1], which is a result of the imbalance between the acidogenic and methanogenic stage [4]. On the other hand, lower I/S ratio results in higher substrate concentrations which in turn yields in higher total methane production per volume of sludge, which is very important for the economic viability of the process. Thus it is important to find the lowest I/S ratio in which the methane yield per gram of volatile solids

Table 1: Codded and actual values of the experimental design.

Treatment	Coding values (X_1 = enzyme load, X_2 = I/S ratio)		Actual values (X_1 = enzyme load, X_2 = I/S ratio)	
	X_1	X_2	X_1	X_2
1	−1	−1	3	0.7
2	1	−1	13	0.7
3	−1	1	3	3.3
4	1	1	13	3.3
5	−1.414	0	0.93	2
6	1.414	0	15.07	2
7	0	−1.414	8	0.16
8	0	1.414	8	3.83
9	0	0	8	2
10	0	0	8	2
11	0	0	8	2

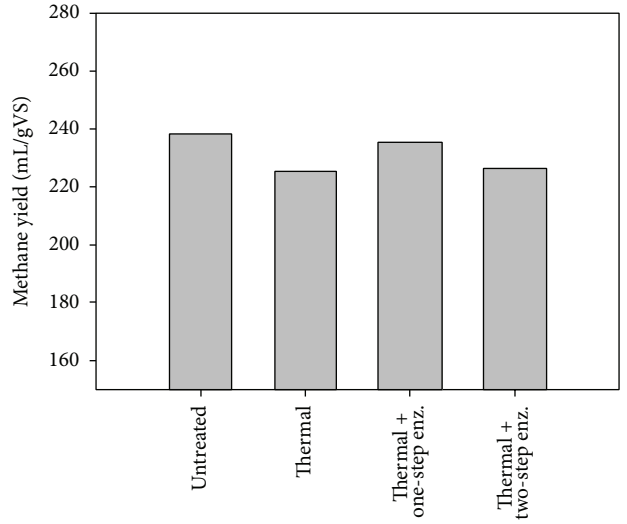

Figure 2: Effect of thermal treatment on methane yield with or without the combination of enzymatic treatment. The values presented are the average of duplicate experiments.

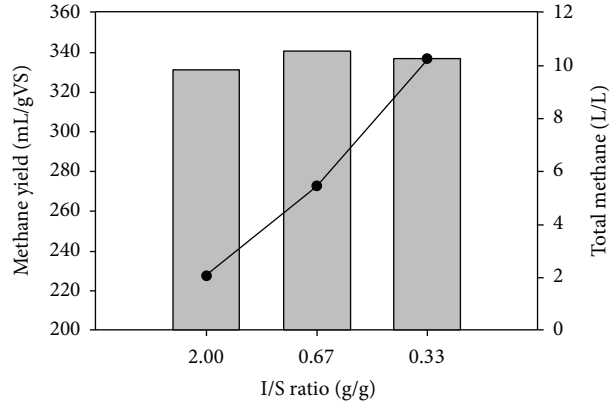

Figure 3: Effect of I/S ratio in methane yield and total methane production from avicel cellulose. The values presented are the average of duplicate experiments.

is not decreasing and at the same time the total production of methane is high.

In order to evaluate the ability of the consortium to act at low I/S ratio, initially microcrystalline cellulose was employed at different I/S ratios (2, 0.67, and 0.33). As can be seen in Figure 3 methane production per gram of VS is increased with decreasing I/S to 0.67, while further decrease to 0.33 resulted in slight decrease of methane potential, which was still above the methane yields at I/S ratio 2. It can be concluded that the used microbial consortium is capable of digesting materials at low I/S ratios which results in higher overall methane production, which in this case increases from 2.1 L CH_2/L to 10.2 L CH_2/L when I/S ratio is decreased from 2 to 0.33.

Subsequently the combined effect of enzyme load and I/S ratio was evaluated by response surface methodology according to circumscribed central composite (CCC) design. 11 experimental combinations came from the experimental design as represented in Table 1 which were done in duplicate resulting in a total of 22 experiments. During the initial fitting of the quadratic model to the obtained results it was found that the R^2 was 0.495, whereas the Q^2 was −0.067, values that indicate that the model was not adequate enough to describe the experimental values and predict values at new experimental combinations. For this reason the values of the experiments at the combination 8 FPU/g sweet sorghum and 0.16 g/g I/S ratio were excluded, as the methane production was inhibited (Table 2). The obtained model is described by the following equation:

$$\text{Met} = 278.708 + 0.716472 \cdot X_1 - 16.9907 \cdot X_2 + 0.014611 \cdot X_1^2 - 1.58786 \cdot X_2^2 + 0.594616 \cdot X_1 \cdot X_2. \quad (2)$$

R^2 was improved to 0.886 and the Q^2 to 0.762 indicating that the model is capable of fitting the experimental data

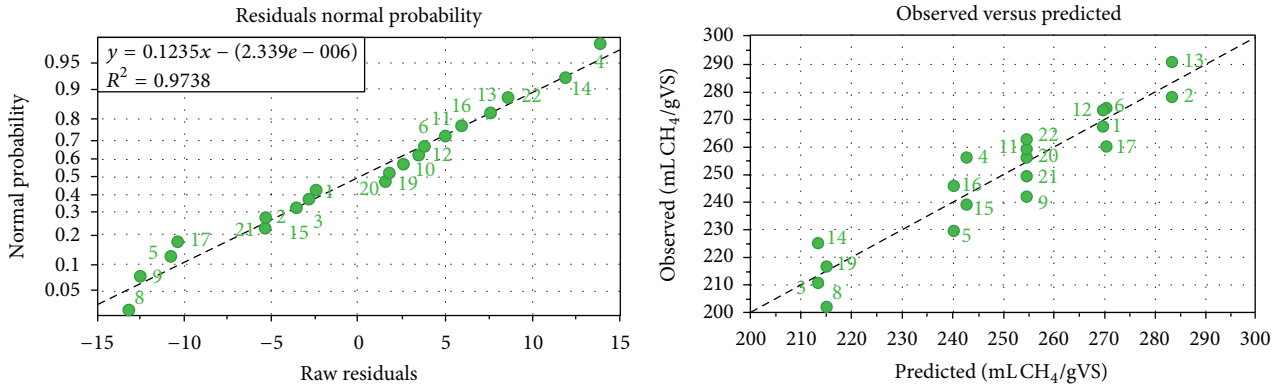

(a) (b)

Figure 4: Diagnostic tools for model evaluation. (a) Residual normal probability and (b) plot of observed values against predicted.

Table 2: Experimental obtained and predicted methane yields.

Treatment	Met (methane yield, mL CH_4/g VS) experimental		Met (methane yield, mL CH_4/g VS) predicted
	A	B	
1	267.15	273.02	269.57
2	277.92	290.82	283.23
3	210.68	225.40	213.51
4	256.48	239.09	242.64
5	229.42	246.11	240.16
6	274.20	260.08	270.41
7	47.11	49.86	—
8	201.86	216.86	215.03
9	242.05	256.17	254.56
10	257.15	249.21	254.56
11	259.60	263.16	254.56

and can efficiently predict new data. Two more factors that describe the efficiency of a model are the model validity and the reproducibility. For the model obtained during this work, both of them were high and found to be 0.735 and 0.849, respectively. Finally, two diagnostics tools were employed to verify the adequacy of the model to fit experimental data, namely, the normal probability plot of residuals and the relationship between predicted and experimental data (Figure 4). Normal probability plot of residuals is made by plotting the observed residuals against the expected values [24] and is used to evaluate the normality of the residuals as well as to detect outliers, whereas plot of experimental obtained data versus predicted ones indicates the efficiency of the model to describe the obtained experimental results. The model obtained during this work is sufficiently describing the experimental result as the values of the data are fairly close to the linear line. This can also be observed at Table 2 where the experimental and predicted values for the duplicate experiments are given.

Figure 5 shows the resulting response surface and contour of the model. It can be observed that low I/S ratio in combination with higher enzyme loadings lead in increased methane yields, where the yields are more affected by the I/S ratio than the enzyme load. As has previously been discussed it is important to find the lowest I/S ratio where the methane yield remains high, in order to increase the total methane production. During this work the highest methane yield (284.37 mL CH_4/gVS) was achieved at a low I/S ratio, equal to 0.7, with the addition of 13 FPU/g resulting in a total production of 4.7 L CH_4/L.

4. Conclusions

The ability of utilization of dried sweet sorghum stalks as raw material for anaerobic digestion was demonstrated. One-step enzymatic treatment of stalks resulted in an increase of the methane production yield compared to thermal treatment which resulted in slight decrease. Finally, the combined effect

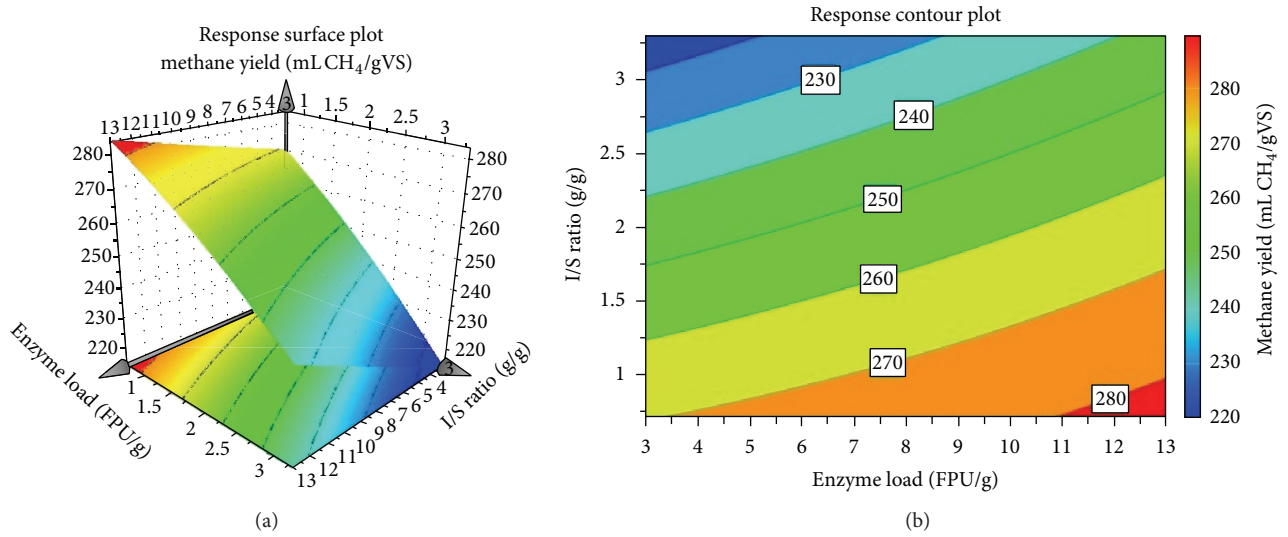

Figure 5: Response surface (a) and contour plot (b) of the methane yield at different combinations of enzyme load and I/S ratio.

of enzyme load and I/S ratio was evaluated resulting in higher yields and total methane production.

Conflict of Interests

The authors declare that there is no conflict of interests regarding the publication of this paper.

Acknowledgment

The authors would like to thank Bio4Energy, a strategic research environment appointed by the Swedish government, for supporting this work.

References

[1] G. K. Kafle, S. Bhattarai, S. H. Kim, and L. Chen, "Effect of feed to microbe ratios on anaerobic digestion of Chinese cabbage waste under mesophilic and thermophilic conditions: biogas potential and kinetic study," *Journal of Environmental Management*, vol. 133, pp. 293–301, 2014.

[2] G. Liu, R. Zhang, H. M. El-Mashad, and R. Dong, "Effect of feed to inoculum ratios on biogas yields of food and green wastes," *Bioresource Technology*, vol. 100, no. 21, pp. 5103–5108, 2009.

[3] A. Mshandete, L. Björnsson, A. K. Kivaisi, S. T. Rubindamayugi, and B. Mattiasson, "Enhancement of anaerobic batch digestion of sisal pulp waste by mesophilic aerobic pre-treatment," *Water Research*, vol. 39, no. 8, pp. 1569–1575, 2005.

[4] N. Adu-Gyamfi, S. R. Ravella, and P. J. Hobbs, "Optimizing anaerobic digestion by selection of the immobilizing surface for enhanced methane production," *Bioresource Technology*, vol. 120, pp. 248–255, 2012.

[5] W. Parawira, "Enzyme research and applications in biotechnological intensification of biogas production," *Critical Reviews in Biotechnology*, vol. 32, no. 2, pp. 172–186, 2012.

[6] A. Jeihanipour, S. Aslanzadeh, K. Rajendran, G. Balasubramanian, and M. J. Taherzadeh, "High-rate biogas production from waste textiles using a two-stage process," *Renewable Energy*, vol. 52, pp. 128–135, 2013.

[7] R. T. Romano, R. Zhang, S. Teter, and J. A. McGarvey, "The effect of enzyme addition on anaerobic digestion of Jose Tall Wheat Grass," *Bioresource Technology*, vol. 100, no. 20, pp. 4564–4571, 2009.

[8] F. Raposo, M. A. de la Rubia, V. Fernández-Cegrí, and R. Borja, "Anaerobic digestion of solid organic substrates in batch mode: an overview relating to methane yields and experimental procedures," *Renewable and Sustainable Energy Reviews*, vol. 16, no. 1, pp. 861–877, 2012.

[9] I. Angelidaki, M. Alves, D. Bolzonella et al., "Defining the biomethane potential (BMP) of solid organic wastes and energy crops: a proposed protocol for batch assays," *Water Science and Technology*, vol. 59, no. 5, pp. 927–934, 2009.

[10] R. A. Labatut, L. T. Angenent, and N. R. Scott, "Biochemical methane potential and biodegradability of complex organic substrates," *Bioresource Technology*, vol. 102, no. 3, pp. 2255–2264, 2011.

[11] Y. Xia, H. H. P. Fang, and T. Zhang, "Recent studies on thermophilic anaerobic bioconversion of lignocellulosic biomass," *RSC Advances*, vol. 3, no. 36, pp. 15528–15542, 2013.

[12] G. Antonopoulou and G. Lyberatos, "Effect of pretreatment of sweet sorghum biomass on methane generation," *Waste and Biomass Valorization*, vol. 4, no. 3, pp. 583–591, 2013.

[13] A. Almodares and M. R. Hadi, "Production of bioethanol from sweet sorghum: a review," *African Journal of Agricultural Research*, vol. 4, no. 9, pp. 772–780, 2009.

[14] F. Wang and C. Z. Liu, "Development of an economic refining strategy of sweet sorghum in the Inner Mongolia region of China," *Energy and Fuels*, vol. 23, no. 8, pp. 4137–4142, 2009.

[15] L. Matsakas and P. Christakopoulos, "Fermentation of liquefacted hydrothermally pretreated sweet sorghum bagasse to ethanol at high-solids content," *Bioresource Technology*, vol. 127, pp. 202–208, 2013.

[16] L. Matsakas and P. Christakopoulos, "Optimization of ethanol production from high dry matter liquefied dry sweet sorghum stalks," *Biomass and Bioenergy*, vol. 51, pp. 91–98, 2013.

[17] S. Fei and L. Ronghou, "Research on solid-state ethanol fermentation using dry sweet sorghum stalk particles with active dry yeast," *Energy and Fuels*, vol. 23, no. 1, pp. 519–525, 2009.

[18] M. Lesteur, V. Bellon-Maurel, C. Gonzalez et al., "Alternative methods for determining anaerobic biodegradability: a review," *Process Biochemistry*, vol. 45, no. 4, pp. 431–440, 2010.

[19] T. K. Ghose, "Measurement of cellulase activities," *Pure and Applied Chemistry*, vol. 59, no. 2, pp. 257–268, 1987.

[20] V. Vivekanand, E. F. Olsen, V. G. H. Eijsink, and S. J. Horn, "Effect of different steam explosion conditions on methane potential and enzymatic saccharification of birch," *Bioresource Technology*, vol. 127, pp. 343–349, 2013.

[21] Y. Zheng, J. Zhao, F. Xu, and Y. Li, "Pretreatment of lignocellulosic biomass for enhanced biogas production," *Progress in Energy and Combustion Science*, vol. 42, pp. 35–53, 2014.

[22] T. Zhang, L. Liu, Z. Song et al., "Biogas production by co-digestion of goat manure with three crop residues," *PLoS ONE*, vol. 8, no. 6, Article ID e66845, 2013.

[23] Y. Chen, J. J. Cheng, and K. S. Creamer, "Inhibition of anaerobic digestion process: a review," *Bioresource Technology*, vol. 99, no. 10, pp. 4044–4064, 2008.

[24] L. Neves, R. Oliveira, and M. M. Alves, "Influence of inoculum activity on the bio-methanization of a kitchen waste under different waste/inoculum ratios," *Process Biochemistry*, vol. 39, no. 12, pp. 2019–2024, 2004.

Hindawi Publishing Corporation
BioMed Research International
Volume 2014, Article ID 765652, 13 pages
http://dx.doi.org/10.1155/2014/765652

Research Article

The Treatment of PPCP-Containing Sewage in an Anoxic/Aerobic Reactor Coupled with a Novel Design of Solid Plain Graphite-Plates Microbial Fuel Cell

Yi-Tang Chang,[1] Chu-Wen Yang,[1] Yu-Jie Chang,[2] Ting-Chieh Chang,[1] and Da-Jiun Wei[1]

[1] *Department of Microbiology, Soochow University, 70 Linhsi Road, Shilin District, Taipei 11102, Taiwan*
[2] *Department of Earth and Life Science, University of Taipei, Taipei 11048, Taiwan*

Correspondence should be addressed to Yi-Tang Chang; ytchang@scu.edu.tw

Received 10 May 2014; Accepted 16 July 2014; Published 14 August 2014

Academic Editor: Ilona Sárvári Horváth

Synthetic sewage containing high concentrations of pharmaceuticals and personal care products (PPCPs, mg/L level) was treated using an anoxic/aerobic (A/O) reactor coupled with a microbial fuel cell (MFC) at hydraulic retention time (HRT) of 8 h. A novel design of solid plain graphite plates (SPGRPs) was used for the high surface area biodegradation of the PPCP-containing sewage and for the generation of electricity. The average COD_{Cr} and total nitrogen removal efficiencies achieved were 97.20% and 83.75%, respectively. High removal efficiencies of pharmaceuticals, including acetaminophen, ibuprofen, and sulfamethoxazole, were also obtained and ranged from 98.21% to 99.89%. A maximum power density of 532.61 mW/cm^2 and a maximum coulombic efficiency of 25.20% were measured for the SPGRP MFC at the anode. Distinct differences in the bacterial community were presented at various locations including the mixed liquor suspended solids and biofilms. The bacterial groups involved in PPCP biodegradation were identified as *Dechloromonas* spp., *Sphingomonas* sp., and *Pseudomonas aeruginosa*. This design, which couples an A/O reactor with a novel design of SPGRP MFC, allows the simultaneous removal of PPCPs and successful electricity production.

1. Introduction

Pharmaceuticals and personal care products (PPCPs) are being paid more public attention as emerging organic contaminants (EOCs) in ecosystems. In Taiwan, the existence of pharmaceuticals pollution can be attributed to incomplete municipal sewage collection systems and inappropriate recycling and treatment programs for waste medical materials. Pharmaceutical sewage can be treated by municipal wastewater treatment plants (WWTPs), but the effluent obtained by such plants introduces residues into the hydrological cycle [1]. Natural surface water systems, such as rivers, reservoirs, and oceans, are widely distributed in Taiwan and are, thus, prone to contamination. Similarly, urban groundwater reservoirs are likely to be contaminated by pharmaceuticals from sewage. The concentration of such pharmaceuticals has been found to range from ng/L to μg/L and can even reach mg/L levels in sanitary landfill leachates. Typical examples of the pharmaceutical drugs found in such sewage in Taiwan include analgesics, antibiotics, and nonsteroidal anti-inflammatory drugs (NSAID); examples are acetaminophen (ACE), sulfamethoxazole (SMX), and ibuprofen (IBU); such compounds are often detected at relatively high concentrations (μg/L) in the influent of municipal WWTPs [2].

Anoxic-aerobic coupled systems (A/O systems) have been applied to the treatment of a wide range of municipal wastewaters and industrial wastewaters of low-to-high strength concentrations. The advantages of A/O systems include a high overall treatment efficiency with respect to BOD and nutrients, a reduced need for sludge disposal, a lower consumption of chemicals, and a greater potential for resource recovery [3]. The combination of aerobic and anoxic degradation pathways in the A/O system has been reported as aiding the overall degradation efficiency of PPCPs. The removal efficiencies for PPCPs in municipal wastewater vary on a case-by-case basis due to differences in the biological processes and the target PPCPs. For example, biofiltration of

wastewater through biological activated carbon has shown good potential for the efficient removal of PPCPs (>90%), but sand biofilters have a poor efficiency [4]. Sulfonamides have been shown to be removed in the range from 18.5% to 37.2% using an anoxic/anaerobic/aerobic (A2O) system, but higher removal efficiencies from 53.3% to 73.3% were obtained using an oxidation ditch [5]. Thus, it is necessary to clarify the contribution to sewage treatment efficiency of each different reactor in an A/O system.

Energy is required to keep the regular operations at an A/O system fully powered, for example, to provide oxygen (O_2) to the aerobic reactor. Recently, microbial fuel cells (MFCs) have been found to be able to provide an innovative renewable energy source that is both green and clean, as well as having a low carbon footprint [6, 7]. The potential for electrical generation of MFCs is being developed and this approach as a source of green energy has the potential to reduce various operational costs (electricity) including aeration and recirculation/process pumping. However, when applied, the two-chamber MFC A/O system is limited in terms of the amount of electrode design. Alternative approaches that can be implemented include improving the electrode design and/or modifying the system by using various chemical catalysts. For example, modifying the cathode by adding a noble metal such as Pt or a nonnoble metal such as Fe^{3+} or Mn^{4+}, which can then act as a chemical mediator, is able to significantly increase the PD of MFCs [8, 9]. Such advances in electricity production either need specific carbon-based materials or have to include noble metals at extremely high cost [10], both of which retard the practical development of such systems for MFCs that are coupled with the biological treatment of wastewater. In addition, some of the above mediators are known to be toxic to the growth of bacteria, which are central to biodegradation.

Graphite electrodes in a MFC system are good in terms of power production compared to various metals, such as iron, aluminum, and stainless steel [11]. Biofilms on the graphite electrodes are known to contribute to power production in the MFC system. Different types of graphite cathode/anode electrodes, including graphite plates, sheets, felts, rods, and papers, have been developed to increase electricity output [12]. In fact, the bacterial biofilm formed on the graphite material is also able to biodegrade sewage, even EOCs. The development of high specific surface area graphite cathode/anode electrodes should result in great benefits in a MFC A/O system in terms of generating electricity and sewage removal. Moreover, the bacterial community structures and their functions are complex in a MFC A/O system. Till now, there has been little information available on the influence of PPCP-containing sewage on the various dynamic bacterial communities present in A/O systems and on electricity generation during biological treatment by an A/O system.

The objective of this study is to design and implement a MFC system that is combined with an A/O reactor and to use this system to process PPCP-containing sewage for the first time. MFC solid plain graphitic plates (SPGRPs) were designed to generate bacterial electricity and to remove PPCPs in a highly effective manner. The removal efficiencies, including COD, N, and P, when treating the sewage, were measured using an integrated MFC A/O system. At the same time, PPCP biodegradation was assessed. The spatial bacterial communities and their major functions were carefully evaluated using biomolecular methods, namely, PCR-DGGE-cloning. The biodiversity of the bacterial communities at various locations, such as mixed liquor suspended solids (MLSS) and biofilms, was compared across the MFC A/O system. This study provides an alternative approach to the biological treatment of municipal/industrial wastewater that contains PPCPs; specifically, it involves the coupling of a two-chamber MFC to an A/O reactor. The specific functions of the various members of the bacterial population present in the reactors were clarified in terms of a series of biochemical reactions within the MFC A/O system.

2. Material and Methods

2.1. Chemicals. Three target pharmaceutical drugs among potential PPCPs were selected for this study, ACE, SMX, and IBU. These drugs are commonly found in WWTP municipal wastewater in Taiwan. ACE was purchased from Fluka at purity of >98%. SMX and IBU were obtained from Sigma-Aldrich at purity of >99% and Sigma at purity of >99.9%, respectively. The organic solvents used in this study were all HPLC grade with purity higher than 99.9%. All other chemicals were reagent grade with purity above 99%. The Milli-Q water was double-distilled and deionized by a Millipore water purification system.

2.2. The MFC A/O System. Figure 1 shows the pilot-scale coupled MFC A/O system used in this study. The sewage influent consisted of a mixture of condensed artificial PPCP-containing sewage and tap water in a stabilized tank (25,000 mL) that was controlled to a temperature between 8°C and 12°C. The anoxic reactor (3,940 mL) was designed as the inner tank and its temperature was controlled to be within the range from 26°C to 29°C, while the aerobic reactor (11,565 mL) was designed as the outer tank. The MFC system consisted of the inner tank (cathode chamber) and outer tank (the anode chamber) separated by two proton exchange membranes (PEM, Nafion N117, DuPont Nafion PFSA membrane). The total area of PEM in the MFC A/O system was 68.40 cm^2 and had the ability to transport hydrogen as protons from the anode (anoxic tank) to the cathode (aerobic tank). SPGRPs (96 mm × 36 mm × 5 mm) with high specific surface areas (20,267.22 mm^2 for each SPGRP) were used for two different purposes in this study, with one set being in the cathode chamber and another set being in the anode chamber. The SPGRPs were fixed by two PTFE-covered stainless steel bars. Copper wires were used to connect all the SPGRPs within the MFC system. The anoxic reactor included eleven SPGRPs that were designed to allow the development of bacterial biofilms on the cathode (called the cathode catalysts or the biocathode) that would increase electricity generation by the MFC. In contrast, the anode chamber consisted of ten SPGRPs that were designed to allow the formation of biofilms that would aid the removal of artificial PPCPs from the sewage.

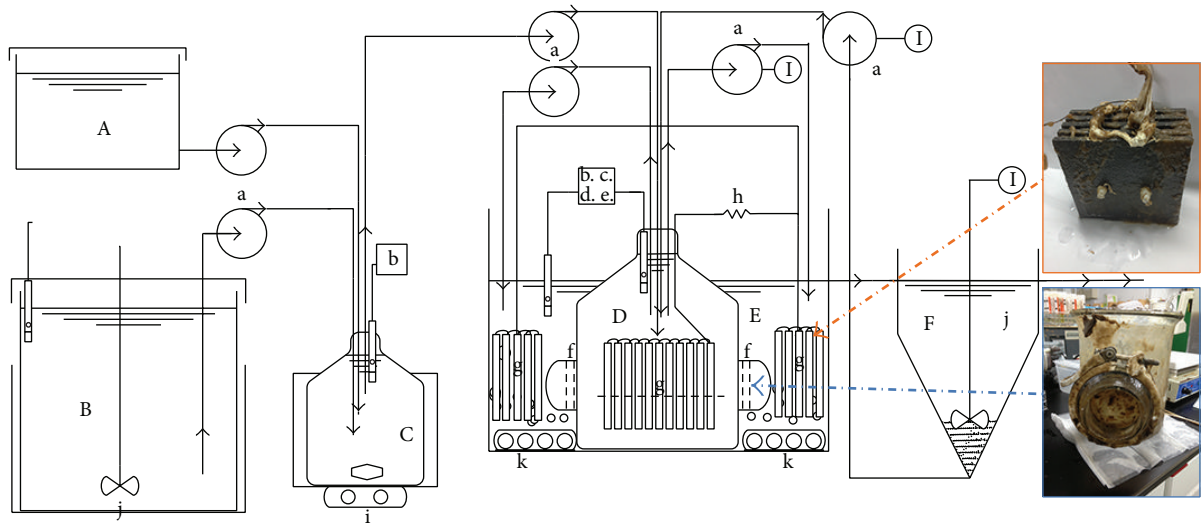

(A) Filtered tap water
(B) Concentrated 30X sewage substrate tank
(C) Mixing tank
(D) Anoxic reactor (anode chamber)
(E) Aerobic reactor (cathode chamber)
(F) Settling clarifier
(I) Sludge recycle route

(a) Peristaltic pump
(b) pH meter
(c) ORP meter
(d) DO meter
(e) Heating rod
(f) Proton exchange membrane (PEM)

(g) Graphite carbon plates (GCP)
(h) Resistance (1 kΩ)
(i) Magnetic stirrer
(j) Overhead stirrer
(k) Air diffusers

Figure 1: Schematic diagram of the A/O reactor and the MFC coupled system.

Table 1: Components of the artificial PPCP-containing sewage (per liter) used in this study.

Component	Weight (mg)
SMX	2
ACE	30
IBU	20
Whole milk (KLIM, Nestlé)	119
Saccharide	30
Urea	11.76
KH_2PO_4	6.3
NH_4Cl	5.6
$FeCl_3$	0.14
Acetic acid (99.7%)	52.64 μL
NaOH (10 N)	Drops were used to adjust the pH to 7.4

2.3. Inoculation and Experimental Operation of the MFC A/O System. The original source of the active sludge used to inoculate the pilot-scale coupled MFC A/O system came from a secondary sedimentation tank at the Neihu WWTP, Taipei, Taiwan, which is used to treat PPCP-contained sewage. To avoid the influence of the complex content found in real sewage during PPCP biodegradation, artificial sewage containing the target PPCPs was used in this study. Table 1 presents the components present in the artificial PPCP-containing sewage used in this study. The COD/N/P ratio of influent artificial sewage is about 257.16 : 13 : 1.96, which is quite close to the best composition (C/N/P = 100 : 5 : 1) for municipal wastewater when carrying out biological treatment at a WWTP. Activated sludge in the settlement tank (154,000 mL) was set up to be 100% recycled into the anoxic reactor because increasing the sludge retention time will reduce the operation costs. Water parameters, including pH, ORP, and DO, were obtained by real-time monitoring of all tanks. Table 2 lists the operating parameters of the MFC A/O system. In order to confirm the ability of the system to remove PPCPs and to be able to observe the shifts in bacterial community present in the MFC A/O system, the influent concentrations of ACE, SMX, and IBU were designated to be 30, 2, and 20 mg/L, respectively, which are about 1,000-fold higher concentrations than those present in sewage effluent from Taiwan. The continuous flow rate of the sewage influent was controlled to be 32.33 mL/min during this experiment. The hydraulic retention time (HRT) was set up to be 8 h, which consisted of 2.04 h in the anoxic reactor and 5.96 h in the aerobic reactor. Two experimental phases were carried out as part of this study. Phase I was designed to have the A/O system coupled with MFC system in steady operation for the biological treatment of artificial sewage without PPCPs and this lasted 95 days. Phase II involved treatment of PPCP-containing sewage and took place immediately after Phase I; this phase lasted for 28 days. The treatment of the PPCPs, the water parameters (COD_{Cr}, N, and P), and the bacterial community present were examined regularly.

2.4. Electricity Measurements and Calculations. Power density (PD) and coulombic efficiency (E_C) were selected to be evaluated as measures of the electricity generation by the MFC system [13]. Voltage (V) was regularly measured

Table 2: Operating parameters for the MFC A/O reactor with a HRT of 8 h (mean ± SD)[2].

Water parameters (unit)	Anoxic reactor (anode chamber)	Aerobic reactor (cathode chamber)
pH	8.07 ± 0.33	7.48 ± 0.31
Temperature (°C)	26.75 ± 1.23	29.58 ± 1.62
ORP (mV)	−393.51 ± 61.9	121.97 ± 42.61
DO (mg L^{-1})	ND[1]	4.22 ± 0.45
MLSS (mg L^{-1})	ND[1]	1956.07 ± 566.51
SVI (mL g^{-1})	ND[1]	218.82 ± 78.15
F/M	ND[1]	0.19 ± 0.1
F/V g BOD (m^3·day)$^{-1}$	ND[1]	0.26 ± 0.14

[1]NA: not available.
[2]Average concentrations in the MFC A/O system during Phase I and Phase II (125 days).

using a multimeter (LTlutron DM-9090, Taiwan) via a data acquisition system and this was converted to PD. PD is the power (P: the definition is the time rate of energy transfer) per cross-sectional area (projected) of the anode (A) according to following equations:

$$I\,(\mathrm{mA}) = \frac{V}{R},$$
$$P\,(\mathrm{mW}) = I \times V, \quad (1)$$
$$\mathrm{PD}\left(\mathrm{mW/m^2}\right) = \frac{P}{A},$$

where P is the power, I is the current (mA), and R is the resistance.

The E_C is calculated based on the ratio of total electrons recovered as I to maximum possible electrons recoverable if all substrate removal produces current; this is calculated using the following equation:

$$E_C = \frac{C_P}{C_{\max}} \times 100\%, \quad (2)$$

where C_P is the total coulombs calculated by integrating the current over time. $C_{\max}$ is the theoretical amount of coulombs that can be produced from the artificial wastewater, calculated using the following equations:

$$C_P = I \times \mathrm{HRT},$$
$$C_{\max} = FfS_{\mathrm{COD}}V_{\mathrm{anode}}, \quad (3)$$

where HRT is hydraulic retention time in the MFC A/O system (s); F is Faraday's constant (96,485 C/mol of electrons); f is the number of moles of electrons produced per mole of sewage (1/8 mol of electrons/g COD); S_{COD} is the difference in COD between the influent and effluent in the anode chamber (anoxic reactor); V_{anode} is the effective volume of anode volume.

2.5. Water Parameters Analysis. Samples of artificial PPCP-containing sewage were initially passed through a 1.20 μm glass-fiber membrane and then refiltered through a 0.45 μm nylon membrane. Samples for water parameter analysis were acquired from the same reactor and at the same time as the microbial samples. Water parameters, including temperature, pH, SS, VSS, and $\mathrm{COD_{Cr}}$, were analyzed and this was done by following the procedures from the Standard Methods for the Examination of Water and Wastewater [14]. Total nitrogen (T-N) and total phosphate (T-P) were measured using test kits, namely, Merck spectroquant Nova 60. NH_4^+–N, NO_2^-–N, NO_3^-–N, and PO_4^{3-}–P were measured by ion chromatography (IC, Metrohm 883 Basic IC, USA). Real-time pH/ORP and DO were monitored using a pH/ORP meter (LTlutron pH/ORP-208 meter, Taiwan) and a DO meter (EZDO, PDO-408, Taiwan), respectively.

2.6. PPCPs Analysis. Filtered sewage samples are dried into a powder on a freeze vacuum evaporator (Labconco, USA) at −50°C. Extracted samples were concentrated by hexane and diluted using acetonitrile (ACN) to adjust the concentration correctly. The stock solution of PPCPs for the HPLC standards was prepared by serial dilution in ACN and stored in dark-brown glass containers at 4°C to prevent photolysis of the PPCPs. Samples and standards were injected into the HPLC system to determine the concentration of PPCPs. The HPLC system was equipped with a UV detector (YL-9100, Young-Lin, Korea) and C18 column (250 × 4.6 mm, Thermo Scientific, USA). The operating conditions of HPLC were as follows: 15 μL injection sample and 1.2 mL/min mobile phase composed grade ACN and 0.02 M phosphoric acid (PA) in the gradient program. The recovery range for the PPCPs in samples was from 75% to 95% and the losses were probably due to limitations of the analytical methods. The detection limit of this approach (MDL) to the analysis of the target PPCPs was 5 μg/L. Triplicate analyses of the PPCPs were carried out on each sample.

2.7. Bacterial Community

2.7.1. DGGE. The genomic DNA of microorganisms involved in the A/O system was extracted from MLSS, SPGRP biofilms, and PEM biofilms in the MFC A/O system using a soil genomic DNA purification kit (Gene Mark, Taiwan). Bacterial 16S rDNA genes were selectively amplified from the purified DNA products by PCR. The V6–V8 region of 16S rDNA was selected using the forward primer 968F-GC clamp and the reverse primer 1392R [15]. The DNA product was separated by DGGE profiling using DCode Universal Mutation Detection System (Bio-Rad Laboratories, Inc., Hercules,

California, USA) and 40% to 65% gradient gel at 60°C and 110 V for 16 h. The acrylamide percentage used for the DGGE electrophoresis gel was 8% and the denaturing agents were formamide and urea. Richness indices (RIs), which are related to the band numbers on the DGGE profiles, were used to represent the variation in biodiversity of the MFC A/O system. This allows the assessment of the changes in richness of the bacterial populations.

2.7.2. Cloning. The genomic DNA of microorganisms involved in the A/O system was extracted from MLSS, GRP biofilms, and PEM biofilms in the MFC A/O system using a soil genomic DNA purification kit (Gene Mark, Taiwan). Bacterial 16S rDNA genes were selectively amplified from the purified DNA products by PCR. Clone libraries were then constructed after amplifying the full length (including the V1–V8 region) of the 16S rRNA using the forward primer E9F and the reverse primer U1510R [16]. The amplicons were purified using an EasyPure PCR/Gel Extraction kit (Bioman, Taiwan). The clean product was then cloned using the pGEM-T Easy Vector Systems kit (Promega, Madison, Wisconsin, USA) and transformed into competent *Escherichia coli* DH5a cells as described by the manufacturer. The transformed *E. coli* was incubated on LB agar plates at 37°C overnight and the next day the blue-white screening method was applied to select all white colonies from each population. Plasmids DNA from each colony was then extracted using an EasyPure Plasmid DNA miniprep kit (Bioman, Taiwan). Plasmids with the correct DNA insert were identified by the PCR amplification using the primers M13-F (5′-GTT-TTC-CCA-GTC-ACG-AC-3′) and M13-R (5′-ACA-GGA-AAC-AGC-TAT-GA-3′). The DNA sequencing of the various 16S rRNA inserts was carried out by the Genomics Company, Taiwan. All sequences were compared with reference microorganisms from the GenBank database using BLAST. The closest 16S rDNA sequences to the 16S rRNA sequences obtained from the bacteria making up the biodegradation bacterial populations were retrieved and all the sequences were then aligned using Clustal X software. A phylogenetic tree was constructed by the neighbor-joining method using Molecular Evolutionary Genetics Analysis, version 5 (MEGA 5.1 Beta 3) software. Bootstrap values of >1,500 (from 5,000 replicates) are indicated as at the nodes in the phylogenic analysis.

3. Results

3.1. Treatment of PPCP-Contained Sewage. Figure 2 outlines the variation in water parameters of the MFC A/O system during Phases I and II (totally 125 days). There is no significant difference in sewage removal when Phase I and Phase II are compared (ANOVA), which indicate that the performance of biological treatment is not affected by the presence of PPCPs. The total removal efficiency of the COD_{Cr} averaged 97.20%. The contributions of the anoxic reactor and aerobic reactor to COD_{Cr} removal were 44.80% and 50.61%, respectively. The total removal of T-N averaged 83.75% for the complete A/O system. In contrast, the total removal of T-P averaged only 39.24%, but this was because the sludge settlement in secondary settlement tank was not disposed

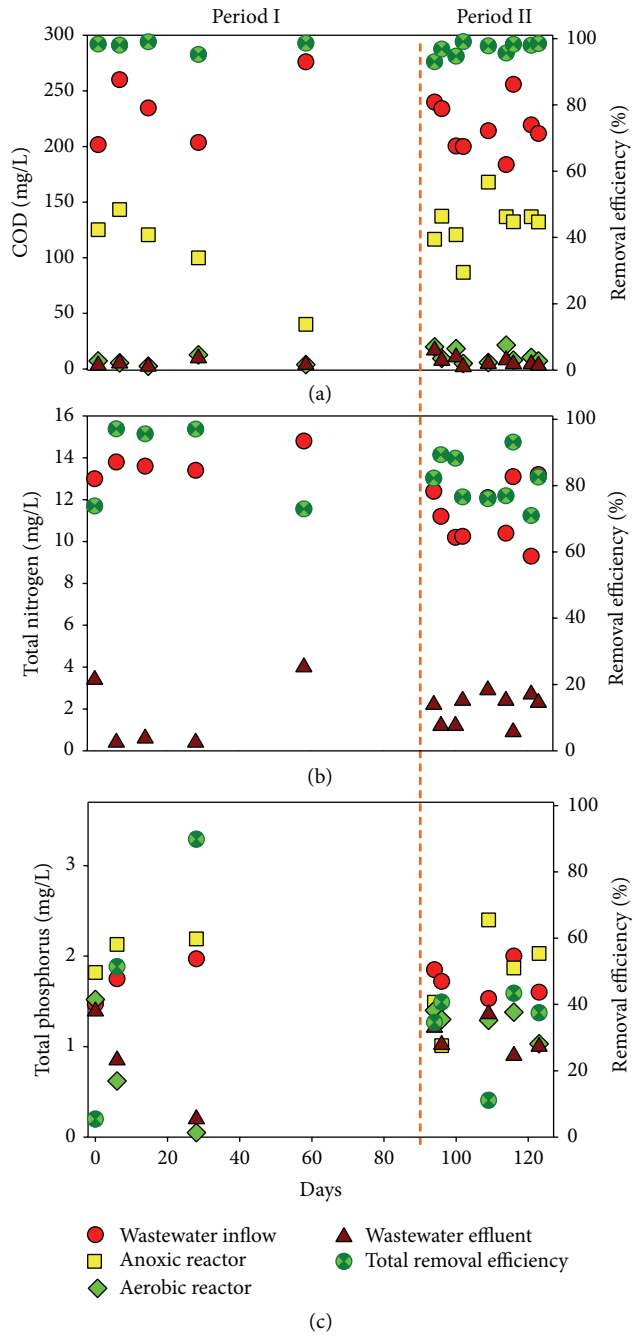

Figure 2: Variation in water parameters in the MFC A/O reactor: (a) COD_{Cr}; (b) T-N; (c) T-P. Phase I = 95 days; Phase II = 28 days.

of on a regular basis. The present MFC A/O system showed a better biological treatment performance compared to a previous study where the removal efficiency for COD_{Cr}, T-N, and T-P during the biological treatment of sewage containing 20 PPCPs by a WWTP at 8 h HRT was found to be 75.0%, 42%, and 66.0%, respectively [17].

Table 3 shows the average concentrations of specific nutrients that were present in the high strength PPCP-containing sewage of the MFC A/O system over Phases I and II.

Table 3: Changes in the sewage nutrients across the MFC A/O system (mean ± SD)[1].

Water parameters (mg/L)	Influent	Anoxic reactor (anode)	Aerobic reactor (cathode)	Effluent
NH_4^+-N	1.767 ± 0.894	9.021 ± 3.623	0.087 ± 0.078	0.036 ± 0.049
NO_2^--N	0.375 ± 0.152	0.258 ± 0.043	0.408 ± 0.211	0.344 ± 0.088
NO_3^--N	1.555 ± 0.501	0.260 ± 0.076	0.335 ± 0.124	1.033 ± 0.670
PO_4^{3-}-P	1.318 ± 0.293	1.777 ± 0.497	0.501 ± 0.201	1.090 ± 0.422

[1] Average concentrations in the MFC A/O system during Phase I and Phase II (125 days).

The SPGRP biofilms within the MFC provided simultaneous nitrification and denitrification in the study. Basically, biofilms on the SPGRP bring about denitrification in the anoxic reactor, while the SPGRP biofilms allow parallel nitrification and aerobic oxidation in the aerobic reactor. The membrane of the PEM contains sulfonic acid groups, which are able to bind the ammonia present during the aerobic nitrification. The concentration of NH_4^+–N in effluent was reduced from 1.767 ± 0.894 mg/L to 0.036 ± 0.009 mg/L in effluent by nitrification/denitrification through the complete A/O reactor process. The total removal efficiency for NH_4^+–N was 97.96%. A significantly increased concentration of NH_4^+–N was found in the anoxic reactor of 9.02 ± 3.62 mg/L because of the mixing of sewage influent and 100% recycled settlement sludge. The concentrations of nitrite and nitrate were found to be decreased in the anoxic reactor. A removal efficiency of 83.28% for nitrate was measured with a biological reduction from 1.555 ± 0.501 mg/L to 0.260 ± 0.076 mg/L. Nitrification was found to occur in aerobic reactor, where the concentration of nitrate was increased from 0.260 mg/L to 1.033 mg/L. Since the A/O process is not designed as a T-P removal system, the low removal efficiency observed is not unexpected. The concentration of PO_4^{3-}–P was slightly decreased from 1.31 ± 0.29 mg/L to 1.090 ± 0.422 mg/L. Moreover, the concentration of T-P averaged 1.8675 ± 0.4412 mg/L in anoxic reactor, which is greater than that of the aerobic reactor at 1.0738 ± 0.500 mg/L. This can be ascribed to intracellular polyphosphate (poly-P) being taken up into the biomass present in the aerobic reactor and then being released in the anoxic reactor. However, the target PPCPs in the present system might have had an effect on nutrient removal in the A/O MFC system. For example, 50–500 mg/L of IBU and ACE have been shown to inhibit nitritation/denitritation and phosphorus uptake/release rates in a sequence of batch reactors [18].

3.2. Occurrence and Removal of PPCPs. Figure 3 shows the variation of PPCP concentration throughout the MFC A/O system. High concentration PPCPs (mg/L level) in the artificial sewage were removed at an efficiency greater than 98% in this MFC A/O system. The PPCP removal performances were compared and this gave the following result (ANOVA, $P < 0.05$): ACE (99.89%) > IBU (99.01%) > SMX (98.21%). A similar trend in terms of removal efficiencies of 99.8-99.9% for ACE, 99.1–99.5% for IBU, and 73.8–80.8% for SMX was found using a conventional activated sludge WWTP system linked to two pilot-scale membrane bioreactor treatment (MBR) systems [19]. In general, antibiotics such as SMX are more resistant to biodegradation in most WWTPs than other pharmaceuticals. It has been reported that 10–400 mg/L SMX is able to inhibit microbial activity in activated sludge by more than 20% [20]. In one study, an average removal efficiency of 65% for SMX was achieved by MBR under anoxic and aerobic conditions [21].

PPCPs at a ppb level could still be detected by HPLC in the effluent of the conventional A/O process. The ACE, SMX, and IBU effluent concentrations were 23.9 ± 2.34 μg/L, 23.7 ± 1.1 μg/L, and 179.9 ± 17.7 μg/L, respectively, and these levels still might pose an ecological risk in terms of the aquatic environment. Since groundwater constitutes the main source of public drinking water supplies in many countries, people who drink PPCPs-contaminated water may suffer an adverse effect on their growth and reproduction. Specific pharmaceuticals at low concentrations (ng/L) have become an important issue, particularly because of their toxicity towards living organisms. For example, about 50% to 90% of the original SMX dose and its metabolites are released into the environment and these then bioaccumulate via biotic factor and abiotic factors in the food chain [22]. SMX induces antibiotic resistance in bacteria and hazard quotients in WWTP effluent have revealed that these chemicals may pose an ecotoxicological risk to algae [23]. The occurrence of ACE has been reported in the aquatic environment and there is an important need to address the potential toxic effects of ACE on nontarget environmentally exposed organisms [24]. Exposure to low concentrations (10–100 ng/L) of IBU has been found to result in a significant decrease in the activity of *Gammarus pulex* [25].

3.3. Electricity Production by the MFC A/O System. Figure 4 demonstrates electricity generation by the MFC A/O system. Initially, polarization curves were obtained by measuring the power generation at various external resistances (from 510 KΩ to 1 Ω) and are shown in Figure 4(a). We selected 1 KΩ to measure I and A during this study. The existence of PPCPs in sewage does not seem to have affected the electric generation (ANOVA). Figure 4(b) presents the average PD, which was found to be 285.15 mW/m^2; furthermore, the maximum PD value achieved during Phase II was 532.61 mW/m^2. The E_C values ranged widely from 2.77% to 25.20% over the 125 days of the study and averaged 12.62% overall. Direct electron transfer from microbial cells to electrodes occurs at very low efficiency and a higher PD by a SPGRP MFC. It modifies the material used as the cathode catalyst in order to increase the efficiency of the oxidation-reduction reaction. In this study, the novel design used here allows the formation

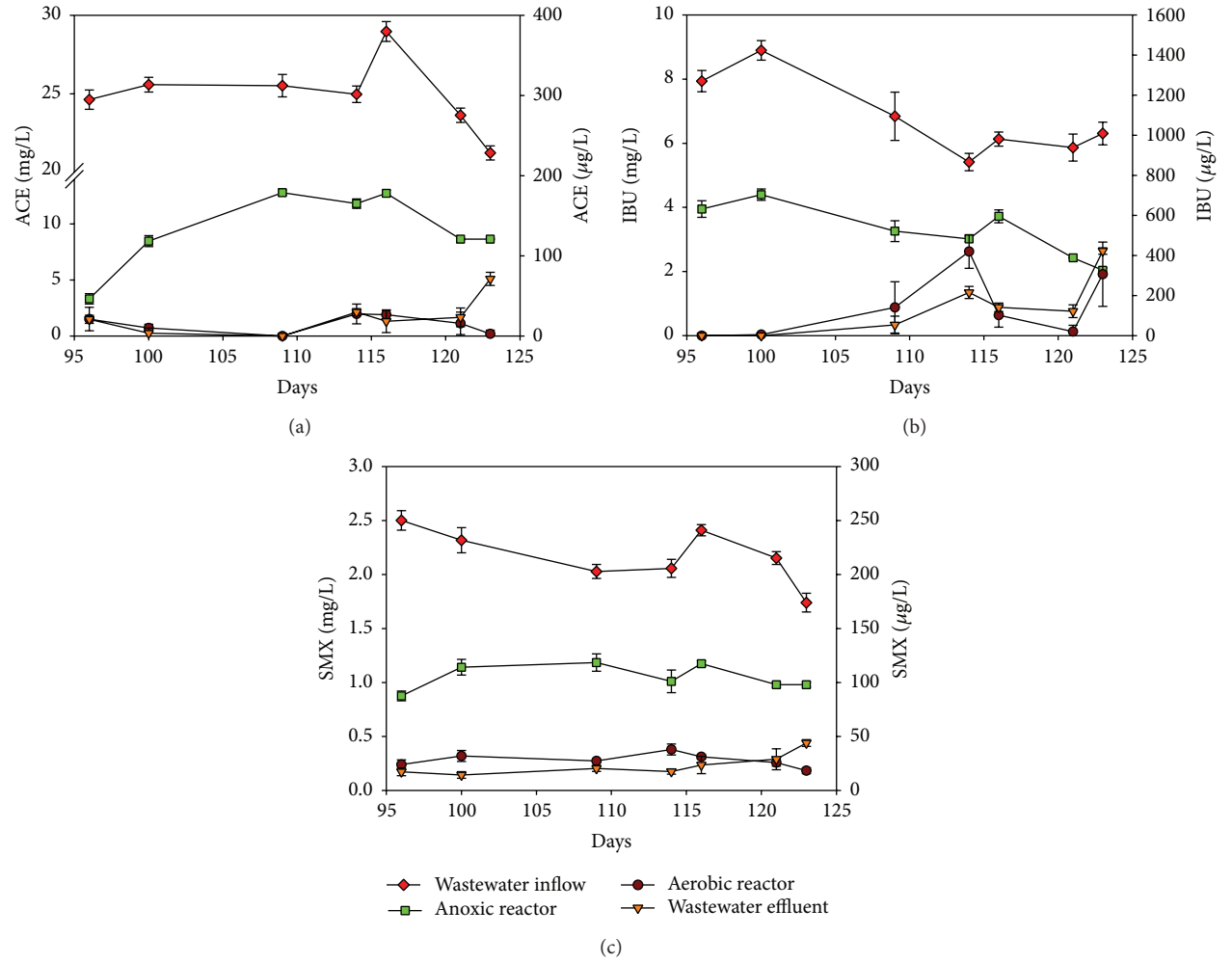

Figure 3: Variation in targeted PPCPs in the MFC A/O system during Phase II: (a) ACE; (b) IBU; (c) SMX. The concentrations in the sewage influent (◆) and in the anoxic reactor (■) are presented on the left-Y axial (mg/L). The concentrations in the aerobic reactor (▼) and in the sewage effluent (●) are presented on the right-Y axial (μg/L).

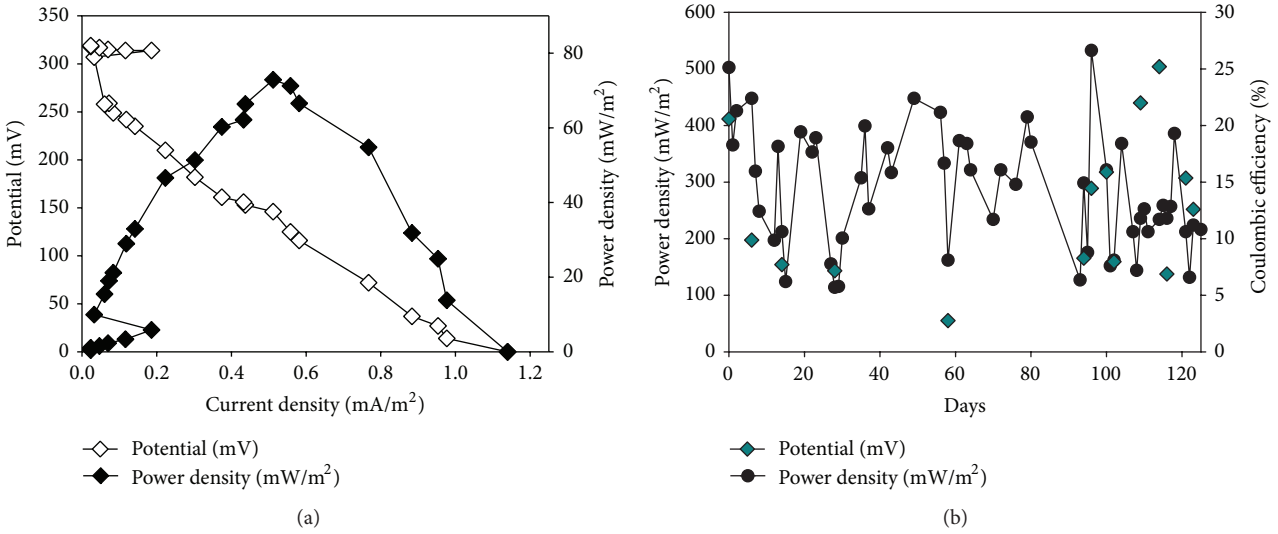

Figure 4: Electrical generation by the A/O reactor coupled with the novel MFC system: (a) polarization curve; (b) power density and coulombic efficiency.

Table 4: The richness index (RI) on the 109th day of Phase II obtained from the DGGE profiles allows assessments of the variation in biodiversity across the various areas of the novel MFC A/O system.

Same bands[1]/different bands[2] (difference ratio[3])		Anoxic reactor (anode)		
		MLSS	SPGRP biofilm	PEM biofilm
Aerobic reactor (cathode)	MLSS	3/18 (85.71%)	7/16 (69.56%)	7/13 (65.00%)
	SPGRP biofilm	7/15 (68.18%)	3/19 (86.36%)	4/16 (80.00%)
	PEM biofilm	5/13 (72.22%)	3/20 (86.96%)	3/18 (85.71%)

[1]Same bands are defined as the same location on the DGGE profile in Figure 3.
[2]Different bands are defined as the total number of different bands obtained when comparing each of two samples.
[3]The difference ratio is defined as the ratio of the number of different bands to all bands present.

of biofilms on the SPGRP, which plays an important role in the generation of electricity. Biofilms were observed to cover a high specific surface area on the SPGRPs forming both the cathode and the anode. Some aerobic bacteria might possibly be acting as cathode catalysts. The performance of a MFC has been found to increase as the biofilm develops on the cathode [26] and a high PD has been found when there is a biofilm covering the anode. This might be because the production of various biointermediates may favor electricity generation. Bacteria are able to use their respiratory chain as part of the oxidative metabolism that occurs at the anode. Nitrite might be converted to nitrate when the cathodic electrode acts as the electron donor due to denitrification in the MFC.

The PD value is higher than that in previous studies using two-chambered MFCs that have had chemical mediators added. For example, an anaerobic-aerobic sequential reactor was reported to generate 387 mW/m^2 PD and 5.2% C_E with 86.4% removal efficiency when high strength dye wastewater was used that comprised 1,000 mg L^{-1} glucose and 200 mg/L Congo red (chemical mediator); this was at a longer HRT of 14.8 h [27]. A MFC shows 91% removal efficiency of high-loading domestic wastewater with the volatile fatty acid/hydrogen production which contained concentrated particular artificial food waste. The overall aim of converting chemical energy into electrical energy was achieved with a C_E of 46% generating 65.33 mA/m^2 at a specific cell potential of 148 mV [28]. However, other factors can affect the generation of electricity in the MFC A/O system. The characteristics of the wastewater can affect the electrical generation performance of MFCs. The slow biodegradations of the PPCPs present in the sewage used in this study might result in more efficient electricity production. Another possible reason is that the mass transfer of protons remains a major constraint affecting the C_E of a MFC. The low C_E values are due to the fact that hydrogen proton exchange through the PEM is retarded by bacterial fouling of the A/O system. It is possible that the high internal electric resistance of the novel design for a MFC system described here might decrease electricity generation performance. Nevertheless, the dual chamber MFC A/O system still is competitive if we are considering the biological treatment efficiency of PPCP sewage and the generation of electricity at the same time.

3.4. The Presence of Specific Bacterial Communities in the MFC A/O System. Figure 5 displays the biodiversity of bacterial community in the MFC A/O systems by comparing their DGGE profiles. Table 4 compares the RI values for the DGGE

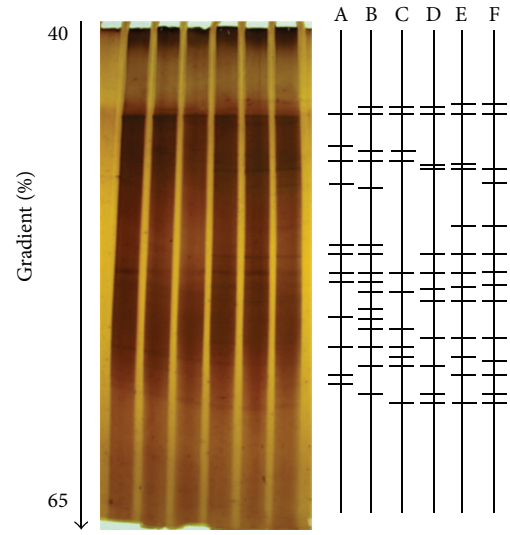

Figure 5: DGGE profiles analysis of the MFC A/O reactor in the MFC A/O system on the 109th day. Lines A, B, and C present the profiles of the MLSS, SPGRP biofilm, and PEM biofilm from the aerobic tank; lines D, E, and F present the profiles of the MLSS, SPGRP biofilm, and PEM biofilm from the anoxic reactor.

bands detected across the different bacterial populations. Distinct differences were found in the bacterial species present at the three sampling locations within the MFC A/O system. The highest difference in band number ratios was 86.96% and this occurred between the SPGRP biofilms in the anoxic reactor and the PEM biofilms in the aerobic reactor. Even the lowest difference in band number ratios was as high as 65.00%, which was between the PEM biofilms in anoxic reactor and MLSS in aerobic reactor. These findings indicate the various different bacterial communities are likely to play distinctly different roles in the two chambers. For example, redox shuttling within the MFC anoxic chamber appears mainly to be present within the SPGRP and PEM biofilms and does not seem to occur within the MLSS biofilm.

Figure 6 provides detailed information on the various bacterial communities in the MFC A/O system at the class-level species using the 16S rDNA clone library. The dominant bacteria in the aerobic reactor were Proteobacteria, including β-Proteobacteria (53.50%), δ-Proteobacteria (14.65%), γ-Proteobacteria (8.92%), and α-Proteobacteria (8.92%). In addition, in terms of the three sampling locations within the reactor, the dominant species at the phylum-level are

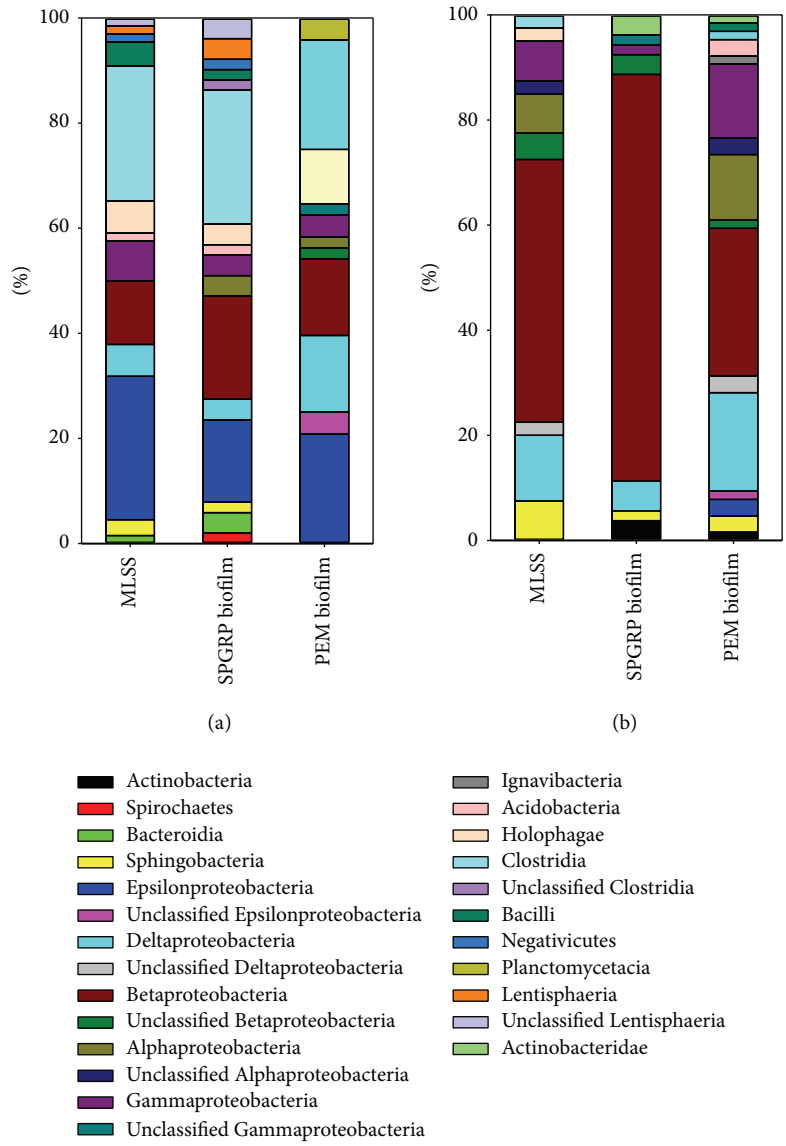

Figure 6: Bacterial community analysis of the MFC A/O reactor. The ratio of identified bacterial species to all bacteria cloned on the 114th day (class level): (a) anoxic reactor; (b) aerobic reactor.

different. The percentage of β-Proteobacteria was 81.13% within the GRP biofilms, compared to 55.0% within the MLSS and 29.69% within the PEM biofilms. The relative abundance of β-Proteobacteria is probably due to the fact that several groups of aerobic or facultative bacteria are well equipped to carry out aromatic degradation. In contrast, higher percentages of α-Proteobacteria, γ-Proteobacteria, δ-Proteobacteria, and Sphingobacteria were found to be present in the MLSS and PEM biofilms, but these groups were found to be much less abundant in the GRP biofilm. Furthermore, the anoxic reactor within the A/O system was found to have a specific dominant bacterial community that included Clostridia-Firmicutes (24.85%), ε-Proteobacteria (23.03%), β-Proteobacteria (15.76%), Bacteroidetes (10.16%), and δ-Proteobacteria (7.88%). Many of these phyla can act as anode-respiring bacteria, which are defined as a bacterial population with a respiration process that can use an anode as their electron acceptor [13]. The percentage of ε-Proteobacteria in the MLSS was 27.27% and in the PEM biofilms was 25.0%, which should be compared with that in the GRP biofilms, which was 15.68%. Clostridia and β-Proteobacteria were dominant in this reactor with ranges from 20.83% to 27.45% and from 12.12% to 19.61% for the three different samples, respectively. Bacterial diversity has been found to vary at the anode of the MFCs when various different substrates are fed. For example, a two-chambered MFC using chocolate industry wastewater as the substrate had the following phyla at the anode: α-Proteobacteria (9.1%), β-Proteobacteria (50.6%), γ-Proteobacteria (0.8%), and Firmicutes (4.9%) [29].

4. Discussion

4.1. Comparison of PPCP Removal in the Anoxic and Anaerobic Reactors. The contribution to PPCP treatment of the

Table 5: Bacteria identified by nucleic acid sequencing of 16S gene clones and by the searching of the GenBank database; these bacteria are associated with the generation of electricity by the MFC A/O system.

Accession number (closest match)	Sequence similarity	Species
KC502887	96%	Uncultured *Geobacter* sp.
FR774807	98%	Uncultured Clostridiales bacterium
FJ269104	96%	Iron-reducing bacterium
DQ234216	99%	Uncultured *Sulfurospirillum* bacterium
JF809001	100%	Uncultured *Leptothrix* sp.
JQ278984	99%	Uncultured Rhodospirillales bacterium
KC517355	87%	*Pelosinus* sp.
JQ086873	97%	Uncultured *Treponema* sp.
CU926806	97%	Uncultured *Lentisphaerae* sp.
KC871534	99%	*Pseudomonas* sp.
AF170354	99%	*Dechloromonas* sp.
HE662651	98%	*Cupriavidus basilensis*

aerobic reactor and of the anoxic reactor was found to be different in this MFC A/O system. The removal efficiency in the anoxic reactor averaged 62.51% for ACE, 51.88% for IBU, and 51.13% for SMX, but there was lower removal efficiency for ACE, IBU, and SMX in the aerobic reactor at 37.86%, 47.14, and 46.84%, respectively. Their biointermediates in the anoxic reactor consist of at least three known compounds (data not shown). Aerobic biodegradation has generally been demonstrated to give a better removal efficiency of COD_{Cr}, which includes most of PPCPs. For example, 50 μg/L of ACE and IBU were biotransformed by greater than 80% after 10 days under aerobic batch biodegradation [30]. The removal efficiency of IBU reached 95 ± 4% in an aerobic nitrification reactor but was only 37 ± 26% in an anoxic denitrification reactor. Very low removal of SMX by biodegradation, 22± 5% was found in an aerobic reactor in one study [31]. In the present MFC A/O system, the anoxic reactor can remove more of the target PPCPs because of the obvious growth of facultative bacteria within the MLSS and SPGRP biofilms. These bacterial populations were able to bring about removal rates for the PPCPs as follows: ACE (62.51%) > IBU (51.88%), both under anoxic condition. In one previous study, there was IBU biodegradation at 28%, with the concentration being 78 mg/L, which contrasted with the result for ACE at 11%, with the concentration being 66.12 mg/L, during anaerobic degradation at 37°C for 56 days [32].

4.2. Bacterial Species Involved in the Generation of Electricity by the MFC A/O System. Using a complex substrate like domestic wastewater that contains high strength PPCPs can help establish a diverse and electrochemically active microbial community using the MFC system. Some species in bacteria population that are able to produce electricity in a MFC were found to be abundant. Extracellular electron transfer was defined as electrons retrieved from the microbial oxidation of the organic substrates, namely, PPCP-containing sewage, in this study; these are then transferred to the anode. Table 5 shows the specific bacterial species identified as being most closely related to the various MFC bacteria that have been identified in MFC systems. Anodophilic consortia, such as Geobacteraceae (identified as *Geobacter* spp. in this study), Clostridiaceae (identified as *Clostridium* spp. in this study, 10.24% clones), and various Proteobacteria species, have been shown to be able to generate a current in an anode chamber and are known to be able to transfer electrons to an electrode. For example, iron-reducing bacteria such as *Shewanella* and *Geobacter* spp. have been described as electrochemically active bacteria in MFC systems [33–35]. A *Leptothrix* sp. has been reported to be a type of Mn-oxidizing bacteria that bioaccumulates Mn oxides that can be used as cathodic reactants. The potential of a MFC that includes the reduction of Mn oxides deposited by *Leptothrix* spp. can be increased to about 300 mV and is able to deliver a current density up to two orders of magnitude higher than that reached using the reduction of O_2 [36]. Rhodospirillales bacterium has been shown to be dominant in a cathodic MLSS rather than a biofilm; one possible reason for this is the fact that this is a light utilizing bacterial group capable of obtaining better illumination in suspension than as a biofilm [33]. *Pelosinus* spp. are capable of fermenting lactate and coupling the oxidation of this compound to Fe^{3+}; and such metal reduction in a microbial fuel cell can produce a maximum PD of 4.1 mW/m^2 [34]. A *Treponema* sp. has been found to be present in a two-chambered PEM MFC that utilized active sludge enriched with chocolate industry wastewater [29]. A Lentisphaerae sp. has been found previously to be associated with the anode of a MFC system [37]. A *Pseudomonas* sp., a facultative anaerobic bacterium, is able to produce pyocyanin as a mediator and then uses these quorum signaling compounds to produce power [35]. A *Dechloromonas* sp. was identified as the most dominant species of anode bacteria in a butyrate-fed two-chamber MFC system [38]. *Cupriavidus basilensis* has been shown to be involved in current production in a microbial fuel cell that used either acetate or phenol as a carbon source; in this case after 72 h in the MFC, 86% of the initial phenol concentration had been removed [39].

4.3. Bacterial Species Involved in the Biodegradation of PPCPs and Aromatic Compounds by the MFC A/O System. Table 6 outlines the specific bacterial species that are equipped

Table 6: Bacteria identified by nucleic acid sequencing of 16S gene clones and by the searching of the GenBank database; these are associated with the biodegradation of PPCP and aromatic compounds in the MFC A/O system.

Accession no (Closest match)	Sequences similarity	Species
KC871534	99%	*Pseudomonas* sp.
AJ620198	99%	*Sphingomonas* sp.
AF170354	99%	*Dechloromonas* sp.
KC871534	96%	Uncultured *Geobacter* sp.
AB636293	97%	Uncultured *Hydrogenophaga* sp.
HE662651	98%	*Cupriavidus* sp.
HQ184339	98%	Uncultured *Zoogloea* sp.
JQ795417	96%	Uncultured Acidobacteria bacterium
KC310815	99%	*Staphylococcus* sp.
JQ723636	96%	Uncultured Sphingobacteriales bacterium
JN540151	95%	Uncultured *Prolixibacter* sp.
JF808996	99%	Uncultured Burkholderiaies bacterium

with the ability to biodegrade aromatic compounds such as PPCPs, and these include bacteria associated with anaerobic biotransformation and aerobic ring cleavage, both of which were identified in the present study. Three species are known to have a direct relationship with PPCP biodegradation. *Dechloromonas* spp., which are β-Proteobacteria, have been detected in an A/O-MBR process that demonstrated good removal efficiency (88.5–99.5%) of antibiotics, including 500 μg/L SMX, at various different HRTs [40]. *Pseudomonas* spp. have been reported to biodegrade many pharmaceutical pollutants. For example, a high concentration of 2,000 mg/L ACE was able to be completely biodegraded as sole carbon source by a *Pseudomonas aeruginosa* isolated from the SBR treatment plant that processed ACE-contaminated wastewater [41]. *Pseudomonas aeruginosa* is also able to biodegrade 1.3% of 6 mg/L SMX when this antibiotic is used as sole carbon source or 5.6% of 6 mg/L SMX when 0.5 g/L glucose is present as an additive [42]. In addition, a *Sphingomonas* sp. strain Ibu-2, which was found in a wastewater treatment plant, was shown to be able to biodegrade 500 mg/L IBU as sole carbon and energy source over 80 hrs [43]. Bacterial communities seem to have adapted to IBU biodegradation best under anoxic conditions. In such circumstances the biological degradation rate constant for IBU with time was found to increase from 16% at the beginning to 75% after 350 days.

The chemical structure of the biological metabolic products derived from PPCPs consists largely of benzene-ring compounds. Anaerobic benzene biodegradation by *Geobacter* sp. has been shown to occur in a petroleum-contaminated aquifer [44]. A *Hydrogenophaga* sp., which is a member of a heterogeneous aerobic benzene-degrading bacterial group, was found during the biological treatment in BTEX groundwater [45]. An overall 95% biodegradation of the lignin-related aromatic compound ferulic acid has been reported to occur with a *Cupriavidus* sp. when ferulic acid is used as a sole carbon and energy source [46]. A *Zoogloea* sp. has been shown to be able to biodegrade 98.6% of lubricating oil over 12 days with a HRT of 6 h. and an inflow rate of 33 L/h [47]. An Acidobacteria bacterium was found to be the dominant bacterial group during PAH bioremediation (3–5 aromatic rings) in soil and was also shown to be able to degrade benzene contaminated groundwater [48, 49]. A *Staphylococcus* sp., when immobilized on vermiculite, was used to remove hydrocarbons; this system used a fluidized bed bioreactor and synthetic water polluted with benzene, toluene, or naphthalene as sole sources of carbon and energy [50]. A Sphingobacteriales bacterium has been identified as part of an ethylbenzene-degrading sulfate-reducing consortium [51]. A *Prolixibacter* sp. has been identified by microbial enrichment to be able to biodegrade chlorinated pesticides that are present in contaminated sites of different geographical habitats of India [52]. A Burkholderiales bacterium has been identified as being able to degrade methyl tert-butyl ether (MTBE), a benzene, toluene, ethylbenzene, and xylene (BTEX) mixture, and tert-butyl alcohol (TBA) [53].

5. Conclusions

The pilot-scale MFC A/O sewage treatment was easily equipped with SPGRPs in order to treat municipal wastewater and to generate electricity in parallel with the biodegradation. The biological treatment of the PPCP-contained sewage demonstrated good performance over the time course of the experiment. A high removal efficiency of the target PPCPs was obtained after biofilms had formed on large specific surface areas available within the MFC A/O system. The ability to generate electricity using the SPGRP MFC is better than previous dual-chamber graphite MFC systems. A total of twenty bacterial species were identified as forming part of the MLSS and SPGRP biofilms and these identifications were used to clarify the possible functions of these microorganisms. These functions included both electrical generation and PPCP biodegradation. Practically, a scale-up of this SPGRP MFC A/O system for the treatment of real PPCP-contained sewage is needed and this should be applied to a commercial operation in the future. This will allow the design, operation, and maintenance of the system to be optimized. Importantly, such a system should be more efficient in terms of power use than conventional systems, without a significant increase in construction costs.

Conflict of Interests

The authors declare that there is no conflict of interests regarding the publication of this paper.

Acknowledgments

The authors thank Professor Ilona Sárvári Horváth for the discussion and comments. Ms. Ruo-Jhen Peng made her great effort to help with the experimental tasks. This work was supported by the National Science Council (NSC) of Taiwan through the project NSC100-2632-B-031-001-MY3.

References

[1] D. W. Kolpin, E. T. Furlong, M. T. Meyer et al., "Pharmaceuticals, hormones, and other organic wastewater contaminants in U.S. streams, 1999–2000: a national reconnaissance," *Environmental Science and Technology*, vol. 36, no. 6, pp. 1202–1211, 2002.

[2] A. Y. Lin, C. Lin, Y. Tsai et al., "Fate of selected pharmaceuticals and personal care products after secondary wastewater treatment processes in Taiwan," *Water Science and Technology*, vol. 62, no. 10, pp. 2450–2458, 2010.

[3] Y. J. Chan, M. F. Chong, C. L. Law, and D. G. Hassell, "A review on anaerobic-aerobic treatment of industrial and municipal wastewater," *Chemical Engineering Journal*, vol. 155, no. 1-2, pp. 1–18, 2009.

[4] J. Reungoat, B. I. Escher, M. Macova, and J. Keller, "Biofiltration of wastewater treatment plant effluent: effective removal of pharmaceuticals and personal care products and reduction of toxicity," *Water Research*, vol. 45, no. 9, pp. 2751–2762, 2011.

[5] L. Zhou, G. Ying, S. Liu et al., "Occurrence and fate of eleven classes of antibiotics in two typical wastewater treatment plants in South China," *Science of the Total Environment*, vol. 452-453, pp. 365–376, 2013.

[6] D. Pant, D. Arslan, G. V. Bogaert et al., "Integrated conversion of food waste diluted with sewage into volatile fatty acids through fermentation and electricity through a fuel cell," *Environmental Technology*, vol. 34, no. 13-14, pp. 1935–1945, 2013.

[7] A. ElMekawy, S. Srikanth, K. Vanbroekhoven, H. D. Wever, and D. Pant, "Bioelectro-catalytic valorization of dark fermentation effluents by acetate oxidizing bacteria in bioelectrochemical system (BES)," *Journal of Power Sources*, vol. 262, pp. 183–191, 2014.

[8] J. Zhang, Y. Zhang, X. Quan et al., "An anaerobic reactor packed with a pair of Fe-graphite plate electrodes for bioaugementation of azo dye wastewater," *Biochemical Engineering Journal*, vol. 63, pp. 31–37, 2012.

[9] Y. Liu, H. Liu, C. Wang, S. X. Hou, and N. Yang, "Sustainable energy recovery in wastewater treatment by microbial fuel cells: stable power generation with nitrogen-doped graphene cathode," *Environmental Science Technology*, vol. 47, no. 23, pp. 13889–13895, 2013.

[10] Y. Alvarez-Gallego, X. Dominguez-Benetton, D. Pant et al., "Development of gas diffusion electrodes for cogeneration of chemicals and electricity," *Electrochimica Acta*, vol. 82, pp. 415–426, 2012.

[11] T. Sangeetha and M. Muthukumar, "Influence of electrode material and electrode distance on bioelectricity production from sago-processing wastewater using microbial fuel cell," *Environmental Progress & Sustainable Energy*, vol. 32, no. 2, pp. 390–395, 2013.

[12] K. Rabaey and W. Verstraete, "Microbial fuel cells: novel biotechnology for energy generation," *Trends in Biotechnology*, vol. 23, no. 6, pp. 291–298, 2005.

[13] L. Alzate-Gaviria, "Microbial fuel cells for wastewater treatment," in *Waste Water-Treatment and Reutilization*, F. Sebastián and G. Einschlag, Eds., InTech, 2011.

[14] APHA, AWWA, and WEF, *Standard Methods for the Examination of Water and Wastewater*, American Public Health Association, American Water Works Association, Water Environment Federation, Washington, DC, USA, 22th edition, 2012, edited by E. W. Rice, R.B. Baird, L. S. Clesceri , A. D. Eaton.

[15] H.-L. Chou, Y.-T. Chang, Y.-F. Liao, and C.-H. Lin, "Biodegradation of decabromodiphenyl ether (BDE-209) by bacterial mixed cultures in a soil/water system," *International Biodeterioration Biodegradation*, vol. 85, pp. 671–682, 2013.

[16] A. L. Reysenbach and N. R. Pace, "Archaea: laboratory manual-thermophiles," F. T. Robb and A. R. Place, Eds., Cold Spring Harbour Laboratory Press, New York, NY, USA, 1995.

[17] S. K. Behera, H. W. Kim, J. Oh, and H. Park, "Occurrence and removal of antibiotics, hormones and several other pharmaceuticals in wastewater treatment plants of the largest industrial city of Korea," *Science of the Total Environment*, vol. 409, no. 20, pp. 4351–4360, 2011.

[18] T. Alvarinoa, K. Evina, S. Malamis, S. Suarez, F. Omil, and F. Fatone, "Inhibition of biomass activity in the via nitrite nitrogen removal processes by veterinary pharmaceuticals," *Bioresource Technology*, vol. 152, pp. 477–483, 2014.

[19] J. Radjenović, M. Petrović, and D. Barceló, "Fate and distribution of pharmaceuticals in wastewater and sewage sludge of the conventional activated sludge (CAS) and advanced membrane bioreactor (MBR) treatment," *Water Research*, vol. 43, no. 3, pp. 831–841, 2009.

[20] F. Ingerslev and B. Halling-Sorensen, "Biodegradability properties of sulfonamides in activated sludge," *Environmental Toxicology and Chemistry*, vol. 19, no. 10, pp. 2467–2473, 2000.

[21] F. I. Hai, X. Li, W. E. Price, and L. D. Nghiem, "Removal of carbamazepine and sulfamethoxazole by MBR under anoxic and aerobic conditions," *Bioresource Technology*, vol. 102, no. 22, pp. 10386–10390, 2011.

[22] S. Thiele-Bruhn, "Pharmaceutical antibiotic compounds in soils—a review," *Journal of Plant Nutrition and Soil Science*, vol. 166, no. 2, pp. 145–167, 2003.

[23] L. H. Santos, M. Gros, S. Rodriguez-Mozaz et al., "Contribution of hospital effluents to the load of pharmaceuticals in urban wastewaters: identification of ecologically relevant pharmaceuticals," *Science of the Total Environment*, vol. 461-462, pp. 302–316, 2013.

[24] S. C. Antunes, R. Freitas, E. Figueira, F. Gonçalves, and B. Nunes, "Biochemical effects of acetaminophen in aquatic species: edible clams Venerupis decussata and *Venerupis philippinarum*," *Environmental Science and Pollution Research*, vol. 20, no. 9, pp. 6658–6666, 2013.

[25] H. J. De Lange, W. Noordoven, A. J. Murk, M. Lürling, and E. T. H. M. Peeters, "Behavioural responses of *Gammarus pulex* (Crustacea, Amphipoda) to low concentrations of pharmaceuticals," *Aquatic Toxicology*, vol. 78, no. 3, pp. 209–216, 2006.

[26] Z. He and L. T. Angenent, "Application of bacterial biocathodes in microbial fuel cells," *Electroanalysis*, vol. 18, no. 19-20, pp. 2009–2015, 2006.

[27] Z. Li, X. Zhang, J. Lin, S. Han, and L. Lei, "Azo dye treatment with simultaneous electricity production in an anaerobic-aerobic sequential reactor and microbial fuel cell coupled system," *Bioresource Technology*, vol. 101, no. 12, pp. 4440–4445, 2010.

[28] E. Elakkiya and M. Matheswaran, "Comparison of anodic metabolisms in bioelectricity production during treatment of dairy wastewater in Microbial Fuel Cell," *Bioresource Technology*, vol. 136, pp. 407–412, 2013.

[29] S. A. Patil, V. P. Surakasi, S. Koul et al., "Electricity generation using chocolate industry wastewater and its treatment in activated sludge based microbial fuel cell and analysis of developed microbial community in the anode chamber," *Bioresource Technology*, vol. 100, no. 21, pp. 5132–5139, 2009.

[30] J. T. Yu, E. J. Bouwer, and M. Coelhan, "Occurrence and biodegradability studies of selected pharmaceuticals and personal care products in sewage effluent," *Agricultural Water Management*, vol. 86, no. 1-2, pp. 72–80, 2006.

[31] S. Suarez, J. M. Lema, and F. Omil, "Removal of pharmaceuticals and personal care products (PPCPs) under nitrifying and denitrifying conditions," *Water Research*, vol. 44, no. 10, pp. 3214–3224, 2010.

[32] S. E. Musson, P. Campo, T. Tolaymat, M. Suidan, and T. G. Townsend, "Assessment of the anaerobic degradation of six active pharmaceutical ingredients," *Science of the Total Environment*, vol. 408, no. 9, pp. 2068–2074, 2010.

[33] K. B. Gregory, D. R. Bond, and D. R. Lovley, "Graphite electrodes as electron donors for anaerobic respiration," *Environmental Microbiology*, vol. 6, no. 6, pp. 596–604, 2004.

[34] S. Choi and J. Chae, "Optimal biofilm formation and power generation in a micro-sized microbial fuel cell (MFC)," *Sensors and Actuators, A: Physical*, vol. 195, pp. 206–212, 2013.

[35] B. E. Logan, "Exoelectrogenic bacteria that power microbial fuel cells," *Nature Reviews Microbiology*, vol. 7, no. 5, pp. 375–381, 2009.

[36] A. Rhoads, H. Beyenal, and Z. Lewandowski, "Microbial fuel cell using anaerobic respiration as an anodic reaction and biomineralized manganese as a cathodic reactant," *Environmental Science and Technology*, vol. 39, no. 12, pp. 4666–4671, 2005.

[37] G. Zhang, K. Wang, Q. Zhao, Y. Jiao, and D. Lee, "Effect of cathode types on long-term performance and anode bacterial communities in microbial fuel cells," *Bioresource Technology*, vol. 118, pp. 249–256, 2012.

[38] K.-J. Chae, M.-J. Choi, J.-W. Lee, K.-Y. Kim, and I. S. Kim, "Effect of different substrates on the performance, bacterial diversity, and bacterial viability in microbial fuel cells," *Bioresource Technology*, vol. 100, no. 14, pp. 3518–3525, 2009.

[39] H. Friman, A. Schechter, Y. Ioffe, Y. Nitzan, and R. Cahan, "Current production in a microbial fuel cell using a pure culture of *Cupriavidus basilensis* growing in acetate or phenol as a carbon source," *Microbial Biotechnology*, vol. 6, no. 4, pp. 425–434, 2013.

[40] S. Xia, R. Jia, F. Feng et al., "Effect of solids retention time on antibiotics removal performance and microbial communities in an A/O-MBR process," *Bioresource Technology*, vol. 106, pp. 36–43, 2012.

[41] B. de Gusseme, L. Vanhaecke, W. Verstraete, and N. Boon, "Degradation of acetaminophen by *Delftia tsuruhatensis* and *Pseudomonas aeruginosa* in a membrane bioreactor," *Water Research*, vol. 45, no. 4, pp. 1829–1837, 2011.

[42] S. Larcher and V. Yargeau, "Biodegradation of sulfamethoxazole by individual and mixed bacteria," *Applied Microbiology and Biotechnology*, vol. 91, no. 1, pp. 211–218, 2011.

[43] R. W. Murdoch and A. G. Hay, "Formation of catechols via removal of acid side chains from ibuprofen and related aromatic acids," *Applied and Environmental Microbiology*, vol. 71, no. 10, pp. 6121–6125, 2005.

[44] J. N. Rooney-Varga, R. T. Anderson, J. L. Fraga, D. Ringelberg, and D. R. Lovley, "Microbial communities associated with anaerobic benzene degradation in a petroleum-contaminated aquifer," *Applied and Environmental Microbiology*, vol. 65, no. 7, pp. 3056–3063, 1999.

[45] A. Fahy, T. J. McGenity, K. N. Timmis, and A. S. Ball, "Heterogeneous aerobic benzene-degrading communities in oxygen-depleted groundwaters," *FEMS Microbiology Ecology*, vol. 58, no. 2, pp. 260–270, 2006.

[46] L. Chai, H. Zhang, W. Yang et al., "Biodegradation of ferulic acid by a newly isolated strain of *Cupriavidus* sp. B-8," *Journal of Central South University*, vol. 20, no. 7, pp. 1964–1970, 2013.

[47] J. Liang, X. J. Wang, Z. L. Gu, D. Z. Zhou, and S. Q. Xie, "Biodegradation of lubricating oil in wastewater with *Zoogloea* sp.," *Pedosphere*, vol. 16, no. 4, pp. 540–544, 2006.

[48] J. Mao, Y. Luo, Y. Teng, and Z. Li, "Bioremediation of polycyclic aromatic hydrocarbon-contaminated soil by a bacterial consortium and associated microbial community changes," *International Biodeterioration and Biodegradation*, vol. 70, pp. 141–147, 2012.

[49] S. Xie, W. Sun, C. Luo, and A. M. Cupples, "Novel aerobic benzene degrading microorganisms identified in three soils by stable isotope probing," *Biodegradation*, vol. 22, no. 1, pp. 71–81, 2011.

[50] J. Taoufik, Y. Zeroual, A. Moutaouakkil et al., "Aromatic hydrocarbons removal by immobilized bacteria (*Pseudomonas* sp., *Staphylococcus* sp.) in fluidized bed bioreactor," *Annals of Microbiology*, vol. 54, no. 2, pp. 189–200, 2004.

[51] T. Nakagawa, S. Sato, Y. Yamamoto, and M. Fukui, "Successive changes in community structure of an ethylbenzene-degrading sulfate-reducing consortium," *Water Research*, vol. 36, no. 11, pp. 2813–2823, 2002.

[52] N. Manickam, A. Pathak, H. S. Saini, S. Mayilraj, and R. Shanker, "Metabolic profiles and phylogenetic diversity of microbial communities from chlorinated pesticides contaminated sites of different geographical habitats of India," *Journal of Applied Microbiology*, vol. 109, no. 4, pp. 1458–1468, 2010.

[53] A. Pruden and M. Suidan, "Effect of benzene, toluene, ethylbenzene, and p-xylene (BTEX) mixture on biodegradation of methyl tert-butyl ether (MTBE) and tert-butyl alcohol (TBA) by pure culture UC1," *Biodegradation*, vol. 15, no. 4, pp. 213–227, 2004.

Hindawi Publishing Corporation
BioMed Research International
Volume 2014, Article ID 350414, 6 pages
http://dx.doi.org/10.1155/2014/350414

Research Article

Enhanced Solid-State Biogas Production from Lignocellulosic Biomass by Organosolv Pretreatment

Safoora Mirmohamadsadeghi,[1] Keikhosro Karimi,[1,2] Akram Zamani,[1] Hamid Amiri,[1] and Ilona Sárvári Horváth[3]

[1] *Department of Chemical Engineering, Isfahan University of Technology, Isfahan 84156-83111, Iran*
[2] *Industrial Biotechnology Group, Institute of Biotechnology and Bioengineering, Isfahan University of Technology, Isfahan 84156-83111, Iran*
[3] *Swedish Centre for Resource Recovery, University of Borås, 50190 Borås, Sweden*

Correspondence should be addressed to Safoora Mirmohamadsadeghi; safoora.mirmohamadsadeghi@ce.iut.ac.ir

Received 15 June 2014; Accepted 18 July 2014; Published 5 August 2014

Academic Editor: Meisam Tabatabaei

Organosolv pretreatment was used to improve solid-state anaerobic digestion (SSAD) for methane production from three different lignocellulosic substrates (hardwood elm, softwood pine, and agricultural waste rice straw). Pretreatments were conducted at 150 and 180°C for 30 and 60 min using 75% ethanol solution as an organic solvent with addition of sulfuric acid as a catalyst. The statistical analyses showed that pretreatment temperature was the significant factor affecting methane production. Optimum temperature was 180°C for elmwood while it was 150°C for both pinewood and rice straw. Maximum methane production was 152.7, 93.7, and 71.4 liter per kg carbohydrates (CH), which showed up to 32, 73, and 84% enhancement for rice straw, elmwood, and pinewood, respectively, compared to those from the untreated substrates. An inverse relationship between the total methane yield and the lignin content of the substrates was observed. Kinetic analysis of the methane production showed that the process followed a first-order model for all untreated and pretreated lignocelluloses.

1. Introduction

Worldwide concerns about the limitations of fossil resources, rising crude oil prices, and greenhouse gas (GHG) emissions have led researchers to seek alternative clean and renewable energy sources, for example, biofuels [1]. Lignocellulosic materials are abundant and renewable feedstocks that have recently been considered for the production of biofuels [2–6]. Compared to liquid biofuels, biogas has been shown to have far better performance with respect to both agricultural land area efficiency and life cycle assessments [7].

Biogas, produced during anaerobic digestion (AD) processes, can be used as a versatile source of energy to produce heat and electricity, either separate or combined, and to propel vehicles. The production of biogas offers other advantages, such as controlling organic waste, reducing greenhouse gas emissions, and producing another economically viable fertilizer [8, 9]. AD processes are classified into liquid anaerobic digestion (LAD) and solid-state anaerobic digestion (SSAD), based on the solid content [10]. LAD operates at a total solid (TS) content of less than 15%, while SSAD is generally called for a TS content of higher than 15% [11]. Smaller specific reactor volume, fewer moving parts, lower energy input for heating, easier handling of the end product, and lower parasitic energy loss are the main advantages of SSAD in comparison with LAD [11–13]. SSAD is specially required with lignocellulosic feedstocks, such as agricultural residues with low moisture content [11, 14]. However, the anaerobic digestion of lignocelluloses is limited by the rate of hydrolysis due to their recalcitrant structure [15]. Therefore, an additional pretreatment process is essential to improve their digestibility [15, 16].

Although different factors, for example, the crystallinity of cellulose and the accessible surface area, may play important roles in the bioconversion of lignocelluloses, the presence of lignin is apparently the most important factor affecting

biodegradability [17–20]. The lignin-carbohydrate matrix limits the digestibility of lignocelluloses since lignin is a hydrophobic polymer that forms a cross-linked network among the carbohydrates. This network is highly resistant to enzymatic and microbial degradations [6, 21]. Hence, the biogas production from lignocelluloses can be improved by a delignification process. Removal of lignin by ethanol is among the most efficient pretreatment techniques in improving bioconversion of lignocelluloses [22, 23]. Furthermore, since lignin is a value added by-product, an additional unique benefit of organosolv pretreatment is unaltered lignin separation [23]. Therefore, using ethanol as an organosolv for pretreatment prior to the AD process has been reported to improve the economy of the process by increasing methane yield and recovery of lignin [24]. To our knowledge, there is no publication in the literature on utilizing organosolv pretreatment prior to SSAD of lignocelluloses.

The main objective of this study was to improve the performance of solid-state anaerobic digestion of three different types of lignocelluloses, that is, elmwood, pinewood, and rice straw, by applying organosolv pretreatments using ethanol under varying conditions. The effects of the pretreatment parameters, that is, temperature and duration time, on the methane yield were determined by solid-state batch anaerobic digestion assays. In addition, the kinetics of the degradation process was investigated for both untreated and pretreated substrates.

2. Material and Methods

2.1. Feedstocks and Inoculum. Elm, a hardwood, pine, a softwood, and rice straw, an agricultural waste, were used as substrates for biogas production. Elmwood and pinewood were obtained from the forest of Isfahan University of Technology (Isfahan, Iran), and rice straw (Sazandegi cultivar, Isfahan, Iran) was sourced from a field in Lenjan Province, Iran. Both elmwood and pinewood were debarked, cut into smaller pieces, and milled to obtain chips of less than 2 cm. The wood chips and the rice straw were partly ball-milled and screened to achieve powder with particle sizes between 295 and 833 μm (20–80 mesh). The screened substrates were then stored in airtight plastic bags at room temperature until use.

Effluent of a 7000 m^3 mesophilic anaerobic digester (Isfahan Municipal Sewage Treatment, Isfahan, Iran) was used as inoculum for the batch digestion assays. Due to its low TS content, the inoculum was centrifuged at 4500 rpm for 30 min to obtain the desirable TS content for the SSAD. The supernatant was discharged, and the remaining sludge was mixed to obtain a homogenous inoculum for SSAD. The inoculum was kept at 37°C for one week for stabilization.

2.2. Organosolv Pretreatment. Ethanol as an organic solvent together with sulfuric acid as catalyst was used for the pretreatments. A predetermined amount of each feedstock was mixed with 75% (v/v) aqueous ethanol solution supplemented with 1% w/w (based on dry mass) sulfuric acid to obtain a solid-to-liquid ratio of 1 : 8 (based on dry mass). The pretreatments were carried out in a 500 mL high-pressure stainless steel batch reactor [25]. After loading the substrate and the acidic ethanol mixture, the reactor was heated at a rate of 3°C/min to the desired temperature, that is, 150 or 180°C, and this temperature was held for 30 or 60 min. Then, the reactor was cooled in an ice bath. Afterwards, the pretreated materials were removed, washed three times with 100 mL aqueous ethanol (75% v/v, 60°C), and left overnight to air dry [24, 26]. The pretreated materials were stored in airtight plastic bags at room temperature until use.

2.3. Solid-State Anaerobic Digestion (SSAD) and Modeling. The untreated and pretreated elmwood, pinewood, and rice straw (1 g dry mass) were mixed with a predetermined amount of inoculum and deionized water to achieve a feed-to-inoculum ratio (F/I) (based on volatile solids (VS) content) of 3 and initial TS content of 21%. Sealable 118 mL glass reactors were used for the anaerobic digestion assays. Anaerobic conditions were provided by purging the reactors with nitrogen gas for about 2 min, and the reactors were then incubated in a convection oven at mesophilic conditions (39 ± 1°C) for 55 days [27]. Inoculum (without adding any substrate) was evaluated as a blank to determine the inoculum's methane production. All digestion assays were run in duplicate. Gas samples were taken and analyzed for produced biogas volume and composition in every 3 days during the first 9 days of the experimental period and then in every 5 or 6 days until 55 days.

The kinetics of the anaerobic digestion process was also evaluated using a first-order kinetic model (1). The first-order kinetic model was linearized as shown in (2) [28]:

$$-\frac{dM}{dt} = kM, \tag{1}$$

$$\ln\left(\frac{M_u}{M_u - M_t}\right) = kt, \tag{2}$$

where t (day) is time and M_u and M_t (L·kg^{-1}CH) are methane yields obtained in 55 days and t days, respectively, and k is the specific rate constant.

2.4. Analytical Methods. Total solid (TS) and volatile solid (VS) contents of the feedstocks and inoculum were measured by drying the samples at 105°C followed by heating the dried residues at 575°C to a constant weight [17]. The untreated and pretreated samples were analyzed for lignin and hemicellulose contents according to the methods presented by Sluiter et al. [29] and Yang et al. [30], respectively. The cellulose content was calculated as the remaining TS, based on an extractive-free basis, assuming that ash, hemicellulose, lignin, and cellulose are the only components of the entire biomass.

Methane and carbon dioxide produced during the anaerobic digestions were analyzed by a gas chromatograph (Sp-3420A, TCD detector, Beijing Beifen Ruili Analytical Instrument Co., China) equipped with a packed column (3 m length and 3 mm internal diameter, stainless steel, Porapak Q column, Chrompack, Germany). The carrier gas was nitrogen at a flow rate of 45 mL/min. The column, injector, and detector temperatures were 40, 100, and 150°C, respectively. A pressure-tight syringe (VICI, Precision Sampling, Inc., USA) with a volume of 250 μL was used for gas sampling and

Table 1: Composition analyses of the inoculum as well as the untreated versus pretreated feedstocks.

Samples	Pretreatment	TS content (%)	VS content (%)	Total lignin* (%)	Hemicellulose (%)	Cellulose (%)
Inoculum	—	5.7	2.7	ND	ND	ND
	Centrifuged	11.7	5.3	ND	ND	ND
Elmwood	Untreated	95.5	94.5	26.2	26.3	46.4
	150°C, 0.5 h	95.5	94.1	25.1	23.4	50.0
	150°C, 1 h	95.5	93.8	23.4	21.5	53.3
	180°C, 0.5 h	96.3	94.4	20.4	21.9	55.7
	180°C, 1 h	94.9	93.6	19.1	21.3	58.1
Pinewood	Untreated	95.1	95.2	26.8	28.0	44.5
	150°C, 0.5 h	95.3	94.6	27.8	20.2	51.3
	150°C, 1 h	95.9	95.1	26.5	21.3	51.4
	180°C, 0.5 h	96.5	95.5	22.1	18.5	58.4
	180°C, 1 h	96.9	95.8	21.1	16.9	60.8
Rice straw	Untreated	95.4	83.9	17.1	50.1	21.5
	150°C, 0.5 h	95.6	83.8	12.2	45.6	29.9
	150°C, 1 h	95.7	83.6	13.4	45.3	28.7
	180°C, 0.5 h	95.9	86.2	11.4	42.3	36.2
	180°C, 1 h	96.0	84.7	10.6	42.2	35.3

ND = not determined.
*Sum of acid soluble lignin (ASL) and acid insoluble lignin (AIL) contents.

injection, enabling taking of gas samples at the bioreactors' actual pressure. Excess gas was released through a needle after each gas sampling to avoid overpressure built-up in the bottles.

All biogas yields were presented at standard conditions.

2.5. Statistical Analysis. Analysis of variance (ANOVA) using Minitab software v. 15 was performed to compare confidence intervals and significance between treatments. The factors were considered significant when the probability (P value) was less than 0.05.

3. Results and Discussion

3.1. Characterization of Inoculum. The inoculum obtained from the industrial biogas plant contained 5.7 and 2.7% TS and VS, respectively (Table 1). In order to achieve a TS content of 21% in SSAD, the inoculum was centrifuged [31] to reach TS and VS contents of 11.7% and 5.3%, respectively (Table 1).

3.2. The Effect of Different Pretreatment Conditions on the Composition of Substrates. Elmwood, pinewood, and rice straw were subjected to organosolv pretreatment using ethanol prior to anaerobic digestion in order to improve the yield of biogas production. The untreated and pretreated materials were characterized, according to their TS, VS, lignin, cellulose, and hemicellulose contents, and results are summarized in Table 1.

Total lignin contents of untreated elmwood and pinewood were 26.2 and 26.8%, respectively, which was much higher than that of untreated rice straw (17.1%).

The various components of the materials were differently affected by the pretreatments. Depending on the pretreatment conditions, the lignin contents were reduced by 4–27% for elmwood, by 1–21% for pinewood, and by 21–37% for rice straw. Increasing the severity of the pretreatment generally resulted in higher lignin removal. A relatively high portion of straw's lignin (37.7%) was removed through pretreatment at 180°C for 60 min, resulting in a pretreated straw with carbohydrate content of over 77% of TS. On the other hand, the organosolv pretreatment of elmwood and pinewood, at 180°C for 60 min, resulted in 27% and 21% lignin removal, respectively, with corresponding CH contents of 72.7% and 72.5% of TS, respectively. In addition to delignification, parts of hemicelluloses were also removed due to the pretreatments. Higher hemicellulose removal was obtained in pretreated pinewoods (28–40%), compared to that in elmwood (11–19%) or straw (9–16%).

3.3. Biogas Production. Organosolv pretreatments in four different conditions were performed on the three different lignocellulosic materials, and the methane yields of the pretreated and untreated materials were then measured through batch SSAD assays. The accumulated methane productions obtained during 55 days of digestion from the untreated and pretreated materials are shown in Figure 1.

Methane production yields from all of the substrates were generally improved by the pretreatments in all conditions. The highest methane yield of 152.7 $L \cdot kg^{-1}$CH was obtained from rice straw pretreated at 150°C for 1 h (Table 2). However increasing the pretreatment temperature resulted in a reduced methane yield. This could be due to the inhibitory products which can be formed at high temperature during the pretreatment. In contrast, the highest yield of methane production from pretreated elmwood (93.7 $L \cdot kg^{-1}$CH) was obtained after pretreatment at 180°C for 1 h; hence, the methane production from elmwood was improved by increasing the severity of the pretreatment. However, the

Table 2: The accumulated methane yields obtained after 55 days of anaerobic digestion from untreated and pretreated lignocellulosic substrates together with the specific rate constants and the regression coefficients calculated from the first-order kinetic model fitting.

Sample	Pretreated conditions	CH_4 ($L{\cdot}kg^{-1}CH$)	k (day^{-1})	r^2
Elmwood	Untreated	54.2 ± 3.5	0.054	0.975
	150°C, 0.5 h	55.4 ± 9.7	0.063	0.934
	150°C, 1 h	63.6 ± 12.3	0.066	0.914
	180°C, 0.5 h	78.7 ± 0.4	0.062	0.961
	180°C, 1 h	93.7 ± 0.9	0.097	0.937
Pinewood	Untreated	38.7 ± 4.1	0.066	0.973
	150°C, 0.5 h	71.4 ± 3.7	0.094	0.981
	150°C, 1 h	63.3 ± 9.3	0.073	0.933
	180°C, 0.5 h	61.1 ± 4.4	0.080	0.979
	180°C, 1 h	56.0 ± 8.5	0.065	0.962
Rice straw	Untreated	115.9 ± 12.8	0.081	0.943
	150°C, 0.5 h	143.3 ± 7.1	0.084	0.946
	150°C, 1 h	152.7 ± 20.2	0.088	0.918
	180°C, 0.5 h	93.8 ± 19.9	0.078	0.991
	180°C, 1 h	113.4 ± 1.6	0.068	0.984

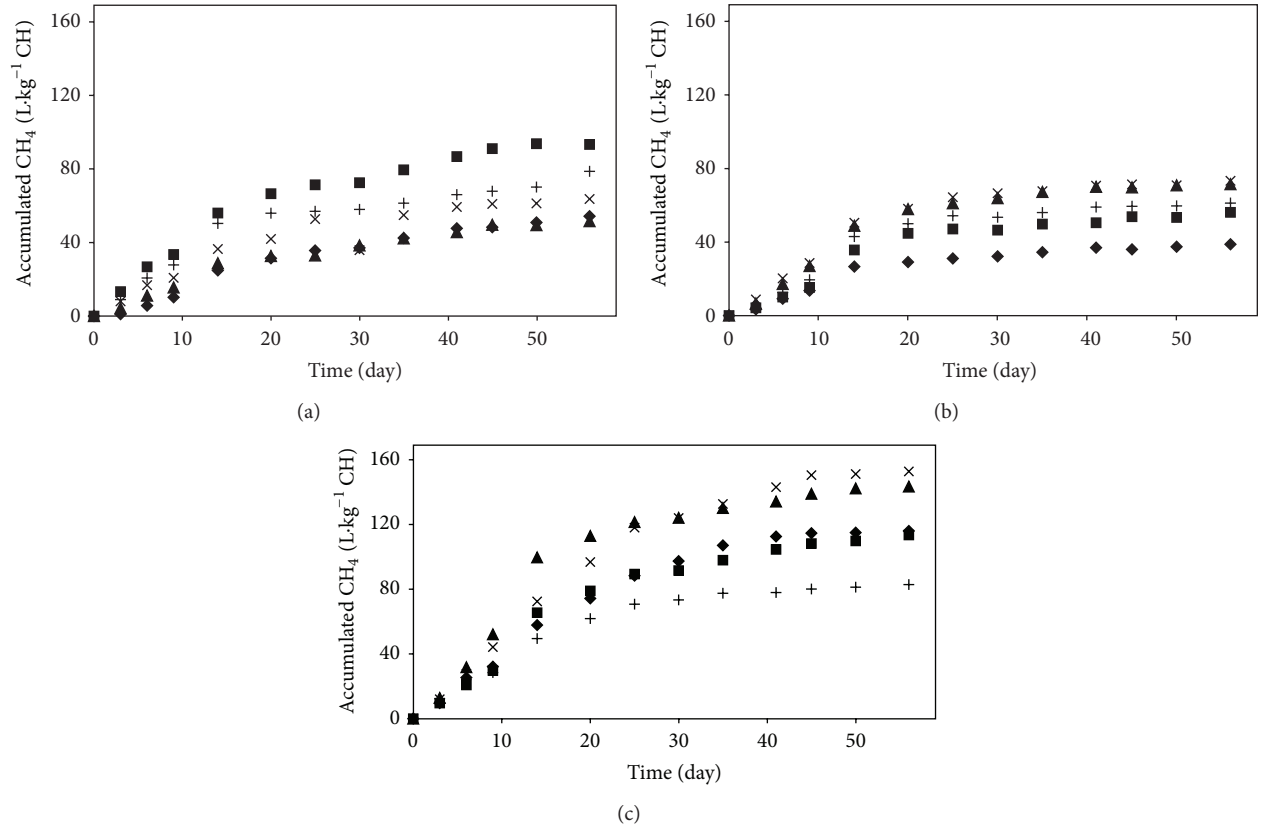

Figure 1: Accumulated methane production from SSAD of untreated and pretreated (a) elmwood, (b) pinewood, and (c) rice straw in different pretreatment conditions. The symbols represent the untreated substrates (◆), the substrates pretreated at 150°C for 0.5 h (▲), at 150°C for 1 h (×), at 180°C for 0.5 h (+), and at 180°C for 1 h (■).

pretreatment of pinewood at 150°C for 0.5 h (the lowest severity) resulted in a methane yield of 71.4 $L{\cdot}kg^{-1}CH$, which showed 84% improvement compared to the methane yield from untreated pinewood. Although pretreating pinewood had a remarkable effect on the yield of methane production (i.e., improvements of 45–84%), the statistical analyses using methane yield as response variable showed that neither temperature nor time, with P values of 0.28 and 0.91, respectively, had a significant effect on methane yield in the case of pinewood. In contrast, pretreatment temperature had

a significant effect on the methane production from elmwood and rice straw; while being similar to that of pinewood, it was concluded that the effect of pretreatment time on methane production from elmwood, pinewood, and rice straw was not significant (P values of 0.14, 0.91, and 0.27, resp.).

Among the untreated samples, the highest methane yield, 115.9 L·kg^{-1}CH, was obtained from rice straw, which had the lowest lignin content among the substrates utilized in this study. The digestion of untreated elmwood and pinewood resulted in methane yields of 54.2 and 38.7 L·kg^{-1}CH, respectively. The presence of pores in the structure of hardwoods which facilitate microorganisms' accessibility might be responsible for the higher yield obtained from elmwood in comparison to that from pinewood [32].

3.4. Methane Production Modeling. The fitting of kinetics data on the first-order model for all of the substrates is shown in Table 2, as well as the accumulated methane yields obtained after 55 days of SSAD. The regression coefficients demonstrated that methane production followed the first-order kinetic model ($r^2 > 0.91$). At the optimum pretreatment conditions for each substrate, that is, 180°C and 1 h, 150°C and 0.5 h, and 150°C and 1 h for elmwood, pinewood, and rice straw, the corresponding k value was at its maximum level, respectively, representing the highest degradation rate for each investigated substrate.

3.5. Relationship between Total Lignin Content and Methane Yield from Lignocellulosic Materials. The effect of lignin content on final methane yield was investigated by comparing methane yield as a function of the materials' lignin content (Figure 2). In line with a previous study [28], an overall inverse relationship between the lignin content of different substrates and the achieved methane yields was observed. However, the low linear regression coefficient of 0.7 confirmed that the content of lignin is not the sole key factor affecting methane yield. The contents of cellulose and hemicellulose, the crystallinity of cellulose, and the accessible surface area may also play important roles affecting methane yields [17–20]. Therefore, further investigations are required to find the specific reason for the observed improvements.

4. Conclusions

Organosolv pretreatment prior to SSAD was an efficient process for improvement of methane production from different types of lignocellulosic materials; however, its effectiveness greatly depended on the type of lignocelluloses. The pretreatment process was more effective on softwood than on hardwood or agricultural waste. Moreover, hardwood needed more severe conditions to be able to achieve maximum improvement during the subsequent batch digestion assays. Lignin content was among the most important factors negatively affecting the methane production from all of the investigated lignocellulosic substrates.

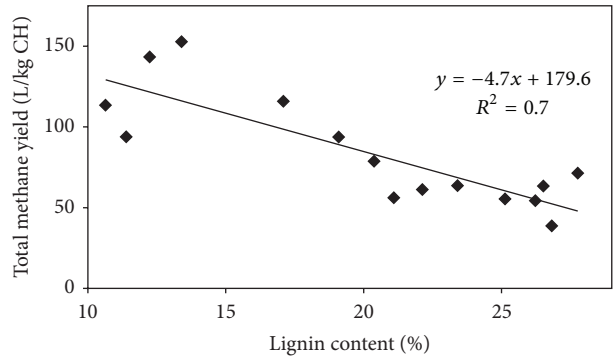

Figure 2: Relationship between lignin content and total methane yield from lignocellulosic substrates (untreated and pretreated elmwood, pinewood, and rice straw).

Conflict of Interests

The authors declare that there is no conflict of interests regarding the publication of this paper.

Authors' Contribution

All experiments and paper preparation were performed by Safoora Mirmohamadsadeghi. The coauthors supervised the experiments and helped with paper preparation.

Acknowledgments

The authors are grateful for financial support from the Region Västra Götaland and the Institute of Biotechnology and Bioengineering, Isfahan University of Technology.

References

[1] D. Deublein and A. Steinhauser, *Biogas from Waste and Renewable Resources: An Introduction*, Wiley, 2008.

[2] E. Gnansounou, "Production and use of lignocellulosic bioethanol in Europe: current situation and perspectives," *Bioresource Technology*, vol. 101, no. 13, pp. 4842–4850, 2010.

[3] J. Hromádko, J. Hromádko, P. Miler, V. Hönig, and M. Cindr, "Technologies in second-generation biofuel production," *Chemicke Listy*, vol. 104, no. 8, pp. 784–790, 2010.

[4] R. E. H. Sims, W. Mabee, J. N. Saddler, and M. Taylor, "An overview of second generation biofuel technologies," *Bioresource Technology*, vol. 101, no. 6, pp. 1570–1580, 2010.

[5] G. Sivakumar, D. R. Vail, J. Xu et al., "Bioethanol and biodiesel: Alternative liquid fuels for future generations," *Engineering in Life Sciences*, vol. 10, no. 1, pp. 8–18, 2010.

[6] S. Kumar, "Hydrothermal processing of biomass for biofuels," *Biofuel Research Journal*, vol. 2, p. 43, 2014.

[7] P. Börjesson and B. Mattiasson, "Biogas as a resource-efficient vehicle fuel," *Trends in Biotechnology*, vol. 26, no. 1, pp. 7–13, 2008.

[8] G. Taleghani and A. S. Kia, "Technical-economical analysis of the Saveh biogas power plant," *Renewable Energy*, vol. 30, no. 3, pp. 441–446, 2005.

[9] M. Balat and H. Balat, "Biogas as a renewable energy source—a review," *Energy Sources, Part A: Recovery, Utilization and Environmental Effects*, vol. 31, no. 14, pp. 1280–1293, 2009.

[10] Y. Li, S. Y. Park, and J. Zhu, "Solid-state anaerobic digestion for methane production from organic waste," *Renewable and Sustainable Energy Reviews*, vol. 15, no. 1, pp. 821–826, 2011.

[11] D. Brown, J. Shi, and Y. Li, "Comparison of solid-state to liquid anaerobic digestion of lignocellulosic feedstocks for biogas production," *Bioresource Technology*, vol. 124, pp. 379–386, 2012.

[12] J. Guendouz, P. Buffière, J. Cacho, M. Carrère, and J. Delgenes, "High-solids anaerobic digestion: comparison of three pilot scales," *Water Science and Technology*, vol. 58, no. 9, pp. 1757–1763, 2008.

[13] Y.-S. Cheng, Y. Zheng, C. W. Yu, T. M. Dooley, B. M. Jenkins, and J. S. Vandergheynst, "Evaluation of high solids alkaline pretreatment of rice straw," *Applied Biochemistry and Biotechnology*, vol. 162, no. 6, pp. 1768–1784, 2010.

[14] R. R. Singhania, A. K. Patel, C. R. Soccol, and A. Pandey, "Recent advances in solid-state fermentation," *Biochemical Engineering Journal*, vol. 44, no. 1, pp. 13–18, 2009.

[15] M. J. Taherzadeh and K. Karimi, "Pretreatment of lignocellulosic wastes to improve ethanol and biogas production: a review," *International Journal of Molecular Sciences*, vol. 9, no. 9, pp. 1621–1651, 2008.

[16] A. Teghammar, K. Karimi, I. Sárvári Horváth, and M. J. Taherzadeh, "Enhanced biogas production from rice straw, triticale straw and softwood spruce by NMMO pretreatment," *Biomass and Bioenergy*, vol. 36, pp. 116–120, 2012.

[17] V. S. Chang and M. T. Holtzapple, "Fundamental factors affecting biomass enzymatic reactivity," in *Proceedings of the 21st Symposium on Biotechnology for Fuels and Chemicals*, Springer, 2000.

[18] L. Laureano-Perez, F. Teymouri, H. Alizadeh, and B. E. Dale, "Understanding factors that limit enzymatic hydrolysis of biomass: Characterization of pretreated corn stover," *Applied Biochemistry and Biotechnology*, vol. 124, no. 1–3, pp. 1081–1099, 2005.

[19] V. P. Puri, "Effect of crystallinity and degree of polymerization of cellulose on enzymatic saccharification," *Biotechnology and Bioengineering*, vol. 26, no. 10, pp. 1219–1222, 1984.

[20] D. P. Koullas, P. Christakopoulos, D. Kekos, B. J. Macris, and E. G. Koukios, "Correlating the effect of pretreatment on the enzymatic hydrolysis of straw," *Biotechnology and Bioengineering*, vol. 39, no. 1, pp. 113–116, 1992.

[21] N. Poornejad, K. Karimi, and T. Behzad, "Ionic liquid pretreatment of rice straw to enhance saccharification and bioethanol production," *Journal of Biomass to Biofuel*, vol. 2, no. 1, pp. 8–15, 2014.

[22] P. Binod, R. Sindhu, R. R. Singhania et al., "Bioethanol production from rice straw: an overview," *Bioresource Technology*, vol. 101, no. 13, pp. 4767–4774, 2010.

[23] X. Zhao, K. Cheng, and D. Liu, "Organosolv pretreatment of lignocellulosic biomass for enzymatic hydrolysis," *Applied Microbiology and Biotechnology*, vol. 82, no. 5, pp. 815–827, 2009.

[24] P. Obama, G. Ricochon, L. Muniglia, and N. Brosse, "Combination of enzymatic hydrolysis and ethanol organosolv pretreatments: Effect on lignin structures, delignification yields and cellulose-to-glucose conversion," *Bioresource Technology*, vol. 112, pp. 156–163, 2012.

[25] H. Amiri, K. Karimi, and S. Roodpeyma, "Production of furans from rice straw by single-phase and biphasic systems," *Carbohydrate Research*, vol. 345, no. 15, pp. 2133–2138, 2010.

[26] H. Amiri, K. Karimi, and H. Zilouei, "Organosolv pretreatment of rice straw for efficient acetone, butanol, and ethanol production," *Bioresource Technology*, vol. 152, pp. 450–456, 2014.

[27] T. L. Hansen, J. E. Schmidt, I. Angelidaki et al., "Method for determination of methane potentials of solid organic waste," *Waste Management*, vol. 24, no. 4, pp. 393–400, 2004.

[28] L. N. Liew, J. Shi, and Y. Li, "Methane production from solid-state anaerobic digestion of lignocellulosic biomass," *Biomass & Bioenergy*, vol. 46, pp. 125–132, 2012.

[29] A. Sluiter, B. Hames, R. Ruiz et al., *Determination of Structural Carbohydrates and Lignin in Biomass*, Laboratory Analytical Procedure, 2008.

[30] H. Yang, R. Yan, H. Chen, C. Zheng, D. H. Lee, and D. T. Liang, "In-depth investigation of biomass pyrolysis based on three major components: Hemicellulose, cellulose and lignin," *Energy and Fuels*, vol. 20, no. 1, pp. 388–393, 2006.

[31] D. Brown and Y. Li, "Solid state anaerobic co-digestion of yard waste and food waste for biogas production," *Bioresource Technology*, vol. 127, pp. 275–280, 2013.

[32] A. Reiterer, G. Sinn, and S. E. Stanzl-Tschegg, "Fracture characteristics of different wood species under mode I loading perpendicular to the grain," *Materials Science and Engineering A*, vol. 332, no. 1-2, pp. 29–36, 2002.

Hindawi Publishing Corporation
BioMed Research International
Volume 2014, Article ID 712197, 8 pages
http://dx.doi.org/10.1155/2014/712197

Research Article

Effects of Psychrophilic Storage on Manures as Substrate for Anaerobic Digestion

Wenche Bergland, Carlos Dinamarca, and Rune Bakke

Department of Process, Energy and Environmental Technology, Telemark University College, 3918 Porsgrunn, Norway

Correspondence should be addressed to Wenche Bergland; wenche.bergland@hit.no

Received 6 May 2014; Revised 19 June 2014; Accepted 24 June 2014; Published 5 August 2014

Academic Editor: Ilona Sárvári Horváth

The idea that storage can enhance manure quality as substrate for anaerobic digestion (AD) to recover more methane is evaluated by studying storage time and temperature effects on manure composition. Volatile fatty acids (VFA) and total dissolved organics (CODs) were measured in full scale pig manure storage for a year and in multiple flasks at fixed temperatures, mainly relevant for colder climates. The CODs generation, influenced by the source of the pig manure, was highest initially (0.3 g COD $L^{-1}d^{-1}$) gradually dropping for 3 months towards a level of COD loss by methane production at 15°C. Methane emission was low (<0.01 g COD $L^{-1}d^{-1}$) after a brief initial peak. Significant CODs generation was obtained during the warmer season (T > 10°C) in the full scale storage and almost no generation at lower temperatures (4–6°C). CODs consisted mainly of VFA, especially acetate. All VFAs were present at almost constant ratios. The naturally separated manure middle layer without sediment and coarser particles is suitable for sludge bed AD and improved further during an optimal storage time of 1–3 month(s). This implies that high rate AD can be integrated with regular manure slurry handling systems to obtain efficient biogas generation.

1. Introduction

Anaerobic digestion of manure can reduce greenhouse gas emissions (GHGE) and odors, produce renewable energy in the form of biogas, and enhance manure fertilizer quality [1]. The largest potential source of methane by AD of wet organic waste is manure, for example, ~40% in Norway; however, only a small fraction of this is realized [2]. The main reason for this is the low energy density of manure, implying low production rates in continuous flow stirred tank reactors (CSTR) currently used for manure AD. Such solutions are not economically sustainable in Norway because the costs of construction and operation of such plants are larger than the value of the methane produced [2]. Some large scale farms have their own CSTR AD solutions that are economically sustainable, for example, in Denmark [3], but agriculture in Norway is dominated by smaller farms where such systems are not profitable [2]. It is assumed that small farms constitute a large fraction of global agriculture also, so that the "Norwegian case" investigated here has international relevance. Manure transport to central AD treatment is used to some extent, especially in Germany, but the sustainability of such solutions is questioned mainly due to transport cost of manure with low biogas potential and greenhouse gas emissions [4]. New process solutions for AD treatment of manure must therefore be developed to realize the enormous total energy potential of this source.

High rate AD (HRAD) reactors may solve this problem by treating more waste in smaller and presumably much cheaper digesters. AD manure treatment that is well integrated with existing farm infrastructure for liquid (slurry) based manure handling is therefore suggested and evaluated here as a strategy for cost-effective biogas generation. Liquid based manure handling systems are common for cattle and pig farms [5] where all excreta are collected in liquid form with some dilution from wash water. Manure from farms using liquid/slurry based handling systems has, for example, 61% of the total theoretical Norwegian manure energy potential of 2480 GWh/a [6]. Manure storage tanks with 8 months minimum hydraulic retention time (HRT) capacity are included in existing farm infrastructure in cold climate countries (e.g., Norway, to comply with government

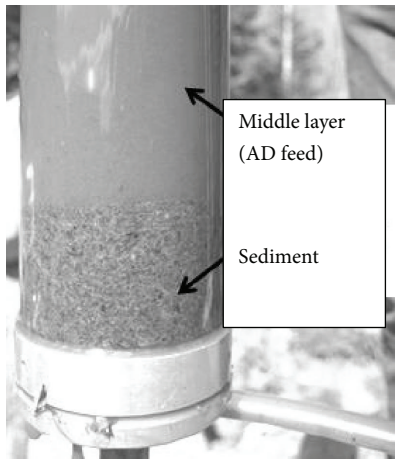

Figure 1: Pig manure sample collected near the bottom of a pig manure storage tank, showing the distinct interface between the sediment and the middle layer.

regulations to avoid pollution and use as fertilizer during the short growth season only). Such storage facilities may serve as the first step in an AD treatment line and/or be used for AD effluent storage in combination with HRAD. Existing pig slurry storage has uncontrolled methane release [7] so treating such slurries by harvesting and using methane has the additional environmental benefit of reducing GHGE from slurry storages.

It has been observed that manure particles disintegrate and hydrolyze during storage [8], thereby improving its quality as AD feed. Examining in greater detail the manure changes during storage is carried out here to evaluate how well manure storage can serve as a first step in an AD treatment line. It has also been observed that manure separates into a floating layer (straw, wood chips, etc.), a bottom sediment layer, and a middle layer with much less suspended solids than the floating and bottom layers. Pig manure separates spontaneously into such distinct layers as seen in Figure 1, implying that potentially suitable high rate AD feed can be taken out from the middle layer at no extra cost. The middle layer may not be best for AD in general, but it is best for sludge bed based HRAD since such reactors require a feed with relatively low particle content and/or low viscosity to avoid losing the culture by flushing out the sludge bed [9].

Several degradation processes, such as those included in the anaerobic digestion model ADM1 [10], can occur during manure storage that can influence the quality of the manure as feed for AD and emissions during storage. The hypothesis tested here is that there is an optimal storage time that depends on the storage temperature. This is based on the assumption that biogas yield will increase if the manure is stored before AD since this will allow particle disintegration and large molecules to hydrolyze into dissolved monosaccharides, amino acids, long chain fatty acids, and VFA that can be converted to methane when used as feed for AD. It is also expected that such easily degradable organic molecules will be degraded all the way to methane in the storage if allowed too long storage.

The aim of the study is to identify an optimal time range for manure storage prior to AD as a function of temperature. The main focus is on Nordic (psychrophilic) conditions including summer temperatures. The evaluation is based on measurements of dissolved organics and methane yield.

2. Materials and Methods

The properties of manure from a pig production farm in southern Norway, Porsgrunn (59.2°N, 9.7°E) were examined during storage. The farm has three production stages/areas: "Sows," "Growers," and "Farrow and Wieners." All animals are fed protein concentrate (14.6% crude protein) added to some grass/straw. The pig production unit uses wood shavings and straw as bedding material. Manure was examined both at controlled temperature conditions and in a storage basin at the farm during one year.

2.1. Sample Collection and Testing Scheme. Manure from the production stage Farrow and Wieners was collected from the manure channel in the barn and stored under controlled conditions at 11°C, 15°C, and 20–23°C for 3 months to monitor the content of easily degradable organics in the liquid manure. 100 mL infusion glass bottles with rubber stopper and metal ring were used. One bottle stored at each temperature was terminated regularly to analyze the liquid content. One bottle was used as parallel for each temperature case, with a total of 17 bottles. Syringe needles were placed through the stoppers of these 17 bottles to release produced biogas.

Manure from all 3 production stages was collected, sieved through a 2 mm sieve, and stored in 54 (100 mL) infusion glass bottles with rubber stopper and metal ring under controlled conditions at 15°C for maximum 4 months to study the effect of the pig production stage on manure development. Three parallel bottles from each pig production stage were terminated regularly to analyze the liquid content. Syringe needles were placed through the stoppers of these 54 bottles to release produced biogas. Sieved manure samples from the 3 production stages were also studied in 1000 mL infusion glass bottles for biogas production monitoring since not enough biogas for volume and composition measurements was produced in the smaller bottles. Syringe needles were placed through the stoppers of these 9 bottles and syringes were connected to the needles to collect biogas samples, to measure volume and composition of the produced biogas.

To evaluate the amount of methane potentially released from the long time storage, the methane potential (B_0) of the sieved manure was measured via volume displacement using 3 parallels of 100 mL medical syringes with 2 mL gradations while stored at 35°C. 30 mL manure (with no inoculum) was placed in each syringe and the biogas production was read regularly, directly as the syringe piston displacement. When enough gas was produced the syringes were emptied and the gas composition measured.

2.2. Manure Handling and Examination at the Farm. Manure handling at the farm involves first manually pushing manure

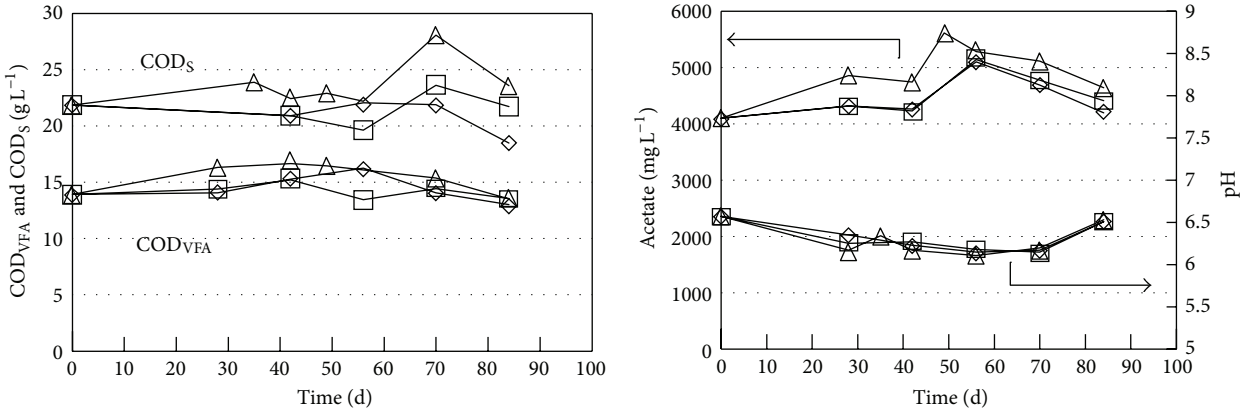

FIGURE 2: Acetate, COD_{VFA}, pH, and COD_S during storage for Farrow and Wieners manure: 11°C (◊), 15°C (□), and 20–23°C (△).

into channels in the floor twice a day, before it is pumped to a 300 m^3 farm building basement storage basin; ~1/3 of the manure comes from each of Farrows and Wieners, Sows, and Growers. The basin manure also contains ~5% of wash water from regular barn washing routines. The content in the basin storage is stirred regularly in order to pump half of the basin volume content each time further to a 1600 m^3 outdoor storage. This gives an average 50 d HRT in the basement storage basin.

Samples were siphoned from the liquid middle layer (Figure 1) during the whole year of 2012. 10–80 liters were collected each time. Temperature was measured in the collected sample immediately after removal from the storage.

2.3. Analysis. Total COD (COD_T), soluble COD (COD_S), total solids (TS), volatile solids (VS), pH, alkalinity, NH_4^+-N, VFAs (acetate, propionate, butyrate, isobutyrate, valerate, and isovalerate), and gas composition were analyzed.

COD, TS, VS, and alkalinity were measured according to US standard 5220D, 2540D, and 2320B, respectively [11]. For CODs determination the samples were first centrifuged at 10000 rpm for 30 minutes and then filtered (0.45 μm). NH_4^+-N concentration was analyzed on filtered samples (0.2 μm) by ion chromatography using a DX-500 ion chromatographic analyzer equipped with a conductivity detector, a SCS1 cation-exchange column (4 × 250 mm) in combination with a Dionex IonPac PCG1 (4 × 50 mm) guard column; 4 mM methane-sulfonic acid was used as the mobile phase. The oven temperature was kept constant at 35°C. VFA were measured by gas chromatography (Hewlett Packard 6890) with a flame ionization detector and a capillary column (FFAP 30 m, inner diameter 0.250 mm, and film 0.5 μm). The oven was programmed to go from 100°C, hold for one minute, to 200°C at a rate of 15°C min^{-1} and then to 230°C at a rate of 100°C min^{-1}. The carrier gas used was helium at 23 mL min^{-1}. The injector and detector temperatures were set to 200°C and 250°C, respectively. Gas composition (CO_2 and CH_4) was quantified by gas chromatography (Hewlett Packard 5890A) equipped with a thermal conductivity detector and two columns connected in parallel: Column 1, CP-Molsieve 5A (10 m × 0.32 mm), and Column 2, CP-PoraBOND Q (50 m × 0.53 mm). The gas carrier was argon at 3.5 bar pressure. The oven temperature was kept constant at 40°C.

3. Results and Discussion

3.1. Farrow and Wieners Manure Storage Test at 3 Temperatures. Only a slight increase in acetate (maximum 30% increase) and total VFA (maximum 20% increase) were observed during storage of Farrow and Wieners manure at 11°C, 15°C, and 20–23°C (Figure 2). No difference in VFA production was observed between 11°C and 15°C, but higher acetate and total VFA concentrations were obtained at 20–23°C. The pH went quickly from 6.5 to 6.2-6.3 at all three temperatures. The pH changes can be explained by both produced VFA and CO_2 [12]. There appears to be a small temperature effect on COD_S with a slight increase at the highest temperature, but all changes are in the range of the standard deviation and therefore not considered as significant. Storage time and temperature of the manure from Farrow and Wieners have therefore little effect on the quality of, for example, AD feed. The low pH implies that there is little risk of methanogenesis and loss of NH_3 during storage of this manure fraction. It may therefore be stored and used for biogas production on demand.

3.2. Comparison between the Pig Production Stages at 15°C

3.2.1. Liquid Properties. Pronounced differences between the manures from the different pig production stages in the way their compositions changed with time were observed when they were all stored at 15°C (Figure 3). The least changes were observed during storage of the manure from the Farrow and Wieners, even though it had the highest initial concentrations of both COD_S and COD_{VFA} and also the lowest initial pH. Manure from Growers had the highest levels of acetate, COD_S (after 30–40 days of storage), and COD_{VFA} (after 78 days of storage). Manure from Sows had the lowest concentration of

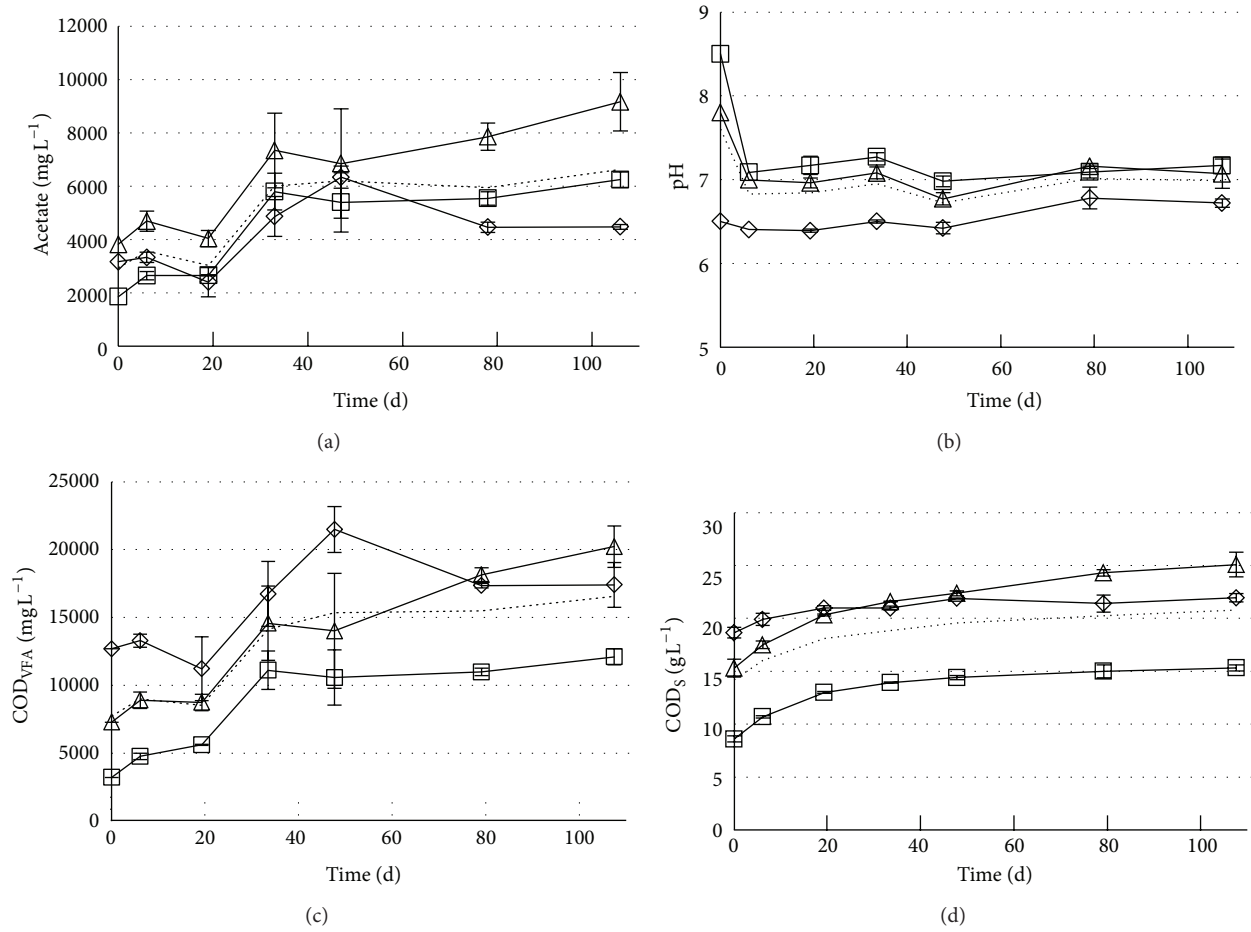

Figure 3: Acetate, COD_{VFA}, pH, and COD_S during storage at 15°C: Sows (□), Growers (△), and Farrow and Wieners (◊), average–dotted line.

soluble organics both as COD_S and COD_{VFA} and also the highest pH. Manure from Sows is therefore expected to give less methane yield than manure from the other stages when used as substrate for AD.

The COD_{VFA} had start values of 3.2, 7.3, and 12.7 g L^{-1} and maximum values of 12.1, 20.2, and 21.5 g L^{-1}, at days 106, 106, and 47 for Sows, Growers, and Farrow and Wieners, respectively. Similar increase in VFA has been observed by others [13]. Acetate, propionate, and butyrate constituted most of the COD_{VFA} content (Figure 4).

The pH started at 8.5, 7.8, and 6.5 for Sows, Growers, and Farrow and Wieners, respectively, dropping quickly to 7.1, 7.1, and 6.4 and staying rather constant for the whole test of 106 days (Figure 3). The soluble organics content (COD_S) increased mainly during the first month (Figures 3 and 5), from 8.6, 15.3, and 18.7 g L^{-1} for Sows, Growers, and Farrow and Wieners, respectively, to 13.9 (61% increase), 21.6 (41% increase), and 21.0 (12% increase) after 33 days, with a maximum of 116, 25, and 23 g L^{-1} at 78, 78, and 47 days, respectively. This implies that one month pig manure storage prior to AD is favorable, assuming that COD_S roughly equals the AD methane production potential. Changes in TS, VS, NH_4-N, and alkalinity concentrations during storage are small and within the range of standard deviations for these parameters (Table 1).

Table 1: Average concentrations and standard deviations during storage at 15°C.

	Sows	Growers	Farrow and Wieners
TS (g L^{-1})	51.9 ± 2.5	78.7 ± 4.1	70.0 ± 3.2
VS (g L^{-1})	34.7 ± 2.1	54.7 ± 3.4	55.5 ± 2.7
NH_4-N (g L^{-1})	2.6 ± 0.2	3.1 ± 0.3	1.9 ± 0.5
Alkalinity (g L^{-1})	15.9 ± 0.6	20.3 ± 1.4	9.8 ± 0.6

3.2.2. Methane Loss. A disadvantage of long term manure storage is the potential for methane loss. Methanogenesis is however a slow process which can be inhibited by pH below 6.5 [14] and high free ammonia concentrations [15] and slowed down by reduced temperatures [8]. Methane production was detected throughout the 15°C laboratory storage test but the rate was close to zero (<0.01 g COD L^{-1}d^{-1}) except during the first week of storage (Figure 5). The methane loss is compared to the COD_S production rate in Figure 5. The COD_S production was higher than but dropping towards the

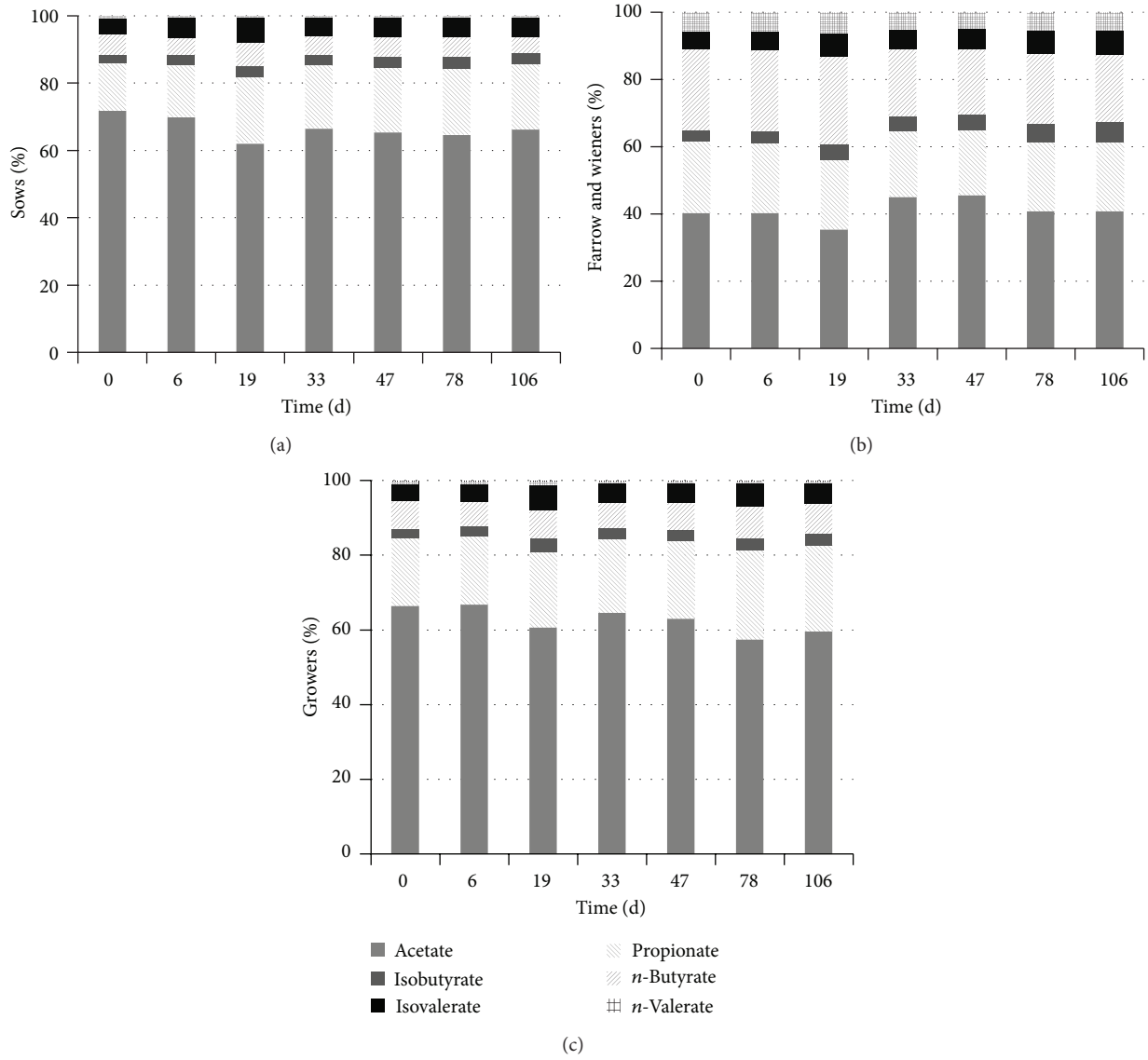

Figure 4: VFA composition during storage at 15°C in manure from Sows, Growers, and Farrow and Wieners.

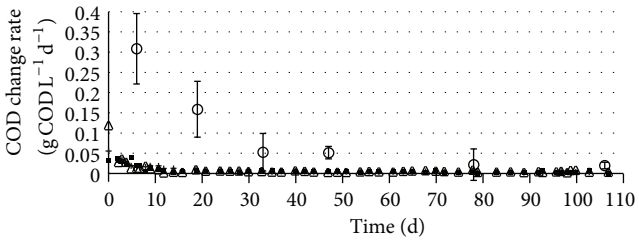

Figure 5: Methane production during storage at 15°C for Sows (■), Growers (△), and Farrow and Wieners (+), and average change in CODs in the 3 manures (○) during storage at 15°C.

methane loss. Real long storage time should be avoided to limit GHGE. The methane loss compared to the methane potential after 33 days is 1.7, 1.0, and 0.7% for Sows, Growers, and Farrow and Wieners, increasing to 2.4, 1.5, and 1.0%, respectively, after 78 days.

3.3. Full Scale Storage. The average monthly air temperatures varied between −5°C and +16°C and in the full scale manure storage basin between +4°C in December and +16°C in July (Figure 6) which is similar to outdoor storage temperatures reported from Sweden, Denmark, and Canada [16–18]. Concentrations of dissolved organics varied throughout the year in phase with temperature changes (Figure 6). Both total VFA and the acetic acid levels were nearly two times higher in the summer compared to the winter. This caused seasonal pH changes from 6.7 in summer to 7.4 in winter. The total content of soluble organics, CODs, did not change as much as the VFA, with values of 11–16 g L^{-1} during the coldest period and 14–19 g L^{-1} during spring, summer, and autumn (Figure 6). This suggests that disintegration and hydrolysis

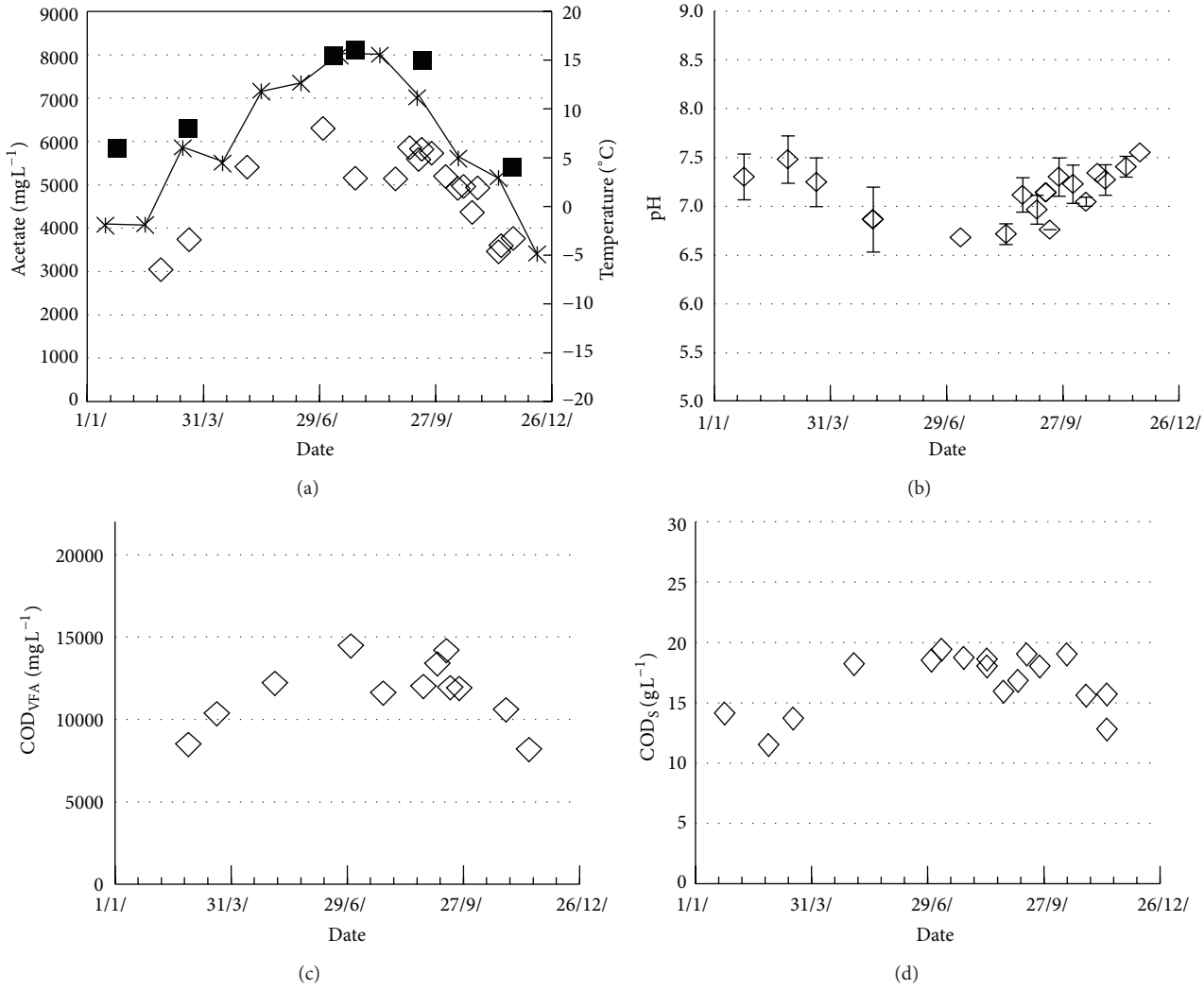

FIGURE 6: Acetate, COD_{VFA}, pH, and COD_S in pig manure during basin storage at the farm. Average monthly air temperature (∗) and temperature in the basin (■).

are less temperature dependent than acidogenesis during manure storage.

3.4. Implications. The study was mainly motivated by the idea that high rate AD reactors may give efficient manure treatment if it is well integrated with existing farm infrastructure for slurry based manure handling systems. The results confirm that such solutions are feasible: pig manure separates by gravity into layers where the main, middle layer is a substrate suitable for high rate AD. This substrate with 50 days average HRT in the full scale case investigated contains easily degradable organics, mainly VFA, at concentrations suitable for high rate AD.

The dissolved organics content in the full scale case (Figure 6) is approximately the same as the average concentrations in the laboratory experiments (Figure 3), implying that these small scale tests yield values realistic for full scale applications and more insight than obtainable in field studies. The laboratory tests suggest that the highest CODs concentration is obtained after 3 months storage with some variations among the different production stages, but where most of the CODs generation is achieved after 1 month. After 3 month storage the CODs generation by hydrolysis has decreased almost to the level of CODs loss by methanogenesis (Figure 5). This implies that the basement storage investigated has a manure retention time (50 d average) ideal for further AD to maximize methane production. During winter, however, little hydrolysis occurs at 4–6°C so that AD feed from this basin will have similar soluble organics concentrations as that of fresh manure towards the end of the winter. The methane production potential of the stored manure is thereby lowest when the farm heat demand is the highest. This is a disadvantage if the generated methane is used for heating purposes, but it may be compensated for by increasing the hydraulic loading rate of the AD.

This investigation is based on the observation that pig manure naturally separates into three layers with a middle

layer with much less suspended solids than the floating and bottom layers (Figure 1) and the assumption that this middle layer is suitable as high rate AD feed. An extensive study to evaluate how suitable this manure middle layer is as feed for sludge bed AD is in progress. The results are not yet published but it is observed that biogas yield is closely related to both the CODs and VFA contents of the feed, implying that these measurements can be used to evaluate the methane potential of such manures. It is also observed that stable methane production (~5 L CH_4 L^{-1} d^{-1}) is obtained at 1 d HRT in lab scale UASB reactors with such manure as the only feed. The proposed concept of combining existing manure storage facilities with high rate AD has, therefore, potential to become a cost-effective individual farm solution for biogas generation.

Only the middle manure layer is used as AD feed in the concept evaluated here, implying that some of the total biogas potential is not directly utilized. Further investigations will be carried out to quantify and limit this loss. The following observations can be relevant for how much methane potential is not recovered by the HRAD approach evaluated here. (1) The top and bottom layers constitute less than 30% of total manure volume. (2) These two layers are kept in the storage for a long time (up to one year) during which disintegration and hydrolysis can transform particles in these layers to CODs that will diffuse into the middle layer and can thereby become part of the utilized AD substrate.

The strongest methane emission from manure occurs during the first hours after it is released from the animals, an effect that can probably not be prevented since it occurs in the barn. Some but very limited and quite constant methane release is observed after the first days of storage (Figure 5), implying that long term storage without or prior to AD for methane recovery will cause some GHGE. This emission must be included when determining optimal storage time prior to AD with respect to "carbon footprint" of such solutions. Optimal storage will, therefore, be less than 3 months during the warmer seasons. This can be achieved in the full scale case investigated by lowering manure HRT simply by changed manure handling routines, maintaining lower liquid level in the storage basin.

4. Conclusion

The amounts of easily degradable organics in pig manure depend on the source of the manure (production stage) and the storage time and temperature. Lab scale results correspond well with measurements from full scale storage of manure from the same barn. Temperature effects on generation of dissolved organics and methane during long term storage from lab tests are therefore useful to understand the processes occurring in farm storage basins.

Slight and quite constant methane emissions were detected through months of storage. The strongest methane emission occurred the first days and is therefore hard to avoid since that is when the manure is in transit from the animals to the storage.

Temperature significantly influenced manure quality during storage. Dissolved organics are generated by disintegration and hydrolysis of particles during storage in the warmest season (manure temperatures 10–15°C) but not at winter temperatures (4–6°C). The manure from the Farrow and Wieners stage, studied in more detail for temperature effects, gained no significant CODs increases.

Most of the dissolved organics are VFA, mainly acetate, and the ratios between the various VFAs remained quite constant for all conditions tested.

The production of dissolved organics showed some variations among manure from the different production stages. The increase of CODs at 15°C were 61%, 41%, and 12% for the three production stages Sows, Growers, and Farrow and Wieners, respectively, after one month.

Dissolved organics generation is highest initially and gradually drops to a low level during the first month at 15°C. The dissolved organics leveled off after three months storage (at 15°C), when the CODs production had dropped almost to the level of the methane production. The full scale basement storage has an average HRT of 50 d so most of the CODs generation potential can therefore be obtained using this storage as pretreatment for AD.

Pig manure separates by gravity into layers where the main, middle layer is a substrate suitable for high rate AD. It is therefore concluded that ordinary basement manure storage basins can be used to make feed with easily degradable organics, mainly VFA, at concentrations suitable for high rate AD. Efficient manure treatment for methane generation by high rate AD integrated with existing farm infrastructure for slurry based manure handling appears to be a promising option that warrants further investigation.

Conflict of Interests

The authors declare that there is no conflict of interests regarding the publication of this paper.

Acknowledgments

The project was supported by the Norwegian Agricultural Authority, Innovation Norway, Research Council of Norway, Ministry of Education and Research, and Telemark University College. The authors wish to thank the farmer, Sondre Skoglund, for the good cooperation in carrying out this project and Mehrdad Torabzadegan for assistance in carrying out the experiments.

References

[1] D. I. Massé, G. Talbot, and Y. Gilbert, "On farm biogas production: a method to reduce GHG emissions and develop more sustainable livestock operations," *Animal Feed Science and Technology*, vol. 166-167, pp. 436–445, 2011.

[2] H. Berglann and K. Krokann, "Biogassproduksjon på basis av husdyrgjødsel—rammebetingelser, økonomi og virkemidler," Norsk Institutt for Landbruksøkonomisk Forskning (NILF), 2011.

[3] R. P. J. M. Raven and K. H. Gregersen, "Biogas plants in Denmark: successes and setbacks," *Renewable and Sustainable Energy Reviews*, vol. 11, no. 1, pp. 116–132, 2007.

[4] P. J. Crutzen, A. R. Mosier, K. A. Smith, and W. Winiwarter, "N_2O release from agro-biofuel production negates global warming reduction by replacing fossil fuels," *Atmospheric Chemistry and Physics*, vol. 8, no. 2, pp. 389–395, 2008.

[5] C. H. Burton and C. Turner, *Manure Management: Treatment Strategies for Sustainable Agriculture*, Edited by J. A. Beck, Silsoe Research Institute, 2003.

[6] H. L. Raadal, V. Schakenda, and J. Morken, "Potensialstudie for biogass i Norge," Østfoldforskning AS and UMB, 2008.

[7] D. I. Massé, L. Masse, S. Claveau, C. Benchaar, and O. Thomas, "Methane emissions from manure storages," *Transactions of the ASABE*, vol. 51, no. 5, pp. 1775–1781, 2008.

[8] S. M. King, S. Barrington, and S. R. Guiot, "In-storage psychrophilic anaerobic digestion of swine manure: acclimation of the microbial community," *Biomass and Bioenergy*, vol. 35, no. 8, pp. 3719–3726, 2011.

[9] G. Lettinga and L. W. H. Pol, "USAB-process design for various types of wastewaters," *Water Science and Technology*, vol. 24, no. 8, pp. 87–107, 1991.

[10] D. Batstone, J. Keller, I. Angelidaki et al., "The IWA anaerobic digestion model no. 1 (ADM1)," *Water Science and Technology*, vol. 45, no. 10, pp. 65–73, 2002.

[11] APHA, *Standard Methods for the Examination of Water and Wastewater*, American Public Health Association / American Water Works Association / Water Environment Federation, Washington, Wash, USA, 19th edition, 1995.

[12] J. W. Paul and E. G. Beauchamp, "Relationship between volatile fatty acids, total ammonia, and pH in manure slurries," *Biological Wastes*, vol. 29, no. 4, pp. 313–318, 1989.

[13] H. B. Møller, S. G. Sommer, and B. K. Ahring, "Biological degradation and greenhouse gas emissions during pre-storage of liquid animal manure," *Journal of Environmental Quality*, vol. 33, no. 1, pp. 27–36, 2004.

[14] Y. Chen, J. J. Cheng, and K. S. Creamer, "Inhibition of anaerobic digestion process: a review," *Bioresource Technology*, vol. 99, no. 10, pp. 4044–4064, 2008.

[15] A. Schnürer and Å. Nordberg, "Ammonia, a selective agent for methane production by syntrophic acetate oxidation at mesophilic temperature," *Water Science and Technology*, vol. 57, no. 5, pp. 735–740, 2008.

[16] S. Husted, "Seasonal variation in methane emission from stored slurry and solid manures," *Journal of Environmental Quality*, vol. 23, no. 3, pp. 585–592, 1994.

[17] L. K. K. Rodhe, J. Abubaker, J. Ascue, M. Pell, and Å. Nordberg, "Greenhouse gas emissions from pig slurry during storage and after field application in northern European conditions," *Biosystems Engineering*, vol. 113, no. 4, pp. 379–394, 2012.

[18] T. K. Flesch, X. P. C. Vergé, R. L. Desjardins, and D. Worth, "Methane emissions from a swine manure tank in western Canada," *Canadian Journal of Animal Science*, vol. 93, no. 1, pp. 159–169, 2013.

Hindawi Publishing Corporation
BioMed Research International
Volume 2014, Article ID 469378, 10 pages
http://dx.doi.org/10.1155/2014/469378

Research Article

Enhanced Ethanol and Biogas Production from Pinewood by NMMO Pretreatment and Detailed Biomass Analysis

Marzieh Shafiei,[1] Keikhosro Karimi,[1,2] Hamid Zilouei,[1] and Mohammad J. Taherzadeh[3]

[1] *Department of Chemical Engineering, Isfahan University of Technology, Isfahan 84156-83111, Iran*
[2] *Industrial Biotechnology Group, Institute of Biotechnology and Bioengineering, Isfahan University of Technology, Isfahan 84156-83111, Iran*
[3] *Swedish Center for Resource Recovery, University of Borås, 501 90 Borås, Sweden*

Correspondence should be addressed to Marzieh Shafiei; m.shafiei@ce.iut.ac.ir

Received 25 May 2014; Accepted 7 July 2014; Published 4 August 2014

Academic Editor: Meisam Tabatabaei

N-Methyl morpholine-N-oxide (NMMO) is an environmentally friendly and commercially applied cellulose solvent that is suggested for pretreatment of lignocelluloses to improve biofuel productions. However, the underlying mechanisms of the improvements have been poorly understood yet. In an attempt to investigate the mechanisms, pinewood powder and chips were pretreated with 85% (w/w) NMMO at 120°C for 1–15 h. The pretreatment improved ethanol production yield from 7.2% (g/g) for the untreated wood powder to 68.1–86.1% (g/g) and from 1.7% (g/g) for the untreated wood chips to 12.6–51.2% (g/g) of theoretical yield. Similarly, the biogas yields of untreated wood chips and powder were improved from 21 and 66 (mL/g volatile solids) by 3.5–6.8- and 2.6–3.4-folds, respectively. SEM micrographs indicated major increase in the wood porosity by the pretreatment, which would confirm increase in the water swelling capacity as well as enzyme adsorption. The analysis of X-ray diffraction showed considerable reduction in the cellulose crystallinity by the pretreatment, while FTIR spectroscopy results indicated reduction of lignin on the wood surface by the pretreatment.

1. Introduction

Lignocelluloses are promising raw materials for production of second generation of ethanol. These relatively cheap and abundant materials may solve the food versus fuel conflict which is a result of production of biofuels from sugar and starch based materials [1, 2]. The process for production of the first generation of bioethanol involves hydrolysis, fermentation, distillation, and dehydration. However, a major challenge of using lignocelluloses is their recalcitrance to saccharification and poor hydrolysis yields. Thus, prior to enzymatic hydrolysis, a pretreatment step is necessary to open up this structure and improve the product yields as well as the process of economy [1, 3, 4]. Similarly, the bottleneck of biogas production process from lignocelluloses is the first step of anaerobic digestion, that is, the rate-limiting hydrolysis step. An efficient pretreatment step can eliminate this bottleneck [1, 3, 4]. In native cell wall of woody biomass, cellulose chains are packed into micro- and macrofibers. Hemicelluloses and lignins are present in the matrix surrounded celluloses and form covalent and noncovalent bindings to cellulose and each other. The whole reinforced composite of the cell wall acts as the main barriers to the production of monomer sugars. Another barrier is the high concentration (50–90%) of lignin in the spaces between cells, that is, cell lamella. Lignin is highly hydrophobic and also inhibits activity of cellulases. Pretreatment can effectively overcome these obstacles by rearranging cellulose, hemicellulose, and lignin to a less recalcitrant structure. Pretreatment can also increase the micro- and macroaccessibility of the hydrolyzing enzymes to the biomass [5]. Among all pretreatment methods, treatment with cellulose solvents such as ionic liquids (ILs) [4, 6, 7], phosphoric acid [8], NaOH/urea [9], and N-methylmorpholine-N-oxide (NMMO) [6, 10, 11] is well known for their high efficiencies. N-Methylmorpholine N-oxide (NMMO) is an industrial

cellulose solvent for fiber making, and pretreatment with this green chemical produces no toxic wastes. This solvent can be almost completely recycled and reused several times [11]. NMMO monohydrate dissolves cellulose via formation of strong hydrogen bonds. These bonds are then broken after addition of the antisolvent, for example, water. As a consequence of the pretreatment, inter- and intrachain hydrogen bonds of cellulose are altered. Thus, the regenerated cellulose is more susceptible to saccharification.

It was previously shown that NMMO pretreatment improved the yields of ethanol from spruce and oak up to 89 and 85.4%, respectively [11]. Furthermore, ethanol production from rice straw [6] and sugarcane bagasse [17] with NMMO pretreatment were studied. This pretreatment was also considered for biogas production from rice straw, triticale straw, and spruce wood [18] as well as birch wood [10]. However, to our knowledge, no previous work on ethanol and biogas production of the NMMO treated pinewood powder and chips has been presented in the literature.

In this study, NMMO pretreatment for ethanol and biogas production enhancement from pinewood powder and chips were investigated. Further experiments were conducted to understand the underlying mechanism of the improvements. Effects of the pretreatment on the wood properties were studied by SEM imaging, cellulose enzyme accessibility, and water swelling capacity. Moreover, the changes in the crystallinity of the substrate were tracked using X-ray diffraction as well as FTIR spectroscopy.

2. Materials and Methods

2.1. Raw Materials and Their Analysis. Pinewood, *Pinus eldarica*, from the forest of Isfahan University of Technology campus (Isfahan, Iran), was used for the biofuel production. After debarking and cutting, a fraction of the wood was milled and screened to achieve a wood powder with particles of less than 1 mm. A fraction was also used as wood chips with approximate dimensions of 0.5 by 0.5 by 0.1 centimeters. The wood was analyzed for carbohydrate and lignin contents according to the standard procedure described by Sluiter et al. [19].

2.2. Pretreatment. A commercial grade of NMMO solution (50%, BASF, Germany) was concentrated to 85% (w/w) solution by vacuum evaporation. An amount of 15 grams of the wood was pretreated by 185 grams of the NMMO solution according to the method described by Shafiei et al. [11]. Briefly, NMMO solution was added to preheated beakers containing wood and mixed by glass rods. The beakers were kept in an oil bath for 1, 3, and 15 hours at 120°C. Afterwards, 150 mL boiling distilled water was added to each of the pretreatment suspensions. The materials were then washed and recovered by vacuum filtration. Freeze-drying was used for dry weight measurement of the pretreated woods at −48°C for 48 h. Similar to the untreated wood, the carbohydrate and lignin contents of the pretreated materials were measured. The pretreated materials were kept in sealable bags at 4°C until use.

2.3. Enzymatic Hydrolysis. The treated and untreated woods were subjected to enzymatic hydrolysis using 15 FPU cellulase (Celluclast 1.5 L, Novozyme, Denmark) and 30 IU β-glucosidase (Novozyme 188, Novozyme, Denmark) per gram of substrate. The hydrolysis was performed at 45°C for 96 h using 5% (w/w) wood (based on the dry weight) in 50 mM sodium citrate buffer (pH 4.8) and 0.4 g/L sodium azide [4]. Sodium azide was added as a metabolite inhibitor in the hydrolysis. Since sodium azide inhibits fermentation, a parallel set of enzymatic hydrolysis without addition of sodium azide was conducted to be used in the fermentation. This hydrolysis was carried out without sample taking to minimize contaminations. The activities of cellulase and β-glucosidase were measured to 70 FPU/mL and 220 IU/mL, respectively, based on the methods described by Adney and Baker [20] and Ximenes et al. [21]. The yield of enzymatic hydrolysis was calculated as (g) produced glucose by hydrolysis/(g) glucan in the biomass/1.111 $*$ 100. The recovery of solid after pretreatment was not considered in the calculations. The glucan content for each wood sample (native or pretreated at different condition) prior to enzymatic hydrolysis was considered for calculation of the yield of the sample.

2.4. Ethanol Fermentation. The liquid fraction, the hydrolysate, was separated by centrifugation under aseptic conditions and supplemented with essential nutrients for the cells. Then, fermentations were performed in 50 mL centrifuge tubes at 32°C for 24 h using high cell density of a flocculating strain of *Saccharomyces cerevisiae* (CCUG 53310, Culture Collection of University of Gothenburg, Sweden). The method used for strain maintenance and inoculum preparation was described by Shafiei et al. [4, 11]. The yield is calculated based on the grams of ethanol produced per grams of ethanol which can theoretically be produced from glucan in each of the wood samples prior to enzymatic hydrolysis. Thus, ethanol yield equals to (g) ethanol in fermentation broth/(g) glucan in the sample/1.111/0.51 $*$ 100.

2.5. Biogas Production. Anaerobic digestion was performed in batch digesters using mesophilic bacteria from a 7000 m^3 biogas digester of Isfahan Municipal Wastewater Treatment (Isfahan, Iran). The inoculum contains bacterial consortia for biogas production which operates at 37°C. Serum glass bottles were filled with 20 mL of inoculum, 0.25 g of the treated or untreated wood, and 5 mL of deionized water and closed with butyl rubber seals and aluminum caps [9]. The digestion was conducted at 37°C for 45 days. Gas mixture containing 80% nitrogen and 20% carbon dioxide was used for initial flushing the bottle's headspace to obtain anaerobic conditions. Water and inoculum were used as a control in order to determine the biogas production of the inoculum. Gas samples were taken from the headspace of the bottles and analyzed for methane and carbon dioxide content by gas chromatography.

2.6. Structural Analysis

2.6.1. Scanning Electron Microscopy (SEM). The microscopic structure of the treated and untreated wood powder was determined by SEM. The dried samples were coated with gold (BAL-TEC SCD 005) and analyzed using SEM microscope (Zeiss, Germany) at 7.5 kV.

2.6.2. Water Swelling Capacity and Enzyme Adsorption. Water swelling capacity, the amount of water adsorbed by the wood, was measured for the untreated and pretreated woods. An amount of 0.1 gram of the samples was put in small bags of nonwoven materials and immersed in water for one hour. Then, the swelling capacity was measured as $(w_2 - w_1)/w_1$, in which w_1 is the weight of the dry materials and w_2 is the final weight of the swollen materials [22].

The cellulase adsorption was evaluated in 15 mL centrifuge tubes containing 1% (w/w) wood sample and 400 mg cellulase per gram of glucan, based on the method developed by Kumar and Wyman [23]. The tubes were shaken at 60 rpm for 2 hours. Then, the tubes were centrifuged for 15 minutes at 4000 rpm. The supernatants were analyzed for protein content based on the Biuret method [24].

2.6.3. X-Ray Diffraction. The crystallinity of cellulose in the treated and untreated wood powder was analyzed using X-ray powder diffraction pattern of the samples. The diffractometer (Philips, X'pert, Netherlands) operated at 40 kV and 30 mA, and the spectra were collected in the range of $2\theta = 10–30^\circ$ with step size of 0.05° and step of 1 s. The crystallinity was calculated according to the method of Segal et al. [25], using $\mathrm{CrI} = ((I_{002} - I_{\mathrm{am}})/I_{\mathrm{am}}) * 100$, in which I_{002} is the intensity of the peak corresponding to crystalline portion of biomass (cellulose) at position of $2\theta = 22.5^\circ$ and I_{am} corresponds to amorphous portion (i.e., hemicellulose, lignin, and cellulose) at position of $2\theta = 18^\circ$ (Figure 5) [26].

2.6.4. FTIR Spectroscopy. The chemical bonds and the crystallinity of the treated and untreated pinewood powder were investigated using a FTIR spectrometer (Bruker) equipped with a universal ATR (Attenuated Total Reflection) accessory and Deuterated triglycine sulfate (DTGS) detector (Bruker Tensor 27 FT-IR). The spectra were collected over using average of 60 scans and resolution of 4 cm^{-1} and at the range of 600–4000 cm^{-1}. Rubberband correction method was used for correction of the spectra baseline [27], and the absorbance values were normalized to 0 and 1 based on the intensity of the maximum peak. Total crystallinity index (TCI = a_{1377}/a_{2922}) and lateral order index (LOI = a_{1421}/a_{893}) as well as the lignin to cellulose ratio (a_{1510}/a_{900}) were determined using the absorption ratios [12, 28].

2.7. Analytical Methods. The composition of metabolites of the hydrolysis and fermentation experiments were measured by HPLC equipped with a RI detector (Jasco International Co., Tokyo, Japan). Sugars were analyzed using an ion-exchange Aminex HPX-87P column (Bio-Rad, Richmond, CA, USA), while ethanol, glycerol, and other metabolites were analyzed using Aminex HPX-87H column (Bio-Rad, Richmond, CA, USA) according to the method described by Shafiei et al. [11]. The methane and carbon dioxide contents of the biogas were measured using a gas chromatograph (Sp-3420A, Propack Q column, TCD detector, Beijing, Beifen Ruili Analytical instrument Co). Helium at flow rate of 25 mL/min was used as a carrier of gas. The column, injector, and detector temperature were controlled at 50, 90, and 140°C, respectively.

Except for the triplicate biogas production experiments, all other experiments were performed in duplicates, and the results are presented as averages of the obtained data.

3. Results and Discussion

Pinewood powder and chips were treated with NMMO at 120°C. The treated and untreated materials were then enzymatically hydrolyzed for 96 h. Afterwards, the hydrolysates were fermented with a flocculating strain *Saccharomyces cerevisiae* for 24 h. Furthermore, the materials were anaerobically digested for biogas production.

3.1. Effect of Pretreatment on the Wood Composition. The compositions of untreated and pretreated wood are presented in Table 1. Glucan content was slightly increased (2–5%) after the pretreatments (Table 1). It can be explained by the loss of the hemicellulosic carbohydrates, that is, xylan (0.8–1.2%) and mannan (1.8–3.2%), by the pretreatment. The hemicelluloses decreased to a higher extent as the pretreatment time increased (Table 1). Overall, the results indicated minor changes in the composition of the treated materials, which is in line with previous studies [4, 6, 11].

3.2. Enzymatic Hydrolysis and Ethanol Production. The effects of pretreatment on the enzymatic hydrolysis yield of pinewood powder and chips are depicted in Figure 1. Significant improvement in the glucose production yields were achieved by the pretreatment (Figure 1). The theoretical glucose yield of untreated wood powder was improved from 11.5% to 74.8–98.9%. The untreated wood chips had a theoretical glucose yield of 4.8% that was improved to 17.7–56.5% by the pretreatment at 120°C for 1–15 h. More enhancements in the saccharification yields were observed with longer pretreatment times, and the maximum yield was achieved by 15 h treatment. However, prolongation of the hydrolysis from 72 to 96 h did not affect the hydrolysis yields.

The high yields of enzymatic hydrolysis are obtained regardless of minor changes in the wood composition after the pretreatment. These data suggest that the improvements in the hydrolysis yields were not due to lignin or hemicellulose removal, but other mechanisms were responsible for the enhancements. The pretreatment was more effective on the wood powder than the wood chips. Pretreatment of the chips for 15 h improved the hydrolysis yield by 11.8-folds, while the improvement for the powder was only 8.6-folds.

Significant improvement in the ethanol yield was observed by the pretreatments (Figure 2). While the theoretical ethanol yields from untreated wood chips and

Table 1: Lignin and carbohydrate contents of untreated and NMMO treated pinewood[1].

Pretreatment time	Glucan (%)	Mannan (%)	Xylan (%)	Galactan (%)	Arabinan (%)	ASL[2] (%)	AINSL[3] (%)
Untreated	41.6 ± 0.5	11.9 ± 0.5	6.1 ± 0.2	1.7 ± 0.2	0.72 ± 0.04	0.6 ± 0.02	26.0 ± 0.4
1 h treated wood	43.1 ± 0.6	10.1 ± 0.3	5.3 ± 0.1	1.7 ± 0.3	0.72 ± 0.04	0.8 ± 0.04	27.0 ± 0.5
3 h treated wood	44.0 ± 0.5	9.6 ± 0.6	5.4 ± 0.2	1.6 ± 0.2	0.74 ± 0.05	0.9 ± 0.02	27.1 ± 0.3
15 h treated wood	46.4 ± 0.8	8.7 ± 0.4	4.9 ± 0.1	1.5 ± 0.2	0.61 ± 0.07	1.5 ± 0.1	27.8 ± 0.6

[1] All data are presented on dry weight basis (treated or untreated). All the given values are means of three determinations ± standard error.
[2] Acid soluble lignin.
[3] Acid insoluble lignin.

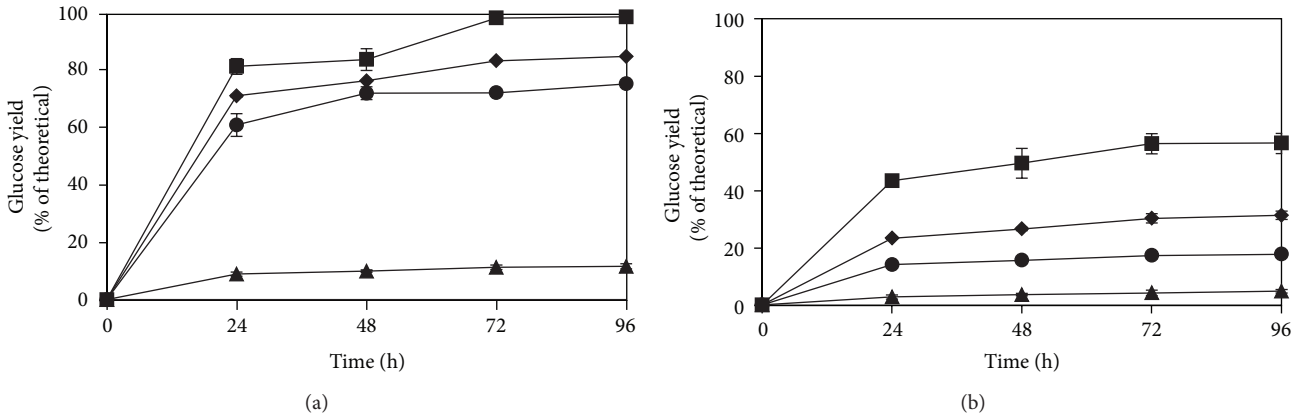

Figure 1: Effects of different pretreatment time and wood size on the hydrolysis yield (the yield of enzymatic hydrolysis was calculated as (g) glucose after hydrolysis/(g) glucan in the untreated or pretreated sample/1.111 ∗ 100) of pinewood powder (a) and chips (b). The symbols correspond to 1 h (●), 3 h (◆), and 15 h (■) pretreatment, and (▲) corresponds to for the untreated wood.

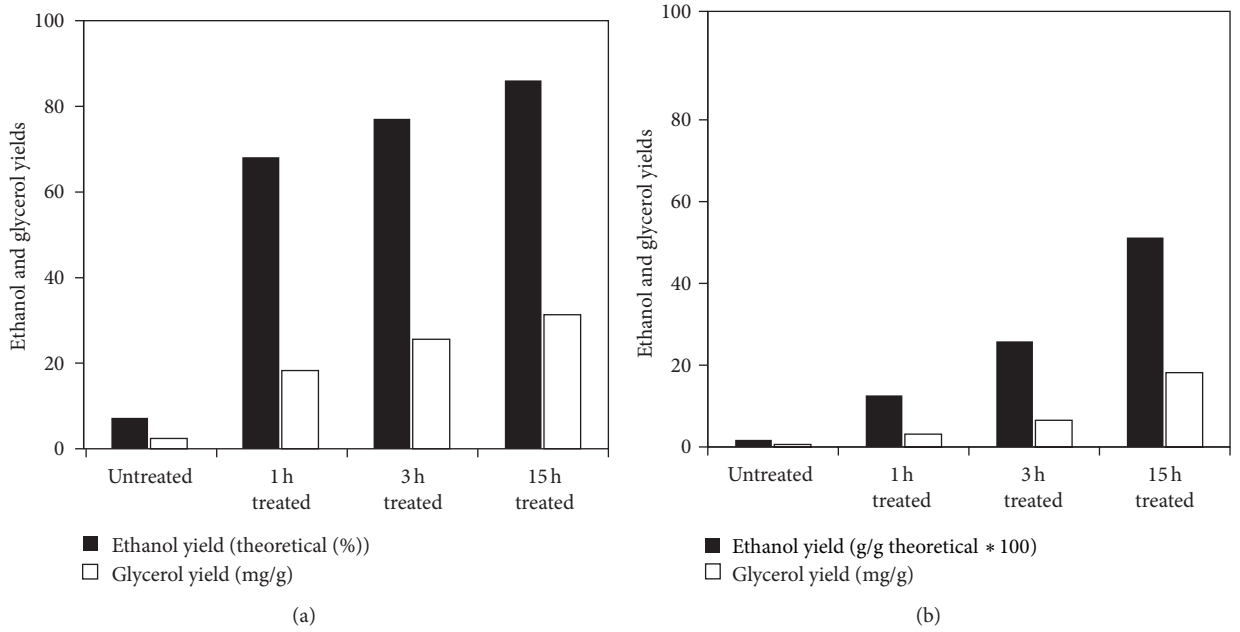

Figure 2: Effects of different pretreatment time and wood size on the ethanol (ethanol yield equals (g) ethanol produced/(g) glucan in the un- or pretreated sample/1.111/0.51 ∗ 100) and glycerol (milligrams of produced glycerol per gram of glucose that can theoretically be produced from the glucan in the treated or nontreated woods) yield of pinewood powder (a) and chips (b).

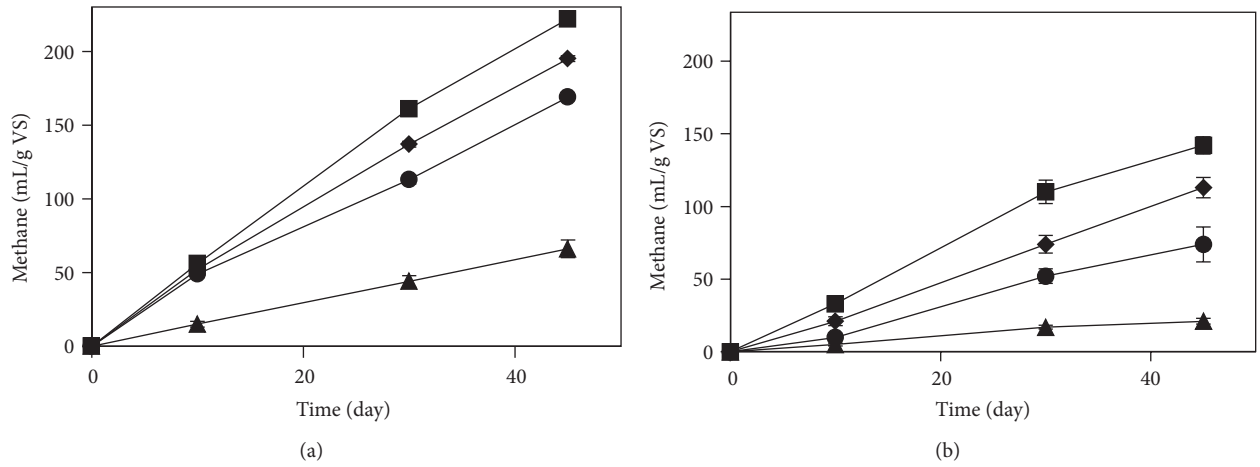

Figure 3: Effects of different pretreatment time and wood size on the methane yield of pinewood powder (a) and chips (b). The symbols correspond to 1 h (●), 3 h (◆), and 15 h (■) treatment, and (▲) corresponds to untreated wood. VS stands for volatile solids.

powder were 1.7% and 7.2%, respectively, the pretreatment improved the yields to respective values of 12.6–51.2% and 68.1–86.1%. More improvements in the ethanol yields were achieved by increasing the pretreatment duration. These improvements were more significant for the wood chips. The ethanol yield of 1 h treated chips and powder was 12.6% and 68.1%, respectively; however, 15 h treatment improved these values by 4.1- and 1.3-folds. Similar improvements in the ethanol and saccharification yield of wood chips and powder were observed in the previous studies [4, 11]. The best yields are comparable with the maximum theoretical ethanol yield of 84–90% obtained by fermentation of pure glucose by similar strain of *S. cerevisiae* [11].

3.3. Biogas Production from Pretreated Pinewood. The pretreatment considerably improved the methane yield of the treated wood powder and chips (Figure 3). The amount of methane produced from the untreated wood chips and powder were 21 and 66 mL/g volatile solid (VS). However, the methane produced from 1, 3, and 15 h treated wood chips increased by 3.5-, 5.4-, and 6.8-folds, respectively. Moreover, the methane yield of 1, 3, and 15 h treated wood powder increased by 2.6-, 3-, and 3.4-folds, respectively. Increase in the pretreatment duration positively enhanced the methane yields for both wood chips and powder.

3.4. Structural Analysis

3.4.1. Scanning Electron Microscopy (SEM). The structural modifications of pinewood powder after pretreatment with NMMO were investigated using SEM, and some of the captured images are presented in Figure 4. The untreated pine powder fibers had a highly compact structure, which was altered to a more accessible structure after the pretreatment. As the pretreatment time increases, more changes in the accessibility to the fibers were observed. The porous materials on the fiber surface of the pretreated wood were previously observed in the treated cellulosic materials. The condensed materials were cellulose microfibrils in the wood chemical or mechanical pulp [29, 30]. For the AFEX treated corn stem, lignin aromatics and hemicellulose oligomers with high and low molecular weight as well as decomposition products of AFEX pretreatment were observed on the outer cell walls [31]. In current study, the ability of NMMO as a cellulose dissolution agent suggests that the porous materials on the fiber surface might be the dissolved cellulose formed by condensation (Figures 4(c2), 4(d1), and 4(d2)). The increase in the ratio of cellulose/lignin on the surface of pretreated wood (Section 3.4.4) confirms the condensation of cellulose on the wood surface after the pretreatment. The cellulose which is condensed after the regeneration has an amorphous form and there is no protecting layer of cell wall matrix around it. Thus, the hydrolysis of the regenerated cellulose is much more convenient compared to the crystalline cellulose inside the cell wall.

While the fiber bundle of wood is intact in the untreated wood (Figures 4(a1) and 4(a2)), the pretreatment obviously opened up the bundle and the cell wall. Therefore, the cell walls and pits (holes on the cell wall for exchange of materials) are visible in Figures 4(b1) and 4(b2). Furthermore, the pores with 2-micrometer diameter are clearly seen in the 3 h and 15 h treated wood powder, while they are missing on the surface of the untreated wood (Figures 4(d1) and 4(d2) versus 4(a1) and 4(a2)). Thus, increase in the porosity as well as increased access to inside of fibers and cells after the pretreatment could be one of the main reasons for the enhanced yields of enzymatic hydrolysis.

Increase in the cellulose accessible surface plays an important role in the improvement of the anaerobic digestion yields. In anaerobic digestion, the size of cellulose-degrading bacteria is in the order of micrometers, and most of these bacteria should be attached to the cellulose surface and produce cellulosome enzymes which are placed on the cell surface [1]. Thus, the increased number of pores and the damaged structure of cell walls help the hydrolyzing bacteria to act more efficiently on the pretreated wood.

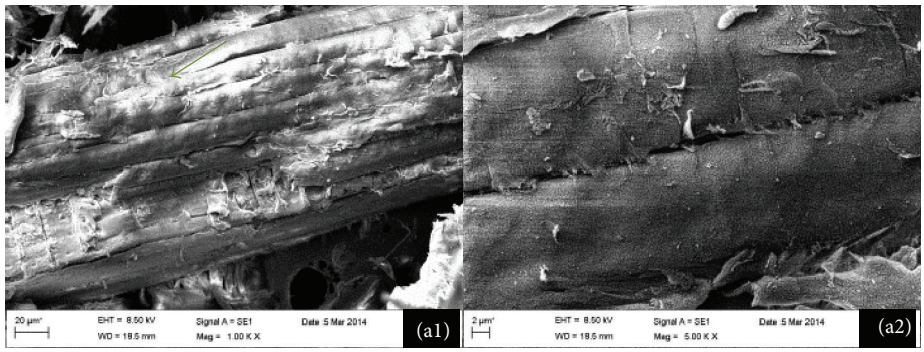

(a)

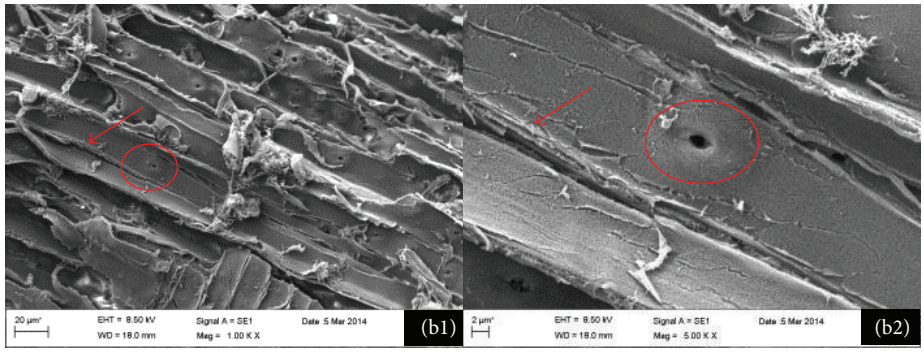

(b)

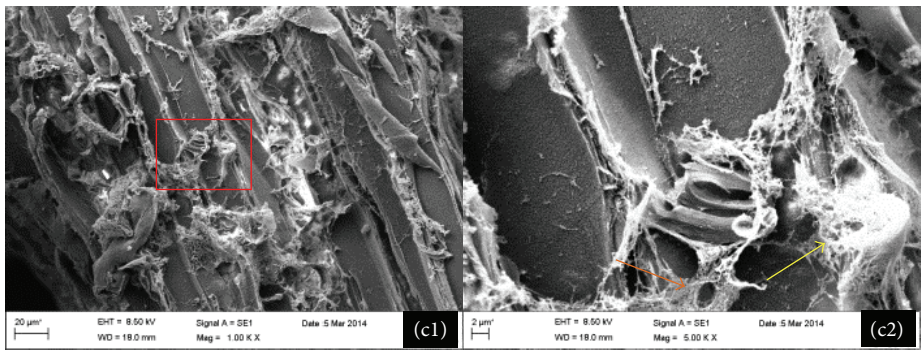

(c)

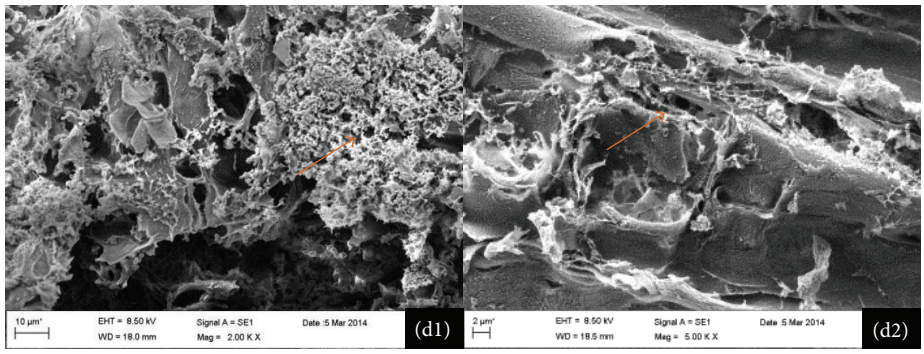

(d)

Figure 4: Scanning electron micrographs of the untreated (a) and NMMO treated pinewood powder for 1 h (b), 3 h (c), and 15 h (d). The magnifications were ×5000 (series 2) and ×1000 (series 1) except for (d1) which is ×2000. The arrows show the fiber bundle (green), opened cell wall (red), pores to the inside of biomass (orange), and condensation of cellulose (yellow). The cell wall pits are shown by red circles.

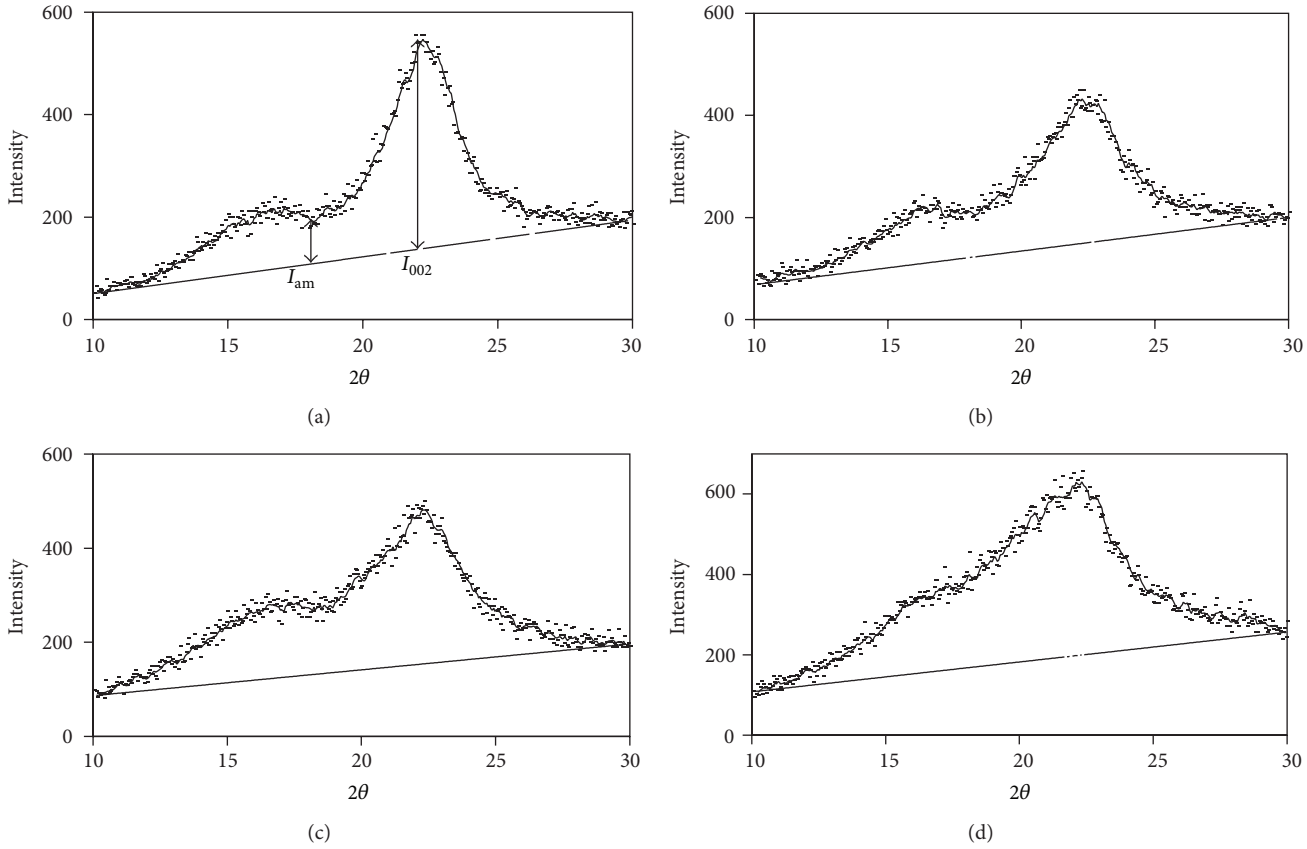

FIGURE 5: X-ray powder diffraction spectra of untreated (a) and NMMO treated pinewood powder for 1 h (b), 3 h (c), and 15 h (d). The trendline of six-point average is presented as the solid line in the spectra, and the base line is drawn from end to end of the spectra.

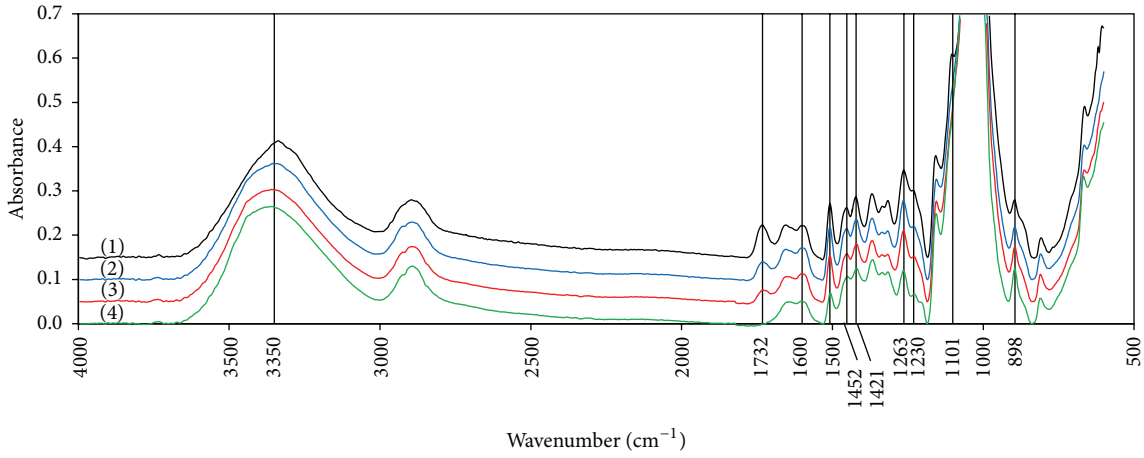

FIGURE 6: The FTIR spectra of untreated (1) and NMMO treated pinewood powder for 1 h (2), 3 h (3), and 15 h (4).

3.4.2. Water Swelling Capacity and Enzyme Adsorption. Water swelling capacity of the treated wood powder and chips was measured, and the results are shown in Table 2. Water swelling capacity of the untreated wood chips and wood powder were 1 and 7.2 (g water/g cellulose), respectively. The pretreatment of the wood chips and powder for 1–15 h increased the swelling capacity to 95–273% and 38–53%, respectively. Moreover, increase in the pretreatment duration resulted in increase of the swelling capacity.

The adsorption of cellulase enzyme on the wood was also measured and presented as relative values (g protein adsorbed/g protein adsorbed by untreated pine chips) (Table 2). Similar to water swelling capacity, increasing trends were observed after the pretreatment with NMMO. This

Table 2: Water swelling capacity and relative enzyme adsorption of the NMMO pretreated and untreated pinewood.

Pretreatment	Wood size	Water swelling capacity (g water/g wood)[1]	Relative enzyme adsorption[2]
Untreated	Powder	7.2	4.0
Pretreated for 1 h	Powder	10.0	4.9
Pretreated for 3 h	Powder	10.7	5.2
Pretreated for 15 h	Powder	11.0	6.7
Untreated	chips	1.0	1.0
Pretreated for 1 h	chips	2.0	1.5
Pretreated for 3 h	chips	3.7	2.7
Pretreated for 15 h	chips	3.8	4.3

[1]The standard deviation of all samples was less than 6.3%.
[2]The standard deviation of all samples was less than 7.2%.

Table 3: The crystallinity of untreated and NMMO treated pinewood powder using FTIR and X-ray spectroscopy.

	Untreated	1 h treated	3 h treated	15 h treated
FTIR				
LOI (a_{1421}/a_{898})	1.06	1.13	1.05	1.00
TCI (a_{1375}/a_{2918})	1.10	1.08	1.16	1.21
Lignin/cellulose (a_{1508}/a_{898})	0.94	0.99	0.83	0.55
X-ray diffraction	0.80	0.71	0.59	0.49

indicates that water swelling capacity and enzyme adsorption are directly related; the sample with higher water adsorption can bind to more enzyme molecules. However, the enzyme adsorption of the wood chips was less than that of wood powder. Furthermore, increasing the pretreatment time increased the adsorption of enzyme on both pine chips and powder. These results are in accordance with the yields of enzymatic hydrolysis of the treated materials, suggesting that more cellulase adsorption results in the higher hydrolysis and fermentation yields [22]. Considering the SEM micrographs (Figure 4), the increases in the water swelling capacity and enzyme adsorption capacity of the pretreated wood can be related to the increase in the wood porosity and enzyme accessibility.

3.4.3. X-Ray Diffraction. The changes in the crystallinity of the untreated and NMMO treated wood are presented in Table 3. Measurement of crystallinity by X-ray diffraction indicates reduction in the crystallinity of wood after pretreatment. The crystallinity reduces to a higher extent as the pretreatment time increases (Figure 5). Table 3 shows the comparison of these results with the values from FTIR spectroscopy. TCI (FTIR) represents the crystallinity of celluloses I and II, while LOI (FTIR) refers exclusively to cellulose I [28]. The crystallinity values obtained from X-ray confirm the reduction of crystallinity after the pretreatment; however, the changes in the TCI and LOI are not significant. This comparison suggests that the calculation of crystallinity of the wood by FTIR spectroscopy might not result in values consistent with the X-ray spectroscopy. The crystallinity measured by FTIR refers to the crystallinity of cellulose. Thus, the presence of hemicellulose and lignin interferes in the measurements. On the other hand, crystallinity, obtained from X-ray diffraction, is the crystallinity of the whole biomass and not cellulose alone [32]. Therefore, it can be concluded that the crystallinity of the whole biomass is reduced by pretreatment.

3.4.4. FTIR Spectroscopy. The FTIR spectra of the untreated and NMMO treated wood powder are shown in Figure 6. FTIR spectroscopy is widely used for structural analysis of cellulose and lignocellulosic materials. The absorption bands and their assigned chemical functional groups are presented in Table 4. Based on the literature data, the absorption bands at 1600, 1508, and 1263 are assigned to the functional groups of lignin [6]. The reduction in the peak intensities at 1508 cm^{-1} (from 0.12 to 0.07) and 1263 cm^{-1} (from 0.2 to 0.12) (Table 4) as a consequence of pretreatment indicates reduction of the lignin, especially the guaiacyl type, on the surface of the treated samples. It also confirms that exposure of the wood to NMMO for a longer time results in more reduction of lignin from the wood surface.

The bands at 1732 and 1230 shows the reduction of lignin and hemicellulose on the wood surface by the pretreatment, while no specific and individual band for hemicellulose reduction is observed.

Cellulose type I is the typical crystalline form of cellulose in the native plant cell wall, while the regenerated celluloses are in the form of cellulose type II and amorphous cellulose [12]. The intensity of the spectra for crystalline cellulose type I at 3352, 1452, 1431, 1162, 1111, and 893 cm^{-1} did not significantly change. The peak for the untreated wood at 3350 cm^{-1} is shifted to 3370 cm^{-1} by the pretreatment. The peak for cellulose II at 1470 is missing in all samples probably

Table 4: Characteristic frequencies and band intensities from the FTIR spectra of the treated and untreated pinewood powder.

Frequency (cm^{-1})	Functional group/band assignment	Untreated powder	1 h treated	3 h treated	15 h treated	Reference
3352 (3447) (no band)	–OH stretching intramolecular hydrogen bonds Cellulose I (3352), cellulose II (3447) Xylan	0.26 (0.18)	0.26 (0.22)	0.25 (0.22)	0.26 (0.24)	[12] [12] [13]
1732	C–O stretching of acetyl or carboxylic acid Hemicellulose and lignin (1730)	0.07	0.04	0.03	0.00	 [6]
1600	C=C Lignin	0.07	0.07	0.06	0.05	[6, 14]
1508	C–C stretching of the aromatic ring, lignin (1510)	0.12	0.12	0.10	0.07	[6]
1452	–OH in plane bending Cellulose I (1455), cellulose II (1470) Asymmetric bending in C–H_3 (1465) lignin –C–H deformation Xylan (1461)	0.11	0.11	0.11	0.11	 [12] [6] [13]
1421	C–H_2 symmetric bending Cellulose II (1419), cellulose I (1431) Weak C–O stretching (1420), aromatic C=C stretch (1433) Lignin (1423), Xylan (1420) [13]	0.14	0.14	0.13	0.13	 [15] [13] [13] [13]
1263	Vibration of guaiacyl rings (1270)	0.20	0.18	0.16	0.12	[14]
1230	C–O stretching in lignin and hemicel. (1235)	0.15	0.12	0.10	0.07	[16]
1101	Ring asymmetric stretching Cellulose I (1111) Cellulose II (1007)	0.46	0.44	0.44	0.49	[12]
898	Asym., out of phase ring stretching Cellulose I (893) Cellulose II, Amorphous Cellulose (895) Xylan (899)	0.13	0.12	0.12	0.12	 [15] [15] [13]

due to the presence of lignin and hemicellulose. Unexpectedly, the peak at 1420 cm^{-1} that is assigned to cellulose II was decreased. At this wave number, the functional groups assigned to lignin and hemicellulose seemed to be more effective than those of cellulose II; hence, the reduction in the peak intensity could be because of reduction in the lignin and hemicellulose content of the wood, rather than cellulose II. Another band assigned to cellulose I is at 1111 cm^{-1} which was clearly disappeared in the NMMO treated samples.

Considering all changes in the FTIR spectra of the wood after NMMO pretreatment, it could be concluded that NMMO altered the distribution of biomass matrix components, for example, condensation of amorphous cellulose on the NMMO treated wood surface and thus reduction in the surface lignin. Furthermore, the regeneration of cellulose I to cellulose II and amorphous cellulose was also possible. However, the wood has a very complex structure, and study of the effects of NMMO pretreatment on pure lignin, cellulose, and hemicellulose by FTIR may help the better understanding of the structural changes by the treatment.

4. Conclusions

Pinewood had a highly recalcitrant structure and the conversion of native pinewood to ethanol and biogas was inefficient. NMMO pretreatment could efficiently improve the yields of ethanol up to 86% of the theoretical yield and the biogas yield up to 222 (mL/g VS) from pinewood. No cellulose loss and minimal compositional changes were among the features of the pretreatment with NMMO. One of the main findings of the current work was that physical removal of lignin and hemicellulose is not necessary to obtain a high cellulose hydrolysis yield. Structural analyses suggested that the improvements were related to increase in the microstructure porosity, reduction in the surface lignin, and decrease in the crystallinity of cellulose. The cellulose solvent NMMO could be a potential reagent for effective pretreatment of lignocellulosic materials in the commercial scale, although the process economy should be considered.

Conflict of Interests

The authors declare no conflict of interests.

Author's Contribution

All experiments and paper preparation were done by Marzieh Shafiei, and the rest of authors supervised the experiments and revised the paper.

Acknowledgments

The authors are grateful for financial support from the Swedish Energy Agency and Institute of Biotechnology and Bioengineering, Isfahan University of Technology.

References

[1] M. J. Taherzadeh and K. Karimi, "Pretreatment of lignocellulosic wastes to improve ethanol and biogas production: a review," *International Journal of Molecular Sciences*, vol. 9, no. 9, pp. 1621–1651, 2008.

[2] N. A. Edama, A. Sulaiman, and S. N. A. Rahim, "Enzymatic saccharification of Tapioca processing wastes into biosugars through immobilization technology," *Biofuel Research Journal*, vol. 1, no. 1, pp. 2–6, 2014.

[3] M. Shafiei, K. Karimi, and M. J. Taherzadeh, "Techno-economical study of ethanol and biogas from spruce wood by NMMO-pretreatment and rapid fermentation and digestion," *Bioresource Technology*, vol. 102, no. 17, pp. 7879–7886, 2011.

[4] M. Shafiei, H. Zilouei, A. Zamani, M. J. Taherzadeh, and K. Karimi, "Enhancement of ethanol production from spruce wood chips by ionic liquid pretreatment," *Applied Energy*, vol. 102, pp. 163–169, 2013.

[5] M. E. Himmel, Ed., *Biomass Recalcitrance, Deconstructing the Plant Cell Wall for Bioenergy*, Blackwell Publishing, 2008.

[6] N. Poornejad, K. Karimi, and T. Behzad, "Improvement of saccharification and ethanol production from rice straw by NMMO and [BMIM][OAc] pretreatments," *Industrial Crops and Products*, vol. 41, no. 1, pp. 408–413, 2013.

[7] N. Poornejad, K. Karimi, and T. Behzad, "Ionic liquid pretreatment of rice straw to enhance saccharification and bioethanol production," *Journal of Biomass to Biofuel*, vol. 1, pp. 8–15, 2014.

[8] F. Moradi, H. Amiri, S. Soleimanian-Zad, M. R. Ehsani, and K. Karimi, "Improvement of acetone, butanol and ethanol production from rice straw by acid and alkaline pretreatments," *Fuel*, vol. 112, pp. 8–13, 2013.

[9] P. Salehian and K. Karimi, "Alkali pretreatment for improvement of biogas and ethanol production from different waste parts of pine tree," *Industrial and Engineering Chemistry Research*, vol. 52, no. 2, pp. 972–978, 2013.

[10] A. Goshadrou, K. Karimi, and M. J. Taherzadeh, "Ethanol and biogas production from birch by NMMO pretreatment," *Biomass and Bioenergy*, vol. 49, pp. 95–101, 2013.

[11] M. Shafiei, K. Karimi, and M. J. Taherzadeh, "Pretreatment of spruce and oak by N-methylmorpholine-N-oxide (NMMO) for efficient conversion of their cellulose to ethanol," *Bioresource Technology*, vol. 101, no. 13, pp. 4914–4918, 2010.

[12] F. Carrillo, X. Colom, J. J. Suñol, and J. Saurina, "Structural FTIR analysis and thermal characterisation of lyocell and viscose-type fibres," *European Polymer Journal*, vol. 40, no. 9, pp. 2229–2234, 2004.

[13] P. K. Adapa, C. Karunakaran, L. G. Tabil et al., "Qualitative and quantitative analysis of lignocellulosic biomass using infrared spectroscopy," in *Proceedings of the CSBE/SCGAB Annual Conference Rodd's Brudenell River Resort*, The Canadian Society for Bioengineering, Prince Edward Island, Canada, 2009.

[14] Y. Liu, Q. Zhong, S. Wang, and Z. Cai, "Correlating physical changes and enhanced enzymatic saccharification of pine flour pretreated by N-methylmorpholine-N-oxide," *Biomacromolecules*, vol. 12, no. 7, pp. 2626–2632, 2011.

[15] S. Y. Oh, I. Y. Dong, Y. Shin et al., "Crystalline structure analysis of cellulose treated with sodium hydroxide and carbon dioxide by means of X-ray diffraction and FTIR spectroscopy," *Carbohydrate Research*, vol. 340, no. 15, pp. 2376–2391, 2005.

[16] C. Li, B. Knierim, C. Manisseri et al., "Comparison of dilute acid and ionic liquid pretreatment of switchgrass: biomass recalcitrance, delignification and enzymatic saccharification," *Bioresource Technology*, vol. 101, no. 13, pp. 4900–4906, 2010.

[17] C. Kuo and C. Lee, "Enhanced enzymatic hydrolysis of sugarcane bagasse by *N*-methylmorpholine-*N*-oxide pretreatment," *Bioresource Technology*, vol. 100, no. 2, pp. 866–871, 2009.

[18] A. Teghammar, K. Karimi, I. Sárvári Horváth, and M. J. Taherzadeh, "Enhanced biogas production from rice straw, triticale straw and softwood spruce by NMMO pretreatment," *Biomass and Bioenergy*, vol. 36, pp. 116–120, 2012.

[19] A. Sluiter, B. Hames, and R. Ruiz, "Determination of structural carbohydrates and lignin in biomass," Laboratory Analytical Procedure NREL/TP-510-42618, 2008.

[20] B. Adney and J. Baker, "Measurement of Cellulase Activities," 2008, http://www.nrel.gov/biomass/pdfs/42628.pdf.

[21] E. A. Ximenes, C. R. Felix, and C. J. Ulhoa, "Production of cellulases by Aspergillus fumigatus and characterization of one β-glucosidase," *Current Microbiology*, vol. 32, no. 3, pp. 119–123, 1996.

[22] A. Goshadrou, K. Karimi, and M. Lefsrud, "Characterization of ionic liquid pretreated aspen wood using semi-quantitative methods for ethanol production," *Carbohydrate Polymers*, vol. 96, no. 2, pp. 440–449, 2013.

[23] R. Kumar and C. E. Wyman, "Cellulase adsorption and relationship to features of corn stover solids produced by leading pretreatments," *Biotechnology and Bioengineering*, vol. 103, no. 2, pp. 252–267, 2009.

[24] C. Verduyn, E. Postma, W. A. Scheffers, and J. P. van Dijken, "Physiology of Saccharomyces cerevisiae in anaerobic glucose-limited chemostat cultures," *Journal of General Microbiology*, vol. 136, no. 3, pp. 395–403, 1990.

[25] L. Segal, J. J. Creely, and A. E. Martin Jr., "An empirical method for estimating the degree of crystallinity of native cellulose using the X-ray diffractometer," *Textile Research Journal*, vol. 29, pp. 786–794, 1959.

[26] R. Kumar, G. Mago, V. Balan, and C. E. Wyman, "Physical and chemical characterizations of corn stover and poplar solids resulting from leading pretreatment technologies," *Bioresource Technology*, vol. 100, no. 17, pp. 3948–3962, 2009.

[27] S. Singh, B. A. Simmons, and K. P. Vogel, "Visualization of biomass solubilization and cellulose regeneration during ionic liquid pretreatment of switchgrass," *Biotechnology and Bioengineering*, vol. 104, no. 1, pp. 68–75, 2009.

[28] X. Colom, F. Carrillo, F. Nogués, and P. Garriga, "Structural analysis of photodegraded wood by means of FTIR spectroscopy," *Polymer Degradation and Stability*, vol. 80, no. 3, pp. 543–549, 2003.

[29] G. Chinga-Carrasco, "Cellulose fibres, nanofibrils and microfibrils: the morphological sequence of MFC components from a plant physiology and fibre technology point of view," *Nanoscale Research Letters*, vol. 6, article 417, 2011.

[30] "Mechanical pulp," http://www.slu.se/sv/institutioner/skogens-produkter/centra/wurc/history-of-wurc/organization/research/mechanical-pulp/.

[31] S. P. S. Chundawat, B. S. Donohoe, L. da Costa Sousa et al., "Multi-scale visualization and characterization of lignocellulosic plant cell wall deconstruction during thermochemical pretreatment," *Energy and Environmental Science*, vol. 4, no. 3, pp. 973–984, 2011.

[32] F. Xu, Y. Shi, and D. Wang, "X-ray scattering studies of lignocellulosic biomass: a review," *Carbohydrate Polymers*, vol. 94, no. 2, pp. 904–917, 2013.

Hindawi Publishing Corporation
BioMed Research International
Volume 2014, Article ID 205636, 7 pages
http://dx.doi.org/10.1155/2014/205636

Research Article

Biotemplated Synthesis of Anatase Titanium Dioxide Nanoparticles via Lignocellulosic Waste Material

Donya Ramimoghadam, Samira Bagheri, and Sharifah Bee Abd Hamid

Nanotechnology & Catalysis Research Centre (NANOCAT), University of Malaya, IPS Building, 50603 Kuala Lumpur, Malaysia

Correspondence should be addressed to Samira Bagheri; samira_bagheri@um.edu.my

Received 29 April 2014; Revised 23 May 2014; Accepted 5 June 2014; Published 15 July 2014

Academic Editor: Meisam Tabatabaei

Anatase titanium dioxide nanoparticles (TiO_2-NPs) were synthesized by sol-gel method using rice straw as a soft biotemplate. Rice straw, as a lignocellulosic waste material, is a biomass feedstock which is globally produced in high rate and could be utilized in an innovative approach to manufacture a value-added product. Rice straw as a reliable biotemplate has been used in the sol-gel method to synthesize ultrasmall sizes of TiO_2-NPs with high potential application in photocatalysis. The physicochemical properties of titanium dioxide nanoparticles were investigated by a number of techniques such as X-ray diffraction analysis (XRD), transmission electron microscopy (TEM), Fourier transform infrared spectroscopy (FTIR), Raman spectroscopy, thermogravimetric analysis (TGA), ultraviolet visible spectra (UV-Vis), and surface area and pore size analysis. All results consensually confirmed that particle sizes of synthesized titanium dioxide were template-dependent, representing decrease in the nanoparticles sizes with increase of biotemplate concentration. Titanium dioxide nanoparticles as small as 13.0 ± 3.3 nm were obtained under our experimental conditions. Additionally, surface area and porosity of synthesized TiO_2-NPs have been enhanced by increasing rice straw amount which results in surface modification of nanoparticles and potential application in photocatalysis.

1. Introduction

Titanium dioxide is an important n-type wide band-gap semiconductor with light absorbing, charge transport, and surface adsorption properties [1]. Three different crystallite structures of brookite, anatase, and rutile have been found for titanium dioxide [2]. Due to the exclusive properties like photoactivity, photostability, being chemically and biologically inert [3], being relatively inexpensive, and high stability [4], titanium dioxide has wide variety of applications including photocatalysis, catalysis, dye sensitized solar cells, and photovoltaic and water-splitting devices [5]. Therefore, exponential growth in research focuses on synthesis, properties, and applications of TiO_2 nanostructures that have been accomplished in recent years.

There are various methods to synthesize titanium dioxide nanostructures such as chemical vapor deposition, microemulsion, chemical precipitation, hydrothermal crystallization, and sol-gel [3, 5]. Sol-gel is one of the most successful techniques to fabricate high photocatalytic titanium dioxide nanostructures [6], with controlled shape and porosity. Moreover, other advantages such as versatile process [7] with high purity, good homogeneity, and low processing temperature [8] can be taken into account for this synthetic technique.

Recently, synthetic methods of TiO_2 nanostructures were accompanied with template-assisted approaches. The templating method is one of the frequently used methods to modify the surface properties of nanomaterials [9]. The surface modification of nanomaterials is mostly applied due to avoiding the agglomeration, increasing the stability and compatibility in different media. It also can assist in creating active sites on the nanomaterials' surface and eventually enhancing their activity. Generally templates are categorized into two major groups of soft and hard templates. Porous solids can be considered as hard templates such as anodic aluminum oxide (AAO) membranes, colloid beads, ordered mesoporous inorganic materials, and zeolites. Conversely, soft templates consist of mostly organic molecules, long-chain polymers, supermolecular aggregates, structure-directing agents, surfactants, gels, micelles, and different types of biological species. Soft templates in order to have special anisotropic

structure not only render more sufficient synthetic process but also have the ability to be easily removed. In addition, it is proven that the effective and high quality encapsulation technique is feasible by soft templating. A variety of materials can be exploited as templates such as nanoporous materials, molecules and supramolecules, colloids, particles, and even biological species named as biotemplates [10].

Waste valorization is a term used for managing waste in the most sustainable way which has attracted a significant amount of attention in recent years [11]. Vast choices of advanced technologies are available to employ the agricultural wastes into novel functional nanomaterials [12]. The rice cultivation procedure results in two types of residues, straw and husk, of which a variety of valuable chemicals can be derived. Rice straw is the stalk of the rice plant that is left over as waste products on the field upon harvesting of the rice grain (i.e., the seeds of rice straw). Rice husk, the main byproduct from rice milling, accounts for roughly 22% of paddy weight, while rice straw to paddy ratio ranges from 1.0 to 4.3. Although the technology for rice husk utilization is well-established worldwide, rice straw is sparingly used as a source of renewable energy [12, 13]. In this regard, recently a lot of efforts have been carried out for conversion of various edible or nonedible biomass feedstocks into biofuels [14].

Various templates have been reported to synthesize metal oxide nanostructures. Moreover, surfactants as subsidiaries of templates have been widely used in the preparation of different nanoparticles with good size distribution and dispersity [15]. Adding diverse surfactants as capping agent into the reaction matrix can help synthesize monodispersed TiO_2 nanoparticles [16]. TiO_2 nanorods can be synthesized with different sizes and shapes through aid of surfactants. Different amines were applied to synthesize TiO_2 nanomaterials as shape controller [16–19]. Another study has reported using sodium stearate and sodium oleate which could change the TiO_2 nanoparticles from round-corner cubes to sharp-edged cubes [20]. In addition, the size distribution of TiO_2 nanorods was largely controlled by the size distribution of anodic alumina membrane (AAM) [19–21]. Moreover, exploiting surfactants such as ammonium carboxylate perfluoropolyether and poly(dimethylaminoethyl methacrylate-block-1H,1H,2H,2H-perfluorooctyl methacrylate) led to increasing the crystal size [22].

Biological materials such as biomolecular structures, viruses, proteins, and DNA have attracted a lot of attention recently. Many studies have investigated the effects of different biotemplates on the synthesis and properties of different metal oxide nanostructures. Gelatin [23, 24], gum [25], starch [22–24, 26], rice straw [27], eggshell membrane [28], bamboo membrane [29], DNA [30], yeast, dandelion pollen, and albumen [28, 29] were all investigated to synthesize metal oxide nanoparticles such as ZnO, TiO_2, and Ag nanoparticles. Applying rice straw as a soft biotemplate appears to be a promising way to synthesize titanium dioxide nanoparticles. Moreover, to the best of our knowledge, no such study on the synthesis of TiO_2-NPs using rice straw as biotemplate is found in the open literature. Therefore, in this study, we investigate the effects of rice straw powder on properties of synthesized TiO_2 nanoparticles via soft, inexpensive, and green template.

2. Experimental

2.1. Materials. All chemicals used in this work were of analytical reagent grade and used as received without any further purification. All the aqueous solutions were prepared using deionized water. Titanium (IV) isopropoxide 98% which was used as a main precursor was purchased from Acros Organics Co., and acetic acid 100% was purchased from Merck Co., Germany. Rice straw was purchased from local market and ground into powder form in milling machine, Fritsch Pulverisette 6 type planetary monomill, Germany.

2.2. Characterization. Powder X-ray diffraction (PXRD) analysis was performed on a Shimadzu diffractometer, XRD-6000 (Tokyo, Japan) equipped with CuKα radiation. The morphology of the titanium dioxide particles was characterized by transmission electron microscopy (TEM) LEO LIBRA-120, Carl Zeiss AG Company (Oberkochen, Germany). Particle size distribution has been calculated using Image J and SPSS software. Surface characterization of the material was carried out using nitrogen gas adsorption-desorption technique at 77 K using Autosorb-6B Quantochrome (FL, USA). Thermogravimetric and differential thermogravimetric analysis (TGA-DTG) were carried out using a Mettler Toledo instrument (Greifensee, Switzerland) using a heating rate of 10°C/min, in the range of 25–1000°C under nitrogen atmosphere. Fourier transform infrared spectra were recorded over the 400–4000 cm^{-1} range using a Perkin-Elmer 100 spectrophotometer (Waltham, MA, USA) under standard conditions. The structural properties were also investigated by inVia Raman microscope, Renishaw (Gloucestershire, UK), in the range of 100–700 cm^{-1}. The UV-VIS-NIR spectrophotometer UV-3600 SHIMADZU was used to determine the optical properties.

2.3. Synthesis of TiO_2 Nanoparticles. In a typical procedure [31], titanium (IV) isopropoxide was dissolved in deionized water (18.2 MΩ cm) and acetic acid with the molar ratio of 1 : 200 : 10. Glacial acetic acid acts as a chelating agent to prevent titanium isopropoxide from the nucleophilic attacks by the water. The solution was stirred for few hours and then different concentrations of rice straw powder 0, 0.25, 0.5, 1, 2, and 4 g were introduced into the solution (the ratio of titanium (IV) isopropoxide to rice straw powder was chosen at 1 : 0.1, 1 : 0.2, 1 : 0.4, 1 : 0.8, and 1 : 1.5 w/w%) and stirred. The mentioned solution was heated at 80°C until formation of the gel. The obtained gel was dried in the oven at 80°C overnight. Finally the dried gel was ground and calcined in a muffle furnace at 500°C for 5 hours.

3. Results and Discussion

3.1. Powder X-Ray Diffraction. To determine the phase of the produced TiO_2-NPs, samples were examined by X-ray

Table 1: The crystalline size of TiO_2-NPs obtained from Scherer's formula.

Samples	2θ (degree)	FWHM (rad)	Size (nm)
0R	25.384	0.0067	20
0.25R	25.385	0.0075	18
0.5R	25.38	0.0090	15
1R	25.346	0.0104	13
2R	25.324	0.0123	11
4R	25.316	0.0135	10

powder diffraction (XRD). Figure 1 shows the XRD patterns of the TiO_2 samples synthesized using different concentrations of rice straw powder after calcinations at 500°C for 5 hours. As clearly seen from Figure 1, all the diffraction peaks of the pure TiO_2 prepared by the conventional sol-gel method can be indexed as anatase (Anatase XRD JCPDS Card number 78-2486). However, Budi et al. [32] reported mesoporous synthesis of titania using starch through sol-gel method involving mixed phases of anatase and rutile applying different concentrations of potato starch.

According to Figure 1, the diffraction peaks of as-synthesized TiO_2 samples were broadened by increasing the concentration of rice straw. This is due to the decrease in the crystalline size. Moreover, no characteristic peaks can be observed in the XRD pattern for rice straw components. The crystalline sizes of the TiO_2-NPs were determined by means of an X-ray line-broadening method by Scherer's formula ($D = K\lambda/\beta\cos\theta$) where λ is the wavelength of X-ray radiation (CuKα = 0.15406 nm), K is a constant taken as 0.9, β is the line width at half maximum height (FWHM) of the peak, and θ is the diffracting angle. The (101) plane with highest intensity peak was chosen to calculate the crystalline size. The average crystalline size of synthesized TiO_2-NPs with different concentrations of rice straw and also without rice straw is listed in Table 1. It is noteworthy to mention that 0R, 0.25R, 0.5R, 1R, 2R, and 4R refer to synthesized TiO_2-NPs using 0.0, 0.25, 0.5, 1, 2, and 4 g rice straw, respectively.

3.2. Transmission Electron Microscopy. In order to understand the effects of biotemplate on the size and morphology of the synthesized TiO_2-NPs, TEM examination was conducted. Figure 2 shows the TEM images and size distributions of the TiO_2-NPs with and without rice straw after calcination at 500°C for 5 hours. The size histograms of the TiO_2-NPs are shown below the relative TEM images. As seen from histograms in Figure 3, the mean particle size of TiO_2 sample prepared without and with 4 g rice straw as biotemplate is 24.0 ± 4.7 nm and 13.0 ± 3.3 nm, respectively. It is notable that size of TiO_2-NPs synthesized using rice straw considerably decreased compared to TiO_2-NPs synthesized without rice straw (all results not shown here). The obtained result from TEM is in agreement with XRD results, representing that smaller size of TiO_2-NPs can be obtained using rice straw as biotemplate which is acting like a directing agent.

Cellulose is the main component of rice straw consisting of mostly polysaccharides. Polysaccharides interfere in various stages of the titanium dioxide synthesis. The biopolymer,

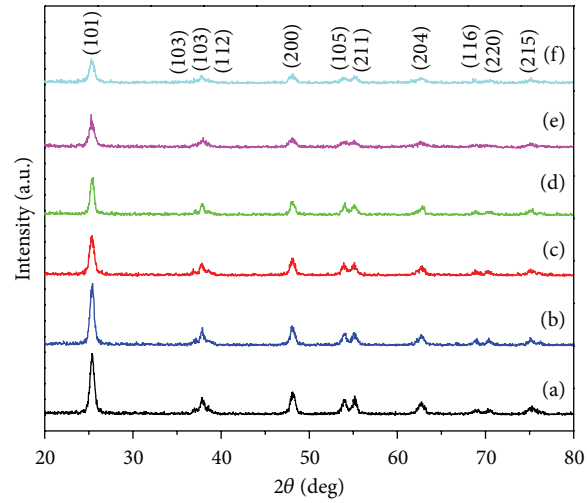

Figure 1: XRD patterns of TiO_2-NPs using different concentrations of rice straw; (a) 0R, (b) 0.25R, (c) 0.5R, (d) 1R, (e) 2R, and (f) 4R (0R, 0.25R, 0.5R, 1R, 2R, and 4R refer to synthesized TiO_2-NPs using 0.0, 0.25, 0.5, 1, 2, and 4 g rice straw, resp.).

which is dispersed in the liquid media, behaves like an organic matrix, binding through their functional groups (hydroxylic or carboxylic groups) to many titanium ions. The initial association of the titanium ions to polysaccharide determines a homogenous dispersion of the ion in well confined spaces. After the change of the initial reaction conditions, in the presence of a precipitation agent, these binding positions provide preferred nucleation and growth sites for the hydrolyzed Ti^{4+}-containing particles, due to the high local suprasaturation in titanium ions. The conversion of oxide precursor to oxide needs heating treatments. The homogeneous dispersion of the cations within the polysaccharide matrix and the low temperature of its thermal degradation shift the balance between nucleation and growth toward the formation of a larger number of smaller oxide crystals [33].

3.3. Fourier Transform Infrared and Raman Spectroscopy. Fourier transform infrared spectroscopy was used to investigate the effects of rice straw as biotemplate on the chemical properties of the TiO_2-NPs prepared by sol-gel method. FTIR spectra were obtained at room temperature in the range of 4000–400 cm^{-1}. Figure 3 shows the FTIR spectra of TiO_2-NPs synthesized using different concentrations of rice straw as a biotemplate. In addition, spectra of TiO_2-NPs sample synthesized using no rice straw are also represented for better comparison.

The bands centered at 1635 cm^{-1} and 3400 cm^{-1} are attributed to δ-H_2O bending and vibration of hydroxyl groups [34]. Band at about 2357 cm^{-1} is assigned to Si–H stretching vibration caused by rice straw components. It is noteworthy to mention that the silicon compound may coexist with other compositions in the rice straw due to the presence of rice straw husk. In addition, absorption bands at around 1430 and 1530 cm^{-1} are attributed to the C–H bending and angular deformation of C–H bond in starch molecule,

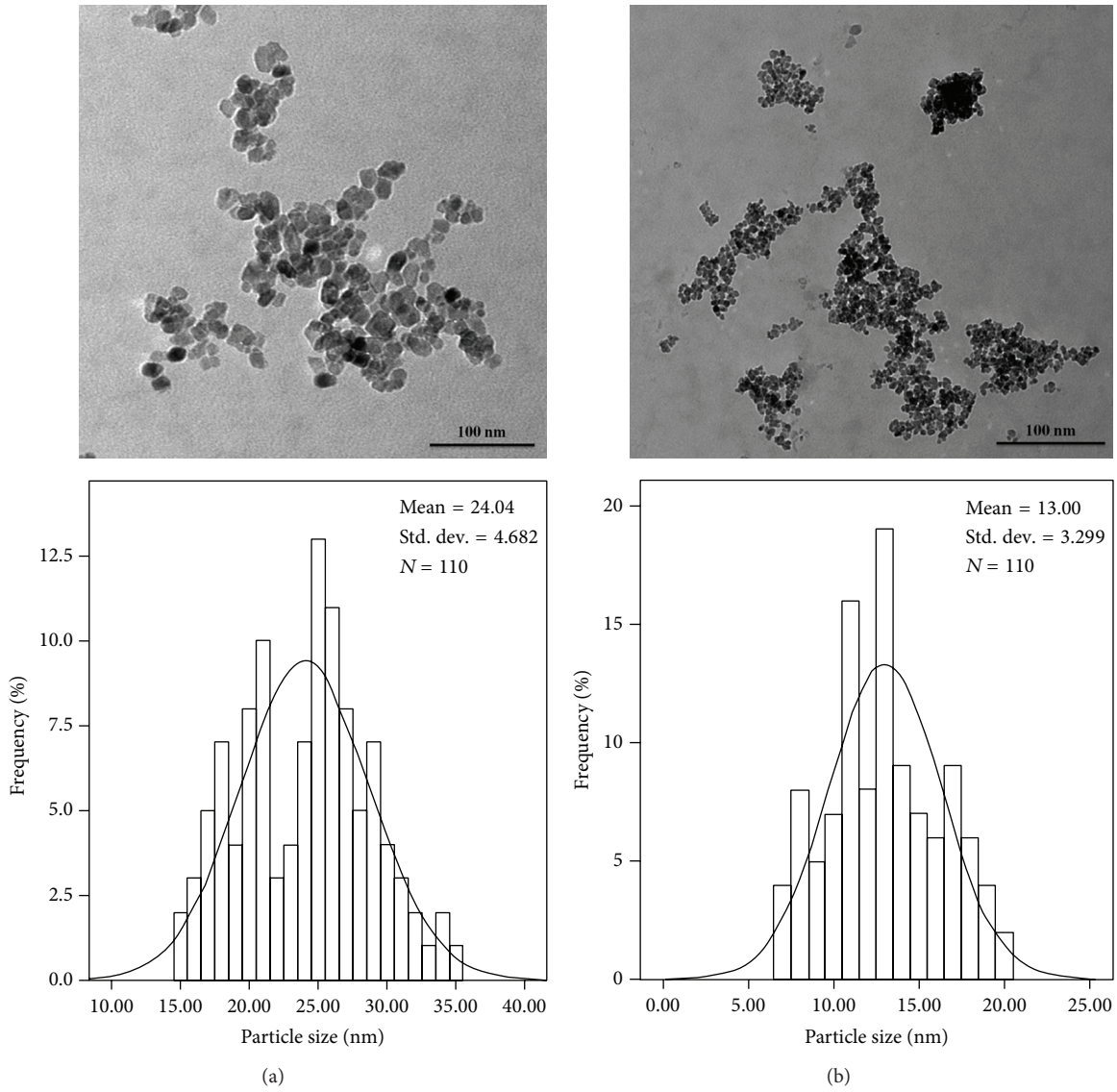

Figure 2: TEM images of TiO_2-NPs prepared using (a) 0R and (b) 4R.

respectively [35]. The band at about 460 cm^{-1} is assigned to O–Ti–O in anatase phase which can be clearly observed in all synthesized TiO_2-NPs samples. A closer look on the FTIR spectra of TiO_2 samples synthesized using different concentrations of rice straw indicates a slight shift to higher wavenumbers in characteristic band of TiO_2 compared to the sample synthesized using no rice straw. This shifting can occur due to the decrease in the particle size of TiO_2-NPs.

The structural properties of the TiO_2-NPs were further investigated by Raman spectroscopy. Figure 4 shows the Raman spectra of TiO_2-NPs synthesized using different concentrations of rice straw as biotemplate along with spectra of TiO_2-NPs sample synthesized using no rice straw as reference. All samples exhibit five distinct Raman-active modes of E_g (145 cm^{-1}), E_g (198 cm^{-1}), B_{1g} (399 cm^{-1}), A_{1g} (516 cm^{-1}), and E_g (640 cm^{-1}) for anatase TiO_2 [36] calcined at 500°C, verifying the materials' phase composition determined by XRD and TEM. Analysis of the Raman spectra by multipeak fitting revealed appreciable shifts of the anatase Raman bands for synthesized TiO_2-NPs using different concentrations of rice straw compared to the reference sample. This behavior is characteristic of size effects raised by biotemplate [31]. Specifically, the lowest frequency and most intense E_g anatase mode shifted from 144 cm^{-1} for the reference to 145 cm^{-1} which is qualitatively consistent with the decrease of the anatase crystalline size.

3.4. Thermogravimetric Analysis. The thermogravimetric and derivative thermogravimetric analysis (TGA/DTG) have been investigated on the TiO_2-NPs synthesized by the sol-gel method using different concentrations of rice straw. Figure 5 shows the TGA-DTG curve of TiO_2-NPs synthesized using 4 g rice straw. It can be clearly seen that TG curve descends until it becomes horizontal around 500°C. The TG and DTA traces show three main regions. The first weight loss

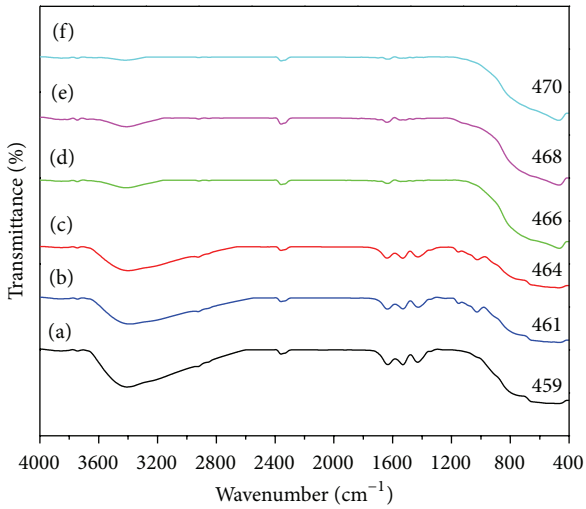

Figure 3: FTIR spectra of TiO_2-NPs synthesized using (a) 0R, (b) 0.25R, (c) 0.5R, (d) 1R, (e) 2R, and (f) 4R.

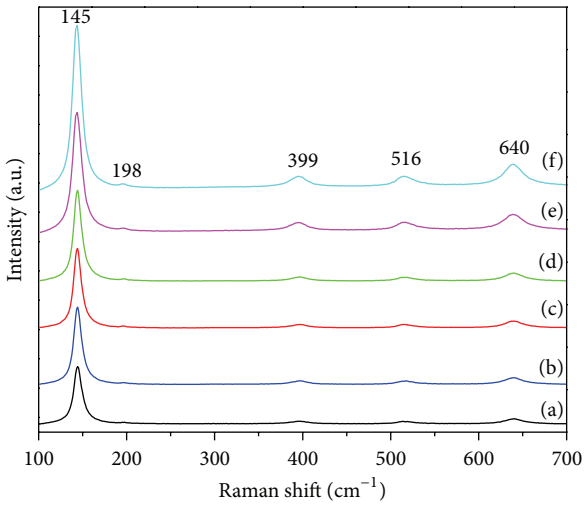

Figure 4: Raman spectra of TiO_2-NPs synthesized using (a) 0R, (b) 0.25R, (c) 0.5R, (d) 1R, (e) 2R, and (f) 4R.

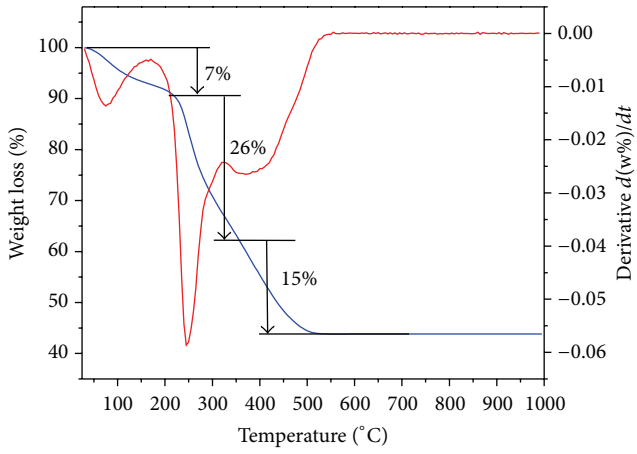

Figure 5: TGA-DTG thermogram of as-synthesized TiO_2-NPs samples synthesized using 4 g rice straw (4R).

below 100°C (7%) is assigned to dehydration of water. The second weight loss from 200 to 300°C (26%) is attributed to the decomposition of rice straw components which are mainly carbohydrates. Similar results were also reported by Ramimoghadam et al. [27]. It is noteworthy to mention that the weight loss percentages of 4, 5, 8, and 15% were observed for TiO_2-NPs synthesized using 0.25, 0.5, 1, and 2 g rice straw. The third step from 350 to 500°C (15%) is related to both the decomposition of the organic group's residuals and the condensation of the TiO_2 anatase phases.

3.5. UV-Visible Spectroscopy. Figure 6 shows the UV-Vis absorption spectra of the TiO_2-NPs using different concentrations of rice straw in comparison with the TiO_2 synthesized using no rice straw as reference. Compared to the very low absorption of the reference TiO_2-NPs, all the TiO_2-NPs synthesized using rice straw exhibit a slight shift of the absorption edge toward the visible region. This red-shift originates from decreasing of the particle size of synthesized TiO_2-NPs.

3.6. Surface Properties. The N_2 adsorption-desorption technique was employed to investigate the effect of rice straw on the surface property of TiO_2-NPs. Figure 7 shows isotherms of TiO_2-NPs synthesized using lowest (0.25R) and highest (4R) amount of rice straw along with reference sample synthesized without rice straw (0R). As seen from Figure 7, all the TiO_2-NPs exhibited Type IV isotherm which is associated with capillary condensation according to IUPAC classification with Type H3 hysteresis loops. The N_2 isotherms varied significantly with the rice straw content, indicating that the TiO_2 porous structure could be controlled by adjusting the amount of rice straw during particle synthesis. Detailed look on isotherms in Figure 6 shows that desorption branch of synthesized samples using rice straw is getting wider compared to sample synthesized without rice straw, representing increase in porosity. In addition, N_2 adsorption-desorption isotherms have clearly shown gradual enhancement in the volume absorbed through pores of the TiO_2 samples using rice straw as biotemplate, representing higher pore volumes for template-assisted TiO_2-NPs. Therefore, it is clear that porosity has been increased during synthesis of TiO_2-NPs by applying rice straw as biotemplate.

The BET surface area and average pore sizes and pore volumes of TiO_2-NPs are listed in Table 2. As seen from the table, the average pore size for the as-obtained samples is between 6.5 and 16.5 nm, indicating increase in the pore size of synthesized samples by adding more rice straw. From surface area values, a consequence can be derived that increasing rice straw concentration in synthesis of TiO_2-NPs could considerably enhance the specific surface area. For example, specific surface area of TiO_2-NPs synthesized using 4 g rice straw was obtained at 97 m^2/g, which is more than twofold in comparison with sample synthesized without rice straw. Results from surface properties are in agreement with obtained particle size from TEM since decrease of particle size could lead to surface area enhancement. It is noteworthy to mention that pore structures play an important role as

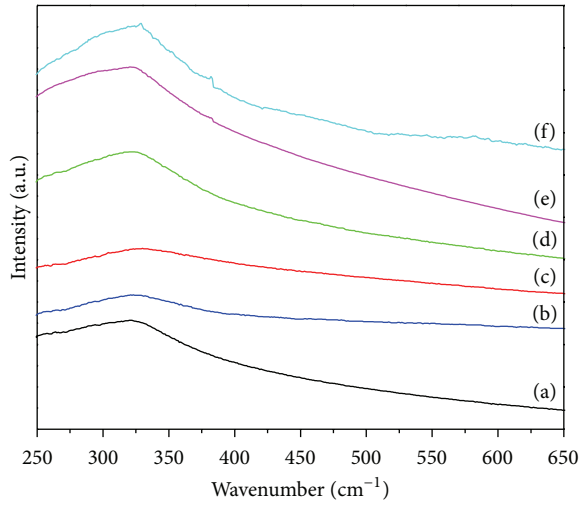

Figure 6: UV-Vis spectra of TiO_2-NPs synthesized using (a) 0R, (b) 0.25R, (c) 0.5R, (d) 1R, (e) 2R, and (f) 4R.

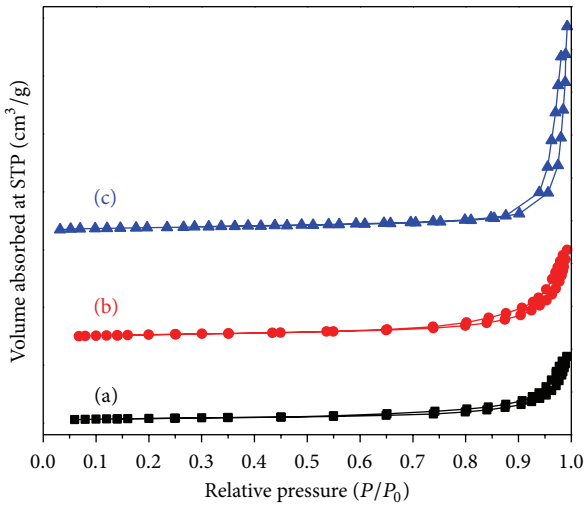

Figure 7: Nitrogen adsorption-desorption isotherms of TiO_2-NPs synthesized using (a) 0R, (b) 0.25R, and (c) 4R.

well. As seen from Table 2, pore volumes of TiO_2 samples improved by increasing the rice straw concentrations, indicating porosity enhancement. In conclusion, surface characteristics of TiO_2-NPs have been modified using rice straw as biotemplate. Increasing in the surface area and porosity of the synthesized TiO_2-NPs can result in high photocatalytic properties under UV light irradiation according to report from Budi et al. [32].

4. Conclusion

Anatase TiO_2 nanoparticles were successfully synthesized by conventional sol-gel method based on the template-assisted waste valorization technique using rice straw. Through this method, highly crystalline TiO_2-NPs with unchanged physical dimensions and minimal agglomeration were prepared. The physicochemical properties of synthesized TiO_2-NPs were investigated by XRD, TEM, FTIR, Raman, UV-Vis spectroscopy, and surface area and porosity analysis indicating that TiO_2-NPs crystallize in the anatase phase with smaller size range and high surface area in the presence of rice straw. This soft template is assumed to self-assemble into well-defined aggregated entities which can restrict and direct the growth of the TiO_2 particles. Modification of the pore volume and size on one hand and decreasing the particle size on the other hand could enhance the surface area of the synthesized TiO_2 nanoparticles up to 97 m^2/g which makes TiO_2-NPs highly potential photocatalyst compared to the titania synthesized using no template. In conclusion, waste valorization approach has dedicated a new pathway to apply sustainable lignocellulosic waste material to fabricate advanced end-products using green chemical technologies.

Table 2: BET surface area and average pore sizes and pore volumes of TiO_2-NPs synthesized using different concentrations of rice straw.

Samples	BET surface area (m^2/g)	Total pores volume (cm^3/g)	Average pore size (nm)
0R	45	0.09	6.5
0.25R	57	0.12	8.7
0.5R	65	0.13	11.3
1R	73	0.16	14.3
2R	89	0.21	15.0
4R	97	0.23	16.5

Conflict of Interests

The authors declare that there is no conflict of interests regarding the publication of this paper.

Acknowledgment

This work was supported by the University of Malaya Research Grant (UMRG RP022-2012A) and also HIR Grant (H-21001-F0032).

References

[1] X. Pan, M. Yang, X. Fu, N. Zhang, and Y. Xu, "Defective TiO_2 with oxygen vacancies: Synthesis, properties and photocatalytic applications," *Nanoscale*, vol. 5, no. 9, pp. 3601–3614, 2013.

[2] S. N. S. A. Ayob and U. Hashim, "Synthesis and characterization of titania nanoparticles via sol-gel method," in *Proceedings of the 2nd IEEE-EMBS Conference on Biomedical Engineering and Sciences (IECBES '12)*, pp. 607–609, December 2012.

[3] S. Valencia, X. Vargas, L. Rios, G. Restrepo, and J. M. Marín, "Sol-gel and low-temperature solvothermal synthesis of photoactive nano-titanium dioxide," *Journal of Photochemistry and Photobiology A: Chemistry*, vol. 251, pp. 175–181, 2013.

[4] A. Fujishima and X. Zhang, "Titanium dioxide photocatalysis: present situation and future approaches," *Comptes Rendus Chimie*, vol. 9, no. 5-6, pp. 750–760, 2006.

[5] N. M. Julkapli, S. Bagheri, and S. B. Abd Hamid, "Recent advances in heterogeneous photocatalytic decolorization of

synthetic dyes," *The Scientific World Journal*, vol. 2014, Article ID 692307, 25 pages, 2014.

[6] J. Yan, G. Wu, N. Guan, L. Li, Z. Li, and X. Cao, "Understanding the effect of surface/bulk defects on the photocatalytic activity of TiO_2: anatase versus rutile," *Physical Chemistry Chemical Physics*, vol. 15, no. 26, pp. 10978–10988, 2013.

[7] X. Chen and S. S. Mao, "Titanium dioxide nanomaterials: synthesis, properties, modifications and applications," *Chemical Reviews*, vol. 107, no. 7, pp. 2891–2959, 2007.

[8] C. Han, H. Lee, and S. Han, "Synthesis of nanocrystalline TiO_2 by sol-gel combustion hybrid method and its application to dye solar cells," *Bulletin of the Korean Chemical Society*, vol. 29, no. 8, pp. 1495–1498, 2008.

[9] F. Zhang, *Modified Ambient Template-Directed Synthesis, Characterization and Applications of One-Dimensional Nanomaterials a Dissertation Presented by Fen Zhang to the Graduate School in Partial Fulfillment of the Requirements for the Degree of Doctor of Philosoph*, Stony Brook University, 2009.

[10] S. Z. Qiao, J. Liu, G. Qing, and M. Lu, "Synthetic chemistry of nanomaterials," in *Modern Inorganic Synthetic Chemistry*, pp. 479–506, Elsevier B.V., New York, NY, USA, 2011.

[11] R. Luque and J. H. Clark, "Valorisation of food residues: waste to wealth using green chemical technologies," *Sustainable Chemical Processes*, vol. 1, no. 1, p. 10, 2013.

[12] S. Kumar, J. S. Upadhyaya, and Y. S. Negi, "Preparation of nanoparticles from corn cobs by chemical treatment methods," *BioResources*, vol. 5, no. 2, pp. 1292–1300, 2010.

[13] M. Tabatabaei, Y. Chisti, A. F. Ismail, and S. Ramakrishna, "Editorial," *Biofuel Research Journal*, vol. 1, 2014.

[14] M. Akia, F. Yazdani, E. Motaee, D. Han, and H. Arandiyan, "A review on conversion of biomass to biofuel by nanocatalysts," *Biofuel Research Journal*, vol. 1, no. 1, pp. 16–25, 2014.

[15] C. Burda, X. Chen, R. Narayanan, and M. A. El-Sayed, "Chemistry and properties of nanocrystals of different shapes," *Chemical Reviews*, vol. 105, no. 4, pp. 1025–1102, 2005.

[16] P. D. Cozzoli, R. Comparelli, E. Fanizza, M. L. Curri, and A. Agostiano, "Photocatalytic activity of organic-capped anatase TiO_2 nanocrystals in homogeneous organic solutions," *Materials Science and Engineering C*, vol. 23, no. 6–8, pp. 701–713, 2003.

[17] T. Sugimoto, X. Zhou, and A. Muramatsu, "Synthesis of uniform anatase TiO_2 nanoparticles by gel-sol method: 3. Formation process and size control," *Journal of Colloid and Interface Science*, vol. 259, no. 1, pp. 43–52, 2003.

[18] T. Sugimoto and X. Zhou, "Synthesis of uniform anatase TiO_2 nanoparticles by the gel-sol method. 2. Adsorption of OH- ions to Ti(OH)4 gel and TiO_2 particles," *Journal of Colloid and Interface Science*, vol. 252, no. 2, pp. 347–353, 2002.

[19] T. Sugimoto, X. Zhou, and A. Muramatsu, "Synthesis of uniform anatase TiO2 nanoparticles by gel-sol method: 1. Solution chemistry of Ti(OH)n(4-n)+ complexes," *Journal of Colloid and Interface Science*, vol. 252, no. 2, pp. 339–346, 2002.

[20] T. Sugimoto, X. Zhou, and A. Muramatsu, "Synthesis of uniform anatase TiO_2 nanoparticles by gel-sol method," *Journal of Colloid and Interface Science*, vol. 259, no. 1, pp. 53–61, 2003.

[21] T. Sugimoto, K. Okada, and H. Itoh, "Synthesis of uniform spindle-type titania particles by the gel-sol method," *Journal of Colloid and Interface Science*, vol. 193, no. 1, pp. 140–143, 1997.

[22] K. T. Lim, H. S. Hwang, W. Ryoo, and K. P. Johnston, "Synthesis of TiO_2 Nanoparticles utilizing hydrated reverse Micelles in CO_2," *Langmuir*, vol. 20, no. 6, pp. 2466–2471, 2004.

[23] T. Maiyalagan, B. Viswanathan, and U. V. Varadaraju, "Fabrication and characterization of uniform TiO_2 nanotube arrays by sol-gel template method," *Bulletin of Materials Science*, vol. 29, no. 7, pp. 705–708, 2006.

[24] L. Miao, S. Tanemura, S. Toh, and K. Kakeko, "Preparation of TiO_2 nanorods by heating sol gel template method," *Journal of the Ceramic Society of Japan*, vol. 112, pp. S1329–S1331, 2004.

[25] M. Darroudi, Z. Sabouri, R. Kazemi Oskuee, A. Khorsand Zak, H. Kargar, and M. H. N. A. Hamid, "Sol-gel synthesis, characterization, and neurotoxicity effect of zinc oxide nanoparticles using gum tragacanth," *Ceramics International*, vol. 8, pp. 9195–9199, 2013.

[26] M. Darroudi, A. Khorsand Zak, M. R. Muhamad, N. M. Huang, and M. Hakimi, "Green synthesis of colloidal silver nanoparticles by sonochemical method," *Materials Letters*, vol. 66, no. 1, pp. 117–120, 2012.

[27] D. Ramimoghadam, M. Z. Bin Hussein, and Y. H. Taufiq-Yap, "Hydrothermal synthesis of zinc oxide nanoparticles using rice as soft biotemplate," *Chemistry Central Journal*, vol. 7, no. 1, article 36, 2013.

[28] D. Yang, L. Qi, and J. Ma, "Eggshell membrane templating of hierarchically ordered macroporous networks composed of TiO_2 tubes," *Advanced Materials*, no. 21, pp. 1543–1546, 2002.

[29] J. Li, X. Shi, L. Wang, and F. Liu, "Synthesis of biomorphological mesoporous TiO_2 templated by mimicking bamboo membrane in supercritical CO_2," *Journal of Colloid and Interface Science*, vol. 315, no. 1, pp. 230–236, 2007.

[30] S. Li, H. Zhu, R. Zhu, X. Sun, S. Yao, and S. Wang, "Impact and mechanism of TiO_2 nanoparticles on DNA synthesis in vitro," *Science in China B: Chemistry*, vol. 51, no. 4, pp. 367–372, 2008.

[31] F. Chekin, S. Bagheri, and S. B. Abd Hamid, "Synthesis of Pt doped TiO_2 nanoparticles: characterization and application for electrocatalytic oxidation of l-methionine," *Sensors and Actuators B: Chemical*, vol. 177, pp. 898–903, 2013.

[32] C. Budi, I. Kartini, and B. Rusdiarso, "Synthesis of mesoporous titania by potato starch templated sol-gel reactions and its characterization," *Indonesian Journal of Chemistry*, vol. 10, no. 1, pp. 26–31, 2010.

[33] D. Visinescu, G. Patrinoiu, A. Tirsoaga, and O. Carp, "Polysaccharides route: a new green strategy for metal oxides synthesis," in *Environmental Chemistry for a Sustainable World*, E. Lichtfouse, J. Schwarzbauer, and D. Robert, Eds., vol. 1, pp. 119–169, Springer, Dordrecht, The Netherlands, 2012.

[34] G. Soler-Illia, A. Louis, and C. Sanchez, "Synthesis and characterization of mesostructured titania-based materials through evaporation-induced self-assembly," *Chemistry of Materials*, vol. 14, no. 2, pp. 750–759, 2002.

[35] S.-J. Bao, C. Lei, M.-W. Xu, C.-J. Cai, and D.-Z. Jia, "Environment-friendly biomimetic synthesis of TiO_2 nanomaterials for photocatalytic application," *Nanotechnology*, vol. 23, no. 20, Article ID 205601, 2012.

[36] S. Bagheri, K. Shameli, and S. B. Abd Hamid, "Synthesis and characterization of anatase titanium dioxide nanoparticles using egg white solution via Sol-Gel method," *Journal of Chemistry*, vol. 2013, Article ID 848205, 5 pages, 2013.

Hindawi Publishing Corporation
BioMed Research International
Volume 2014, Article ID 169705, 8 pages
http://dx.doi.org/10.1155/2014/169705

Research Article

Overexpression of D-Xylose Reductase (*xyl*1) Gene and Antisense Inhibition of D-Xylulokinase (*xyiH*) Gene Increase Xylitol Production in *Trichoderma reesei*

Yuanyuan Hong,[1,2] Mehdi Dashtban,[1,3] Greg Kepka,[1,4] Sanfeng Chen,[2] and Wensheng Qin[1]

[1] *Department of Biology, Lakehead University, Thunder Bay, ON, Canada P7B 5E1*
[2] *State Key Laboratory for Agrobiotechnology and College of Biological Sciences, China Agricultural University, Beijing 100193, China*
[3] *School of Environmental Sciences, University of Guelph, Guelph, ON, Canada N1G 2W1*
[4] *Instrumentation Laboratory, Lakehead University, 955 Oliver Road, Thunder Bay, ON, Canada P7B 5E1*

Correspondence should be addressed to Wensheng Qin; wqin@lakeheadu.ca

Received 22 March 2014; Accepted 18 May 2014; Published 11 June 2014

Academic Editor: Meisam Tabatabaei

T. reesei is an efficient cellulase producer and biomass degrader. To improve xylitol production in *Trichoderma reesei* strains by genetic engineering, two approaches were used in this study. First, the presumptive D-xylulokinase gene in *T. reesei* (*xyiH*), which has high homology to known fungi D-xylulokinase genes, was silenced by transformation of *T. reesei* QM9414 strain with an antisense construct to create strain S6-2-2. The expression of the *xyiH* gene in the transformed strain S6-2-2 decreased at the mRNA level, and D-xylulokinase activity decreased after 48 h of incubation. This led to an increase in xylitol production from undetectable levels in wild-type *T. reesei* QM9414 to 8.6 mM in S6-2-2. The *T. reesei* Δxdh is a xylose dehydrogenase knockout strain with increased xylitol production compared to the wild-type *T. reesei* QM9414 (22.8 mM versus undetectable). The copy number of the xylose reductase gene (*xyl*1) in *T. reesei* Δxdh strain was increased by genetic engineering to create a new strain Δ9-5-1. The Δ9-5-1 strain showed a higher *xyl*1 expression and a higher yield of xylose reductase, and xylitol production was increased from 22.8 mM to 24.8 mM. Two novel strains S6-2-2 and Δ9-5-1 are capable of producing higher yields of xylitol. *T. reesei* has great potential in the industrial production of xylitol.

1. Introduction

D-Xylitol is a five-carbon polyol, which can be naturally found in various fruits and vegetables. Xylitol has similar sweetness to sucrose but lower energy value than sucrose; it has been used as sugar substitute in foods, medicine, and chemical industry. Unfortunately, the natural content of D-xylitol in fruits and vegetables is very low [1]. On an industrial scale, D-xylitol is mainly produced by chemical reduction of D-xylose from biomass hydrolysates. The biosynthesis of D-xylitol using microorganisms has gained popularity due to environmental and economic considerations using the current industrial production method [2]. Many microorganisms are able to produce D-xylitol, including bacteria, fungi, and yeasts. These include four species of *Candida, Saccharomyces, Debaryomyces, Pichia, Hansenula, Torulopsis, Kloeckera, Trichosporon, Cryptococcus, Rhodotorula, Monilia, Kluyveromyces, Pachysolen, Enterobacter liquefaciens, and Corynebacterium* spp. [3].

In bacteria, D-xylose is converted to D-xylulose by xylose isomerase in a single step (Figure 1(b)). In yeasts and fungi, however, the conversion of D-xylose to D-xylulose occurs using a two-step process: a reduction step followed by an oxidation step (Figure 1(a)). D-Xylose is first reduced to D-xylitol by xylose reductase (XR) and then D-xylitol is oxidized to D-xylulose by xylitol dehydrogenase (XDH). D-Xylulose can be further metabolized to xylulose-5-phosphate

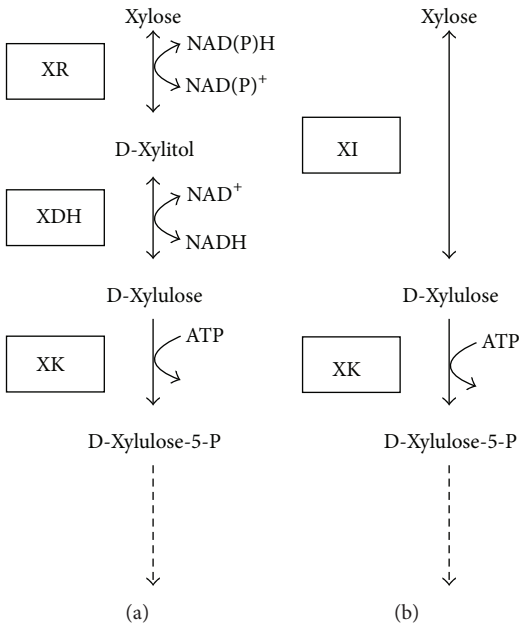

Figure 1: Metabolic pathway for xylose utilization. (a) The XR-XDH pathway in yeast and fungi. (b) The XI pathway in bacteria. XR: xylose reductase. XDH: xylitol dehydrogenase. XK: D-xylulokinase. XI: xylose isomerase [4].

by xylulokinase (XK). Xylulose-5-phosphate can enter the pentose phosphate pathway.

Lignocellulosic wastes are largely produced by a variety of industries such as forestry, agriculture, and food. *T. reesei* is an efficient biomass degrader and is a prolific industrial cellulase and hemicellulase producing fungus.

Studies have been carried out for xylitol production in yeast, especially in *Candida* species and *Saccharomyces cerevisiae* [5–7]. However, fewer studies have been completed on xylitol production in *T. reesei*. These include cloning of xylose reductase (*xyl*1) and xylitol dehydrogenase (*xdh*1) in *T. reesei* [8, 9] and antisense inhibition strategies for inhibition of xylitol dehydrogenase (XDH) in *T. reesei*. The novel strains constructed in these studies were ultimately shown to be capable of accumulating xylitol [10].

Two approaches were taken in this study in order to increase the xylitol production in *T. reesei*. In the first approach, the D-xylulokinase gene (*xyiH*) in the xylose utilization pathway in *T. reesei* was silenced; in the second one, the xylose reductase gene (*xyl*1) was overexpressed in a *T. reesei* Δxdh strain.

2. Materials and Methods

2.1. Medium. The fungal strains were grown and maintained on potato dextrose agar (PDA) containing 15.0 gL^{-1} starch, 20.0 gL^{-1} D-glucose, and 18.0 gL^{-1} agar. Strains were grown in 250 mL flasks, on a rotary shaker (200 rpm) at 30°C and in 50 mL of minimum medium containing 1.4 gL^{-1} $(NH_4)_2SO_4$, 5 gL^{-1} KH_2PO_4, 0.3 gL^{-1} urea, 0.3 gL^{-1} $MgSO_4{\cdot}7H_2O$, 0.3 gL^{-1} $CaCl_2$, 0.005 gL^{-1} $FeSO_4{\cdot}7H_2O$, 0.0016 gL^{-1} $MnSO_4{\cdot}H_2O$, 0.0014 gL^{-1} $ZnSO_4{\cdot}7H_2O$, and 0.002 gL^{-1} $CoCl_2$, pH 5.5, with the respective carbon source.

2.2. Construction of Vectors. *T. reesei* genomic DNA was extracted using a Fungi/Yeast Genomic DNA Isolation Kit (Norgen Biotek, Canada). The 1932 bp D-xylulokinase gene (*xyiH*) was amplified with PCR using xyiH primers (xyiH up and xyiH down, Table S3; see Supplementary Material available online at http://dx.doi.org/10.1155/2014/169705) designed according to DNA sequence of *T. reesei* QM6a.

Fungal total RNA was extracted using an Ambion RNA extraction kit (Invitrogen, Canada) and cDNA was constructed using a Fermentas first strand cDNA synthesis kit (Fermentas, Canada). For RNA interference of the D-xylulokinase gene in *T. reesei* QM9414, plasmid pSilent-1 (Table S2) and primers S1 and S2 were used to clone the partial D-xylulokinase gene of *T. reesei* QM9414 named fragment 1. Additionally, primers S3 and S4 were used to clone the partial D-xylulokinase gene of *T. reesei* QM9414 which was named fragment 2. Fragment 1 was digested by *Xho* I and *Hind* III, inserted into pSilent-1, which resulted in pSilent-1-fragment1. Fragment 2 was digested by *Kpn* I and *Bgl* II and inserted into pSilent-1-fragment1, resulting in pSilent-xyiH.

Plasmid pPtef1-hph (Table S2) was used for *T. reesei* QM9414 xylose reductase gene overexpression. First, the hygromycin B phosphotransferase (*hph*) gene in pPtef1-hph vector was replaced by phleomycin gene (*ble*). The *ble* gene was cloned from plasmid pBC-phleo by primers ble up and ble down. Then, the *ble* gene fragment was digested by *Xba* I and *Nsi* I and inserted into plasmid pPtef1-hph, which resulted in plasmid pPtef1-ble. By using primers xyl up and A2, the xylose reductase gene (*xyl*1) was amplified. The *xyl*1 terminator was amplified using primers B1 and xyl down. Finally, these two fragments were fused using Fusion PCR. The fused fragment was digested by *Cla* I and *Hind* III and inserted into pPtef1-ble, resulting in plasmid pPtef1-ble-xyl.

2.3. Measurement of Xylitol. During the incubation period, aliquots of 500 μL were extracted at 24 h intervals and centrifuged (16060 rcf for 5 min). The resultant supernatants were kept at 4°C for further substrate and product analyses. These supernatants were used to determine the extracellular concentration of xylitol produced by the *T. reesei* strains. The supernatant was appropriately diluted, followed by filtration using 0.2 μm syringe filters (Ultident, Canada). Ultimately, they were analyzed by high-performance anion exchange chromatography with pulsed amperometric detection (HPAE-PAD) using a Dionex ICS3000 system (Dionex, Sunnyvale, USA) equipped with a 3 × 150 mm CarboPac PA20 carbohydrate column and guard. 52 mM NaOH (isocratic) eluent was used at a flow rate of 0.5 mL min^{-1} and with a full loop injection volume of 25 μL. The column was maintained at 30°C, and a gold (Au) electrode with quadruple potential was used.

2.4. Preparation of T. reesei Cell-Free Extract. Mycelia were harvested by filtration and were washed extensively with cold tap water. 1 g of mycelia was blotted dry with paper towels

and ground in 3 mL of extraction buffer (0.1 M Tris-HCl pH: 6.5–7.5, 1 mM EDTA, and 5 mM β-mercaptoethanol) to a fine powder under liquid nitrogen with mortar and pestle. Finally, the suspension was homogenized by sonication for 10 min (1 s burst and 1 s cooling period) on ice followed by centrifugation at 10,000 g for 20 min at 4°C. The supernatant was used as the cell-free extract [11].

2.5. Measurement of Xylose Reductase Activities. The xylose reductase activities of *T. reesei* Δxdh and Δ9-5-1 were measured using a 200 μL reaction. The 200 μL reaction contained 20 μL cell-free extract, 50 mM sodium phosphate buffer (pH: 6.5), 100 mM D-xylose, and 0.2 mM NADPH. Background activities (without xylose) were also measured at room temperature. Absorbance changes at 340 nm were continuously monitored. One unit of xylose reductase is defined as the amount of enzyme which converts 1 μM NADPH to NADP per minute at room temperature, $\varepsilon = 6.22\,\text{mM}^{-1}\,\text{cm}^{-1}$ [12]. The xylose reductase activities were normalized by the concentrations of protein.

2.6. Measurement of D-Xylulokinase Activities. The D-xylulokinase activities of *T. reesei* QM9414 and S6-2-2 were measured using a 200 μL reaction. The 200 μL reaction contained 20 μL cell-free extract, 50 mM glycylglycine (pH: 7.8), 2 mM ATP, 0.5 mM PEP, 3 mM reduced glutathione, 0.1 mM NADH, 2 mM $MgCl_2$, 1 mM D-xylulose, 5 mM NaF, 5 mM KCN, 10 UmL^{-1} lactate dehydrogenase, and 10 UmL^{-1} pyruvate kinase. The reaction was initiated by addition of the cell extract. Background activities (without lactate dehydrogenase and pyruvate kinase) were also measured at room temperature. Absorbance changes at 340 nm were continuously monitored. One unit of D-xylulokinase is defined as the amount of enzyme which converts 1 μM NADH to NAD per minute at room temperature, $\varepsilon = 6.22\,\text{mM}^{-1}\,\text{cm}^{-1}$ [13]. The D-xylulokinase activities were normalized by the concentrations of protein.

2.7. Preparation of T. reesei Protoplast and Transformation. Protoplasts of different *T. reesei* strains used in this study were prepared according to Szewczyk et al. [14]. The protoplasts were then transformed with a pSilent-xyiH construct containing a hygromycin B phosphotransferase (*hph*) expression cassette as the selection marker or a pPtef1-ble-xyl vector containing a phleomycin (*ble*) expression cassette as the selection marker according to the method described by Szewczyk. The pSilent-xyiH transformants were screened on PDA plate containing 50 μgml^{-1} hygromycin as the selection marker. The pPtef1-ble-xyl transformants were screened on PDA plate containing 100 μgml^{-1} phleomycin as the selection marker. Single spore separation was done to ensure a pure culture. The integration of pSilent-xyiH into the genome of *T. reesei* QM9414 was confirmed using primers S1 and S2 (Table S3). Also, the integration of pPtef1-ble-xyl into the genome of *T. reesei* Δxdh was confirmed using ble primers (up and down) (Table S3).

2.8. Quantitative Real-Time PCR (qRT-PCR). Prior to RNA extraction, mycelia were disrupted and homogenized using a motorized homogenizer (Silentcrusher M, Heidolph, Elk Grove Village, IL). Fungal total RNA was extracted using an Ambion RNA extraction kit (Invitrogen, Canada) according to the manufacturer's instructions and extracted RNA was stored at −80°C until used. The quality and integrity of the total RNA were determined using an Experion Automated Electrophoresis Station and RNA HighSens Chips (Bio-Rad, Hercules, CA). cDNA was constructed using a Fermentas first strand cDNA synthesis kit (Fermentas, Canada) according to the manufacturer's instructions and stored in −20°C until the real-time PCR analyses. The *xyiH* and *xyl*1 (target genes) gene specific primers (Table S3) were used for qRT-PCR analyses and glyceraldehyde-3-phosphate dehydrogenase (*gpd1*) primers (Table S3) were used as the housekeeping gene. qRT-PCR data were normalized using *gpd1* as the housekeeping gene. The experiments were performed using a Bio-Rad CFX96 Touch Real-Time PCR Detection System (Bio-Rad, Hercules, CA) with each well containing the following: 10 μL Sso FastTM EvaGreenW Supermix (Bio-Rad, Canada), 5.0 μL of appropriately diluted cDNA, 1.0 μL of each primer (final concentration of 500 nM each) (Table S1), and 3.0 μL of double distilled water with a total well volume of 20 μL. Preliminary experiments have been done to obtain the optimal annealing temperature of each primer, the amplification efficiencies of all primers, and the optimal concentration of cDNA. Based on the preliminary results the cDNA was diluted 100-fold. The optimal RT-PCR cycling was 120 s at 98°C followed by 40 cycles of 5 s at 98°C and 5 s at 58°C. Three technical replicates were tested for each transformant to ensure consistency and accuracy. To ensure specificity of primers, melt curves were produced for each RT-PCR experiment. All primers were shown to amplify specific sequences and showed only one melting temperature on the melting curve. Serial dilutions of cDNA and a temperature gradient were used in RT-PCR in order to determine the efficiencies of all reactions and were found to be between 90 and 110% efficient. *gpd1* primers (Table S3) were used for the reference gene and data were normalized using *gpd1* primers.

For each gene (target or housekeeping) and each biological replication, ΔCt was calculated by subtracting the Ct number of the housekeeping gene from that of the target gene [15]. The ΔΔCt values were calculated using the below equation [15]:

$$\Delta\Delta\text{Ct} = \Delta\text{Ct reference} - \Delta\text{Ct target}. \quad (1)$$

The expression ratio was calculated according to the below equation:

$$\text{Ratio} = 2^{-\Delta\Delta\text{Ct}}. \quad (2)$$

3. Results

3.1. Cloning of the D-Xylulokinase Gene (xyiH) of T. reesei QM9414. The genome of wild-type *T. reesei* QM6a with approximately 34 MB was subjected to genome sequence by the US Department of Energy Joint Genome Institute [16] and is available online (http://genome.jgi-psf.org/

```
1    ATGAGTGAGG AAAAGGGGCC CCTTTACCTG GGCTTTGACC TCTCAACCCA GCAACTCAAA
           xyiH up
61   GGTCTGTCCA ACTCCCCTCC CAGCCCATCT ATACCCTCAT ATAAACCACC ACAACCTCAA
121  GGTGACAGTC CACTAACACA ACACATCACA CAACACAGCC ATCGTCGTCA ACTCCAATCT
181  CAAATCCATA GCCGAGGCCA AAGTCGACTT TGACCAAGAC TTTGGCCCCC AGTACGGCAT
241  CCAAAAGGGC GTCCACGTGC GCGAGTCCAC CGGCGAGGTC TTCGCCCCCG TCGCCCTATG
301  GCTGGAATCC CTCGACCTCG TCCTGAGCCG GCTCTCCAAG GCGATGCACC CGCTGCCCAT
361  GAGCCGCATC CGCGGCGTCA GCGGCTCCGG CCAGCAGCAC GGCGCCGTCT TCTGGAACGC
421  GAGCGCCGAG GAGCTGCTGG GCGGGCTGGA TGCGGCCAAG GGGTCGTTGG TCGAGCAGCT
481  CAGGGGCGCG CTGGCGCATG AGTTTGCGCC CAACTGGCAG GATCACAGTA CGCAGGAGGA
541  GTTGGTTGCG TTTGATGCCG AGCTCGGGGA TAGGGAGAAG CTGGCTGAGG TTACGGGCAG
601  CGGTGCCCAT CATGCAAGTC TTTCCCGGTC CCTTATGAGC TTCTCCAGTC ATCTGCTATC
661  TTCCCCCTTT TGACGCCATA TGCTAACATG AAGGACCCTC CTTGCCTTGT CGCCTTACAG
721  AGATTCACCG GCCTCCAAAT CATGCGCATC AGGCGCGTCC TCCCCCAAGT CTACGCAAAC
781  GCAAAGCGCA TCTCCCTCGT CTCCTCCTGG CTCGCCTCCG TCCTCATGGG CTCCATCGCG
841  CCCCTCGACG TCAGCGATGT CTGCGGCATG AACCTCTGGG ACATCCCTAA TCAAGCCTGG
901  AGCGAGAAGC TGCTCGCCCT CTCCGGGGGC GGCGGCCTGG ACGGCGCGGC CAACCTGCGA
961  CGGAAGCTCG GCGAGCCGCG CATGGACGGC GGCGGCTCCA TGGGCAGCAT CTCGAGGTAC
1021 TACGTGTCCA AGTACGGCTT CAGCCCGGAG TGTCAGATCA CGCCCTTCAC GGGGGACAAC
1081 CCGGCGACGA TCCTTGCGCT GCCGCTGAGG CCGCTGGATG CCATTGTTTC GCTGGGCACG
1141 TCGACGACGT TTCTGATGAA CACGCCTGCG TACAAGCCGG ATGGCTCGTA CCACTTCTTC
1201 AACCATCCCA CGACGCCCGG CAACTACATG TTCATGCTCT GCTACAAAAA CGGCGGTCTC
1261 GCGCGCGAGA AGGTGCGCGA CACCCTCCCC AAGCCCGAGG GCGGCGCCAC AGGCTGGGAG
1321 ACGTTCAATG AGGCCATCAT GGCCACGAAG CCCCTGGGCA TCGAAAGCGA CGGCGATCGC
1381 GCCAAGCTCG GGCTGTACTT TTACCTCCGG GAGACGGTGC CCAACATCCG CGCCGGAACA
1441 TGGCGCTTCA CGTGCAGGCA GGACGGCAGC GACCTGCAGG AGGCGCGCGA GGCTTGGCCC
1501 AAGGAGGCCG ACGCGCGCGC CATTGTCGAG TCGCAGGCCC TGTCCATGCG CCTGCGCTCG
1561 CAGAAGCTCG TCCACAGCCC GCGCGACGGG CTCCCCGCGC AGCCGCGGCG CATCTACGTC
1621 GTCGGCGGCG GGTCGCTGAA CCCGGCCATC ACGCGCGTGC TCGGCGAGGT GCTCGGCGGC
1681 GCCGACGGCG TGTACAAGCT CGACGTCGGG GGCAACGCGT GCGCGCTGGG CGGCGCGTAC
1741 AAGGCGCTGT GGGCGCTGGA GCGCAAGGAC GGCGAGACGT TTGACGACCT CATTGGGGGG
1801 CGGTGGACCG AGGAGGGATC CATTGACAAG GTGGACGTTG GCTATCGCGA GGGGACGTAT
1861 GAGCGGTATG GCAAGGTGCT GGGGGCGTTT GAGGAGATGG AGAGGAGGTT GCTTGCGGAG
1921 GAGGAGCACT AG
       xyiH down
```

Figure 2: The proposed D-xylulokinase gene of *T. reesei* QM6a. Exons are shown in black while introns are presented in red color.

Trire2/Trire2.home.html). Because the D-xylulokinase gene sequences of fungi are known to have high similarities, the D-xylulokinase gene sequence of *Aspergillus* was used to identify a homologous gene in *T. reesei* QM6a with high similarity (about 61% of identity) to *Aspergillus* D-xylulokinase. The length of the identified gene in *T. reesei* QM6a was 1932 bp and includes two introns and motifs for the FGGY domains identified in other D-xylulokinase genes (Figure 2). Primers (Table S3) were designed from the predicted gene sequence for *T. reesei* QM6a used to amplify a PCR product of the same size (1932 bp) as the predicted sequence. The same primers (xyiH up and xyiH down) were also used to amplify the same gene from *T. reesei* QM9414 genomic DNA and the D-xylulokinase gene of QM9414 was named *xyiH*.

3.2. Higher Xylitol Production by T. reesei Strains S6-2-2 and Δ9-5-1. *T. reesei* QM9414 protoplast transformation with the pSilent-xyiH construct (Figure 3(a)) resulted in five clones which exhibited RNA interference of the D-xylulokinase gene. In this first approach, these five clones and the parent strain *T. reesei* QM9414 were cultured in minimum medium supplemented with xylose (25 gL^{-1}) and glucose (10 gL^{-1}) as

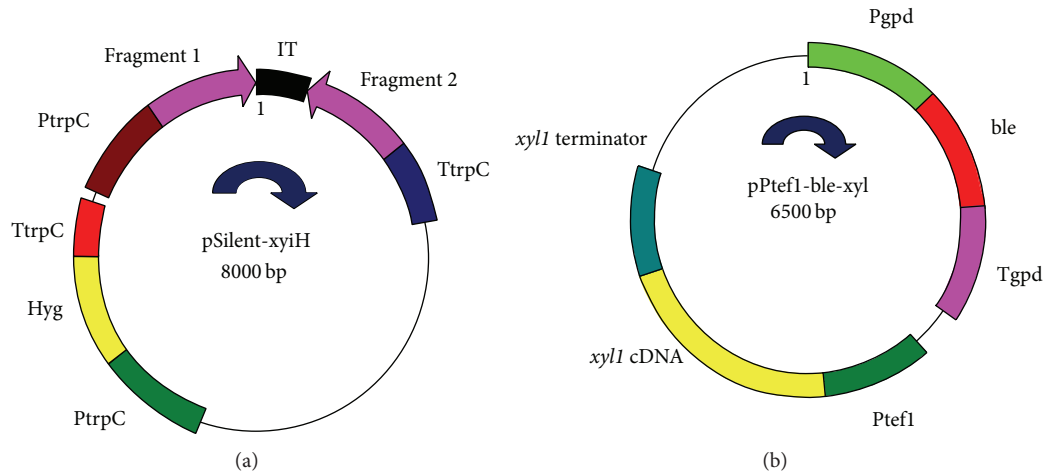

FIGURE 3: (a) The structure of pSilent-xyiH vector. PtrpC: promoter of *trpC* gene. TtrpC: terminator of *trpC* gene. Hyg: hygromycin antibiotic resistance gene. (b) The structure of pPtef1-ble-xyl vector. Pgpd: promoter of *gpd* gene. Tgpd: terminator of *gpd* gene. ble: phleomycin antibiotic resistance gene.

carbon sources. The results showed that the highest xylitol production was achieved by one of the five positive clones named S6-2-2 (data not shown). While *T. reesei* QM9414 has no detectable xylitol production, the S6-2-2 mutant strain showed xylitol production of 8.6 mM after 6 days of incubation (Figure 4(a)). However, prolonging the incubation time (days 6 to 13) did not increase the xylitol production by *T. reesei* S6-2-2.

For the second approach to increasing xylitol production by *T. reesei*, the *T. reesei* Δxdh strain was subjected to overexpression of the xylose reductase gene. The *T. reesei* xylose dehydrogenase knockout strain Δxdh produced 22.8 mM of xylitol after 12 days of incubation. Four positive clones with enhanced copies of xylose reductase gene from the *T. reesei* Δxdh strain were obtained by transferring the pPtef1-ble-xyl cassette (Figure 3(b)) into the *T. reesei* Δxdh protoplast. The four positive clones and Δxdh were cultured in minimum medium supplemented with xylose (25 gL^{-1}) and glucose (10 gL^{-1}) as the sole carbon sources. The highest xylitol production was obtained for one of the four positive clones which was named Δ9-5-1, with production of 24.8 mM after 11 days of incubation (Figure 4(b)). Our results indicated that xylitol production by our transformed strains showed a similar trend as the parent strain (Figure 4(b)).

3.3. D-Xylulokinase Activity Measurement of T. reesei S6-2-2 and QM9414 Strains. D-Xylulokinase activity was measured in *T. reesei* strains S6-2-2 and its parent strain (*T. reesei* QM9414) (Figure 5). No significant difference ($P > 0.05$) in the D-xylulokinase activities of *T. reesei* S6-2-2 and QM9414 was detected after 36 h of incubation using xylose (25 gL^{-1}) and glucose (10 gL^{-1}) as the sole carbon sources. However, lower D-xylulokinase activity was obtained for *T. reesei* S6-2-2 strain compared to *T. reesei* QM9414 after 48 h of incubation ($P < 0.05$) (Figure 5).

3.4. Xylose Reductase Activity Measurement of T. reesei Δ9-5-1 and Δxdh Strains. *T. reesei* strains including Δ9-5-1 and its parent strain Δxdh were subjected to xylose reductase activity measurement (Figure 6). Higher xylose reductase activity was obtained for the *T. reesei* Δ9-5-1 strain compared to the parent strain Δxdh using xylose (25 gL^{-1}) and glucose (10 gL^{-1}) as the sole carbon sources after 36 h and 48 h of incubation, especially after 36 h incubation ($P < 0.05$) (Figure 6).

3.5. Expression of xyiH and xyl Genes in T. reesei Strains S6-2-2 and Δ9-5-1. *T. reesei* strains including S6-2-2 and Δ9-5-1 were subjected to quantitative real-time PCR (qRT-PCR) to investigate the expression levels of *xyiH* and *xyl* genes, respectively. qRT-PCR results showed that the expression of the *xyiH* gene in S6-2-2 is much lower than QM9414 after 36 and 48 h of incubation time (Figure 7(a)). This indicated that the *xyiH* gene in the *T. reesei* S6-2-2 strain was partially silenced compared to the *xyiH* expression in the parent strain *T. reesei* QM9414. This was also confirmed by the higher xylitol production (8.6 mM) of the S6-2-2 mutant strain when compared to *T. reesei* QM9414 with no detectable xylitol production (Figure 4(a)).

Additionally, the expression of the *xyl* gene in the *T. reesei* Δ9-5-1 strain was compared to its parent strain *T. reesei* Δxdh (Figure 7(b)). Our results indicated that the expression of the *xyl* gene in Δ9-5-1 is higher than *T. reesei* Δxdh after 36 and 48 h of incubation (Figure 7(b)). These are also well in line with the results obtained for the enzyme activities experiments of the *T. reesei* strains (D-xylose reductase activities, Figure 6). This was also confirmed by the high xylitol production of the xylose reductase gene (*xyl*1) overexpressed in the *T. reesei* Δxdh strain (Δ9-5-1 strain, Figure 4(b)).

3.6. Growth Experiments of T. reesei Strains. *T. reesei* strains were grown in minimum medium containing xylose or

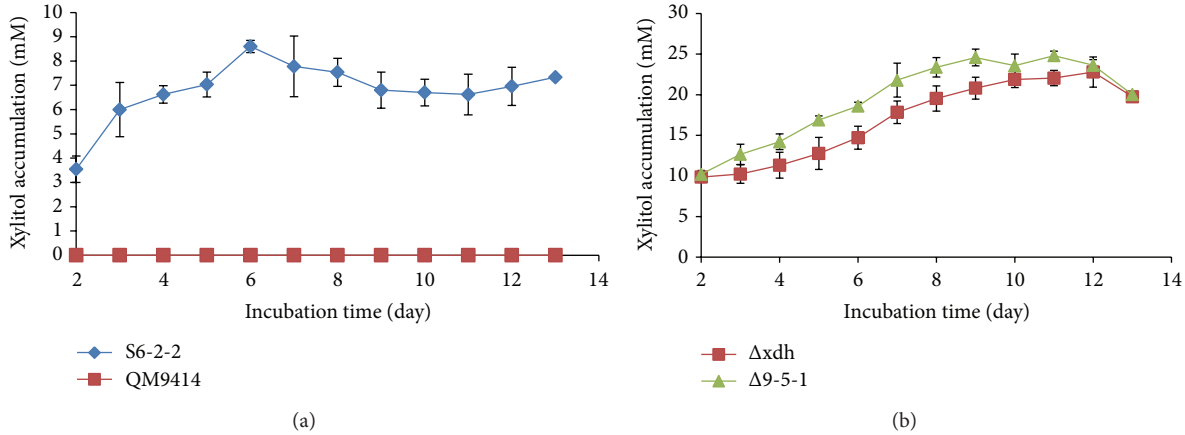

Figure 4: (a) Xylitol production by *T. reesei* QM9414 and S6-2-2. Red square represents *T. reesei* QM9414; green triangle represents *T. reesei xyiH* gene silenced strain S6-2-2. (b) Xylitol production by *T. reesei* Δxdh and Δ9-5-1 strains. Blue square represents *T. reesei xdh* gene knockout mutant Δxdh; purple triangle represents *xyl*1 gene overexpressed *T. reesei* Δ9-5-1 strain.

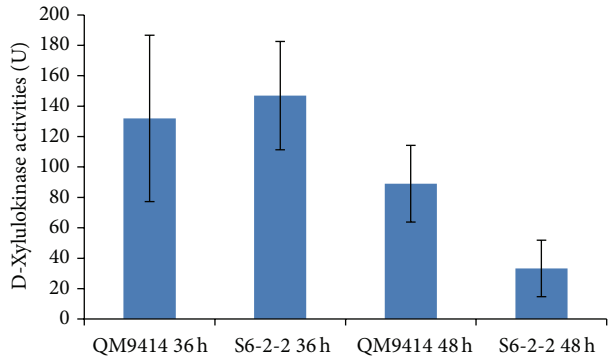

Figure 5: D-Xylulokinase activities of *T. reesei* QM9414 and S6-2-2 strains. D-Xylulokinase activities of *T. reesei* QM9414 and *T. reesei xyiH* gene silenced strain S6-2-2 were measured after 36 h and 48 h of incubation.

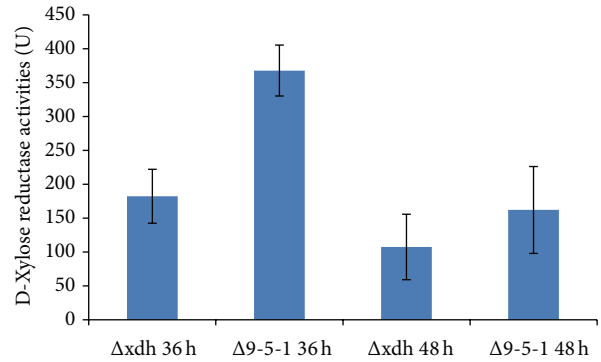

Figure 6: D-Xylose reductase activities of *T. reesei* Δxdh and Δ9-5-1 strains. Xylose reductase activities of *T. reesei xdh* gene knockout mutant Δxdh strain and *T. reesei xyl*1 gene overexpressed Δ9-5-1 strain were measured after 36 and 48 h of incubation.

glucose ($10\,gL^{-1}$) as the sole carbon sources. Our results indicated that *T. reesei* QM9414, S6-2-2, Δxdh, and Δ9-5-1 showed very similar growth patterns when glucose was used as the sole carbon source (Figure 8(a)). However, when xylose was used as the sole carbon source, *T. reesei* QM9414 grew faster than the other strains including S6-2-2, Δxdh, and Δ9-5-1 (Figure 8(b)). This could be a result of blocking of the xylose pathway in *T. reesei* S6-2-2, Δxdh, and Δ9-5-1 strains.

4. Discussion

The *T. reesei* transformants were subcultured using the antibiotic for three generations. After the third generation, genomic DNA was extracted and screened for the presence of the transformed genes using PCR. Finally, the obtained positive transformants were subjected to single spore isolation. The isolated single spores were subcultured and rescreened using gene specific primers and PCR method. Using the method, we were able to obtain stable positive transformants. Since xylose is needed for the induction and expression of *T. reesei* genes such as D-xylulokinase (*xyiH*) and D-xylose reductase (*xyl*1), cDNA should be extracted from mycelia grown using medium supplemented with xylose for the study and cloning of these genes.

Our results showed that silencing the D-xylulokinase gene in *T. reesei* was more efficient than overexpressing the xylose reductase gene (*xyl*1) with over 8 and 1.08 times xylitol production compared to levels produced by their parent strains, respectively. When D-xylulokinase gene (*xyiH*) was silenced, xylitol production increased from 0 to 8.6 mM. However, when the D-xylose reductase gene (*xyl*1) was overexpressed, xylitol production increased only marginally from 22.8 mM to 24.8 mM. This lower level of increase in xylitol production may be due to a limitation of accessible NADPH which is required for transforming xylose into xylitol. In *Candida utilis*, for example, two enzymes involved in the pentose phosphate pathway (PPP) including glucose-6-phosphate dehydrogenase and 6-phosphogluconate dehydrogenase are responsible for the production of the required NADPH [17]. A study by Ahmad et al. [5] showed that

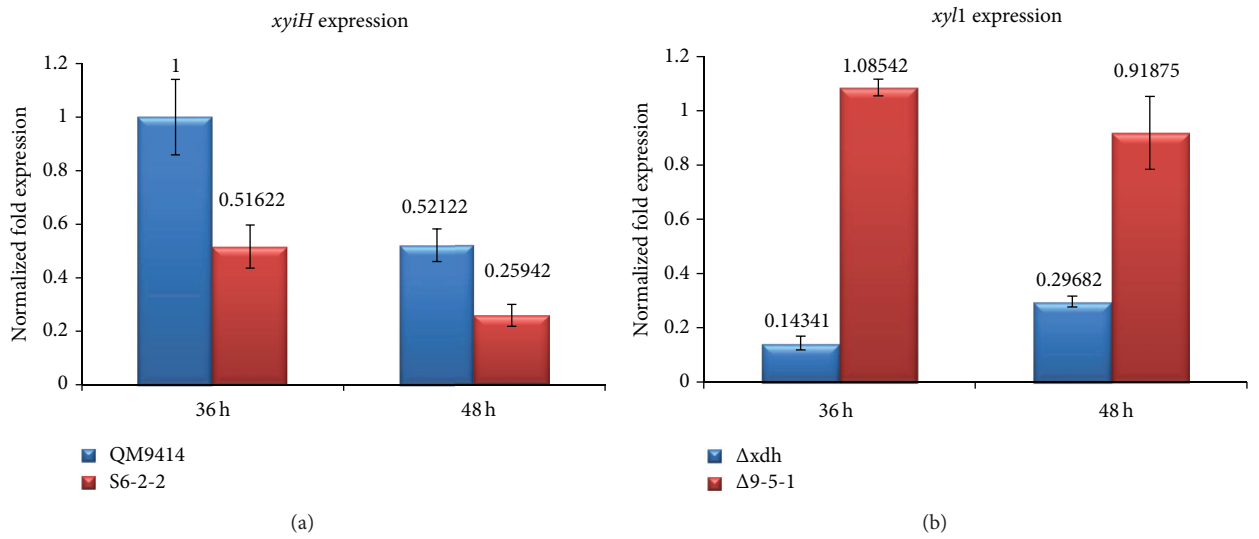

Figure 7: (a) D-Xylulokinase gene (*xyiH*) expression of *T. reesei* QM9414 and S6-2-2. D-Xylulokinase gene (*xyiH*) expression was measured after 36 and 48 h of incubation. (b) D-Xylose reductase gene (*xyl*1) expression of *T. reesei* Δxdh and Δ9-5-1. D-Xylose reductase gene (*xyl*1) expression was measured after 36 and 48 h of incubation.

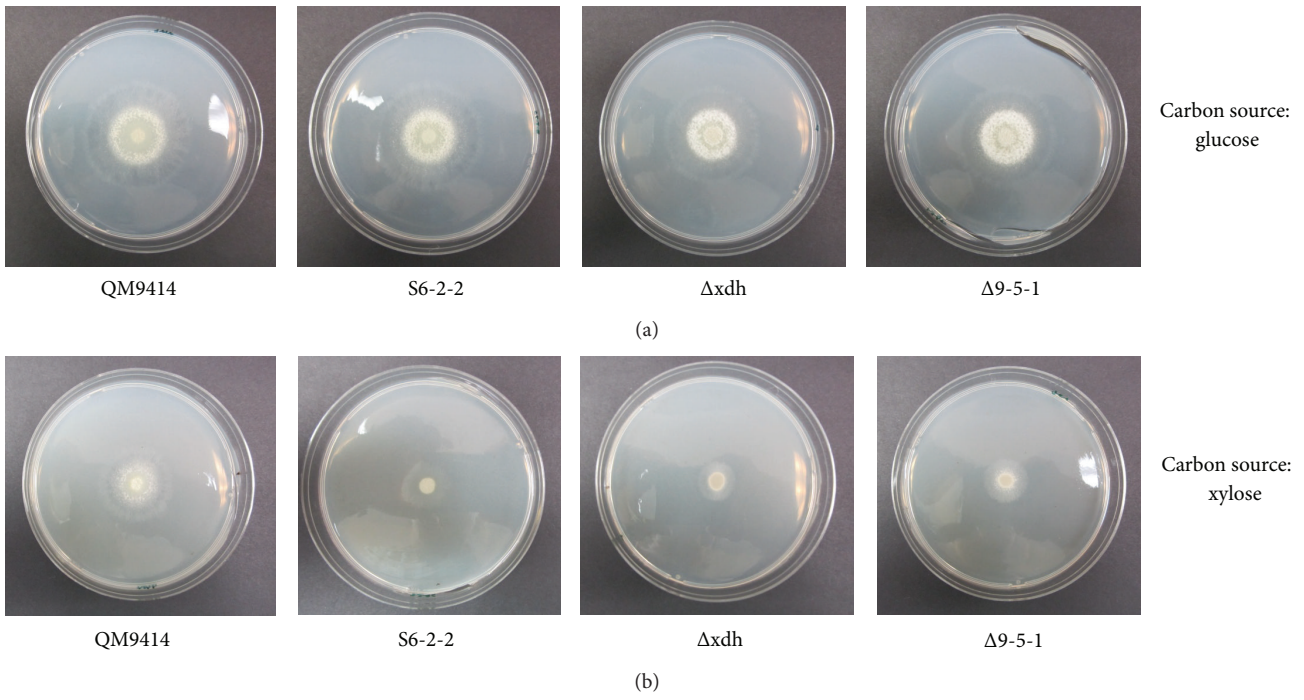

Figure 8: Growth of *T. reesei* QM9414, S6-2-2, Δxdh, and Δ9-5-1 using glucose (a) or xylose (b) as the sole carbon sources, respectively. S6-2-2: *T. reesei xyiH* gene silenced strain; Δxdh: *T. reesei xdh* gene knockout mutant strain; Δ9-5-1: *xyl* gene overexpressed *T. reesei* Δxdh strain.

overexpression of these two enzymes led to an increase in xylitol production in *Candida tropicalis*.

Although xylitol production by *T. reesei* is not as high as that reported in yeast, the advantage of *T. reesei* is their ability to use biomass directly. Yeastscan only use biomass hydrolysates to produce xylitol or to ferment biomass with other microorganisms to produce xylitol. In contrast, genetically engineered *T. reesei* strains can use biomass directly to produce xylitol [18]. Additionally, *T. reesei* grows rapidly and there is no need for strict control of growth conditions, ultimately lowering xylitol production costs compared to the use of yeast strains. Additional improvements to improve

xylitol production by *T. reesei* can be made,including genetic engineering of several genes in xylose metabolic pathway simultaneously; adjustment of fermentation conditions like carbon sources, nitrogen sources, and trace elements; and employing biomass directly to produce xylitol.

5. Conclusion

By using RNA interference of D-xylulokinase gene or overexpression of xylose reductase gene based on xylitol dehydrogenase knockout strain, two *T. reesei* strains S6-2-2 and Δ9-5-1 were obtained in this study. The genetically modified strains obtained have potential applications for industrial xylitol production.

Conflict of Interests

The authors declare that there is no conflict of interests regarding the publication of this paper.

Acknowledgments

The authors thank Dr. Irina Druzhinina, Dr. Tianhong Wang, and Dr. Bernhard Seiboth for providing strain *T. reesei QM6a*, *T. reesei* QM9414, and *T. reesei* Δxdh, respectively.

References

[1] T. Pepper and P. M. Olinger, "Xylitol in sugar-free confections," *Food Technology*, vol. 42, pp. 98–106, 1988.

[2] E. Winkelhausen and S. Kuzmanova, "Microbial conversion of D-xylose to xylitol," *Journal of Fermentation and Bioengineering*, vol. 86, no. 1, pp. 1–14, 1998.

[3] H. Horitsu, Y. Yahashi, K. Takamizawa, K. Kawai, T. Suzuki, and N. Watanabe, "Production of xylitol from D-xylose by *Candida tropicalis*: optimization of production rate," *Biotechnology and Bioengineering*, vol. 40, no. 9, pp. 1085–1091, 1992.

[4] K. Karhumaa, R. G. Sanchez, B. Hahn-Hägerdal, and M.-F. Gorwa-Grauslund, "Comparison of the xylose reductase-xylitol dehydrogenase and the xylose isomerase pathways for xylose fermentation by recombinant *Saccharomyces cerevisiae*," *Microbial Cell Factories*, vol. 6, article 5, 2007.

[5] I. Ahmad, W. Y. Shim, W. Y. Jeon, B. H. Yoon, and J.-H. Kim, "Enhancement of xylitol production in *Candida tropicalis* by co-expression of two genes involved in pentose phosphate pathway," *Bioprocess and Biosystems Engineering*, vol. 35, no. 1-2, pp. 199–204, 2012.

[6] B. S. Ko, D.-M. Kim, B. H. Yoon et al., "Enhancement of xylitol production by attenuation of intracellular xylitol dehydrogenase activity in *Candida tropicalis*," *Biotechnology Letters*, vol. 33, no. 6, pp. 1209–1213, 2011.

[7] J. Hallborn, M. Walfridsson, U. Airaksinen et al., "Xylitol production by recombinant *Saccharomyces cerevisiae*," *Biotechnology*, vol. 9, no. 11, pp. 1090–1095, 1991.

[8] B. Seiboth, C. Gamauf, M. Pail, L. Hartl, and C. P. Kubicek, "The D-xylose reductase of *Hypocrea jecorina* is the major aldose reductase in pentose and D-galactose catabolism and necessary for β-galactosidase and cellulase induction by lactose," *Molecular Microbiology*, vol. 66, no. 4, pp. 890–900, 2007.

[9] R. Lunzer, Y. Mamnun, D. Haltrich, K. D. Kulbe, and B. Nidetzky, "Structural and functional properties of a yeast xylitol dehydrogenase, a Zn^{2+}-containing metalloenzyme similar to medium-chain sorbitol dehydrogenases," *Biochemical Journal*, vol. 336, no. 1, pp. 91–99, 1998.

[10] T. H. Wang, Y. H. Zhong, W. Huang, T. Liu, and Y. W. You, "Antisense inhibition of xylitol dehydrogenase gene, xdh1 from *Trichoderma reesei*," *Letters in Applied Microbiology*, vol. 40, no. 6, pp. 424–429, 2005.

[11] L. Hartl, C. P. Kubicek, and B. Seiboth, "Induction of the gal pathway and cellulase genes involves no transcriptional inducer function of the galactokinase in *Hypocrea jecorina*," *Journal of Biological Chemistry*, vol. 282, no. 25, pp. 18654–18659, 2007.

[12] R. H. W. Maas, J. Springer, G. Eggink, and R. A. Weusthuis, "Xylose metabolism in the fungus Rhizopus oryzae: effect of growth and respiration on L(+)-lactic acid production," *Journal of Industrial Microbiology and Biotechnology*, vol. 35, no. 6, pp. 569–578, 2008.

[13] C. Guo, P. He, D. Lu, A. Shen, and N. Jiang, "Cloning and molecular characterization of a gene coding D-xylulokinase (CmXYL3) from *Candida maltosa*," *Journal of Applied Microbiology*, vol. 101, no. 1, pp. 139–150, 2006.

[14] E. Szewczyk, T. Nayak, C. E. Oakley et al., "Fusion PCR and gene targeting in *Aspergillus nidulans*," *Nature protocols*, vol. 1, no. 6, pp. 3111–3120, 2006.

[15] J. S. Yuan, A. Reed, F. Chen, and C. N. Stewart Jr., "Statistical analysis of real-time PCR data," *BMC Bioinformatics*, vol. 7, article 85, 2006.

[16] D. Martinez, R. M. Berka, B. Henrissat et al., "Genome sequencing and analysis of the biomass-degrading fungus Trichoderma reesei (syn. Hypocrea jecorina)," *Nature Biotechnology*, vol. 26, no. 5, pp. 553–560, 2008.

[17] P. M. Bruinenberg, J. P. Van Dijken, and W. A. Scheffers, "An enzymic analysis of NADPH production and consumption in *Candida utilis*," *Journal of General Microbiology*, vol. 129, no. 4, pp. 965–971, 1983.

[18] M. Dashtban, G. Kepka, B. Seiboth, and W. Qin, "Xylitol production by genetically engineered trichoderma reesei strains using barley straw as feedstock," *Applied Biochemistry and Biotechnology*, vol. 169, no. 2, pp. 554–569, 2013.

Hindawi Publishing Corporation
BioMed Research International
Volume 2014, Article ID 435631, 8 pages
http://dx.doi.org/10.1155/2014/435631

Research Article

Particulate Size of Microalgal Biomass Affects Hydrolysate Properties and Bioethanol Concentration

Razif Harun,[1,2] Michael K. Danquah,[3] and Selvakumar Thiruvenkadam[2]

[1] *Department of Chemical Engineering, Monash University, Clayton, VIC 3800, Australia*
[2] *Department of Chemical and Environmental Engineering, Universiti Putra Malaysia, 43400 Serdang, Malaysia*
[3] *Department of Chemical and Petroleum Engineering, Curtin University of Technology, 98009 Sarawak, Malaysia*

Correspondence should be addressed to Razif Harun; mh_razif@upm.edu.my

Received 28 February 2014; Revised 3 May 2014; Accepted 6 May 2014; Published 29 May 2014

Academic Editor: Rajeev Kumar

Effective optimization of microalgae-to-bioethanol process systems hinges on an in-depth characterization of key process parameters relevant to the overall bioprocess engineering. One of the such important variables is the biomass particle size distribution and the effects on saccharification levels and bioethanol titres. This study examined the effects of three different microalgal biomass particle size ranges, $35\,\mu\text{m} \le x \le 90\,\mu\text{m}$, $125\,\mu\text{m} \le x \le 180\,\mu\text{m}$, and $295\,\mu\text{m} \le x \le 425\,\mu\text{m}$, on the degree of enzymatic hydrolysis and bioethanol production. Two scenarios were investigated: single enzyme hydrolysis (cellulase) and double enzyme hydrolysis (cellulase and cellobiase). The glucose yield from biomass in the smallest particle size range ($35\,\mu\text{m} \le x \le 90\,\mu\text{m}$) was the highest, 134.73 mg glucose/g algae, while the yield from biomass in the larger particle size range ($295\,\mu\text{m} \le x \le 425\,\mu\text{m}$) was 75.45 mg glucose/g algae. A similar trend was observed for bioethanol yield, with the highest yield of 0.47 g EtOH/g glucose obtained from biomass in the smallest particle size range. The results have shown that the microalgal biomass particle size has a significant effect on enzymatic hydrolysis and bioethanol yield.

1. Introduction

The utilization of microalgae to produce a variety of products such as fine organic chemicals, food, animal feed, and food supplements have been discovered in the past [1–3]. Current interest has been on the development of biofuels, such as bioethanol, from microalgae as a nonedible feedstock. Aside from its renewable and sustainable benefits, the high carbohydrate composition of microalgal biomass can be converted to fermentable sugars for microbial conversion to bioethanol [4, 5]. One of such biomass saccharification methods is via enzymatic hydrolysis.

Enzymatic hydrolysis is a well-established process and provides mild operating conditions, high sugar yields, high selectivity, and minimal by-products formation [6, 7], hence a more preferred method of hydrolyzing fermentation substrates. However, process conditions and parameters during enzymatic hydrolysis require detailed optimization for maximum product conversion. One of the important parameters that influence the effectiveness of enzymatic hydrolysis is biomass particle size. Fundamentally, smaller particle size biomass presents a large specific surface area, thus increasing the contact areas between the enzymes and the interparticle bonding of the material during the hydrolysis process [8].

Previous attention has been focused on the effect of particle size on enzymatic hydrolysis of either cellulosic (such as cotton, plant, and fibers) or lignocellulosic biomass (such as corn, sugarcane, and wheat). Pedersen and Meyer [9] reported that smaller biomass particle size (53–149 μm) increased glucose release up to 90% after 24 h hydrolysis of wheat straw biomass. The finding was in accordance with those reported by Dasari and Eric Berson [10] and Carvalho et al. [11] who used sawdust and lemon, respectively, as hydrolysis substrates. Biomass particulate size reduction also results in enhancing the hydrolysis rate [10, 12]. This can be explained by the easy access to enzyme active sites by smaller biomass particles. Contrary to this, Ballesteros et al. [13, 14] have reported that larger particle size biomass significantly

increases hydrolysis rates and sugar recoveries (particularly glucose) compared to smaller particle size biomass. These conflicting views call for further studies on the characteristic effects of biomass particle size on the degree and effectiveness of enzymatic hydrolysis. To the best of our knowledge, no similar work has been performed on the carbohydrates of microalgae biomass and the concomitant effect on bioethanol yields. Therefore, this study aims to investigate the effect of particle size on enzymatic hydrolysis of microalgal biomass. The glucose yields and the physical properties of the substrate during the hydrolysis process are examined and discussed. Also, the kinetic investigation of enzyme hydrolysis and the effects on glucose and bioethanol yields are presented.

2. Materials and Methods

2.1. Substrate Preparation. Culture samples of *Chlorococcum infusionum* obtained from Bio-fuels Pty Ltd (Victoria, Australia) were centrifuged (Heraeus Multifuge 3 S-R, Germany) at 4500 × g for 10 mins and the supernatant was discarded. The microalgal cake was dried in a laboratory oven at 60°C for 24 h (Model 400, Memmert, Germany). The dried biomass was pulverized for 1 min using a hammer mill (N.V Tema, Germany). The different particle sizes were separated by passing the milled sample through a series of cascaded stainless steel sieves (until the desired biomass sizes were partitioned in the following ranges: $35\,\mu\text{m} \leq x \leq 90\,\mu\text{m}$, $125\,\mu\text{m} \leq x \leq 180\,\mu\text{m}$, and $295\,\mu\text{m} \leq x \leq 425\,\mu\text{m}$). The samples were stored at room temperature before further analysis.

2.2. Enzyme Activity. The enzymes used in this study were cellulase from *Trichoderma reesei* (ATCC 26921) and cellobiase from *Aspergillus niger* (Novozyme 188), purchased from Sigma Aldrich, Australia. The activity of cellulase measured at 1.0 units/mg solid means that one unit of cellulase liberates 1.0 μmol of glucose from cellulose in 1 h at pH 5.0. The cellobiase activity was determined as 250 units/mg.

2.3. Enzymatic Hydrolysis. Varying quantities of microalgal biomass in powder form (0.2–1.0 g) within three different particle size ranges $35\,\mu\text{m} \leq x \leq 90\,\mu\text{m}$, $125\,\mu\text{m} \leq x \leq 180\,\mu\text{m}$, and $295\,\mu\text{m} \leq x \leq 425\,\mu\text{m}$ were loaded with a constant cellulase mass of 20 mg and a cellobiase volume of 1.0 mL. The samples were hydrolysed in shake flasks with 10 mM of 100 mL sodium acetate buffer at pH 4.8 and were placed in an incubator (LH Fermentation Ltd., Buckinghamshire, England) at 40°C for 48 h with 200 RPM agitation. Samples were taken at 5 h intervals and the enzymatic hydrolysis process was halted by heating the hydrolysate to ~90°C for 10 min. The samples were then cooled to room temperature and stored in a freezer at −75°C (Ultraflow freezer, Plymouth, USA) for further analysis.

2.4. Bioethanol Production. *Saccharomyces cerevisiae*, purchased from Lalvin, Winequip Products Pty Ltd. (Victoria, Australia), was used in the microbial fermentation process for bioethanol production. The culture was prepared by dissolving 5.0 g of dry yeast powder in 50 mL sterile warm water (~40°C) and the pH was adjusted to 7 by 1 M NaOH addition. The yeast was cultured in YDP medium with composition in g/L given as follows: 10 g yeast extract, 20 g peptone, and 20 g glucose. The yeast was harvested after 24 h and washed to eliminate the sugars then transferred into 500 mL Erlenmeyer flask containing 100 mL of the sugar-containing liquid medium obtained after the hydrolysis process. The flasks were tightly sealed and nitrogen gas was bubbled through to create an oxygen-free environment for bioethanol production. The flasks were incubated at 30°C under 200 RPM shaking. The pH was maintained at 7 by adding 1 M NaOH solution. The fermentation continued for 50 h and samples for analysis were taken after every 4 h.

2.5. Chemical Analysis. The biomass was pretreated using a sonicator to break down the cell walls. Phenol-sulphuric acid method was used to quantify the total carbohydrate in the biomass. Note that Table 1 is a presaccharification data, presenting the existence of different carbohydrate forms entrapped in the microalgae system. Microalgal biomass and the hydrolysate compositions were analyzed by HPLC using a 250 mm × 4.6 mm Prevail Carbohydrate ES Column. The HPLC system consists of the following accessory instruments: a detector (ELSD, Alltech 3300), quaternary gradient pump (Model 726, Alltech), degasser (Model 591500M Elite degassing system, Alltech), autosampler (Model 570, Alltech), and system controller (Model 726300M, Alltech). The mobile phase was a mixture of acetonitrile and water (85 : 15) and the operating flow rate was 1 mL/min. 30 μL sample was injected at 50°C. The sample was filtered through a 13 mm membrane filter prior to injection. The sugar concentrations were evaluated using a calibration curve generated from HPLC-grade sugars.

The ethanol concentration was analyzed using gas chromatography (GC) (Model 7890A, Agilent, USA). The GC unit consists of an autosampler, flame ion detector (FID), and HP-FFAP column (50 m × 0.20 mm × 0.33 μm). The injector, detector, and oven temperatures were maintained at 150°C, 200°C, and 120°C, respectively. Nitrogen gas was used as the carrier gas. The bioethanol concentration was quantified using a calibration curve prepared by injecting different concentrations of a standard ethanol (0.1–10% v/v).

2.6. Fourier Transform Infrared Spectroscopy (FTIR). The polymorphs of the resulting hydrolysate from the hydrolysis process were determined by FTIR. FTIR spectra of hydrolysed samples were recorded on a Nicolet 6700 FTIR (Fischer Scientific, Australia) equipped with Thermo Scientific iD3 ATR accessory (Fischer Scientific, Australia), and the spectra were run and processed with OMNIC software (Version 7.0 ThermoNicolet). The dried hydrolysis samples were loaded on the sample holder and the spectrum was recorded at an average of 32 scans with a spectral resolution of 4 cm^{-1} from 400 to 4000 cm^{-1}. Sample spectra were recorded as absorbance values at each data point in triplicates.

Table 1: Biomass composition of the microalgal species.

Component	Composition (% w/w)
Total carbohydrate	32.52
Xylose	9.54
Mannose	4.87
Glucose	15.22
Galactose	2.89
Starch	11.32
Others*	56.16

*Lipids, protein, and ash.

2.7. Viscosity Measurement. The hydrolysate viscosities were determined using a modular advanced rheometer system (Haake Mars, Thermo Electron Corp., Germany). The system is equipped with a stainless steel measuring plate (MP 660, 60 mm) and a rotor (PP60H, 60 mm). The temperature was set to 30°C, the frequency was maintained at 1.5 Hz, and the gap between the parallel plates was kept at 1 mm. The hydrolysed samples were measured for 5 min at different shear rates ranging from 50 to 500 s^{-1}.

3. Results and Discussion

3.1. Substrate Carbohydrate Composition. According to Table 1, carbohydrate constitutes up to 32% of the dry weight of *C. infusionum* biomass with the major fermentable sugar component being glucose (15.2%), followed by xylose (9.5%), mannose (4.9%), and galactose (2.9%). This strain also contains starch at 11.3% dry weight. The total carbohydrates present in the biomass could be made available for bioethanol production under optimal saccharification and microbial fermentation conditions. The remaining biomass composition could represent lipids, protein, and ash that is available in microalgal strain. Unlike both red and brown algae, the cell wall of most green algae has high cellulose content, ranging up to 70% of the dry weight [15, 16]. The composition of the carbohydrate content in the unicellular microalgal specie per unit mass does not vary greatly among fractions of different particle size. For intact microalgae cells, the carbohydrates are well distributed within the cell membrane and this gives a uniform carbohydrate composition in the membrane.

3.2. FTIR Analysis. The spectra of hydrolyzed biomass with different particle sizes were examined using FTIR techniques and the results are shown in Figure 1. Two types of hydrolysates were compared in this study: single enzyme hydrolysate with only cellulase and double enzyme hydrolysate with both cellulase and cellobiase. These two scenarios are denoted by Case 1 and Case 2, respectively. The FTIR spectra represent samples taken at the end of the hydrolysis process. The spectrum of nonpretreated powdered microalgae within the size range of 295 $\mu m \leq x \leq 425$ μm was analyzed for comparison. According to Murdock and Wetzel [17], the reference absorption peaks for major

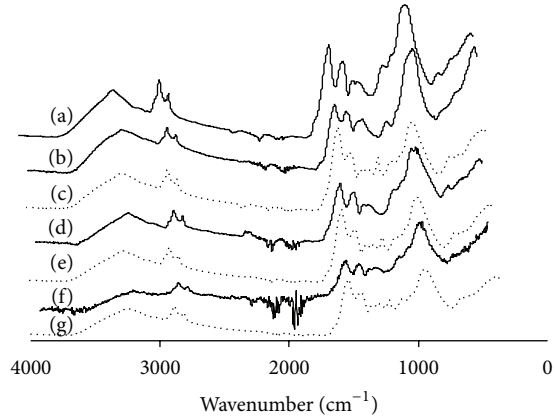

Figure 1: FTIR spectra for microalgal biomass with different particle sizes under different Cases. (a) Nonpretreated microalgal biomass (original powdered sample); Case 1 (cellulase only): (b) 35 $\mu m \leq x \leq 90$ μm, (d) 125 $\mu m \leq x \leq 180$ μm, and (f) 295 $\mu m \leq x \leq 425$ μm; Case 2 (cellulase + cellobiase): (c) 35 $\mu m \leq x \leq 90$ μm, (e) 125 $\mu m \leq x \leq 180$ μm, and (g) 295 $\mu m \leq x \leq 425$ μm.

microalgal compositions are ~1100–900 cm^{-1} for polysaccharides (cellulose and starch), ~2970–2850 cm^{-1} for lipids, and 1750–1500 cm^{-1} for proteins and carboxylic groups. Since we wish to convert complex carbohydrates in the biomass to produce fermentable sugars for bioethanol production, only polysaccharide peaks are of interest. The microalgal biomass used in this study showed a relatively high amount of polysaccharides since a strong absorption peak was recorded around 1100 cm^{-1} to 1000 cm^{-1} in the powdered microalgal sample as summarized in Figure 1. It was observed that the degree of polysaccharides absorption decreased as the biomass particle size decreased. This indicates that more polysaccharides were converted to fermentable sugars in the case of biomass with smaller particle size during the hydrolysis process. Based on the individual spectrum, sugar conversions were calculated by referring to the peak heights of nonpretreated samples. The hydrolysis of cellulose with the addition of cellobiase (Case 2) generated hydrolysis conversion of 90, 78, and 64% of the biomass in the particle size ranges 35 $\mu m \leq x \leq 90$ μm, 125 $\mu m \leq x \leq 180$ μm, and 295 $\mu m \leq x \leq 425$ μm, respectively. A lower degree of hydrolysis was observed without cellobiase addition (Case 1) of 41, 29, and 18% for biomass in the particle size ranges 35 $\mu m \leq x \leq 90$ μm, 125 $\mu m \leq x \leq 180$ μm, and 295 $\mu m \leq x \leq 425$ μm, respectively. Cellulase contains cellobiohydrolases, endoglucanases, and β-glucosidase that function to efficiently hydrolyse cellulose. The hydrolysis of cellulose to cellobiose is the rate-limiting step, and this limitation is resolved by cellobiohydrolases which hydrolyse cellulose to cellobiose and cellotriose. However, the small amount of β-glucosidase in cellulase hinders the cellulolysis process; hence, the addition of β-glucosidase helps cellulase to hydrolyse the intermediate product, cellobiose, to form glucose in a faster reaction time while minimizing product inhibition during the cellulolytic process [18–25]. Furthermore, the kinetics of molecular activation drawdown is faster in the double enzyme case

and this favors forward production of fermentable subunits during the hydrolysis process. The total crystallinity index (TCI) of the hydrolyzed biomass was calculated as reported by Nelson and O'Connor [19]. From the calculations, the TCI of all the hydrolysed samples decreased when compared with the nonhydrolysed biomass. Decreasing biomass crystallinity has been reported to increase enzymatic hydrolysis rates [26]. Although the polysaccharides were degraded during hydrolysis, FTIR spectra analysis showed that the structure of the hydrolysed monomers remained intact for bioethanol production.

3.3. Glucose Yield. Table 2 shows the yield of glucose for different assays. The rate of glucose release was rapid at the beginning of hydrolysis and slowed down until the end of the hydrolysis process. This profile is typical of batch hydrolysis [9]. Note that the enzymes involved in the study are not hydrolysing starch composition thus not accounted for potential glucose for the fermentation process. It was found that biomass with smaller particle size generated higher glucose yields and this observation was the same for both Case 1 and Case 2. The highest glucose yields were 75.45 mg/g biomass and 134.73 mg/g biomass for Cases 1 and 2, respectively, for biomass in the smallest particle size range of $35\,\mu\text{m} \leq x \leq 90\,\mu\text{m}$. The lowest glucose yields were 26.01 mg/g biomass and 61.55 mg/g biomass for Cases 1 and 2, respectively, for biomass in the largest particle size range of $295\,\mu\text{m} \leq x \leq 425\,\mu\text{m}$. Smaller biomass particle size increases the interactions with the enzymes during hydrolysis due to the presence of a large exposed surface area [12]. Hence, smaller microalgal biomass particle size is required to achieve higher glucose yield. The amount of microalgal biomass loaded in the hydrolysis process also showed a significant effect on glucose yields. Although the same microalgal biomass particle size was used in assay numbers 1, 2, and 3, different glucose yields of 111.08 mg/g biomass, 125.77 mg/g biomass, and 134.73 mg/g biomass were achieved. When examining the effect of different substrate concentrations on glucose yield within the same particle size range in Case 2, it was found that the glucose yield increased with increasing substrate concentration. This trend was however not observed in Case 1 containing cellulose enzyme. Therefore, high yield of glucose from increasing substrate concentration is dependent on the balanced composition of cellulosic enzyme components to minimize product inhibition [27]. Furthermore, a significant increase in glucose yield was observed when the second enzyme (cellobiase) was introduced to the assays (Case 2). The glucose yields in Case 2 were almost the double compared to those obtained in Case 1. From the collision theory perspective, the kinetics of molecular activation drawdown is faster in the double enzyme case and this favors forward production of fermentable subunits. The kinetics of this double enzyme effect is demonstrated with the scheme below.

Mechanism of enzymatic hydrolysis of cellulase, Case 1:

$$S + E \underset{k_{-1}}{\overset{k_1}{\Longleftrightarrow}} \text{SE} \xrightarrow{k_2} P + E, \tag{1}$$

where S is the substrate concentration, E is the enzyme concentration, SE is the concentration of substrate-enzyme complex, P is the product concentration, and k_1, k_{-1}, k_2 are rate constants.

The rates of change in SE concentration and product formation are

$$\frac{d\text{SE}}{dt} = k_1 S \times E - k_{-1}\text{SE} - k_2\text{SE}, \tag{2}$$

$$\frac{dP}{dt} = k_2\text{SE}. \tag{3}$$

For substrate mass balance, the substrate concentration (S) is written as

$$S = S_o - \text{SE} - P. \tag{4}$$

Substituting (4) into (2) gives

$$\frac{d\text{SE}}{dt} = k_1 \left(S_0 - \text{SE} - P\right) \times E - k_{-1}\text{SE} - k_2\text{SE}. \tag{5}$$

Applying equilibrium and steady state conditions to (5) gives

$$\text{SE} = \frac{\left(S_0 - P\right) E}{K_e + E}, \tag{6}$$

where K_e is the equilibrium constant

$$K_e = \frac{k_{-1} + k_2}{k_1}. \tag{7}$$

The simplified equation (6) may be written as follows at initial conditions:

$$\left(\frac{dP}{dt}\right)_{P_0} = \frac{k_2\ S_0\ E_0}{K_e + E_0}, \tag{8}$$

where $(dP/dt)_{P_0}$ denotes the product formation at the initial conditions.

The mechanism of the enzymatic hydrolysis of cellulase (E_1) and cellobiase (E_2), Case 2, is

$$\begin{aligned} S_C + E_1 &\underset{k_{-1}}{\overset{k_1}{\Longleftrightarrow}} S_C E_1 \xrightarrow{k_2} S_{CB} + E_1, \\ S_{CB} + E_2 &\underset{k'_{-1}}{\overset{k'_1}{\Longleftrightarrow}} S_{CB} E_2 \xrightarrow{k'_2} P + E_2, \end{aligned} \tag{9}$$

where S_C, S_{CB}, and P are concentrations of cellulose, cellobiose, and glucose, respectively.

By following the same procedure as in Case 1, simplified equation for Case 2 at the initial conditions is

$$\left(\frac{dP}{dt}\right)_{P_0} = \frac{k'_2 E_2 \left(S_{C_0} - S_C E_{1_0} - S_{CB_0}\right)}{K'_e + E_{2_0}}, \tag{10}$$

$$K'_e = \frac{k'_2 + k'_{-1}}{k'_1}, \tag{11}$$

Table 2: Yield of glucose released after 48 h of hydrolysis.

Assay number	Particle size, μm	Algae loading, g/L	mg glucose/g algal biomass	
			Cellulase (Case 1)	Cellulase + cellobiase (Case 2)
1	$35 \le x \le 90$	25	54.21	111.08
2	$35 \le x \le 90$	50	44.48	125.77
3	$35 \le x \le 90$	100	75.45	134.73
4	$125 \le x \le 180$	25	30.24	68.79
5	$125 \le x \le 180$	50	27.96	85.88
6	$125 \le x \le 180$	100	27.63	114.54
7	$295 \le x \le 425$	25	26.01	68.79
8	$295 \le x \le 425$	50	26.43	92.61
9	$295 \le x \le 425$	100	30.24	102.29

where k_1', k_{-1}', and k_2' are rate constants and K_e' is the equilibrium constant.

Equations (8) and (10) can be rewritten as follows.

For Case 1,

$$\frac{1}{v} = \frac{K_e}{V_0}\left[\frac{1}{S_o}\right] + \frac{1}{V_0}, \tag{12}$$

where

$$V_0 = k_2 E. \tag{13}$$

For Case 2,

$$\frac{1}{v} = \frac{K_e'}{V_0'}\left[\frac{1}{S_{\mathrm{CB}}}\right] + \frac{1}{V_0'}, \tag{14}$$

where

$$V_0' = k_2'\left(E_T - S_C E_1\right). \tag{15}$$

From the mathematical derivation, K_m which is the equilibrium constant is K_e for Case 1 and K_e' for Case 2. Also, $V_{\max}$ which is the maximum forward velocity is $1/V_0$ for Case 1 and $1/V_0'$ for Case 2, where V_0 and V_0' occur at their respective initial enzyme concentration. As can be seen in Table 3, Lineweaver-Burk plot analysis of (12) and (14) shows that the K_m value for Case 1 is higher than Case 2 and the $V_{\max}$ value for Case 1 is lower than Case 2. The lower value of K_m and the higher value of $V_{\max}$ obtained from Case 2 confirm that the introduction of cellobiase significantly increases the combined enzyme-substrate affinity and the hydrolysis rate.

Table 3: K_m and $V_{\max}$ for hydrolysis of cellulose by cellulase (Case 1) and cellulase + cellobiase (Case 2).

Case number	Enzyme	Hydrolysis of cellulose	
		K_m	$V_{\max}$
1	Cellulase	18.81	35.05
2	Cellulase + cellobiase	18.23	135.83

3.4. Ethanol Yield. The produced hydrolysates were used as substrates in *Saccharomyces cerevisiae* fermentations for bioethanol production. This yeast strain has widely been utilized for bioethanol production because it is easy to culture and has a high ethanol tolerance. This could allow fermentation to continue under 16-17% v/v ethanol concentrations [28]. Figure 2 shows the bioethanol yields for both Cases 1 and 2 using biomass with different particle sizes. The trend in bioethanol yield for the different particle size biomass was in agreement with the glucose yields; biomass with smaller particle size displayed higher glucose concentrations to generate higher bioethanol yields. It can be observed that available glucose in the hydrolysate was completely consumed after 48 h of fermentation. The highest bioethanol yield of 0.47 g ethanol/g glucose was obtained when hydrolysed under Case 2 with the smallest particle size biomass ($35\,\mu\mathrm{m} \le x \le 90\,\mu\mathrm{m}$) at 100 g/L microalgae concentration, whereas the lowest bioethanol yield of 0.05 g ethanol/g glucose was obtained when hydrolysed under Case 1 with the largest particle size biomass ($295\,\mu\mathrm{m} \le x \le 425\,\mu\mathrm{m}$) at 25 g/L microalgae concentration. Assays in Case 2 produced up to 50% more bioethanol yields than the assays in Case 1, reaching a maximum bioethanol yield of 0.47 g/g glucose compared to 0.19 g/g glucose, as represented by assay number 3 in both cases. Hydrolysate produced in the presence of cellobiase generated higher bioethanol yields due to the presence of high glucose concentrations.

3.5. Viscosity Analysis. The purpose of the viscosity study is to understand the influence of the rheological properties of the hydrolysate during hydrolysis and how this affects the fermentation process for bioethanol production. The viscosity measurements were performed under different shear rates ($50–500\ \mathrm{s}^{-1}$) using hydrolysates obtained from biomass with different particle sizes for an equivalent substrate concentration of 100 g/L. Figure 3 shows the viscosity data of the different particle size biomass for both Cases 1 and 2 with samples taken after the hydrolysis process. A decreasing trend of viscosity was observed with increasing shear rate and biomass with smaller particle sizes displaying higher viscosities. For biomass in the same particle size range, Case 2 showed

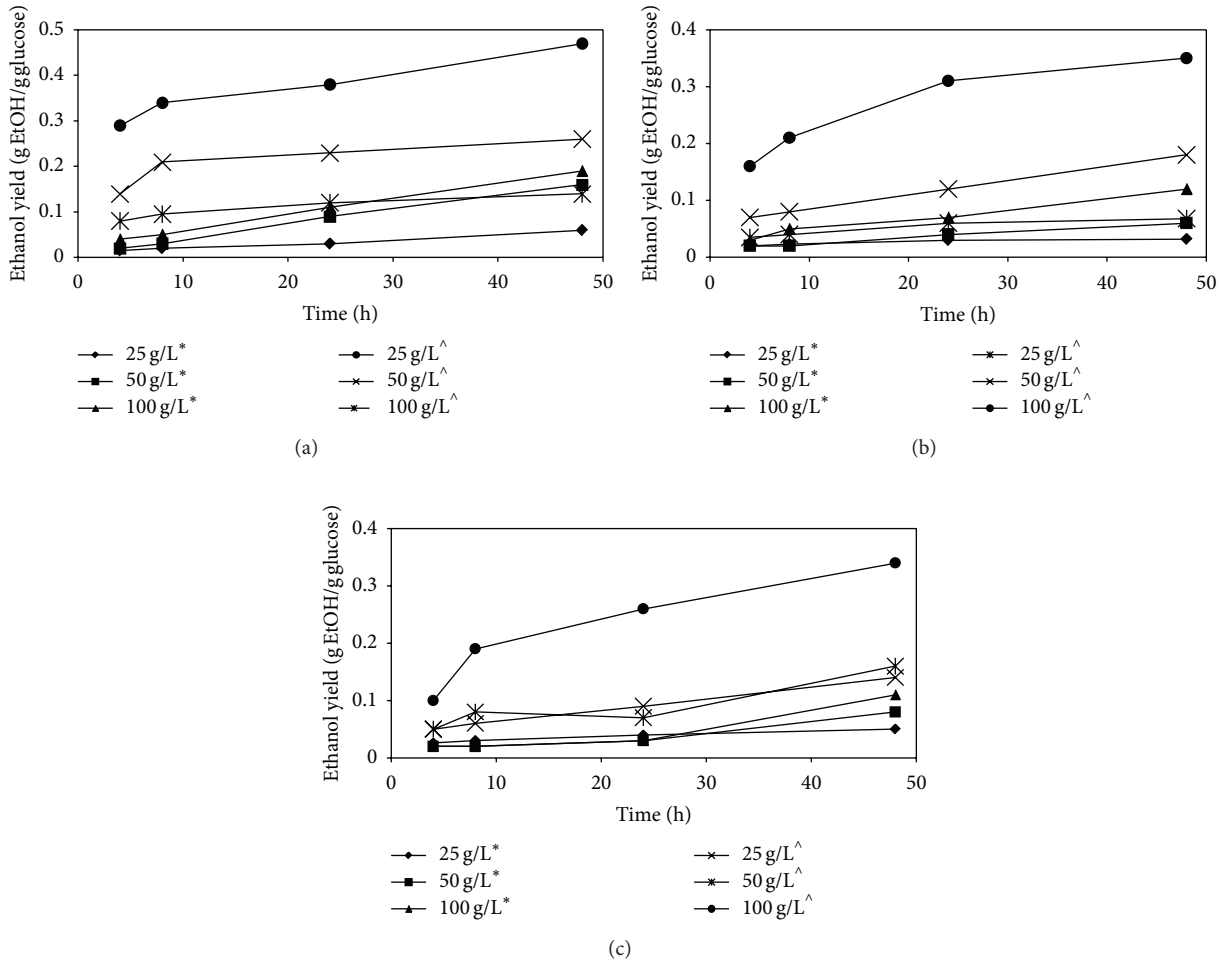

Figure 2: Yield of bioethanol after 48 h fermentation of microalgal biomass with different particle sizes for both cases: (a) 35 μm $\leq x \leq$ 90 μm, (b) 125 μm $\leq x \leq$ 180 μm, and (c) 295 μm $\leq x \leq$ 425 μm (*Case 1: cellulase; ^Case 2: cellulase + cellobiase).

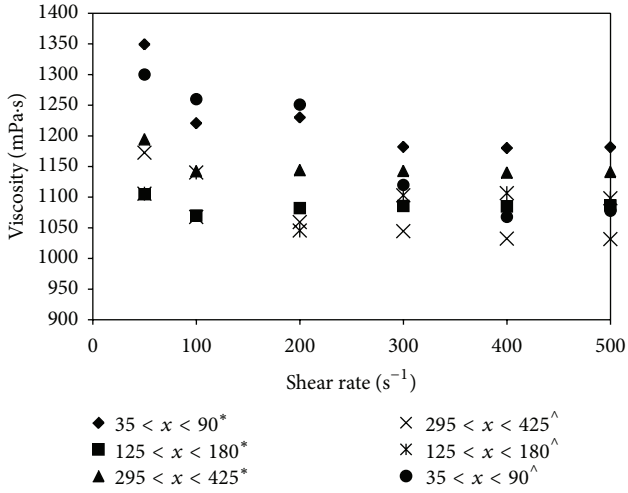

Figure 3: Viscosity versus shear rate for the different particle size biomass. A decreasing trend in viscosity was observed with increasing shear rate (*Case 1: cellulase; ^Case 2: cellulase + cellobiase; substrate concentration: 100 g/L).

a slightly higher viscosity than Case 1. The effective enzyme-substrate interactions associated with smaller particle size biomass result in a more viscous hydrolysate than large size particles as more water molecules are consumed per unit volume, exceeding the reduction of total solids concentration [29].

We also studied the viscosity profile of the hydrolysates over the time course of hydrolysis and the data is presented in Figure 4. The hydrolysate viscosities for both Cases 1 and 2 reduced with hydrolysis time with a significant decrease which was observed at the initial stage of hydrolysis between 4 and 24 h. This is probably due to the faster initial kinetics, structural changes, and/or the release of intercalating molecules in the cell wall. Decreasing viscosity during hydrolysis is caused by cellulose degradation as the structure and solid concentration change during the cellulolytic activity caused by the enzymes [10].

The profiles of viscosity and bioethanol production were superimposed to understand their relationship during the enzymatic hydrolysis process as shown in Figure 5. It can be seen that bioethanol yield increases with lower viscosities.

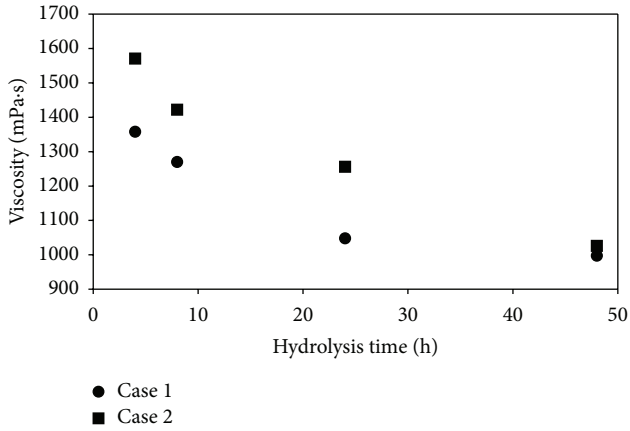

Figure 4: Hydrolysate viscosity profiles during hydrolysis for single-enzyme (Case 1: cellulase) and double-enzyme (Case 2: cellulase + cellobiase) conditions. The viscosity of the hydrolysates in both cases decreased with hydrolysis time. The data presented is for assay number 1 in both cases (substrate concentration: 25 g/L).

This trend also matches glucose yields as higher released glucose produces higher bioethanol yields. The results show that less viscous slurry is required to produce high glucose yields under effective mixing.

4. Conclusion

This paper is the premier study on the effect of particle size of microalgal biomass on enzymatic hydrolysis and bioethanol production. The results show that the highest glucose and bioethanol yields were obtained using biomass with smaller particle size ($35\,\mu\text{m} \leq x \leq 90\,\mu\text{m}$) at a substrate concentration of 100 g/L. The addition of the second enzyme, cellobiase, increases the glucose yield, thus increasing the bioethanol yield. This was confirmed by a kinetic investigation of the double enzyme process using the rapid equilibrium model. The viscosity of the hydrolysate also influences glucose yield. Lower viscosities result in higher glucose yields. Overall, microalgal biomass particle size has a significant effect on enzymatic hydrolysis and bioethanol production.

Abbreviations

S:	Substrate concentration, g/L
E:	Enzyme concentration, g/L
SE:	Concentration of substrate-enzyme complex
P:	Product concentration, g/L
k_1, k_{-1}, k_2, k_1', k_{-1}', and k_2':	Rate constants, g/L
K_e, K_e':	Equilibrium constant, g/L
$(dP/dt)_{P_0}$:	Product formation at the initial conditions
E_1:	Enzyme I (cellulase) concentration, g/L
E_2:	Enzyme II (cellobiase) concentration, g/L

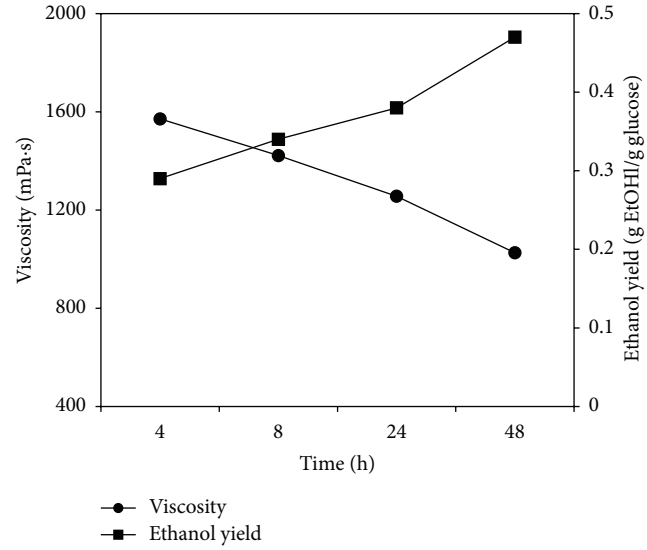

Figure 5: Relationship between hydrolysate viscosity and bioethanol yield. Bioethanol yield increases with lower hydrolysate viscosities. The data presented is for assay number 1 of Case 2 (substrate concentration: 25 g/L).

S_C:	Cellulose concentration, g/L
S_{CB}:	Cellobiose concentration, g/L
$S_C E_1$:	Concentration of cellulose-cellulase complex
$S_{CB} E_2$:	Concentration of cellobiose-cellobiase complex
K_m:	Michaelis constant, g/L
V_{max}:	Maximum rate of hydrolysis, g/L·min.

Conflict of Interests

The authors declare that there is no conflict of interests regarding the publication of this paper.

Acknowledgments

This work has been supported by the Department of Chemical Engineering, Monash University, Australia, and the Ministry of Higher Education, Malaysia.

References

[1] R. Harun, M. Singh, G. M. Forde, and M. K. Danquah, "Bioprocess engineering of microalgae to produce a variety of consumer products," *Renewable and Sustainable Energy Reviews*, vol. 14, no. 3, pp. 1037–1047, 2010.

[2] V. K. Dhargalkar and X. N. Verlecar, "Southern Ocean seaweeds: a resource for exploration in food and drugs," *Aquaculture*, vol. 287, no. 3-4, pp. 229–242, 2009.

[3] J. L. Fortman, S. Chhabra, A. Mukhopadhyay et al., "Biofuel alternatives to ethanol: pumping the microbial well," *Trends in Biotechnology*, vol. 26, no. 7, pp. 375–381, 2008.

[4] S. P. Choi, M. T. Nguyen, and S. J. Sim, "Enzymatic pretreatment of *Chlamydomonas reinhardtii* biomass for ethanol production," *Bioresource Technology*, vol. 101, no. 14, pp. 5330–5336, 2010.

[5] R. Harun, M. K. Danquah, and G. M. Forde, "Microalgal biomass as a fermentation feedstock for bioethanol production," *Journal of Chemical Technology and Biotechnology*, vol. 85, no. 2, pp. 199–203, 2010.

[6] Y. Zheng, Z. Pan, R. Zhang, and B. M. Jenkins, "Kinetic modeling for enzymatic hydrolysis of pretreated creeping wild ryegrass," *Biotechnology and Bioengineering*, vol. 102, no. 6, pp. 1558–1569, 2009.

[7] Y. Sun and J. J. Cheng, "Dilute acid pretreatment of rye straw and bermudagrass for ethanol production," *Bioresource Technology*, vol. 96, no. 14, pp. 1599–1606, 2005.

[8] L. T. Fan, Y. H. Lee, and D. H. Beardmore, "Mechanism of the enzymatic hydrolysis of cellulose: effects of major structural features of cellulose on enzymatic hydrolysis," *Biotechnology and Bioengineering*, vol. 22, pp. 177–199, 1980.

[9] M. Pedersen and A. S. Meyer, "Influence of substrate particle size and wet oxidation on physical surface structures and enzymatic hydrolysis of wheat straw," *Biotechnology Progress*, vol. 25, no. 2, pp. 399–408, 2009.

[10] R. K. Dasari and R. Eric Berson, "The effect of particle size on hydrolysis reaction rates and rheological properties in cellulosic slurries," *Applied Biochemistry and Biotechnology*, vol. 137–140, no. 1–12, pp. 289–299, 2007.

[11] L. M. J. Carvalho, R. Borchetta, and É. M. M. da Silva, "Effect of enzymatic hydrolysis on particle size reduction in lemon juice (*Citrus limon*, L.)," *Brazilian Journal of Food Technology*, vol. 4, pp. 277–282, 2006.

[12] A.-I. Yeh, Y.-C. Huang, and S. H. Chen, "Effect of particle size on the rate of enzymatic hydrolysis of cellulose," *Carbohydrate Polymers*, vol. 79, no. 1, pp. 192–199, 2010.

[13] I. Ballesteros, J. M. Oliva, A. A. Navarro, A. González, J. Carrasco, and M. Ballesteros, "Effect of chip size on steam explosion pretreatment of softwood," *Applied Biochemistry and Biotechnology A: Enzyme Engineering and Biotechnology*, vol. 84–86, pp. 97–110, 2000.

[14] I. Ballesteros, J. M. Oliva, M. J. Negro, P. Manzanares, and M. Ballesteros, "Enzymic hydrolysis of steam exploded herbaceous agricultural waste (*Brassica carinata*) at different particule sizes," *Process Biochemistry*, vol. 38, no. 2, pp. 187–192, 2002.

[15] B. Baldan, P. Andolfo, L. Navazio, C. Tolomio, and P. Mariani, "Cellulose in algal cell wall: an "in situ" localization," *European Journal of Histochemistry*, vol. 45, no. 1, pp. 51–56, 2001.

[16] K. Sander and G. S. Murthy, "Enzymatic degradation of microalgal cell walls," in *Proceedings of the American Society of Agricultural and Biological Engineers Annual International Meeting*, pp. 2489–2500, Reno, Nev, USA, June 2009.

[17] J. N. Murdock and D. L. Wetzel, "FT-IR microspectroscopy enhances biological and ecological analysis of algae," *Applied Spectroscopy Reviews*, vol. 44, no. 4, pp. 335–361, 2009.

[18] D. S. Domozych, M. Ciancia, J. U. Fangel, M. D. Mikkelsen, P. Ulvskov, and W. G. Willats, "The cell walls of green algae: a journey through evolution and diversity," *Frontiers in Plant Science*, vol. 3, article 82, 2012.

[19] M. L. Nelson and R. T. O'Connor, "Relation of certain infrared bands to cellulose crystallinity and crystal latticed type. Part I. Spectra of lattice types I, II, III and of amorphous cellulose," *Journal of Applied Polymer Science*, vol. 8, pp. 1311–1324, 1964.

[20] R. Sposina Sobral Teixeira, A. Sant'Ana da Silva, H.-W. Kim et al., "Use of cellobiohydrolase-free cellulase blends for the hydrolysis of microcrystalline cellulose and sugarcane bagasse pretreated by either ball milling or ionic liquid [Emim][Ac]," *Bioresource Technology*, vol. 149, pp. 551–555, 2013.

[21] C. Divne, J. Ståhlberg, T. Reinikainen et al., "The three-dimensional crystal structure of the catalytic core of cellobiohydrolase I from *Trichoderma reesei*," *Science*, vol. 265, no. 5171, pp. 524–528, 1994.

[22] Y.-S. Liu, J. O. Baker, Y. Zeng, M. E. Himmel, T. Haas, and S.-Y. Ding, "Cellobiohydrolase hydrolyzes crystalline cellulose on hydrophobic faces," *Journal of Biological Chemistry*, vol. 286, no. 13, pp. 11195–11201, 2011.

[23] J. Jalak and P. Väljamäe, "Mechanism of initial rapid rate retardation in cellobiohydrolase catalyzed cellulose hydrolysis," *Biotechnology and Bioengineering*, vol. 106, no. 6, pp. 871–883, 2010.

[24] S. Al-Zuhair, "The effect of crystallinity of cellulose on the rate of reducing sugars production by heterogeneous enzymatic hydrolysis," *Bioresource Technology*, vol. 99, no. 10, pp. 4078–4085, 2008.

[25] M. Chauve, H. Mathis, D. Huc, D. Casanave, F. Monot, and N. L. Ferreira, "Comparative kinetic analysis of two fungal β-glucosidases," *Biotechnology for Biofuels*, vol. 3, article 3, 2010.

[26] L. Liu and H. Chen, "Enzymatic hydrolysis of cellulose materials treated with ionic liquid [BMIM]Cl," *Chinese Science Bulletin*, vol. 51, no. 20, pp. 2432–2436, 2006.

[27] Q. Gan, S. J. Allen, and G. Taylor, "Kinetic dynamics in heterogeneous enzymatic hydrolysis of cellulose: an overview, an experimental study and mathematical modelling," *Process Biochemistry*, vol. 38, no. 7, pp. 1003–1018, 2003.

[28] G. P. Casey and W. M. Ingledew, "Ethanol tolerance in yeasts," *Critical Reviews in Microbiology*, vol. 13, no. 3, pp. 219–280, 1986.

[29] K. W. Dunaway, R. K. Dasari, N. G. Bennett, and R. Eric Berson, "Characterization of changes in viscosity and insoluble solids content during enzymatic saccharification of pretreated corn stover slurries," *Bioresource Technology*, vol. 101, no. 10, pp. 3575–3582, 2010.